



HAL
open science

Membrane biogenesis in Apicomplexa parasites: How trafficking and recycling lipid sources for dynamic membrane remodeling sustain parasite survival within its human host

Christophe-Sébastien Arnold

► **To cite this version:**

Christophe-Sébastien Arnold. Membrane biogenesis in Apicomplexa parasites: How trafficking and recycling lipid sources for dynamic membrane remodeling sustain parasite survival within its human host. Microbiology and Parasitology. Université Grenoble Alpes [2020-..], 2023. English. NNT : 2023GRALV034 . tel-04281000

HAL Id: tel-04281000

<https://theses.hal.science/tel-04281000>

Submitted on 12 Nov 2023

HAL is a multi-disciplinary open access archive for the deposit and dissemination of scientific research documents, whether they are published or not. The documents may come from teaching and research institutions in France or abroad, or from public or private research centers.

L'archive ouverte pluridisciplinaire **HAL**, est destinée au dépôt et à la diffusion de documents scientifiques de niveau recherche, publiés ou non, émanant des établissements d'enseignement et de recherche français ou étrangers, des laboratoires publics ou privés.

THÈSE

Pour obtenir le grade de

DOCTEUR DE L'UNIVERSITÉ GRENOBLE ALPES

École doctorale : CSV- Chimie et Sciences du Vivant

Spécialité : Virologie - Microbiologie - Immunologie

Unité de recherche : IAB : Epigenetics, Environment, Cell Plasticity, Cancer (UGA / Inserm U1209 / CNRS UMR 5309)

Biogenèse membranaire chez les parasites Apicomplexa : trafic et recyclage lipidique pour le remodelage membranaire permettant la survie du parasite chez son hôte humain

Membrane biogenesis in Apicomplexa parasites: How trafficking and recycling lipid sources for dynamic membrane remodeling sustain parasite survival within its human host

Présentée par :

Christophe-Sébastien ARNOLD

Direction de thèse :

Cyrille BOTTE

DIRECTEUR DE RECHERCHE, CNRS

Yoshiki YAMARYO-BOTTE

RESPONSABLE THE PLATFORM DU LIPIDOMIC,

Directeur de thèse

Co-encadrante de thèse

Rapporteurs :

Dominique SOLDATI-FAVRE

PROFESSEUR, Université de Genève

Frédéric DOMERGUE

CHARGE DE RECHERCHE HDR, CNRS délégation Aquitaine

Thèse soutenue publiquement le **11 mai 2023**, devant le jury composé de :

Cyrille BOTTE

DIRECTEUR DE RECHERCHE, CNRS délégation Alpes

Simon GRAS

DOCTEUR EN SCIENCES, Ludwig-Maximilians - Universität München

Dominique SOLDATI-FAVRE

PROFESSEUR, Université de Genève

Corinne MERCIER

PROFESSEUR DES UNIVERSITES, Université Grenoble-Alpes

Frédéric DOMERGUE

CHARGE DE RECHERCHE HDR, CNRS délégation Aquitaine

Francesca GIORDANO

CHARGE DE RECHERCHE HDR, INSERM délégation Paris Ile-de-France Sud

Directeur de thèse

Examinateur

Rapporteuse

Présidente

Rapporteur

Examinatrice

Invités :

Yoshiki Yamaryo-Botté

DOCTEUR EN SCIENCES, Université Grenoble-Alpes



Acknowledgments

To Cyrille and Yoshiki, my bosses, it is hard to find the right words after all you have done for me. All you taught about the apicomplexan field, the research world in general. Thank you, Yoshiki, for the good time learning about GC-MS analysis and maintenance, and for sharing pieces of advice about my future career and life. Thank you, Cyrille, for being a good boss, for having shown me the unseeing world of research and institutions, for the good time at conferences and beside the lab, and for the enthusiasm you always have shown. Thank you, Nick my mini-boss, who taught me all I know about *Toxoplasma* cellular biology, molecular technics, and cell cultures, for your time, patience, and help during my PhD. My time in the lab could have not been better than it was!

Thank you, Sarah, Nyamekye (Mitch), my young PhD fellows, and Celia (sorry again for your knee..) for the moments and talks we have shared in and out of the lab! Thank you, Serena, my PhD twin, without whom this journey would have not been the same, even if you finished a little bit before me. These were three great years of shared cups of coffee, pipettes, and parasites!

To all the Apicos, Sam, Delphine, Marie-France, Catherine, and Pierre, for being so cheerful, and helpful. Thank you all to have shared your experiences, your time, and your kindness with me, I really appreciated each moment we have spent together.

A special thanks to all of my jury members: my reporters, Pr. Dominique Soldati-Favre, and Dr. Frédéric Domergue; my examiners, Pr. Corinne Mercier, Dr. Francesca Giordano and Dr. Simon Gras for being on my side to close this amazing adventure!

I would also like to thank my PhD CSI members Dr. Sébastien Besteiro, Dr. Juliette Jouhet, and Dr. Ludovic Pelosi for their guidance throughout my PhD from CSI #1 to CSI #3.

Last but not least, I would like to thank my family, my loving parents who always provided me with all their support and love, and without whom none of this would have been possible. They gave me the love of discovery and curiosity and they pushed me forward to be who I am today. Finally, I would like to thank my lovely wife Aurélia, who has supported me during my entire PhD, giving me strength and courage, always supportive and present for me in any circumstances.

Abstract

Apicomplexan parasites are responsible for severe diseases such as malaria, which kills almost half a million people yearly, and toxoplasmosis, which chronically infects nearly one-third of the population worldwide. These infections affect humans and livestock and have serious social and economic impacts, which are more important in developing countries. These diseases are caused by unicellular and obligate intracellular parasites, whose proliferation depends on the acquisition of lipids through the massive scavenging from their hosts and their own *de novo* synthesis capabilities. These parasites use these two sources to form a lipidic "patchwork" essential for their development. While the synthesis of both fatty acids and phospholipids is widely studied, little is known about the transport of those lipids. Which transporters are involved in the lipidic transport within the parasite and between these different intracellular compartments? To answer this question, I focused my interest and PhD project on major Apicomplexa lipid transporters of the P-type ATPase family: a P5 ATPase, FLP12, which subgroup's substrate affinity remains poorly known, and a P4 ATPase, FLP2, predicted to "flip" phospholipids.

Most Apicomplexan parasites have a relic plant-like plastid called the apicoplast, a non-photosynthetic organelle capable of synthesizing short fatty acids *via* its prokaryotic fatty acid synthesis pathway (FASII). These fatty acids are either exported out of the apicoplast or directly used to form lyso- or phosphatidic acid for parasite membrane biogenesis. How these different lipids are exported outside the apicoplast remains unknown. During my thesis, I identified and characterized a novel P5-ATPase in *Toxoplasma*, *TgFLP12*, which localizes in the apicoplast membranes. Phylogenetic analysis of *TgFLP12* revealed that it belongs to a new subgroup of P5-ATPase, P5C. The shutdown of *TgFLP12* expression was lethal to the parasite by slowing down its intracellular replication. Analysis of the lipidome and lipid fluxes by GC-MS combined with isotopic metabolic markers showed that *TgFLP12* is essential for the incorporation of myristic acid from the FASII in the different classes of lipids used for membrane biogenesis. In the absence of *TgFLP12*, the parasites lost most fatty acids derived from FASII. Only the complementation by short fatty acids similar to those made by FASII restored the growth of the parasites. The data obtained by these different approaches, and the presence of a *TgFLP12* homolog in most Apicomplexa bearing an apicoplast point to *TgFLP12* being the apicoplast fatty exporter that likely replaced the canonical chloroplast fatty acid exporter usually found in photosynthetic organisms.

The second part of my project focused on the characterization of a P4 ATPase, named *TgFLP2*, present in the trans-Golgi network of the parasite, and essential for its survival. P4-ATPases are known to be involved in the maintenance of membrane asymmetry allowing membrane curvatures necessary for vesicular trafficking. I showed that in *Toxoplasma*, *TgFLP2* plays an essential role in most of the known trans-Golgi vesicular trafficking. Its deletion was notably critical for the import of the content of micronemes, secretory organelles essential for the active invasion and egress of the parasite from the host. Furthermore, we showed that *TgFLP2* also plays a central role in the newly discovered endocytosis machinery of the parasite, allowing the trafficking of vesicles essential for the completion of endocytosis. *TgFLP2* was also shown to be essential for the lipid homeostasis of the parasite and its deletion led to a rapid decrease of its phosphatidylethanolamine (PE) composition. A similar phenotype was also observed after the deletion of *Neo1p* and *Drs2p*, the two P4-ATPases present in the yeast Golgi. All these elements demonstrated the central role of *TgFLP2* in the control of trans-Golgi vesicular trafficking and illustrated its central role in the regulation of parasite intracellular trafficking.

Résumé

Les parasites du phylum des Apicomplexes sont responsables de graves maladies telles que le paludisme, qui tue encore presque un demi-million de personnes par an, ou la toxoplasmose dont près d'un tiers de la population mondiale est chroniquement infecté. Ces infections touchent à la fois les humains et les élevages et ont de forts impacts sociaux et économiques, plus importants encore dans les pays en développement. Ces maladies sont causées par des parasites unicellulaires et obligatoirement intracellulaires, dont la prolifération dépend de l'acquisition massive de lipides par deux mécanismes : détournement des ressources lipidiques de l'hôte et synthèse *de novo*. Ces parasites utilisent ces deux sources pour former un « patchwork » essentiel à leur développement. Alors que la synthèse d'acides gras et de phospholipides a été largement étudiée, le transport de ces lipides reste méconnu. Quels transporteurs sont impliqués dans le trafic de lipides au sein du parasite et entre ses différents organites ? Pour répondre à cette question, j'ai étudié et caractérisé durant ma thèse différents transporteurs de lipides de la famille des P-type ATPases, une P5 ATPase, FLP12, sous-groupe dont l'affinité de substrat reste mal connue et une P4-ATPase, FLP2, prédite pour « flipper » des phospholipides dans les membranes lipidiques.

La plupart des Apicomplexes possèdent un organite dérivé d'un chloroplaste, nommé l'apicoplaste, capable de synthétiser des acides gras courts grâce à sa voie procaryotique de synthèse des acides gras (FASII). Ces acides gras sont soit exportés hors de l'apicoplaste, soit utilisés pour former de l'acide lyso- ou phosphatidique, précurseur membranaire central. Le processus par lequel ces différents lipides sont exportés hors de l'apicoplaste reste inconnu. Au cours de ma thèse, j'ai étudié le rôle d'une P5-ATPase *TgFLP12* chez *Toxoplasma*. Cette P5-ATPase a été localisée dans les membranes de l'apicoplaste. L'analyse phylogénétique de *TgFLP12* a révélé qu'elle appartient à un nouveau sous-groupe de P5-ATPase, P5C. L'arrêt de l'expression de *TgFLP12* s'est révélé létal pour le parasite et ralentit sa répllication intracellulaire. L'analyse du lipidome par GC-MS combinée à des marquages métaboliques ont montré que *TgFLP12* est une protéine essentielle pour l'incorporation d'acide myristique issu de la FASII dans les différentes classes de lipides. Seule la complémentation exogène par des acides gras similaires à ceux produits par la FASII a permis de rétablir la croissance parasitaire. Les résultats de ces différentes approches, ainsi que la présence de l'homologue de FLP12 chez tous les Apicomplexes portant un apicoplaste, pointent *TgFLP12* comme étant l'exporteur d'acide gras de l'apicoplaste en l'absence du transporteur canonique du chloroplaste présent chez les organismes photosynthétiques.

La seconde partie de mon projet de thèse a porté sur la caractérisation d'une P4-ATPase, *TgFLP2*, présent dans le Golgi du parasite et qui est essentiel à sa survie. Les P4-ATPases sont impliquées dans le maintien de l'asymétrie membranaire permettant la courbure membranaire nécessaire au trafic vésiculaire. Chez *Toxoplasma*, j'ai montré que *TgFLP2* joue un rôle essentiel dans le contrôle du trafic vésiculaire issu du réseau trans-Golgi. Sa délétion est néfaste au trafic du contenu des micronèmes, organelles de sécrétion essentiels pour l'invasion et la sortie active du parasite de son hôte. *TgFLP2* joue un rôle central dans les processus nouvellement découverts d'endocytose parasitaire, permettant l'acquisition de nutriments issus de l'hôte. *TgFLP2* est essentielle pour l'homéostasie lipidique du parasites et sa suppression entraine une rapide baisse dans sa composition en phosphatidyléthanolamine (PE). Ce phénotype est similaire à celui observé lors de l'inactivation de ses homologues chez la levure, *Neo1p* et *Drs2p*, deux P4 également localisées dans le Golgi. Tous ces éléments pointent le rôle central de *TgFLP2* dans le contrôle du trafic vésiculaire trans-Golgi du parasite et illustre son importance pour sa survie.

Table of Contents

| | |
|---|----|
| <i>Acknowledgments</i> | 3 |
| <i>Abstract</i> | 4 |
| <i>Résumé</i> | 6 |
| <i>Abbreviations</i> | 13 |
| <i>Introduction:</i> | 19 |
| <i>Chapter I: Introduction to Apicomplexa parasites</i> | 21 |
| Apicomplexa belong to the superphylum of Alveolata | 21 |
| <i>Toxoplasma gondii</i> and toxoplasmosis | 22 |
| <i>Plasmodium</i> spp and human malaria..... | 23 |
| Life cycles | 24 |
| <i>T. gondii</i> life cycle (Figure 2) | 24 |
| Asexual development within the intermediate mammal host | 24 |
| Sexual development within the definitive felid host | 25 |
| <i>Plasmodium</i> life cycle (Figure 3) | 27 |
| Asexual development within the intermediate human host | 27 |
| Sexual development within the final <i>Anopheles</i> host | 27 |
| Dissection of Apicomplexa’s ultrastructure | 30 |
| General structures (Figure 4)..... | 30 |
| The inner membrane complex, an Alveolata specificity | 30 |
| The apical complex, big gun for a small parasite | 30 |
| Secretory organelles..... | 31 |
| (1) Micronemes..... | 31 |
| (2) Rhoptries..... | 32 |
| (3) Dense granules. C..... | 32 |
| Mitochondria | 33 |
| Apicoplast, the memory of plant ascendance..... | 34 |
| Heme synthesis pathway..... | 35 |
| Iron-sulfur cluster synthesis pathway..... | 35 |
| Isoprenoid synthesis pathway..... | 36 |
| Fatty acid synthesis type II pathway..... | 36 |

| | |
|--|-----------|
| Chapter II: Lipids in Apicomplexa | 39 |
| Lipid definition..... | 39 |
| Phospholipids are the major lipids of membranes..... | 39 |
| Phosphatidic acid (PA)..... | 39 |
| Phosphatidylcholine (PC)..... | 41 |
| Phosphatidylethanolamine (PE): | 41 |
| Phosphatidylserine (PS): | 41 |
| Phosphatidylinositol (PI):..... | 42 |
| Phosphatidylthreonine (PT): | 42 |
| Cardiolipin (CL) and phosphatidylglycerol (PG):..... | 43 |
| Phospholipids are not the only important lipids for membranes | 43 |
| Sphingolipids (SL)..... | 43 |
| Cholesterol (Chol). | 44 |
| Lipids can be stored | 47 |
| Chapter III Membrane trafficking and lipid transporters: how do lipids circulate within the cell? | 48 |
| Membranes are highly dynamic cell components | 48 |
| General introduction to eukaryote vesicular trafficking | 48 |
| Vesicular trafficking in Apicomplexa: exocytosis | 50 |
| Vesicular trafficking in Apicomplexa: the endocytosis..... | 51 |
| Non-vesicular lipid transfer <i>via</i> lipid transporters. | 53 |
| Eukaryote cytosolic and luminal lipid transporters, roles, and regulations (Figure 10)..... | 53 |
| Fatty acyl binding proteins (FABP) | 53 |
| Acyl-CoA binding proteins (ACBP)..... | 54 |
| Sterol carrier proteins (SCP)..... | 55 |
| Plant lipid transfer proteins (PLTP) | 55 |
| Other small LTPs, Sec14, PITP, and ORP | 56 |
| Repeating β -groove (RBG) domain LTPs:..... | 57 |
| To cross membranes, lipids require membranous transporters (Figure 11) | 58 |
| Flippases | 59 |
| Floppases | 60 |
| Scramblases | 61 |
| Fatty acid exporters (FAX), FA exit door for plastids? (Figure 12)..... | 61 |
| Apicomplexa lipid transporters: what do we know so far?..... | 63 |

| | |
|--|-----|
| References to chapters I, II, and III..... | 65 |
| <i>Scientific questions and aims of my thesis</i> | 85 |
| <i>Results</i> | 87 |
| <i>Chapter IV: Toxoplasma gondii apicoplast uses a new type of P5-ATPase for fatty acid export, which is essential for parasite survival</i> | 89 |
| Chapter IV Summary | 89 |
| Abstract | 90 |
| Introduction | 91 |
| Results | 95 |
| <i>TgFLP12</i> belongs to a new clade of P5-ATPase. | 95 |
| <i>TgFLP12</i> is an apicoplast membrane protein. | 97 |
| <i>TgFLP12</i> is essential for tachyzoite development and apicoplast integrity. | 98 |
| <i>TgFLP12</i> deletion alters parasite short FA chain content. | 100 |
| Disruption of <i>TgFLP12</i> causes a defect in apicoplast FASII activity as revealed by ¹³ C lipid flux analysis. | 102 |
| | 102 |
| <i>TgFLP12</i> is responsible for free fatty acid export from the apicoplast..... | 105 |
| Discussion | 109 |
| Acknowledgments | 112 |
| Material and Methods | 112 |
| <i>Toxoplasma gondii</i> strains and cultures: | 112 |
| Generation of inducible knockdown FLP12 line in <i>T. gondii</i> : | 112 |
| Immunofluorescence assay:..... | 113 |
| Phylogenetic analysis of P5-ATPases: | 113 |
| Western blot analysis: | 114 |
| Plaque assays in <i>T. gondii</i> mutants: | 114 |
| Replication assay in <i>T. gondii</i> mutants:..... | 114 |
| Electron microscopy:..... | 115 |
| Lipidomic analysis: | 115 |
| Fluxomic analysis: | 116 |
| Statistics and graphs:..... | 116 |
| Supplementary figures | 118 |
| References to chapter IV | 126 |

Chapter V: *TgFLP2*, a flippase that controls trans-Golgi vesicular trafficking and endocytosis in *Toxoplasma gondii*..... 131

Chapter V Summary..... 131

Abstract 133

Introduction..... 134

Results..... 139

TgFLP2 belongs to the sub-family of P4B-ATPases. 139

TgFLP2 is an essential putative Golgi flippase. 140

Disruption of *TgFLP2* impairs the trafficking of microneme content. 142

TgFLP2 is essential for endocytosis trafficking. 146

TgFLP2 is essential for correct membrane homeostasis. 147

Discussion 149

TgFLP2 could act as a PE/PS flippases like *ScNeo1p*. 150

Toxoplasma vesicular trafficking is dependent on *TgFLP2*. 151

Plasmodium homolog *PfATP8* could play a similar role as *TgFLP2*. 153

Acknowledgments 154

Material and Methods 154

Toxoplasma gondii strains and cultures: 154

Generation of inducible knockdown *TgFLP2* line:..... 154

Immunofluorescence assay:..... 155

Prediction of protein structure: 155

Egress assay: 155

Microneme secretion assay:..... 156

Phylogenetic analysis of P4-ATPases: 156

Western blot analysis: 156

Plaque assays in *T. gondii* mutants: 156

Replication assay in *T. gondii* mutants:..... 157

Electron microscopy:..... 157

Lipidomic analysis: 157

Fluxomic analysis: 158

Generation of inducible knockdown *PfFLP2* line in *Plasmodium falciparum*: 158

Statistics and graphs:..... 159

Supplementary figures..... 160

References to chapter V 166

| | |
|--|------------|
| <i>Chapter VI: General discussion and future perspectives</i> | 171 |
| <i>TgFLP12, a FA exporter of the apicoplast</i> | 172 |
| <i>TgFLP2, a pivotal element of <i>Toxoplasma</i> vesicular trafficking</i> | 173 |
| Apicoplast transporters remain poorly known | 175 |
| Parasite’s transportome, the Achille heel of Apicomplexa? | 176 |
| Membrane contact sites in Apicomplexa | 177 |
| Last word | 177 |
| References to chapter VI | 179 |
| <i>Annex</i> | 182 |

Abbreviations

| Abbreviation: | Definition: |
|----------------------|---|
| 5-ALA | 5-Aminolevulinic acid |
| ABC | ATP binding cassette |
| ACAT1/2 | Acyl-CoA cholesterol acyl transferases 1/2 |
| ACBP | Acyl-CoA binding protein |
| ACP | Acyl-carrier protein |
| ACS | Acyl-CoA synthetase |
| AGPAT | Acyl glycerol-3-phosphate transferase |
| AIDS | Acquired immunodeficiency syndrome |
| AMA1 | Apical membrane antigen 1 |
| AP1/2 | Clathrin adaptor 1/2 |
| APR | apical polar ring |
| Arf1 | ADP-ribosylation factor 1 |
| Arp2/3 | Actin Related Protein 2/3 complex |
| ASP5 | Aspartyl protease 5 |
| ATc | Anhydrotetracycline |
| ATG | Autophagy-related protein |
| ATP | Adenosine triphosphate |
| ATR _x 1 | Apicoplast thioredoxin 1 |
| ATS1 / ATS2 | Acyltransferase 1 & 2 |
| AV | Apical vesicle |
| C/EPT | Choline/ethanolamine phosphotransferase |
| CDC50 | Cell division control protein 50 |
| CDP | Cytidine biphosphate |
| CDS2 | CDP-DAG synthase 2 |
| cGMP | Cyclic guanosine monophosphate |
| Chol | Cholesterol |
| CIA | Cytosolic iron-sulfur cluster assembly |
| CL | Cardiolipin |
| CoA | Coenzyme A |
| COPI / COPII | Coat protein I/II |
| CPB | Cathepsin protease B |
| CPL | Cathepsin protease L |
| CPN60 | Chaperonin 60 |
| CPO | Coproporphyrinogen III oxidase |
| CPO-III | Coproporphyrinogen III |
| CRAL-TRIO | Cellular retinaldehyde-binding protein and TRIO guanine exchange factor |
| CRT | Chloramphenicol resistance transporter |
| DAG | Diacylglycerol |
| DAMPP | Dimethylallyl diphosphate |
| DG | Dense granule |

| | |
|------------|--|
| DGAT | Diacylglycerol acyltransferase |
| DHSM | Dihydrosphingomyelin |
| DNA | Deoxyribonucleic acid |
| DOXP | 1-Deoxy-D-xylulose 5-phosphate (non-mevalonate) pathway |
| DrpB/C | Dynamamin B/C |
| DV | Digestive vacuole |
| ELC | Endosome-like compartment |
| ELO A/B/C | Elongases A/B/C |
| EPC | Ethanolaminephosphoryl-ceramide |
| Eps15 | Epidermal growth factor receptor protein substrate 15 |
| ER | Endoplasmic reticulum |
| ERAD | ER-associated degradation |
| ESCRT | Endosomal sorting complexes required for transport machinery |
| EXP2 | Pore-forming protein 2 |
| FA | Fatty acid |
| FabB/F | β -ketoacyl-ACP synthases I/II |
| FabG | β -ketoacyl-ACP reductase |
| FabI | Enoyl-ACP reductase |
| FABP | Fatty acid binding protein |
| FabZ | β -hydroxyacyl-ACP dehydratase |
| FASII | Type fatty acid synthesis pathway |
| FAX | Fatty acid exporter |
| Fe-S | Iron-sulfur cluster |
| FFA | Free fatty acid |
| FFAT | Two phenylalanines in an acid tract motif |
| FLP | Flippase |
| FRM1 | Formin 1 |
| GC-MS | Gas chromatography-mass spectrometry |
| GFP | Green fluorescent protein |
| GPAT | Glycerol-3-phosphate acyltransferase |
| GPI-anchor | Glycosylphosphatidylinositol-anchor |
| GRA | Granule dense protein |
| GRASP | Golgi reassembly and stacking protein |
| H.O.S.T. | Host organelle-sequestering tubulostructures |
| HA | Hemagglutinin |
| HCCU | Host cell cytosol uptake |
| HDL | High-density lipoprotein particles |
| HFF | Human foreskin fibroblast |
| HP-TLC | High performance thin layer chromatography |
| IAA | Indole-3-acetic acid (auxin) |
| IFA | Immunofluorescence assay |
| iKD | Inducible knock-down |
| IMC | inner membrane complex |

| | |
|------------------------|--|
| IMM | Inner membrane of mitochondria |
| IP3 | inositol triphosphate |
| IPC | Inositolphosphoryl-ceramide |
| IPP | Isopentenyl pyrophosphate |
| ISC | Iron-sulfur cluster |
| IVN | Intravacuolar network |
| KIC1-9 | Kelch13 interaction candidates 1-9 |
| LACS | Long-chain acyl-CoA synthetase |
| LB | Lipid body |
| LD | Lipid droplet |
| LDL | Low-density lipoprotein particles |
| Lem3 | Alkylphosphocholine resistance protein (CDC50) |
| LPA | Lysophosphatidic acid |
| LPC | Lysophosphatidylcholine |
| LPL | Lysophospholipid |
| LTP | Lipid transfer protein |
| M2AP | MIC2-associated protein |
| MAF1 | Mitochondrial association factor 1 |
| mAID | Mini auxin degron system |
| MCS | Membrane contact site |
| MDR | Multidrug resistance proteins |
| MEP | methylerythritol phosphate |
| MHC | Major histocompatibility complex |
| MIC | Microneme protein |
| MID | Mass isotopomer distribution |
| MMV | Medicines for Malaria Venture |
| M β CD | Methyl β -cyclodextran |
| N-WASP | Neural Wiskott-Aldrich syndrome protein |
| ORP | OSBP related protein |
| OSBP | Oxysterol binding protein |
| PA | Phosphatidic acid |
| PC | Phosphatidylcholine |
| PCR | Preconoidal rings |
| PDH | Pyruvate dehydrogenase |
| PE | Phosphatidylethanolamine |
| PG | Phosphatidylglycerol |
| PGP | Phosphatidylglycerophosphate |
| PH | Pleckstrin homology domain |
| PI | Phosphatidylinositol |
| PI ₍₃₎ P | Phosphatidylinositol-3-monophosphate |
| PI _(3,5) P2 | Phosphatidylinositol-3,5-biphosphate |
| PI ₍₄₎ P | Phosphatidylinositol-4-monophosphate |
| PI _(4,5) P2 | Phosphatidylinositol-4,5-biphosphate |

| | |
|--------|---|
| PI-LPC | PI -phospholipase C |
| PIP | Phosphatidylinositol phosphate |
| PIPKI | Type I phosphatidylinositol-4-phosphate 5-kinase |
| PITP | PI transfer protein |
| PL | Phospholipid |
| PLSCR | Phospholipid scramblase |
| PLVAC | Plant-like vacuolar compartment |
| PMT | PE methyl transferase |
| PPIX | Protoporphyrin IX |
| PS | Phosphatidylserine |
| PSDmt | PS decarboxylase (mitochondrial) |
| PSDpv | PS decarboxylase (PV) |
| PSS | PS synthase |
| PSS2 | PS synthase 2 |
| PT | Phosphatidylthreonine |
| PTS | PT synthase |
| PV | Parasitophorous vacuole |
| PVM | Parasitophorous vacuole membrane |
| RBC | Red blood cell |
| RFP | Red fluorescent protein |
| RGB | Repeating β -groove |
| RNA | Ribonucleic acid |
| RON | Rhoptry neck protein |
| ROP | Rhoptry bulbous body protein |
| RSA | Rhoptry secretory apparatus |
| SAFA | Saturated fatty acid |
| SAG1 | Surface antigen |
| SCP | Sterol carrier protein |
| Sec14 | CRAL-TRIO |
| SERCA | sarco/endoplasmic reticulum Ca^{2+} -ATPase |
| SL | Sphingolipid |
| SM | Sphingomyelin |
| SNARE | Soluble N-ethylmaleimide-sensitive-factor attachment protein receptor |
| SPT | Serine palmitoyl transferase |
| Stx | Syntaxin |
| SUF | Sulfur formation (Fe-S cluster biogenesis pathways) |
| TAG | Triacylglycerol |
| TCA | Tricarboxylic acid |
| TEM | Transmission electron microscopy |
| TET | Tetracycline-controlled transcriptional activation |
| TEXEL | Toxoplasma export motif |
| TGD | Trigalactosyl-diacylglycerol |
| TIC | Translocon on the inner chloroplast membrane |

| | |
|-------|--|
| TM | Transmembrane domain |
| TOC | Translocon on the outer chloroplast membrane |
| TPT | Triose phosphate transporter |
| UFA | Unsaturated fatty acid |
| VAMP4 | Vesicle associated membrane protein 4 |
| VPS | Vacuolar protein sorting-associated protein |
| WT | Wild-type |

Introduction:

- **Chapter I: Introduction to Apicomplexa parasites**
- **Chapter II: Lipids in Apicomplexa**
- **Chapter III: Membrane trafficking and lipid transporters, how do lipids circulate within the cell?**

Chapter I: Introduction to Apicomplexa parasites

Apicomplexa belong to the superphylum of Alveolata

Apicomplexa belong to the superphylum of Alveolata, which groups unicellular protozoans that are either free-living phototrophs or mixotrophs, free-living heterotrophs or parasitic symbiotes. Alveolates are defined by the presence of flat vesicles underneath the plasma membrane as well as mitochondria with tubular cristae. The phylum of Alveolata presents a wide range of organisms divided into three major groups (Fast *et al.*, 2002; Nash *et al.*, 2008) (**Figure 1A**). (1) Ciliates comprising over seven thousand species, are characterized by cilia that can beat synchronously or in waves and participate to the coordination of directed movements or food ingestion. Ciliates include the textbook case genus *Paramecium*, which possesses an oral groove for food acquisition (bacteria ingestion). Ingested food is translocated to the food vacuole, and debris are eliminated *via* the anal pore where exocytosis events take place. (2) Dinoflagellates that group photosynthetic, heterotrophic, or mixotrophic protozoans. They are an important part of the plankton and play a key role in ocean oxygenation being essential photosynthetic symbiotes of corals. And finally, (3) Apicomplexa parasites that comprise more than six thousand species infecting a wide range of intermediate and final hosts including humans and livestock, with a massive social and economic burden. Apicomplexa comprise three major subgroups:

- Cryptosporidians which include *Cryptosporidium* infecting livestock and humans, are responsible for severe childhood diarrhea (Pane and Putignani, 2022) (**Figure 1B**).
- Gregarines infect numerous insects and invertebrates which makes them successful parasites. From a few micrometers, they can reach millimeters, making them one of the largest eukaryotic cells, and contrary to parasites from the two other families, they mostly develop in an extracellular lifestyle (Boisard and Florent, 2020).
- Coccidiomorphs to which belong Coccidians, including *Toxoplasma gondii* (**Figure 1C**) and Haemosporidia, which include intraerythrocytic Alveolata parasites with the *Plasmodium* subspecies (**Figure 1D**).

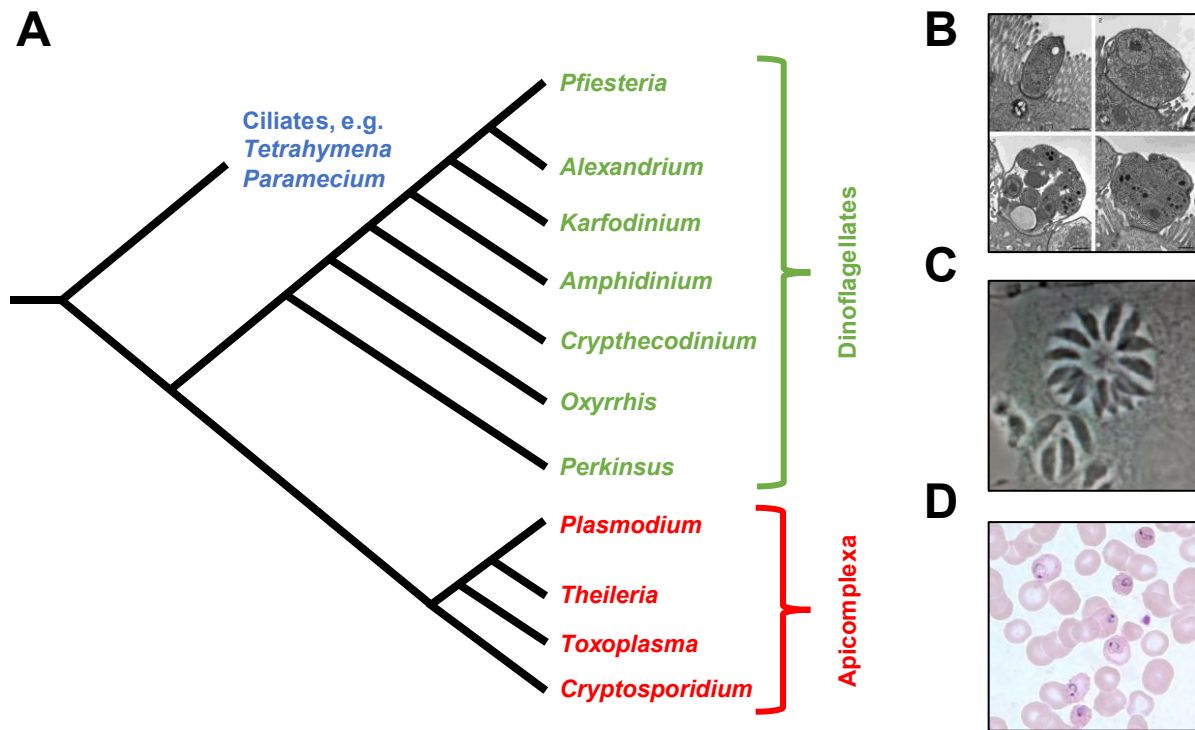


Figure 1: Evolution of Apicomplexa and diversity

(A) Simplified diagram of the Alveolata superfamily including Apicomplexa parasites, adapted from Nash *et al.*, 2008. (B) Electron micrographs of different developmental stages of *Cryptosporidium parvum* infecting piglet gut (Tzipori and Ward, 2002). (C) *Toxoplasma gondii* tachyzoite infecting human foreskin fibroblasts. (D) *Plasmodium falciparum* blood stage, all the parasites (violet) that infect erythrocytes are synchronized in ring stage.

***Toxoplasma gondii* and toxoplasmosis**

Toxoplasma gondii chronically infects about one-third of the human population worldwide and is the pathogenic agent of toxoplasmosis. The prevalence of *Toxoplasma*-infected patients varies according to cultural habits. Countries such as France or Brazil with high consumption of raw meat have a high prevalence of *Toxoplasma*-positive persons close to 40 % and 60 % respectively. Cultural changes such as the reduction of meat consumption affect these figures and tend to modify them. *Toxoplasma* infection is usually harmless, asymptomatic, or may cause flu-like illness in immunocompetent patients. However, the major problem is the ability of the parasite to chronically infect non-dividing tissues such as muscle cells, brain neurons, or eye tissue. When the patient's immune defenses decline, due to aging, immunosuppressive therapy (organ transplantation), chemotherapy, or co-infection with AIDS, the parasites move from the chronic to the acute stage and cause ocular or encephalitis toxoplasmosis, which can result in the patient's death (Edwards and Dubey, 2013; Pawełczyk *et al.*, 2022; Vittecoq *et al.*, 2012). *Toxoplasma* infection can also be fatal to the fetus of primo-infected women because the mother's immune system, confronted with

the parasite for the first time, cannot prevent the parasite from infecting the fetus, and impairing its brain development (Garweg *et al.*, 2022).

There do not exist sub-species of *Toxoplasma*, but it exists several types of strains depending on their ability to manipulate their hosts. Type I is highly virulent and does not convert to chronic infection. Type II, mostly prevalent in Europe and North America, is less lethal than type I, instead, it rapidly converts to a chronic phase and persists within its host during its lifespan. Type III is less prevalent in humans and mainly infects livestock, and is mostly found in South America. Currently, no vaccine exists against *Toxoplasma*, and current treatments are based on antiparasitic molecules pyrimethamine associated with sulfadiazine or antibiotics targeting the essential prokaryotic-origin organelle, the apicoplast. All have severe side effects such as allergies, nausea, stomach pain, muscle weakness, and depression, and cannot treat all phases of the disease. Currently, there is indeed no treatment available against the chronic bradyzoite stage.

***Plasmodium* spp and human malaria**

Despite important efforts to eradicate malaria across the world, malaria cases and deaths that were decreasing since 2000 are on the rise since 2014 with more than 245 million cases and close to 620 000 deaths in 2021 (World malaria report, 2022). Malaria is caused by Apicomplexa *Plasmodium* subspecies, which are divided into more than 150 species but four are considered non-zoonotic parasites: *P. ovale*, *P. malariae*, *P. vivax* and *P. falciparum* (“CDC Malaria,” 2020). The two last species are the most predominant with *vivax* localized to South-East Asia, and representing around 40 to 50 % of malaria cases, and *falciparum* principally present in Africa, where it is responsible for almost 100 % of malaria cases in the past 5 years. *Plasmodium vivax* is not as lethal as *falciparum* but can form “dormant” hypnozoites within the liver, which causes a resurgence of the disease years after the contagious mosquito bit. This creates a serious problem for malaria eradication (Habtamu *et al.*, 2022). *Plasmodium falciparum* contrary to *vivax* cannot form hypnozoites.

Plasmodium spp are transmitted to humans *via* the bite of an infected *Anopheles* female mosquito. However, ~100 species of mosquitoes can transmit malaria in endemic areas. Human malaria is characterized by two phases, one asymptomatic, after the mosquito bit the parasite reaches the liver to silently replicate, and one symptomatic, when parasites heavily infect red blood cells (erythrocytes) causing their destruction and thus anemia, fever, headache, nausea, and diarrhea. Treatments targeting the liver stage are considered prophylactic, and treatments targeting the blood

stage are symptomatic. Malaria treatments are based on a combination of active compounds to prevent the development of resistance. For the past century malaria treatments were based on quinine and chloroquine but nowadays all endemic regions are affected by parasites resistant to these compounds (Plowe, 2005; Uhlemann and Krishna, 2005; World Health Organization, 2006). The problem was and is the abuse of quinine as a prophylactic treatment in the prevention of malaria infection. Current treatments are based on the recent 2015 Nobel prize in physiology and medicine molecule artemisinin identified in the *Artemisia annua* plant used in ancestral Chinese medicine as an infusion to treat malaria-induced fever. The use of *Artemisia* infusion as a low-cost and efficient treatment to cure malaria is still under debate: *in vitro* efficiency has been demonstrated on *vivax* hypnozoite, *vivax*, and *falciparum* liver and blood stages (Ashraf *et al.*, 2022), but the irregularity in the infusion preparation and use of sublethal doses can lead to the rapid spread of resistances that have already emerged in South-East Asia (Phyo and Nosten, 2018).

Life cycles

Apicomplexa parasites are obligate intracellular parasites. During invasion of the host, parasites create a niche hidden from the immune system and distinct from host phagosomes or lysosomes called the parasitophorous vacuole (PV). These parasites can either replicate sexually within their final host, cats for *T. gondii* or *Anopheles* mosquitoes for *Plasmodium* spp., or replicate asexually within their intermediate hosts.

***T. gondii* life cycle (Figure 2)**

Asexual development within the intermediate mammal host

Toxoplasma is virtually able to infect all nucleated cells of warm-blooded animals (Almeria and Dubey, 2021). Intermediate hosts meaning humans, farm animals, birds, rodents, ... are infected *via* the ingestion of oocysts excreted in felid feces and present in the environment, consumption of not properly washed vegetables, or direct contact with domestic cat feces. Humans are also infected directly by the consumption of cysts containing chronic-stage parasites called bradyzoites in undercooked meat. Once in the intermediate host, sporozoites from oocysts or bradyzoites from cysts convert to the acute, highly replicative stage known as tachyzoites. Tachyzoite parasites divide by endodyogeny, meaning that two daughter cells are newly formed within the mother cell and then burst out at the end of the division. Tachyzoites end up invading macrophages that they use as a cab to travel around the body to reach muscles and brain nerves. Once within non-dividing tissues parasites, tachyzoites convert into slow-dividing chronic stage bradyzoites and form latent

tissue cysts protected from the immune system clearance by the cyst's wall. Cysts persist within the host during the lifespan until the host's death, or until a weakening of the immune system allows the conversion back to tachyzoites causing the disease.

Sexual development within the definitive felid host

Toxoplasma is known to control the behavior of its host. Studies on rodents demonstrated that *Toxoplasma*-infected mice have repression of fear and were no longer discouraged by cat smell (Vyas *et al.*, 2007), concomitantly increasing the chance of cysts in mice to reach the final host, cats. Cysts in rodents are ingested by cats (domestic or wild) and within the cat's gut the cyst wall bursts and releases trophozoites that invade the intestine epithelium and divide through schizogony. The absence of the delta-6-desaturase in felines' intestines leads to the accumulation of linoleic acid, which induces *Toxoplasma* sexual commitment and trophozoites undergo gamogony with the development of male and female gametes (Martorelli Di Genova *et al.*, 2019). Male and female gametes fuse to form oocysts and are released into the environment *via* the cat's feces. Once in the environment, the oocyst sporulates forming sporozoites, and can be ingested either by mammals in which the asexual cycle occurs, or can be ingested by other cats where the sexual cycle repeats.

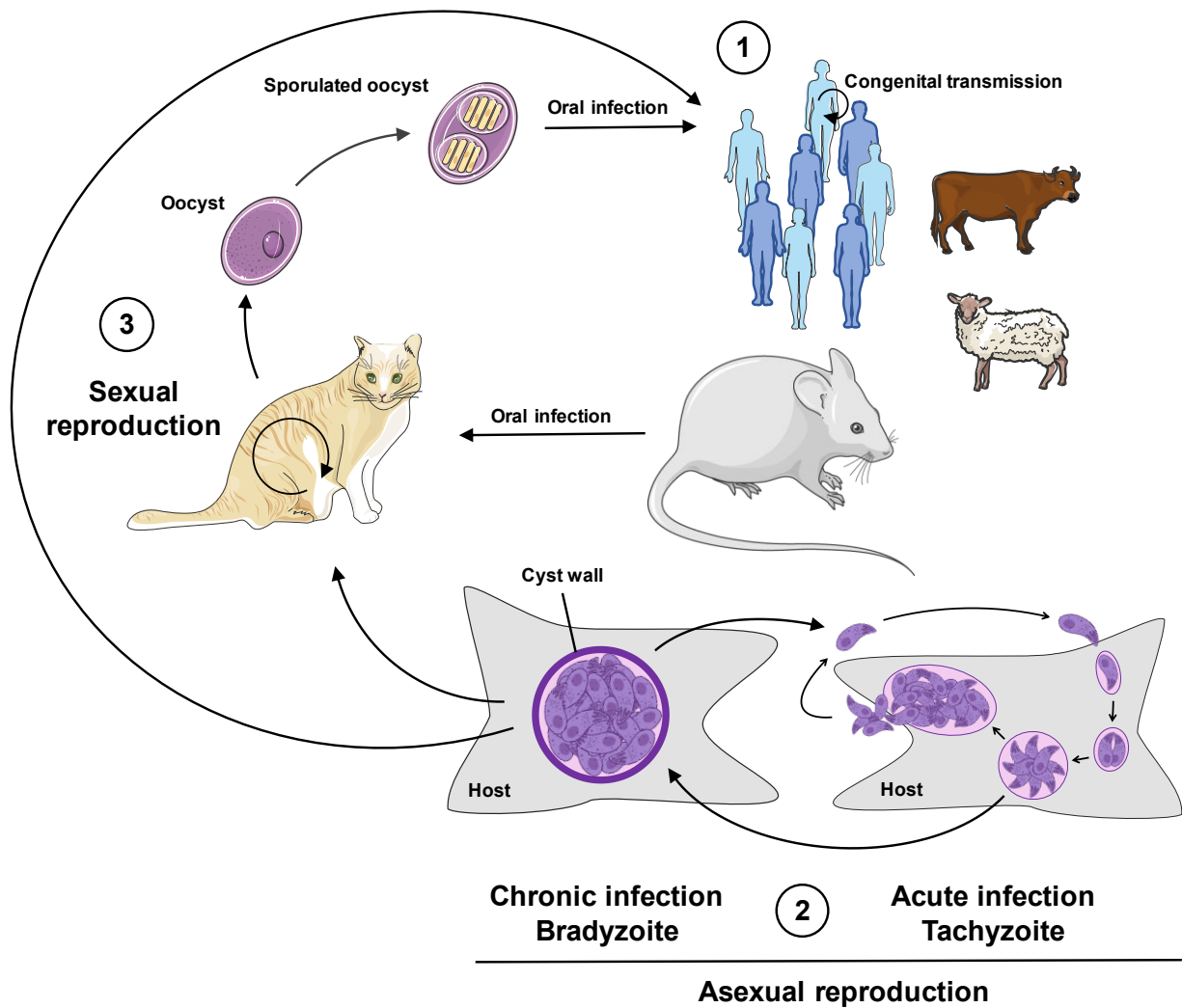


Figure 2: *Toxoplasma* life cycle

(1) Mammal and bird hosts are infected *via* the oral ingestion of sporulated oocysts or tissue cysts. Congenital transmission to the fetus can occur in the case of primo-infected women. (2) Within the intermediate hosts, parasites undergo asexual reproduction. Tachyzoites, the rapid replicative form responsible for the acute phase of the infection, rapidly invade the cell and replicate in their parasitophorous vacuole by endodyogeny up to ~32 parasites. Tachyzoites egress from the cell and the lytic cycle re-starts. Parasites migrate to slow-dividing tissues (muscles, neurons) and convert to the persistent slow-dividing bradyzoite form. Bradyzoites persist within cysts during the host life-span and can convert to rapid replicative tachyzoites when the host immune system declines. (3) Cysts within rodents are ingested by cats, the definitive host. Cats lack the $\Delta 6$ -desaturase, normally present in mammal intestines, creating an accumulation of linoleic acid, which is sensed by the parasite and induces sexual conversion. Parasites trophozoites divide by schizogony (similar to endodyogeny but forming multiple daughter cells instead of 2), before proceeding the gamogony forming male and female gametes. Fertilization leads to the formation of an oocyst that sporulates and is excreted within cat's feces. Oocysts are environmentally-resistant and can persist in nature for years before being ingested by a new intermediate host. Parts of the figure were drawn using pictures from Servier Medical Art. Servier Medical Art by Servier is licensed under a Creative Commons Attribution 3.0 Unported License (<https://creativecommons.org/licenses/by/3.0/>).

***Plasmodium* life cycle (Figure 3)**

Asexual development within the intermediate human host

In opposite to *Toxoplasma*, *Plasmodium* only infects and replicates within specific cell types, namely hepatocytes and erythrocytes. Anopheles mosquitoes inject sporozoites into the intermediate host during the blood meal through their salivary glands. They cross the derma to the bloodstream and rapidly reach the liver, within 30-60 minutes (Phillips *et al.*, 2017) where they cross the sinusoidal barrier and undergo transversal invasion, which consists of the invasion of several hepatocytes into a transient vacuole before switching to productive invasion (Arredondo *et al.*, 2021; Loubens *et al.*, 2021). Within hepatocytes, a single sporozoite rapidly divides, and forms an hepatic schizont leading to thousands of progenies. This step is known as exoerythrocytic schizogony (Tuteja, 2007). Then hepatic cells burst releasing merozoites into the bloodstream. Merozoites reach the lungs with a high dioxygen concentration, and merozoites in turn burst to release merozoites that are now able to invade erythrocytes and begin the intraerythrocytic cycle that lasts for 4 to 8 days (Phillips *et al.*, 2017). Parasites divide by schizogony (intraerythrocytic schizogony) into erythrocytes. During this cycle the parasite development starts with the ring stage, followed by the trophozoite stage which is the step of nuclear division and mitochondria/apicoplast elongation/branching, and finally, the schizont stage where a single polynucleated cell divides forming up to 32 individual merozoites that egress for the cell and re-invade a new erythrocyte and the cycle continues. Each cycle lasts around 48 hours and this stage corresponds to the symptomatic phase of the infection, causing severe anemia, nausea, diarrhea, headache, and fever that reaches a peak every 36-72 hours corresponding to the erythrocyte lysis (Phillips *et al.*, 2017). When host resources are running out, parasites are able to detect the lack of nutrients such as a decrease in lysophosphatidylcholine (LPC), the main building block of phosphatidylcholine (PC), which is the major component of the lipid membrane, and commit to gametogenesis (Brancucci *et al.*, 2017).

Sexual development within the final *Anopheles* host

Male and female gametes are ingested by another *Anopheles* mosquito during a blood meal, similar to *Toxoplasma*, *Plasmodium* also controls its host behavior by controlling its host smell, realizing a cocktail of compounds increasing mosquito attraction and thus chances to reach its final host (De Moraes *et al.*, 2014). The male and female gametes mature within the mosquito's gut to form flagellated microgametes and macrogametes. Gametes fuse and form a zygote that matures to an ookinete now able to invade the gut epithelium and form an oocyst, in which parasites undergo

several rounds of replication and form sporozoites. Sporozoites egress from the gut epithelium and reach the salivary glands. During the next blood feed, the mosquito will infect a new human host with mature sporozoites, and the asexual reproduction of the parasite will repeat itself.

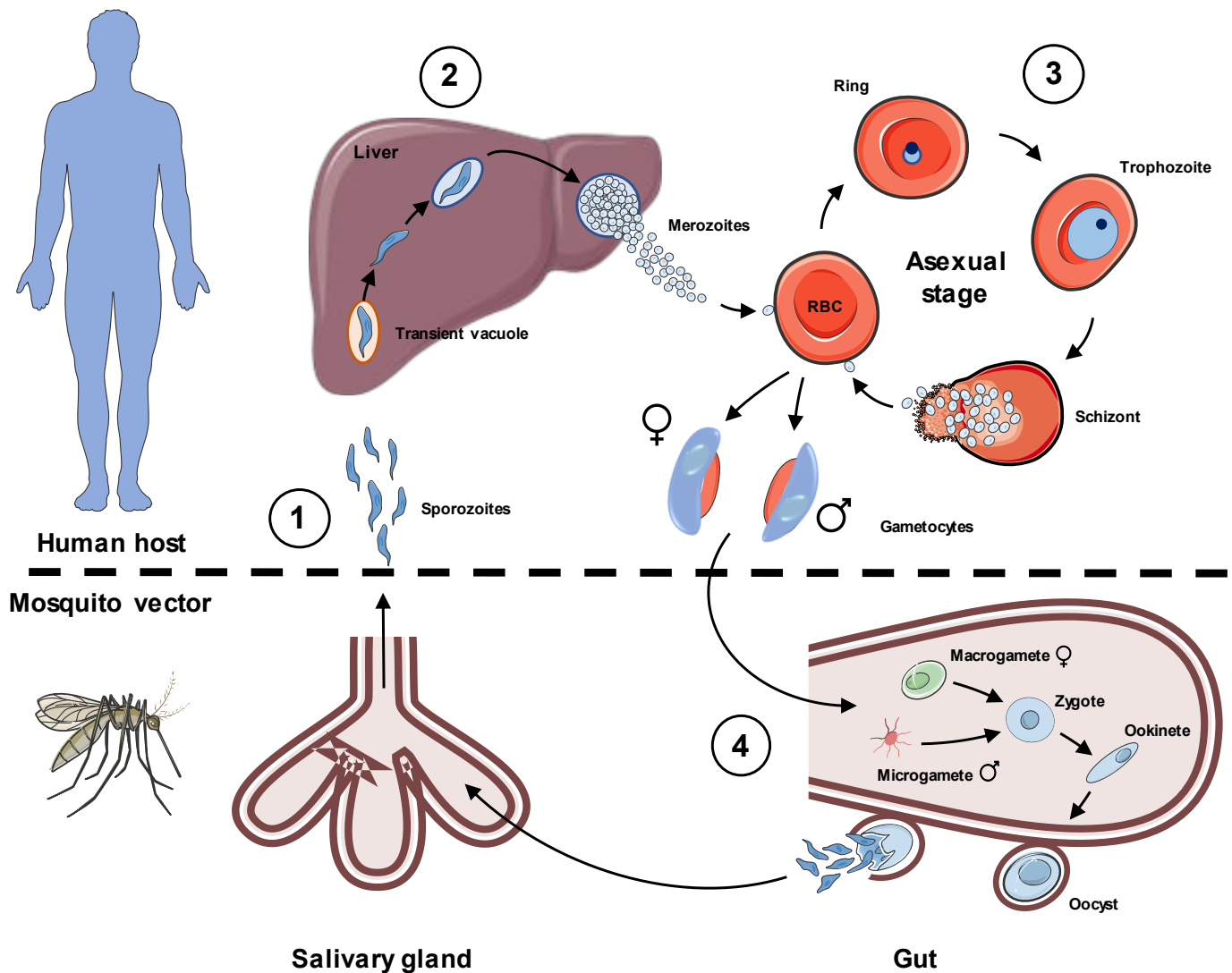


Figure 3: *Plasmodium falciparum* life cycle

(1) During a blood meal, the female *Anopheles* mosquito injects sporozoites that rapidly reach the liver through the bloodstream. Sporozoites cross the sinusoidal barrier and transiently infect hepatocytes before switching to productive invasion. Exoerythrocytic schizogony generates thousands of progenies from a single original sporozoite. (2) Merozoites are released in the bloodstream, infect red blood cells (RBC), and start the intraerythrocytic cycle. Early trophozoites, or rings, undergo organelles elongation and branching in parallel with DNA replication to form mature trophozoites. Poly-nucleated trophozoites divide to form schizonts that release merozoites that re-invade new RBC. Parasites can sense the nutritional status of the host and under stress conditions, RBC-stage parasites stop replicating and commit to sexual conversion forming male and female gametes. (4) During another blood meal, a new *Anopheles* mosquito uptakes the parasite's gametes. Within the gut, male and female gametes form flagellated microgametes and macrogametes respectively, which fuse to form a zygote that evolves into an invasive ookinete. The ookinete invades the gut's epithelium, forming an oocyst dividing into sporozoites. Sporozoites burst from the gut's epithelium and reach the mosquito's salivary glands before being injected into a new human host during the next blood meal. Parts of the figure were drawn using pictures from Servier Medical Art. Servier Medical Art by Servier is licensed under a Creative Commons Attribution 3.0 Unported License (<https://creativecommons.org/licenses/by/3.0/>).

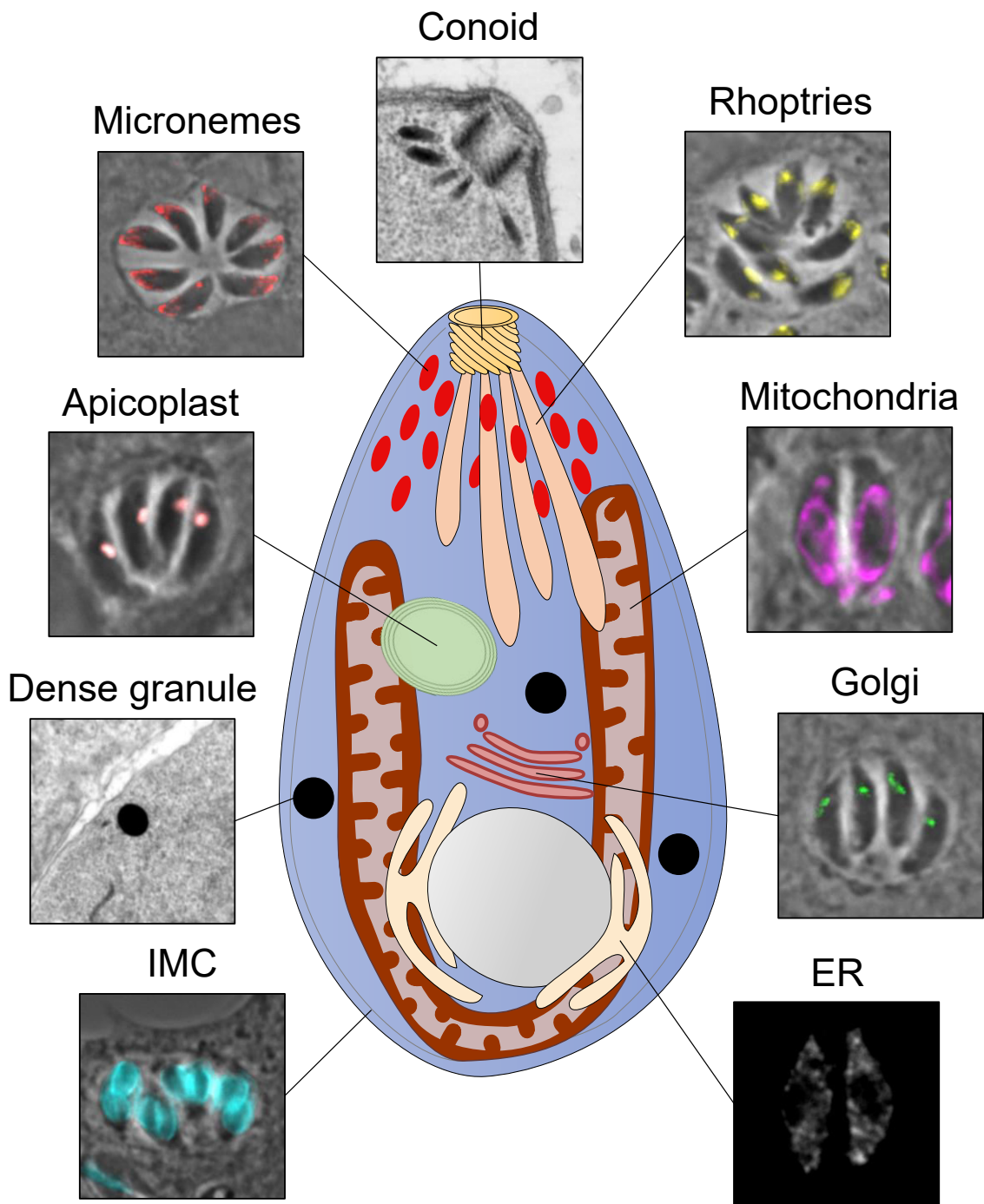


Figure 4: Apicomplexa ultrastructure

Conoid and dense granule structures are shown by electron micrographs realized on *Toxoplasma gondii* tachyzoite (this PhD). The immunofluorescence images are made using different intracellular markers: rhoptries = RON2-4; mitochondria = TOM40; Golgi = GRASP; endoplasmic reticulum (ER) = Der1; inner membrane complex (IMC) = IMC1; apicoplast = CPN60; micronemes = AMA1.

Dissection of Apicomplexa's ultrastructure

General structures (Figure 4)

Apicomplexa are eukaryotic parasites. As such, they are nucleated cells with common features like the endoplasmic reticulum (smooth and rough), the Golgi apparatus, and a single mitochondrion. A secretory pathway is present in Apicomplexa and goes through the ER and the Golgi apparatus, but was repurposed mainly for parasites invasion and egress with the acquisition of apical secretory organelles named micronemes and rhoptries. Apicomplexa, while intracellular replicate, within a vacuole called the parasitophorous vacuole (PV) with a membrane (the PVM) made of a mix of host and parasite membrane and matured by parasite effectors named GRA proteins that originate and are secreted from dense granules (DG). The plant origin of Apicomplexa left some relics: the plant-like vacuolar compartment (PLVAC) in *Toxoplasma*, the food vacuole in *Plasmodium*, which both play a similar role to the plant vacuole by being ion storage compartments (calcium, zinc). The PLVAC and the food vacuole also play the role of lysosomal compartments and are involved in endocytosis and nutrient acquisition (Dou *et al.*, 2014; Stasic *et al.*, 2022). All Apicomplexa, except for the *Cryptosporidium* genus, possess a chloroplast-relic named apicoplast that has lost the photosynthetic ability and is the resident place of essential metabolic pathways.

The inner membrane complex, an Alveolata specificity

The IMC is specific to the superphylum of Alveolata. The IMC corresponds to flattened vesicles located beneath the plasma membrane and interconnected with the cytoskeleton. The IMC is essential for cytokinesis. It covers the nascent parasites underneath the plasma membrane. Starting at the apical pole, the forming IMCs are derived from the Golgi material and bind to the centrosomes (Harding and Meissner, 2014; Kono *et al.*, 2013). Then the IMCs form rings on the apical pole of the daughter parasites and during the development of the cells the IMC recruits, in At first, the glideosome machinery and then recruits the alveolin network (Kono *et al.*, 2013) for conoid assembly and subpellicular microtubules organization (Tosetti *et al.*, 2020). The IMC plays an essential role in gliding motility as the glideosome machinery is located in between the IMC and the plasma membrane and uses an actin-myosin motor to allow parasite motility (Harding and Meissner, 2014).

The apical complex, big gun for a small parasite

Apicomplexa parasites are unicellular and polarized cells, with a basal pole and an apical pole. Their ability to invade a host resides in the complex structure present in the apical region. The

conoid is a complex cytoskeleton structure composed of spiraling tubulin fibers, subpellicular microtubules, preconoidal rings (PCR), and apical polar ring (APR) 1 and 2 that connect the conoid to the IMC and the subpellicular microtubules respectively, (Haase *et al.*, 2022; Koreny *et al.*, 2021; Tosetti *et al.*, 2020). Presence of a conoid is a shared feature among Coccidian and for a long time it was presumed absent from Haemosporidia and their sister clade Myzozoa (dinoflagellate and *Chromera*). However, conoids were recently identified in invasive forms of these taxa: sporozoites, merozoites, ookinetes (Koreny *et al.*, 2021). The conoid is extruded in extracellular parasites and allows parasite attachment, motility, and entry into the host cell. Conoid extrusion is due to F-actin attachment to the preconoidal rings and its polymerization by formin 1 (FRM1), then F-actin is fluxed toward the APR by myosin H (MyoH), that it binds. MyoH then promotes conoid extrusion. After conoid extrusion F-actin is fluxed to the pellicle by MyoA to promote parasite motility (Dos Santos Pacheco *et al.*, 2022). Conoid extrusion is sensitive to changes in the environment, the presence of 3 % ethanol or pH acidification or exogenous phosphatidic acid (ePA) induce conoid extrusion (Del Carmen *et al.*, 2009; Katris *et al.*, 2020). These external signal trigger an intracellular signaling through the cGMP pathway that leads to calcium release from the ER and induces extrusion of the conoid (Bullen *et al.*, 2019).

Secretory organelles

Apicomplexa are weaponized with secretory organelles essential for parasite invasion, egress, and host control. These organelles are known as (1) micronemes, (2) rhoptries, and (3) dense granules. All are formed from the Golgi apparatus but then use divergent pathways to be matured and secreted.

(1) Micronemes. Their number and shape vary according to the parasite's species or life stage. In *Toxoplasma*, micronemes are divided into two categories, apical micronemes, and peripheral micronemes (Kremer *et al.*, 2013). They contain proteins called microneme proteins, which possess a wide range of biological functions. Perforin-like proteins present in micronemes allow parasites to egress by forming pores into the PVM of the host cell membrane (Deligianni *et al.*, 2013; Kafsack and Carruthers, 2010). Extracellular parasites attach to the host cell and secrete microneme proteins that contain adhesins called MICs, which bind to host surface antigens such as collagen or sialic acid and allow parasite gliding motility (Dubois and Soldati-Favre, 2019; Tomley and Soldati, 2001). Once parasites tightly attach to the host cell, microneme proteins such as the complexes MIC/M2AP or MIC1/4/6 bind to a host receptor and make the connection to the parasite

glideosome (Zhu *et al.*, 2021, p. 4), which is an Apicomplexa-specific machinery using a myosin motor complex, cytoskeleton F-actin, and plasma membrane docking proteins, that generate the forward movement (gliding motility), which allows parasite entry within the host cell (Fréchal and Soldati-Favre, 2013; Opitz and Soldati, 2002). Another microneme protein called AMA1 also participates in the formation of the moving junction associated with RON proteins secreted by the rhoptries into the host cell forming a complex at the interface of the host and the parasite, which leads to the entry of the parasite and the formation of the PV (Fernandes *et al.*, 2022, p. 1; Lamarque *et al.*, 2014).

(2) Rhoptries. They are shared among Apicomplexa and their number varies depending on the organism: 1 in *Cryptosporidium* spp., 8-12 in *Toxoplasma*, 2 in *Eimeria* and *Plasmodium* spp. (Burrell *et al.*, 2022; Mageswaran *et al.*, 2021; Martinez *et al.*, 2022; Segev-Zarko *et al.*, 2022). They are composed of a neck and a bulb. Recent findings have shown that rhoptries dock to the apical vesicle (AV). *Toxoplasma* and *Eimeria* opposite to *Plasmodium* possess several AV aligned on the two intra-conoid microtubules but only the most apical one serves for rhoptry docking. Upon calcium stimulation, the AV associates with another apical structure termed rhoptry secretory apparatus (RSA) forming a rosette composed of a repetition of 8 complexes of anchor proteins (A-I, A-II, A-III), the central density, an anterior and posterior central channels and radiating spokes (Mageswaran *et al.*, 2021), being the gatekeeper of rhoptry discharge through the fusion of the AV with the plasma membrane. Rhoptry proteins are secreted only in extracellular parasites, after microneme secretion, and attachment to the host cell surface that trigger intracellular signaling and calcium release inducing rhoptry discharge. Sequentially, the neck content, aka RON proteins, is discharged first and releases a set of proteins involved in the parasite's invasion, such as formation of the moving junction (RON2/4/5/8) (Ben Chaabene *et al.*, 2021; Besteiro *et al.*, 2011). Then the bulb content, aka ROP proteins, is discharged and is composed of effectors for host behavior manipulation (Hakimi *et al.*, 2017; Ihara and Nishikawa, 2021).

(3) Dense granules. Contrarily to rhoptries and micronemes, DGs are not apical organelles but are spread around the cytoplasm and are not conserved throughout the phylum. DG are likely conserved among cyst-forming apicomplexan parasites such as *Toxoplasma gondii* and *Neospora caninum*. They have been named due to their electron-dense crystalline protein core, which means that they appear as deep dark round-shape vesicles by transmission electron microscopy. DGs contain and secrete GRA proteins involved in host behavior manipulation (Ihara and Nishikawa, 2021), nutrient acquisition through the PV and PVM maturation (Griffith *et al.*, 2022; Mayoral *et*

al., 2022; Rivera-Cuevas *et al.*, 2021; Romano *et al.*, 2017). DGs find their origin in the canonical secretory pathway: most GRA proteins possess a signal peptide, are translated, and translocated into the rough ER. GRA proteins inserted into the parasite plasma membrane possess a transmembrane (TM) domain that allows their insertion into the ER membrane. Secreted GRAs aggregate and may mask the TM domain, but can also count on chaperone proteins such as GRA45, which has a similar structure to small heat shock protein, and prevent premature membrane insertion (Braun *et al.*, 2008; Griffith *et al.*, 2022; Wang *et al.*, 2020). GRA proteins transit to the Golgi apparatus, where GRA with a TEXEL motif (*Toxoplasma* export motif) are matured by the aspartyl protease ASP5 for correct targeting upon secretion (Coffey *et al.*, 2018, 2015). Mature DGs bud from the trans-Golgi network and traffic to the plasma membrane where the secretion mechanism across the IMC and the plasma membrane remains unclear. It has been suggested that apical annuli may play the exit gate for DG secretion (Griffith *et al.*, 2022). Once secreted GRA proteins play an essential role in host control such as suppressing the antigen presentation by MHC-I or MHC-II, by GRA2-9 (Leroux *et al.*, 2015; Rommereim *et al.*, 2019), parasite dissemination into the host with GRA28 (ten Hoeve *et al.*, 2022) as well as an essential role in host nutrients acquisition, example: GRA2, GRA6, and GRA7 are essential for host Rab vesicles scavenging through the intravacuolar network (IVN) (Romano *et al.*, 2017), GRA64 and GRA14 for the recruitment of host ESCRT machinery at the PVM for nutrient acquisition (Mayoral *et al.*, 2022; Rivera-Cuevas *et al.*, 2021), or host organelle recruitment like mitochondria *via* MAF1 (Blank *et al.*, 2021).

Mitochondria

Apicomplexa possess a single mitochondrion (except for the *Cryptosporidium* genus that possesses a mitosome) with one of the smallest genomes in the eukaryotic realm, *i.e.* 6 kb, that encoded only three proteins (Usey and Huet, 2022). The rest of the mitochondrial proteins are encoded within the parasite nucleus. Apicomplexa mitochondria have conserved essential metabolic pathways, divergent enough from their host to be druggable. As in other eukaryotes, Apicomplexa mitochondria is the powerhouse of the cell, and the place of the respiratory chain. While complex I is missing in Apicomplexa, complexes II, III, and IV are composed of more subunits than their human homologs. It is also the case for the complex V, F₁F₀-ATP synthase, which is composed of close to 30 subunits in Apicomplexa compared to 18 subunits for the human F₁F₀-ATP synthase (Maclean *et al.*, 2022). The reason for this increased number of subunits remains unknown but the characterization of specific *Toxoplasma* subunits has revealed their essentiality for the assembly of

the different complexes and parasite survival (Maclean *et al.*, 2021). The structure of Apicomplexa complex V explains the tubular cristae structure of their mitochondria, forming a hexamer bending the mitochondria's inner membrane, disrupting this hexameric structure and impairing the cristae structure (Mühleip *et al.*, 2021). In *Plasmodium*, intraerythrocytic asexual replication relies on glycolytic fermentation and ATP synthesis by F₁F₀-ATP synthase is dispensable, but not in mosquito sexual replication (Jacot *et al.*, 2016; Sturm *et al.*, 2015). This divergence of the Apicomplexa respiratory chain makes it a perfect drug target in the fight against Apicomplexa diseases. Atovaquone is an inhibitor of the Apicomplexa complex III and is already one of the main drug used against *Plasmodium* infection (Siregar *et al.*, 2015). The Apicomplexa mitochondrion is the place of the heme synthesis pathway shared with the apicoplast, an iron-sulfur cluster synthesis (ISC), the tricarboxylic acid (TCA) cycle that fuels the respiratory chain in reducing agents (Jacot *et al.*, 2016; Sheiner *et al.*, 2013). Apicomplexa energy metabolism relies on glucose, glycolysis, the TCA cycle, and the respiratory chain. As another source of energy, β -oxidation consumes fatty acids to generate ATP. *Toxoplasma* possesses all enzymes of the β -oxidation except for the mitochondrial transporter carnitine palmitoyltransferase, which allows the entry of palmitic acid (C16:0) into the mitochondrion to fuel the β -oxidation, and the situation in *Plasmodium* is more complex where another enzyme of the β -oxidation is absent. Yet there is no evidence of mitochondrial β -oxidation activity in Apicomplexa and its existence is still controversial (**Figure 5**).

Apicoplast, the memory of plant ascendance

The apicoplast is a non-photosynthetic organelle (that has been lost in the genus *Cryptosporidium*), acquired from a primary endosymbiosis of a cyanobacterium to evolve as a chloroplast, then Chromoalveolate acquired the apicoplast from a secondary endosymbiosis event of a red alga (van Dooren and Striepen, 2013). The apicoplast thus possesses four membranes, the two innermost membranes being those of the original chloroplast while the periplastid membrane originates from the red alga plasma membrane and the outermost membrane comes from the endomembrane. The apicoplast genome encodes approximately thirty genes, and to maintain the endosymbiont as a novel organelle, gene transfer occurred between the plast and the nucleus. Nuclear-encoded apicoplast proteins need to reach their final destination and are so addressed to the apicoplast. Most of the apicoplast stromal proteins harbor a bipartite signal, which is composed of a signal peptide for ER translocation, in the ER the signal peptide is cleaved revealing a transient peptide for apicoplast localization (DeRocher *et al.*, 2000; Waller *et al.*, 2000). How apicoplast proteins reach

the outermost membrane remains unclear, but vesicular trafficking between the ER and the apicoplast is privileged. Indeed, disrupting the R-SNARE *TgVAMP4* blocks the entrance of the stromal ACP and CPN60 as well as the membranous proteins ATrx1 and ATrx2 (Cao *et al.*, 2021). To cross the periplastid membrane, parasites possess a plastid-localized ER-associated degradation (ERAD) system, and its disruption impairs the translocation of proteins to the apicoplast followed by the loss of the plastid and death of the parasite (Agrawal *et al.*, 2009; Fellows *et al.*, 2017; Spork *et al.*, 2009). However, localization of this ERAD complex to the periplastid membrane remains uncertain. The two inner membranes of the apicoplast, which correspond to the ancestral chloroplast, possess protein translocons at the outer and inner chloroplast membrane (TOC/TIC) homologs, which recognize the transient peptide for the protein import into the stroma of the apicoplast (Glaser *et al.*, 2012; Glaser and Higgins, 2012; Sheiner *et al.*, 2015, p. 75).

Despite the loss of photosynthesis, the apicoplast has conserved essential metabolic pathways and its absence from the human host makes it a perfect drug target (**Figure 5**).

Heme synthesis pathway. Heme plays an essential role in redox reaction and the electron transport chain. This pathway is essential for the development of *Toxoplasma* but can be dispensable in *Plasmodium* depending on the life stage. In the intraerythrocytic life stage where the parasite evolved in a heme-rich environment, the pathway is dispensable (Yeh and DeRisi, 2011). By contrast, the heme synthesis pathway is critical in the liver (Kloehn *et al.*, 2021a; Rathnapala *et al.*, 2017) and the mosquito stages (Nagaraj *et al.*, 2013). The pathway, as mentioned in the mitochondria section, is shared between the two organelles, with the first step in the mitochondrion, the next four steps are in the apicoplast and convert 5-aminolevulinic acid (5-ALA) to coproporphyrinogen III, which exits the apicoplast into the cytosol *via* an unknown path, to be converted to protoporphyrinogen IX by CPO. The two last steps into the mitochondrion allow the formation of the heme (Dooren *et al.*, 2012).

Iron-sulfur cluster synthesis pathway. Iron-sulfur (Fe-S) clusters are presumed to be one of the oldest catalysts for the synthesis of metabolites, genome maintenance (DNA replication and repair), and functionality of the translation machinery (biogenesis of ribosome and tRNAs modification) (Lill, 2009). Apicomplexa, as plants and algae, possess the three eukaryotic pathways, with the cytosolic CIA and the mitochondrial ISC while the apicoplast possesses the SUF Fe-S cluster synthesis pathway. The three pathways are essential for parasite survival (Aw *et al.*, 2021; Pamukcu *et al.*, 2021). In *Toxoplasma* and *Plasmodium*, the SUF pathway generates Fe-

S clusters to the isoprenoid synthesis pathway (IspG and IspH), the FASII pathway (LipA), and apicoplast protein translation (MiaB for tRNA modification) (Renaud *et al.*, 2022; Swift *et al.*, 2022).

Isoprenoid synthesis pathway. Isoprenoids serve multi-biological functions in the cell: protein, and tRNA prenylation, synthesis of the coenzyme Q for the mitochondrial electron transport chain, vitamins. They also are critical components of membrane lipids (Guggisberg *et al.*, 2014). Apicomplexa harbor a plant-like methylerythritol phosphate (MEP) pathway, responsible for the synthesis of the isoprenoid precursor isopentenyl pyrophosphate (IPP), which is critical for both *Toxoplasma* and *Plasmodium* survival (Nair *et al.*, 2011; Yeh and DeRisi, 2011). Nevertheless, the IPP synthesis is the only apicoplast pathway essential during the blood stage (Yeh and DeRisi, 2011) in a synthetic nutrient-rich environment, and parasite growth can be inhibited by the action of fosmidomycin.

Fatty acid synthesis type II pathway. Fatty acids (FA) are the building blocks of phospholipids (PL) and neutral lipids, diacylglycerols (DAG), triacylglycerols (TAG), and cholesteryl esters (Chol-FA). FA are either massively scavenged from the host or *de novo* synthesized within the apicoplast, which possesses the prokaryotic fatty acid synthesis type II pathway (FASII), and can synthesize both the saturated short fatty acid chains myristic, and palmitic acids (C14:0, and C16:0, respectively).

FASII is a multi-enzymatic complex that uses acetyl-CoA generated from imported phosphoenolpyruvate, converted back to pyruvate, which is dehydrogenated and associated with a coenzyme A by pyruvate dehydrogenase (PDH) to form the acetyl-CoA pool. Then the CoA is replaced by an acyl carrier protein (ACP) essential for the initiation and the elongation of the FA chain by FASII. Elongation of the newly synthesized FA is performed by the β -ketoacyl-ACP synthases I/II (FabB/F), the β -ketoacyl-ACP reductase (FabG), the β -hydroxyacyl-ACP dehydratase (FabZ), and the enoyl-ACP reductase (FabI). After several rounds of elongation the FASII generates a C8:0 FA (octanoyl-ACP) used for a positive feedback loop to activate the PDH, and after a few other rounds, produces the short FAs C14:0 and C16:0 (Goodman and McFadden, 2007; Sharma *et al.*, 2007; Shears *et al.*, 2015).

Chloroplasts use *de novo* FAs for galactolipid synthesis and photosynthesis, but this pathway is lost in Apicomplexa, and FASII fatty acid has been repurposed for the synthesis of

lysophosphatidic acid (LPA) and phosphatidic acid (PA) *via* the conserved plant acyltransferases called ATS1 and ATS2 that serve for bulk phospholipids and membrane biogenesis (Amiar *et al.*, 2020, 2016). FASII is essential for the integrity of the apicoplast and the survival of *Toxoplasma*, but in *Plasmodium* the pathway has been shown to be dispensable during the acute blood stage (Yeh and DeRisi, 2011) and essential during liver (Yu *et al.*, 2008) and mosquito stages (Vaughan *et al.*, 2009). Recent evidence re-questions the essentiality of the pathway during the blood stage as growth assays on FASII mutants have shown that the parasites were no longer able to survive in poor nutritional environment and may illustrate the FASII activity flexibility for parasite survival during the acute infection (Amiar *et al.*, 2020; Shunmugam *et al.*, 2022).

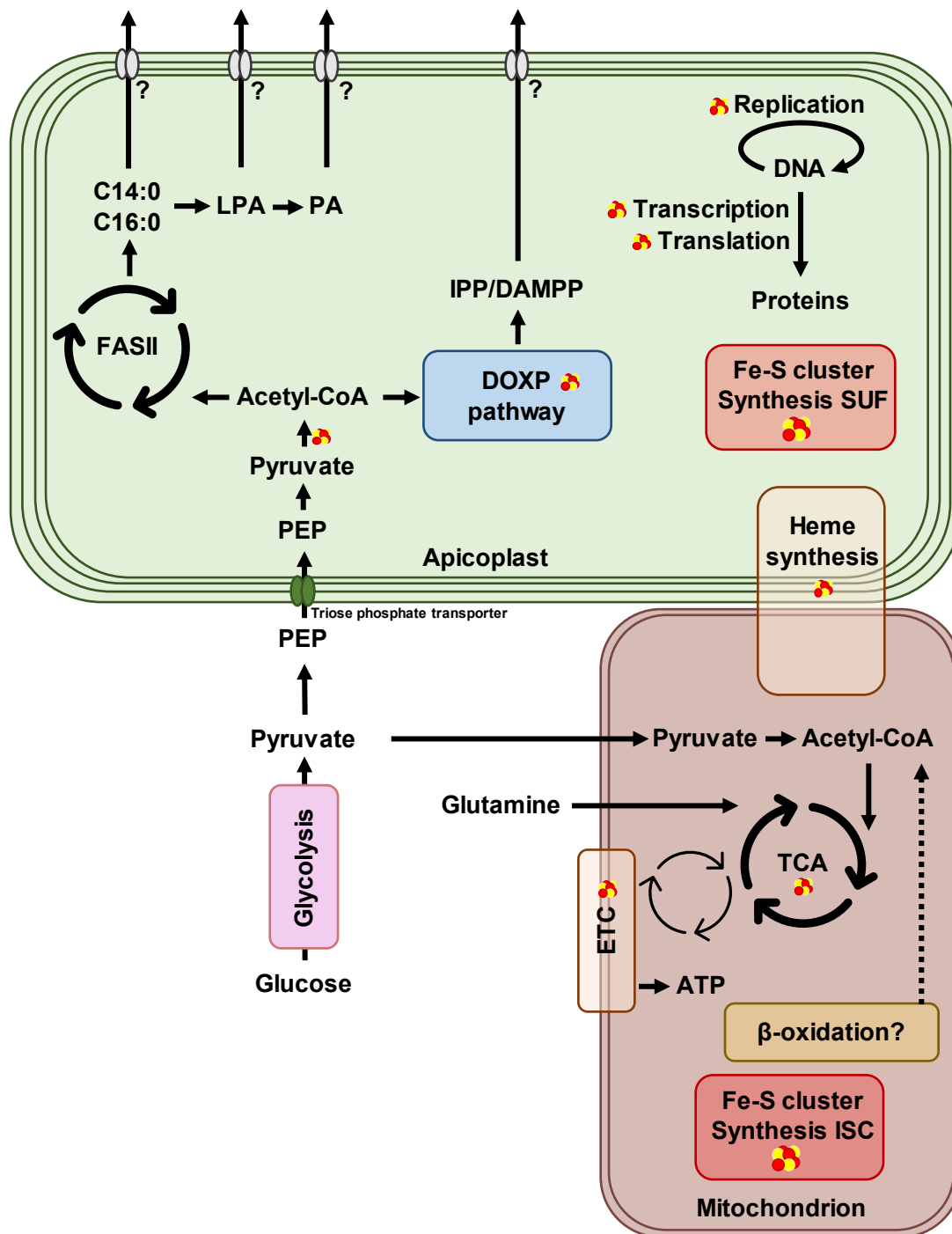


Figure 5: Apicoplast and mitochondrion metabolic pathways

Scavenged glucose is the main carbon source for endosymbiotic organelle metabolism. The apicoplast hosts the type II fatty acid synthesis pathway (FASII) providing FAs, the DOXP isoprenoid synthesis pathway providing IPP and DAMPP, the heme synthesis pathway shared with the mitochondrion, and the iron-sulfur cluster synthesis pathway (SUF) providing Fe-S clusters essential for the conversion of pyruvate to acyl-CoA, enzymes of the DOXP pathway but also for housekeeping functions (DNA replication, transcription, and protein translation) and to form the heme. The mitochondrion hosts the tricarboxylic acid cycle (TCA) providing reductive power to the electron transport chain (ETC) for ATP synthesis. It also possesses a Fe-S cluster synthesis pathway (ISC) essential for the correct function of the TCA cycle and the ETC. Apicoplast exporters in grey are unknown.

Chapter II: Lipids in Apicomplexa

Lipid definition

Lipids are major metabolites of life. They are defined as organic compounds insoluble in water but soluble in organic solvents. They include fats, vitamins, waxes, phospholipids, etc. Lipids are involved in cell structural components, signaling, and energy storage.

Phospholipids are the major lipids of membranes

The plasma membrane and the organelle's membranes and envelopes serve as barriers between the extracellular environment, the cytosol, and the lumen of the different organelles, maintaining the characteristics of each compartment such as ion gradients or metabolic pathways. Membranes are made of a lipid bilayers mainly composed of phospholipids held together by noncovalent interactions. They adopt this particular structure thanks to their physical properties and shapes. A phospholipid is an amphiphilic molecule. It is a lipid that contains a hydrophobic tail made of two fatty acid chains attached to the position 1 and 2 on a glycerol-3-phosphate (G3P) backbone *via* an ester bond and a hydrophilic head that comprises the phosphate of the glycerol-3-phosphate backbone, which is attached to different radicals depending on the nature of the considered phospholipid. Because of the two FAs, they generally adopt a cylinder shape that forces them to naturally assemble into a bilayer with their FA tails within the hydrophobic core of the membrane, and their hydrophobic heads popping out into the hydrophilic compartment. Lysophospholipids, which adopt an inverted cone shape naturally form micelles made of one single lipid layer. Phospholipids' bilayer properties depend on the nature of their phospholipids.

Phosphatidic acid (PA). PA is made of two FAs and a glycerol-3-phosphate. It constitutes the sole precursor of each class of phospholipids, and plays an essential role in membrane biogenesis. The absence of a radical group on the phosphate induces a trapezoid shape and generates positive membrane curvature important for cytokinesis (Amiar *et al.*, 2020) and vesicular trafficking. The PA can be dephosphorylated to form diacylglycerol (DAG), which can be esterified with a third FA and form a triacylglycerol (TAG) for lipid storage (Dass *et al.*, 2021). PA can additionally play a role as a signaling molecule (Arisz *et al.*, 2009; Bisio *et al.*, 2019; Katris *et al.*, 2020; Wang *et al.*, 2006). Apicomplexa are able of PA *de novo* synthesis, the apicoplast possesses plant relics of acyltransferases called ATS1 and ATS2. In the chloroplast, they are responsible for the synthesis of galactolipids for the plast integrity and photosynthesis, while in the apicoplast, they have been

repurposed for the synthesis of LPA and PA, respectively (Amiar *et al.*, 2020, 2016). Apicomplexa genomes also encode ER/cytosolic LPA/PA synthesis enzymes, glycerol-3-phosphate acyl transferase (GPAT), and acyl glycerol-3-phosphate acyl transferase (AGPAT) (Amiar *et al.*, 2020) but their roles in parasite lipidome and survival remain unknown.

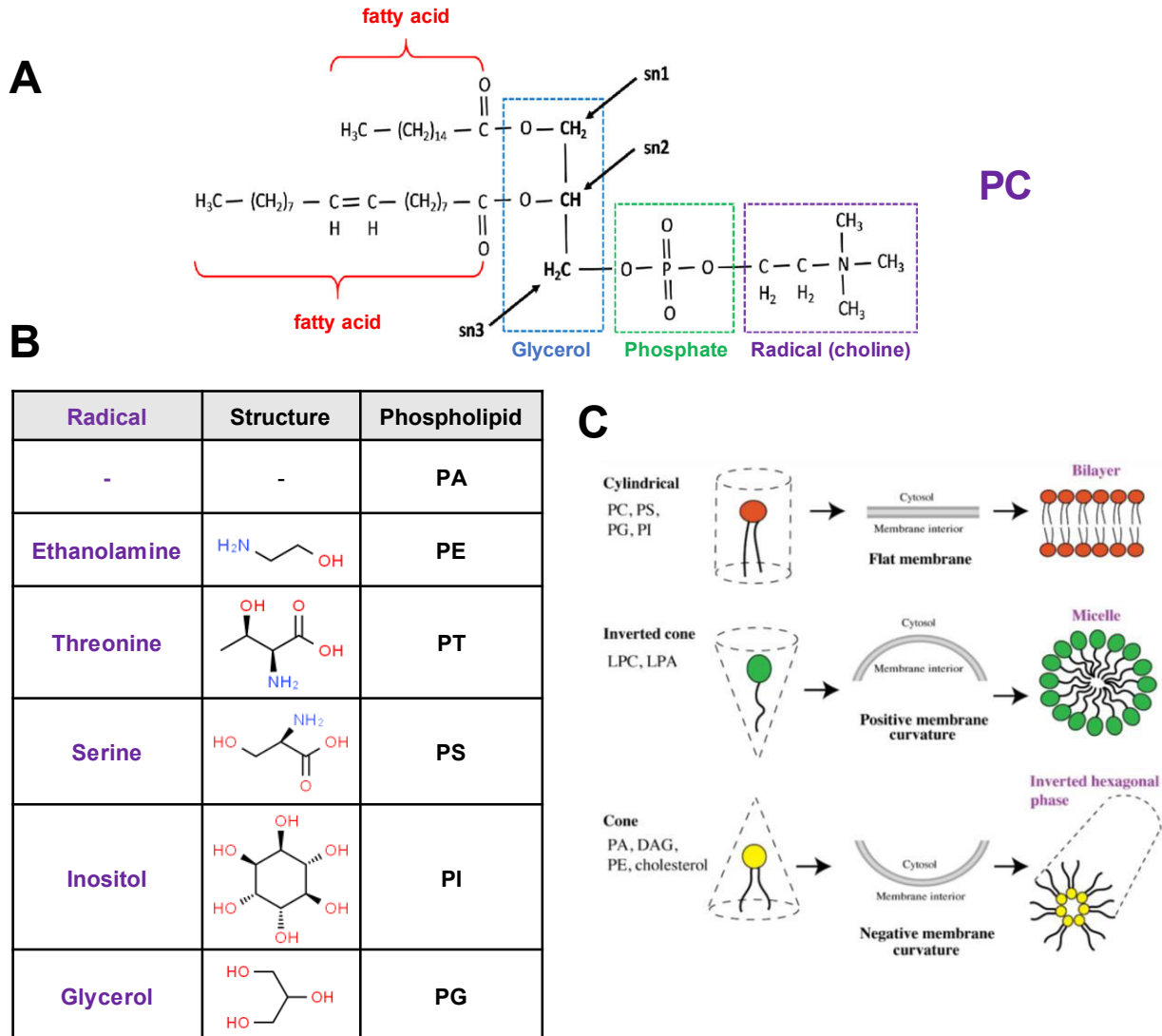


Figure 6: Phospholipid's structure

(A) General organization of a phospholipid, the phosphatidylcholine (PC) in which two FA chains are esterified on a glycerol-3-phosphate backbone. The phosphate position sn3 is linked to a radical that defines the phospholipid species (adapted from MacDonald *et al.*, 2019). (B) Table of the different radicals defining the phospholipids (structures are from ChemSpider). (C) Phospholipids spatial shape inducing membrane curvatures (adapted from Zhukovsky *et al.*, 2019).

Phosphatidylcholine (PC). PC is the major component of eukaryotic membranes and corresponds to ~75 % of *Toxoplasma* and between 20 to 55 % of *Plasmodium* blood-stage phospholipids. PC assembles to a planar bilayer (**Figure 6A, B**) and is crucial for parasite proliferation. The ratio PC/LPC is important for apicoplast maintenance (Lévêque *et al.* 2017), and differentiation, low level of LPC during the blood stage reduces the number of merozoites and triggers the expression of a transcription factor for sexual commitment (Brancucci *et al.*, 2017; Kilian *et al.*, 2018). PC is synthesized from scavenged resources (host PC/LPC or choline). Choline is used through the Kennedy pathway where choline is CDP-activated and then transferred to a DAG by a choline/ethanolamine phosphotransferase (C/EPT) (Gibellini and Smith, 2010; Kilian *et al.*, 2018; Sampels *et al.*, 2012) (**Figure 7**). Mammals can synthesize PC from PE by multiple steps of methylation converting the ethanolamine to choline and *Plasmodium* has conserved a functional PE methyl transferase (PMT) (Witola *et al.*, 2008) important for growth and survival but there is no PMT activity reported in *Toxoplasma* (Gupta *et al.*, 2005) (**Figure 7**).

Phosphatidylethanolamine (PE): PE is the second most abundant phospholipid of eukaryotic membranes. It can be *de novo* synthesized by the Kennedy pathway or the CDP-DAG pathway (**Figure 7**). *Toxoplasma* and *Plasmodium* can form ethanolamine from serine but not from ceramide like Kinetoplastida. Both *Toxoplasma* and *Plasmodium* phosphorylate the ethanolamine and activate it with a CDP to be transferred on DAG by C/EPT to form PE and *Toxoplasma* possesses a gene duplication EPT also responsible for ethanolamine transfer on a DAG (Ramakrishnan *et al.*, 2013). PE can also be sourced by the CDP-DAG pathway from which a PA is converted to an activated CDP-DAG molecule used to synthesize phosphatidylserine (PS) and PE is generated by PS decarboxylation (**Figure 7**). *Toxoplasma* possesses two PS decarboxylases (one in the mitochondria and one in the PV), that have a compensatory activity depending on the nutritional environment (Hartmann *et al.*, 2014). In both parasites, PE synthesis from the Kennedy pathway is essential for parasite survival (Déchamps *et al.*, 2010; Sampels *et al.*, 2012), whereas PE sourced by PS decarboxylation is important for parasite growth but not survival (Hartmann *et al.*, 2014; Vial *et al.*, 1982) (**Figure 7**). As PA, PE also adopts a trapezoid shape inducing negative membrane curvature (Peeters *et al.*, 2022) and plays a role in vesicle budding, trafficking, and membrane fusion (Wu *et al.*, 2016) (**Figure 6B and C**).

Phosphatidylserine (PS): PS is one of the most abundant phospholipids in Apicomplexa (~5-15 %). Within the human host, PS is localized on the cytosolic leaflet of the phospholipid bilayer

and is actively maintained as such, PS exposure on the extracellular side is an apoptotic signal recognized by the immune system, which induces the programmed cell death. Interestingly, it has been shown that *Plasmodium*-infected hepatocytes showed a decreased exposure of PS to avoid parasite phagocytic clearance (Burda *et al.*, 2017), but in infected erythrocytes, PS exposure increase causing red blood cell attachment within the blood vessel to avoid clearance by the spleen (Eda and Sherman, 2002). Still, in *Plasmodium*, PS synthesis mainly occurs *via* the CDP-DAG pathway from serine and CDP-DAG, by a bacterial-type PS synthase (PSS) (Elabbadi *et al.*, 1997), whereas PS synthesis in *Toxoplasma* likely occurred by head group exchange with PE by the PS synthase 2 (PSS2) (Gupta *et al.*, 2005) (**Figure 7**).

Phosphatidylinositol (PI): PI synthesis is conserved in all Eukaryotes including Apicomplexa. PI is synthesized from myo-inositol, a cyclic sugar alcohol of six carbons, either scavenged or *de novo* synthesized from glucose. Myo-inositol is then assembled to form PI through the CDP-DAG pathway by PI synthase (1 in *Plasmodium* and 2 in *Toxoplasma* stage dependent) (Séron *et al.*, 2000; Wengelnik and Vial, 2007), and serves as a precursor for phosphatidylinositol phosphate molecules (PIPs) (**Figure 7**).

PI and PIPs are essential lipids for signaling events. Phospholipase PI-LPC, recruited at the plasma membrane after induction of the cGMP signaling pathway, cuts the PI_(4,5)P₂ releasing DAG and IP₃, which induces calcium release from the ER leading to microneme secretion (Bisio *et al.*, 2019; Tanzifi *et al.*, 2020). PIPs are crucial for the synthesis of glycosylphosphatidylinositol-anchored proteins, playing a major role in the immune system evasion with the rapid variation of surface antigens (SAGs) (Lekutis *et al.*, 2001), but also for organelle maintenance with the regulation of the apicoplast homeostasis (Daher *et al.*, 2016, 2015), or protein export in *Plasmodium* (Bhattacharjee *et al.*, 2012) and thus parasite survival.

Phosphatidylthreonine (PT): PT is only present in very low abundance in eukaryotic cells and PT appears to be a by-product of PS synthesis due to the close similarity to serine and threonine. However, coccidian parasites such as *Toxoplasma*, exclusively possess an ER-localized phosphatidylthreonine synthase (PTS) evolved from the PSS, responsible for the transfer of a threonine onto an activated CDP-DAG to form PT (Arroyo-Olarte *et al.*, 2015) (**Figure 7**). In *Toxoplasma*, PT appears to be more abundant than PS, its synthesis is essential for both acute and chronic stage, and PT plays an essential role in parasite gliding motility and thus parasite egress *via* the regulation of calcium homeostasis (Arroyo-Olarte *et al.*, 2015; Kuchipudi *et al.*, 2016).

Cardiolipin (CL) and phosphatidylglycerol (PG): cardiolipin is a unique phospholipid synthesized and localized into the inner membrane of mitochondria (IMM) where its abundance can reach 15-20 % of the phospholipids composing the IMM. CL plays an important role in the different mitochondrial metabolic processes such as the assembly of supercomplexes of the ETC, mitochondria biogenesis, protein import, IMM cristae formation, and ATP synthesis (Paradies *et al.*, 2019). CL synthesis is conserved among all Eukaryotes and starts from the PA, which is activated to form a CDP-DAG, then a phosphatidyl group is added to the DAG by a phosphatidylglycerophosphate (PGP) synthase to form PGP, which is dephosphorylated by a PGP phosphatase to form phosphatidylglycerol (PG) (**Figure 7**). The prokaryotic CL synthesis pathway assembles CL from two PGs with the release of glycerol (Schlame, 2008). PG and CL synthesis is essential for parasite survival as the deletion of one of the CDP-DAG synthase, the prokaryotic one *TgCDS2*, abrogates PG synthesis and illustrates the tight metabolite exchanges between the apicoplast and the mitochondria as *TgCDS2* localized to the apicoplast and the PG and PL synthesis localized to the mitochondria (Kong *et al.*, 2017) (**Figure 7**).

To sum up, the synthesis of phospholipids in Apicomplexa parasites possesses both the CDP-DAG pathway and the Kennedy pathway. The Kennedy pathway is responsible for the assembly of PC and PE, the major phospholipid classes from scavenged resources (choline, ethanolamine, LPC, etc.) with the transfer of CDP-activated precursor on DAG. The CDP-DAG pathway fuels the synthesis of the PS, PT, PI/PIP, and PG/CL *via* the activation of DAG with a CDP and further assembly of the different phospholipids with the specific compartments with PS and PT in the ER, PI, and PIPs in the Golgi apparatus and PG/CL within the mitochondria.

Phospholipids are not the only important lipids for membranes

While phospholipids are the major components of the membrane, other non-glyceride lipids play an important structural role in the membrane. Sphingolipids represent near to 10 % of the membrane lipids and sterols including cholesterol and cholesteryl esters that reach 20-30 % of the lipid present in the membrane (Coones *et al.*, 2021).

Sphingolipids (SL). SLs are different from PLs as the PLs possess a glycerol backbone, whereas SLs possess a sphingoid base backbone made from aliphatic amino alcohols mainly serine forming sphingosine. SLs are synthesized from ceramide sourced by the assembly of serine with a palmitic acid (C16:0) by a serine palmitoyl transferase (SPT) to form 3-ketosphinganine, this

compound is reduced to form sphinganine, which is esterified with a FA by a ceramide synthase (CERS) and becomes dihydroceramide. The final step is catalyzed by desaturase to make ceramide, which serves as the precursor for all sphingolipids, meaning sphingomyelin (SM), inositolphosphoryl-ceramide (IPC), and ethanolaminephosphoryl-ceramide (EPC). In the lipidic membrane, SLs play an essential role in the formation of lipid rafts or lipid microdomains that control the membrane fluidity and membrane protein trafficking (Pike, 2009). Apicomplexa can scavenge SL from their host but can also *de novo* synthesize SLs (Coppens, 2013). *De novo* synthesis pathway of SLs is shared and conserved among Eukaryotes and Apicomplexa: Coccidia, Haemosporidia, Cryptosporidia, but absent from Piroplasmida and Gregarina (Nyonda *et al.*, 2022).

In *Toxoplasma*, sphingolipids play an essential role in rhoptry secretion. Indeed rhoptry membranes are enriched in SM compared to the whole tachyzoite with a ratio SM/PC that increases from 0.18 in tachyzoite to 0.32 in the fraction rhoptry-enriched (Besteiro *et al.*, 2008). Disruption of SL synthesis impairs tachyzoite growth and bradyzoite establishment as well as the secretion of rhoptries and thus the formation of the e-vacuole, formed after parasite attachment and rhoptries discharge into a new host cell and that precedes the formation of PV (Nyonda *et al.*, 2022).

In *Plasmodium*, SL synthesis is important for both asexual and sexual parasites. However, gametes present a sex-specific lipid composition and SLs are a central element of the differences. In asexual parasites, SM is the main sphingolipid but in male and female gametes, there is an enrichment of dihydrosphingomyelin (DHSM) from 2 % in asexual parasites to 20 % and 35 % in male and female gametes respectively (Ridgway *et al.*, 2022). While SM synthesis is not critical for males, it plays an essential role in the survival of male gametes, which are killed selectively by the addition of the SM synthase inhibitor GT11 (Ridgway *et al.*, 2022).

Cholesterol (Chol). Cholesterol is a sterol made of a rigid ring structure, the gonane, a hydroxyl group in position 3, and a short non-polar hydrocarbon tail. It is a key component of membranes of eukaryotic cells. Cholesterol is inserted in the phospholipid bilayer with its hydroxyl group that interacts with the polar head of phospholipids, while the ring structure and the hydrocarbon tail interact with the FA chains. In abundance, cholesterol can go up to 30 %, which corresponds to a ratio of Chol-PL close to 1-1 (van Meer *et al.*, 2008). Cholesterol plays an important structural role in modifying membrane fluidity. Together with sphingolipids, it is enriched in lipid rafts, and generally helps in the organization of the lipid membrane, acts as a facilitator stabilizer of protein

complexes (Coskun and Simons, 2011; Fantini and Barrantes, 2013). In Eukaryotes, cholesterol is made from acetyl-CoA generated by the mitochondria, exported to the cytosol, and synthesized *via* the mevalonate pathway in the cytosol and the ER (Sitaula and Burris, 2016).

Alveolates, including Apicomplexa have conserved the mevalonate pathway in the apicoplast but they have lost the gene for sterol synthesis and are thus auxotroph for cholesterol (Desmond and Gribaldo, 2009). Their survival thus relies on their capacity to scavenge cholesterol from the host (Coppens, 2013; Maier and van Ooij, 2022; Romano *et al.*, 2017). *Plasmodium* spp. niche in a cholesterol-rich environment within the human host, *i.e.* the hepatic cells that synthesize large quantities of cholesterol and recycle it from the circulating low-density lipoprotein particles (LDL), and the erythrocytes where the parasite scavenges cholesterol from the high-density lipoprotein particles (HDL) present in the blood (Grellier *et al.*, 1990) or directly from the erythrocyte membrane that contains up to 50 % of the circulating cholesterol (Chakrabarti *et al.*, 2017; Turner *et al.*, 2012). Cholesterol in the malaria parasite plays an essential role in invasion and nutrient uptake in hepatocytes and erythrocytes. Treatment with a cholesterol remover, methyl β -cyclodextran (M β CD), blocks parasite cell entry as well as uptake of small molecules, probably by affecting the fluidity of the PVM and affecting the correct assembly of the pore-forming protein EXP2 (Ahiya *et al.*, 2022; Bano *et al.*, 2007; Dluzewski *et al.*, 1985; Maier and van Ooij, 2022; Silvie *et al.*, 2006). Cholesterol is also essential for the sexual development of *Plasmodium*. Gametes indeed contain around 20 % cholesterol compared to 13 % in asexual parasites and an increase in the concentration of cholesteryl ester (cholesterol esterified with a FA chain) by 4 times (Ridgway *et al.*, 2022). This increase in cholesterol can be explained by the need of the parasite to deform the membrane during the gamogony and to store this precious resource as access to cholesterol in the mosquito is limited compared to the human host, mosquitos being like *Plasmodium*, auxotroph for cholesterol (Maier and van Ooij, 2022; Ridgway *et al.*, 2022).

Similar to the *Plasmodium* liver stage, intracellular *Toxoplasma* scavenges cholesterol from host internalized LDL processed in the host endo-lysosomes (Coppens *et al.*, 2000) but also from the host lipid droplets, which are the storage place of the cell for neutral lipids such as cholesteryl esters (Nolan *et al.*, 2017). Once internalized by the parasite *via* an ATP binding cassette (ABC) transporter G subfamily present in the PV and the plasma membrane, and contrary to *Plasmodium*, cholesterol is then stored in parasite lipid droplets after its esterification by two acyl-CoA cholesterol acyl transferases (ACAT1 and ACAT2) present in the ER. Chemical blocked or genetic ablation of the *Tg*ACATs lead to the inhibition of the parasite growth, reduction in lipid droplet s'

number and size, decrease in cholesteryl ester, and an accumulation of free cholesterol in the parasite's plasma membrane that collapses (Lige *et al.*, 2013).

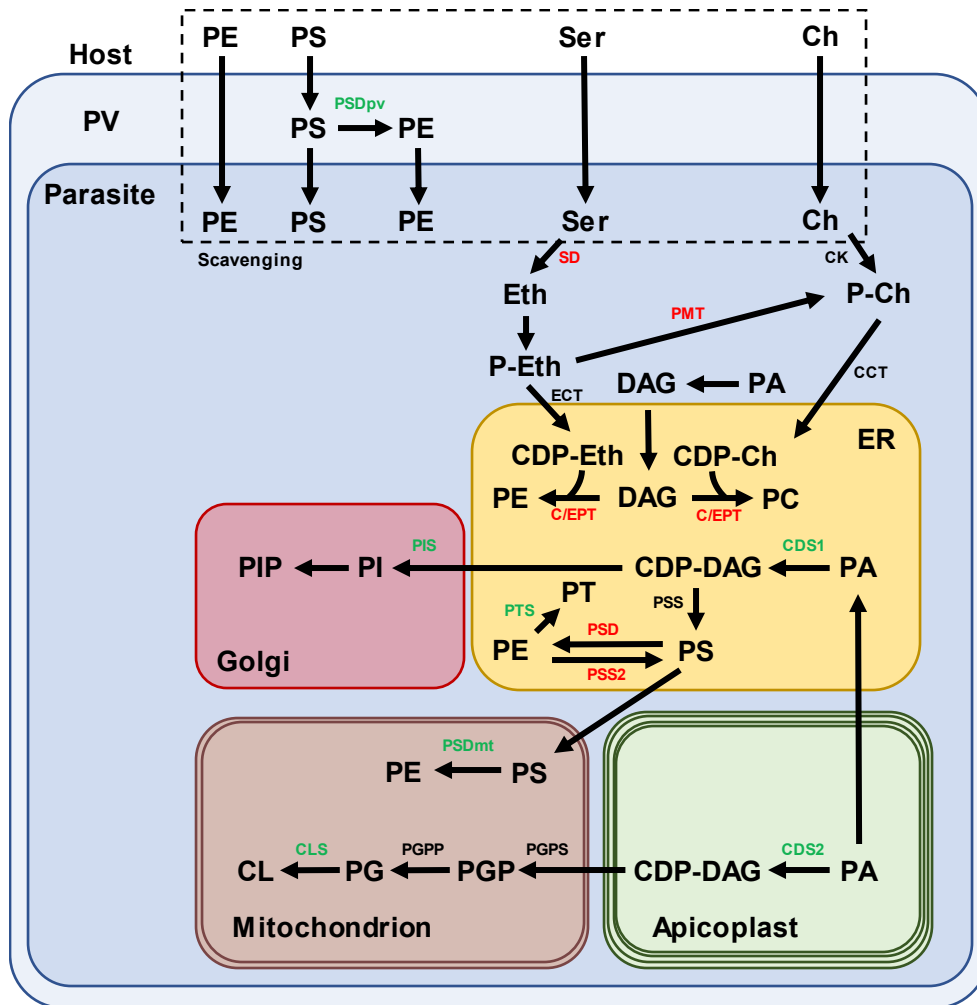


Figure 7: Schematic representation of overall phospholipid synthesis in *Toxoplasma* and *Plasmodium* parasites

Green enzymes are characterized in *Toxoplasma* while red enzymes are characterized in *Plasmodium*. Abbreviation used, PE = phosphatidylethanolamine; PS = phosphatidylserine; PC = phosphatidylcholine; PT = phosphatidylthreonine; PI = phosphatidylinositol; PIP = phosphatidylinositol phosphate; PG = phosphatidylglycerol; PGP = phosphatidylglycerol-phosphate; CL = cardiolipin; PA = phosphatidic acid; DAG = diacylglycerol; Ch = choline; Ser = serine; Eth = ethanolamine; P-Eth = phosphoethanolamine; P-Ch = phosphocholine; CDP = cytidine diphosphate; CDS1/2 = CDP-DAG synthetases 1/2; PSDmt / PSDpv = PS decarboxylases mitochondrial / parasitophorous vacuole; CLS = cardiolipin synthase; PGPP = phosphatidylglycerol-phosphate phosphatase; PGPS = phosphatidylglycerol-phosphate synthase; PIS = phosphatidylinositol synthase; PSS = phosphatidylserine synthase; PSS2 = phosphatidylserine synthase 2; PTS = phosphatidylthreonine synthase; C/EPT = choline / ethanolamine phosphate cytidyltransferase; ECT = ethanolamine-phosphate cytidyltransferase; CCT = choline-phosphate cytidyltransferase; PMT = phosphoethanolamine N- methyltransferase; SD = serine decarboxylase; CK = choline kinase. Boxes colour code: yellow = endoplasmic reticulum; red = Golgi apparatus; brown = mitochondrion; green = apicoplast.

Lipids can be stored

In eukaryotic cells, lipids are stored in lipid bodies (LBs) also known as lipid droplets (LDs). Lipid bodies are micelles made of a monolayer of phospholipids, mainly PC composed of C18:1/C18:1 or C18:1/C16:1 FA chains and containing TAG, DAG, cholesteryl ester, that found their origins in the ER membrane leaflet (Blanchette-Mackie *et al.*, 1995; Tauchi-Sato *et al.*, 2002). LD biogenesis starts in the ER membrane, place of the G3P pathway: FAs are first activated with the transfer of a CoA on a free fatty acid chain by acyl-CoA synthase (ACS), and acyls-CoA are esterified on a G3P backbone by acyl transferases recruited at the level of the ER membrane (GPAT, AGPAT) to form LPA and PA (Agarwal *et al.*, 2017). To produce the DAG storage molecules, cells possess a PA phosphatase (PAP) called LIPIN that hydrolyses the phosphate from the PA, thus releasing a DAG (Fang *et al.*, 2014). A third acyl transferase, a diacylglycerol acyl transferase (DGAT), esterifies a third acyl chain on the DAG to form TAG fueling the LDs (Yen *et al.*, 2008). LDs serve as lipid storage for membrane biogenesis and cell division but also as energy storage. When needed, FAs stored in the LD can be released *via* the action of lipases and channeled toward the mitochondria or the peroxisome for processing by β -oxidation for energy production.

The *Toxoplasma* genome contains the genes of the prokaryotic PA synthesis localized within the apicoplast (Amiar *et al.*, 2020, 2016), as well as the eukaryotic G3P pathway, namely *TgGPAT*, *TgAGPAT*, *TgDGAT1/2*, and *TgLIPIN* (Amiar *et al.*, 2020; Dass *et al.*, 2021; Quittnat *et al.*, 2004). Constant scavenged lipids are channeled toward lipid storage within LDs, and inducible ablation of *TgLIPIN* illustrates its role in preventing parasite death from lipotoxicity: without LIPIN, parasites over-produce phospholipids and membranes and contain a reduced TAG/DAG ratio and LD numbers (Dass *et al.*, 2021). Channeling this constant flux into LDs prevents parasite death. Blocking the DGAT activity with the DGAT inhibitor T863 leads to a disruption of the normal ER structure, results in ER swelling and membranous tubules, a phenotype that is exaggerated upon the addition of exogenous unsaturated FAs (Nolan *et al.*, 2018).

Chapter III Membrane trafficking and lipid transporters: how do lipids circulate within the cell?

Membranes are highly dynamic cell components

General introduction to eukaryote vesicular trafficking

Protein sorting, plasma membrane homeostasis, exocytosis, endocytosis, or signaling events are biological processes that are all regulated by vesicular trafficking. Unlike LDs, vesicles are composed of a phospholipid bilayer, that can transport solutes, soluble or membranous proteins, vitamins, sugars, and nutrients in a general manner. They are responsible for trafficking between different cellular compartments.

The secretion pathway is a vesicle-mediated trafficking that involves the rough ER, the Golgi apparatus, post-Golgi vesicles, the early and late endosomes, the lysosomes, and the plasma membrane. The vesicular trafficking starts from a donor compartment in which a membrane curvature occurs, facilitated by the membrane asymmetry causing the accumulation of specific phospholipids on one side of the phospholipid bilayer, creating positive and negative curvatures that initiate the vesicle budding. As mentioned in chapter 2, phospholipid shapes and charges vary depending on their classes. For example, the accumulation of PS on the cytosolic leaflet induces curvature and the accumulation of negative charges recruits vesicle coating protein complexes (Takeda *et al.*, 2014). This budding is amplified by the recruitment of specific coatomer proteins, also involved in the correct addressing of the vesicle (**Figure 8**). As such coatomers, COPII coats vesicle budding from the rough ER and addressed to the cis Golgi. The return is ensured by COPI which coats vesicle budding from the cis Golgi targeting the ER (Bonifacino and Glick, 2004). Vesicles trafficking between the plasma membrane, the Golgi, and the endosomal compartments are coated with clathrin (Bonifacino and Glick, 2004). The nascent vesicle is detached from the donor compartment *via* the action of dynamins that polymerize around the vesicle neck and pinch the membrane with the energy from GTP hydrolysis. As main actors of this vesicular trafficking small GTPases called Rab proteins play an essential role in vesicle budding, and trafficking along the microtubules *via* kinesin proteins. Rab proteins also facilitate the vesicle fusion with the correct target membrane by directly interacting with the tethering proteins inserted in the receiving membrane, thus facilitating the formation of the SNARE complex (Li and Marlin, 2015; Stenmark, 2009). SNAREs (soluble N-ethylmaleimide-sensitive factor attachment protein receptors) are also

critical for the correct addressing of the vesicle of the membrane fusion with the right compartment. The v-SNARE inserts in the cytosolic leaflet of the vesicles, after docking *via* the Rab and tethering proteins, thus forming a complex with the t-SNARE inserted in the target membrane, which pulls the two membranes in close vicinity and allows membrane fusion and release of the vesicle content (Bonifacino and Glick, 2004; Koike and Jahn, 2019; Südhof and Rothman, 2009) (**Figure 8**).

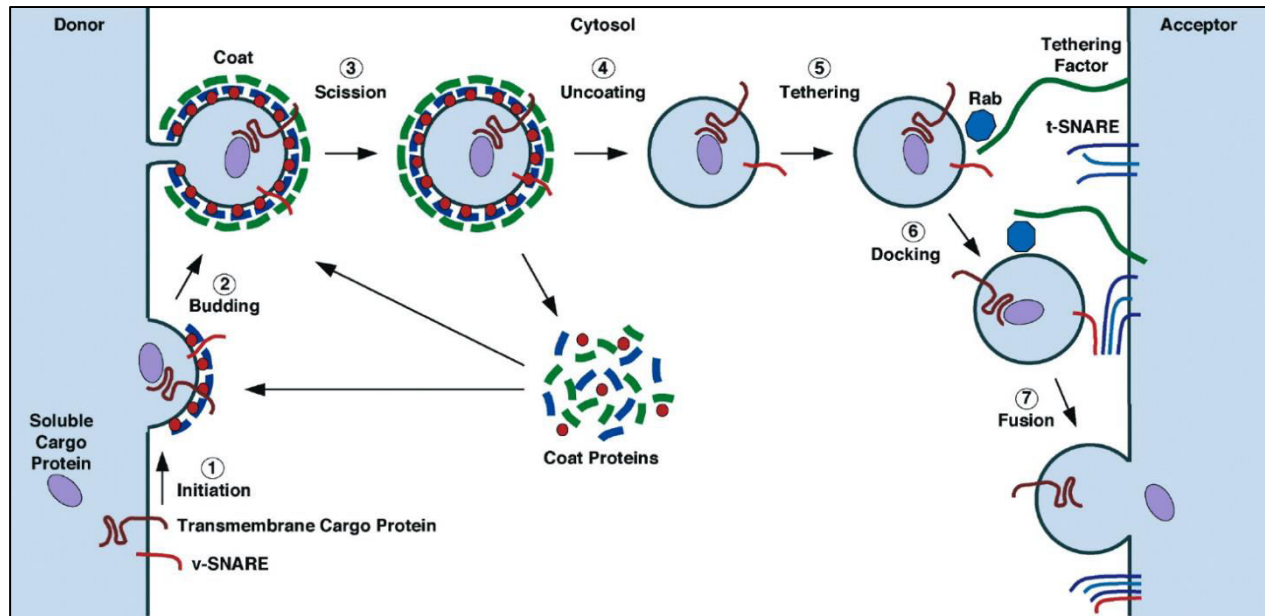


Figure 8: Vesicle budding and fusion

(1) Membrane curvature induces the recruitment of small GTPases (in red), such as Arf proteins, and coat adaptor complex proteins such as AP1 or AP2 (in blue). Transmembrane cargo proteins allow soluble cargo to be exported *via* the nascent vesicle and gathered with v-SNAREs to the coat assembly. (2) The vesicle budding is ensured by the recruitment of coat proteins like COPI, COPII, and clathrin. (3) The vesicle is released from the donor membrane by the action of dynamins that polymerized at the neck of the vesicle and pinch the membrane. (4) The vesicle coat is disassembled by inactivation of small GTPases or the action of uncoating enzymes. (5) Association of GTP-bound Rab proteins (on the vesicle) with tethering factors (on the acceptor membrane) initiates the docking of the vesicle. (6) V-SNAREs on the vesicle associate with the t-SNAREs on the target membrane, and the complex triggers the membrane fusion. (7) The vesicle content is released into the target compartment and v-SNAREs are recycled back to the donor compartment. The figure is adapted from Bonifacino and Glick, 2004.

Phospholipids and more specifically PIPs are essential for intracellular vesicular trafficking. The various organelles possess specific protein and lipid compositions responsible for the correct addressing of intracellular vesicles, the Rab or the SNARE proteins, PI₄P for the Golgi, PI₃P and PI_{3,5}P₂ for the early and the late endosomes, respectively (Kim *et al.*, 2011; McCrea and De Camilli, 2009). PIS localized at the ER and synthesized PI, which is exported to the Golgi and serves as precursor for the synthesis of PI₄P by a PI 4-kinase at the level of the cytosolic leaflet of the Golgi, PI₄P is then used either as a substrate for PI_{4,5}P₂ synthesis or the recruitment of the vesicle budding machinery comprising the small GTPase Arf1, the Epsin R involved in the retrograde trafficking from the endosomes to the Golgi *via* the interaction to Golgi PI₄P, and the clathrin adaptor protein

AP1, recruiting the vesicle coating protein clathrin, which is responsible for the addressing from the Golgi to the endosomes (Downes *et al.*, 2005; Mills *et al.*, 2003; Saint-Pol *et al.*, 2004). Similar to PI4P in the Golgi membrane, PI_{4,5}P₂ generated by PIPKs at the plasma membrane, is responsible for the recruitment of the AP2 complex, Espin 1-3, and dynamins at the sites of endocytosis for endocytic vesicle budding and release (Ford *et al.*, 2002; Itoh *et al.*, 2001, 2001; Zheng *et al.*, 1996). PI_{4,5}P₂ also regulates actin polymerization through the recruitment and the regulation of N-WASP and the Arp2/3 complex, which drive the force for membrane deformation and vesicle budding (Engqvist-Goldstein and Drubin, 2003).

Vesicular trafficking in Apicomplexa: exocytosis

Apicomplexa have repurposed the secretion for the synthesis of the apical secretory organelles, namely rhoptries, and micronemes. Starting within the rough ER, secreted proteins are synthesized, then exported toward the Golgi apparatus, probably *via* the Sec1 family protein SLY1, which is known to interact with the Golgi core SNARE fusion complex syntaxin Sed5p, also known as Stx5. Recent findings identified two important ER-resident SNARE proteins, Stx18 and Stx19 as being critical for the secretory system (Cao *et al.*, 2021). Microneme and rhoptry proteins traffic from the Golgi to the endosome-like compartment (ELC) using vesicles budding from the trans-Golgi network. Apicomplexa have conserved an AP1, which forms a complex recruiting Arf1 and clathrin. AP1 also seems to mediate the traffic of lateral microneme and rhoptry proteins, essential for the biogenesis the apical secretory organelles (Venugopal *et al.*, 2017). Additionally, disruption of *TgAP1* highlighted the biogenesis of apical micronemes and supposedly clathrin-independent trafficking. Newly formed vesicles are detached from the Golgi by the action of the dynamin *TgDrpB* that disruption impairs rhoptry and microneme biogenesis (Breinich *et al.*, 2009) (**Figure 9**).

The vacuolar protein sorting VPS45, the SNAREs Stx16, and Stx6 mediate and regulate the vesicular trafficking between the trans-Golgi network and the ELC, and are critical for the nascent IMC. The ELC then serves as a central hub for Apicomplexa vesicular trafficking and is the place that crosses the endocytosis and the exocytosis events (McGovern *et al.*, 2018). From ELC, rhoptry and microneme proteins take different paths to reach their specific destinations: microneme proteins somehow intersect with the ingested proteins and ended up in the micronemes (McGovern *et al.*, 2018), rhoptry proteins transit *via* their specific pre-rhoptry compartment before maturation and are addressed to the rhoptries. Addressing of rhoptry and microneme contents seems to be

dependent on Stx12. In contrast, the biogenesis of these apical organelles appears not affected by transmission electron microscopy after deletion of Stx12 (Bisio *et al.*, 2020; Cao *et al.*, 2021) (Figure 9).

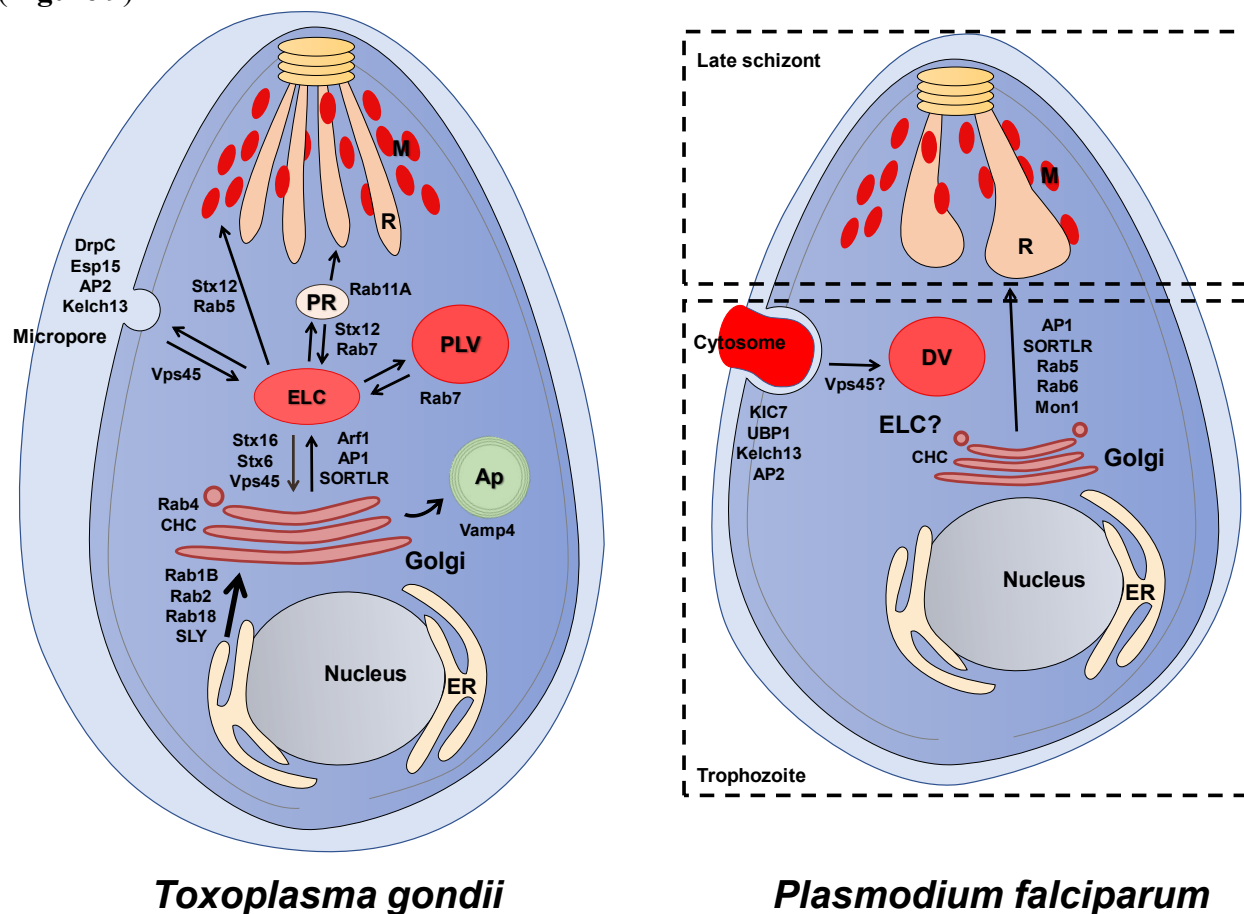


Figure 9: Schematic representation of Apicomplexa secretory pathway and endocytosis

Relevant proteins involved in the *Toxoplasma gondii* tachyzoite and the *Plasmodium falciparum* blood stage are annotated. In *Plasmodium* blood stage, apical organelles biogenesis occurs only in late schizonts, whereas endocytosis through the cytosome occurs in early, mid, and late trophozoites. Abbreviation used, ELC = endosome-like compartment; PLV = plant-like vacuolar compartment; PR = pre-rhoptry; ER = endoplasmic reticulum; M = micronemes; R = rhoptries; Ap = apicoplast; DV = digestive vacuole. Adapted from (Bisio *et al.*, 2021; Spielmann *et al.*, 2020).

Vesicular trafficking in Apicomplexa: the endocytosis.

Apicomplexa use endocytosis to acquire nutrients and resources from their hosts. Primarily, endocytosis is known to happen in *Plasmodium* during the intraerythrocytic stage. The parasite ingests a large quantity of hemoglobin from the RBC, up to two third of the RBC cytosol content, to supply its need in material and space to properly develop. This process has been termed host cell cytosol uptake (HCCU) (Francis *et al.*, 1997; Hanssen *et al.*, 2012; Sherman, 1977; Spielmann *et al.*, 2020). The internalized material is then addressed to a lysosome-like compartment called the digestive vacuole (DV) where the hemoglobin is digested by the parasite to release amino acids used for its development, and the heme is neutralized into a non-toxic pigment, hemozoin

(Sherman, 1977) (**Figure 9**). The mechanism surrounding this uptake remains unclear but two structures frequently appear to be involved, the cytosome and the phagotroph. Both are host cytosol-filled invaginations of the parasite plasma membrane and the PVM. The difference is that the phagotroph is larger and with a wider neck than the cytosome and it does not have a collar (Milani *et al.*, 2015; Spielmann *et al.*, 2020). Few proteins have been characterized to be directly involved in *Plasmodium* endocytosis. Among them, *PfVPS45* is critical for the correct addressing of host cytosol-filled vesicles to the DV. Deletion of this protein induces the accumulation of cytosol-filled vesicles, which are mistargeted and no longer reach the DV (Jonscher *et al.*, 2019). Other proteins such as SNAREs, dynamins, PI₃P kinase, or Rab proteins are suspected to be involved in the HCCU and addressing to the DV but experimental validations are needed to confirm their roles (Spielmann *et al.*, 2020). Recently, a donut-shape structure essential for the early formation of the cytosome has been identified. It comprises surprisingly 1/ the *PfAP2* homolog, regardless the involvement of clathrin in the process, the *Plasmodium* 2/ *Eps15*, 3/ *Kelch13* which is known to be involved in artemisinin resistance, and 4/ unknown proteins associated to *Kelch13*, named *Kelch13* interaction candidates KIC1-9 (Birnbaum *et al.*, 2020; Spielmann *et al.*, 2020). *Plasmodium* cytosome thus appears to be the closest endocytic structure present in its cousin *Toxoplasma*, the micropore (**Figure 9**).

The *Toxoplasma*'s micropore has recently been shown to be related to endocytosis in both intra- and extracellular tachyzoites. It is, as the cytosome, an invagination of the parasite's plasma membrane but filled with PV content instead of PVM and host cytosol. A structure similar to the one of the *Plasmodium* cytosome neck is conserved in *Toxoplasma*. *Kelch13*, *AP2*, and *Eps15* have also been localized to the micropore and shown to be essential for parasite endocytotic event and survival (Koreny *et al.*, 2022). The dynamin *DrpC*, previously identified to localize at the basal pole during endodyogeny suggests a role in pinching the individual daughter cells. This second micropore-localization thus suggests a dual role of this highly divergent dynamin in pinching the plasma membrane at the basal pole at the end of the endodyogeny (Amiar *et al.*, 2020) and at the micropore for material internalization (Koreny *et al.*, 2022). As in *Plasmodium*, *TgVPS45* deletion impairs the ingestion of host material with the presence of enlarged micropores but it also affects the homeostasis of the PLVAC and the ELC (Bisio *et al.*, 2020). Internalized materials transit through the parasite ELC, and intersect with the microneme proteins, which traffic to the apical pole and end up in the PLVAC. Ingested proteins are digested *via* the action of the proteases *CPL* and *CPB*, which have been localized to the PLVAC, their deletion leading to the accumulation of

host material within the PLVAC. Amino acids are then transferred to the cytosol *via* the CRT transporter (McGovern *et al.*, 2018). Endocytosis is poorly characterized in the *Toxoplasma* chronic bradyzoite. Further investigation will be required to identify the mechanism involved in the ingestion of host material (Kannan *et al.*, 2021) (**Figure 9**).

Studying endocytosis in Apicomplexa reveals to be critical in the fight against Apicomplexa, firstly because it is an essential pathway: the development of *Plasmodium* blood stages relies on hemoglobin acquisition and all *Toxoplasma* life stages are dependent on massive host scavenging; Secondly because the Apicomplexa endocytosis pathway is the battlefield between drugs fighting Apicomplexa vs. the parasites' drug resistance development. Chloroquine is an anti-malaria compound that blocks the polymerization of the heme into hemozoin within the DV. Hemozoin is highly toxic for the parasite. As a response to chloroquine treatment, a mutation appeared to a DV transporter now known as the chloroquine-resistant transporter (CRT). This mutation prevents the accumulation of chloroquine and limits its action (Martin and Kirk, 2004). Kelch13, an essential protein of both *Plasmodium* cytosome and *Toxoplasma* micropore has recently been shown to be involved in the resistance against one the latest anti-malaria compound, artemisinin (Balikagala *et al.*, 2021; Kampoun *et al.*, 2022; Talundzic *et al.*, 2018).

Non-vesicular lipid transfer *via* lipid transporters.

Because of their hydrophobicity and their solubility in solvents, the large majority of lipids cannot circulate freely through the cell. Nevertheless, the smallest lipid, i.e., FAs can circulate freely. Lipid transporters prevent circulating FAs, to act as detergents and cause damages to lipidic membranes, by the creation of pores or micelles that could lead to cell death. Lipids can move around the cell and between cells *via* vesicular trafficking as seen above but they can also be transported by specific soluble or membranous lipid transporters to facilitate their exchange between the different intracellular compartments.

Eukaryote cytosolic and luminal lipid transporters, roles, and regulations (Figure 10)

Fatty acyl binding proteins (FABP)

FABPs are soluble lipid transporters that bind to FAs and also to other lipid compounds such as eicosanoids. These are derivatives of the arachidonic acid. They play important signaling roles in the inflammatory response. FABPs also transport retinoids which are derivatives of the vitamin A

(Chmurzyńska, 2006; Richieri *et al.*, 2000; Smathers and Petersen, 2011). While a large number of FABPs have been identified, they do not present a high degree of discrimination between FAs within the same tissue. However, in different animals, a relative FA specificity exists depending on the tissues suggesting different roles in FA metabolism (Richieri *et al.*, 2000). These transporters are responsible for the exchange of lipids between different intracellular compartments such as the peroxisome, the mitochondria, or the ER. The human genome encodes close to ten FABP isoforms. These have specific tissue localizations including liver, heart, intestine, adipocyte, brain, myelin, testis, epidermis. As an example of FABP functions, three of the 10 identified in humans are localized to the brain: FABP3, 5, and 7 with essential functions for brain development, FABP7 for neuron migration, and FABP3/5 in neuron differentiation (Liu *et al.*, 2010). FABPs are also involved in pathologies such as 1/ glioblastoma in which FABP 7 plays an important role in promoting the migration of the tumor cells, 2/ the Down Syndrome (DS) that presents the characteristic phenotype of mental retardation and where patients suffering from DS show an increased expression of FABP7 and a decreased expression of FABP3 (Cheon *et al.*, 2003).

Acyl-CoA binding proteins (ACBP)

As another acyl ester binding protein, ACBPs are small lipid carriers (~10 kDa), which bind with a high affinity (C12:0-C26:0) FAs and they can be activated with a CoA by acyl-CoA synthetases (ACS). ACBPs have versatile roles in cells as intermediates and regulators in lipid metabolism. For examples, they provide FAs for β -oxidation, they allow glycerolipid and sphingolipid synthesis, vesicle trafficking, and cell signaling (Lung and Chye, 2016). Depletion of the yeast ACBP homolog *ScAcb1p* leads to an important reduction in growth, accumulation of cytosolic vesicles, multilayered membranes, and fragmented vacuoles (FÆRGEMAN *et al.*, 2004). In plants, ACBPs have been classified into four classes: small ACBPs (class I), ankyrin-repeat ACBPs (class II), large ACBPs (class III), and kelch-ACBPs (class IV). The presence of at least one of each class in plants indicates non-redundant functions. The four classes have been characterized as highly conserved class I. One such class I ACBP is *AtACBP6*, which is involved in pollen, seed, and seedling development. It also plays an important role in freezing resistance (Hsiao *et al.*, 2014; Liao *et al.*, 2014; Lung and Chye, 2016). Class II ankyrin-ACBPs possess an N-terminal transmembrane domain that allows an endomembrane localization, and the C-terminal ankyrin domain for protein-protein interactions with proteins involved in abscisic acid, hypoxia, and heavy metal stress responses (Du *et al.*, 2013; Schmidt *et al.*, 2018; Xiao *et al.*, 2008a) but also in freezing tolerance and embryo development (Chen *et al.*, 2010; Du *et al.*, 2010; Lung and Chye, 2016).

Class III large ACBPs, localize to the endomembranes or the apoplast and contrary to the other classes the class III ACBPs have their ACB domain in C-terminal instead of N-terminal. Large *AtACBP3* revealed itself not only to bind to acyl-CoA but also to PC and PE, which could explain their role in leaf senescence by regulating phospholipid metabolism (Xiao *et al.*, 2010). The last family of ACBPs, the kelch-ACBPs, bind to C18:1 acyl-CoA and PC through the kelch domain in addition to the ACB domain (Xiao *et al.*, 2009). Like class II ACBPs with an ankyrin domain, the kelch domain may also help to identify protein partners. Class IV ACBPs play different roles in embryogenesis, lipid metabolism, and defense reaction (Hsiao *et al.*, 2014; Li *et al.*, 2008; Xiao *et al.*, 2008b).

Sterol carrier proteins (SCP)

SCPs are none specific lipid transporters. The SCP gene encodes two SCP proteins with different roles in lipid metabolism. SCP-x is a peroxisomal 3-ketoacyl-CoA thiolase involved in the oxidation of branched-chain lipids for bile acid formation from cholesterol and detoxification *via* oxidation of branched-FA (Fuchs *et al.*, 2001; Kannenberg *et al.*, 1999). SCP2 is a small soluble non-specific lipid transporter that can bind to cholesterol, free-FA, acyl-CoA, LPA, PI, sphingolipids, or signaling molecules (leukotrienes, prostaglandins, ...). SCP2 regulates lipid rafts and microdomains at the plasma membrane (Schroeder *et al.*, 2007) and was originally identified as being required for isoprenoid and cholesterol metabolisms (Ericsson *et al.*, 1993; Kesav *et al.*, 1992).

Plant lipid transfer proteins (PLTP)

PLTPs also called non-specific LTPs (nsLTPs). They are also small proteins (~7-9 kDa), found in plants that bind to a large range of lipids such as FA, (C10:0-C18:0) acyl-CoA, sterols, LPLs/PLs, and galactolipids. They are divided in two categories, nsLTP1s and nsLTP2s (Arondel and Kader, 1990; Cheng *et al.*, 2004; Dubiela *et al.*, 2017; Han *et al.*, 2001; Missaoui *et al.*, 2022; Nazeer *et al.*, 2019; Shenkarev *et al.*, 2017). The localization of these nsLTPs varies depending on the developmental stage of the plant: nsLTP1s are expressed in the aerial organ while nsLTP2s are in the roots, and both are expressed in the seed (Douliez *et al.*, 2000). At the cellular level, the localization is also dynamic: nsLTPs can be secreted, or attached to the external side of the plasma membrane after post-translational modifications with the addition of a GPI anchor, being released by the action of phospholipases (Ambrose *et al.*, 2013; Edstam *et al.*, 2013; Wei and Zhong, 2014). Inside the cell, nsLTPs localization varies between the apoplast, the plasma membrane and the cytosol but depending on the organism they can also localize to atypical compartments such as

vacuoles or the glyoxysomes (Ambrose *et al.*, 2013; Finkina *et al.*, 2016; Kielbowicz-Matuk *et al.*, 2008). Still, in plants, nsLTPs play an important role in plant defenses against bacteria and fungi (Ben Hsouna *et al.*, 2021; Roy-Barman *et al.*, 2006; Safi *et al.*, 2015; Schmitt *et al.*, 2021), in response to abiotic stresses such as drought, cold, or oxidative stress but also during germination and cuticle formation (Chen *et al.*, 2017; Fang *et al.*, 2020; Safi *et al.*, 2015; Song *et al.*, 2020). In human health, nsLTPs are responsible for food allergies. Their resistance to high-temperature and proteolysis protects them from denaturation (Palacin *et al.*, 2010; Salminen *et al.*, 2018) thus preserving the specific binding of IgEs that trigger the allergic reaction (Costa *et al.*, 2022; Cuadrado *et al.*, 2021).

Other small LTPs, Sec14, PITP, and ORP

Despite their specificities, all these transporters' families have in common to act in the transport of PI (Lipp *et al.*, 2020), which is a crucial lipid for vesicular trafficking and signaling events as seen in chapter 2. In yeast, Sec14p is a well-known lipid transporter that belongs to the CRAL-TRIO super-family. It participates in the regulation of the Golgi PI₄P pool, furnishing PI to Pik1. It also participates to the regulation of DAG abundance for vesicle fission (Shemesh *et al.*, 2003). While Sec14 is mostly known for its interactions with PC and mainly PI, other members of the family have been shown to bind to PE and PS. They members are Sfh1p, which is proposed to be the PS/PE exchanger between the ER and the endosomes (Mizuike *et al.*, 2019). Sfh3p binds to PI as Sec14p. It binds also to sterols and is an actor of the ergosterol metabolism and it contribute to the utilization of lipids stored in LD rich in TAG and Chol-ester (Ren *et al.*, 2014).

As other transporters of PI, PI transfer proteins (the PITPs family) are divided in two classes (Lipp *et al.*, 2020). The class I PITPs comprise brain PITP α and liver PITP β that can bind to PI and PC. PIPT α is involved in exocytosis of secretory vesicles (Hay and Martin, 1993), providing PI for PI_{3,4,5}P₃ by PI3K (Kular *et al.*, 1997). It is also involved in signaling cascades through PIP cleavage by phospholipases (Kauffmann-Zeh *et al.*, 1995). The PITP β function is still unclear but it seems that it participates to sustain the PI₄P pool in the Golgi, providing PI from the ER (Carvou *et al.*, 2010). Class II PITPs do not bind to PC in addition to PI but they bind to PA (Garner *et al.*, 2012), and are essential for signaling cascades through PIPs cleavage. As such, they participate in the PI cycle, recycling PA to the ER to be converted into PI, which is then transported back to the plasma membrane to be phosphorylated (SoHui Kim *et al.*, 2013; Kim *et al.*, 2015).

Oxysterol-binding proteins (OSBPs) were the first identified OSBP-related proteins (ORPs). They are recruited to the Golgi *via* the recognition of PI₄P by a pleckstrin-homology (PH) domain and to the ER thanks to the presence of a FFAT motif that mediates interaction with ER-inserted VAP. More recent ORPs have been identified. They have allowed subdivision in six sub-families. Based on their conservation or class of their PH and their FFAT domain (Lehto *et al.*, 2001; Lipp *et al.*, 2020). The ORP characterization has mainly been performed by the characterization of one of the “simplest” ORP proteins, *i.e.*, Osh4p, which can transfer sterols between membranes (Raychaudhuri *et al.*, 2006). In addition, Osh4p has been demonstrated to bind to PI₄P and it has been proposed to act as a sterol/PI exchanger following a PI₄P gradient to regulate the sterol distribution within the cell (de Saint-Jean *et al.*, 2011; Lipp *et al.*, 2020). This model is supported by previous work that showed an opposite role of Osh4p to Sec14p by downregulating PI₄P in the Golgi membrane. The repression of Osh4p indeed abrogates the lethality of the Sec14p deletion (Fairn *et al.*, 2007; Fang *et al.*, 1996). A deeper analysis of ORP family members has revealed that ORP5/8 and their yeast homologs Osh6/7p play a role in distributing the PS from the ER to the plasma membrane, and recycling back PI₄P to the ER, thus preventing PI_{4,5}P₂ accumulation (Chung *et al.*, 2015; Lipp *et al.*, 2020; Maeda *et al.*, 2013; Moser von Filseck *et al.*, 2015).

Repeating β -groove (RBG) domain LTPs:

It is a recently identified family of large eukaryotic LTPs (above 2000 residues), with the characteristic to form a large groove made of β -sheets (Neuman *et al.*, 2022). This family comprises VPS13, ATG2, SHIP164, hobbit, and tweek sub-families, which are present at membrane contact sites. These proteins ensure the transfer of phospholipids between different intracellular organelles, mostly from the ER, for *de novo* membrane generation (Guillén-Samander *et al.*, 2021; Hanna *et al.*, 2022; Kumar *et al.*, 2018; Neuman *et al.*, 2022, 2021; Toulmay *et al.*, 2022; Valverde *et al.*, 2019). They are important for lipid homeostasis and correct vesicular trafficking events as the disruption of such transporters impairs the subcellular distribution of PI_{4,5}P₂ in the hobbit and tweek mutants (John Peter *et al.*, 2022; Neuman *et al.*, 2021), PE deliverance to ER by Csf1 (Toulmay *et al.*, 2022). Furthermore, hobbit mutation results in the loss of exocytosis whereas SHIP164 and tweek seem to be involved in endocytosis (Hanna *et al.*, 2022; Verstreken *et al.*, 2009). One of the most characterized RBGs is ATG2, shown to bridge the ER and the autophagosome at membrane contact sites. ATG2 fuels the autophagosome membrane development with phospholipids *via* its interaction with the autophagosome receptor ATG9 (Ghanbarpour *et al.*, 2021; Valverde *et al.*, 2019). Mutations of VPS13 subfamily members have

been connected to neurological disorders such as the Cohen syndrome or the Parkinson's disease. In a general manner, disruption of RBGs severely impacts animal development and physiology (Neuman *et al.*, 2022).

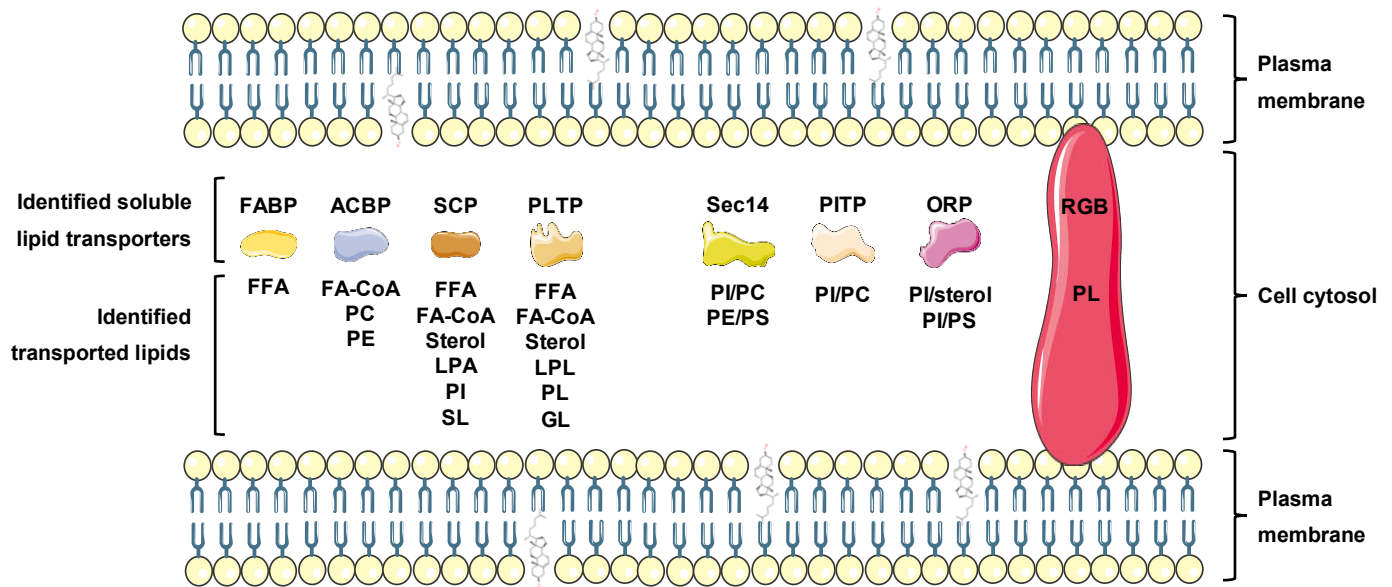


Figure 10: Soluble lipid transporters

Lipid transporters: FABP = fatty acid binding protein; ACBP = acyl-CoA binding protein; SCP = sterol carrier protein; PLTP = plan lipid transfer protein; PITP = phosphatidylinositol transfer protein; ORP = oxysterol binding protein (OSBP) related protein; RGE = repeating β -groove domain. Lipid substrates: FFA = free fatty acid; FA-CoA = acyl-CoA; PC = phosphatidylcholine; PE = phosphatidylethanolamine; PI = phosphatidylinositol; PS = phosphatidylserine; LPA = lysophosphatidic acid; LPL = lysophospholipids; PL = phospholipids; SL = sphingolipids; GL = galactolipids. Parts of the figure were drawn using pictures from Servier Medical Art. Servier Medical Art by Servier is licensed under a Creative Commons Attribution 3.0 Unported License (<https://creativecommons.org/licenses/by/3.0/>).

To cross membranes, lipids require membranous transporters (Figure 11)

The transporters/exchangers described above allow the non-vesicular transfer of lipids, namely FAs, acyl-CoAs, phospholipids, sterols, etc., between organelles and/or the plasma membrane at membrane contact sites. However, most *de novo* lipid synthesis pathways occur within endocompartments, *e.g.*, the ER, the Golgi, chloroplasts, or mitochondria. To maintain the membrane homeostasis and correct cellular functions, such as vesicular trafficking, membrane biogenesis, or cell division, lipids need to be distributed through the membrane bi-layers. As a brief reminder of the plasma membrane structure, both luminal/cytosolic and extracellular faces are hydrophilic. This is at these faces that polar heads of lipids aggregate. While the lipid tails form the hydrophobic core of the membrane. Because of this structure, the natural flipping of lipids from a

lipid leaflet to the other one happens spontaneously very slowly. To regulate this process, the cell thus requires energy and specific transporters.

Flippases

They are two kinds of unidirectional transporters that use the energy from the hydrolysis of ATP to flip phospholipids across the membrane: the flippases, which transport phospholipids from the extracellular/luminal side toward the cytosol, and the floppases, which ensure the opposite direction. Flippases are a group of large membranous transporters also known as P4-ATPases or aminophospholipid ATPases, which belong to the superfamily of P-type ATPases. This superfamily includes cation transporters P1-, P2-, and P3-ATPases, among which are found the well-known P2-ATPases, the Sarco(endo)plasmic reticulum calcium-ATPases (SERCA) (Berchtold *et al.*, 2000; Nemirovskaya and Sharlo, 2022), and the Na⁺/K⁺ pump involved in action potential formation in nerves (Jorgensen *et al.*, 2003). Flippases or P4-ATPases are essential to maintain the membrane asymmetry. In eukaryotic cells, the distribution of membrane lipids is indeed unequal with a large accumulation of PC, SM, and few PE but no PS on the exoplasmic side while the cytoplasmic side concentrates all the PS, a large proportion of PE and PC, the PI/PIP and some SM (Paulusma and Oude Elferink, 2006). P4-ATPases are divided in three subfamilies: P4A is conserved in all eukaryotes. P4B was lost in plants and seems to function as a monomer without the usual P4-ATPase β -subunit CDC50. An intermediate P4C subfamily seems similar in function to P4B but closer to P4A on the phylogenetic aspect (Palmgren *et al.*, 2019). In erythrocytes, disruption of the plasma membrane localized P4-ATPase, ATP81B, results in an abnormal exposition of PS on the extracellular side of the cell, which is an apoptotic signal recognized by the immune system to induce programmed cell death. In contrast in platelets, external exposition of PS is a normal process that occurs during the coagulation allowing platelets to aggregate and be cleared by macrophages. In addition to the plasma membrane, P4-ATPases also localize to the endosomes/Golgi complexes (Andersen *et al.*, 2016). The majority of flippases flip PS, but some can also flip PE or PC (Andersen *et al.*, 2016; Bai *et al.*, 2020; Roland and Graham, 2016; Wehman *et al.*, 2011). Work on the *Saccharomyces* model, which possesses five P4-ATPases, Drs2p, Dnf1/2/3, and Neo1p, have revealed the importance of the flippases. Drs2p was shown to be involved in protein trafficking through vesicular budding at the trans-Golgi network. This supported the previous model of flippases providing lipid imbalance on the cytosolic leaflet, thus creating membrane curvatures for the recruitment of AP1 and coat proteins, such as clathrin, and thus vesicle budding (Graham, 2004; Liu *et al.*, 2008). Disruption of these P4-ATPases led to a

decrease in membrane asymmetry, a defect in protein trafficking, exocytosis, and endocytosis events (Alder-Baerens *et al.*, 2006; Graham, 2004; Hua *et al.*, 2002; Takeda *et al.*, 2014). Drs2p flipping activity was shown to be positively regulated by the interaction with PI₄P, which is highly abundant in the Golgi membrane. Drs2p was also shown to be regulated by Gea2p, an Arf-GEF protein essential for vesicle budding: the C-terminal domain of Gea2p inhibits the Drs2p activity (Natarajan *et al.*, 2009) once in the endosome when recycled to the Golgi, Drs2p interacts with Rcy1p and the Arf-GAP protein Gsc1p (Hanamatsu *et al.*, 2014; Sakane *et al.*, 2006).

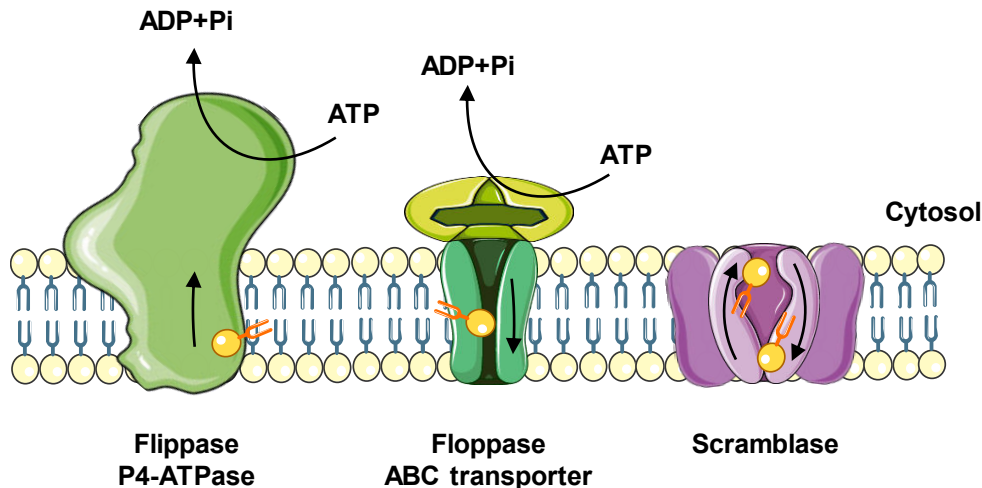


Figure 11: Membrane lipid transporters

Flippases and floppases use the energy of the hydrolysis of ATP to flip lipids against their concentration gradient and they participate in generating membrane asymmetry. Scramblases are bidirectional. They use the concentration gradient force to flip lipids, and participate to distribute lipids across the membrane bilayer. Parts of the figure were drawn using pictures from Servier Medical Art. Servier Medical Art by Servier is licensed under a Creative Commons Attribution 3.0 Unported License (<https://creativecommons.org/licenses/by/3.0/>).

Floppases

ATP binding cassette (ABC) transporters have first been described as multidrug resistance proteins (MDR) but they were also rapidly shown to bind to lipids (Borst *et al.*, 2000). They catalyze the transport of molecules in the opposite direction of flippases, meaning from the cytosol toward the luminal or the extracellular space. ABC transporters can either secrete their substrate if the acceptor is present, or, if the substrate is soluble in water, they can act as a floppase in the case of lipids/phospholipids in the absence of acceptor. In that case, the lipids will just be translocated from a membrane leaflet to the other. MDR3 or ABCB4 is shown to be a PC exporter involved in the secretion of PC in the bile. Another ABC transporter, ABC1 or ACBA1, is involved in cholesterol release for collection by HDL. The plant chloroplasts possess a prokaryotic-like ABC transporter called trigalactosyl-diacylglycerol (TGD) involved in the import of PA from the ER to the

chloroplast for galactolipid synthesis required for the photosynthesis (Fan *et al.*, 2015; Li-Beisson *et al.*, 2017; Lu *et al.*, 2007; Lu and Benning, 2009). Some ABC transporters such as the ABCD1 in plant peroxisome bind to FAs and present a supplementary function. They indeed also possess a fatty acyl-CoA thioesterase activity essential for FA metabolism like β -oxidation (De Marcos Lousa *et al.*, 2013), or they are responsible for the import of FA into the ER (ACBA9) (Sangwoo Kim *et al.*, 2013).

Scramblases

Contrary to ABC and P4-ATPase transporters, scramblases are bidirectional lipid transporters. They localize to the plasma membrane, the Golgi, and the ER. Still, in the erythrocyte membrane, where ATP8B1 maintains PS on the cytosolic side, cell stimulation triggers calcium release, which inhibits the action of ATP8B1 and activates PLSCR1, a scramblase located in diverse membranes of the cell. Scramblases including PLSCR1 use the concentration gradient force to flip lipids. They participate to counteract membrane asymmetry by redistributing PE and PS to the exoplasmic/luminal leaflet of the membrane. Generally, scramblases are essential for membrane expansion and thus for autophagy. As such, the autophagosome scramblase ATG9 redistributes phospholipids from the ER *via* ATG2 (Noda, 2021) or TMEM41B and VMP1, two ER scramblases that regulate the formation of autophagosomes but also regulate LD (Li *et al.*, 2021).

Fatty acid exporters (FAX), FA exit door for plastids? (Figure 12)

All FAs in plants provide from the chloroplast. They can either be directly used in the plast for LPA/PA and galactolipids synthesis or they can exit the chloroplast to reach the ER membrane for phospholipid, sphingolipid synthesis for membrane biogenesis or synthesis of neutral lipids for storage (Li *et al.*, 2016). Seven fatty acid exporters (FAXs) have been identified and four were predicted to localize to the chloroplast inner membrane (Li *et al.*, 2015). FAX1, FAX2, and FAX4 have now been shown to indeed localize to the inner membrane of the apicoplast but also to bind and facilitate the transport of FFAs from the chloroplast's stroma to the ER (Li *et al.*, 2020, 2015; Tian *et al.*, 2019). Once at the cytosolic side of the chloroplast membranes, FFAs are activated by an acyl CoA synthetase, LACS9, which is attached to the outer membrane of the plast, and newly formed acyl-CoAs are translocated into the ER *via* ABCA9 to be used by the eukaryotic lipid synthesis pathway (Li *et al.*, 2016; Li-Beisson *et al.*, 2017).

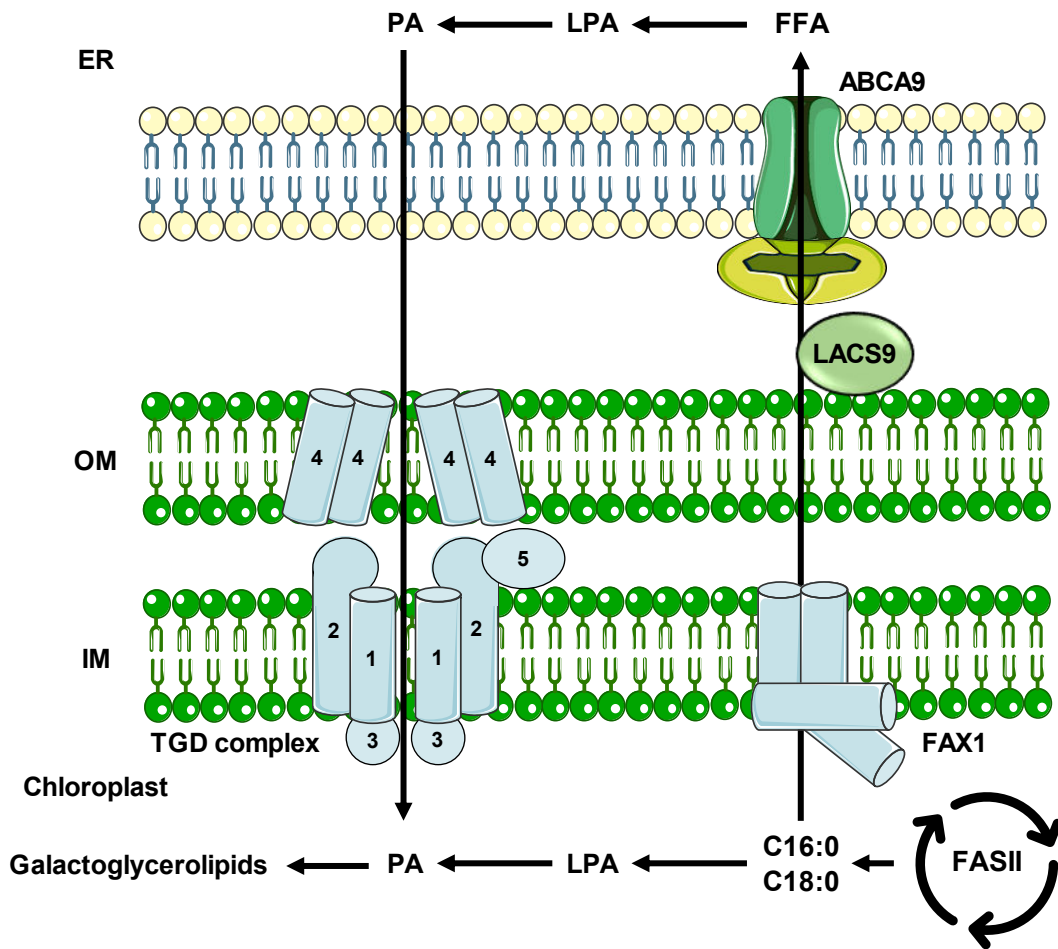


Figure 12: Lipid transfer through the chloroplast membranes

Chloroplast FASII generates FA chains C16:0 and C18:0. These FAs are exported to the ER *via* the fatty acid exporters (7 FAXs exist, 4 are predicted to localize in the chloroplast membranes. FAX1, 2 and 4 have confirmed localization and function in FA export). Exported FAs are activated by the long chain acyl-CoA synthetase 9 (LACS9) and imported into the ER by the ABC transporter ABCA9. In the ER and the chloroplast, FAs are esterified on a glycerol backbone to form LPA and PA. PA generated in the ER is imported back to the chloroplast *via* the ABC transporter trigalactosyldiacylglycerol (TGD1, 2, 3, 4 and 5), and is used to form galactoglycerolipids. Parts of the figure were drawn using pictures from Servier Medical Art. Servier Medical Art by Servier is licensed under a Creative Commons Attribution 3.0 Unported License (<https://creativecommons.org/licenses/by/3.0/>).

Apicomplexa lipid transporters: what do we know so far?

All these transporters/exchangers described above highlight the tight control exerted by the cell on the regulation of its membrane and lipid homeostasis *via* a large diversity of substrates. If some transporters are redundant in function, their specific localization and expression profile make their disruption lethal most of the time.

Despite the importance of lipid acquisition/scavenging and *de novo* synthesis, Apicomplexa possess only a few identified and characterized lipid transporters. For instance, the *Toxoplasma* genome encodes two ACBPs, one cytosolic and one recruited to the mitochondrial membrane and essential for cardiolipin metabolism (Fu *et al.*, 2019, 2018). In addition, an SCP2 is present in *Toxoplasma* and plays a synergic role with *Tg*ACBP1 in glycerides and phospholipids synthesis (Fu *et al.*, 2019). *Plasmodium* genomes encode five ACBPs but only one has been studied and has shown that, compared to the bovine ACBP, *Pf*ACBP can bind to shorter acyl-CoA (van Aalten *et al.*, 2001). Surprisingly, no FATB nor PLTP have been identified in both *Toxoplasma* and *Plasmodium* genomes (“PlasmoDB”; “ToxoDB”). However, the expression of the host FATB3 and 5 along with key enzymes involved in host TAG synthesis, is upregulated in the case of *Toxoplasma* infection, increasing TAG acquisition to supply the parasite large need for lipids (Hu *et al.*, 2017).

Parasite survival relies on the apicoplast-resident metabolic pathway, in which the prokaryotic FASII synthesizes short-chain FAs, C14:0 and C16:0, that are used directly within the apicoplast by plant-like ATS1 and ATS2 for LPA and PA synthesis (Amiar *et al.*, 2020, 2016). Studies of the ATS1 and 2 showed that only apicoplast LPA (over PA) is essential for parasite survival and that LPA exits the apicoplast for bulk PL synthesis. These studies also revealed that, like in the chloroplast, FAs must exit the apicoplast in a separate manner, but none of the canonical lipid transporters present in the chloroplast, FAX or TGD transporters, are present in the apicoplast. Several transporters have been identified in the apicoplast but only the apicoplast phosphate translocator (APT) in *Toxoplasma* and its *Plasmodium* homolog triose phosphate transporter (TPT) have been characterized (Kloehn *et al.*, 2021b).

The autophagy pathway is partially conserved in *Toxoplasma*. Among the conserved proteins, the RGB ATG9 and the scramblase ATG2 have been identified. While the ATG2 function remains unclear, ATG9 was shown to be essential for both tachyzoites and bradyzoites, and its disruption leads to severe morphological defects (Nguyen *et al.*, 2017; Smith *et al.*, 2021). None of *Toxoplasma*'s scramblases have been characterized. One has been characterized in *Plasmodium*,

*Pf*PLSCR. It was shown to flip PE and PS. This scramblase has different intracellular localizations depending on the life stage and it is not essential for the blood stages (Haase *et al.*, 2020). A second scramblase has been identified and shown to be important for sporozoites invasion within hepatocytes but its flipping activity remains to be determined (Cha *et al.*, 2021).

Among the different lipid transporter families, Apicomplexa conserved several aminophospholipid flippases. *Toxoplasma* and *Plasmodium* possess respectively six and five P4-ATPases, and most of them are crucial for the acute asexual development of both parasites (Bisio *et al.*, 2021; Chen *et al.*, 2021; Weiner and Kooij, 2016). Three of the *Toxoplasma* flippases, ATP2A, ATP2B, and GC, localize at the apical pole, the essential place for apical organelle secretion, and ATP2B along with its CDC50 partner is crucial for correct microneme secretion by maintaining the PS asymmetry at the plasma membrane and particularly at the apical pole (Bisio *et al.*, 2021). GC, present in two copies in *Plasmodium*, is a P4-ATPase fused to a guanylate cyclase, that acts as a PA sensor which triggers GC cGMP synthesis and, through the cGMP signaling cascade, leads to calcium release from the ER and thus microneme secretion (Bisio *et al.*, 2019; Nofal *et al.*, 2021). Other flippases are localized to the endo/plasma membrane, the Golgi. One is not expressed in tachyzoites suggesting a function dependent on the parasite life stage (Bisio *et al.*, 2021; Chen *et al.*, 2021; Katris *et al.*, 2020). While their essentiality and localization have been assessed, flippases' role in Apicomplexa lipid metabolism and cellular function remains poorly known.

References to chapters I, II, and III

- Agarwal, A.K., Tunison, K., Dalal, J.S., Nagamma, S.S., Hamra, F.K., Sankella, S., Shao, X., Auchus, R.J., Garg, A., 2017. Metabolic, Reproductive, and Neurologic Abnormalities in Agpat1-Null Mice. *Endocrinology* 158, 3954–3973. <https://doi.org/10.1210/en.2017-00511>
- Agrawal, S., van Dooren, G.G., Beatty, W.L., Striepen, B., 2009. Genetic Evidence that an Endosymbiont-derived Endoplasmic Reticulum-associated Protein Degradation (ERAD) System Functions in Import of Apicoplast Proteins. *J Biol Chem* 284, 33683–33691. <https://doi.org/10.1074/jbc.M109.044024>
- Ahiya, A.I., Bhatnagar, S., Morrisey, J.M., Beck, J.R., Vaidya, A.B., 2022. Dramatic Consequences of Reducing Erythrocyte Membrane Cholesterol on Plasmodium falciparum. *Microbiol Spectr* 10, e0015822. <https://doi.org/10.1128/spectrum.00158-22>
- Alder-Baerens, N., Lisman, Q., Luong, L., Pomorski, T., Holthuis, J.C.M., 2006. Loss of P4 ATPases Drs2p and Dnf3p Disrupts Aminophospholipid Transport and Asymmetry in Yeast Post-Golgi Secretory Vesicles. *Molecular Biology of the Cell* 17, 11.
- Almeria, S., Dubey, J.P., 2021. Foodborne transmission of Toxoplasma gondii infection in the last decade. An overview. *Research in Veterinary Science* 135, 371–385. <https://doi.org/10.1016/j.rvsc.2020.10.019>
- Ambrose, C., DeBono, A., Wasteneys, G., 2013. Cell Geometry Guides the Dynamic Targeting of Apoplastic GPI-Linked Lipid Transfer Protein to Cell Wall Elements and Cell Borders in Arabidopsis thaliana. *PLOS ONE* 8, e81215. <https://doi.org/10.1371/journal.pone.0081215>
- Amiar, S., Katris, N.J., Berry, L., Dass, S., Duley, S., Arnold, C.-S., Shears, M.J., Brunet, C., Touquet, B., McFadden, G.I., Yamaro-Botté, Y., Botté, C.Y., 2020. Division and Adaptation to Host Environment of Apicomplexan Parasites Depend on Apicoplast Lipid Metabolic Plasticity and Host Organelle Remodeling. *Cell Reports* 30, 3778-3792.e9. <https://doi.org/10.1016/j.celrep.2020.02.072>
- Amiar, S., MacRae, J.I., Callahan, D.L., Dubois, D., van Dooren, G.G., Shears, M.J., Cesbron-Delauw, M.-F., Maréchal, E., McConville, M.J., McFadden, G.I., Yamaro-Botté, Y., Botté, C.Y., 2016. Apicoplast-Localized Lysophosphatidic Acid Precursor Assembly Is Required for Bulk Phospholipid Synthesis in Toxoplasma gondii and Relies on an Algal/Plant-Like Glycerol 3-Phosphate Acyltransferase. *PLoS Pathog* 12, e1005765. <https://doi.org/10.1371/journal.ppat.1005765>
- Andersen, J.P., Vestergaard, A.L., Mikkelsen, S.A., Mogensen, L.S., Chalat, M., Molday, R.S., 2016. P4-ATPases as Phospholipid Flippases—Structure, Function, and Enigmas. *Front. Physiol.* 7. <https://doi.org/10.3389/fphys.2016.00275>
- Arisz, S.A., Testerink, C., Munnik, T., 2009. Plant PA signaling via diacylglycerol kinase. *Biochimica et Biophysica Acta (BBA) - Molecular and Cell Biology of Lipids*, Phospholipase D 1791, 869–875. <https://doi.org/10.1016/j.bbalip.2009.04.006>
- Arondel, V., Kader, J.C., 1990. Lipid transfer in plants. *Experientia* 46, 579–585. <https://doi.org/10.1007/BF01939696>
- Arredondo, S.A., Schepis, A., Reynolds, L., Kappe, S.H.I., 2021. Secretory Organelle Function in the Plasmodium Sporozoite. *Trends in Parasitology* 37, 651–663. <https://doi.org/10.1016/j.pt.2021.01.008>
- Arroyo-Olarte, R.D., Brouwers, J.F., Kuchipudi, A., Helms, J.B., Biswas, A., Dunay, I.R., Lucius, R., Gupta, N., 2015. Phosphatidylthreonine and Lipid-Mediated Control of Parasite Virulence. *PLoS Biol* 13, e1002288. <https://doi.org/10.1371/journal.pbio.1002288>
- Ashraf, K., Tazeri, S., Arnold, C.-S., Amanzougaghene, N., Franetich, J.-F., Vantaux, A., Soulard, V., Bordessoulles, M., Cazals, G., Bousema, T., Gemert, G.-J., Grand, R., Dereuddre-Bosquet, N., Barale, J.-C., Witkowski, B., Snounou, G., Duval, R., Botté, C., Mazier, D., 2022. Artemisinin-independent inhibitory activity of Artemisia sp. infusions against different Plasmodium stages including relapse-causing hypnozoites. *Life Science Alliance* 5, e202101237. <https://doi.org/10.26508/lsa.202101237>

- Aw, Y.T.V., Seidi, A., Hayward, J.A., Lee, J., Makota, F.V., Rug, M., van Dooren, G.G., 2021. A key cytosolic iron–sulfur cluster synthesis protein localizes to the mitochondrion of *Toxoplasma gondii*. *Molecular Microbiology* 115, 968–985. <https://doi.org/10.1111/mmi.14651>
- Bai, L., You, Q., Jain, B.K., Duan, H.D., Kovach, A., Graham, T.R., Li, H., 2020. Transport mechanism of P4 ATPase phosphatidylcholine flippases. *eLife* 9, e62163. <https://doi.org/10.7554/eLife.62163>
- Balikagala, B., Fukuda, N., Ikeda, M., Katuru, O.T., Tachibana, S.-I., Yamauchi, M., Opio, W., Emoto, S., Anywar, D.A., Kimura, E., Palacpac, N.M.Q., Odongo-Aginya, E.I., Ogwang, M., Horii, T., Mita, T., 2021. Evidence of Artemisinin-Resistant Malaria in Africa. *New England Journal of Medicine* 385, 1163–1171. <https://doi.org/10.1056/NEJMoa2101746>
- Bano, N., Romano, J.D., Jayabalasingham, B., Coppens, I., 2007. Cellular interactions of *Plasmodium* liver stage with its host mammalian cell. *Int J Parasitol* 37, 1329–1341. <https://doi.org/10.1016/j.ijpara.2007.04.005>
- Ben Chaabene, R., Lentini, G., Soldati-Favre, D., 2021. Biogenesis and discharge of the rhoptries: Key organelles for entry and hijack of host cells by the Apicomplexa. *Molecular Microbiology* 115, 453–465. <https://doi.org/10.1111/mmi.14674>
- Ben Hsouna, A., Ben Saad, R., Dhifi, W., Mnif, W., Brini, F., 2021. Novel non-specific lipid-transfer protein (TdLTP4) isolated from durum wheat: Antimicrobial activities and anti-inflammatory properties in lipopolysaccharide (LPS)-stimulated RAW 264.7 macrophages. *Microbial Pathogenesis* 154, 104869. <https://doi.org/10.1016/j.micpath.2021.104869>
- Berchtold, M.W., Brinkmeier, H., Müntener, M., 2000. Calcium ion in skeletal muscle: its crucial role for muscle function, plasticity, and disease. *Physiol Rev* 80, 1215–1265. <https://doi.org/10.1152/physrev.2000.80.3.1215>
- Besteiro, S., Bertrand-Michel, J., Lebrun, M., Vial, H., Dubremetz, J.-F., 2008. Lipidomic analysis of *Toxoplasma gondii* tachyzoites rhoptries: further insights into the role of cholesterol. *Biochemical Journal* 415, 87–96. <https://doi.org/10.1042/BJ20080795>
- Besteiro, S., Dubremetz, J.-F., Lebrun, M., 2011. The moving junction of apicomplexan parasites: a key structure for invasion. *Cellular Microbiology* 13, 797–805. <https://doi.org/10.1111/j.1462-5822.2011.01597.x>
- Bhattacharjee, S., Stahelin, R.V., Speicher, K.D., Speicher, D.W., Haldar, K., 2012. Endoplasmic reticulum PI(3)P lipid binding targets malaria proteins to the host cell. *Cell* 148, 201–212. <https://doi.org/10.1016/j.cell.2011.10.051>
- Birnbaum, J., Scharf, S., Schmidt, S., Jonscher, E., Hoeijmakers, W.A.M., Flemming, S., Toenhake, C.G., Schmitt, M., Sabitzki, R., Bergmann, B., Fröhlke, U., Mesén-Ramírez, P., Blancke Soares, A., Herrmann, H., Bártfai, R., Spielmann, T., 2020. A Kelch13-defined endocytosis pathway mediates artemisinin resistance in malaria parasites. *Science* 367, 51–59. <https://doi.org/10.1126/science.aax4735>
- Bisio, H., Chaabene, R.B., Sabitzki, R., Maco, B., Marq, J.B., Gilberger, T.-W., Spielmann, T., Soldati-Favre, D., 2020. The ZIP Code of Vesicle Trafficking in Apicomplexa: SEC1/Munc18 and SNARE Proteins. *mBio* 11, e02092-20. <https://doi.org/10.1128/mBio.02092-20>
- Bisio, H., Krishnan, A., Marq, J.-B., Soldati-Favre, D., 2021. *Toxoplasma gondii* phosphatidylserine flippase complex ATP2B-CDC50.4 critically participates in microneme exocytosis (preprint). *Cell Biology*. <https://doi.org/10.1101/2021.11.25.470034>
- Bisio, H., Lunghi, M., Brochet, M., Soldati-Favre, D., 2019. Phosphatidic acid governs natural egress in *Toxoplasma gondii* via a guanylate cyclase receptor platform. *Nat Microbiol* 4, 420–428. <https://doi.org/10.1038/s41564-018-0339-8>
- Blanchette-Mackie, E.J., Dwyer, N.K., Barber, T., Coxey, R.A., Takeda, T., Rondinone, C.M., Theodorakis, J.L., Greenberg, A.S., Londos, C., 1995. Perilipin is located on the surface layer of intracellular lipid droplets in adipocytes. *Journal of Lipid Research* 36, 1211–1226. [https://doi.org/10.1016/S0022-2275\(20\)41129-0](https://doi.org/10.1016/S0022-2275(20)41129-0)
- Blank, M.L., Xia, J., Morcos, M.M., Sun, M., Cantrell, P.S., Liu, Y., Zeng, X., Powell, C.J., Yates, N., Boulanger, M.J., Boyle, J.P., 2021. *Toxoplasma gondii* association with host mitochondria requires key mitochondrial protein import machinery. *Proc Natl Acad Sci U S A* 118, e2013336118. <https://doi.org/10.1073/pnas.2013336118>

- Boisard, J., Florent, I., 2020. Why the –omic future of Apicomplexa should include gregarines. *Biology of the Cell* 112, 173–185. <https://doi.org/10.1111/boc.202000006>
- Bonifacino, J.S., Glick, B.S., 2004. The Mechanisms of Vesicle Budding and Fusion. *Cell* 116, 153–166. [https://doi.org/10.1016/S0092-8674\(03\)01079-1](https://doi.org/10.1016/S0092-8674(03)01079-1)
- Borst, P., Zelcer, N., van Helvoort, A., 2000. ABC transporters in lipid transport. *Biochimica et Biophysica Acta (BBA) - Molecular and Cell Biology of Lipids* 1486, 128–144. [https://doi.org/10.1016/S1388-1981\(00\)00053-6](https://doi.org/10.1016/S1388-1981(00)00053-6)
- Brancucci, N.M.B., Gerdt, J.P., Wang, C., De Niz, M., Philip, N., Adapa, S.R., Zhang, M., Hitz, E., Niederwieser, I., Boltryk, S.D., Laffitte, M.-C., Clark, M.A., Grüning, C., Ravel, D., Blancke Soares, A., Demas, A., Bopp, S., Rubio-Ruiz, B., Conejo-Garcia, A., Wirth, D.F., Gendaszewska-Darmach, E., Duraisingh, M.T., Adams, J.H., Voss, T.S., Waters, A.P., Jiang, R.H.Y., Clardy, J., Marti, M., 2017. Lysophosphatidylcholine Regulates Sexual Stage Differentiation in the Human Malaria Parasite *Plasmodium falciparum*. *Cell* 171, 1532-1544.e15. <https://doi.org/10.1016/j.cell.2017.10.020>
- Braun, L., Travier, L., Kieffer, S., Musset, K., Garin, J., Mercier, C., Cesbron-Delauw, M.-F., 2008. Purification of *Toxoplasma dense granule* proteins reveals that they are in complexes throughout the secretory pathway. *Molecular and Biochemical Parasitology* 157, 13–21. <https://doi.org/10.1016/j.molbiopara.2007.09.002>
- Breinich, M.S., Ferguson, D.J.P., Foth, B.J., van Dooren, G.G., Lebrun, M., Quon, D.V., Striepen, B., Bradley, P.J., Frischknecht, F., Carruthers, V.B., Meissner, M., 2009. An alveolate specific dynamin is required for the biogenesis of specialised secretory organelles in *Toxoplasma gondii*. *Curr Biol* 19, 277–286. <https://doi.org/10.1016/j.cub.2009.01.039>
- Bullen, H.E., Bisio, H., Soldati-Favre, D., 2019. The triumvirate of signaling molecules controlling *Toxoplasma* microneme exocytosis: Cyclic GMP, calcium, and phosphatidic acid. *PLoS Pathog* 15, e1007670. <https://doi.org/10.1371/journal.ppat.1007670>
- Burda, P.-C., Caldelari, R., Heussler, V.T., 2017. Manipulation of the Host Cell Membrane during *Plasmodium* Liver Stage Egress. *mBio* 8, e00139-17. <https://doi.org/10.1128/mBio.00139-17>
- Burrell, A., Marugan-Hernandez, V., Wheeler, R., Moreira-Leite, F., Ferguson, D.J.P., Tomley, F.M., Vaughan, S., 2022. Cellular electron tomography of the apical complex in the apicomplexan parasite *Eimeria tenella* shows a highly organised gateway for regulated secretion. *PLoS Pathog* 18, e1010666. <https://doi.org/10.1371/journal.ppat.1010666>
- Cao, S., Yang, J., Fu, J., Chen, H., Jia, H., 2021. The Dissection of SNAREs Reveals Key Factors for Vesicular Trafficking to the Endosome-like Compartment and Apicoplast *via* the Secretory System in *Toxoplasma gondii*. *mBio* 12, e01380-21. <https://doi.org/10.1128/mBio.01380-21>
- Carvou, N., Holic, R., Li, M., Futter, C., Skippen, A., Cockcroft, S., 2010. Phosphatidylinositol- and phosphatidylcholine-transfer activity of PITPbeta is essential for COPI-mediated retrograde transport from the Golgi to the endoplasmic reticulum. *J Cell Sci* 123, 1262–1273. <https://doi.org/10.1242/jcs.061986>
- CDC Malaria [WWW Document], 2020. URL <https://www.cdc.gov/dpdx/malaria/index.html> (accessed 12.16.22).
- Cha, S.-J., Kim, M.-S., Na, C.H., Jacobs-Lorena, M., 2021. *Plasmodium* sporozoite phospholipid scramblase interacts with mammalian carbamoyl-phosphate synthetase 1 to infect hepatocytes. *Nat Commun* 12, 6773. <https://doi.org/10.1038/s41467-021-27109-7>
- Chakrabarti, R.S., Ingham, S.A., Kozlitina, J., Gay, A., Cohen, J.C., Radhakrishnan, A., Hobbs, H.H., 2017. Variability of cholesterol accessibility in human red blood cells measured using a bacterial cholesterol-binding toxin. *eLife* 6, e23355. <https://doi.org/10.7554/eLife.23355>
- Chen, K., Günay-Esiyok, Ö., Klingenberg, M., Marquardt, S., Pomorski, T.G., Gupta, N., 2021. Aminoglycerophospholipid flipping and P4-ATPases in *Toxoplasma gondii*. *Journal of Biological Chemistry* 296, 100315. <https://doi.org/10.1016/j.jbc.2021.100315>
- Chen, Q.-F., Xiao, S., Qi, W., Mishra, G., Ma, J., Wang, M., Chye, M.-L., 2010. The Arabidopsis *acbp1acbp2* double mutant lacking acyl-CoA-binding proteins ACBP1 and ACBP2 is embryo lethal. *New Phytol* 186, 843–855. <https://doi.org/10.1111/j.1469-8137.2010.03231.x>

- Chen, Y., Ma, J., Zhang, X., Yang, Y., Zhou, D., Yu, Q., Que, Y., Xu, L., Guo, J., 2017. A Novel Non-specific Lipid Transfer Protein Gene from Sugarcane (NsLTPs), Obviously Responded to Abiotic Stresses and Signaling Molecules of SA and MeJA. *Sugar Tech* 19, 17–25. <https://doi.org/10.1007/s12355-016-0431-4>
- Cheng, C.-S., Samuel, D., Liu, Y.-J., Shyu, J.-C., Lai, S.-M., Lin, K.-F., Lyu, P.-C., 2004. Binding Mechanism of Nonspecific Lipid Transfer Proteins and Their Role in Plant Defense. *Biochemistry* 43, 13628–13636. <https://doi.org/10.1021/bi048873j>
- Cheon, M.S., Kim, S.H., Fountoulakis, M., Lubec, G., 2003. Heart type fatty acid binding protein (H-FABP) is decreased in brains of patients with Down syndrome and Alzheimer's disease. *J Neural Transm Suppl* 225–234. https://doi.org/10.1007/978-3-7091-6721-2_20
- Chmurzyńska, A., 2006. The multigene family of fatty acid-binding proteins (FABPs): Function, structure and polymorphism. *J Appl Genet* 47, 39–48. <https://doi.org/10.1007/BF03194597>
- Chung, J., Torta, F., Masai, K., Lucast, L., Czapla, H., Tanner, L.B., Narayanaswamy, P., Wenk, M.R., Nakatsu, F., De Camilli, P., 2015. INTRACELLULAR TRANSPORT. PI4P/phosphatidylserine countertransport at ORP5- and ORP8-mediated ER-plasma membrane contacts. *Science* 349, 428–432. <https://doi.org/10.1126/science.aab1370>
- Coffey, M.J., Dagley, L.F., Seizova, S., Kapp, E.A., Infusini, G., Roos, D.S., Boddey, J.A., Webb, A.I., Tonkin, C.J., 2018. Aspartyl Protease 5 Matures Dense Granule Proteins That Reside at the Host-Parasite Interface in *Toxoplasma gondii*. *mBio* 9, e01796-18. <https://doi.org/10.1128/mBio.01796-18>
- Coffey, M.J., Sleeb, B.E., Uboldi, A.D., Garnham, A., Franco, M., Marino, N.D., Panas, M.W., Ferguson, D.J., Enciso, M., O'Neill, M.T., Lopaticki, S., Stewart, R.J., Dewson, G., Smyth, G.K., Smith, B.J., Masters, S.L., Boothroyd, J.C., Boddey, J.A., Tonkin, C.J., 2015. An aspartyl protease defines a novel pathway for export of *Toxoplasma* proteins into the host cell. *eLife* 4, e10809. <https://doi.org/10.7554/eLife.10809>
- Coones, R.T., Green, R.J., Frazier, R.A., 2021. Investigating lipid headgroup composition within epithelial membranes: a systematic review. *Soft Matter* 17, 6773–6786. <https://doi.org/10.1039/D1SM00703C>
- Coppens, I., 2013. Targeting lipid biosynthesis and salvage in apicomplexan parasites for improved chemotherapies. *Nat Rev Microbiol* 11, 823–835. <https://doi.org/10.1038/nrmicro3139>
- Coppens, I., Sinai, A.P., Joiner, K.A., 2000. *Toxoplasma gondii* Exploits Host Low-Density Lipoprotein Receptor-Mediated Endocytosis for Cholesterol Acquisition. *J Cell Biol* 149, 167–180.
- Coskun, Ü., Simons, K., 2011. Cell Membranes: The Lipid Perspective. *Structure* 19, 1543–1548. <https://doi.org/10.1016/j.str.2011.10.010>
- Costa, J., Bavaro, S.L., Benedé, S., Diaz-Perales, A., Bueno-Diaz, C., Gelencser, E., Klueber, J., Larré, C., Lozano-Ojalvo, D., Lupi, R., Mafrá, I., Mazzucchelli, G., Molina, E., Monaci, L., Martín-Pedraza, L., Piras, C., Rodrigues, P.M., Roncada, P., Schrama, D., Cirkovic-Velickovic, T., Verhoeckx, K., Villa, C., Kuehn, A., Hoffmann-Sommergruber, K., Holzhauser, T., 2022. Are Physicochemical Properties Shaping the Allergenic Potency of Plant Allergens? *Clinic Rev Allerg Immunol* 62, 37–63. <https://doi.org/10.1007/s12016-020-08810-9>
- Cuadrado, C., Sanchiz, Á., Linacero, R., 2021. Nut Allergenicity: Effect of Food Processing. *Allergies* 1, 150–162. <https://doi.org/10.3390/allergies1030014>
- Daher, W., Morlon-Guyot, J., Alayi, T.D., Tomavo, S., Wengelnik, K., Lebrun, M., 2016. Identification of *Toxoplasma* TgPH1, a pleckstrin homology domain-containing protein that binds to the phosphoinositide PI(3,5)P2. *Molecular and Biochemical Parasitology* 207, 39–44. <https://doi.org/10.1016/j.molbiopara.2016.03.011>
- Daher, W., Morlon-Guyot, J., Sheiner, L., Lentini, G., Berry, L., Tawk, L., Dubremetz, J.-F., Wengelnik, K., Striepen, B., Lebrun, M., 2015. Lipid kinases are essential for apicoplast homeostasis in *Toxoplasma gondii*. *Cell Microbiol* 17, 559–578. <https://doi.org/10.1111/cmi.12383>
- Dass, S., Shunmugam, S., Berry, L., Arnold, C.-S., Katris, N.J., Duley, S., Pierrel, F., Cesbron-Delauw, M.-F., Yamaro-Botté, Y., Botté, C.Y., 2021. *Toxoplasma* LIPIN is essential in channeling host lipid fluxes through membrane biogenesis and lipid storage. *Nat Commun* 12, 2813. <https://doi.org/10.1038/s41467-021-22956-w>

- De Marcos Lousa, C., van Roermund, C.W.T., Postis, V.L.G., Dietrich, D., Kerr, I.D., Wanders, R.J.A., Baldwin, S.A., Baker, A., Theodoulou, F.L., 2013. Intrinsic acyl-CoA thioesterase activity of a peroxisomal ATP binding cassette transporter is required for transport and metabolism of fatty acids. *Proc. Natl. Acad. Sci. U.S.A.* 110, 1279–1284. <https://doi.org/10.1073/pnas.1218034110>
- De Moraes, C.M., Stanczyk, N.M., Betz, H.S., Pulido, H., Sim, D.G., Read, A.F., Mescher, M.C., 2014. Malaria-induced changes in host odors enhance mosquito attraction. *Proc Natl Acad Sci U S A* 111, 11079–11084. <https://doi.org/10.1073/pnas.1405617111>
- de Saint-Jean, M., Delfosse, V., Douguet, D., Chicanne, G., Payraastre, B., Bourguet, W., Antonny, B., Drin, G., 2011. Osh4p exchanges sterols for phosphatidylinositol 4-phosphate between lipid bilayers. *J Cell Biol* 195, 965–978. <https://doi.org/10.1083/jcb.201104062>
- Déchamps, S., Wengelnik, K., Berry-Sterkers, L., Cerdan, R., Vial, H.J., Gannoun-Zaki, L., 2010. The Kennedy phospholipid biosynthesis pathways are refractory to genetic disruption in *Plasmodium berghei* and therefore appear essential in blood stages. *Mol Biochem Parasitol* 173, 69–80. <https://doi.org/10.1016/j.molbiopara.2010.05.006>
- Del Carmen, M.G., Mondragón, M., González, S., Mondragón, R., 2009. Induction and regulation of conoid extrusion in *Toxoplasma gondii*. *Cellular Microbiology* 11, 967–982. <https://doi.org/10.1111/j.1462-5822.2009.01304.x>
- Deligianni, E., Morgan, R.N., Bertuccini, L., Wirth, C.C., Silmon de Monerri, N.C., Spanos, L., Blackman, M.J., Louis, C., Pradel, G., Siden-Kiamos, I., 2013. A perforin-like protein mediates disruption of the erythrocyte membrane during egress of *Plasmodium berghei* male gametocytes. *Cellular Microbiology* 15, 1438–1455. <https://doi.org/10.1111/cmi.12131>
- DeRocher, A., Hagen, C.B., Froehlich, J.E., Feagin, J.E., Parsons, M., 2000. Analysis of targeting sequences demonstrates that trafficking to the *Toxoplasma gondii* plastid branches off the secretory system. *Journal of Cell Science* 113, 3969–3977. <https://doi.org/10.1242/jcs.113.22.3969>
- Desmond, E., Gribaldo, S., 2009. Phylogenomics of sterol synthesis: insights into the origin, evolution, and diversity of a key eukaryotic feature. *Genome Biol Evol* 1, 364–381. <https://doi.org/10.1093/gbe/evp036>
- Dluzewski, A.R., Rangachari, K., Wilson, R.J., Gratzer, W.B., 1985. Relation of red cell membrane properties to invasion by *Plasmodium falciparum*. *Parasitology* 91 (Pt 2), 273–280. <https://doi.org/10.1017/s003118200005736x>
- Dooren, G.G. van, Kennedy, A.T., McFadden, G.I., 2012. The Use and Abuse of Heme in Apicomplexan Parasites [WWW Document]. <https://home-liebertpub-com.proxy.insermbiblio.inist.fr/ars>. <https://doi.org/10.1089/ars.2012.4539>
- Dos Santos Pacheco, N., Brusini, L., Haase, R., Tosetti, N., Maco, B., Brochet, M., Vadas, O., Soldati-Favre, D., 2022. Conoid extrusion regulates glideosome assembly to control motility and invasion in Apicomplexa. *Nat Microbiol* 7, 1777–1790. <https://doi.org/10.1038/s41564-022-01212-x>
- Dou, Z., McGovern, O.L., Di Cristina, M., Carruthers, V.B., 2014. *Toxoplasma gondii* Ingests and Digests Host Cytosolic Proteins. *mBio* 5, e01188-14. <https://doi.org/10.1128/mBio.01188-14>
- Douliez, J.-P., Michon, T., Elmorjani, K., Marion, D., 2000. Mini Review: Structure, Biological and Technological Functions of Lipid Transfer Proteins and Indolines, the Major Lipid Binding Proteins from Cereal Kernels. *Journal of Cereal Science* 32, 1–20. <https://doi.org/10.1006/jcers.2000.0315>
- Downes, C.P., Gray, A., Lucocq, J.M., 2005. Probing phosphoinositide functions in signaling and membrane trafficking. *Trends in Cell Biology* 15, 259–268. <https://doi.org/10.1016/j.tcb.2005.03.008>
- Du, Z.-Y., Chen, M.-X., Chen, Q.-F., Xiao, S., Chye, M.-L., 2013. Arabidopsis acyl-CoA-binding protein ACBP1 participates in the regulation of seed germination and seedling development. *The Plant Journal* 74, 294–309. <https://doi.org/10.1111/tpj.12121>
- Du, Z.-Y., Xiao, S., Chen, Q.-F., Chye, M.-L., 2010. Arabidopsis acyl-CoA-binding proteins ACBP1 and ACBP2 show different roles in freezing stress. *Plant Signal Behav* 5, 607–609. <https://doi.org/10.4161/psb.11503>

- Dubiela, P., Aina, R., Polak, D., Geiselhart, S., Humeniuk, P., Bohle, B., Alessandri, S., Conte, R.D., Cantini, F., Borowski, T., Bublin, M., Hoffmann-Sommergruber, K., 2017. Enhanced Prp 3 IgE-binding activity by selective free fatty acid-interaction. *Journal of Allergy and Clinical Immunology* 140, 1728-1731. <https://doi.org/10.1016/j.jaci.2017.06.016>
- Dubois, D.J., Soldati-Favre, D., 2019. Biogenesis and secretion of micronemes in *Toxoplasma gondii*. *Cellular Microbiology* 21, e13018. <https://doi.org/10.1111/cmi.13018>
- Eda, S., Sherman, I.W., 2002. Cytoadherence of malaria-infected red blood cells involves exposure of phosphatidylserine. *Cell Physiol Biochem* 12, 373–384. <https://doi.org/10.1159/000067908>
- Edstam, M.M., Blomqvist, K., Eklöf, A., Wennergren, U., Edqvist, J., 2013. Coexpression patterns indicate that GPI-anchored non-specific lipid transfer proteins are involved in accumulation of cuticular wax, suberin and sporopollenin. *Plant Mol Biol* 83, 625–649. <https://doi.org/10.1007/s11103-013-0113-5>
- Edwards, J.F., Dubey, J.P., 2013. *Toxoplasma gondii* abortion storm in sheep on a Texas farm and isolation of mouse virulent atypical genotype T. *gondii* from an aborted lamb from a chronically infected ewe. *Veterinary Parasitology* 192, 129–136. <https://doi.org/10.1016/j.vetpar.2012.09.037>
- Elabbadi, N., Ancelin, M.L., Vial, H.J., 1997. Phospholipid metabolism of serine in *Plasmodium*-infected erythrocytes involves phosphatidylserine and direct serine decarboxylation. *Biochem J* 324, 435–445.
- Engqvist-Goldstein, A.E.Y., Drubin, D.G., 2003. Actin assembly and endocytosis: from yeast to mammals. *Annu Rev Cell Dev Biol* 19, 287–332. <https://doi.org/10.1146/annurev.cellbio.19.111401.093127>
- Ericsson, J., Appelkvist, E.L., Runquist, M., Dallner, G., 1993. Biosynthesis of dolichol and cholesterol in rat liver peroxisomes. *Biochimie* 75, 167–173. [https://doi.org/10.1016/0300-9084\(93\)90074-3](https://doi.org/10.1016/0300-9084(93)90074-3)
- FÆRGEMAN, N.J., FEDDERSEN, S., CHRISTIANSEN, J.K., LARSEN, M.K., SCHNEITER, R., UNGERMANN, C., MUTENDA, K., ROEPSTORFF, P., KNUDSEN, J., 2004. Acyl-CoA-binding protein, Acb1p, is required for normal vacuole function and ceramide synthesis in *Saccharomyces cerevisiae*. *Biochemical Journal* 380, 907–918. <https://doi.org/10.1042/bj20031949>
- Fairn, G.D., Curwin, A.J., Stefan, C.J., McMaster, C.R., 2007. The oxysterol binding protein Kes1p regulates Golgi apparatus phosphatidylinositol-4-phosphate function. *Proc Natl Acad Sci U S A* 104, 15352–15357. <https://doi.org/10.1073/pnas.0705571104>
- Fan, J., Zhai, Z., Yan, C., Xu, C., 2015. Arabidopsis TRIGALACTOSYLDIACYLGLYCEROL5 Interacts with TGD1, TGD2, and TGD4 to Facilitate Lipid Transfer from the Endoplasmic Reticulum to Plastids. *Plant Cell tpc.15.00394*. <https://doi.org/10.1105/tpc.15.00394>
- Fang, M., Kearns, B.G., Gedvilaite, A., Kagiwada, S., Kearns, M., Fung, M.K., Bankaitis, V.A., 1996. Kes1p shares homology with human oxysterol binding protein and participates in a novel regulatory pathway for yeast Golgi-derived transport vesicle biogenesis. *EMBO J* 15, 6447–6459.
- Fang, Z., He, Y., Liu, Y., Jiang, W., Song, J., Wang, S., Ma, D., Yin, J., 2020. Bioinformatic identification and analyses of the non-specific lipid transfer proteins in wheat. *Journal of Integrative Agriculture* 19, 1170–1185. [https://doi.org/10.1016/S2095-3119\(19\)62776-0](https://doi.org/10.1016/S2095-3119(19)62776-0)
- Fang, Z., Wang, S., Du, X., Shi, P., Huang, Z., 2014. Phosphatidate phosphatase-1 is functionally conserved in lipid synthesis and storage from human to yeast. *Acta Biologica Hungarica* 65, 481–492. <https://doi.org/10.1556/abiol.65.2014.4.11>
- Fantini, J., Barrantes, F.J., 2013. How cholesterol interacts with membrane proteins: an exploration of cholesterol-binding sites including CRAC, CARC, and tilted domains. *Front Physiol* 4, 31. <https://doi.org/10.3389/fphys.2013.00031>
- Fast, N.M., Xue, L., Bingham, S., Keeling, P.J., 2002. Re-examining Alveolate Evolution Using Multiple Protein Molecular Phylogenies. *Journal of Eukaryotic Microbiology* 49, 30–37. <https://doi.org/10.1111/j.1550-7408.2002.tb00336.x>
- Fellows, J.D., Cipriano, M.J., Agrawal, S., Striepen, B., 2017. A Plastid Protein That Evolved from Ubiquitin and Is Required for Apicoplast Protein Import in *Toxoplasma gondii*. *mBio* 8, e00950-17. <https://doi.org/10.1128/mBio.00950-17>

- Fernandes, P., Loubens, M., Le Borgne, R., Marinach, C., Ardin, B., Briquet, S., Vincensini, L., Hamada, S., Hoareau-Coudert, B., Verbavatz, J.-M., Weiner, A., Silvie, O., 2022. The AMA1-RON complex drives Plasmodium sporozoite invasion in the mosquito and mammalian hosts. *PLoS Pathog* 18, e1010643. <https://doi.org/10.1371/journal.ppat.1010643>
- Finkina, E.I., И, Ф.Е., Melnikova, D.N., H, M.Д., Bogdanov, I.V., B, Б.И., Ovchinnikova, T.V., B, O.T., 2016. Lipid Transfer Proteins As Components of the Plant Innate Immune System: Structure, Functions, and Applications. *Acta Naturae* 8, 47–61. <https://doi.org/10.32607/20758251-2016-8-2-47-61>
- Ford, M.G.J., Mills, I.G., Peter, B.J., Vallis, Y., Praefcke, G.J.K., Evans, P.R., McMahon, H.T., 2002. Curvature of clathrin-coated pits driven by epsin. *Nature* 419, 361–366. <https://doi.org/10.1038/nature01020>
- Francis, S.E., Sullivan, D.J., Goldberg, E. D., 1997. Hemoglobin Metabolism in the Malaria Parasite *Plasmodium Falciparum*. *Annual Review of Microbiology* 51, 97–123. <https://doi.org/10.1146/annurev.micro.51.1.97>
- Frénel, K., Soldati-Favre, D., 2013. Un complexe moléculaire unique à l'origine de la motilité et de l'invasion des Apicomplexes. *Med Sci (Paris)* 29, 515–522. <https://doi.org/10.1051/medsci/2013295015>
- Fu, Y., Cui, X., Fan, S., Liu, J., Zhang, X., Wu, Y., Liu, Q., 2018. Comprehensive Characterization of *Toxoplasma* Acyl Coenzyme A-Binding Protein TgACBP2 and Its Critical Role in Parasite Cardiolipin Metabolism. *mBio* 9. <https://doi.org/10.1128/mBio.01597-18>
- Fu, Y., Cui, X., Liu, J., Zhang, X., Zhang, H., Yang, C., Liu, Q., 2019. Synergistic roles of acyl-CoA binding protein (ACBP1) and sterol carrier protein 2 (SCP2) in *Toxoplasma* lipid metabolism. *Cellular Microbiology* 21, e12970. <https://doi.org/10.1111/cmi.12970>
- Fuchs, M., Hafer, A., Münch, C., Kannenberg, F., Teichmann, S., Scheibner, J., Stange, E.F., Seedorf, U., 2001. Disruption of the sterol carrier protein 2 gene in mice impairs biliary lipid and hepatic cholesterol metabolism. *J Biol Chem* 276, 48058–48065. <https://doi.org/10.1074/jbc.M106732200>
- Garner, K., Hunt, A.N., Koster, G., Somerharju, P., Groves, E., Li, M., Raghu, P., Holic, R., Cockcroft, S., 2012. Phosphatidylinositol Transfer Protein, Cytoplasmic 1 (PITPNC1) Binds and Transfers Phosphatidic Acid. *J Biol Chem* 287, 32263–32276. <https://doi.org/10.1074/jbc.M112.375840>
- Garweg, J.G., Kieffer, F., Mandelbrot, L., Peyron, F., Wallon, M., 2022. Long-Term Outcomes in Children with Congenital Toxoplasmosis—A Systematic Review. *Pathogens* 11, 1187. <https://doi.org/10.3390/pathogens11101187>
- Ghanbarpour, A., Valverde, D.P., Melia, T.J., Reinisch, K.M., 2021. A model for a partnership of lipid transfer proteins and scramblases in membrane expansion and organelle biogenesis. *Proc Natl Acad Sci U S A* 118, e2101562118. <https://doi.org/10.1073/pnas.2101562118>
- Gibellini, F., Smith, T.K., 2010. The Kennedy pathway—De novo synthesis of phosphatidylethanolamine and phosphatidylcholine. *IUBMB Life* 62, 414–428. <https://doi.org/10.1002/iub.337>
- Glaser, S., Higgins, M.K., 2012. Overproduction, purification and crystallization of PfTic22, a component of the import apparatus from the apicoplast of *Plasmodium falciparum*. *Acta Crystallogr Sect F Struct Biol Cryst Commun* 68, 351–354. <https://doi.org/10.1107/S1744309112004952>
- Glaser, S., van Dooren, G.G., Agrawal, S., Brooks, C.F., McFadden, G.I., Striepen, B., Higgins, M.K., 2012. Tic22 is an essential chaperone required for protein import into the apicoplast. *J Biol Chem* 287, 39505–39512. <https://doi.org/10.1074/jbc.M112.405100>
- Goodman, C.D., McFadden, G.I., 2007. Fatty acid biosynthesis as a drug target in apicomplexan parasites. *Curr Drug Targets* 8, 15–30. <https://doi.org/10.2174/138945007779315579>
- Graham, T.R., 2004. Flippases and vesicle-mediated protein transport. *Trends in Cell Biology* 14, 670–677. <https://doi.org/10.1016/j.tcb.2004.10.008>
- Grellier, P., Rigomier, D., Schrével, J., 1990. [In vitro induction of *Plasmodium falciparum* schizogony by human high density lipoproteins (HDL)]. *C R Acad Sci III* 311, 361–367.
- Griffith, M.B., Pearce, C.S., Heaslip, A.T., 2022. Dense granule biogenesis, secretion, and function in *Toxoplasma gondii*. *Journal of Eukaryotic Microbiology* 69, e12904. <https://doi.org/10.1111/jeu.12904>

- Guggisberg, A.M., Amthor, R.E., Odom, A.R., 2014. Isoprenoid Biosynthesis in *Plasmodium falciparum*. *Eukaryotic Cell* 13, 1348–1359. <https://doi.org/10.1128/EC.00160-14>
- Guillén-Samander, A., Leonzino, M., Hanna, M.G., Tang, N., Shen, H., De Camilli, P., 2021. VPS13D bridges the ER to mitochondria and peroxisomes *via* Miro. *J Cell Biol* 220, e202010004. <https://doi.org/10.1083/jcb.202010004>
- Gupta, N., Zahn, M.M., Coppens, I., Joiner, K.A., Voelker, D.R., 2005. Selective Disruption of Phosphatidylcholine Metabolism of the Intracellular Parasite *Toxoplasma gondii* Arrests Its Growth*. *Journal of Biological Chemistry* 280, 16345–16353. <https://doi.org/10.1074/jbc.M501523200>
- Haase, R., Dos Santos Pacheco, N., Soldati-Favre, D., 2022. Nanoscale imaging of the conoid and functional dissection of its dynamics in Apicomplexa. *Current Opinion in Microbiology* 70, 102226. <https://doi.org/10.1016/j.mib.2022.102226>
- Haase, S., Condron, M., Miller, D., Cherkaoui, D., Jordan, S., Gulbis, J.M., Baum, J., 2020. Identification and characterization of a phospholipid scramblase in the malaria parasite *Plasmodium falciparum* (preprint). *Microbiology*. <https://doi.org/10.1101/2020.06.22.165258>
- Habtamu, K., Petros, B., Yan, G., 2022. *Plasmodium vivax*: the potential obstacles it presents to malaria elimination and eradication. *Trop Dis Travel Med Vaccines* 8, 27. <https://doi.org/10.1186/s40794-022-00185-3>
- Hakimi, M.-A., Olias, P., Sibley, L.D., 2017. *Toxoplasma* Effectors Targeting Host Signaling and Transcription. *Clin Microbiol Rev* 30, 615–645. <https://doi.org/10.1128/CMR.00005-17>
- Han, G.W., Lee, J.Y., Song, H.K., Chang, C., Min, K., Moon, J., Shin, D.H., Kopka, M.L., Sawaya, M.R., Yuan, H.S., Kim, T.D., Choe, J., Lim, D., Moon, H.J., Suh, S.W., 2001. Structural basis of non-specific lipid binding in maize lipid-transfer protein complexes revealed by high-resolution X-ray crystallography. Edited by D. Rees. *Journal of Molecular Biology* 308, 263–278. <https://doi.org/10.1006/jmbi.2001.4559>
- Hanamatsu, H., Fujimura-Kamada, K., Yamamoto, T., Furuta, N., Tanaka, K., 2014. Interaction of the phospholipid flippase Drs2p with the F-box protein Rcy1p plays an important role in early endosome to trans-Golgi network vesicle transport in yeast. *J Biochem* 155, 51–62. <https://doi.org/10.1093/jb/mvt094>
- Hanna, M.G., Suen, P.H., Wu, Y., Reinisch, K.M., De Camilli, P., 2022. SHIP164 is a chorein motif lipid transfer protein that controls endosome–Golgi membrane traffic. *Journal of Cell Biology* 221, e202111018. <https://doi.org/10.1083/jcb.202111018>
- Hanssen, E., Knoechel, C., Dearnley, M., Dixon, M.W.A., Le Gros, M., Larabell, C., Tilley, L., 2012. Soft X-ray microscopy analysis of cell volume and hemoglobin content in erythrocytes infected with asexual and sexual stages of *Plasmodium falciparum*. *Journal of Structural Biology* 177, 224–232. <https://doi.org/10.1016/j.jsb.2011.09.003>
- Harding, C.R., Meissner, M., 2014. The inner membrane complex through development of *Toxoplasma gondii* and *Plasmodium*. *Cell Microbiol* 16, 632–641. <https://doi.org/10.1111/cmi.12285>
- Hartmann, A., Hellmund, M., Lucius, R., Voelker, D.R., Gupta, N., 2014. Phosphatidylethanolamine Synthesis in the Parasite Mitochondrion Is Required for Efficient Growth but Dispensable for Survival of *Toxoplasma gondii*. *J Biol Chem* 289, 6809–6824. <https://doi.org/10.1074/jbc.M113.509406>
- Hay, J.C., Martin, T.F., 1993. Phosphatidylinositol transfer protein required for ATP-dependent priming of Ca²⁺-activated secretion. *Nature* 366, 572–575. <https://doi.org/10.1038/366572a0>
- Hsiao, A.-S., Haslam, R.P., Michaelson, L.V., Liao, P., Chen, Q.-F., Sooriyaarachchi, S., Mowbray, S.L., Napier, J.A., Tanner, J.A., Chye, M.-L., 2014. Arabidopsis cytosolic acyl-CoA-binding proteins ACBP4, ACBP5 and ACBP6 have overlapping but distinct roles in seed development. *Biosci Rep* 34, e00165. <https://doi.org/10.1042/BSR20140139>
- Hu, X., Binns, D., Reese, M.L., 2017. The coccidian parasites *Toxoplasma* and *Neospora* dysregulate mammalian lipid droplet biogenesis. *J Biol Chem* 292, 11009–11020. <https://doi.org/10.1074/jbc.M116.768176>

- Hua, Z., Fatheddin, P., Graham, T.R., 2002. An Essential Subfamily of Drs2p-related P-Type ATPases Is Required for Protein Trafficking between Golgi Complex and Endosomal/Vacuolar System. *MBoC* 13, 3162–3177. <https://doi.org/10.1091/mbc.e02-03-0172>
- Ihara, F., Nishikawa, Y., 2021. *Toxoplasma gondii* manipulates host cell signaling pathways *via* its secreted effector molecules. *Parasitology International* 83, 102368. <https://doi.org/10.1016/j.parint.2021.102368>
- Itoh, T., Koshiba, S., Kigawa, T., Kikuchi, A., Yokoyama, S., Takenawa, T., 2001. Role of the ENTH domain in phosphatidylinositol-4,5-bisphosphate binding and endocytosis. *Science* 291, 1047–1051. <https://doi.org/10.1126/science.291.5506.1047>
- Jacot, D., Waller, R.F., Soldati-Favre, D., MacPherson, D.A., MacRae, J.I., 2016. Apicomplexan Energy Metabolism: Carbon Source Promiscuity and the Quiescence Hyperbole. *Trends in Parasitology* 32, 56–70. <https://doi.org/10.1016/j.pt.2015.09.001>
- John Peter, A.T., van Schie, S.N.S., Cheung, N.J., Michel, A.H., Peter, M., Kornmann, B., 2022. Rewiring phospholipid biosynthesis reveals resilience to membrane perturbations and uncovers regulators of lipid homeostasis. *EMBO J* 41, e109998. <https://doi.org/10.15252/embj.2021109998>
- Jonscher, E., Flemming, S., Schmitt, M., Sabitzki, R., Reichard, N., Birnbaum, J., Bergmann, B., Höhn, K., Spielmann, T., 2019. PfVPS45 Is Required for Host Cell Cytosol Uptake by Malaria Blood Stage Parasites. *Cell Host & Microbe* 25, 166-173.e5. <https://doi.org/10.1016/j.chom.2018.11.010>
- Jorgensen, P.L., Hakansson, K.O., Karlsh, S.J.D., 2003. Structure and mechanism of Na,K-ATPase: functional sites and their interactions. *Annu Rev Physiol* 65, 817–849. <https://doi.org/10.1146/annurev.physiol.65.092101.142558>
- Kafsack, B.F.C., Carruthers, V.B., 2010. Apicomplexan perforin-like proteins. *Commun Integr Biol* 3, 18–23.
- Kampoun, T., Srichairatanakool, S., Prommana, P., Shaw, P.J., Green, J.L., Knuepfer, E., Holder, A.A., Uthaiyibull, C., 2022. Apicoplast ribosomal protein S10-V127M enhances artemisinin resistance of a Kelch13 transgenic *Plasmodium falciparum*. *Malar J* 21, 302. <https://doi.org/10.1186/s12936-022-04330-3>
- Kannan, G., Thaprawat, P., Schultz, T.L., Carruthers, V.B., 2021. Acquisition of Host Cytosolic Protein by *Toxoplasma gondii* Bradyzoites. *mSphere* 6, e00934-20. <https://doi.org/10.1128/mSphere.00934-20>
- Kannenberg, F., Ellinghaus, P., Assmann, G., Seedorf, U., 1999. Aberrant oxidation of the cholesterol side chain in bile acid synthesis of sterol carrier protein-2/sterol carrier protein-x knockout mice. *J Biol Chem* 274, 35455–35460. <https://doi.org/10.1074/jbc.274.50.35455>
- Katris, N.J., Yamaro-Botte, Y., Janouškovec, J., Shunmugam, S., Arnold, C.-S., Yang, A.S.P., Vardakis, A., Stewart, R.J., Sauerwein, R., McFadden, G.I., Tonkin, C.J., Cesbron-Delauw, M.-F., Waller, Ross.F., Botte, C.Y., 2020. Rapid kinetics of lipid second messengers controlled by a cGMP signalling network coordinates apical complex functions in *Toxoplasma* tachyzoites (preprint). *Microbiology*. <https://doi.org/10.1101/2020.06.19.160341>
- Kauffmann-Zeh, A., Thomas, G.M., Ball, A., Prosser, S., Cunningham, E., Cockcroft, S., Hsuan, J.J., 1995. Requirement for phosphatidylinositol transfer protein in epidermal growth factor signaling. *Science* 268, 1188–1190. <https://doi.org/10.1126/science.7761838>
- Kesav, S., McLaughlin, J., Scallen, T.J., 1992. Participation of sterol carrier protein-2 in cholesterol metabolism. *Biochemical Society Transactions* 20, 818–824. <https://doi.org/10.1042/bst0200818>
- Kielbowicz-Matuk, A., Rey, P., Rorat, T., 2008. The organ-dependent abundance of a *Solanum* lipid transfer protein is up-regulated upon osmotic constraints and associated with cold acclimation ability. *J Exp Bot* 59, 2191–2203. <https://doi.org/10.1093/jxb/ern088>
- Kilian, N., Choi, J.-Y., Voelker, D.R., Ben Mamoun, C., 2018. Role of phospholipid synthesis in the development and differentiation of malaria parasites in the blood. *J Biol Chem* 293, 17308–17316. <https://doi.org/10.1074/jbc.R118.003213>
- Kim, SoHui, Kedan, A., Marom, M., Gavert, N., Keinan, O., Selitrennik, M., Laufman, O., Lev, S., 2013. The phosphatidylinositol-transfer protein Nir2 binds phosphatidic acid and positively regulates phosphoinositide signalling. *EMBO Rep* 14, 891–899. <https://doi.org/10.1038/embor.2013.113>

- Kim, Sangwoo, Yamaoka, Y., Ono, H., Kim, H., Shim, D., Maeshima, M., Martinoia, E., Cahoon, E.B., Nishida, I., Lee, Y., 2013. AtABCA9 transporter supplies fatty acids for lipid synthesis to the endoplasmic reticulum. *Proc. Natl. Acad. Sci. U.S.A.* 110, 773–778. <https://doi.org/10.1073/pnas.1214159110>
- Kim, Y.J., Guzman-Hernandez, M.L., Balla, T., 2011. A highly dynamic ER-derived phosphatidylinositol-synthesizing organelle supplies phosphoinositides to cellular membranes. *Dev Cell* 21, 813–824. <https://doi.org/10.1016/j.devcel.2011.09.005>
- Kim, Y.J., Guzman-Hernandez, M.-L., Wisniewski, E., Balla, T., 2015. Phosphatidylinositol-Phosphatidic Acid Exchange by Nir2 at ER-PM Contact Sites Maintains Phosphoinositide Signaling Competence. *Dev Cell* 33, 549–561. <https://doi.org/10.1016/j.devcel.2015.04.028>
- Kloehn, J., Harding, C.R., Soldati-Favre, D., 2021a. Supply and demand—heme synthesis, salvage and utilization by Apicomplexa. *The FEBS Journal* 288, 382–404. <https://doi.org/10.1111/febs.15445>
- Kloehn, J., Lacour, C.E., Soldati-Favre, D., 2021b. The metabolic pathways and transporters of the plastid organelle in Apicomplexa. *Current Opinion in Microbiology* 63, 250–258. <https://doi.org/10.1016/j.mib.2021.07.016>
- Koike, S., Jahn, R., 2019. SNAREs define targeting specificity of trafficking vesicles by combinatorial interaction with tethering factors. *Nat Commun* 10, 1608. <https://doi.org/10.1038/s41467-019-09617-9>
- Kong, P., Ufermann, C.-M., Zimmermann, D.L.M., Yin, Q., Suo, X., Helms, J.B., Brouwers, J.F., Gupta, N., 2017. Two phylogenetically and compartmentally distinct CDP-diacylglycerol synthases cooperate for lipid biogenesis in *Toxoplasma gondii*. *J Biol Chem* 292, 7145–7159. <https://doi.org/10.1074/jbc.M116.765487>
- Kono, M., Prusty, D., Parkinson, J., Gilberger, T.W., 2013. The apicomplexan inner membrane complex. *Frontiers in Bioscience-Landmark* 18, 982–992. <https://doi.org/10.2741/4157>
- Koreny, L., Mercado-Saavedra, B.N., Klinger, C.M., Barylyuk, K., Butterworth, S., Hirst, J., Rivera-Cuevas, Y., Zaccai, N.R., Holzer, V.J.C., Klingl, A., Dacks, J.B., Carruthers, V.B., Robinson, M.S., Gras, S., Waller, R.F., 2022. Stable and ancient endocytic structures navigate the complex pellicle of apicomplexan parasites. <https://doi.org/10.1101/2022.06.02.494549>
- Koreny, L., Zeeshan, M., Barylyuk, K., Tromer, E.C., van Hooff, J.J.E., Brady, D., Ke, H., Chelaghma, S., Ferguson, D.J.P., Eme, L., Tewari, R., Waller, R.F., 2021. Molecular characterization of the conoid complex in *Toxoplasma* reveals its conservation in all apicomplexans, including *Plasmodium* species. *PLoS Biol* 19, e3001081. <https://doi.org/10.1371/journal.pbio.3001081>
- Kremer, K., Kamin, D., Rittweger, E., Wilkes, J., Flammer, H., Mahler, S., Heng, J., Tonkin, C.J., Langsley, G., Hell, S.W., Carruthers, V.B., Ferguson, D.J.P., Meissner, M., 2013. An Overexpression Screen of *Toxoplasma gondii* Rab-GTPases Reveals Distinct Transport Routes to the Micronemes. *PLoS Pathog* 9, e1003213. <https://doi.org/10.1371/journal.ppat.1003213>
- Kuchipudi, A., Arroyo-Olarte, R.D., Hoffmann, F., Brinkmann, V., Gupta, N., 2016. Optogenetic monitoring identifies phosphatidylthreonine-regulated calcium homeostasis in *Toxoplasma gondii*. *Microb Cell* 3, 215–223. <https://doi.org/10.15698/mic2016.05.500>
- Kular, G., Loubtchenkov, M., Swigart, P., Whatmore, J., Ball, A., Cockcroft, S., Wetzker, R., 1997. Cooperation of phosphatidylinositol transfer protein with phosphoinositide 3-kinase gamma in the formylmethionyl-leucylphenylalanine-dependent production of phosphatidylinositol 3,4,5-trisphosphate in human neutrophils. *Biochem J* 325 (Pt 2), 299–301. <https://doi.org/10.1042/bj3250299>
- Kumar, N., Leonzino, M., Hancock-Cerutti, W., Horenkamp, F.A., Li, P., Lees, J.A., Wheeler, H., Reinisch, K.M., De Camilli, P., 2018. VPS13A and VPS13C are lipid transport proteins differentially localized at ER contact sites. *J Cell Biol* 217, 3625–3639. <https://doi.org/10.1083/jcb.201807019>
- Lamarque, M.H., Roques, M., Kong-Hap, M., Tonkin, M.L., Rugarabamu, G., Marq, J.-B., Penarete-Vargas, D.M., Boulanger, M.J., Soldati-Favre, D., Lebrun, M., 2014. Plasticity and redundancy among AMA–RON pairs ensure host cell entry of *Toxoplasma* parasites. *Nat Commun* 5, 4098. <https://doi.org/10.1038/ncomms5098>

- Lehto, M., Laitinen, S., Chinetti, G., Johansson, M., Ehnholm, C., Staels, B., Ikonen, E., Olkkonen, V.M., 2001. The OSBP-related protein family in humans. *Journal of Lipid Research* 42, 1203–1213. [https://doi.org/10.1016/S0022-2275\(20\)31570-4](https://doi.org/10.1016/S0022-2275(20)31570-4)
- Lekutis, C., Ferguson, D.J.P., Grigg, M.E., Camps, M., Boothroyd, J.C., 2001. Surface antigens of *Toxoplasma gondii*: variations on a theme. *International Journal for Parasitology, Life in Vacuoles-A strategy for Parasite Survival* 31, 1285–1292. [https://doi.org/10.1016/S0020-7519\(01\)00261-2](https://doi.org/10.1016/S0020-7519(01)00261-2)
- Leroux, L.-P., Dasanayake, D., Rommereim, L.M., Fox, B.A., Bzik, D.J., Jardim, A., Dzierszynski, F.S., 2015. Secreted *Toxoplasma gondii* molecules interfere with expression of MHC-II in interferon gamma-activated macrophages. *International Journal for Parasitology* 45, 319–332. <https://doi.org/10.1016/j.ijpara.2015.01.003>
- Lévêque, M.F., Berry, L., Yamaro-Botté, Y., Nguyen, H.M., Galera, M., Botté, C.Y., Besteiro, S., 2017. TgPL2, a patatin-like phospholipase domain-containing protein, is involved in the maintenance of apicoplast lipids homeostasis in *Toxoplasma*. *Molecular Microbiology* 105, 158–174. <https://doi.org/10.1111/mmi.13694>
- Li, G., Marlin, M.C., 2015. Rab Family of GTPases. *Methods Mol Biol* 1298, 1–15. https://doi.org/10.1007/978-1-4939-2569-8_1
- Li, H.-Y., Xiao, S., Chye, M.-L., 2008. Ethylene- and pathogen-inducible Arabidopsis acyl-CoA-binding protein 4 interacts with an ethylene-responsive element binding protein. *Journal of Experimental Botany* 59, 3997–4006. <https://doi.org/10.1093/jxb/ern241>
- Li, N., Gügel, I.L., Giavalisco, P., Zeisler, V., Schreiber, L., Soll, J., Philippar, K., 2015. FAX1, a Novel Membrane Protein Mediating Plastid Fatty Acid Export. *PLoS Biol* 13, e1002053. <https://doi.org/10.1371/journal.pbio.1002053>
- Li, N., Meng, H., Li, S., Zhang, Z., Zhao, X., Wang, S., Liu, A., Li, Q., Song, Q., Li, X., Guo, L., Li, H., Zuo, J., Luo, K., 2020. Two Plastid Fatty Acid Exporters Contribute to Seed Oil Accumulation in Arabidopsis1. *Plant Physiol* 182, 1910–1919. <https://doi.org/10.1104/pp.19.01344>
- Li, N., Xu, C., Li-Beisson, Y., Philippar, K., 2016. Fatty Acid and Lipid Transport in Plant Cells. *Trends in Plant Science* 21, 145–158. <https://doi.org/10.1016/j.tplants.2015.10.011>
- Li, Y.E., Wang, Y., Du, X., Zhang, T., Mak, H.Y., Hancock, S.E., McEwen, H., Pandzic, E., Whan, R.M., Aw, Y.C., Lukmantara, I.E., Yuan, Y., Dong, X., Don, A., Turner, N., Qi, S., Yang, H., 2021. TMEM41B and VMP1 are scramblases and regulate the distribution of cholesterol and phosphatidylserine. *Journal of Cell Biology* 220, e202103105. <https://doi.org/10.1083/jcb.202103105>
- Liao, P., Chen, Q.-F., Chye, M.-L., 2014. Transgenic Arabidopsis Flowers Overexpressing Acyl-CoA-Binding Protein ACBP6 are Freezing Tolerant. *Plant and Cell Physiology* 55, 1055–1071. <https://doi.org/10.1093/pcp/pcu037>
- Li-Beisson, Y., Neunzig, J., Lee, Y., Philippar, K., 2017. Plant membrane-protein mediated intracellular traffic of fatty acids and acyl lipids. *Current Opinion in Plant Biology* 40, 138–146. <https://doi.org/10.1016/j.pbi.2017.09.006>
- Lige, B., Sampels, V., Coppens, I., 2013. Characterization of a second sterol-esterifying enzyme in *Toxoplasma* highlights the importance of cholesterol storage pathways for the parasite. *Mol Microbiol* 87, 951–967. <https://doi.org/10.1111/mmi.12142>
- Lill, R., 2009. Function and biogenesis of iron–sulphur proteins. *Nature* 460, 831–838. <https://doi.org/10.1038/nature08301>
- Lipp, N.-F., Ikhlef, S., Milanini, J., Drin, G., 2020. Lipid Exchangers: Cellular Functions and Mechanistic Links With Phosphoinositide Metabolism. *Front Cell Dev Biol* 8, 663. <https://doi.org/10.3389/fcell.2020.00663>
- Liu, K., Surendhran, K., Nothwehr, S.F., Graham, T.R., 2008. P4-ATPase Requirement for AP-1/Clathrin Function in Protein Transport from the *trans* -Golgi Network and Early Endosomes. *MBoC* 19, 3526–3535. <https://doi.org/10.1091/mbc.e08-01-0025>
- Liu, R.-Z., Mita, R., Beaulieu, M., Gao, Z., Godbout, R., 2010. Fatty acid binding proteins in brain development and disease. *Int. J. Dev. Biol.* 54, 1229–1239. <https://doi.org/10.1387/ijdb.092976rl>

- Loubens, M., Vincensini, L., Fernandes, P., Briquet, S., Marinach, C., Silvie, O., 2021. Plasmodium sporozoites on the move: Switching from cell traversal to productive invasion of hepatocytes. *Mol Microbiol* 115, 870–881. <https://doi.org/10.1111/mmi.14645>
- Lu, B., Benning, C., 2009. A 25-Amino Acid Sequence of the Arabidopsis TGD2 Protein Is Sufficient for Specific Binding of Phosphatidic Acid. *Journal of Biological Chemistry* 284, 17420–17427. <https://doi.org/10.1074/jbc.M109.016014>
- Lu, B., Xu, C., Awai, K., Jones, A.D., Benning, C., 2007. A Small ATPase Protein of Arabidopsis, TGD3, Involved in Chloroplast Lipid Import. *Journal of Biological Chemistry* 282, 35945–35953. <https://doi.org/10.1074/jbc.M704063200>
- Lung, S.-C., Chye, M.-L., 2016. Deciphering the roles of acyl-CoA-binding proteins in plant cells. *Protoplasma* 253, 1177–1195. <https://doi.org/10.1007/s00709-015-0882-6>
- Maclean, A.E., Bridges, H.R., Silva, M.F., Ding, S., Ovcariakova, J., Hirst, J., Sheiner, L., 2021. Complexome profile of *Toxoplasma gondii* mitochondria identifies divergent subunits of respiratory chain complexes including new subunits of cytochrome bc1 complex. *PLoS Pathog* 17, e1009301. <https://doi.org/10.1371/journal.ppat.1009301>
- Maclean, A.E., Hayward, J.A., Huet, D., van Dooren, G.G., Sheiner, L., 2022. The mystery of massive mitochondrial complexes: the apicomplexan respiratory chain. *Trends in Parasitology* 38, 1041–1052. <https://doi.org/10.1016/j.pt.2022.09.008>
- Maeda, K., Anand, K., Chiapparino, A., Kumar, A., Poletto, M., Kaksonen, M., Gavin, A.-C., 2013. Interactome map uncovers phosphatidylserine transport by oxysterol-binding proteins. *Nature* 501, 257–261. <https://doi.org/10.1038/nature12430>
- Mageswaran, S.K., Guérin, A., Theveny, L.M., Chen, W.D., Martinez, M., Lebrun, M., Striepen, B., Chang, Y.-W., 2021. In situ ultrastructures of two evolutionarily distant apicomplexan rhoptry secretion systems. *Nat Commun* 12, 4983. <https://doi.org/10.1038/s41467-021-25309-9>
- Maier, A.G., van Ooij, C., 2022. The role of cholesterol in invasion and growth of malaria parasites. *Front Cell Infect Microbiol* 12, 984049. <https://doi.org/10.3389/fcimb.2022.984049>
- Martin, R.E., Kirk, K., 2004. The malaria parasite's chloroquine resistance transporter is a member of the drug/metabolite transporter superfamily. *Mol Biol Evol* 21, 1938–1949. <https://doi.org/10.1093/molbev/msh205>
- Martinez, M., Chen, W.D., Cova, M.M., Molnár, P., Mageswaran, S.K., Guérin, A., John, A.R.O., Lebrun, M., Chang, Y.-W., 2022. Rhoptry secretion system structure and priming in *Plasmodium falciparum* revealed using in situ cryo-electron tomography. *Nat Microbiol* 7, 1230–1238. <https://doi.org/10.1038/s41564-022-01171-3>
- Martorelli Di Genova, B., Wilson, S.K., Dubey, J.P., Knoll, L.J., 2019. Intestinal delta-6-desaturase activity determines host range for *Toxoplasma* sexual reproduction. *PLoS Biol* 17, e3000364. <https://doi.org/10.1371/journal.pbio.3000364>
- Mayoral, J., Guevara, R.B., Rivera-Cuevas, Y., Tu, V., Tomita, T., Romano, J.D., Gunther-Cummins, L., Sidoli, S., Coppens, I., Carruthers, V.B., Weiss, L.M., 2022. Dense Granule Protein GRA64 Interacts with Host Cell ESCRT Proteins during *Toxoplasma gondii* Infection. *mBio* 13, e01442-22. <https://doi.org/10.1128/mbio.01442-22>
- McCrea, H.J., De Camilli, P., 2009. Mutations in phosphoinositide metabolizing enzymes and human disease. *Physiology (Bethesda)* 24, 8–16. <https://doi.org/10.1152/physiol.00035.2008>
- McGovern, O.L., Rivera-Cuevas, Y., Kannan, G., Narwold, A., Carruthers, V.B., 2018. Intersection of Endocytic and Exocytic Systems in *Toxoplasma gondii*. *Traffic* 19, 336–353. <https://doi.org/10.1111/tra.12556>
- Milani, K.J., Schneider, T.G., Taraschi, T.F., 2015. Defining the Morphology and Mechanism of the Hemoglobin Transport Pathway in *Plasmodium falciparum*-Infected Erythrocytes. *Eukaryot Cell* 14, 415–426. <https://doi.org/10.1128/EC.00267-14>
- Mills, I.G., Praefcke, G.J.K., Vallis, Y., Peter, B.J., Olesen, L.E., Gallop, J.L., Butler, P.J.G., Evans, P.R., McMahon, H.T., 2003. EpsinR : an AP1/clathrin interacting protein involved in vesicle trafficking. *Journal of Cell Biology* 160, 213–222. <https://doi.org/10.1083/jcb.200208023>

- Missaoui, K., Gonzalez-Klein, Z., Pazos-Castro, D., Hernandez-Ramirez, G., Garrido-Arandia, M., Brini, F., Diaz-Perales, A., Tome-Amat, J., 2022. Plant non-specific lipid transfer proteins: An overview. *Plant Physiology and Biochemistry* 171, 115–127. <https://doi.org/10.1016/j.plaphy.2021.12.026>
- Mizuike, A., Kobayashi, S., Rikukawa, T., Ohta, A., Horiuchi, H., Fukuda, R., 2019. Suppression of respiratory growth defect of mitochondrial phosphatidylserine decarboxylase deficient mutant by overproduction of Sfh1, a Sec14 homolog, in yeast. *PLoS One* 14, e0215009. <https://doi.org/10.1371/journal.pone.0215009>
- Moser von Filseck, J., Čopič, A., Delfosse, V., Vanni, S., Jackson, C.L., Bourguet, W., Drin, G., 2015. INTRACELLULAR TRANSPORT. Phosphatidylserine transport by ORP/Osh proteins is driven by phosphatidylinositol 4-phosphate. *Science* 349, 432–436. <https://doi.org/10.1126/science.aab1346>
- Mühleip, A., Kock Flygaard, R., Ovcariškova, J., Lacombe, A., Fernandes, P., Sheiner, L., Amunts, A., 2021. ATP synthase hexamer assemblies shape cristae of *Toxoplasma* mitochondria. *Nat Commun* 12, 120. <https://doi.org/10.1038/s41467-020-20381-z>
- Nagaraj, V.A., Sundaram, B., Varadarajan, N.M., Subramani, P.A., Kalappa, D.M., Ghosh, S.K., Padmanaban, G., 2013. Malaria Parasite-Synthesized Heme Is Essential in the Mosquito and Liver Stages and Complements Host Heme in the Blood Stages of Infection. *PLoS Pathog* 9, e1003522. <https://doi.org/10.1371/journal.ppat.1003522>
- Nair, S.C., Brooks, C.F., Goodman, C.D., Strum, A., McFadden, G.I., Sundriyal, S., Anglin, J.L., Song, Y., Moreno, S.N.J., Striepen, B., 2011. Apicoplast isoprenoid precursor synthesis and the molecular basis of fosmidomycin resistance in *Toxoplasma gondii*. *J Exp Med* 208, 1547–1559. <https://doi.org/10.1084/jem.20110039>
- Nash, E.A., Nisbet, R.E.R., Barbrook, A.C., Howe, C.J., 2008. Dinoflagellates: a mitochondrial genome all at sea. *Trends in Genetics* 24, 328–335. <https://doi.org/10.1016/j.tig.2008.04.001>
- Natarajan, P., Liu, K., Patil, D.V., Sciorra, V.A., Jackson, C.L., Graham, T.R., 2009. Regulation of a Golgi flippase by phosphoinositides and an ArfGEF. *Nat Cell Biol* 11, 1421–1426. <https://doi.org/10.1038/ncb1989>
- Nazeer, M., Waheed, H., Saeed, M., Ali, S.Y., Choudhary, M.I., Ul-Haq, Z., Ahmed, A., 2019. Purification and Characterization of a Nonspecific Lipid Transfer Protein 1 (nsLTP1) from Ajwain (*Trachyspermum ammi*) Seeds. *Sci Rep* 9, 4148. <https://doi.org/10.1038/s41598-019-40574-x>
- Nemirovskaya, T.L., Sharlo, K.A., 2022. Roles of ATP and SERCA in the Regulation of Calcium Turnover in Unloaded Skeletal Muscles: Current View and Future Directions. *Int J Mol Sci* 23, 6937. <https://doi.org/10.3390/ijms23136937>
- Neuman, S.D., Cavanagh, A.T., Bashirullah, A., 2021. The Hob proteins: Putative, novel lipid transfer proteins at ER-PM contact sites. *Contact (Thousand Oaks)* 4. <https://doi.org/10.1177/25152564211052376>
- Neuman, S.D., Levine, T.P., Bashirullah, A., 2022. A novel superfamily of bridge-like lipid transfer proteins. *Trends in Cell Biology* 32, 962–974. <https://doi.org/10.1016/j.tcb.2022.03.011>
- Nguyen, H.M., El Hajj, H., El Hajj, R., Tawil, N., Berry, L., Lebrun, M., Bordat, Y., Besteiro, S., 2017. *Toxoplasma gondii* autophagy-related protein ATG9 is crucial for the survival of parasites in their host. *Cellular Microbiology* 19, e12712. <https://doi.org/10.1111/cmi.12712>
- Noda, N.N., 2021. Atg2 and Atg9: Intermembrane and interleaflet lipid transporters driving autophagy. *Biochimica et Biophysica Acta (BBA) - Molecular and Cell Biology of Lipids* 1866, 158956. <https://doi.org/10.1016/j.bbalip.2021.158956>
- Nofal, S.D., Patel, A., Blackman, M.J., Flueck, C., Baker, D.A., 2021. Plasmodium falciparum Guanylyl Cyclase-Alpha and the Activity of Its Appended P4-ATPase Domain Are Essential for cGMP Synthesis and Blood-Stage Egress. *mBio* 12, e02694-20. <https://doi.org/10.1128/mBio.02694-20>
- Nolan, S.J., Romano, J.D., Coppens, I., 2017. Host lipid droplets: An important source of lipids salvaged by the intracellular parasite *Toxoplasma gondii*. *PLoS Pathog* 13, e1006362. <https://doi.org/10.1371/journal.ppat.1006362>
- Nolan, S.J., Romano, J.D., Kline, J.T., Coppens, I., 2018. Novel Approaches To Kill *Toxoplasma gondii* by Exploiting the Uncontrolled Uptake of Unsaturated Fatty Acids and Vulnerability to Lipid

- Storage Inhibition of the Parasite. *Antimicrob Agents Chemother* 62, e00347-18, /aac/62/10/e00347-18.atom. <https://doi.org/10.1128/AAC.00347-18>
- Nyonda, M.A., Kloehn, J., Sosnowski, P., Krishnan, A., Lentini, G., Maco, B., Marq, J.-B., Hannich, J.T., Hopfgartner, G., Soldati-Favre, D., 2022. Ceramide biosynthesis is critical for establishment of the intracellular niche of *Toxoplasma gondii*. *Cell Rep* 40, 111224. <https://doi.org/10.1016/j.celrep.2022.111224>
- Opitz, C., Soldati, D., 2002. ‘The glideosome’: a dynamic complex powering gliding motion and host cell invasion by *Toxoplasma gondii*. *Molecular Microbiology* 45, 597–604. <https://doi.org/10.1046/j.1365-2958.2002.03056.x>
- Palacin, A., Bartra, J., Muñoz, R., Diaz-Perales, A., Valero, A., Salcedo, G., 2010. Anaphylaxis to Wheat Flour-Derived Foodstuffs and the Lipid Transfer Protein Syndrome: A Potential Role of Wheat Lipid Transfer Protein Tri a 14. *IAA* 152, 178–183. <https://doi.org/10.1159/000265539>
- Palmgren, M., Østerberg, J.T., Nintemann, S.J., Poulsen, L.R., López-Marqués, R.L., 2019. Evolution and a revised nomenclature of P4 ATPases, a eukaryotic family of lipid flippases. *Biochimica et Biophysica Acta (BBA) - Biomembranes* 1861, 1135–1151. <https://doi.org/10.1016/j.bbamem.2019.02.006>
- Pamukcu, S., Cerutti, A., Bordat, Y., Hem, S., Rofidal, V., Besteiro, S., 2021. Differential contribution of two organelles of endosymbiotic origin to iron-sulfur cluster synthesis and overall fitness in *Toxoplasma*. *PLOS Pathogens* 17, e1010096. <https://doi.org/10.1371/journal.ppat.1010096>
- Pane, S., Putignani, L., 2022. Cryptosporidium: Still Open Scenarios. *Pathogens* 11, 515. <https://doi.org/10.3390/pathogens11050515>
- Paradies, G., Paradies, V., Ruggiero, F.M., Petrosillo, G., 2019. Role of Cardiolipin in Mitochondrial Function and Dynamics in Health and Disease: Molecular and Pharmacological Aspects. *Cells* 8, 728. <https://doi.org/10.3390/cells8070728>
- Paulusma, C.C., Oude Elferink, R.P.J., 2006. Diseases of intramembranous lipid transport. *FEBS Letters* 580, 5500–5509. <https://doi.org/10.1016/j.febslet.2006.06.067>
- Pawelczyk, A., Bednarska, M., Caraballo Cortés, K., Glamkowska-Sady, M., Kowalska, J., Uszyńska-Kałuża, B., Radkowski, M., Welc-Fałęciak, R., 2022. Seronegative Infection with *Toxoplasma gondii* in Asymptomatic Human Immunodeficiency Virus Type 1 (HIV-1)-Infected Patients and in Blood Donors. *J Clin Med* 11, 638. <https://doi.org/10.3390/jcm11030638>
- Peeters, B.W.A., Piët, A.C.A., Fornerod, M., 2022. Generating Membrane Curvature at the Nuclear Pore: A Lipid Point of View. *Cells* 11, 469. <https://doi.org/10.3390/cells11030469>
- Phillips, M.A., Burrows, J.N., Manyando, C., van Huijsduijnen, R.H., Van Voorhis, W.C., Wells, T.N.C., 2017. Malaria. *Nat Rev Dis Primers* 3, 1–24. <https://doi.org/10.1038/nrdp.2017.50>
- Phyo, A.P., Nosten, F., 2018. The Artemisinin Resistance in Southeast Asia: An Imminent Global Threat to Malaria Elimination. <https://doi.org/10.5772/intechopen.76519>
- Pike, L.J., 2009. The challenge of lipid rafts. *J Lipid Res* 50, S323–S328. <https://doi.org/10.1194/jlr.R800040-JLR200>
- PlasmoDB [WWW Document], n.d. URL <https://plasmodb.org/plasmo/app/> (accessed 1.26.23).
- Plowe, C.V., 2005. Antimalarial drug resistance in Africa: strategies for monitoring and deterrence. *Curr Top Microbiol Immunol* 295, 55–79. https://doi.org/10.1007/3-540-29088-5_3
- Quittnat, F., Nishikawa, Y., Stedman, T.T., Voelker, D.R., Choi, J.-Y., Zahn, M.M., Murphy, R.C., Barkley, R.M., Pypaert, M., Joiner, K.A., Coppens, I., 2004. On the biogenesis of lipid bodies in ancient eukaryotes: synthesis of triacylglycerols by a *Toxoplasma* DGAT1-related enzyme. *Molecular and Biochemical Parasitology* 138, 107–122. <https://doi.org/10.1016/j.molbiopara.2004.08.004>
- Ramakrishnan, S., Serricchio, M., Striepen, B., Bütikofer, P., 2013. Lipid Synthesis in Protozoan Parasites: a Comparison Between Kinetoplastids and Apicomplexans. *Prog Lipid Res* 52, 10.1016/j.plipres.2013.06.003. <https://doi.org/10.1016/j.plipres.2013.06.003>
- Rathnapala, U.L., Goodman, C.D., McFadden, G.I., 2017. A novel genetic technique in *Plasmodium berghei* allows liver stage analysis of genes required for mosquito stage development and demonstrates that de novo heme synthesis is essential for liver stage development in the malaria parasite. *PLoS Pathog* 13, e1006396. <https://doi.org/10.1371/journal.ppat.1006396>

- Raychaudhuri, S., Im, Y.J., Hurley, J.H., Prinz, W.A., 2006. Nonvesicular sterol movement from plasma membrane to ER requires oxysterol-binding protein-related proteins and phosphoinositides. *J Cell Biol* 173, 107–119. <https://doi.org/10.1083/jcb.200510084>
- Ren, J., Pei-Chen Lin, C., Pathak, M.C., Temple, B.R.S., Nile, A.H., Mousley, C.J., Duncan, M.C., Eckert, D.M., Leiker, T.J., Ivanova, P.T., Myers, D.S., Murphy, R.C., Brown, H.A., Verdaasdonk, J., Bloom, K.S., Ortlund, E.A., Neiman, A.M., Bankaitis, V.A., 2014. A phosphatidylinositol transfer protein integrates phosphoinositide signaling with lipid droplet metabolism to regulate a developmental program of nutrient stress-induced membrane biogenesis. *Mol Biol Cell* 25, 712–727. <https://doi.org/10.1091/mbc.E13-11-0634>
- Renaud, E.A., Pamukcu, S., Cerutti, A., Berry, L., Lemaire-Vieille, C., Yamaryo-Botté, Y., Botté, C.Y., Besteiro, S., 2022. Disrupting the plastidic iron-sulfur cluster biogenesis pathway in *Toxoplasma gondii* has pleiotropic effects irreversibly impacting parasite *viability*. *J Biol Chem* 298, 102243. <https://doi.org/10.1016/j.jbc.2022.102243>
- Richieri, G.V., Ogata, R.T., Zimmerman, A.W., Veerkamp, J.H., Kleinfeld, A.M., 2000. Fatty Acid Binding Proteins from Different Tissues Show Distinct Patterns of Fatty Acid Interactions. *Biochemistry* 39, 7197–7204. <https://doi.org/10.1021/bi000314z>
- Ridgway, M.C., Cihalova, D., Brown, S.H.J., Tran, P., Mitchell, T.W., Maier, A.G., 2022. Analysis of sex-specific lipid metabolism of *Plasmodium falciparum* points to the importance of sphingomyelin for gametocytogenesis. *Journal of Cell Science* 135, jcs259592. <https://doi.org/10.1242/jcs.259592>
- Rivera-Cuevas, Y., Mayoral, J., Di Cristina, M., Lawrence, A.-L.E., Olafsson, E.B., Patel, R.K., Thornhill, D., Waldman, B.S., Ono, A., Sexton, J.Z., Lourido, S., Weiss, L.M., Carruthers, V.B., 2021. *Toxoplasma gondii* exploits the host ESCRT machinery for parasite uptake of host cytosolic proteins. *PLoS Pathog* 17, e1010138. <https://doi.org/10.1371/journal.ppat.1010138>
- Roland, B.P., Graham, T.R., 2016. Decoding P4-ATPase Substrate Interactions. *Crit Rev Biochem Mol Biol* 51, 513–527. <https://doi.org/10.1080/10409238.2016.1237934>
- Romano, J.D., Nolan, S.J., Porter, C., Ehrenman, K., Hartman, E.J., Hsia, R., Coppens, I., 2017. The parasite *Toxoplasma* sequesters diverse Rab host vesicles within an intravacuolar network. *Journal of Cell Biology* 216, 4235–4254. <https://doi.org/10.1083/jcb.201701108>
- Rommereim, L.M., Fox, B.A., Butler, K.L., Cantillana, V., Taylor, G.A., Bzik, D.J., 2019. Rhoptry and Dense Granule Secreted Effectors Regulate CD8+ T Cell Recognition of *Toxoplasma gondii* Infected Host Cells. *Front Immunol* 10, 2104. <https://doi.org/10.3389/fimmu.2019.02104>
- Roy-Barman, S., Sautter, C., Chattoo, B.B., 2006. Expression of the lipid transfer protein Ace-AMP1 in transgenic wheat enhances antifungal activity and defense responses. *Transgenic Res* 15, 435–446. <https://doi.org/10.1007/s11248-006-0016-1>
- Safi, H., Saibi, W., Alaoui, M.M., Hmyene, A., Masmoudi, K., Hanin, M., Brini, F., 2015. A wheat lipid transfer protein (TdLTP4) promotes tolerance to abiotic and biotic stress in *Arabidopsis thaliana*. *Plant Physiology and Biochemistry* 89, 64–75. <https://doi.org/10.1016/j.plaphy.2015.02.008>
- Saint-Pol, A., Yélamos, B., Amessou, M., Mills, I.G., Dugast, M., Tenza, D., Schu, P., Antony, C., McMahon, H.T., Lamaze, C., Johannes, L., 2004. Clathrin Adaptor epsinR Is Required for Retrograde Sorting on Early Endosomal Membranes. *Developmental Cell* 6, 525–538. [https://doi.org/10.1016/S1534-5807\(04\)00100-5](https://doi.org/10.1016/S1534-5807(04)00100-5)
- Sakane, H., Yamamoto, T., Tanaka, K., 2006. The Functional Relationship between the Cdc50p-Drs2p Putative Aminophospholipid Translocase and the Arf GAP Gcs1p in Vesicle Formation in the Retrieval Pathway from Yeast Early Endosomes to the TGN. *Cell Structure and Function* 31, 87–108. <https://doi.org/10.1247/csf.06021>
- Salminen, T.A., Eklund, D.M., Joly, V., Blomqvist, K., Matton, D.P., Edqvist, J., 2018. Deciphering the Evolution and Development of the Cuticle by Studying Lipid Transfer Proteins in Mosses and Liverworts. *Plants* 7, 6. <https://doi.org/10.3390/plants7010006>
- Sampels, V., Hartmann, A., Dietrich, I., Coppens, I., Sheiner, L., Striepen, B., Herrmann, A., Lucius, R., Gupta, N., 2012. Conditional Mutagenesis of a Novel Choline Kinase Demonstrates Plasticity of Phosphatidylcholine Biogenesis and Gene Expression in *Toxoplasma gondii*. *J Biol Chem* 287, 16289–16299. <https://doi.org/10.1074/jbc.M112.347138>

- Schlame, M., 2008. Thematic Review Series: Glycerolipids. Cardiolipin synthesis for the assembly of bacterial and mitochondrial membranes. *J Lipid Res* 49, 1607–1620. <https://doi.org/10.1194/jlr.R700018-JLR200>
- Schmidt, R.R., Fulda, M., Paul, M.V., Anders, M., Plum, F., Weits, D.A., Kosmacz, M., Larson, T.R., Graham, I.A., Beemster, G.T.S., Licausi, F., Geigenberger, P., Schippers, J.H., van Dongen, J.T., 2018. Low-oxygen response is triggered by an ATP-dependent shift in oleoyl-CoA in *Arabidopsis*. *Proc Natl Acad Sci U S A* 115, E12101–E12110. <https://doi.org/10.1073/pnas.1809429115>
- Schmitt, A., Roy, R., Carter, C.J., 2021. Nectar antimicrobial compounds and their potential effects on pollinators. *Current Opinion in Insect Science, Ecology * Parasites/Parasitoids/Biological control* 44, 55–63. <https://doi.org/10.1016/j.cois.2021.03.004>
- Schroeder, F., Atshaves, B.P., McIntosh, A.L., Gallegos, A.M., Storey, S.M., Parr, R.D., Jefferson, J.R., Ball, J.M., Kier, A.B., 2007. Sterol Carrier Protein-2: New roles in regulating lipid rafts and signaling. *Biochim Biophys Acta* 1771, 700–718. <https://doi.org/10.1016/j.bbali.2007.04.005>
- Segev-Zarko, L., Dahlberg, P.D., Sun, S.Y., Pelt, D.M., Kim, C.Y., Egan, E.S., Sethian, J.A., Chiu, W., Boothroyd, J.C., 2022. Cryo-electron tomography with mixed-scale dense neural networks reveals key steps in deployment of *Toxoplasma* invasion machinery. *PNAS Nexus* 1, pgac183. <https://doi.org/10.1093/pnasnexus/pgac183>
- Séron, K., Dzierszynski, F., Tomavo, S., 2000. Molecular cloning, functional complementation in *Saccharomyces cerevisiae* and enzymatic properties of phosphatidylinositol synthase from the protozoan parasite *Toxoplasma gondii*. *Eur J Biochem* 267, 6571–6579. <https://doi.org/10.1046/j.1432-1327.2000.01749.x>
- Sharma, S., Sharma, S.K., Modak, R., Karmodiya, K., Surolia, N., Surolia, A., 2007. Mass Spectrometry-Based Systems Approach for Identification of Inhibitors of *Plasmodium falciparum* Fatty Acid Synthase. *Antimicrob Agents Chemother* 51, 2552–2558. <https://doi.org/10.1128/AAC.00124-07>
- Shears, M.J., Botté, C.Y., McFadden, G.I., 2015. Fatty acid metabolism in the *Plasmodium* apicoplast: Drugs, doubts and knockouts. *Molecular and Biochemical Parasitology* 199, 34–50. <https://doi.org/10.1016/j.molbiopara.2015.03.004>
- Sheiner, L., Fellows, J.D., Ovcariakova, J., Brooks, C.F., Agrawal, S., Holmes, Z.C., Bietz, I., Flinner, N., Heiny, S., Mirus, O., Przyborski, J.M., Striepen, B., 2015. *Toxoplasma gondii* Toc75 Functions in Import of Stromal but not Peripheral Apicoplast Proteins. *Traffic* 16, 1254–1269. <https://doi.org/10.1111/tra.12333>
- Sheiner, L., Vaidya, A.B., McFadden, G.I., 2013. The metabolic roles of the endosymbiotic organelles of *Toxoplasma* and *Plasmodium* spp. *Curr Opin Microbiol* 16, 452–458. <https://doi.org/10.1016/j.mib.2013.07.003>
- Shemesh, T., Luini, A., Malhotra, V., Burger, K.N.J., Kozlov, M.M., 2003. Prefission constriction of Golgi tubular carriers driven by local lipid metabolism: a theoretical model. *Biophys J* 85, 3813–3827. [https://doi.org/10.1016/S0006-3495\(03\)74796-1](https://doi.org/10.1016/S0006-3495(03)74796-1)
- Shenkarev, Z.O., Melnikova, D.N., Finkina, E.I., Sukhanov, S.V., Boldyrev, I.A., Gizatullina, A.K., Mineev, K.S., Arseniev, A.S., Ovchinnikova, T.V., 2017. Ligand Binding Properties of the Lentil Lipid Transfer Protein: Molecular Insight into the Possible Mechanism of Lipid Uptake. *Biochemistry* 56, 1785–1796. <https://doi.org/10.1021/acs.biochem.6b01079>
- Sherman, I.W., 1977. Amino acid metabolism and protein synthesis in malarial parasites. *Bull World Health Organ* 55, 265–276.
- Shunmugam, S., Arnold, C.-S., Dass, S., Katris, N.J., Botté, C.Y., 2022. The flexibility of Apicomplexa parasites in lipid metabolism. *PLoS Pathog* 18, e1010313. <https://doi.org/10.1371/journal.ppat.1010313>
- Silvie, O., Charrin, S., Billard, M., Franetich, J.-F., Clark, K.L., van Gemert, G.-J., Sauerwein, R.W., Dautry, F., Boucheix, C., Mazier, D., Rubinstein, E., 2006. Cholesterol contributes to the organization of tetraspanin-enriched microdomains and to CD81-dependent infection by malaria sporozoites. *J Cell Sci* 119, 1992–2002. <https://doi.org/10.1242/jcs.02911>
- Siregar, J.E., Kurisu, G., Kobayashi, T., Matsuzaki, M., Sakamoto, K., Mi-ichi, F., Watanabe, Y., Hirai, M., Matsuoka, H., Syafruddin, D., Marzuki, S., Kita, K., 2015. Direct evidence for the atovaquone

- action on the Plasmodium cytochrome bc1 complex. *Parasitology International*, SI: Kazuyuki Tanabe's Gedenkschrift 64, 295–300. <https://doi.org/10.1016/j.parint.2014.09.011>
- Sitaula, S., Burris, T.P., 2016. Cholesterol and Other Steroids, in: Bradshaw, R.A., Stahl, P.D. (Eds.), *Encyclopedia of Cell Biology*. Academic Press, Waltham, pp. 173–179. <https://doi.org/10.1016/B978-0-12-394447-4.10021-5>
- Smathers, R.L., Petersen, D.R., 2011. The human fatty acid-binding protein family: Evolutionary divergences and functions. *Human Genomics* 5, 170. <https://doi.org/10.1186/1479-7364-5-3-170>
- Smith, D., Kannan, G., Coppens, I., Wang, F., Nguyen, H.M., Cerutti, A., Olafsson, E.B., Rimple, P.A., Schultz, T.L., Mercado Soto, N.M., Di Cristina, M., Besteiro, S., Carruthers, V.B., 2021. Toxoplasma TgATG9 is critical for autophagy and long-term persistence in tissue cysts. *eLife* 10, e59384. <https://doi.org/10.7554/eLife.59384>
- Song, X., Li, E., Song, H., Du, G., Li, S., Zhu, H., Chen, G., Zhao, C., Qiao, L., Wang, J., Yu, S., Sui, J., 2020. Genome-wide identification and characterization of nonspecific lipid transfer protein (nsLTP) genes in *Arachis duranensis*. *Genomics* 112, 4332–4341. <https://doi.org/10.1016/j.ygeno.2020.07.034>
- Spielmann, T., Gras, S., Sabitzki, R., Meissner, M., 2020. Endocytosis in Plasmodium and Toxoplasma Parasites. *Trends in Parasitology* 36, 520–532. <https://doi.org/10.1016/j.pt.2020.03.010>
- Spork, S., Hiss, J.A., Mandel, K., Sommer, M., Kooij, T.W.A., Chu, T., Schneider, G., Maier, U.G., Przyborski, J.M., 2009. An Unusual ERAD-Like Complex Is Targeted to the Apicoplast of Plasmodium falciparum. *Eukaryot Cell* 8, 1134–1145. <https://doi.org/10.1128/EC.00083-09>
- Stasic, A.J., Moreno, S.N.J., Carruthers, V.B., Dou, Z., 2022. The Toxoplasma plant-like vacuolar compartment (PLVAC). *J Eukaryot Microbiol* 69, e12951. <https://doi.org/10.1111/jeu.12951>
- Stenmark, H., 2009. Rab GTPases as coordinators of vesicle traffic. *Nat Rev Mol Cell Biol* 10, 513–525. <https://doi.org/10.1038/nrm2728>
- Sturm, A., Mollard, V., Cozijnsen, A., Goodman, C.D., McFadden, G.I., 2015. Mitochondrial ATP synthase is dispensable in blood-stage Plasmodium berghei rodent malaria but essential in the mosquito phase. *Proc Natl Acad Sci U S A* 112, 10216–10223. <https://doi.org/10.1073/pnas.1423959112>
- Südhof, T.C., Rothman, J.E., 2009. Membrane Fusion: Grappling with SNARE and SM Proteins. *Science* 323, 474–477. <https://doi.org/10.1126/science.1161748>
- Swift, R.P., Rajaram, K., Elahi, R., Liu, H.B., Prigge, S.T., 2022. Roles of Ferredoxin-Dependent Proteins in the Apicoplast of Plasmodium falciparum Parasites. *mBio* 13, e03023-21. <https://doi.org/10.1128/mbio.03023-21>
- Takeda, M., Yamagami, K., Tanaka, K., 2014. Role of Phosphatidylserine in Phospholipid Flippase-Mediated Vesicle Transport in Saccharomyces cerevisiae. *Eukaryot Cell* 13, 363–375. <https://doi.org/10.1128/EC.00279-13>
- Talundzic, E., Ravishankar, S., Kelley, J., Patel, D., Plucinski, M., Schmedes, S., Ljolje, D., Clemons, B., Madison-Antenucci, S., Arguin, P.M., Lucchi, N.W., Vannberg, F., Udhayakumar, V., 2018. Next-Generation Sequencing and Bioinformatics Protocol for Malaria Drug Resistance Marker Surveillance. *Antimicrob Agents Chemother* 62, e02474-17. <https://doi.org/10.1128/AAC.02474-17>
- Tanzifi, A., Khoshi, A., Emami, S., Sarvi, S., Sharif, M., Montazeri, M., Moghbeli, M., Daryani, A., 2020. The effect of edelfosine on GRA1 and MIC3 expressions in acute toxoplasmosis. *Parasitol Res* 119, 1371–1380. <https://doi.org/10.1007/s00436-020-06601-x>
- Tauchi-Sato, K., Ozeki, S., Houjou, T., Taguchi, R., Fujimoto, T., 2002. The Surface of Lipid Droplets Is a Phospholipid Monolayer with a Unique Fatty Acid Composition*. *Journal of Biological Chemistry* 277, 44507–44512. <https://doi.org/10.1074/jbc.M207712200>
- ten Hoeve, A.L., Braun, L., Rodriguez, M.E., Olivera, G.C., Bougdour, A., Belmudes, L., Couté, Y., Saeij, J.P.J., Hakimi, M.-A., Barragan, A., 2022. The Toxoplasma effector GRA28 promotes parasite dissemination by inducing dendritic cell-like migratory properties in infected macrophages. *Cell Host & Microbe* 30, 1570-1588.e7. <https://doi.org/10.1016/j.chom.2022.10.001>

- Tian, Y., Lv, X., Xie, G., Wang, L., Dai, T., Qin, X., Chen, F., Xu, Y., 2019. FAX2 Mediates Fatty Acid Export from Plastids in Developing Arabidopsis Seeds. *Plant and Cell Physiology* 60, 2231–2242. <https://doi.org/10.1093/pcp/pcz117>
- Tomley, F.M., Soldati, D.S., 2001. Mix and match modules: structure and function of microneme proteins in apicomplexan parasites. *Trends in Parasitology* 17, 81–88. [https://doi.org/10.1016/S1471-4922\(00\)01761-X](https://doi.org/10.1016/S1471-4922(00)01761-X)
- Tosetti, N., Dos Santos Pacheco, N., Bertiaux, E., Maco, B., Bournonville, L., Hamel, V., Guichard, P., Soldati-Favre, D., 2020. Essential function of the alveolin network in the subpellicular microtubules and conoid assembly in *Toxoplasma gondii*. *eLife* 9, e56635. <https://doi.org/10.7554/eLife.56635>
- Toulmay, A., Whittle, F.B., Yang, J., Bai, X., Diarra, J., Banerjee, S., Levine, T.P., Golden, A., Prinz, W.A., 2022. Vps13-like proteins provide phosphatidylethanolamine for GPI anchor synthesis in the ER. *J Cell Biol* 221, e202111095. <https://doi.org/10.1083/jcb.202111095>
- ToxoDB [WWW Document], n.d. URL <https://toxodb.org/toxo/app> (accessed 1.26.23).
- Turner, S., Voogt, J., Davidson, M., Glass, A., Killion, S., Decaris, J., Mohammed, H., Minehira, K., Boban, D., Murphy, E., Luchoomun, J., Awada, M., Neese, R., Hellerstein, M., 2012. Measurement of Reverse Cholesterol Transport Pathways in Humans: In Vivo Rates of Free Cholesterol Efflux, Esterification, and Excretion. *J Am Heart Assoc* 1, e001826. <https://doi.org/10.1161/JAHA.112.001826>
- Tuteja, R., 2007. Malaria – an overview. *The FEBS Journal* 274, 4670–4679. <https://doi.org/10.1111/j.1742-4658.2007.05997.x>
- Uhlemann, A.C., Krishna, S., 2005. Antimalarial multi-drug resistance in Asia: mechanisms and assessment. *Curr Top Microbiol Immunol* 295, 39–53. https://doi.org/10.1007/3-540-29088-5_2
- Usey, M.M., Huet, D., 2022. Parasite powerhouse: A review of the *Toxoplasma gondii* mitochondrion. *J Eukaryot Microbiol* 69, e12906. <https://doi.org/10.1111/jeu.12906>
- Valverde, D.P., Yu, S., Boggavarapu, V., Kumar, N., Lees, J.A., Walz, T., Reinisch, K.M., Melia, T.J., 2019. ATG2 transports lipids to promote autophagosome biogenesis. *J Cell Biol* 218, 1787–1798. <https://doi.org/10.1083/jcb.201811139>
- van Aalten, D.M.F., Milne, K.G., Zou, J.Y., Kleywegt, G.J., Bergfors, T., Ferguson, M.A.J., Knudsen, J., Jones, T.A., 2001. Binding site differences revealed by crystal structures of Plasmodium falciparum and bovine acyl-CoA binding protein I Edited by R. Huber. *Journal of Molecular Biology* 309, 181–192. <https://doi.org/10.1006/jmbi.2001.4749>
- van Dooren, G.G., Striepen, B., 2013. The Algal Past and Parasite Present of the Apicoplast. *Annu. Rev. Microbiol.* 67, 271–289. <https://doi.org/10.1146/annurev-micro-092412-155741>
- van Meer, G., Voelker, D.R., Feigenson, G.W., 2008. Membrane lipids: where they are and how they behave. *Nat Rev Mol Cell Biol* 9, 112–124. <https://doi.org/10.1038/nrm2330>
- Vaughan, A.M., O'Neill, M.T., Tarun, A.S., Camargo, N., Phuong, T.M., Aly, A.S.I., Cowman, A.F., Kappe, S.H.I., 2009. Type II fatty acid synthesis is essential only for malaria parasite late liver stage development. *Cellular Microbiology* 11, 506–520. <https://doi.org/10.1111/j.1462-5822.2008.01270.x>
- Venugopal, K., Werkmeister, E., Barois, N., Saliou, J.-M., Poncet, A., Huot, L., Sindikubwabo, F., Hakimi, M.A., Langsley, G., Lafont, F., Marion, S., 2017. Dual role of the *Toxoplasma gondii* clathrin adaptor AP1 in the sorting of rhoptry and microneme proteins and in parasite division. *PLoS Pathog* 13, e1006331. <https://doi.org/10.1371/journal.ppat.1006331>
- Verstreken, P., Ohshima, T., Haueter, C., Habets, R.L.P., Lin, Y.Q., Swan, L.E., Ly, C.V., Venken, K.J.T., De Camilli, P., Bellen, H.J., 2009. Tweek, an evolutionarily conserved protein, is required for synaptic vesicle recycling. *Neuron* 63, 203–215. <https://doi.org/10.1016/j.neuron.2009.06.017>
- Vial, H.J., Thuet, M.J., Philippot, J.R., 1982. Phospholipid Biosynthesis in Synchronous Plasmodium falciparum Cultures I. *The Journal of Protozoology* 29, 258–263. <https://doi.org/10.1111/j.1550-7408.1982.tb04023.x>
- Vittecoq, M., Elguero, E., Lafferty, K.D., Roche, B., Brodeur, J., Gauthier-Clerc, M., Missé, D., Thomas, F., 2012. Brain cancer mortality rates increase with *Toxoplasma gondii* seroprevalence in France. *Infect Genet Evol* 12, 496–498. <https://doi.org/10.1016/j.meegid.2012.01.013>

- Vyas, A., Kim, S.-K., Giacomini, N., Boothroyd, J.C., Sapolsky, R.M., 2007. Behavioral changes induced by *Toxoplasma* infection of rodents are highly specific to aversion of cat odors. *Proc Natl Acad Sci U S A* 104, 6442–6447. <https://doi.org/10.1073/pnas.0608310104>
- Waller, R.F., Reed, M.B., Cowman, A.F., McFadden, G.I., 2000. Protein trafficking to the plastid of *Plasmodium falciparum* is *via* the secretory pathway. *EMBO J* 19, 1794–1802. <https://doi.org/10.1093/emboj/19.8.1794>
- Wang, X., Devaiah, S.P., Zhang, W., Welti, R., 2006. Signaling functions of phosphatidic acid. *Progress in Lipid Research* 45, 250–278. <https://doi.org/10.1016/j.plipres.2006.01.005>
- Wang, Y., Sangaré, L.O., Paredes-Santos, T.C., Hassan, M.A., Krishnamurthy, S., Furuta, A.M., Markus, B.M., Lourido, S., Saeij, J.P.J., 2020. Genome-wide screens identify *Toxoplasma gondii* determinants of parasite fitness in IFN γ -activated murine macrophages. *Nat Commun* 11, 5258. <https://doi.org/10.1038/s41467-020-18991-8>
- Wehman, A.M., Poggioli, C., Schweinsberg, P., Grant, B.D., Nance, J., 2011. The P4-ATPase TAT-5 inhibits the budding of extracellular vesicles in *C. elegans* embryos. *Curr Biol* 21, 1951–1959. <https://doi.org/10.1016/j.cub.2011.10.040>
- Wei, K., Zhong, X., 2014. Non-specific lipid transfer proteins in maize. *BMC Plant Biology* 14, 281. <https://doi.org/10.1186/s12870-014-0281-8>
- Weiner, J., Kooij, T., 2016. Phylogenetic profiles of all membrane transport proteins of the malaria parasite highlight new drug targets. *Microb Cell* 3, 511–521. <https://doi.org/10.15698/mic2016.10.534>
- Wengelnik, K., Vial, H.J., 2007. Characterisation of the phosphatidylinositol synthase gene of *Plasmodium* species. *Research in Microbiology* 158, 51–59. <https://doi.org/10.1016/j.resmic.2006.11.005>
- Witola, W.H., El Bissati, K., Pessi, G., Xie, C., Roepe, P.D., Mamoun, C.B., 2008. Disruption of the *Plasmodium falciparum* PfPMT Gene Results in a Complete Loss of Phosphatidylcholine Biosynthesis *via* the Serine-Decarboxylase-Phosphoethanolamine-Methyltransferase Pathway and Severe Growth and Survival Defects. *J Biol Chem* 283, 27636–27643. <https://doi.org/10.1074/jbc.M804360200>
- World Health Organization (Ed.), 2006. Guidelines for the treatment of malaria. World Health Organization, Geneva.
- World malaria report, W., 2022. World malaria report 2022.
- Wu, Y., Takar, M., Cuentas-Condori, A.A., Graham, T.R., 2016. Neo1 and phosphatidylethanolamine contribute to vacuole membrane fusion in *Saccharomyces cerevisiae*. *Cell Logist* 6, e1228791. <https://doi.org/10.1080/21592799.2016.1228791>
- Xiao, S., Chen, Q.-F., Chye, M.-L., 2009. Light-regulated *Arabidopsis* ACBP4 and ACBP5 encode cytosolic acyl-CoA-binding proteins that bind phosphatidylcholine and oleoyl-CoA ester. *Plant Physiology and Biochemistry* 47, 926–933. <https://doi.org/10.1016/j.plaphy.2009.06.007>
- Xiao, S., Gao, W., Chen, Q.-F., Chan, S.-W., Zheng, S.-X., Ma, J., Wang, M., Welti, R., Chye, M.-L., 2010. Overexpression of *Arabidopsis* Acyl-CoA Binding Protein ACBP3 Promotes Starvation-Induced and Age-Dependent Leaf Senescence. *The Plant Cell* 22, 1463–1482. <https://doi.org/10.1105/tpc.110.075333>
- Xiao, S., Gao, W., Chen, Q.-F., Ramalingam, S., Chye, M.-L., 2008a. Overexpression of membrane-associated acyl-CoA-binding protein ACBP1 enhances lead tolerance in *Arabidopsis*. *Plant J* 54, 141–151. <https://doi.org/10.1111/j.1365-313X.2008.03402.x>
- Xiao, S., Li, H.-Y., Zhang, J.-P., Chan, S.-W., Chye, M.-L., 2008b. *Arabidopsis* acyl-CoA-binding proteins ACBP4 and ACBP5 are subcellularly localized to the cytosol and ACBP4 depletion affects membrane lipid composition. *Plant Mol Biol* 68, 571–583. <https://doi.org/10.1007/s11103-008-9392-7>
- Yeh, E., DeRisi, J.L., 2011. Chemical Rescue of Malaria Parasites Lacking an Apicoplast Defines Organelle Function in Blood-Stage *Plasmodium falciparum*. *PLoS Biol* 9, e1001138. <https://doi.org/10.1371/journal.pbio.1001138>
- Yen, C.-L.E., Stone, S.J., Koliwad, S., Harris, C., Farese, R.V., 2008. DGAT enzymes and triacylglycerol biosynthesis. *J Lipid Res* 49, 2283–2301. <https://doi.org/10.1194/jlr.R800018-JLR200>

- Yu, M., Santha Kumar, T.R., Nkrumah, L.J., Coppi, A., Retzlaff, S., Li, C.D., Kelly, B.J., Moura, P.A., Lakshmanan, V., Freundlich, J.S., Valderramos, J.-C., Vilcheze, C., Siedner, M., Tsai, J.H.-C., Falkard, B., Sidhu, A. bir S., Purcell, L.A., Gratraud, P., Kremer, L., Waters, A.P., Schiehser, G., Jacobus, D.P., Janse, C.J., Ager, A., Jacobs, W.R., Sacchettini, J.C., Heussler, V., Sinnis, P., Fidock, D.A., 2008. The Fatty Acid Biosynthesis Enzyme FabI Plays a Key Role In the Development of Liver Stage Malarial Parasites. *Cell Host Microbe* 4, 567–578. <https://doi.org/10.1016/j.chom.2008.11.001>
- Zheng, J., Cahill, S.M., Lemmon, M.A., Fushman, D., Schlessinger, J., Cowburn, D., 1996. Identification of the binding site for acidic phospholipids on the pH domain of dynamin: implications for stimulation of GTPase activity. *J Mol Biol* 255, 14–21. <https://doi.org/10.1006/jmbi.1996.0002>
- Zhu, J., Wang, Y., Cao, Y., Shen, J., Yu, L., 2021. Diverse Roles of TgMIC1/4/6 in the Toxoplasma Infection. *Frontiers in Microbiology* 12. <https://doi.org/10.3389/fmicb.2021.666506>

Scientific questions and aims of my thesis

Apicomplexa development and survival are highly dependent on the parasite's capacity to scavenge lipid resources from their hosts and *de novo* synthesis. While assembly and synthesis pathways focus most studies on Apicomplexa lipid metabolism, there still exists a significant knowledge gap concerning the different metabolite transporters. Lipids above other metabolites cannot easily circulate through the cell: they require specific transporters. Our team and others have established that 1/ parasites are capable of FFA, LPA, and PA *de novo* synthesis *via* the prokaryotic FASII pathway, and plant-like acyltransferases, all located in the apicoplast; 2/ that these lipids can exit the apicoplast and participate in parasite membrane biogenesis by being incorporated and form the lipidic patchwork made together with the scavenged FAs and lipids. The plant chloroplast possesses different lipid transporters specific for FFA export and PA import but none of them are conserved in the apicoplast. Nonetheless, different eukaryote models showed that membrane trafficking is dependent on the action of phospholipid flippases but no such mechanism has yet been described in Apicomplexa parasites.

My PhD project focused on better understanding how lipids circulate through the parasite and what is the molecular mechanism behind the membrane biogenesis and trafficking. I thus investigated essential-predicted lipid transporters among the P-type ATPase superfamily and more precisely, two candidates: 1/ one from the poorly characterized P5-ATPase family, which was suggested from the close homology to P4 to act as a lipid transporter in different endocompartments, *i.e.*, the ER, the vacuole, or the lysosome, and 2/ one canonical P4-ATPase. We hypothesized that these P-type ATPases could be key components of parasites' lipid metabolism and play crucial roles in parasite membrane biogenesis.

To achieve these goals and elucidate the role of these two candidates, my PhD work followed the objectives presented below:

- generation of tagged and inducible knock-down lines in *Toxoplasma* and *Plasmodium*;
- state-of-the-art phenotypic characterization (localization, essentiality, morphology, ...);
- functional characterization by performing comprehensive lipidomic analyses and metabolite labeling by gas-chromatography mass-spectrometry;
- developing a strong scientific/professional network.

Results

- **Chapter IV: *Toxoplasma gondii* apicoplast uses a new type of P5-ATPase for fatty acid export, which is essential for parasite survival**
- **Chapter V: *TgFLP2*, a lipid flippase that controls trans-Golgi vesicular trafficking and endocytosis in *Toxoplasma gondii***

Author contributions:

My contribution for this project was as described below:

- Conceptualization (CSA, CYB, YYB, NJK)
- Generation of the mutants lines (CSA)
- Metabolite labeling, lipid extraction, lipidomics analysis (CSA, YYB)
- All phenotypic characterization (CSA)
- Phylogeny background (JJ)
- Microscopy imaging, EM sample preparation (CSA, LB)
- Results and interpretation (CSA, CYB, YYB)
- Manuscript writing and corrections (CSA, CYB, YYB)

More precisely, for this work, I personally generated the tagged and the inducible lines, performed all the state-of-the-art phenotypic characterization (plaque assays, intracellular replication assays). I performed all the lipidomics (lipid extraction, isotope labeling, extraction, analysis, and interpretation), the fluorescence imaging and the growth complementation. TEM pictures were acquired by Laurence Berry, and the phylogenetic analysis was performed by Jan Janouškovec. I did the writing of the manuscript in parallel with corrections by my PIs.

Chapter IV: *Toxoplasma gondii* apicoplast uses a new type of P5-ATPase for fatty acid export, which is essential for parasite survival

Chapter IV Summary

Most apicomplexan parasites depend on a plast acquired by secondary endosymbiosis of a photosynthetic red algae and named the apicoplast. This plast, which is derived from an ancestral chloroplast, has conserved the capacity to synthesize fatty acids (FAs) and phospholipid precursors lyso- and phosphatidic acids. These lipids are then exported outside of the apicoplast for elongation and desaturation in the ER. Then, these lipids serve for membrane biogenesis or lipid storage to sustain the parasite's rapid replication rate. However, contrary to the chloroplast, none of the apicoplast lipid transporters has been characterized or even identified. In this study, we characterized a putative transporter of the apicoplast, *TgFLP12*, in the Apicomplexa model *Toxoplasma gondii*, and showed that it participates in short FAs export from the apicoplast.

Below are summarized the major findings of this study:

- *TgFLP12* belongs to a newly identified subfamily of P5-ATPases, P5C, conserved in basic land plants, fungi, and SAR supergroup including alveolates;
- *TgFLP12* is essential for tachyzoite development and apicoplast integrity;
- lack of *TgFLP12* reduces incorporation of apicoplast FASII main product, the myristic acid (C14:0), into major lipid classes;
- parasite lipid labeling showed that early disruption of *TgFLP12* leads to an increase in FASII activity, which is shut down on the long term;
- labeling of parasite elongation showed that *TgFLP12* activity is not altered by its disruption and that lipids still exit the apicoplast by another route as a longer chain palmitic acid (C16:0), probably as LPA or PA;
- finally, only medium complementation with exogenous lipids, mainly short FAs, partially rescued the growth of parasites lacking *TgFLP12*.

***Toxoplasma gondii* apicoplast uses a new type of P5-ATPase for fatty acid export, which is essential for parasite survival.**

(Submitted in *Nature Communications*)

Christophe-Sebastien Arnold¹, Serena Shunmugam¹, Jan Janouškovec^{2,3}, Laurence Berry⁴, Samuel Duley¹, Yoshiki Yamaro-Botté¹, Nicholas J. Katris^{1*}, Cyrille Y. Botté^{1*}

¹Apicolipid Team, Institute for Advanced Biosciences, CNRS UMR5309, Université Grenoble Alpes, INSERM U1209, Grenoble, France.

²Centre Algatech, Institute of Microbiology of the Czech Academy of Sciences, Novohradská 237, Třeboň, 37901, Czech Republic.

³School of Biological Sciences, University of Southampton, SO17 1BJ Southampton, UK

⁴Laboratory of Pathogen Host Interactions, Université Montpellier, France.

* Equal senior and corresponding authors. To whom correspondence should be sent, cyrille.botte@univ-grenoble-alpes.fr

Abstract

Apicomplexan parasites are responsible for major human diseases such as toxoplasmosis and malaria. These obligate intracellular parasites possess a relict non-photosynthetic chloroplast named the apicoplast, which is essential for their survival. Although apicoplast *de novo* synthetic capacities have been well studied, none of the metabolite exporters required for parasite survival has been identified thus far. The absence of canonical chloroplast-like fatty acid, and more generally, lipid transporters in the apicoplast of Apicomplexa raises the question of how can these parasites allow the essential flux of fatty acids from the apicoplast. We thus searched for unusual and/or orphan transporters in the P-type ATPase family from *Toxoplasma gondii*, a model Apicomplexa. We identified an atypical P5-ATPase, which we named *TgFLP12*, and which belongs to a newly identified P5C-ATPase sub-clade. *TgFLP12* localizes to the apicoplast membranes and a comprehensive lipidomic characterization of a deletional mutant line revealed that *TgFLP12* had a negative impact on the incorporation of apicoplast myristic acid into phospholipids and neutral lipids. *TgFLP12* mutant fitness was increased by the addition of exogenous free fatty acids or lysophosphatidic acid. This study underlines the essential role that *TgFLP12* plays in lipid export from apicoplast and starts to scratch the surface of the unanswered question of what are the apicoplast metabolite exporters.

Introduction

The phylum Apicomplexa includes unicellular infectious pathogens that are responsible for major human diseases with heavy human and economic burdens (www.who.org). *Toxoplasma gondii*, the agent of human toxoplasmosis, a global infectious chronic disease that affects about a third of the world population, and *Plasmodium falciparum*, responsible for the most lethal human malaria, affecting hundreds of millions and killing about half a million people every year, both belong to the phylum Apicomplexa. Following their active and rapid invasion into a host cell using their specialized apical complexes, these obligate intracellular parasites require large amounts of specific nutrients to generate their daughter cells, propagate and survive. One such class of key nutrients required for parasite survival are lipids, whose acquisition, synthesis, trafficking, and homeostasis are critical for the intracellular development of parasitic Apicomplexa (Shunmugam *et al.*, 2022).

To maintain intracellular development, as well as a high asexual division rate, Apicomplexa need large amounts of lipids, which they obtain through a combination of host cell scavenging, and *de novo* synthesis *via* the parasite's metabolic pathways. Fatty acids (FA) are the pivotal lipid building block at the center of all scavenging, synthesis, and trafficking pathways. The parasite can sense and metabolically adapts the activity of each FA acquisition pathway (host scavenging *vs de novo* synthesis).

The current consensus is that, on one hand, the parasite constantly and massively scavenges FA directly from the host cell and its external environment (Dass *et al.*, 2021b; Nolan *et al.*, 2018, 2017; Shunmugam *et al.*, 2022). This constant flux of host FA is channeled towards parasite lipid storages, i.e. lipid droplets (LD), by *Tg*LIPIN, in the form of triacylglycerol (TAG). LDs are then timely mobilized specifically during parasite division to allow parasite propagation, and avoid lipotoxic/lethal accumulation of FA in the parasite (Dass *et al.*, 2021b).

On the other hand, most Apicomplexa harbor a relict non-photosynthetic plastid named the apicoplast, which was acquired by the secondary endosymbiosis of a red algal ancestor (Köhler *et al.*, 1997; McFadden *et al.*, 1996; Wilson *et al.*, 1996). The apicoplast harbors a prokaryotic type II fatty acid synthesis pathway (FASII) that is essential for parasite survival depending on the parasite life stage and host nutrient content (Amiar *et al.*, 2016b; Vaughan *et al.*, 2009; Waller *et al.*, 1998; Yu *et al.*, 2008). More particularly, the apicoplast FASII acts as the second pivotal provider of FA for the parasite, it plays critical roles when host lipid content varies and becomes lower: the parasite



Figure 1: TgFLP12, a novel P5-ATPase

Maximum likelihood phylogeny of P5-ATPases. The tree was derived by using the best-fit model (LG+F+R7) in IQ-TREE and shows two sets of UFBoot2 supports at branches (1000 replicates). The first set corresponds to P5-ATPase only (114 sequences as shown here) and the second set corresponds to a global dataset of P-type ATPase (207 sequences; Figure S1). The rooting of the P5 clade is shown by the dashed line. Black dots indicate 100/100 support. Dashes indicate supports <80 or a different topology in one of the analyses (supports are not shown where <80 in both analyses). P5 in blue have been characterized and TgFLP12 is in red.

senses it and up-regulates apicoplast FASII activity so it becomes an essential provider of FA for membrane biogenesis and parasite survival (Amiar *et al.*, 2016b; Krishnan *et al.*, 2020; Liang *et al.*, 2020; van Schaijk *et al.*, 2014).

Unlike in photosynthetic plastids, where the FASII essentially provides FA for the *de novo* synthesis of galactolipids that are essential for chloroplast biogenesis and photosynthesis (Nakamura *et al.*, 2007), the function of the apicoplast FASII has been repurposed to fit the obligate intracellular lifestyle of apicomplexan parasites (Amiar *et al.*, 2016b). We, and others, showed that instead of fueling plastidial galactolipid synthesis, the apicoplast FASII provides FA for the bulk synthesis of all parasite phospholipids, which then allows membrane biogenesis and parasite survival (Amiar *et al.*, 2016b). More precisely, stable isotope labeling and lipidomics showed that the parasite uses glycolytic intermediates to generate short FA C12:0, C14:0, and C16:0 *via* the apicoplast FASII. These FA are (i) used *via* a plant-like acyltransferase TgATS1/G3PAT to form a central lysophosphatidic acid (LPA) precursor that is exported to the ER and combined with host scavenged FA to form an “obligate patchwork PA”, as a central precursor for bulk phospholipid synthesis. FA can also be (ii) directly exported from the apicoplast to the ER, for further elongation and later incorporation for bulk phospholipid synthesis as well. Hence, FA (and LPA) have to be exported from the apicoplast to reach ER and cytosol for further elongation and incorporation into phospholipids.

Despite the apparent importance of trafficking metabolites to and from the apicoplast, only a handful of apicoplast transporters have been identified thus far (Boucher *et al.*, 2018; Kloehn *et al.*, 2021b; Mullin *et al.*, 2006; Sayers *et al.*, 2018a). Importantly, although essential chloroplast lipid transporters have been identified and characterized in plants, such as ABC transporters for PA export called TGDs (Fan *et al.*, 2015; Lu *et al.*, 2007; Roston *et al.*, 2011), and fatty acid exporters (FAXs) (Li *et al.*, 2020, 2015). No homolog could be found in Apicomplexa, suggesting their potential loss during evolution. Taken together, this leads to the central question: What is (are) the transporter(s) responsible for exporting lipids and FA from the apicoplast of apicomplexan parasites?

P-Type ATPases are ubiquitous membrane-bound and selective transporters that use the energy from ATP hydrolysis to transport substrates to the cytosol across the plasma or organellar membrane. They are divided into 5 sub-families based on their substrate specificities (Palmgren and Nissen, 2011a). P1-, P2- and P3-ATPases are known as cationic transporters, one famous

example of P2-ATPase being the SERCA protein that triggers calcium release from the ER in most eukaryotes (Nemirovskaya and Sharlo, 2022). The two last families P4 and P5, are present only in eukaryotic cells and have so-called “giant substrates”. P4-ATPases are known as amino-phospholipid flippases that can transport lipids across biological membranes with key roles for lipid trafficking, lipid homeostasis, and membrane asymmetry. Their presence and essential roles, notably for microneme secretion and parasite invasion/egress, have recently been revealed in *Toxoplasma* (Bisio *et al.*, 2021, 2019; Bullen *et al.*, 2016; Günay-Esiyok *et al.*, 2019; Günay-Esiyok and Gupta, 2020; Katris *et al.*, 2020). The last and least characterized sub-family, the P5-ATPase, is the most peculiar because it has no defined canonical substrate. The P5-ATPase is currently divided into two clades: the P5A and P5B, which localize to the ER membranes, and the vacuole or lysosome membrane respectively (Palmgren and Nissen, 2011a).

In this study, we identified a novel putative P5-ATPase transporter in *Toxoplasma gondii*, which we named *TgFLP12*. *TgFLP12* localizes to the apicoplast and is critical for parasite survival. Using lipidomics, lipid flux analyses by stable isotope labeling, and substrate complementation

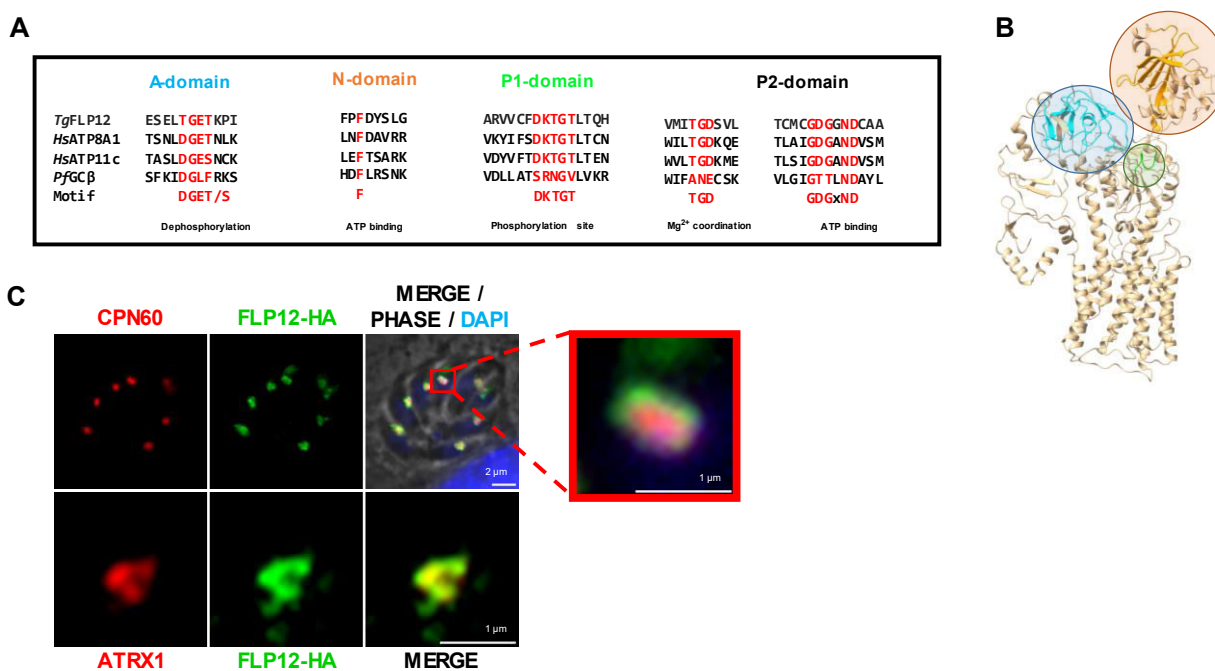


Figure 2: *TgFLP12*, a putative transporter of the apicoplast

(A) Cytosolic P-type ATPase conserved domains, A-domain = Actuator domain (blue), N-domain = Nucleotide domain (orange), and P1- and P2-domains = Phosphorylation domain (green and black). (B) Phyre2 3D model based on yeast P5-ATPase homology and obtained with ChimeraX 1.2.5, blue = A-domain, orange = N-domain, and green = phosphorylation site. (C) *TgFLP12*-HA apicoplast localization was determined by IFA with intracellular markers and observed by epifluorescence (top panel) or confocal (lower panel) microscopy. Blue = Hoechst, Red = apicoplast markers (Stromal CPN60 and outer-most membrane ATRx1), and green = 3xHA tag.

approaches on an inducible *TgFLP12* knock-down parasite line, we reveal that, unlike plant and algal chloroplasts, the apicoplast of *T. gondii* uses *TgFLP12* as its FA exporter to maintain lipid synthesis, membrane biogenesis, and parasite survival. This further reveals the complex metabolic pathways put in place by Apicomplexa through their evolution as obligate intracellular parasites to provide the lipids essential for their propagation.

Results

TgFLP12 belongs to a new clade of P5-ATPase

We hypothesized that apicoplast FA transporter might fall in the P-type ATPase transporter family. To identify such possible ATPase involved in the apicoplast lipid transfer in *Toxoplasma gondii*, we screened its genome for P-type ATPase transporters, using the sequence of known P-type ATPases from *Saccharomyces*. Several P-type transporters have already been identified and characterized in *Toxoplasma*, such as the ER-resident P2-ATPase transporter *TgSERCA*, located in the ER membrane for calcium storage (Nagamune *et al.*, 2008), the P3-ATPase *PMA1* involved in bradyzoite differentiation (Holpert *et al.*, 2006), as well as several lipid P4-ATPases involved in parasite microneme secretion, invasion, and egress (Bisio *et al.*, 2021, 2019; Chen *et al.*, 2021).

This allowed us to identify a total of 18 putative P-Type ATPases in *T. gondii* (**Figure 1, Figure Supp 1**): 8 putative cation transporters belonging to families P1, 2, and 3 Types ATPases, 6 putative P4-ATPases/lipid flippases, and two putative P5A/B ATPases. Interestingly, the phylogenetic screening allowed us to identify two peculiar P-type ATPases of which, *TGME49_289070*, which we named *TgFLP12* due to its twelve transmembrane domains. *TgFLP12* bore all typical cytosolic domains found in P-Type ATPases, the actuator (A)-domain (**Figure 2 A, B**, light blue), the nucleotide-binding domain (orange), and support domain (green) (N-domain and P2-domain respectively) and the Phosphorylation domain (P1-domain) (**Figure 2 A, B**). Phylogenetic analysis of *TgFLP12*, which allowed the identification of its homolog in *Plasmodium falciparum* (PF3D7_0504000), showed that both proteins belong to the P5-ATPase subfamily. Interestingly, it seemed that the gene has independently duplicated in *Cryptosporidium* (an Apicomplexan parasite devoid of apicoplast) and coccidians, both bearing different copies of the gene with different predicted localization (Barylyuk *et al.*, 2020). P5-ATPases are known to be subdivided into two clades. The P5A clade members have been localized into the ER membrane where they can export mistargeted mitochondrial (McKenna *et al.*, 2020) or import small Wnt proteins (T. Li *et al.*, 2021a).

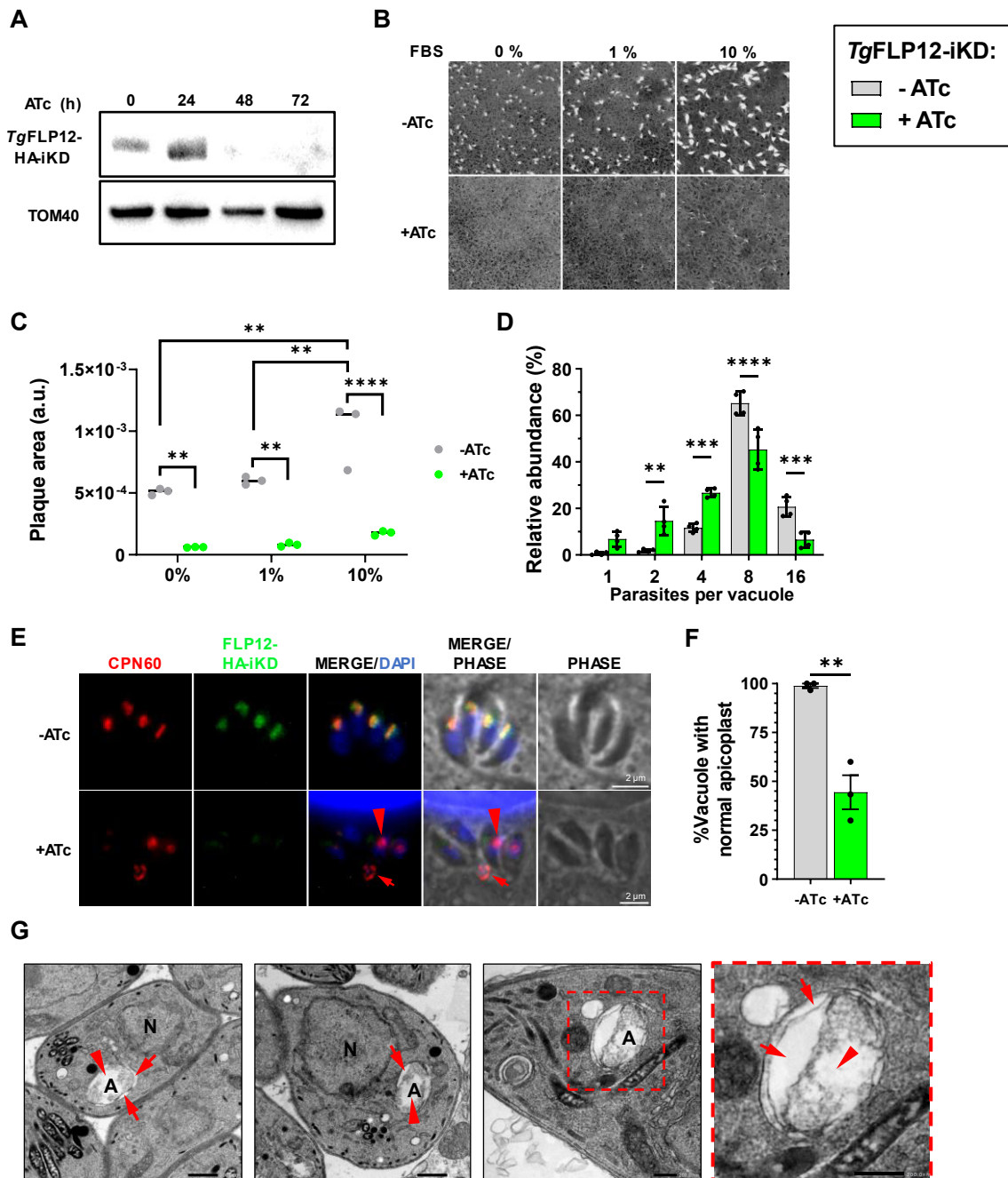


Figure 3: *TgFLP12* disruption is detrimental to tachyzoite development and apicoplast maintenance

(A) Inducible knockdown of *TgFLP12* in the *TgFLP12*-HA line after promoter replacement. *TgFLP12* was detected by western-blot using Rt anti-HA antibody, and complete shutdown of the protein occurred after 48h of ATc treatment (Numbers indicate hours of culture). TOM40 (lower panel) served as a loading control. (B) Detrimental effect of *TgFLP12* loss shown by plaque assays performed in the absence (-) or presence (+) of ATc and with different FBS concentrations (0, 1, and 10%) and fixed after 7 days. (C) Plaque size quantification and statistics from plaque assay panel (B), two-way Anova, and means are compared from 3 independent experiments. (D) The absence of *TgFLP12* reduced the intracellular replication of *Toxoplasma* tachyzoites, two-way Anova multiple comparisons, error bars represent +/- SD from 4 independent experiments. (E) Apicoplast disruption in absence of *TgFLP12* revealed by IFA and using an anti-CPN60 antibody, Blue = Hoechst, Red = apicoplast marker CPN60, and green = 3xHA tag. (F) Statistical analysis of the apicoplast disruption after complete shutdown of *TgFLP12* expression, error bars represent +/- SD from 3 independent experiments. (G) Transmission electron microscopy showing apicoplast morphology after 48 h of ATc treatment on *TgFLP12*-iKD, apicoplast appeared swelling and accumulating electron light material in the stroma (redhead arrows) as well as in the intermembrane spaces (red arrows).

ns $p > 0.05$, * $p \leq 0.05$, ** $p \leq 0.01$, *** $p \leq 0.001$, and **** $p \leq 0.0001$.

The P5B clade ATPases, usually localize at vacuolar or lysosomal membranes, and recent data show that one member could transport polyamine-containing molecules (spermidine/spermine) from the lysosome to the cytosol (De La Hera *et al.*, 2013; Van Veen *et al.*, 2021). Surprisingly, *TgFLP12* does not cluster to any of the previously mentioned P5A- or P5B-ATPases but rather to a third and newly identified clade that we called P5C-ATPase. The P5C clade is absent from animals, yeasts, and

flowering plants, but is present in a range of other eukaryotes including fungi, basal land plants such as mosses, and numerous protists such as diatoms, oomycetes and alveolates (**Figure 1**). This data suggests that *TgFLP12* is a novel P5C-ATPase in *Toxoplasma gondii* that could transport some type of macromolecule.

***TgFLP12* is an apicoplast membrane protein**

The localization of *TgFLP12* was unclear based on existing information. *TgFLP12* has no predicted N-terminal targeting sequence, such as the bipartite signal characteristic of apicoplast targeting. Its predicted localization by HyperLOPIT (Barylyuk *et al.* 2020, ToxoDB.org) suggests that it would be a Golgi and/or Plasma membrane protein whereas immunofluorescence assay (IFA) on its murine malaria agent (*P. berghei*) homolog revealed an apicoplast localization (Sayers *et al.* 2018). Thus, to determine the actual localization of *TgFLP12* *in vivo* in *Toxoplasma*, we generated an HA-tagged *TgFLP12* parasite line by inserting the coding sequencing of a triple hemagglutinin (3xHA) epitope-tag to the 3' end of *TgFLP12* gene using the pLIC strategy (Huynh and Carruthers, 2009), all validated by a PCR screen (**Figure Supp 2 A, B**). Immunofluorescence assays (IFAs) revealed that, *TgFLP12*-HA co-localized with the apicoplast stromal marker, chaperonin 60 (CPN60) (**Figure 2 C**) similar to the *P. berghei* homolog (Sayers *et al.*, 2018b). More specifically, we observed an accumulation of the HA signal on the periphery of the apicoplast (**Figure 2 C**), suggesting localization in the apicoplast membranes. To confirm this hypothesis, we performed further IFAs with the apicoplast outermost membrane marker, Apicoplast Thioredoxin 1 (ATR_x1) using confocal microscopy. This confirmed the apicoplast localization and revealed a robust colocalization of ATR_x1 with the 3xHA signal (**Figure 2 C**, lower panel), strongly pointing at an apicoplast membrane localization of *TgFLP12*. Western-blot analysis further confirmed the predicted molecular weight of *TgFLP12* at ~220 KDa (**Figure Supp 2 E**).

***TgFLP12* is essential for tachyzoite development and apicoplast integrity**

To investigate the functional role of *TgFLP12*, and following its negative phenotypic score of -3.25 (Sidik *et al.* 2016, ToxoDB.org), an inducible knock-down strain was generated. Using the promoter replacement TATi-TET system facilitated by a CRISPR-Cas9 approach (Bullen *et al.*, 2016) (**Fig Supp 2 A**) in the *TgFLP12*-HA strain we obtained the *TgFLP12*-HA-iKD strain. Integration of the exogenous promoter to the correct locus was confirmed by PCR (**Figure Supp 2 D, E**). The depletion of the *TgFLP12* protein was confirmed by western blot after 48 h of anhydrotetracycline (ATc) treatment (**Figure 3 A**).

We then performed a plaque assay on the inducible KD strain to assess its role in parasite development. The disruption of *TgFLP12* induced a drastic reduction of the plaque size in the presence of ATc, demonstrating the importance of the protein for intracellular development (**Figure 3 B, C**). As a negative control, the ATc treatment showed no effect on parasite development and plaque size in the parental strain (**Figure Supp 2 F**). We, and others, have recently revealed that the parasite can adapt its metabolic program to host nutrient content and that some proteins become more or less important if the host corresponding nutrient is high or low (Amiar *et al.*, 2020b; Dass *et al.*, 2021b; Krishnan *et al.*, 2020; Shunmugam *et al.*, 2022; Walsh *et al.*, 2022). To assess whether *TgFLP12* had a more specific role in cases under fluctuating nutrient content, *TgFLP12*-iKD was grown under high, normal, or low nutrient/lipid content at 10%, 1%, or 0% FBS content, respectively, as previously described (Dass *et al.*, 2021b). We performed plaque assays and found no significant change in plaque size between the different nutrient conditions despite a slight trend to size increase with increasing concentration of FBS (**Figure 3 B, C**). All parasite lines lacking *TgFLP12* displayed very low or almost absence of growth in any nutrient conditions compared to the WT, suggesting that *TgFLP12* essentiality is directly not dependent on nutrient availability.

To further assess the importance and role of *TgFLP12* for parasite intracellular development, we conducted replication assays in the *TgFLP12*-HA-iKD line and compared it to the WT. Tachyzoite replication was likewise significantly impacted upon the disruption of *TgFLP12*: there was a significant decrease in the number of large vacuoles with a drop from ~65% to ~45% for vacuoles with 8-stage parasites and ~20% to ~6% for vacuoles with 16 parasites, and a significant accumulation in small vacuoles (1-, 2- and 4-stage parasites) in the absence of *TgFLP12* by 3 days pre-treatment and 24 h for the assay of ATc treatment (**Figure 3 D**). These data further demonstrate that *TgFLP12* depletion reduces *Toxoplasma* division rate and therefore reduces parasite fitness.

Since *TgFLP12* is essential and localizes to the apicoplast, we sought to determine whether the depletion of *TgFLP12* could impact the biogenesis, morphology, or presence of the organelle. To do so, we conducted IFA using the stromal apicoplast marker CPN60 to scrutinize the apicoplast (**Figure 3 E**). In WT parasites (i.e. *TgFLP12*-HA-iKD in absence of ATc), the apicoplast forms a single dot per parasite located on the apical part of the parasite. The addition of ATc, which suppresses *TgFLP12*, led to the loss of the apicoplast in most parasites within the same vacuole and/or a swelling of the few ones remaining (**Figure 3 E**, lower panel red head arrow). Furthermore, the apicoplast was also sometimes found as a signal at the residual body (**Figure 3 D**, lower panel red arrows). This mislocalization of fluorescence in the *TgFLP12*-depleted parasites was quantified and 60% of vacuoles presented a CPN60 signal that localized to the residual body (**Figure 3 F**). Together, this data demonstrates that *TgFLP12* is essential for *Toxoplasma* tachyzoite development and the maintenance of the apicoplast. While the apicoplast is disrupted by *TgFLP12* deletion, *Toxoplasma* mitochondria was not affected after ATc treatment and *TgFLP12* loss, as the intracellular parasites have conserved their lasso shape-like form (**Figure Supp 3**). Similar results were previously obtained in the apicoplast ACP (a key enzyme of the FASII pathway) mutant deletion of the protein led to the disruption of the apicoplast but the mitochondria remained unchanged (Mazumdar *et al.*, 2006).

Transmission electron microscopy was performed on parasites treated and untreated with ATc for 48h. Parasites depleted for *TgFLP12* were mostly similar to WT parasites with soundly shaped apical machinery (micronemes, rhoptries, and conoid), and no visible change in the mitochondria, ER, nucleus, or Golgi apparatus. The only change observed was an enlarged apicoplast with the accumulation of low-density material within the stroma (redhead arrows) as well as between the membranes (red arrows; **Figure 3 G**). Down-regulation of *TgFLP12* rapidly led to a morphological change of the apicoplast within 48 h (**Figure 3 G**) that resulted in the longer-term, to the loss of the plast (**Figure 3** Error! Reference source not found. **E**, lower panel).

Because *TgFLP12* belongs to a family of macromolecule transporters, its disruption leads to an alteration of the apicoplast within a short time after repression, and the apicoplast is a place of *de novo* lipid synthesis, we decided to determine the impact of *TgFLP12* loss on the parasite lipid content.

TgFLP12 deletion alters parasite short FA chain content

Since *TgFLP12* could act as a lipid transporter of the apicoplast, we investigated the lipidome of *TgFLP12*-depleted parasites. *TgFLP12*-HA-iKD parasites were grown for three days with ATc (+ATc, green bars) and harvested to compare to the untreated one (-ATc, grey bars). The total lipid was extracted and its total fatty acid was determined by gas chromatography and mass spectrometry (GC-MS, Agilent 7890B-5977A). The total fatty acids abundance did not significantly change between parasites with and without ATc (**Figure 4 A**). However, their fatty acid composition had significant differences, FA species are commonly labeled Cx:y, x being the number of carbon that

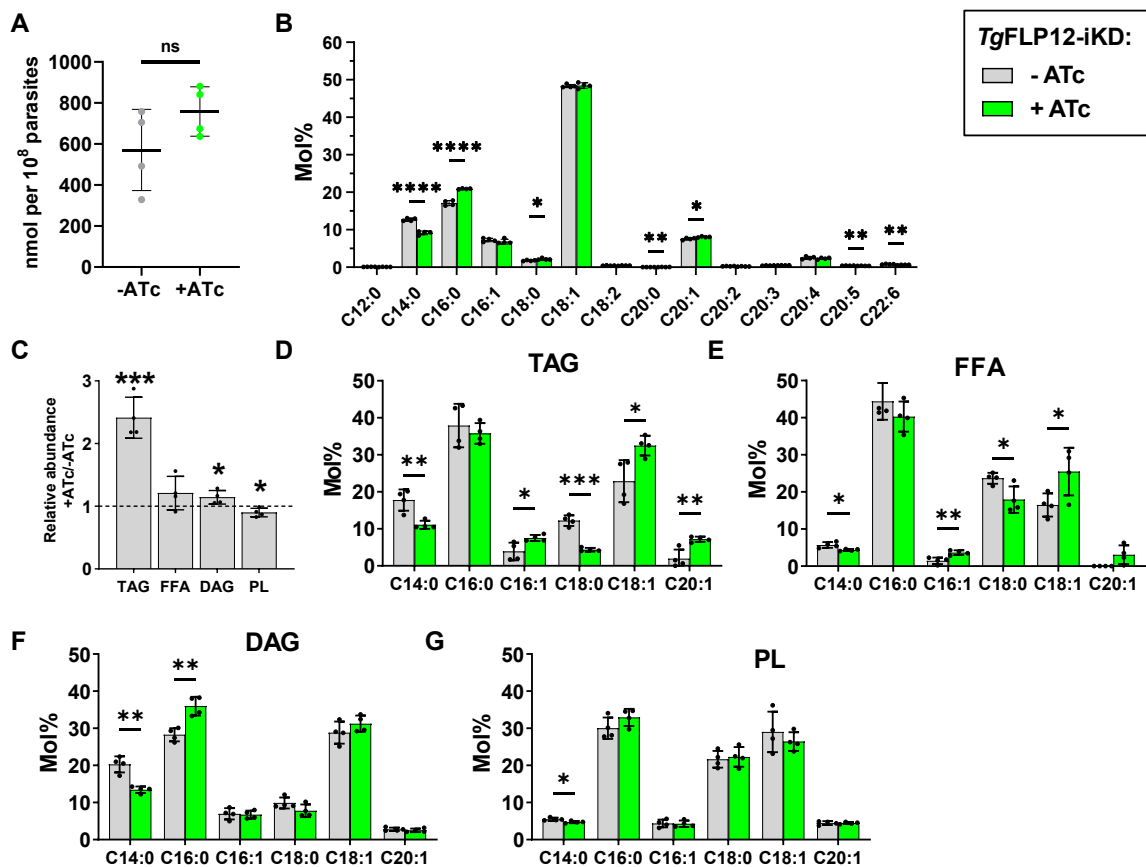


Figure 4: Lipidomic analysis of *TgFLP12* revealed a general decrease in the composition of myristic acid

(A) FA total amount, quantified by GC-MS is unchanged after *TgFLP12* repression, error bars represent +/- SD of 4 independent experiments. (B) FA composition in Mol% of *TgFLP12* lacking parasites (+ATc) compared to parasites harboring *TgFLP12*, error bars represent +/- SD of 4 independent experiments. (C) Lipid composition revealed by one dimension TLC and GC-MS showed a decrease in phospholipids and an increase in neutral lipid TAG and DAG in parasites without *TgFLP12* (+ATc) compared to parasites with *TgFLP12*, error bars represent +/- SD of 4 independent experiments. Major FA relative abundance of (D) triacylglycerols (TAG), (E) free fatty acids (FFA), (F) diacylglycerols (DAG), and (G) phospholipids (PL), error bars represent +/- SD of 4 independent experiments. ns $p > 0.05$, * $p \leq 0.05$, ** $p \leq 0.01$, *** $p \leq 0.001$, and **** $p \leq 0.0001$.

made the chain and γ the number of unsaturation. The relative abundance of myristic acid (C14:0) decreased and that of palmitic acid (C16:0) increased (**Figure 4 B**). Since C14:0 originate from *de novo* fatty acid synthesis by FASII in the apicoplast, *TgFLP12* may be involved in the export of lipid products containing short-chain fatty acid C14:0.

We also observed a slight but significant increase in the relative abundance for C18:0, C20:0, and 20:1 and a decrease in C20:5, 22:6 FA. These results were the impact of *TgFLP12* deletion as the parental strain Δ Ku80 TATi showed no change in the FA quantity (**Figure Supp 4 A**) and FA composition (**Figure Supp 4 B**) upon ATc treatment.

In order to see the detailed difference of fatty acids in each lipid species, total lipid was separated by high-performance thin layer chromatography (HPTLC). *TgFLP12* mutant had a different composition of lipids that a slight but significant decrease in phospholipids compared to WT parasites (**Figure 4 C**) and a ~2.5-fold increase in the composition of TAG as well as a significant increase in diacylglycerol (DAG) (**Figure 4 C**). Free fatty acids (FFA) seemed to be more abundant in *TgFLP12*+ATc compared to *TgFLP12*-ATc but the difference was not significant. We next measured how *TgFLP12*-depleted tachyzoites differ in individual phospholipid species, which are known to have different structural and signaling roles. Using a targeted phospholipid-specific analysis, we found that levels of most phospholipids were not significantly different between *TgFLP12*-ATc and *TgFLP12*+ATc parasites. However, there was a significant decrease in phosphatidylcholine (PC) the major membrane phospholipid in *TgFLP12*-depleted parasites compared to *TgFLP12*-ATc (**Figure Supp 4 C**). This decreased PC supported the previously observed decrease in total PLs (**Figure 4 C**).

TAG had a significant decrease in its composition of C14:0 and C18:0 in *TgFLP12*+ATc compared to *TgFLP12*-ATc and an increase in the composition of C16:1, 18:1, and C20:1 after the shutdown of *TgFLP12* (**Figure 4 E**). Building blocks of the different classes of lipids, FFA had a composition in FA almost identical to TAG, with a significant decrease in the composition of C14:0 and C18:0, and a significant increase in C16:1, 18:1 (**Figure 4 F**). DAG had a significant decrease in C14:0 and an increase in C16:0 relative abundance (**Figure 4 G**). Despite previously observing a significant reduction in phospholipid composition (**Figure 4 C**), all phospholipids together only showed a small yet significant decrease in C14:0 while all other FA species composition did not seem affected by the depletion of *TgFLP12* (**Figure 4 H**). The common feature we observed for all the different lipid families was a significant decrease in myristic acid C14:0 composition which

was also observed in the global lipid FA composition. Myristic acid is known to be made by the apicoplast which is consistent with our apicoplast localization of *TgFLP12*. The general decrease in short FA C14:0 suggested an inhibition of the apicoplast FASII activity while the increase in TAG suggested an increase in FA scavenging.

Disruption of *TgFLP12* causes a defect in apicoplast FASII activity as revealed by ^{13}C lipid flux analysis

Since the loss of *TgFLP12* leads to a decrease in the composition of C14:0 which are produced in the apicoplast, FASII may have lower activity in the absence of *TgFLP12*. To determine if the FASII activity in the apicoplast was reduced in the absence of *TgFLP12*, we performed state-of-the-art stable isotope labeling. Briefly, *TgFLP12*-iKD parasites were grown 72 h in presence of 8 mM ^{13}C -U-Glucose and in the presence or absence of ATc, and FA content in harvested parasites was analyzed by GC-MS. FAs made by the parasite appeared to have a mass shift of M+1 for each ^{13}C carbon incorporated within the chain. First, the real abundance of ^{13}C carbon labeled FA to each FA species was determined. The abundance of labeled FA was similar in both WT and *TgFLP12* mutants suggesting that FASII is still active in the *TgFLP12* mutant during the 72 h of incubation with ^{13}C -U-Glucose (**Figure 5 A**). Surprisingly, in some fatty acid species such as C16:0, C18:0, and 18:1, the abundance of ^{13}C labeled FA was higher in the mutant while the abundance of C14:0 did not change suggesting there is some alteration of FASII activity or the fate of FAs from the FASII (**Figure 5 A**).

Although the abundance of C14:0 made by FASII during 72 h did not alter, its mass isotopomer distribution (MID) changed importantly (**Figure 5 B**). Both WT and mutant had the ^{13}C incorporation up to the M+14, fully labeled with ^{13}C , suggesting the FASII is fully active in both with a two by two increase of the mass typical from the FASII activity. However, in the mutant, the species fully labeled, i.e. C14:0 M+14 is lower than that of WT. This is consistent with the lower abundance of C14:0 in the total fatty acids (**Figure 4 B**). In C16:0 MID, the mutant contained a higher abundance of C16:0 M+14 than that of WT (**Figure 5 C**). This suggests two possibilities: FAs myristic acid, C14:0 underwent another round of elongation through the FASII pathway and then was exported outside of the apicoplast as palmitic acid C16:0 to be elongated. Parasites could also have been incubated for too long with ^{13}C -U-Glucose, with the increased activity in the mutant the culture was running out of labeled glucose and the last steps of elongation within the apicoplast occurred with unlabeled carbons. Also, the increased activity could have occurred during the loss of *TgFLP12* as the total protein shutdown happened after 48 h of ATc treatment.

To test these hypotheses, we treated the parasite culture with ATc for 48 h (two-day pre-treatment) before the addition of ^{13}C -U-Glucose and further incubation for 24 h before parasites harvest, lipid extraction, and analysis (**Figure Supp 5 B**). Interestingly, labeled FA abundance of each FA species showed a general decrease of labeled FA in the mutant yet significant for C16:0 and C18:1 (**Figure 5 D**). This confirmed that the increase in FASII activity previously observed for 72 h was certainly happening during the loss of *TgFLP12*. Labeling after the complete loss of the protein showed a decrease in the FASII activity. MID profiles of C14:0 (**Figure 5 E**) and C16:0 (**Figure 5 F**) revealed a significant decrease in the ^{13}C incorporation within all FA chains for both products, consistent with the drop in C14:0 composition.

Previous studies illustrated that FASII products exit the apicoplast to reach the ER to be elongated. To determine if *TgFLP12* had an impact on FA elongation into the ER, we measured parasite elongation activity by complementing the culture media with 8 mM ^{13}C -U-Acetate, which is used by the ER elongases (ELO A, B, and C) to elongate/desaturate FA (**Figure Supp 5 A**). Elongated FAs were measured and quantified by GC-MS (Dubois *et al.*, 2018a; Ramakrishnan *et al.*, 2012a). After complete repression of *TgFLP12* for 48 h and 24 h of incubation with ^{13}C -U-Acetate, we observed that parasite elongation was still active. While FAs made by FASII were affected, the real abundance of the elongated FAs showed no difference between the WT and the mutant (**Figure 5 G**). As for the measurement of FASII activity, the elongation had been measured for 24 h after complete repression of *TgFLP12*, to avoid acetate degradation. MID of long-chain FAs C20:0 (**Figure 5 H**) and C24:0 (**Figure 5 I**) showed an accumulation of M+4 and M+8 products respectively in the mutant, meaning that more C20:0 and 24:0 have been elongated from C16:0 chains, which probably originated in the apicoplast. This was also observed for other elongation products like C18:0, C18:2, C20:1, and C22:0 (**Figure supp 7 D, F, G, and H** respectively).

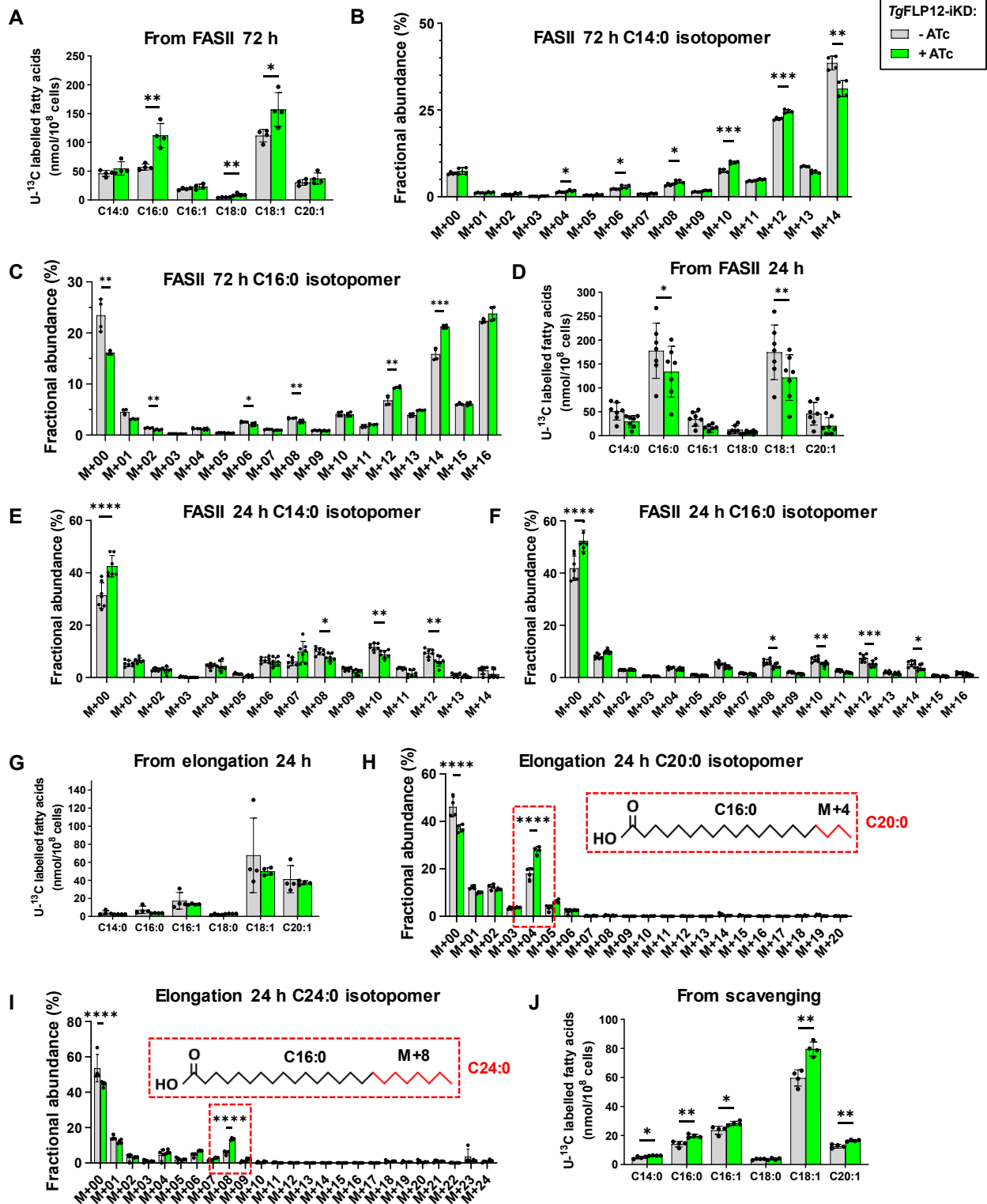


Figure 5: ¹³C labeling revealed a decrease in FASII activity and an increase in lipid scavenging in absence of TgFLP12

(A) TgFLP12-iKD FA abundances with ¹³Carbon incorporated by parasite *de novo* FASII in the presence and absence of ATc after 72 h incubation 8 mM ¹³C-U-Glucose, error bars represent +/- SD from 4 independent experiments. Mass isotopomer distribution of (B) C14:0 and (C) C16:0 showing the incorporation of ¹³C by FASII 72 h into the FA chains, M+ indicates the number of ¹³carbon incorporated per chain, error bars represent +/- SD from 4 independent experiments. (D) TgFLP12-iKD FA abundances with ¹³Carbon incorporated by parasite *de novo* FASII in the presence and absence of ATc after 24 h incubation with 8 mM ¹³C-U-Glucose after complete loss of TgFLP12 = 48 h incubation with ATc before ¹³C-U-Glucose addition, error bars represent +/- SD from 7 independent experiments. Mass isotopomer distribution of (E) C14:0 and (F) C16:0 showing the incorporation of ¹³C by FASII 24 h into the FA chains, M+ indicates the number of ¹³carbon incorporated per chain, error bars represent +/- SD from 7 independent experiments. (G) TgFLP12-iKD FA abundances with ¹³Carbon incorporated by parasite elongation in the presence and absence of ATc after 24 h incubation with 8 mM ¹³C-U-Acetate, error bars represent +/- SD from 4 independent experiments. Mass isotopomer distribution of (H) C20:0 and (I) C24:0 showing the incorporation of ¹³C by elongation 24 h into the FA chains, M+ indicates the number of ¹³carbon incorporated per chain, error bars represent +/- SD from 4 independent experiments. (J) TgFLP12-iKD FA abundances with ¹³Carbon incorporated by the host and scavenged by the parasite in the presence and absence of ATc, error bars represent +/- SD from 4 independent experiments. ns p > 0.05, *p ≤ 0.05, **p ≤ 0.01, ***p ≤ 0.001, and ****p ≤ 0.0001.

As previously reported in Amiar *et al.* 2020 and Shunmugam, Dass *et al.* 2021, *de novo* FASII and host lipid scavenging work as a balance, each being increased when the other is decreased and vice-versa. To examine the contribution of host scavenging to TgFLP12 depleted parasites and specifically examine if host scavenging is altered during TgFLP12 shutdown, we used a novel labeling experiment in which tachyzoites are grown on host fibroblasts pre-fed with ¹³C-U-Glucose (Dass *et al.*, 2021b). The host cells are seeded into new flasks and are grown in the presence of ¹³C-U-Glucose which was then incorporated into host lipids *via* the mammalian cytosolic FASI system. We analyzed the global fatty acid abundance of TgFLP12-iKD -ATc or +ATc grown on pre-labeled HFF, and we found that TgFLP12 depleted parasites scavenged significantly more C14:0, C16:0, C16:1, C18:1 and C20:1 (**Figure 5 J**), which is broadly the opposite of the general decrease observed in FASII after total loss of TgFLP12, and consistent with the complementary roles of the two lipid sources. Analysis of the major lipid classes PLs, TAGs, DAGs, and FFAs sourced by host scavenging revealed that TgFLP12+ATc had a nearly 6-fold increase in neutral lipid TAG and FFA (**Figure Supp 4 D**). Global increase in neutral lipids (**Figure 4 C**) is supported by increased scavenging fluxed toward neutral lipids (**Figure 5 J, Figure Supp 4D**) and is correlated with the previous work on TgLIPIN (Dass *et al.*, 2021) showing that scavenged lipids are fluxed to lipid storage (**Figure Supp 4 D**). The apicoplast is the sole place for *de novo* FA synthesis, lipid products i.e. FFA, LPA, and PA need to be exported outside of the apicoplast for lipid reshuffle, phospholipid synthesis and thus membrane biogenesis (Amiar *et al.*, 2016b).

TgFLP12 is responsible for free fatty acid export from the apicoplast

TgFLP12 depletion impacts the global lipid composition of the parasite, particularly C14:0 the main product of the apicoplast. P5- as P4-ATPases are known to be giant substrate transporters. To determine which lipid classes were affected by TgFLP12 depletion, lipids labeled with ¹³C by

FASII for 72 h were separated by 1D HP-TLC and quantified by GC-MS. No difference was observed in the abundance of PL, TAG, and DAG originating from FASII. Despite the FASII activity increases at 72 h, the abundance of FFA sourced by FASII was reduced by 30 % in the *TgFLP12* mutant (**Figure 6 A**). Moreover, the incorporation of ¹³C by FASII in only C14:0 from FFA was significantly reduced in the mutant (**Figure 6 B**), the same feature was observed on DAG and PL from FASII but not on TAG (**Figure Supp 8 A, B, and C**). These different elements suggested a default for short apicoplast C14:0 to exit the apicoplast and fueled the bulk of FFA for membrane synthesis as well as lipid storage.

As mentioned previously, the apicoplast is the place of essential metabolic pathways, like FASII or heme synthesis, which require yet unknown exporters for their final metabolites to exit the apicoplast (Kloehn *et al.*, 2021b). Recent findings on P5-ATPases have shown some of them to be polyamine transporters (De La Hera *et al.*, 2013; Van Veen *et al.*, 2021). Based on the flexibility of *Toxoplasma* to rescue essential enzymatic pathways by scavenging, we decided to perform plaque assays supplemented with known scavenged metabolites and observe if we rescued the $\Delta TgFLP12$ death phenotype.

Previous data from this study collectively strongly suggests that *TgFLP12* plays a role in facilitating the export of lipid products from the apicoplast. Specifically, *TgFLP12* seems to have a role in the export of lipids with C14:0 FA chains or the C14:0 chain itself. To test this, we attempted to complement, or rescue the phenotype of *TgFLP12* depleted parasites with possible substrates, 60 μ M FFA C14:0, 60 μ M FFA C16:0, 60 μ M LPA C14:0 and 60 μ M LPA C16:0, similar to previous studies (Amiar *et al.*, 2016b; Krishnan *et al.*, 2020). The addition of LPA C14:0 or LPA C16:0 or FFA C14:0 or FFA C16:0 is not detrimental for the parasite growth as plaques appeared in complemented cultures of *TgFLP12*-ATc like in the uncomplemented one. LPA C16:0 seemed to benefit the parasites' growth (**Figures 6 C and D**).

The addition of exogenous C14:0, C16:0 FFA, or LPA, improved the growth of parasites lacking for *TgFLP12* as plaques were observed in culture complemented with either FFA or LPA (**Figure 6 C, D**). A stronger rescue was observed for FFA C14:0 as more and bigger plaques were observed compared to the other lipid species tested. The number and size of plaques decreased gradually for FFA C16:0, LPA C14:0, and LPA C16:0 in this order (**Figure 6 D, E**).

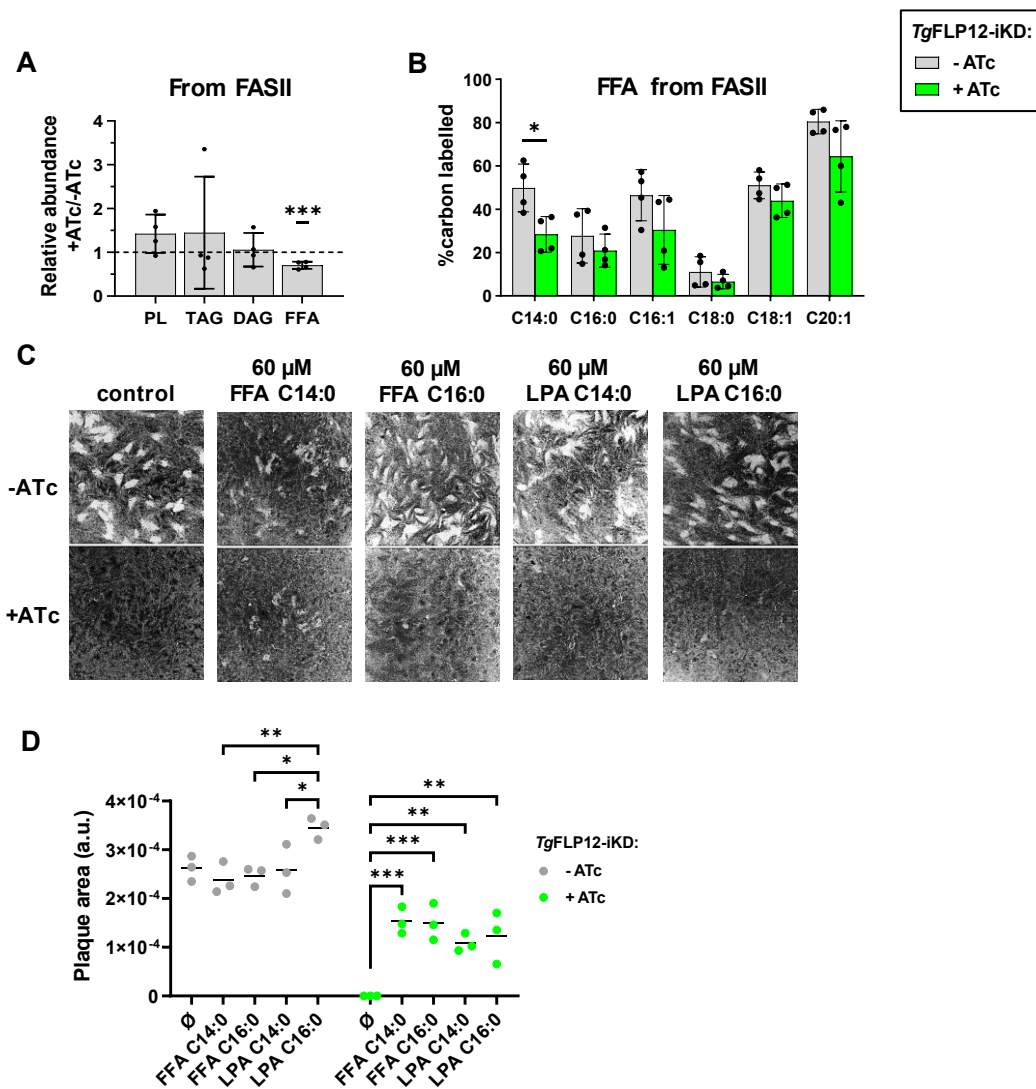


Figure 6: *TgFLP12* is responsible for the exit of FFA from the apicoplast

(A) Relative abundance of TAG, DAG, PL, and FFA originated from parasite FASII, error bars represent +/- SD from 4 independent experiments. (B) Percentage of ¹³C incorporation in major FA species of FFA made by parasite FASII in presence (-ATc) and absence (+ATc) of *TgFLP12*, error bars represent +/- SD from 4 independent experiments. (C) Plaque assays complemented with possible *TgFLP12* substrates, FFA C14:0 or C16:0, and LPA C14:0 or C16:0. (D) Plaque size quantification and statistics from plaque assay panel (C), two-way Anova, and means are compared from 3 independent experiments. ns $p > 0.05$, * $p \leq 0.05$, ** $p \leq 0.01$, *** $p \leq 0.001$, and **** $p \leq 0.0001$.

To assess the heme synthesis pathway, we complemented the culture media with 5-ALA (5-aminolevulinic acid) 300 μ M, already use to complement the CPO mutant, the enzyme that catalyzes the cytosolic step of the heme synthesis after the apicoplast exit (Krishnan *et al.*, 2020), or PPIX (protoporphyrin IX) 300 μ M. Neither 5-ALA nor PPIX was able to restore the growth in *TgFLP12* treated with ATc compared to the *TgFLP12* treated with ATc but not complemented (Figure Sup 7 D).

P5B-ATPases the closest P5 subfamily to the new clade to which *TgFLP12* belongs, have been shown to regulate polyamine trafficking from lysosomes. To assess if *TgFLP12* plays a role in polyamine synthesis, we have cultured *TgFLP12* in the absence or presence of ATc and supplemented the media with spermidine 30 μ M or spermine 30 μ M in 1 mM aminoguanidine to prevent ROS generation from polyamines. Polyamines showed no toxicity as *TgFLP12* -ATc complemented and uncomplemented with polyamines showed similar plaques sizes. Similarly to 5-ALA and PPIX neither spermidine nor spermine was able to complement *TgFLP12* (Figure Supp 7 D).

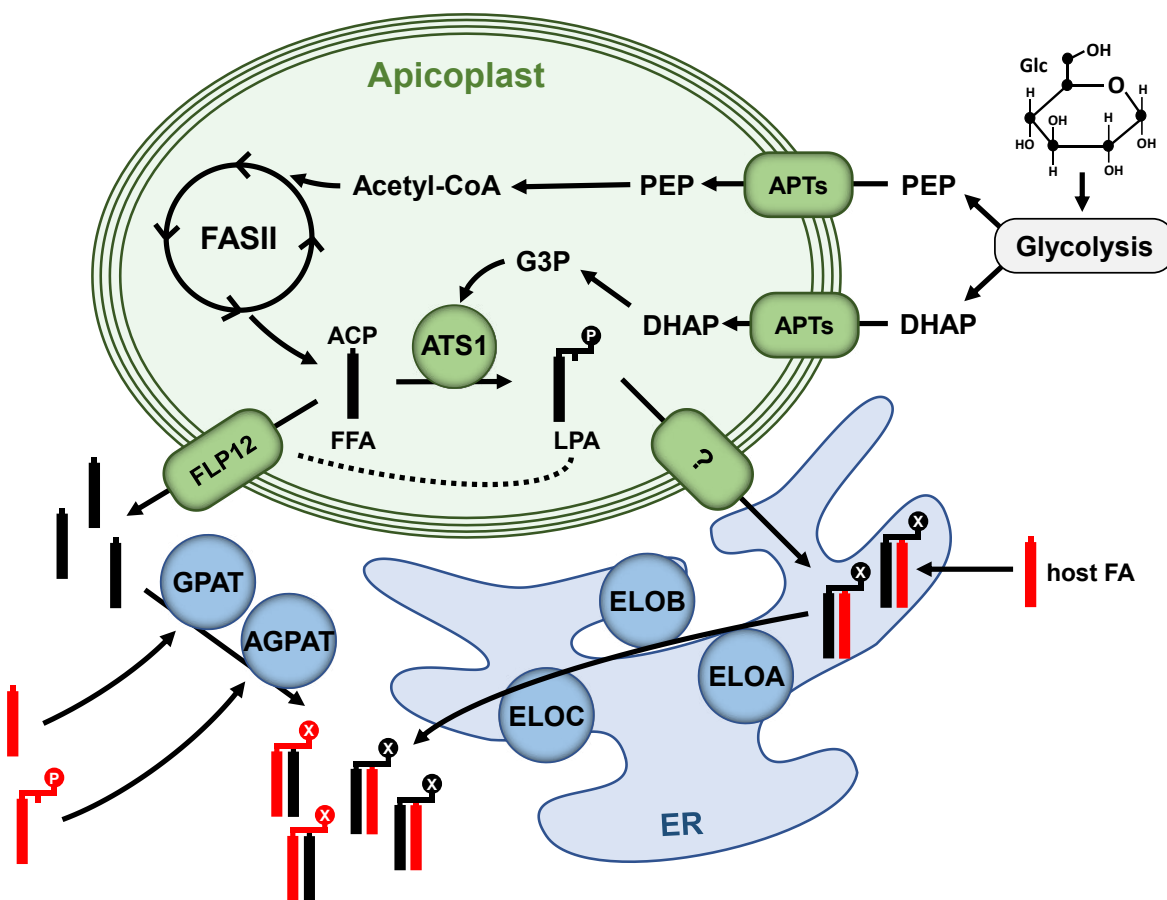


Figure 7: Proposed model for *TgFLP12* function in *Toxoplasma gondii* lipid metabolism

Scavenged glucose is proceeded through the parasite glycolysis pathway. Glycolysis products PEP and DHAP are imported to the apicoplast stroma *via* APT transporters. DHAP is used to form G3P and PEP is converted back to pyruvate and then proceeded to finally form acetate-CoA, which is used by the FASII pathway to generate short FA chains, C14:0. From Amiar *et al.*, 2016, we know that apicoplast FAs can be esterified on a G3P backbone by ATS1 to form LPA, that exit the apicoplast to reach the ER *via* an unknown pathway. This exported LPA serves for phospholipids synthesis and FAs are elongated by the three ER elongases ELO A/B/C. This study suggests the role of *TgFLP12* as an FFA exporter that allows the exit of C14:0 from the apicoplast to be used by the cytosolic acyl-transferases GPAT, AGPAT, etc., and participates to fuel the bulk of phospholipids. PEP = phosphoenolpyruvic acid; DHAP = dihydroxyacetone phosphate; G3P = glycerol-3-phosphate; APTs = apicoplast phosphate transporter; FASII = fatty acid synthesis pathway type II; ACP = acyl-carrier protein; FFA = free fatty acid; ATS1= acyl-transferase 1; LPA = lysophosphatidic acid; ELO = elongase; GPAT = glycerol acyl-transferase; acyl glycerol acyl-transferase.

These results consolidate the lipidomics data which indicate that *TgFLP12* plays a role in exporting lipids from the FASII pathway outside of the apicoplast, with a higher affinity for FFA than LPA and a higher affinity for C14:0 length chain compare to C16:0 chain.

Discussion

P-type ATPases are transporters that export their substrate from the extracellular or lumen space to the cytosol. This study focuses on an essential apicoplast exporter, *TgFLP12* that belongs to a newly identified clade from the sub-family of P5-ATPase never described before, which we called P5C-ATPases. Although absent in most laboratory model species, the new P5C-ATPase family is present in a broad range of eukaryotes and is strongly resolved in the phylogeny pointing to a potentially conserved substrate specificity different from the other P5 clades (**Figure 1, Figure Supp 1**). The relationship between P5B-ATPases and P5C-ATPases remains unclear because P5B-ATPases do not form a strongly supported clade and members of neither group have been functionally characterized in different taxa. The P5C-ATPase family shows several examples of secondary gene duplication events, including two specific to *Cryptosporidium*. The origin of the coccidian P5C-ATPase duplication is more difficult to pinpoint because deep relationships between apicomplexan sequences are not confidently resolved (support >95). While *TgFLP12* colocalized with ATRx1 at the outermost membrane of the apicoplast (**Figure 2 C**), a LOPIT experiment in *Toxoplasma* predicted its paralog to localize to the rhoptries. Rhoptries are present in all apicomplexans, which may help to explain why P5C-ATPase is present in the apicoplast-lacking *Cryptosporidium*. Indeed, since P5C-ATPase is found in many non-photosynthetic eukaryotes (**Figure 1**), the apicoplast FA transport in apicomplexans is apparently a derived state. Notably, P5A has been recently shown to transport proteins across the ER membrane (T. Li *et al.*, 2021a) and P5B to export polyamines from the lysosome to cytosol (De La Hera *et al.*, 2013; Van Veen *et al.*, 2021). Given that the ER and lysosomal membranes are topologically equivalent with both, the membrane of (Golgi-derived) rhoptries and the outermost membrane of the apicoplast, it appears likely that P5 and P5C-ATPases were both ancestrally functionally connected with the endomembrane system.

Despite the essentiality of the apicoplast metabolic pathways, little is known about metabolite importers and exporters involved in these pathways as summarized in a recent review (Kloehn *et al.*, 2021b). *TgFLP12* is a putative transporter of the apicoplast, and our data demonstrate that its disruption is deleterious for the apicoplast integrity (**Figure 3 D, E**) as well as the parasite survival

(**Figure 3 B, C**). From this, we wanted to elucidate the metabolic pathway in, which *TgFLP12* was involved.

In *Plasmodium*, putative transporters have been localized or predicted to localize to the apicoplast (Boucher *et al.*, 2018; Sayers *et al.*, 2018b). Among these transporters, is a *TgFLP12* homolog (*Pf3D7_0504000*, *PbANKA_1103600*) with a confirmed apicoplast localization by endogenous tagging. Straight KO of *Plasmodium berghei* FLP12 homolog demonstrated that its absence did not affect parasite growth during the erythrocytic life cycle (Sayers *et al.*, 2018b). Investigation from Yeh *et al* 2011 (Yeh and DeRisi, 2011), showed the only apicoplast pathway essential for *Plasmodium* blood stage survival was the isoprenoid synthesis pathway as the addition of exogenous IPP was sufficient to maintain an apicoplast-free parasite culture indefinitely. In *Toxoplasma*, intermediate elements of this isoprenoid synthesis pathway (FPP and GGPP) are scavenged from the host (Li *et al.*, 2013), which reduces the essentiality of this pathway in *Toxoplasma* tachyzoite compare to *Plasmodium* blood stage. Plus the essentiality of *TgFLP12* for *Toxoplasma* survival (this study), these elements indicate that *TgFLP12* and its *Plasmodium* homologs are not involved in the isoprenoid metabolite transportation.

Toxoplasma possesses three iron-sulfur cluster pathways, the mitochondria iron-sulfur cluster (ISC) pathway which delivers Fe-S clusters to mitochondrial apoproteins and also fuels with precursors the cytosolic Fe-S cluster assembly machinery (CIA) (Aw *et al.*, 2021; Pamukcu *et al.*, 2021b). Like plants and algae, the Apicomplexa plastid apicoplast also harbors a Fe-S cluster synthesis pathway known as the SUF pathway. All three pathways are essential for normal parasite growth. While the ISC pathway needs a transporter (ATP binding cassette: ABC.B7 in Yeast) to deliver the CIA pathway precursor from the mitochondria to the cytosol, the apicoplast SUF pathway seems to not exporter metabolite and act as an apicoplast housekeeping pathway regulating isoprenoid synthesis (*via TgIspH* and *TgIspG*), the FASII pathway (*via TgLipA*), redox state (*via TgFd*) and apicoplast gene transcription (*via TgMiaB*) (Renaud *et al.*, 2022b). Meaning that *TgFLP12* does not seem to be a transporter involved in this pathway.

Despite the photosynthetic origin of the apicoplast, the organelle lacks the canonical chloroplast lipid transporters such as fatty acid exporters FAX1 (Li *et al.*, 2015) and FAX2 or the ABC transporter, TGDs (Fan *et al.*, 2015; Lu *et al.*, 2007; Lu and Benning, 2009; Roston *et al.*, 2011), for the import of PA to the chloroplast from ER for galactoglycerolipid synthesis. The close proximity of P5-ATPases to P4-ATPases on the phylogenetic aspect already raised the question of

P5 being involved in lipid transfer. In this study, we deeply investigated the lipidome of parasites lacking *TgFLP12*, and we found a decrease in short fatty acid chains myristic acid, C14:0 in the mutant (**Figure 4 B**). Myristic acid, is one of the main products of the apicoplast FASII. We investigated FASII activity with stable isotope labeling coupled with mass spectrometry and revealed that during the loss of *TgFLP12*, labeling for 72 h without ATc pre-treatment, the FASII activity increased (**Figure 5 A**), while after the complete loss, 48h ATc pre-treatment followed by 24 h activity labeling, the FASII activity was reduced (**Figure 5 D**). MID analysis of C14:0 and 16:0 labeled over 72 h showed an accumulation of total chain length M-2 products (**Figure 5 B and C**). One explanation could be that in absence of *TgFLP12* lipidic products from the apicoplast FASII were no longer exported outside of the plast and their availability in the cytosol was reduced. So the parasite increased the activity of FASII trying to compensate. However, the increased activity led to the accumulation of the potential *TgFLP12* substrate within the apicoplast (**Figure 3 G**) that caused the loss of the organelle (**Figure 3 E**) and so a drop of the FASII activity after the complete loss of the transporter (**Figure 5 D**). Lipid separation combined with FASII labeling revealed that only FFA were decreased upon *TgFLP12* disruption (**Figure 6 A**). *Toxoplasma* growth flexibility has already been illustrated in different mutants of the FASII pathway or lipid synthesis within the apicoplast. The addition of exogenous lipid products, short-chain FFA (Krishnan *et al.*, 2020), or LPA (Amiar *et al.*, 2016b) have successfully restored parasite growth. Both FFA (C14:0 and C16:0) and LPA (C14:0 and C16:0) were able to partially restore the growth in *TgFLP12* mutant, but a specificity appeared for FFA over LPA and C14:0 over C16:0 (**Figure 6 B and C**). These results suggest that *TgFLP12* substitutes FAX proteins present in the chloroplast and preferentially exports C14:0 FFA outside of the apicoplast.

This study reveals the essential role of short FFA originating from FASII to be exported outside of the apicoplast. We propose that *TgFLP12* plays the role of the missing fatty acid exporter in the apicoplast, these exported FA can then be used by cytosolic/ER acyl-transferases (Amiar *et al.*, 2020b; Quittnat *et al.*, 2004) such as GPAT for LPA synthesis, AGPAT for PA synthesis or DGAT for TAG synthesis and plays a role in forming the lipidic patchwork previously reported in *TgATS1* (**Figure 7**). Our data from parasite elongation also revealed that in the mutant, more elongation products originated from C16:0 FA (**Figure 5 H, I, Figure supp 7**). Linked to previous data obtained for the *TgATS1* mutant, we suggest that accumulated FFA C14:0 into the apicoplast undergo another cycle of elongation by the FASII and are then used by *TgATS1* to produce LPA.

Our elongation measurements support that LPA generated by *Tg*ATS1 can exit the apicoplast to reach the ER where FA chains are elongated by ELO A/B/C (**Figure 7**).

The apicoplast is a perfect drug target because of its specificity to the Apicomplexa phylum and absence from the human host and the conservation of essential metabolic pathways derived from a prokaryotic origin. While essential metabolite synthesis has been well studied over the last two decades since the apicoplast discovery, little is known about the transportation and trafficking of these metabolites. The characterization of *Tg*FLP12 illustrates the importance of such transporters for parasite survival. Its conservation among Apicomplexa and the total absence of this new clade of P5-ATPase from the human host make FLP12 a potential new target for the development of treatment against Apicomplexa-caused diseases.

Acknowledgments

This work was supported by Agence Nationale de la Recherche, France (Project ApicoLipiAdapt grant ANR-21-CE44-0010), The Fondation pour la Recherche Médicale (FRM EQU202103012700), Laboratoire d'Excellence Parafrap, France (grant ANR-11-LABX-0024), LIA-IRP CNRS Program (Apicolipid project), the Université Grenoble Alpes (IDEX ISP-IRGA Apicolipid), Région Auvergne Rhone-Alpes for the lipidomics analyses platform (Grant IRICE Project GEMELI), the CEFIPRA *via* a Collaborative Research Program Grant (Project 6003-1). JJ was supported by the Junior STAR grant no. 21-19798M from the Czech Science Foundation.

Material and Methods

Toxoplasma gondii strains and cultures:

Human foreskin fibroblasts (HFF) are cultured in Dulbecco's Modified Eagle's Medium (DMEM, Life Technologies) supplemented with 10 % fetal bovine serum (FBS) (Gibco), 2 mM glutamine (Gibco) and 25 µg/mL gentamicin (Gibco) at 37°C and 5% CO₂.

T. gondii tachyzoites (RH-Δku80, HA strains, and inducible knock-down strains) were maintained in human foreskin fibroblasts (HFF) using Dulbecco's Modified Eagle's Medium (DMEM, Life Technologies) supplemented with 1% fetal bovine serum (FBS) (Life Technologies), 2 mM glutamine and 25 µg/mL gentamicin at 37°C and 5% CO₂.

Generation of inducible knockdown FLP12 line in *T. gondii*:

To introduce the endogenous tag at the 3' end of the genes of interest, the open reading frames of *Tg*FLP12 were amplified by PCR. Amplicons were cloned into the plasmid LIC-HA3-CAT vector.

After those plasmids were linearized with XbaI and transfected into the RH- Δ ku80 strain. Inducible KD strains have been generated *TgFLP12* by amplification of a mycophenolic acid resistance cassette, TATi sequence, and the inducible promoter TET from the plasmid pT8TATi1-HX-tetO7S1. For tag insertion or iKD, 50 μ g of PCR products were co-transfected with 50 μ g plasmid Sibley Cas9 coding for the endonuclease CRISPR-Cas9 and the appropriate protospacer (guide RNA) generated on the platform CHOP-CHOP (chopchop.cbu.uib.no). RH- Δ ku80 strains were transfected with pLIC-*TgFLP12*-HA. The promoter replacements for inducible knockouts were then transfected into cells with their respective 3' HA tags. Electroporations were performed in a 2-mm cuvette in a BTX ECM 630 (Harvard Apparatus, at 1,100 V, 25 Ω , and 25 μ F). Stable lines expressing the constructs (endogenous tagging or exogenous promoter) were selected in media with 30 μ g/ml chloramphenicol or 25 μ g/ml mycophenolic acid and 50 μ g/ml xanthine according to the resistance cassette of the insert transfected and cloned by limiting dilution.

Screenings of the parasite clones with correct HA element insertion and promoter replacement were done using primers pair in Table 1, Figure supp 2. PCRs were performed with TaKara primestar max polymerase.

Immunofluorescence assay:

Primary rabbit anti-CPN60 antibodies were used at a dilution of 1:500, rabbit anti-IMC1 at 1:500, rat anti-HA (Roche) at 1:500, and mouse anti-ATRx1 at 1:500. Secondary AlexaFluor 488- and 546-conjugated goat anti-rat and anti-rabbit antibodies (Life Technologies) were used at 1:1000 dilutions, respectively. Parasites were fixed in PBS containing 2% paraformaldehyde for 15 min at room temperature. Samples were permeabilized with 0.1% Triton X-100 in PBS for 10 min at room temperature before blocking in PBS containing 2% FBS and incubation with primary antibodies then secondary antibodies diluted in the blocking solution. Labeled parasites were stained with Hoechst (1:10,000, Life Technologies) for 20 min and then washed three times in PBS then H₂O. Coverslips were mounted onto slides before observation using a Zeiss epifluorescent microscope.

Phylogenetic analysis of P5-ATPases:

We first used the *TgFLP12* sequence to retrieve related entries from Uniprot by BLASTP and complemented this set by characterized P-ATPases from the literature (Axelsen and Palmgren, 1998; Benito *et al.*, 2004; Rodríguez-Navarro and Benito, 2010). The preliminary dataset was expanded by additional BLASTP searches against GenBank nr and VEuPathDb. The sampling of the global P-ATPase dataset was optimized to 207 sequences (Figure S1) by several rounds of tree

reconstruction in FastTree v2.1.11 (-lg -gamma parameters). A subset of 114 sequences comprising only P5-ATPases was then created from the global dataset (**Figure 1**). All species present in this subset (except *Thermochaetoides thermophila* whose P5B sequence was added later from PDB) had their genomes exhaustively searched for P5-ATPase sequences. Final matrices for the global P-ATPase and P5-ATPase datasets were prepared by using the local pair alignment (-linsi) in MAFFT v7.505 and hypervariable site removal in BMGE v1.12 under relaxed criteria (-m BLOSUM30 -b 3 -g 0.4). Best maximum likelihood trees were computed by using the best fits models (LG+F+R8 for P-ATPase and LG+F+R7 for P5-ATPase) in IQ-TREE v2.2.0, each with 1000 UFBoot2 supports.

Western blot analysis:

Proteins were harvested from scraped, needled (G26 needle), and filtered parasite cultures before counting by hemocytometer. Proteins were normalized and extracted by the addition of sample buffer to the parasite and boiled at 95°C for 5 min. Equal volumes of protein samples were loaded and separated on a 4-12% gradient SDS-polyacrylamide (Life Technologies) and transferred to a nitrocellulose membrane. Incubation of the membrane with primary antibodies rat anti-HA (Roche) and rabbit anti-TOM40 followed by incubation with Horse radish peroxidase (HRP) goat anti-rat and anti-rabbit conjugated antibodies (Thermo Scientific). Revelation was done using the Biorad Chemidoc imager after incubation membrane staining with Luminata Crescendo Western HRP detection kit (Millipore).

Plaque assays in *T. gondii* mutants:

The extracellular parasites were harvested after filtration and counted by hemocytometer. HFF monolayers were infected with ~1,000 mutant parasites and allowed to develop under normal culture conditions or culture medium supplemented with 0.5 µg/ml anhydrotetracycline (ATc) for 10 days untouched before staining with Crystal Violet (Sigma) and cell growth assessment by light microscopy for the presence of intact HFF. The average plaque areas (particles) were analyzed using ImageJ software.

Replication assay in *T. gondii* mutants:

TgFLP12-HA-iKD mutants were pre-treated 3 days with 0.5 µg/ml ATc before replication assay. In 4-well plates (with coverslips) equal numbers of parasites were allowed to invade confluent HFF cells for 2h. After invasion, the plates were washed (x3) with ED1 (DMEM, 1% FBS) and parasites were grown for 24h with or without ATc (0.5 µg/ml). These coverslips were

then processed for IFA and the number of parasites per vacuole was calculated (n = 4 independent experiments).

Electron microscopy:

TgFLP12-iKD parasites were grown 48 h in the presence and absence of ATc, in labteks (Nunk, Thermofisher). The labteks containing parasite-infected HFF were fixed in 0.1 M cacodylate buffer with 2.5 % glutaraldehyde for 2 h and kept at 4°C until further processing. During processing, samples were fixed again for 1 h with 1 % osmium tetroxide in cacodylate buffer followed by overnight treatment in 2 % uranyl acetate in distilled water. After dehydration in graded series of acetonitrile, samples were progressively impregnated in Epon812, the wells were then filled with fresh resin and allowed to polymerize for 48 h at 60°C. Ultrathin 70 nm sections were obtained with a Leica UCT Ultramicrotome and collected on copper grids. Grids were poststained with uranyl acetate and lead citrate before their observation on a Jeol1200EXII Transmission Electron Microscope. All chemicals were from Electron Microscopy Sciences.

Lipidomic analysis:

To extract lipids, *T. gondii* tachyzoites were grown on 175 cm² HFF cultures. Freshly egressed parasites (~10⁸ parasites equivalent) were quenched in a bath of pure ethanol/dry ice, then needed, filtered, and counted by hemocytometer before centrifugation. Pellets were washed 3x times in cold PBS to eliminate lipids from the culture media before conservation at -80°C. Internal standard 10 μmol FFA C13:0 and 10 μmol PC C21:0 (Avanti Polar lipids) are added to samples and lipids are extracted following the Bligh and Dyer modified by Folch protocol (Ramakrishnan S, *et al*; 2012), FAs are methanolized by Trimethylsulfonium hydroxide (TMSH) by gas-chromatography coupled with mass-spectrometry (Agilent 5977A-7890B) (GC-MS), fatty acid methyl esters were identified by their mass spectrum and retention time compared to authentic standards.

Phospholipid, DAG/TAG/FFA analyses: The extracted total lipid extracted (as above) was separated by one-dimensional silica gel high-performance thin-layer chromatography (HPTLC, Merck). The 1st and 2nd solvent systems used were chloroform/methanol/water/ acetic acid, 25:15:2:4 (v/v/v/v) and hexane/MTBE/acetic acid, 35:15:0.5 (v/v/v), respectively. For DAG, TAG, FFA, and PL analysis, the total lipid fraction was separated by 1D-HPTLC using hexane/diethyl ether/formic acid, 80:20:2 (v/v/v) as solvent system. The spots correlating to DAG, TAG, FFA, and PL on the HPTLC plate were scraped off, and lipids were methanolized with 200 μL 0.5 M

methanolic HCl in the presence of 1 nmol pentadecanoic acid (C15:0) as internal standard at 85 °C for 4 h. The resulting FAMES were extracted with hexane and analyzed by GC-MS (Agilent).

Fluoromic analysis:

Confluent T175 HFF cultures are set up for FASII ¹³C carbon labeling, the culture medium is discarded and replaced with ED1% (-) Glucose complemented with 500 μL 800 mM U-¹³C-Glucose or 500 μL 800 mM U-¹²C-Glucose as a control for ¹³C natural abundance. Freshly egressed parasites are loaded on the previous HFF U-¹³C-Glucose / U-¹²C-Glucose and incubated for 72 hours before parasites harvest and lipid extraction for GC-MS analysis. Scavenging was assessed as described in Dass *et al.* 2021, T175 are set up with HFF grown for 5 days in D10% (-)Glucose complemented with 500 μL 800 mM U-¹³C-Glucose. Confluent T175 HFF pre-labeled cultures are set up for scavenging assay, the culture medium is discarded, cells are washed with ED1% (3x) and new ED1% is added. Freshly egressed parasites are loaded on the previous HFF pre-labeled with U-¹³C-Glucose and incubated for 72 h before parasites harvest and lipid extraction for GC-MS analysis.

Statistics and graphs:

Graphs and statistical analysis were made using GraphPad Prism8. Graphs represent means and error bars represent standard errors of means. All data were analyzed with the two-tailed unpaired student's t-test (except when mentioned). All p values are represented by asterisks in figures as follows: ns = p > 0.05, * = p < 0.05, ** = p < 0.01, *** = p < 0.001, and **** = p < 0.0001. We consider all p-values lower than 0.05 to be significant.

Table 1: Oligonucleotide sequences used in this study.

| Oligo ID: | Sequence: |
|---|---|
| <i>TgFLP12</i> pLIC Forward | TACTTCCAATCCAATTTAGCgaagccggtaaagttc gatcgc |
| <i>TgFLP12</i> pLIC Reverse | aaccatgagattatcagactctccagg |
| <i>TgFLP12</i> HR1 promoter replacement | Tggtactcgatccttctcgacagctgaatggtgctgg cctccgccatgttgcggatccgggg |
| <i>TgFLP12</i> HR2 promoter replacement | Cggaggcggagcggaggaggatctgttgatggctgc tccatCATtttgataccctaggaattcactcgt |
| Reverse Cas9 plasmid | AACTTGACATCCCCATTTAC |
| <i>TgFLP12</i> gRNA Forward Cas9 plasmid | gcggtttgtcatgggagtGTTTTAGAGCTAGAAAT AGCAAG |
| <i>TgFLP12</i> Forward screen #1 | caggcttggatgaggtac |
| <i>TgFLP12</i> Reverse screen #2 | GTCGATGTAATATACATTCGCAGACGG |
| <i>TgFLP12</i> Forward screen #3 | cggggagtgtcaccatgt |
| <i>TgFLP12</i> Reverse screen #4 | ccgatccagctccgacgatac |

Supplementary figures

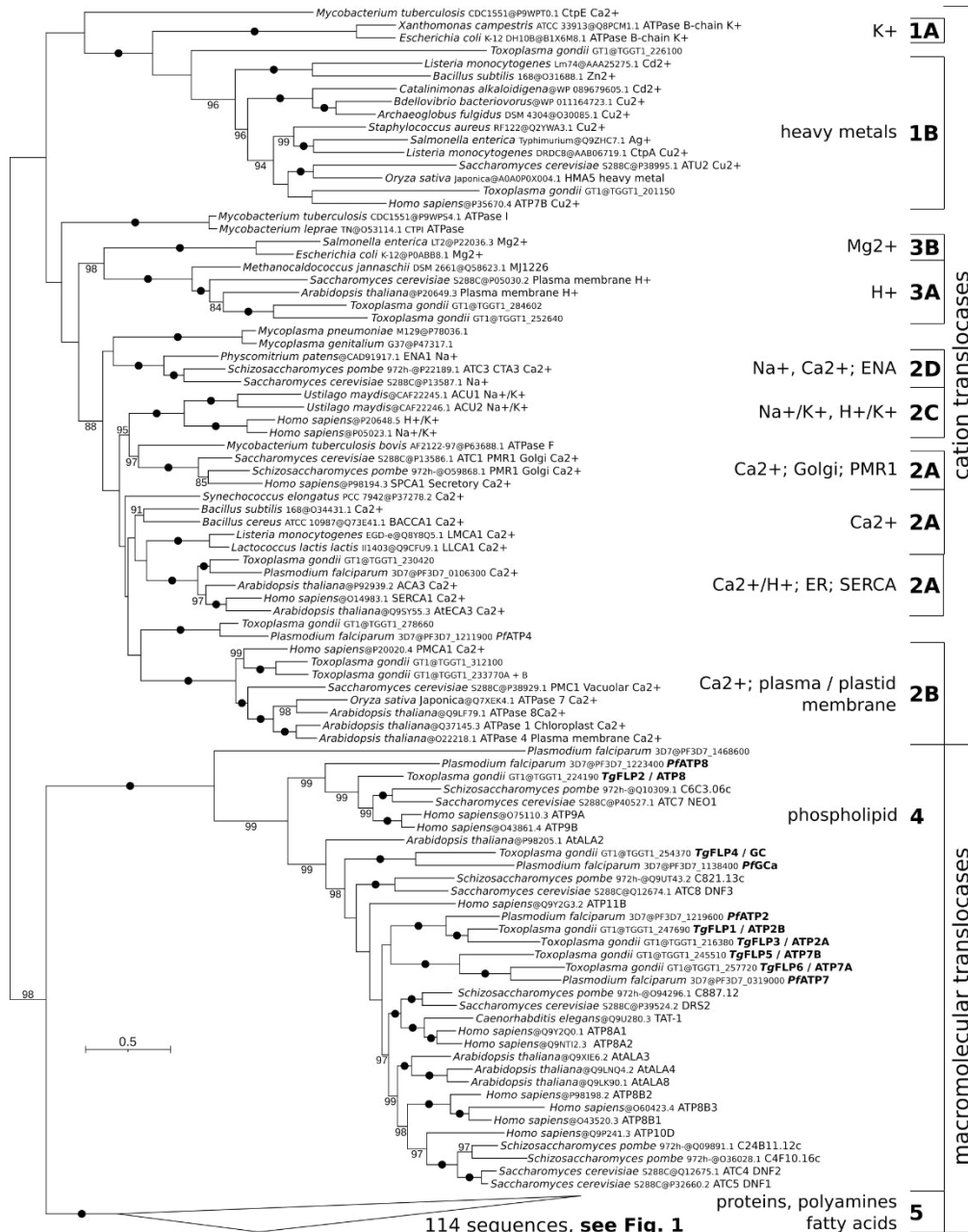


Figure Supp 1: Phylogeny of the P-Type ATPases family

Maximum likelihood phylogeny of P-type ATPases. The tree was derived by using the best-fit model (LG+F+R8) in IQ-TREE and UFBoot2 supports at branches (1000 replicates). The supports from the compacted P5-ATPase are shown in Figure 1. Black dots indicate 100 support. Supports <80 are no shown.

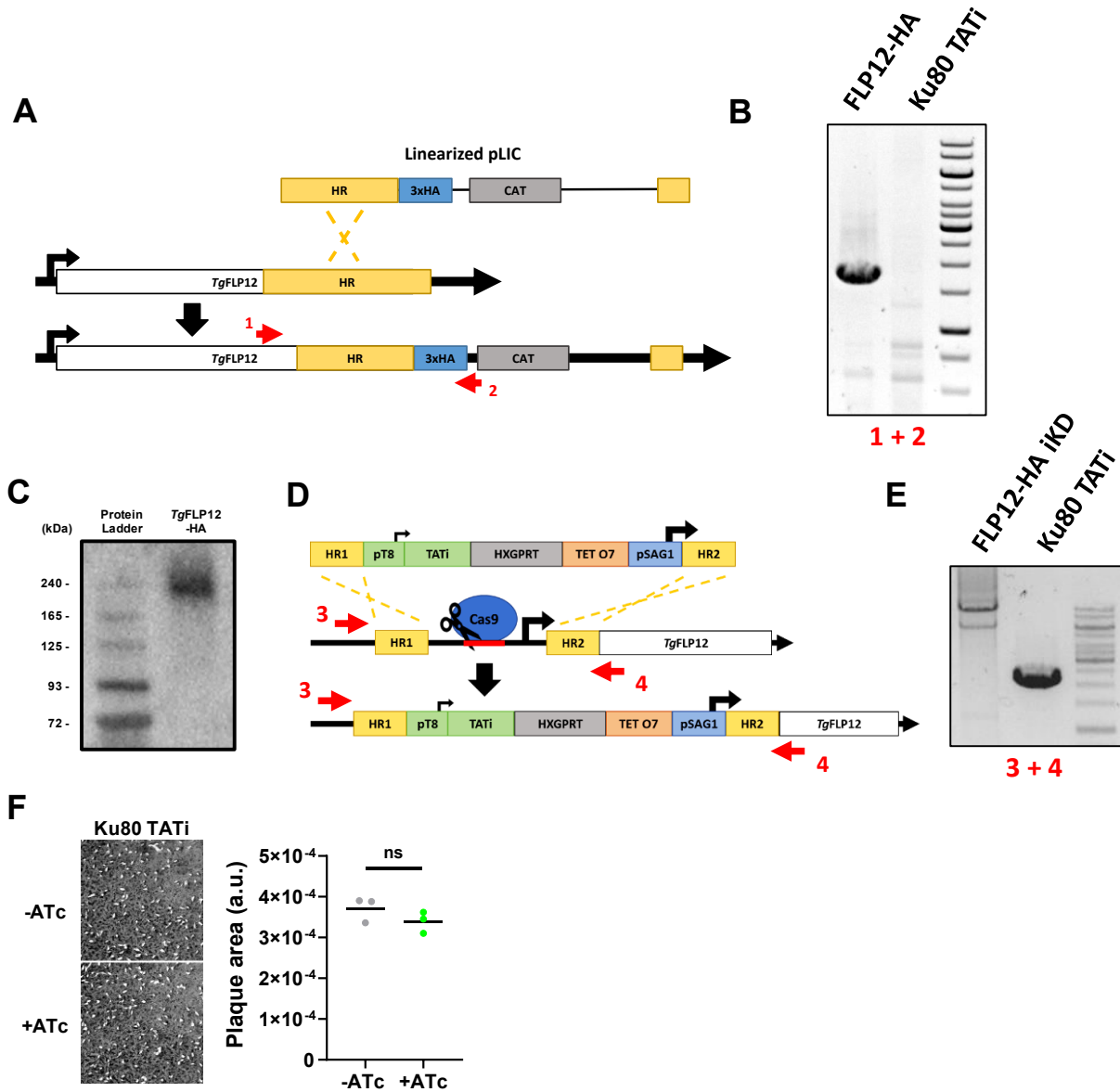


Figure Supp 2: Molecular constructions of *TgFLP12* tagged and inducible knock-down line

(A) Triple HA tag insertion by double homologous recombination using the pLIC system. HR = homologous region; CAT = chloramphenicol acetyltransferase. (B) Confirmation by PCR of the tag integration using pair of primers 1 and 2. Transgenic element is absent from the parental strain Δ Ku80. (C) Visualization of *TgFLP12*-HA by western blot. Molecular weight around ~220 KDa. (D) Gene promoter replacement using the TET system, CRISPR approach, and homologous recombination. (E) Confirmation by PCR of promoter replacement using pair of primers 3 and 4. Size shift of promoter integration is present in the *TgFLP12*-HA-iKD different from the parental strain Δ Ku80. (F) Plaque assay and plaque size quantification of parental strain Ku80 TATi, showing no difference after treatment or not with ATc.

ns $p > 0.05$, * $p \leq 0.05$, ** $p \leq 0.01$, *** $p \leq 0.001$, and **** $p \leq 0.0001$.

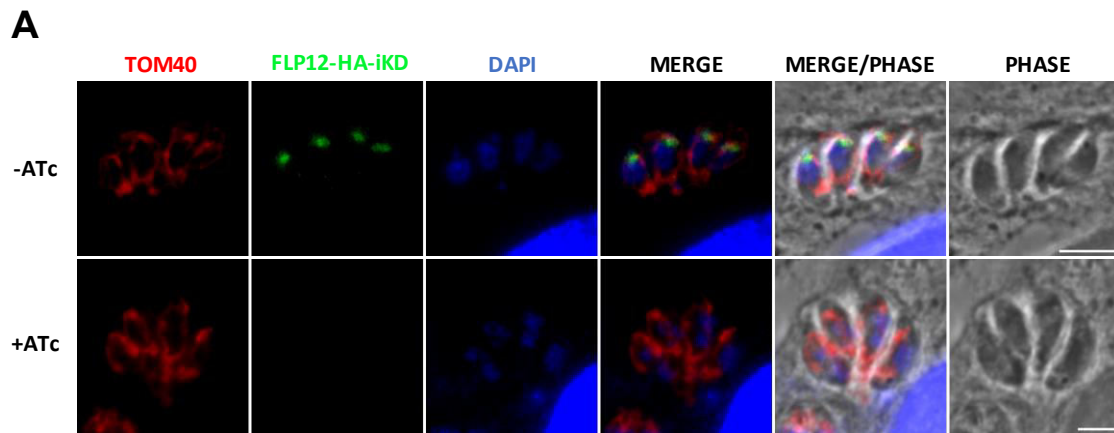


Figure Supp 3: *TgFLP12* absence does not impact the morphological shape of the mitochondria

(A) Mitochondria IFA revealed no effect of *TgFLP12* deletion, Blue = Hoechst, Red = mitochondria marker TOM40, and green = 3xHA tag.

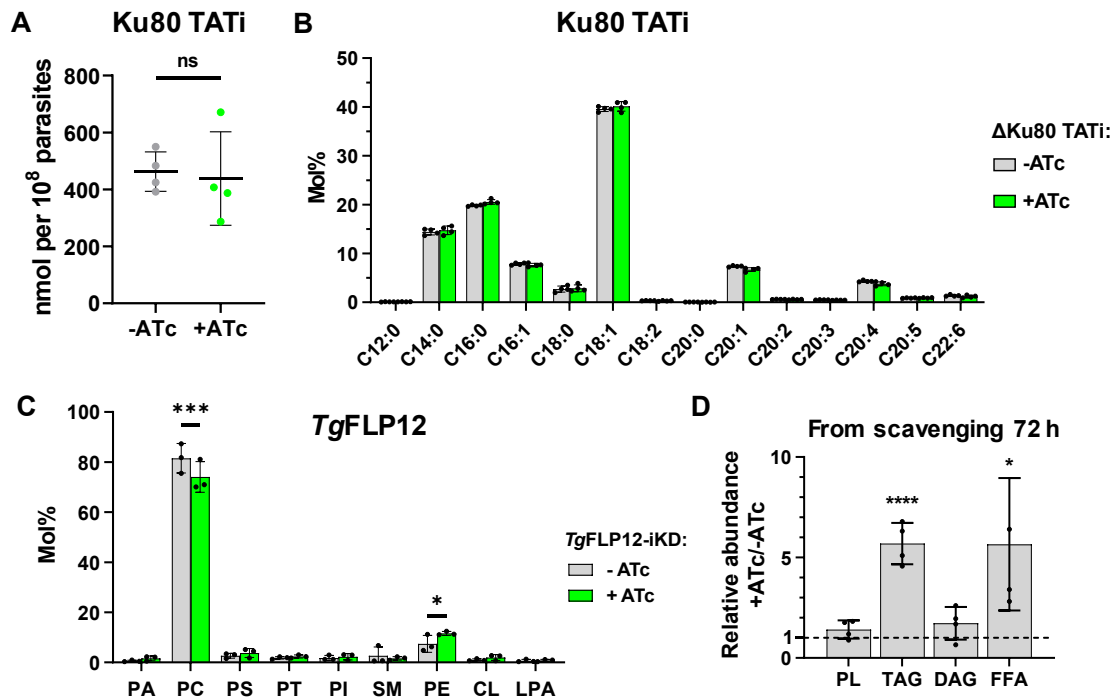


Figure Supp 4: Lipidomic on parental strain that shows no difference upon ATc treatment

(A) FA total amount, quantified by GC-MS is unchanged after ATc treatment on the parental line Δ Ku80 TATi, error bars represent +/- SD of 4 independent experiments. (B) FA composition in Mol% of parental line Δ Ku80 TATi treated with +ATc, compared to parasites untreated, error bars represent +/- SD of 4 independent experiments. (C) Lipid classes, from parasites *TgFLP12-iKD* treated with ATc or not, separated by 2D-TLC and analyzed by GC-MS, error bars represent +/- SD of 3 independent experiments. (D) Relative abundance of the different lipid classes made from scavenged lipids, revealed that neutral lipids TAG and FFA from scavenged lipids increase after addition of ATc, error bars represent +/- SD from 4 independent experiments.

ns $p > 0.05$, * $p \leq 0.05$, ** $p \leq 0.01$, *** $p \leq 0.001$, and **** $p \leq 0.0001$.

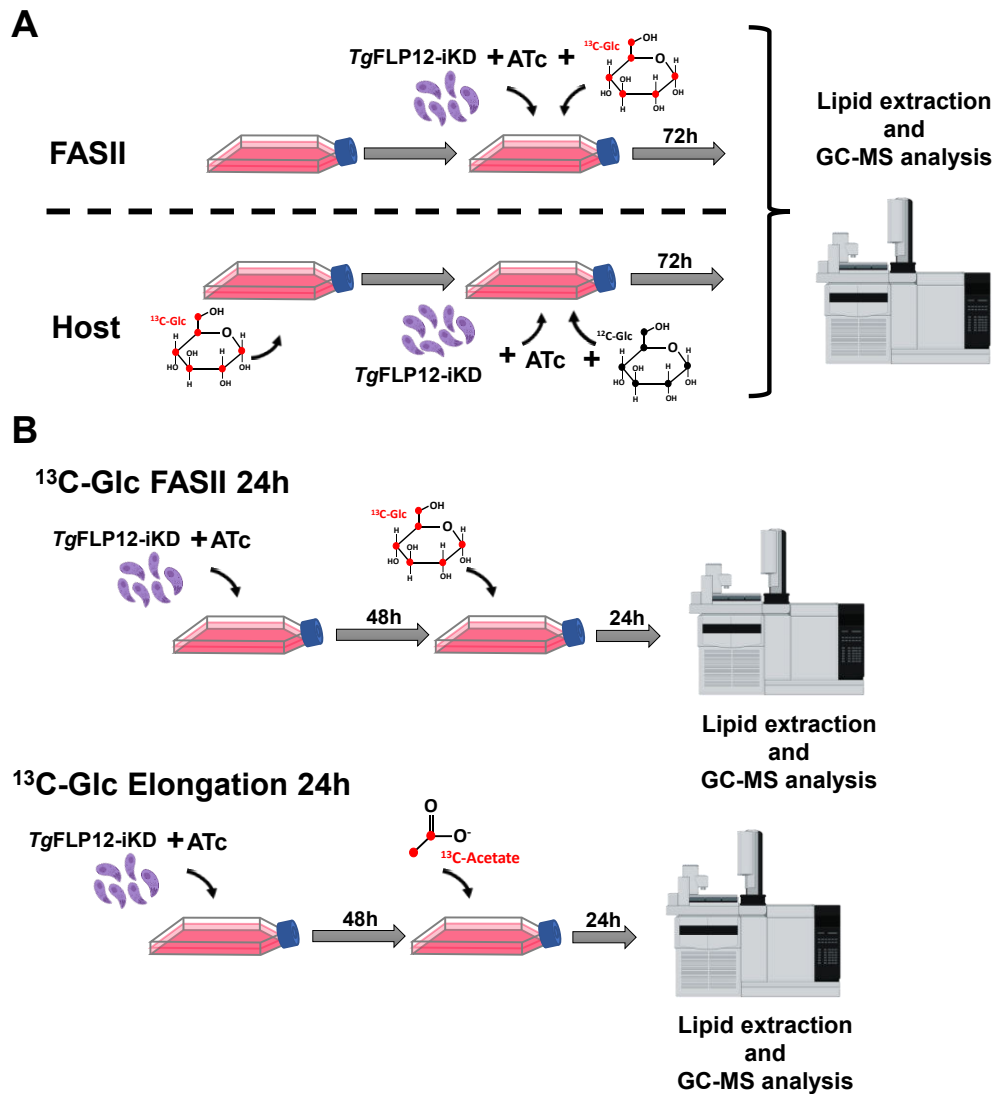
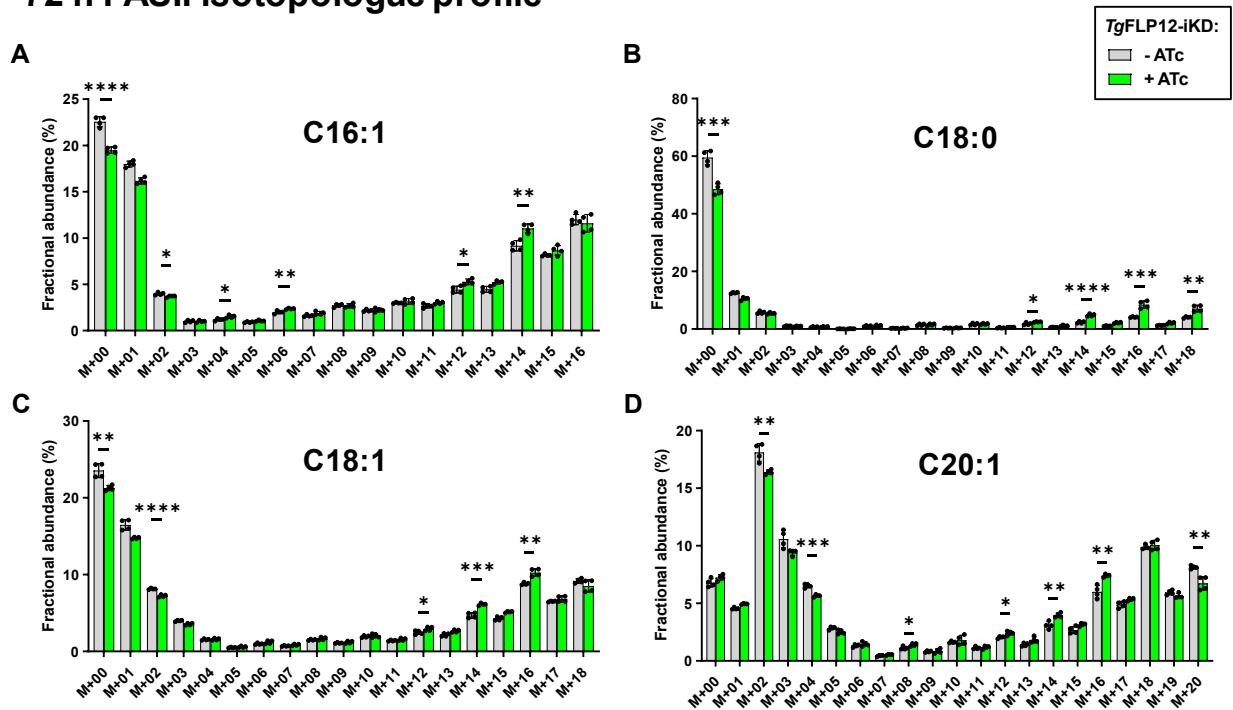


Figure Supp 5: Schematic of stable isotope labelling to measure FASII activity, parasite elongation or scavenging from the host

(A) Labelling of FA made by FASII, confluent HFF are infected with *TgFLP12-iKD* with or without ATc, in media glucose-free. Cultures are complemented with 8 mM U-¹³C-Glucose and grown for 72 h. Labelling of FA made by the host to measure scavenging capacities, HFF are cultured with media glucose-free and complemented with 8 mM U-¹³C-Glucose until they reached full confluency. Media with labelled glucose is washed out and cells are infected with *TgFLP12-iKD* with or without ATc, in regular media and grown for 72 h. (B) FASII labelling on 24 h after total loss of *TgFLP12*. Confluent HFF are infected with *TgFLP12-iKD* with or without ATc for 48 h, then media is replaced by media glucose-free complemented with 8 mM U-¹³C-Glucose and cultured for an extra 24 h. Parasite elongation is measured in the same manner, but U-¹³C-Glucose is replaced by 8 mM U-¹³C-Acetate.

72 h FASII isotopologue profile



24 h FASII isotopologue profile

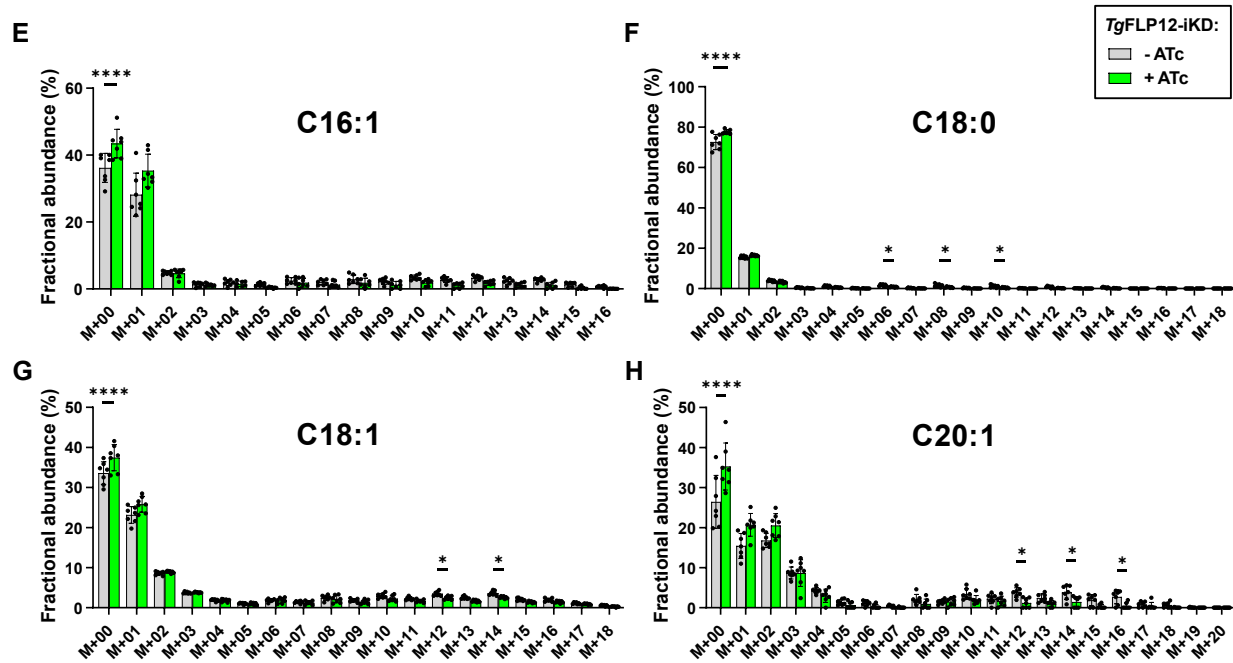


Figure Supp 6: Isotopologue distribution profile of FAs de novo synthesized by apicoplast FASII

(A) C16:1, (B) C18:0, (C) C18:1, and (D) C20:1 show the incorporation of ^{13}C by parasite FASII 72 h into the FA chains, M+ indicates the number of ^{13}C carbon incorporated per chain, error bars represent \pm SD from 4 independent experiments. (E) C16:1, (F) C18:0, (G) C18:1, and (H) C20:1 show the incorporation of ^{13}C by parasite FASII 24 h into the FA chains, M+ indicates the number of ^{13}C carbon incorporated per chain, error bars represent \pm SD from 4 independent experiments. ns $p > 0.05$, * $p \leq 0.05$, ** $p \leq 0.01$, *** $p \leq 0.001$, and **** $p \leq 0.0001$.

ER isotopologue profiles 24 h

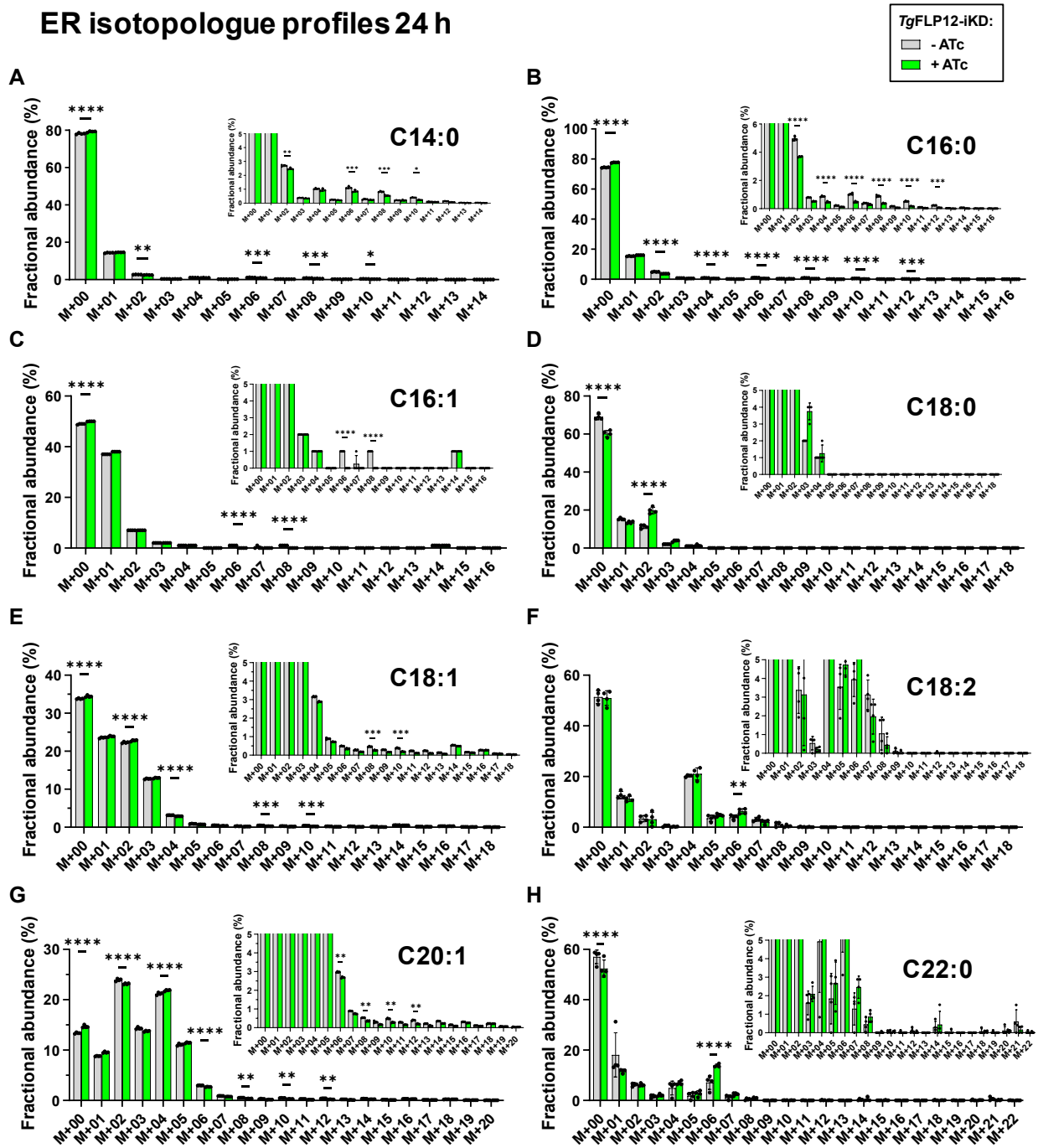


Figure Supp 7: Isotopologue distribution profile of FAs elongated by the parasite

(A) C14:0, (B) C16:0, (C) C16:1, (D) C18:0, (E) C18:1, (F) C18:2, (G) C20:1 and (H) C22:0 showing the incorporation of ^{13}C by elongation 24 h into the FA chains, M+ indicates the number of ^{13}C carbon incorporated per chain, error bars represent +/- SD from 4 independent experiments.

ns $p > 0.05$, * $p \leq 0.05$, ** $p \leq 0.01$, *** $p \leq 0.001$, and **** $p \leq 0.0001$.

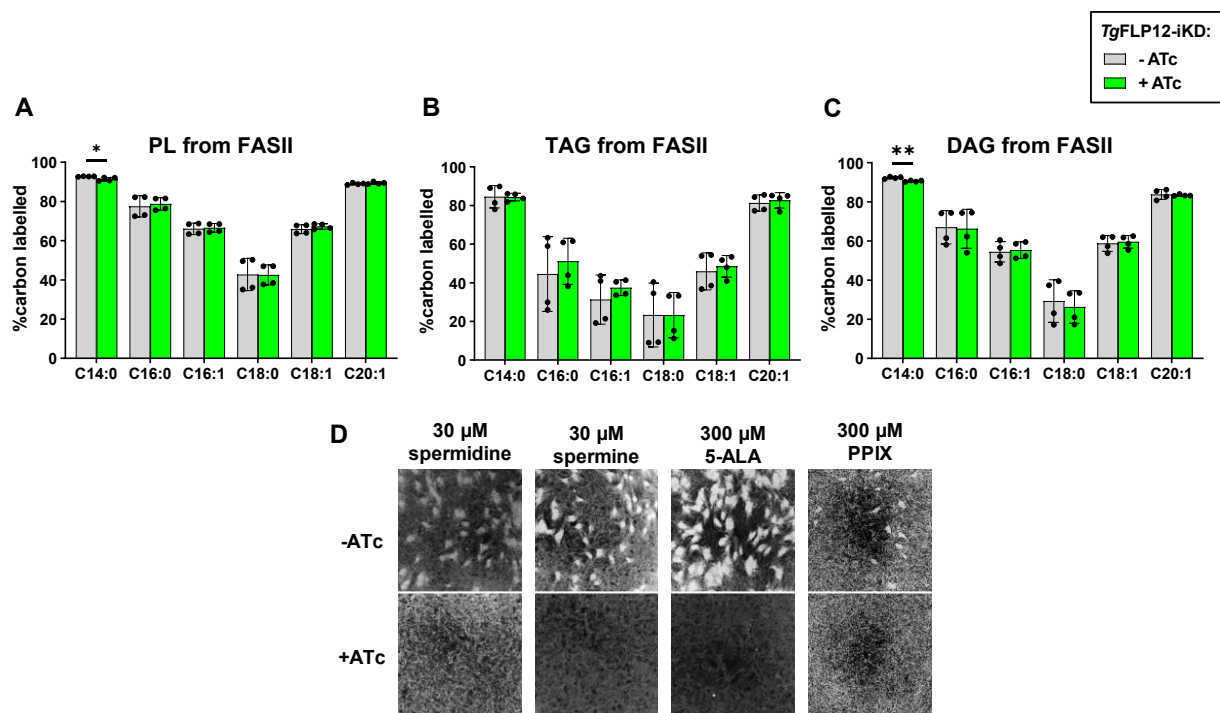


Figure Supp 8: *TgFLP12*-iKD, complementation assay

Percentage of ^{13}C incorporation in major FA species of PL (A), TAG (B), and DAG (C) made by parasite FASII in presence (-ATc) and absence (+ATc) of *TgFLP12*, error bars represent +/- SD from 4 independent experiments. (D) Plaque assays complemented with possible *TgFLP12* substrates, spermidine, spermine, 5-ALA, and PPIX. ns $p > 0.05$, * $p \leq 0.05$, ** $p \leq 0.01$, *** $p \leq 0.001$, and **** $p \leq 0.0001$.

References to chapter IV

- Amiar, S., Katris, N.J., Berry, L., Dass, S., Duley, S., Arnold, C.-S., Shears, M.J., Brunet, C., Touquet, B., McFadden, G.I., Yamaro-Botté, Y., Botté, C.Y., 2020. Division and Adaptation to Host Environment of Apicomplexan Parasites Depend on Apicoplast Lipid Metabolic Plasticity and Host Organelle Remodeling. *Cell Rep* 30, 3778-3792.e9. <https://doi.org/10.1016/j.celrep.2020.02.072>
- Amiar, S., MacRae, J.I., Callahan, D.L., Dubois, D., van Dooren, G.G., Shears, M.J., Cesbron-Delauw, M.-F., Maréchal, E., McConville, M.J., McFadden, G.I., Yamaro-Botté, Y., Botté, C.Y., 2016. Apicoplast-Localized Lysophosphatidic Acid Precursor Assembly Is Required for Bulk Phospholipid Synthesis in *Toxoplasma gondii* and Relies on an Algal/Plant-Like Glycerol 3-Phosphate Acyltransferase. *PLoS Pathog.* 12, e1005765. <https://doi.org/10.1371/journal.ppat.1005765>
- Aw, Y.T.V., Seidi, A., Hayward, J.A., Lee, J., Makota, F.V., Rug, M., van Dooren, G.G., 2021. A key cytosolic iron–sulfur cluster synthesis protein localizes to the mitochondrion of *Toxoplasma gondii*. *Molecular Microbiology* 115, 968–985. <https://doi.org/10.1111/mmi.14651>
- Axelsen, K.B., Palmgren, M.G., 1998. Evolution of substrate specificities in the P-type ATPase superfamily. *J Mol Evol* 46, 84–101. <https://doi.org/10.1007/pl00006286>
- Barylyuk, K., Koreny, L., Ke, H., Butterworth, S., Crook, O.M., Lassadi, I., Gupta, V., Tromer, E., Mourier, T., Stevens, T.J., Breckels, L.M., Pain, A., Lilley, K.S., Waller, R.F., 2020. A Comprehensive Subcellular Atlas of the *Toxoplasma* Proteome *via* hyperLOPIT Provides Spatial Context for Protein Functions. *Cell Host Microbe* 28, 752-766.e9. <https://doi.org/10.1016/j.chom.2020.09.011>
- Benito, B., Garciadeblás, B., Schreier, P., Rodríguez-Navarro, A., 2004. Novel p-type ATPases mediate high-affinity potassium or sodium uptake in fungi. *Eukaryot Cell* 3, 359–368. <https://doi.org/10.1128/EC.3.2.359-368.2004>
- Bisio, H., Krishnan, A., Marq, J.-B., Soldati-Favre, D., 2021. *Toxoplasma gondii* phosphatidylserine flippase complex ATP2B-CDC50.4 critically participates in microneme exocytosis (preprint). *Cell Biology*. <https://doi.org/10.1101/2021.11.25.470034>
- Bisio, H., Lunghi, M., Brochet, M., Soldati-Favre, D., 2019. Phosphatidic acid governs natural egress in *Toxoplasma gondii* *via* a guanylate cyclase receptor platform. *Nat Microbiol* 4, 420–428. <https://doi.org/10.1038/s41564-018-0339-8>
- Boucher, M.J., Ghosh, S., Zhang, L., Lal, A., Jang, S.W., Ju, A., Zhang, S., Wang, X., Ralph, S.A., Zou, J., Elias, J.E., Yeh, E., 2018. Integrative proteomics and bioinformatic prediction enable a high-confidence apicoplast proteome in malaria parasites. *PLoS Biol* 16, e2005895. <https://doi.org/10.1371/journal.pbio.2005895>
- Bullen, H.E., Jia, Y., Yamaro-Botté, Y., Bisio, H., Zhang, O., Jemelin, N.K., Marq, J.-B., Carruthers, V., Botté, C.Y., Soldati-Favre, D., 2016. Phosphatidic Acid-Mediated Signaling Regulates Microneme Secretion in *Toxoplasma*. *Cell Host Microbe* 19, 349–360. <https://doi.org/10.1016/j.chom.2016.02.006>
- Chen, K., Günay-Esiyok, Ö., Klingeberg, M., Marquardt, S., Pomorski, T.G., Gupta, N., 2021. Aminoglycerophospholipid flipping and P4-ATPases in *Toxoplasma gondii*. *Journal of Biological Chemistry* 296, 100315. <https://doi.org/10.1016/j.jbc.2021.100315>
- Dass, S., Shunmugam, S., Berry, L., Arnold, C.-S., Katris, N.J., Duley, S., Pierrel, F., Cesbron-Delauw, M.-F., Yamaro-Botté, Y., Botté, C.Y., 2021a. *Toxoplasma* LIPIN is essential in

- channeling host lipid fluxes through membrane biogenesis and lipid storage. *Nat Commun* 12, 2813. <https://doi.org/10.1038/s41467-021-22956-w>
- Dass, S., Shunmugam, S., Berry, L., Arnold, C.-S., Katris, N.J., Duley, S., Pierrel, F., Cesbron-Delauw, M.-F., Yamaro-Botté, Y., Botté, C.Y., 2021b. Toxoplasma LIPIN is essential in channeling host lipid fluxes through membrane biogenesis and lipid storage. *Nat Commun* 12, 2813. <https://doi.org/10.1038/s41467-021-22956-w>
- De La Hera, D.P., Corradi, G.R., Adamo, H.P., De Tezanos Pinto, F., 2013. Parkinson's disease-associated human P5B-ATPase ATP13A2 increases spermidine uptake. *Biochemical Journal* 450, 47–53. <https://doi.org/10.1042/BJ20120739>
- Dubois, D., Fernandes, S., Amiar, S., Dass, S., Katris, N.J., Botté, C.Y., Yamaro-Botté, Y., 2018. Toxoplasma gondii acetyl-CoA synthetase is involved in fatty acid elongation (of long fatty acid chains) during tachyzoite life stages. *J. Lipid Res.* 59, 994–1004. <https://doi.org/10.1194/jlr.M082891>
- Fan, J., Zhai, Z., Yan, C., Xu, C., 2015. Arabidopsis TRIGALACTOSYLDIACYLGLYCEROL5 Interacts with TGD1, TGD2, and TGD4 to Facilitate Lipid Transfer from the Endoplasmic Reticulum to Plastids. *Plant Cell tpc.15.00394*. <https://doi.org/10.1105/tpc.15.00394>
- Günay-Esiyok, Ö., Gupta, N., 2020. Chimeras of P4-ATPase and Guanylate Cyclase in Pathogenic Protists. *Trends in Parasitology* 36, 382–392. <https://doi.org/10.1016/j.pt.2020.01.009>
- Günay-Esiyok, Ö., Scheib, U., Noll, M., Gupta, N., 2019. An unusual and vital protein with guanylate cyclase and P4-ATPase domains in a pathogenic protist. *Life Sci Alliance* 2, e201900402. <https://doi.org/10.26508/lsa.201900402>
- Holpert, M., Gross, U., Bohne, W., 2006. Disruption of the bradyzoite-specific P-type (H⁺)-ATPase PMA1 in Toxoplasma gondii leads to decreased bradyzoite differentiation after stress stimuli but does not interfere with mature tissue cyst formation. *Molecular and Biochemical Parasitology* 146, 129–133. <https://doi.org/10.1016/j.molbiopara.2005.11.004>
- Huynh, M.-H., Carruthers, V.B., 2009. Tagging of endogenous genes in a Toxoplasma gondii strain lacking Ku80. *Eukaryot Cell* 8, 530–539. <https://doi.org/10.1128/EC.00358-08>
- Katris, N.J., Yamaro-Botte, Y., Janouškovec, J., Shunmugam, S., Arnold, C.-S., Yang, A.S.P., Vardakis, A., Stewart, R.J., Sauerwein, R., McFadden, G.I., Tonkin, C.J., Cesbron-Delauw, M.-F., Waller, Ross.F., Botte, C.Y., 2020. Rapid kinetics of lipid second messengers controlled by a cGMP signalling network coordinates apical complex functions in Toxoplasma tachyzoites (preprint). *Microbiology*. <https://doi.org/10.1101/2020.06.19.160341>
- Kloehn, J., Lacour, C.E., Soldati-Favre, D., 2021. The metabolic pathways and transporters of the plastid organelle in Apicomplexa. *Current Opinion in Microbiology* 63, 250–258. <https://doi.org/10.1016/j.mib.2021.07.016>
- Köhler, S., Delwiche, C.F., Denny, P.W., Tilney, L.G., Webster, P., Wilson, R.J., Palmer, J.D., Roos, D.S., 1997. A plastid of probable green algal origin in Apicomplexan parasites. *Science* 275, 1485–1489. <https://doi.org/10.1126/science.275.5305.1485>
- Krishnan, A., Kloehn, J., Lunghi, M., Chiappino-Pepe, A., Waldman, B.S., Nicolas, D., Varesio, E., Hehl, A., Lourido, S., Hatzimanikatis, V., Soldati-Favre, D., 2020. Functional and Computational Genomics Reveal Unprecedented Flexibility in Stage-Specific Toxoplasma Metabolism. *Cell Host & Microbe* 27, 290-306.e11. <https://doi.org/10.1016/j.chom.2020.01.002>

- Li, N., Gügel, I.L., Giavalisco, P., Zeisler, V., Schreiber, L., Soll, J., Philippar, K., 2015. FAX1, a Novel Membrane Protein Mediating Plastid Fatty Acid Export. *PLoS Biol* 13, e1002053. <https://doi.org/10.1371/journal.pbio.1002053>
- Li, N., Meng, H., Li, S., Zhang, Z., Zhao, X., Wang, S., Liu, A., Li, Q., Song, Q., Li, X., Guo, L., Li, H., Zuo, J., Luo, K., 2020. Two Plastid Fatty Acid Exporters Contribute to Seed Oil Accumulation in *Arabidopsis*1. *Plant Physiol* 182, 1910–1919. <https://doi.org/10.1104/pp.19.01344>
- Li, T., Yang, X., Feng, Z., Nie, W., Fang, Z., Zou, Y., 2021. P5A ATPase controls ER translocation of Wnt in neuronal migration. *Cell Rep* 37, 109901. <https://doi.org/10.1016/j.celrep.2021.109901>
- Li, Z.-H., Ramakrishnan, S., Striepen, B., Moreno, S.N.J., 2013. *Toxoplasma gondii* Relies on Both Host and Parasite Isoprenoids and Can Be Rendered Sensitive to Atorvastatin. *PLoS Pathog* 9, e1003665. <https://doi.org/10.1371/journal.ppat.1003665>
- Liang, X., Cui, J., Yang, X., Xia, N., Li, Y., Zhao, J., Gupta, N., Shen, B., 2020. Acquisition of exogenous fatty acids renders apicoplast-based biosynthesis dispensable in tachyzoites of *Toxoplasma*. *J Biol Chem* 295, 7743–7752. <https://doi.org/10.1074/jbc.RA120.013004>
- Lu, B., Benning, C., 2009. A 25-Amino Acid Sequence of the *Arabidopsis* TGD2 Protein Is Sufficient for Specific Binding of Phosphatidic Acid. *Journal of Biological Chemistry* 284, 17420–17427. <https://doi.org/10.1074/jbc.M109.016014>
- Lu, B., Xu, C., Awai, K., Jones, A.D., Benning, C., 2007. A Small ATPase Protein of *Arabidopsis*, TGD3, Involved in Chloroplast Lipid Import. *Journal of Biological Chemistry* 282, 35945–35953. <https://doi.org/10.1074/jbc.M704063200>
- Mazumdar, J., H. Wilson, E., Masek, K., A. Hunter, C., Striepen, B., 2006. Apicoplast fatty acid synthesis is essential for organelle biogenesis and parasite survival in *Toxoplasma gondii*. *Proc Natl Acad Sci U S A* 103, 13192–13197. <https://doi.org/10.1073/pnas.0603391103>
- McFadden, G.I., Reith, M.E., Munholland, J., Lang-Unnasch, N., 1996. Plastid in human parasites. *Nature* 381, 482–482. <https://doi.org/10.1038/381482a0>
- McKenna, M.J., Sim, S.I., Ordureau, A., Wei, L., Harper, J.W., Shao, S., Park, E., 2020. The endoplasmic reticulum P5A-ATPase is a transmembrane helix dislocase. *STRUCTURAL BIOLOGY* 16.
- Mullin, K.A., Lim, L., Ralph, S.A., Spurck, T.P., Handman, E., McFadden, G.I., 2006. Membrane transporters in the relict plastid of malaria parasites. *Proc Natl Acad Sci U S A* 103, 9572–9577. <https://doi.org/10.1073/pnas.0602293103>
- Nagamune, K., Moreno, S.N., Chini, E.N., Sibley, L.D., 2008. Calcium regulation and signaling in apicomplexan parasites. *Subcell Biochem* 47, 70–81. https://doi.org/10.1007/978-0-387-78267-6_5
- Nakamura, Y., Tsuchiya, M., Ohta, H., 2007. Plastidic Phosphatidic Acid Phosphatases Identified in a Distinct Subfamily of Lipid Phosphate Phosphatases with Prokaryotic Origin*. *Journal of Biological Chemistry* 282, 29013–29021. <https://doi.org/10.1074/jbc.M704385200>
- Nemirovskaya, T.L., Sharlo, K.A., 2022. Roles of ATP and SERCA in the Regulation of Calcium Turnover in Unloaded Skeletal Muscles: Current View and Future Directions. *Int J Mol Sci* 23, 6937. <https://doi.org/10.3390/ijms23136937>
- Nolan, S.J., Romano, J.D., Coppens, I., 2017. Host lipid droplets: An important source of lipids salvaged by the intracellular parasite *Toxoplasma gondii*. *PLoS Pathog* 13, e1006362. <https://doi.org/10.1371/journal.ppat.1006362>
- Nolan, S.J., Romano, J.D., Kline, J.T., Coppens, I., 2018. Novel Approaches To Kill *Toxoplasma gondii* by Exploiting the Uncontrolled Uptake of Unsaturated Fatty Acids and

- Vulnerability to Lipid Storage Inhibition of the Parasite. *Antimicrob Agents Chemother* 62, e00347-18, /aac/62/10/e00347-18.atom. <https://doi.org/10.1128/AAC.00347-18>
- Palmgren, M.G., Nissen, P., 2011. P-type ATPases. *Annu Rev Biophys* 40, 243–266. <https://doi.org/10.1146/annurev.biophys.093008.131331>
- Pamukcu, S., Cerutti, A., Bordat, Y., Hem, S., Rofidal, V., Besteiro, S., 2021. Differential contribution of two organelles of endosymbiotic origin to iron-sulfur cluster synthesis and overall fitness in *Toxoplasma*. *PLoS Pathog* 17, e1010096. <https://doi.org/10.1371/journal.ppat.1010096>
- Quittnat, F., Nishikawa, Y., Stedman, T.T., Voelker, D.R., Choi, J.-Y., Zahn, M.M., Murphy, R.C., Barkley, R.M., Pypaert, M., Joiner, K.A., Coppens, I., 2004. On the biogenesis of lipid bodies in ancient eukaryotes: synthesis of triacylglycerols by a *Toxoplasma* DGAT1-related enzyme. *Molecular and Biochemical Parasitology* 138, 107–122. <https://doi.org/10.1016/j.molbiopara.2004.08.004>
- Ramakrishnan, S., Docampo, M.D., Macrae, J.I., Pujol, F.M., Brooks, C.F., van Dooren, G.G., Hiltunen, J.K., Kastaniotis, A.J., McConville, M.J., Striepen, B., 2012. Apicoplast and endoplasmic reticulum cooperate in fatty acid biosynthesis in apicomplexan parasite *Toxoplasma gondii*. *J. Biol. Chem.* 287, 4957–4971. <https://doi.org/10.1074/jbc.M111.310144>
- Renaud, E.A., Pamukcu, S., Cerutti, A., Berry, L., Lemaire-Vieille, C., Yamaryo-Botté, Y., Botté, C.Y., Besteiro, S., 2022. Disruption of the plastid-hosted iron-sulfur cluster biogenesis pathway in *Toxoplasma gondii* has pleiotropic effects irreversibly impacting parasite viability. <https://doi.org/10.1101/2022.03.18.484844>
- Rodríguez-Navarro, A., Benito, B., 2010. Sodium or potassium efflux ATPase a fungal, bryophyte, and protozoal ATPase. *Biochim Biophys Acta* 1798, 1841–1853. <https://doi.org/10.1016/j.bbamem.2010.07.009>
- Roston, R., Gao, J., Xu, C., Benning, C., 2011. Arabidopsis chloroplast lipid transport protein TGD2 disrupts membranes and is part of a large complex: TGD2 involved in chloroplast lipid transport. *The Plant Journal* 66, 759–769. <https://doi.org/10.1111/j.1365-313X.2011.04536.x>
- Sayers, C.P., Mollard, V., Buchanan, H.D., McFadden, G.I., Goodman, C.D., 2018a. A genetic screen in rodent malaria parasites identifies five new apicoplast putative membrane transporters, one of which is essential in human malaria parasites. *Cellular Microbiology* 20. <https://doi.org/10.1111/cmi.12789>
- Sayers, C.P., Mollard, V., Buchanan, H.D., McFadden, G.I., Goodman, C.D., 2018b. A genetic screen in rodent malaria parasites identifies five new apicoplast putative membrane transporters, one of which is essential in human malaria parasites. *Cell Microbiol* 20. <https://doi.org/10.1111/cmi.12789>
- Shunmugam, S., Arnold, C.-S., Dass, S., Katris, N.J., Botté, C.Y., 2022. The flexibility of Apicomplexa parasites in lipid metabolism. *PLoS Pathog* 18, e1010313. <https://doi.org/10.1371/journal.ppat.1010313>
- Sidik, S.M., Huet, D., Ganesan, S.M., Huynh, M.-H., Wang, T., Nasamu, A.S., Thiru, P., Saeij, J.P.J., Carruthers, V.B., Niles, J.C., Lourido, S., 2016. A Genome-wide CRISPR Screen in *Toxoplasma* Identifies Essential Apicomplexan Genes. *Cell* 166, 1423-1435.e12. <https://doi.org/10.1016/j.cell.2016.08.019>
- van Schaijk, B.C.L., Kumar, T.R.S., Vos, M.W., Richman, A., van Gemert, G.-J., Li, T., Eappen, A.G., Williamson, K.C., Morahan, B.J., Fishbaugher, M., Kennedy, M., Camargo, N., Khan, S.M., Janse, C.J., Sim, K.L., Hoffman, S.L., Kappe, S.H.I., Sauerwein, R.W., Fidock, D.A., Vaughan, A.M., 2014. Type II fatty acid biosynthesis is essential for

- Plasmodium falciparum* sporozoite development in the midgut of *Anopheles* mosquitoes. *Eukaryot Cell* 13, 550–559. <https://doi.org/10.1128/EC.00264-13>
- Van Veen, S., Martin, S., Schuermans, M., Vangheluwe, P., 2021. Polyamine Transport Assay Using Reconstituted Yeast Membranes. *Bio Protoc* 11, e3888. <https://doi.org/10.21769/BioProtoc.3888>
- Vaughan, A.M., O'Neill, M.T., Tarun, A.S., Camargo, N., Phuong, T.M., Aly, A.S.I., Cowman, A.F., Kappe, S.H.I., 2009. Type II fatty acid synthesis is essential only for malaria parasite late liver stage development. *Cellular Microbiology* 11, 506–520. <https://doi.org/10.1111/j.1462-5822.2008.01270.x>
- Waller, R.F., Keeling, P.J., Donald, R.G., Striepen, B., Handman, E., Lang-Unnasch, N., Cowman, A.F., Besra, G.S., Roos, D.S., McFadden, G.I., 1998. Nuclear-encoded proteins target to the plastid in *Toxoplasma gondii* and *Plasmodium falciparum*. *Proc Natl Acad Sci U S A* 95, 12352–12357. <https://doi.org/10.1073/pnas.95.21.12352>
- Walsh, D., Katris, N.J., Sheiner, L., Botté, C.Y., 2022. *Toxoplasma* metabolic flexibility in different growth conditions. *Trends in Parasitology* 38, 775–790. <https://doi.org/10.1016/j.pt.2022.06.001>
- Wilson, R.J., Denny, P.W., Preiser, P.R., Rangachari, K., Roberts, K., Roy, A., Whyte, A., Strath, M., Moore, D.J., Moore, P.W., Williamson, D.H., 1996. Complete gene map of the plastid-like DNA of the malaria parasite *Plasmodium falciparum*. *J Mol Biol* 261, 155–172. <https://doi.org/10.1006/jmbi.1996.0449>
- Yeh, E., DeRisi, J.L., 2011. Chemical Rescue of Malaria Parasites Lacking an Apicoplast Defines Organelle Function in Blood-Stage *Plasmodium falciparum*. *PLoS Biol* 9, e1001138. <https://doi.org/10.1371/journal.pbio.1001138>
- Yu, M., Santha Kumar, T.R., Nkrumah, L.J., Coppi, A., Retzlaff, S., Li, C.D., Kelly, B.J., Moura, P.A., Lakshmanan, V., Freundlich, J.S., Valderramos, J.-C., Vilcheze, C., Siedner, M., Tsai, J.H.-C., Falkard, B., Sidhu, A. bir S., Purcell, L.A., Gratraud, P., Kremer, L., Waters, A.P., Schiehsler, G., Jacobus, D.P., Janse, C.J., Ager, A., Jacobs, W.R., Sacchettini, J.C., Heussler, V., Sinnis, P., Fidock, D.A., 2008. The Fatty Acid Biosynthesis Enzyme *FabI* Plays a Key Role In the Development of Liver Stage Malarial Parasites. *Cell Host Microbe* 4, 567–578. <https://doi.org/10.1016/j.chom.2008.11.001>

Chapter V: *TgFLP2*, a flippase that controls trans-Golgi vesicular trafficking and endocytosis in *Toxoplasma gondii*

Chapter V Summary

P4-ATPases are phospholipid transporters involved in creating membrane phospholipid asymmetry inducing membrane curvatures. They are important for correct vesicular trafficking and thus for membrane recycling, exocytosis, and endocytosis. The parasitic lifestyle of Apicomplexa has repurposed the secretion pathway for the synthesis of secretory organelles, essential for egress, invasion, scavenging, and host control. Parasites also possess specific places for endocytosis events and ingestion of host material, the micropore in *Toxoplasma gondii* or the cytosome in *Plasmodium*. *T. gondii* possesses six flippases. One is not expressed in the tachyzoite life stage, three are located at the apical pole and play a role in microneme secretion, or environmental sensing, and two are localized to the parasite endomembrane system. This study revealed the importance of the Golgi flippase, *TgFLP2*, for correct vesicular trafficking within the parasite.

Below are summarized the major findings of the study:

- *TgFLP2* belongs to the subfamily of P4B-ATPases, and structural prediction suggests that its substrate specificity could be the same as the yeast flippase *ScNeolp*;
- *TgFLP2* is localized to the Golgi apparatus and is essential for parasite survival and intracellular replication. The parasite fitness cannot be increased by changing the nutritional status of the host;
- deletion of *TgFLP2* impacts microneme proteins localization but not the biogenesis of the organelles;
- lack of *TgFLP2* is deleterious for endocytosis, vesicles formed at the micropore can no longer detach from the plasma membrane;
- disruption of *TgFLP2* also impacts the general lipid homeostasis of the parasite with a negative impact on both scavenging and FASII activity.

Author contributions

My contribution for this project was as described below (CSA):

- Conceptualization (CSA, CYB, YYB)
- Generation of the mutants lines (CSA)
- Metabolite labeling, lipid extraction, lipidomic analyses (CSA, YYB)
- All phenotypic characterizations (CSA, SG, NQ)
- Microscopy imaging, EM sample preparation (CSA, LB)
- Results and interpretation (CSA, CYB, YYB)
- Manuscript writing and correction (CSA, CYB, YYB)

More precisely, for this work, I personally generated the inducible/tagged parasite lines (*Toxoplasma* and *Plasmodium*), performed all the state-of-the-art phenotypic characterization (invasion, egress, microneme secretion assays, plaque assays, intracellular replication assays). I performed the *in silico* analysis of the TgFLP2 structure, all the lipidomic analyses and their interpretation, and fluorescence imaging. TEM pictures were acquired by Laurence Berry, and the endocytosis assays were performed by Simon Gras. I did the writing of the manuscript in parallel with the corrections from my PIs.

Tg*FLP2, a lipid flippase that controls trans-Golgi vesicular trafficking and endocytosis in *Toxoplasma gondii

Christophe-Sebastien Arnold¹, Simon Gras², Nyamekye A. Quansah¹, Serena Shunmugam¹, Laurence Berry³, Sarah Charital¹, Samuel Duley¹, Yoshiki Yamaro-Botté¹, Nicholas J. Katris¹, Cyrille Y. Botté^{1*}

¹Apicolipid Team, Institute for Advanced Biosciences, CNRS UMR5309, Université Grenoble Alpes, INSERM U1209, Grenoble, France.

²Lehrstuhl für experimentelle Parasitologie, Ludwig-Maximilians-Universität, LMU, Tierärztliche Fakultät, München, Germany.

³Laboratory of Pathogen Host Interactions, Université Montpellier, France.

*Corresponding author

To whom correspondence should be sent, cyrille.botte@univ-grenoble-alpes.fr

Abstract

The parasitic lifestyle of Apicomplexa, such as *Toxoplasma gondii* or *Plasmodium falciparum*, is ensured by extremely efficient capacities to scavenge resources from the host. Parasites secrete effectors through apical organelles, micronemes, and rhoptries, which allow the fast exit and entry of the host cell. Scavenged resources actively get into the parasitophorous vacuole, and are then ingested by endocytosis into the parasite. However, little is known about this last step. P4-ATPases are known to be involved in generating membrane curvatures for vesicular trafficking and are involved in both exo- and endocytosis. Here, the role of a Golgi P4B-ATPase, *Tg*FLP2, was shown to control parasite lipid homeostasis and regulate the formation of endocytosis vesicles at the level of the micropore. Depletion of *Tg*FLP2 has also shown its importance for the correct addressing of micronemes proteins but not rhoptries. This study illustrates the central position of *Tg*FLP2, which presumably generates membrane curvatures in the Golgi, controlling parasite post-Golgi vesicular trafficking with a role in exo- and endocytosis.

Introduction

Toxoplasma gondii and *Plasmodium falciparum*, which belong to the superphylum of Apicomplexa, are obligate intracellular parasites and represent a severe threat to humans by leading to the death of hundreds of thousands each year. To ensure their intracellular propagation Apicomplexa parasites require large amounts of lipids, which are acquired from two sources: (i) host scavenging, and (ii) *de novo* synthesis, recycling and assembly by the parasite *de novo* synthesis machinery. Both pathways for lipid acquisition and synthesis are essential for parasite membrane biogenesis.

Parasites are able to *de novo* fatty acid (FA) synthesis, thanks to a vegetal relic-plastid named the apicoplast, obtained from the secondary endosymbiosis of ancestral red algae. This organelle has lost the photosynthesis ability but essential metabolic pathways remained (heme synthesis pathway, DOXP pathway, iron-sulfur cluster synthesis pathway, and type II fatty acid synthesis pathway (FASII)). Previous studies on the apicoplast have demonstrated the presence of two plant-like acyltransferases named ATS1 and ATS2, involved in the synthesis of lysophosphatidic acid (LPA) (Amiar *et al.*, 2016a) and phosphatidic acid (PA) (Amiar *et al.*, 2020a) respectively, by adding fatty acid chains (made by the FASII) onto a glycerol-3-phosphate backbone. The LPA and PA serve as the major precursors for the *de novo* synthesis of all phospholipid classes and need to be exported toward the endoplasmic reticulum (ER), where the fatty acid chains can be elongated and desaturated by the three elongases (ELO A/B/C) found in the ER (Dubois *et al.*, 2018b; Ramakrishnan *et al.*, 2012b, 2015a).

These parasites also acquire lipids, proteins, and other nutrients by massive scavenging from the host, using their parasitophorous vacuole membrane (PVM) and effectors sent to the host to manipulate its behavior. To ensure its survival, the parasite recruits host organelles (mitochondria, Rab vesicles, ER, etc.) and internalized their content in the parasitophorous vacuole (PV) by several mechanisms like the recruitment of the host ESCRT machinery, or the intravacuolar network. Once in the PV, the host material is ingested by the parasite by endocytosis and targeted to a lysosome-like compartment called the plant-like vacuolar compartment (PLVAC), to be proceeded and digested by lipases and proteases for nutrient acquisition. Lipid scavenging is constant and used to form the lipidic patchwork, with parasite *de novo* lipids, essential for the bulk of phospholipids and membrane biogenesis (Amiar *et al.*, 2016a). Moreover, this constant flux is also forwarded to lipid storage *via* the metabolic switch TgLIPIN, which senses the host's nutritional status and catalyzes

the dephosphorylation of PA, forming diacylglycerol (DAG) used *via* the glycerolipid pathway for triacylglycerol (TAG) and lipid droplet synthesis (Dass *et al.*, 2021a).

In Apicomplexa parasites, the mechanism that controls endocytosis remains poorly known. This process is extremely fast and depends on well-orchestrated vesicular trafficking. The admitted hypothesis to describe those endocytic events is that in *Toxoplasma*, the micropore and its equivalent in *Plasmodium* the cytosome, are assumed to be the place for endocytosis. Recent works revealed the recruitment of proteins related to endocytosis at the level of these structures, such as coated protein clathrin adaptor protein AP2, Kelch13, ESP15, and the dynamin DrpC (Koreny *et al.*, 2022; Ma *et al.*, 2016; Spielmann *et al.*, 2020; Wan *et al.*, 2023). Internalized material transits through the endosome-like compartments (ELCs) to reach the digestive vacuole or the PLVAC, and disruption of the trans-Golgi/ELC VPS45 impairs endocytosis in *Plasmodium* (Jonscher *et al.*, 2019) and induces enlarged micropore in *Toxoplasma* (Bisio *et al.*, 2020). While endocytosis and exocytosis adopt distinct trafficking pathways in mammalian and model systems, Apicomplexa endocytosis and exocytosis do intersect at the level of the ELCs.

To invade their hosts, Apicomplexa do not rely on phagocytosis like other intracellular pathogens but instead actively enter the host thanks to the secretion of effectors, that allow their attachment, the active entry with the formation of the PV, the shutdown of the host immune response and the nutrient acquisition (Ben Chaabene *et al.*, 2021; Dubois and Soldati-Favre, 2019). Such effectors are located within secretory organelles namely, micronemes, rhoptries, and dense granules, which are the result of parasites re-wiring the exocytosis pathway. Rhoptry and microneme immature proteins enter the secretory pathway in the ER and follow the anterograde trafficking to the Golgi, then they are translocated to the ELCs using *TgSORTL* where the pro-peptides are cleaved and the proteins become mature (Venugopal and Marion, 2018). Rhoptries and micronemes are both apical organelles but from the ELCs, their contents traffic through different pathways (McGovern *et al.*, 2018; Venugopal *et al.*, 2017). Micronemes have been shown to intersect the ingested material addressed to the PLVAC, whereas rhoptry proteins transit through the pre-rhoptry compartments before reaching the rhoptries without crossing the ingested material (McGovern *et al.*, 2018). The process by which microneme sorting differs from material addressed to the PLVAC remains unclear.

Membrane trafficking/recycling along with endocytosis and exocytosis are dependent on cell vesicular trafficking. Vesicles bud from a donor membrane, travel within the cell using the

cytoskeleton, and fuse with the target membrane. The initial step in the vesicle budding is the membrane curvature, which is then amplified by the recruitment of proteins involved in coating the vesicles, such as Arf-GTPase, AP1, and clathrin (Liu *et al.*, 2008). The accumulation of certain species of lipids induces membrane curvatures due to their spatial shape, conical or trapezoid creating positive or negative curvatures respectively (McMahon and Boucrot, 2015). Anionic phospholipids accumulation like phosphatidylserine (PS) participates in the formation of membrane curvature *via* the recruitment of Arf1 for clathrin assembly, or Gsc1 for trafficking to the Golgi from the endosome in yeast (Xu *et al.*, 2013).

The accumulation of charged lipids and specific shapes, both depend on membrane phospholipid asymmetry. Phospholipids are the major component of lipidic membranes which are formed of two layers of phospholipids, the FA tails facing each other's forming the hydrophobic core and the polar head being exposed to the cytosol or luminal or extracellular space. But phospholipids flipping from one layer to the other one is a high-energy demanding process or occurs very slowly. To catalyze this transfer, cells bear specific phospholipid transporters. Flippases use the energy of the hydrolysis of ATP and catalyze the phospholipid transfer toward the cytosolic face. Floppases also use the energy of the ATP consumption and catalyze in the opposite direction. Finally, the scramblases are bidirectional and participate in membrane symmetry using the concentration gradient force of the different lipid species (Daleke, 2003; van Meer, 2011).

Flippases or P4-ATPases, are aminophospholipid transporters and are essential for vesicular trafficking. Their principal substrates are PS and phosphatidylethanolamine (PE) (Andersen *et al.*, 2016; Bai *et al.*, 2021; Wehman *et al.*, 2011), which are two important lipids for membrane curvatures. The yeast model *Saccharomyces* possesses five flippases, Golgi Drs2p and Neo1p, and plasma membrane, endosomes Dnf1, 2, and 3. All are important in endocytosis and exocytosis, with Drs2p, and Dnf1, 2, and 3 presenting some redundant functions while Neo1p is essential on its own. *Toxoplasma* and *Plasmodium* encode respectively six and five P4-ATPases, some are essential to maintain the plasma membrane asymmetry, and play an essential role in environmental sensing and microneme secretion (Bisio *et al.*, 2021, 2019; Katris *et al.*, 2020) but none of them has yet been shown to participate in the endomembrane vesicular trafficking that are crucial for many pathways including organelle biogenesis, and/or parasite exocytosis and endocytosis.

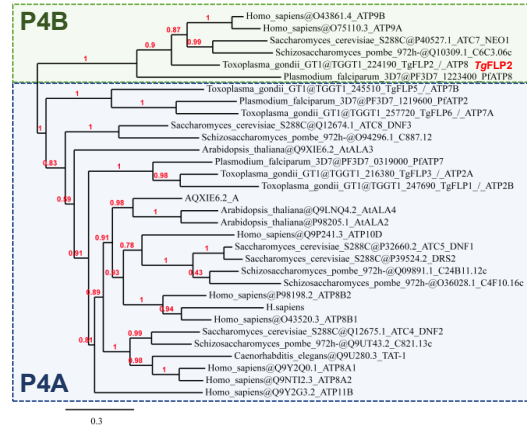
In this study, we reveal the roles of an essential P4-ATPase, TgFLP2, in *Toxoplasma gondii* as the central regulator for Trans-Golgi vesicular trafficking. We show that TgFLP2 is essential for the

proper trafficking and localization of microneme proteins. We further show that the ELCs morphologies are also dependent on the activity of *TgFLP2*. Furthermore, our work reveal that *TgFLP2* is absolutely required for the endocytosis pathway. Lipidomics reveal that *TgFLP2* is important to maintain proper parasite lipid homeostasis, and more particularly with PE. Taken, together, our study an essential component for the post-Golgi vesicular trafficking and plays a role in both endocytosis and correct addressing of microneme contents, but not rhoptries illustrating once more the divergent trafficking paths between micronemes and rhoptries.

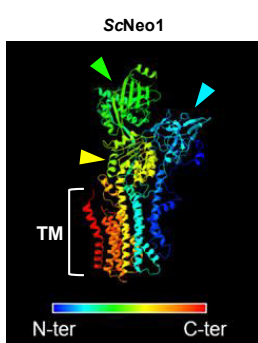
A

| ID | Phenotypic score* | LOPIT** | Confirmed localization*** | Plasmodium homologue |
|----------------|-------------------|-------------|---------------------------|---------------------------|
| TgFLP1 / ATP2B | -1.5 | PM | Apical | ATP2 |
| TgFLP2 / ATP8 | -5.24 | Golgi | Golgi | ATP8 |
| TgFLP3 / ATP2A | -0.43 | - | Apical | ATP2 |
| TgFLP4 / GC | -3.56 | PM integral | Apical/PM | GC α GC β |
| TgFLP5 / ATP7B | -3.76 | PM integral | Sp/PM | ATP7 |
| TgFLP6 / ATP7A | -0.38 | - | - | ATP7 |

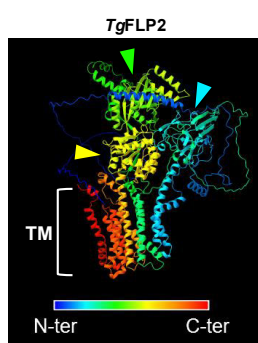
B



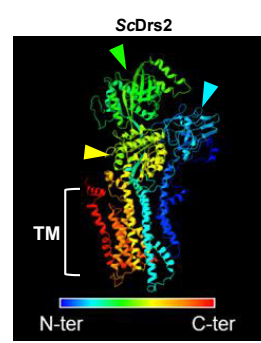
C



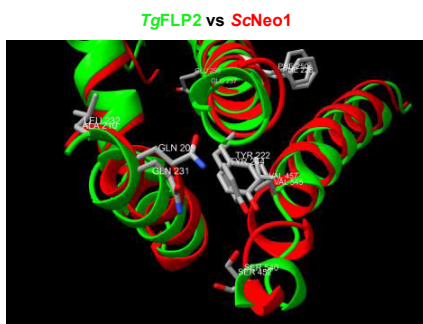
D



E



F



G

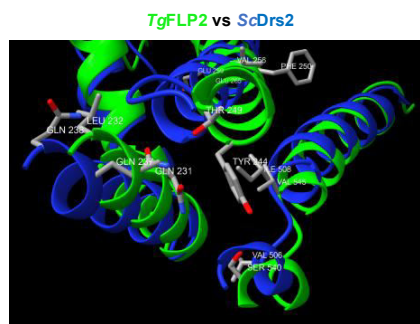


Figure 1: TgFLP2, a parasite P4B-ATPase

(A) *Toxoplasma gondii* P4-ATPases and their homologs in *Plasmodium falciparum*, along with associated fitness scores predicted in Sidik *et al.*, 2016, predicted localization by the LOPIT in Barylyuk *et al.*, 2020, and confirmed localization in Chen *et al.*, 2021 and Bisio *et al.*, 2022. PM: plasma membrane, ER: endoplasmic reticulum, Sp: secretory pathway. (B) Maximum likelihood phylogeny of Apicomplexa P4-type ATPases with homologs from yeast (*Saccharomyces cerevisiae* and *Schizosaccharomyces pombe*), human (*Homo sapiens*), plant (*Arabidopsis thaliana*), and worm (*Caenorhabditis elegans*). Node support values are indicated. (C) Crystal structure of ScNeo1 (Bai *et al.*, 2021), (D) AlphaFold2 predicted structure of TgFLP2, (E) Crystal structure of ScDrs2 (Timcenko *et al.*, 2019), for (C), (D), and (E) cyan arrow: actuator domain, green arrow: nucleotide binding site, yellow arrow: phosphorylation site, TM: transmembrane domains. (F-G) Overlay of AlphaFold FLP2 predicted transmembrane domains (in green) on crystal structures of *Saccharomyces* Neo1 in red (F), or Drs2 in blue (G) transmembrane domains and essential residues for Neo1 activity of TM1, TM2, and TM4.

Results

TgFLP2 belongs to the sub-family of P4B-ATPases

Toxoplasma genome encodes for five P4-ATPases (Bisio *et al.*, 2021; Chen *et al.*, 2021) plus one atypical flippase coupled to a guanylate cyclase called GC (**Figure 1A**), all have conserved the different essential domains for the flippase activity namely, the phosphorylation domain, the actuator domain, and the nucleotide-binding domain. Two P4-ATPases were localized to the apical pole and characterized to be essential for plasma membrane lipid asymmetry and parasite invasion (Bisio *et al.*, 2021). One did not appear to be expressed in *Toxoplasma* tachyzoite life stage and two remained poorly characterized. In the present study, we decided to investigate the role of ATP8, also named TgFLP2 (TGME49_224190). The phylogenetic analysis illustrated the common evolution of flippases in *Toxoplasma* and *Plasmodium* as they cluster together in two distinct groups, ATP2s, ATP7s belong to P4A-ATPases, and TgFLP2 and its *Plasmodium* homolog belong to P4B-ATPases (**Figure 1B**). *Plasmodium* genome encodes for two GC, α and β , and *Toxoplasma* genome encodes for one, but it appears to be the opposite for ATP8 and 2 for which *Toxoplasma* possesses two gene copies of each while *Plasmodium* possesses only one (**Figure 1B**). Concerning FLP2, both parasites possess only one copy. This divergence between the two parasites could be explained by the two distinct life cycles and the different cell types they encounter. For example, *Plasmodium* had not conserved all proteins that form the conoid and apical flippases could play an important role in invasive forms (merozoite, sporozoite, or ookinete) that require the secretion of apical organelles but could become unnecessary in non-invasive forms (Koreny *et al.*, 2021).

The predicted 3-dimensional structure of TgFLP2 was obtained using Colabfold (Mirdita *et al.*, 2022), which is based on the AlphaFold2 algorithm (Jumper *et al.*, 2021; Varadi *et al.*, 2022), and molecular graphics were made using ChimeraX (Goddard *et al.*, 2018; Pettersen *et al.*, 2021) (**Figures 1D, F, G**). TgFLP2 structure was compared to the crystal structures of P4B-ATPase Neo1p (Bai *et al.*, 2021) (**Figures 1C and 1F**) and P4A-ATPase Drs2p (Timcenko *et al.*, 2019) (**Figures 1E and G**). Structure comparison revealed that TgFLP2 predicted structure matches Neo1p and Drs2p crystal structures, and possessed the characteristic domains shared between all P-type ATPases (**Figure 1D**), the actuator domain (cyan arrow), the nucleotide-binding domain (green arrow), and the phosphorylation domain (yellow arrow). The notable difference of TgFLP2 compared to yeast flippases was the presence of a long N-terminal tail for which the structure prediction generated a low b-factor, 19.9 out of 100 (orange), indicating a poor structural prediction

confidence (**Figure supp 1A**). The electrostatic surface potential of this N-terminal tail revealed two domains electrically charged, one negatively which seemed placed close to the nucleotide-binding site and the actuator domain, and one positively at the opposite closer to the phosphorylation domain (**Figure supp 1B**). These two domains could presumably play a role as regulators of the *TgFLP2* activity. Comparison of the transmembrane domains (TMs) of *TgFLP2* with the TMs from *ScNeo1p* (**Figure 1F**) and *ScDrs2p* (**Figure 1G**), more precisely the TM1, TM2, and TM4 showed that *TgFLP2* TMs have conserved essential residues essential for *ScNeo1p* activity and specificity (**Figure 1F**). *TgFLP2* possesses the entry gate residues GLN231 and LEU232 that match spatial position of *ScNeo1p* GLN209 and ALA210, SER540, and VAL545 corresponding to *ScNeo1p* SER454 and VAL457, which are essential to maintain membrane asymmetry. And *TgFLP2* also conserved the residues PHE250 and GLU259 matching with *ScNeo1p* PHE228 and GLU237 important for cold resistance, and the TYR244 that corresponds to the TYR222 which defines the specificity of *Neo1p*. In Yeast, the substitution of TYR222 with a SER can rescue membrane asymmetry defects in the $\Delta drs2p$ strain (Huang *et al.*, 2020). Almost all these residues are not conserved in *ScDrs2p* (**Figure 1G**), which is coherent with the phylogenetic background of *TgFLP2* that placed it in the P4B-ATPase sub-family to which *ScNeo1p* belongs.

***TgFLP2* is an essential putative Golgi flippase**

To elucidate the role of *TgFLP2* in *Toxoplasma*, we generated an inducible knock-down and tagged line by fusing the endogenous locus with the recent HA mini auxin degron system within a Ku80 knockout strain expressing the transgenic element TIR (Brown *et al.*, 2018), and correct genomic insertion was confirmed by PCR (**Figure supp 2A**). *TgFLP2*-HA-mAID transgenic line efficiently expressed the HA-tagged which revealed a punctate signal by immunofluorescence assay (IFA) localized above the nucleus (**Figures 2A and B**). To determine the localization of *TgFLP2*, IFAs coupled to co-staining with anti-HA and different intracellular markers were performed and revealed that *TgFLP2* did not colocalize with the apicoplast stromal marker CPN60, or the ER marker SERCA, or the PLVAC marker CPL (**Figure 2A**). The HA-signal did seem to be in close vicinity with the ELC's marker pro-M2AP but did not colocalize properly (**Figure 2A**), although the HA-signal best match was the Golgi marker GRASP-RFP expressed on a transient vector (**Figures 2B and C**) confirming the Golgi localization predicted by the hyperLOPIT (Barylyuk *et*

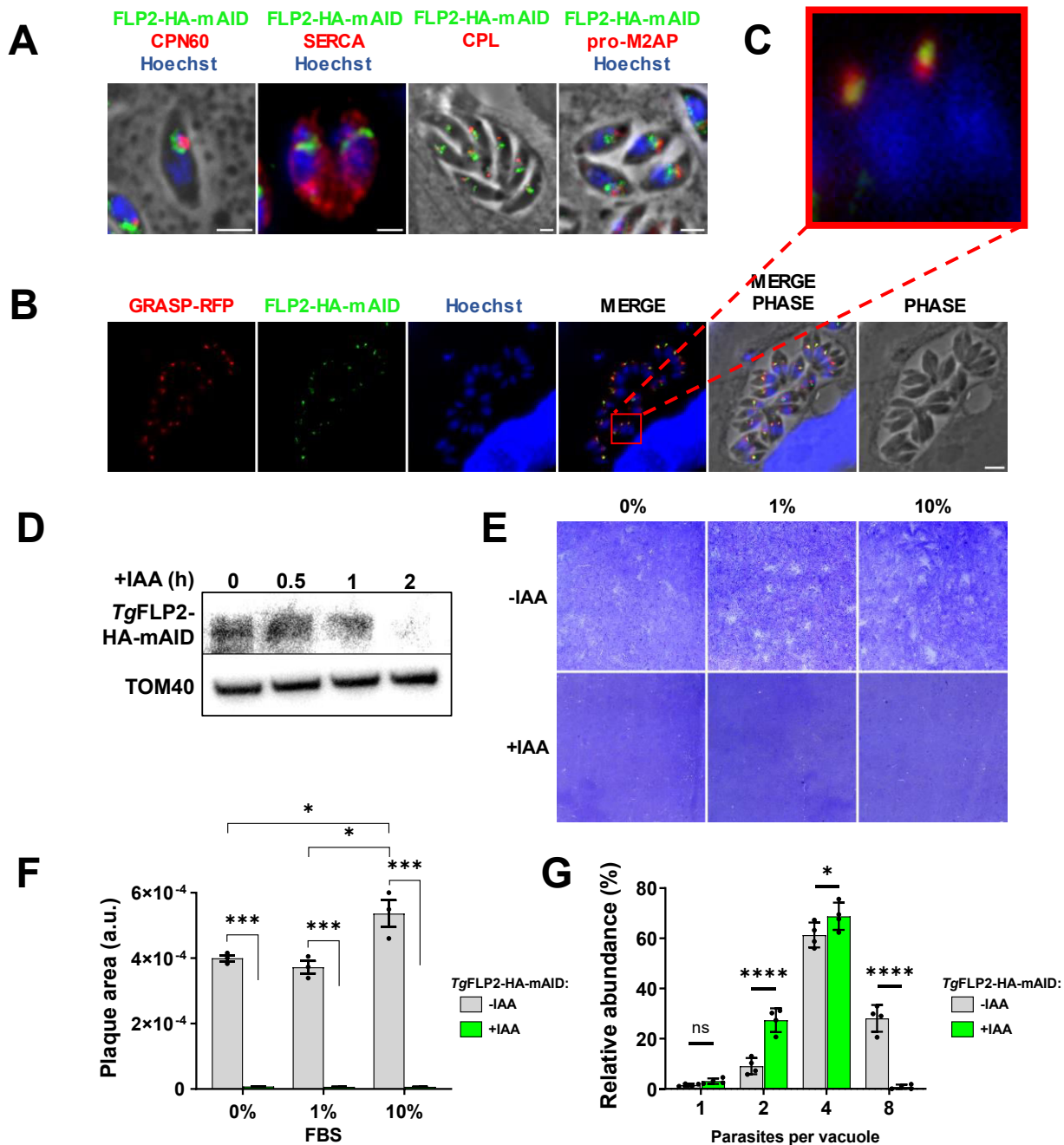


Figure 2: TgFLP2 is an essential Golgi protein

(A) Immunofluorescence assays of TgFLP2-HA-mAID using anti-HA along with antibodies targeting different intracellular markers, CPN60: apicoplast, SERCA: endoplasmic reticulum, CPL: plant-like vacuolar compartment, pro-M2AP: endosomes-like compartments, scale bar = 2 μ m. (B) Confirmation of the Golgi localization of TgFLP2 with the transient expression of the Golgi marker GRASP-RFP in TgFLP2-HA-mAID and revealed by immunofluorescence assay using anti-HA, scale bar = 2 μ m. (C) Zoom of merge (B). (D) Inducible knockdown of TgFLP2 after IAA addition. TgFLP2 was detected by western-bot using Rt anti-HA antibody, and a complete shutdown of the protein occurred after 2 h of IAA treatment (numbers indicate hours of culture). TOM40 (lower panel) served as a loading control. (E) Detrimental effect of TgFLP2 loss shown by plaque assays performed in the absence (-) or presence (+) of IAA and with different FBS concentrations (0, 1, and 10%) and fixed after 7 days. (F) Plaque size quantification and statistic from plaque assay panel (E), unpaired t-test, mean +/- SD from 3 independent experiments. * $p \leq 0.05$, ** $p \leq 0.01$, *** $p \leq 0.001$, and **** $p \leq 0.0001$. (G) Absence of TgFLP2 reduced the intracellular replication of *Toxoplasma* tachyzoites, two-way Anova multiple comparisons, and mean +/- SD from 4 independent experiments.

al., 2020), and the localization previously reported (Chen *et al.*, 2021). The mAID system rapidly led to protein degradation within 2 h after auxin addition (Figure 2D). To assess the essentiality of

TgFLP2 and determine if the nutrient environment can rescue a potential growth defect, plaque assays were performed in different FBS concentrations (starve condition 0%, poor condition 1%, and rich condition 10%). Independently from the FBS concentration, deletion of *TgFLP2* is deleterious for the parasite growth as no plaque was detected after 7 days (**Figures 2E and F**). This data illustrates the critical role of *TgFLP2* for parasite survival regardless of the increased fitness in a nutrient-rich environment observed in WT (**Figure 2F**). For the rest of this study, the reference culture media used was 1% FBS. *TgFLP2* disruption also impaired parasite intracellular development. Replication assay showed a significant accumulation of small vacuoles of 2- and 4-stage parasites, while the large vacuoles of 8-stage parasites drastically dropped from 30 % to less than 1 % in presence of IAA (**Figure 2G**).

The Golgi apparatus is the central place of vesicular trafficking and flippases have been shown to play critical roles to control exocytosis and endocytosis events. In *Saccharomyces* model, the two flippases Neo1p and Drs2p, regulates the vesicular traffic around the Golgi and the endosomes, however, in *Toxoplasma*, the secretion pathway has been repurposed for the biogenesis of apical organelles and the presence of a single essential flippase FLP2 suggests that it could play a dual role in both endocytosis and apical organelle biogenesis.

Disruption of *TgFLP2* impairs the trafficking of microneme content

Micronemes and rhoptries are both generated from the Golgi apparatus, pro-microneme, and pro-rhoptry proteins transit to the ELCs where they are processed to form mature microneme and rhoptry proteins. Both microneme and rhoptry biogenesis pathways share common effectors as *TgSORTLR*, a GPI-anchor, or the clathrin-adaptor protein AP1 located in the trans-Golgi network and essential for both apical organelles biogenesis (Sloves *et al.*, 2012; Venugopal *et al.*, 2017). But the two pathways also possess divergences, as micronemes' journey to the apical pole intersects with internalized material in the ELCs, while rhoptry content transit through the pre-rhoptries before reaching the mature rhoptries. Flippases are known to facilitate vesicular trafficking, and thus we investigated the impact of *TgFLP2* depletion on the parasite micronemes and rhoptries. ELCs, rhoptries, and micronemes were assessed by IFA using antibodies targeting specific markers of these organelles.

The ELCs are the crossing-rod of rhoptries, micronemes, and internalized materials, and are the first step after the trans-Golgi network. To determine if ELCs were affected by the depletion of *TgFLP2*, we realized IFA using the antibody targeting pro-M2AP, a pro-microneme protein,

matured in the ELCs to become M2AP and reach the micronemes. Observation by epifluorescent microscopy revealed that, in untreated parasites, ELCs mostly appeared as a punctuate signal in the apical area but in about 10 % of the counted parasites, appeared diffused (**Figures 3A top panel and B**). This proportion trended to change upon 24 h of IAA treatment, with a ratio closer to 50:50,

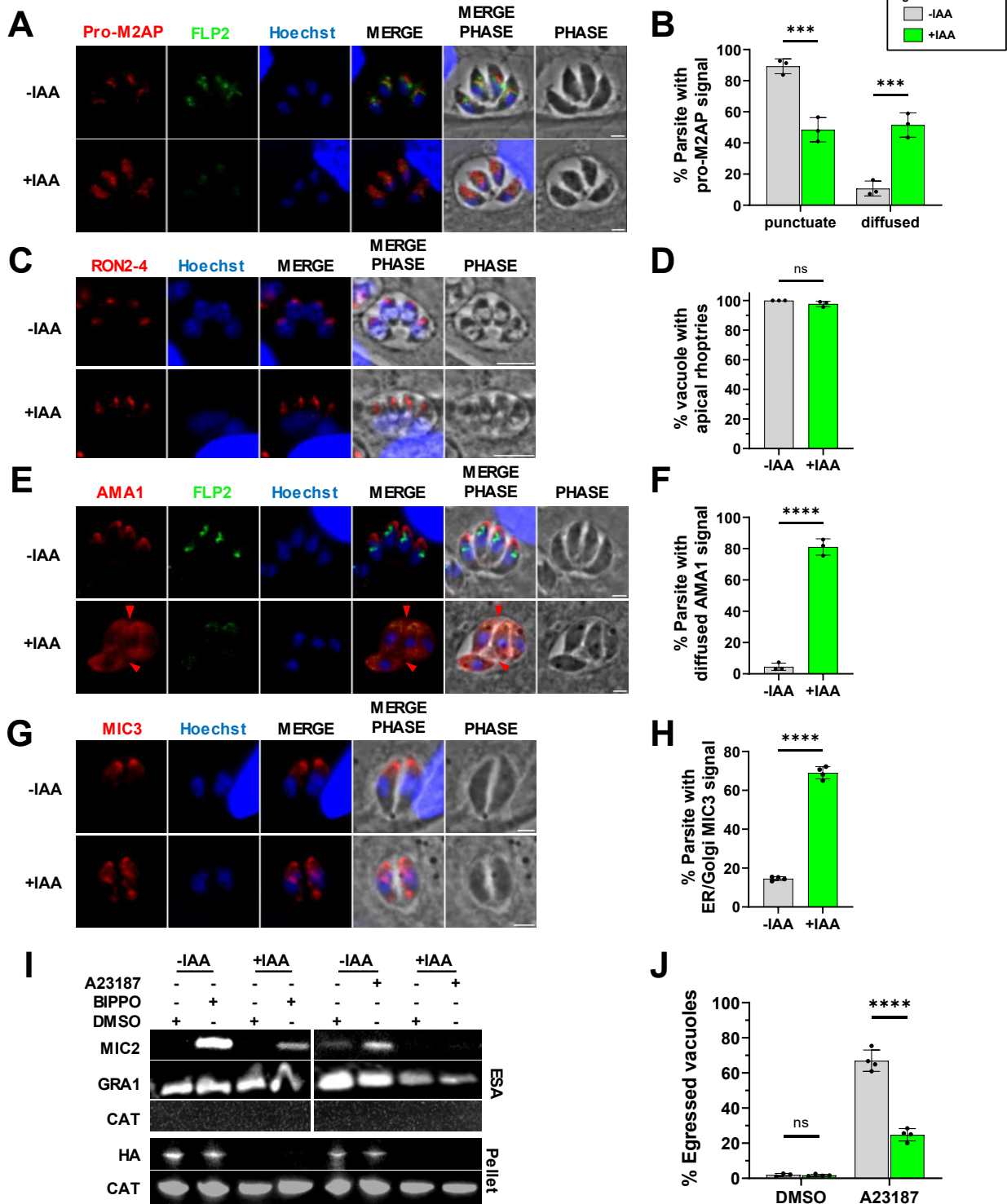


Figure 3: *TgFLP2* controls microneme content targeting

(A) Morphology of ELCs observed by IFA upon *TgFLP2* downregulation +IAA, pro-M2AP: ELCs, scale bar = 2 μm . (B) Quantification of pro-M2AP signal shape in A, punctuate (upper panel) or diffused (lower panel), unpaired t-test, mean \pm SD from 3 independent experiments, *** $p \leq 0.001$. (C) Localization of Rhoptries observed by IFA upon *TgFLP2* downregulation, +IAA, RON2-4: rhoptry's neck, scale bar = 5 μm . (D) Quantification of RON2-4 signal position in C, unpaired t-test, mean \pm SD from 3 independent experiments, ns $p > 0.05$. (E-G) Localization of micronemes observed by IFA upon *TgFLP2* downregulation, +IAA, AMA1 (E), red arrows showing signal in the PV, and MIC3 (G), scale bar = 2 μm . (F-H) Quantification of AMA1 (F) and MIC3 (H) signal position in E and G respectively, unpaired t-test, mean \pm SD from minimum 3 independent experiments, **** $p \leq 0.0001$. (I) Microneme secretion of extracellular *TgFLP2*-HA-mAID stimulated with A23187, or BIPPO of DMSO, and treated or not with IAA for 24 h. ESA: excreted-secreted antigens, Pellet: pellet fraction, MIC2: microneme ESA, GRA1: dense granules ESA, CAT: catalase (cytosolic marker), HA: *TgFLP2*-HA-mAID. (J) Egress assay of *TgFLP2*-HA-mAID grown for 30 h with or without IAA and before stimulation with DMSO or A23187 for 5 min. The percentage of egressed vacuoles is determined, unpaired t-test, mean \pm SD from minimum 4 independent experiments, ns $p > 0.05$, **** $p \leq 0.0001$

revealing that *TgFLP2* is important for the correct morphology of the ELCs (**Figures 3A lower panel and B**).

Rhoptries are elongated eggplant-like shaped organelles composed of a bulb connected to the apical pole *via* the neck. The impact of *TgFLP2* on rhoptries was assessed the same way as for the ELCs, using instead an antibody targeting the rhoptry-neck protein RON2-4. Surprisingly, localization of the RON2-4 signal remained unchanged despite the absence of *TgFLP2* (**Figures 3D and E**).

Finally, to assess the impact of *TgFLP2* on the micronemes, we performed IFA using different antibodies targeting microneme proteins (MIC3 and AMA1) and looked by fluorescent microscopy at transgenic parasites treated or not with IAA for 24 h. Microneme signals were normally localized at the apex of the parasites with signals that were close to the parasite plasma membrane (**Figure 3E and G top panels**). Once *TgFLP2* depleted, the AMA1 signal appeared to be diffused / perinuclear in $\sim 80\%$ of the counted parasites and even localized in the PV (**Figures 3E and F**). MIC3 localization compared to AMA1 localization is timely regulated and is known to accumulate as pro-MIC3 within the secretory pathway in recently replicated parasites (El Hajj *et al.*, 2008). In untreated parasites, $\sim 15\%$ presented a retained signal with the ER/Golgi but this was further exaggerated up to $\sim 70\%$ after 24 h of IAA treatment (**Figures 3G and H**). To confirm the defect in micronemes reaching the correct localization, direct microneme secretion on extracellular parasites and parasite active egress from its host, which depends on microneme secretion, were tested. Secretion assay revealed that microneme secretion was affected upon IAA treatment, with no MIC2 band detected by western blot after secretion stimulation with A23187 that induced Ca^{2+} release from the ER or a reduced band intensity after stimulation with BIPPO that leads to cGMP accumulation, compare to *TgFLP2* harboring parasites (-IAA) (**Figure 3I**). In addition to the defect in microneme secretion, *TgFLP2* depleted parasites also presented a severe reduction of the egress efficiency with a total of egressed vacuoles ~ 3 -fold less in cultures treated with IAA compared to

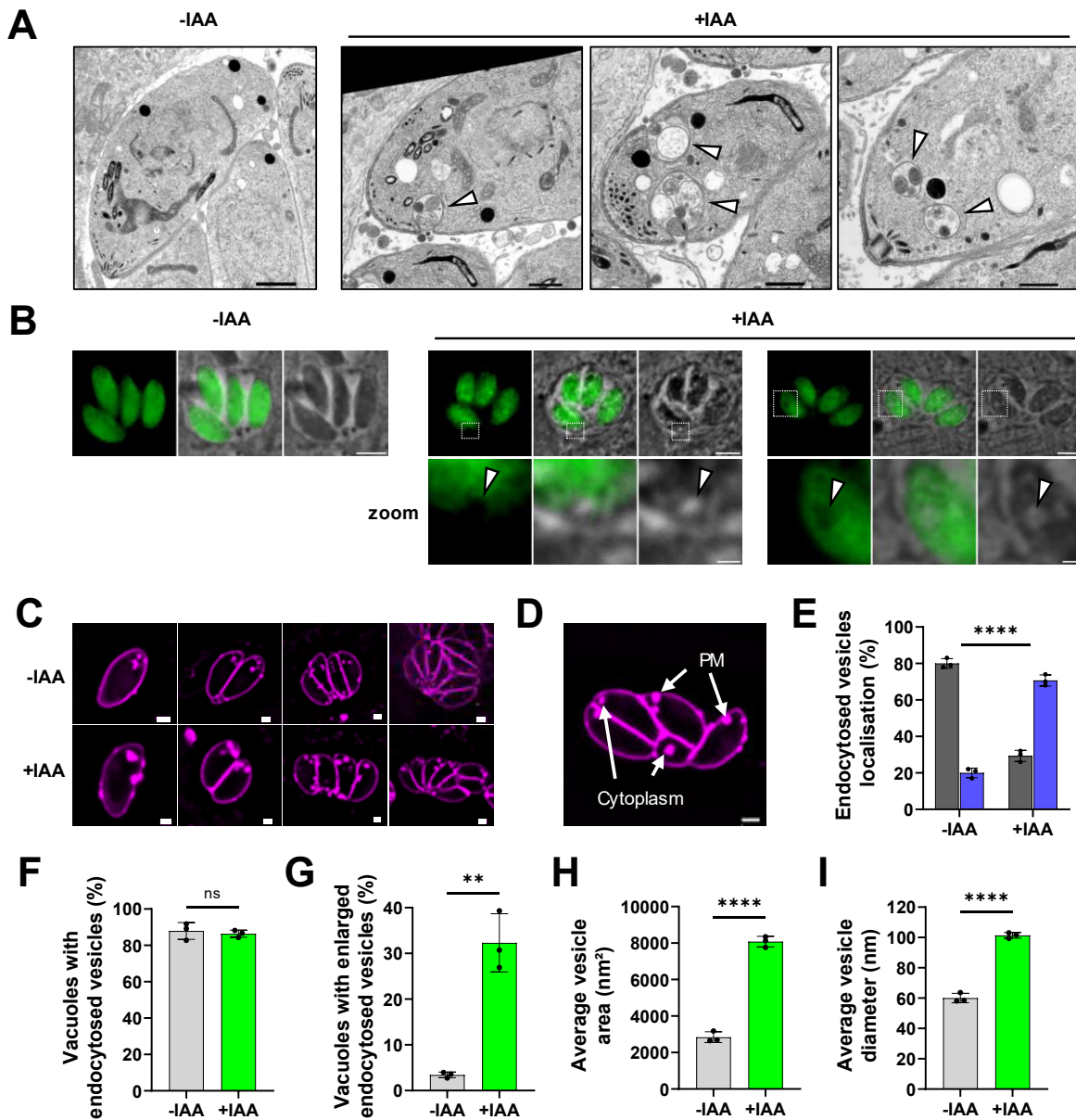


Figure 4: *TgFLP2* regulates endocytosis vesicle formation

(A) Transmission electron microscopy on *TgFLP2*-HA-mAID treated or not with IAA for 24 h. White arrows indicate enlarged structures containing similar materials found in the PV. Scale bar = 1 μ m for -IAA, and 500 nm for +IAA. (B) *TgFLP2*-HA-mAID parasites expressing a cytosolic GFP and observed by IFA after 24 h with or without IAA treatment. Lower panels are the zoom of the white dotted square on upper panels, white arrows indicate light spots in the GFP visible in brightfield. Scale bar = 2 μ m top panels, and 1 μ m lower panels. (C) Representative picture of the *TgFLP2*-HA-mAID control (-IAA) and knock-down (+IAA) at different stages of replication. Scale bar = 1 μ m. (D) Illustration of the different localization quantified in (E), with the endocytic vesicles touching the PM and the fully cytosolic one. Scale bar = 1 μ m. (E) Localization percentage of the endocytic vesicles. Black: Cytoplasm localization, Bleu: In contact with the plasma membrane (PM). Unpaired t-test, mean \pm SD from minimum 3 independent experiments, **** $p \leq 0.0001$. (F) Percentage of vacuole with observable endocytic event between *TgFLP2*-HA-mAID control (-IAA) and knock-down (+IAA). Unpaired t-test, mean \pm SD from minimum 3 independent experiments, ** $p \leq 0.01$. (G) Percentage of vacuole with visible enlarged endocytic vesicles between *FLP2*-HA-mAID control (-IAA) and knock-down (+IAA). Unpaired t-test, mean \pm SD from minimum 3 independent experiments, ns $p > 0.05$. (H) Average endocytic vesicle area between *TgFLP2*-HA-mAID control (-IAA) and knock-down (+IAA). Unpaired t-test, mean \pm SD from minimum 3 independent experiments, **** $p \leq 0.0001$. (I) Average endocytic vesicle diameter between *TgFLP2* control and knock-down. Unpaired t-test, mean \pm SD from minimum 3 independent experiments, **** $p \leq 0.0001$.

cultures untreated (Figure 3J). Together, these results indicate that *TgFLP2* plays an important role in addressing micronemes proteins to the apical pole through the ELCs. However, this is not the

case for rhoptry proteins illustrating the divergence in reaching their mature organelles.

***TgFLP2* is essential for endocytosis trafficking**

Because of the impact of *TgFLP2*-HA-mAID down-regulation on micronemes, it was expected to observe a morphological impact on the micronemes. To assess their morphology, transmission electron microscopy (TEM) was performed on parasites treated for 24 h with IAA and control. Surprisingly, no visible change was observed on rhoptries as expected, but also on micronemes that still appeared rod-shaped and clustered around the conoid (**Figure Supp 3A**). This observation suggests that *TgFLP2* plays a role in the correct import of the microneme content but not directly in the biogenesis of the organelles.

The most interesting observation was the presence of abnormal membranous structures, filled with electron light materials vesicles in absence of *TgFLP2*, which were absent from control parasites (**Figure 4A**). These structures could have been vesicles involved in exocytosis or endocytosis. The first element of response was that the materials inside these structures were similar to the internalized vesicles present in the PV. The second was that the number of events per parasite was comprised between one to three, and their positions in the parasite close to the apical pole suggested that it could be enlarged micropores, the proposed place for endocytosis in *Toxoplasma* (Spielmann *et al.*, 2020; Wan *et al.*, 2023). This was further supported by the transfection of a cytosolic GFP in the *TgFLP2*-HA-mAID strain and revelations by IFA. Untreated parasites showed a diffused homogenous GFP signal in the parasite's cytosol. But in treated parasites, some lighter dots were visible with a lighter GFP signal (white arrows), which matches light dots also visible in brightfield (**Figure 4B**). These observations reminded the membranous structures observed by TEM. The fact that these dots were not filled with GFP signal also indicated that these vesicles were probably issued from endocytosis.

Close homology to *ScNeo1p* and conservation of essential residues already suggested that *TgFLP2* could play a similar role in *Toxoplasma* than the yeast flippase. *ScNeo1p* is involved in endocytosis events and vesicle recycling to the Golgi from the early endosome (Hua *et al.*, 2002; Wicky *et al.*, 2004). To confirm, the involvement of *TgFLP2* in endocytosis was assessed *via* an endocytosis assay which consist to grief a Halo-tag to SAG1, a plasma membrane surface marker, in the *TgFLP2*-HA-mAID strain and to measure the formation of endocytosis vesicle through the internalization of SAG1-Halo by fluorescent microscopy. Both IAA-treated and untreated parasites expressed the Halo tag at the plasma membrane, and both showed dotted signals which were the

endocytosis vesicles (**Figure 4C**, **Figure Supp 3B**). Using this new strain, endocytosis vesicle localization and size can be quantified. Two localizations were discriminated, vesicles attached to the plasma membrane or internalized in the cytosol (**Figure 4D**). In control parasites (-IAA), 80 % of the vesicles were localized in the cytosol vs ~70 % that stayed attached to the plasma membrane after IAA treatment (**Figure 4E**). Deletion of *TgFLP2* did not affect the formation of endocytosis vesicles as these events occurred in knock-down parasites as frequently as in the control (**Figure 4F**). However, *TgFLP2* deletion did affect the size of these vesicles, 30 % of the vacuoles presented enlarged vesicles (**Figure 4G**), with an increased area from 2800 nm² to 8000 nm² and an increased diameter from 60 to 101 nm (**Figure 4H and I**). This assay confirmed the nature of the membrane structures observed by TEM, and highlight the role of *TgFLP2* in regulating the endocytosis vesicles that stay blocked at the plasma membrane and are expanding in its absence.

***TgFLP2* is essential for correct membrane homeostasis**

Vesicular trafficking, endo- and, exocytosis are regulated by lipidic microdomains and membrane asymmetry generated by flippases. *TgFLP2* is a putative P4-ATPase and to determine its role in *Toxoplasma* lipidome, we performed lipidomic analysis on parasites treated or not with IAA for 12 h and analyzed their FA content by GC-MS. Total FA content was unchanged upon *TgFLP2* repression (**Figure 5A**), however, looking at the detailed FA composition we observed several significant changes. Short FA chains C16:0, and C18:0 increased while long FA chains C18:2, C20:1, C22:1, and C22:6 decreased, this is also the case for C12:0 and C16:1 (**Figure 5B**). The notable point was that the composition in unsaturated FA (UFA) trended to decrease compared to the composition in saturated FA (SAFA), which can alter the physical properties of the membrane and certainly impairs the vesicular trafficking, thus SAFA and UFA percentages were determined and revealed a slight but significant decrease of the UFA in the absence of *TgFLP2* (**Figure 5C**). This change not that impressive remained visible at the parasite scale while *TgFLP2* was restricted to the Golgi apparatus, and the decrease of the UFA composition suggested that the membrane fluidity was reduced, which can also reduce the formation of membrane curvatures. These observations were specific to *TgFLP2* deletion and not due to IAA addition as the parental line osTIR was treated for 48 h with IAA and no change was observable in the total FA amount as well as the FA composition (**Figures Supp 4A and B**).

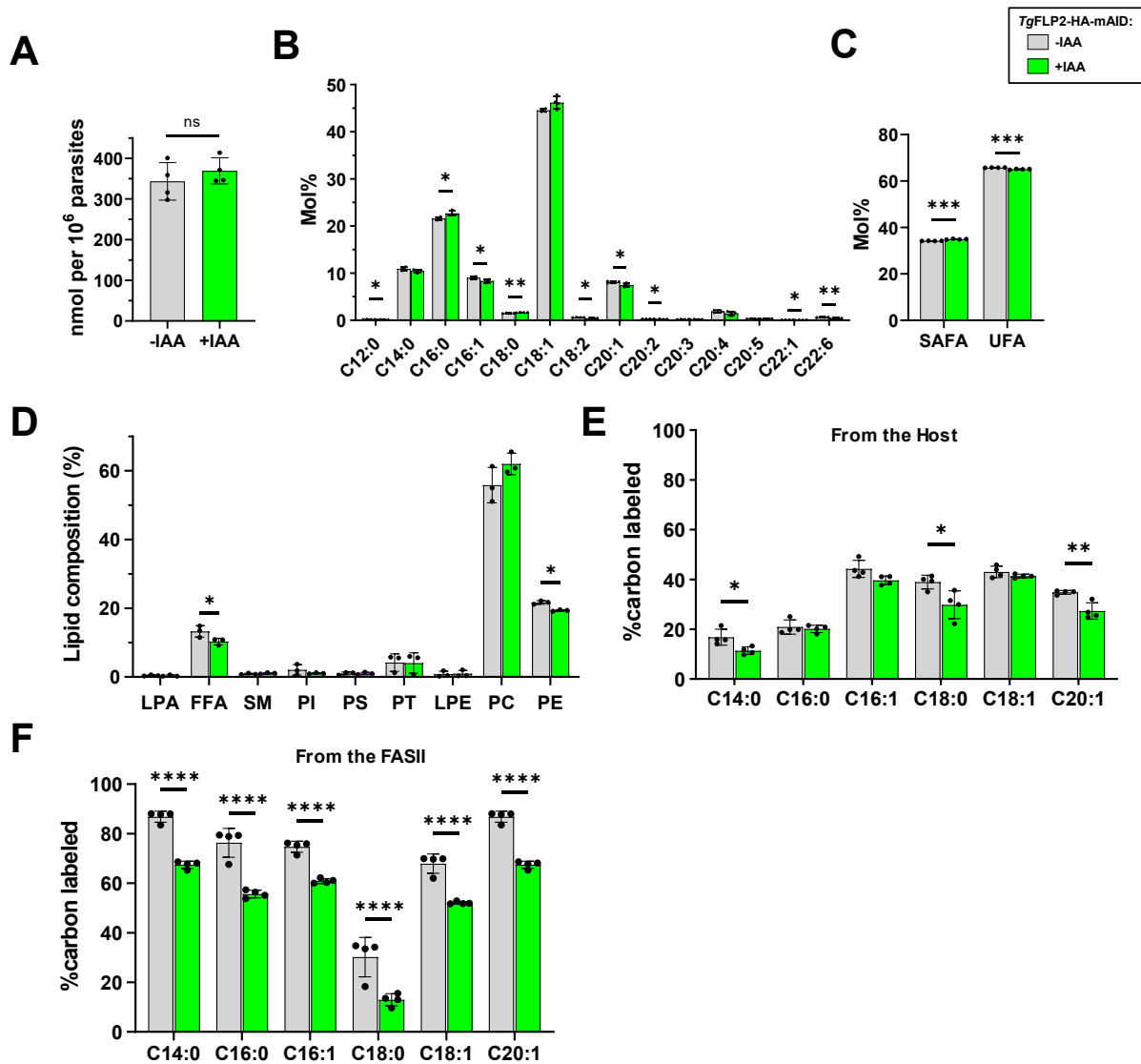


Figure 5: *TgFLP2* deletion impacts *Toxoplasma* lipidic homeostasis

(A) *TgFLP2*-HA-mAID FA total amount, quantified by GC-MS is unchanged after 12 h with or without IAA treatment. Unpaired t-test, mean \pm SD of 4 independent experiments, ns $p > 0.05$. (B) *TgFLP2*-HA-mAID FA composition in Mol% after 12 h with or without IAA treatment, Unpaired t-test, mean \pm SD of 4 independent experiments, * $p \leq 0.05$; ** $p \leq 0.01$. (C) *TgFLP2*-HA-mAID Mol% of saturated FA (SAFA) vs unsaturated (UFA) after 12 h with or without IAA treatment, Unpaired t-test, mean \pm SD of 4 independent experiments, *** $p \leq 0.001$. (D) Lipid classes, from *TgFLP2*-HA-mAID, treated with IAA or not for 12 h, separated by 2D-TLC and analyzed by GC-MS, Unpaired t-test, mean \pm SD of 3 independent experiments, * $p \leq 0.05$. (E) *TgFLP2*-HA-mAID 13 C incorporation % in FA by parasite *de novo* FASII grown in 8 mM 13 C-U-Glucose for 48 h and treated for 24 h with or without IAA before the harvest, Unpaired t-test, mean \pm SD of 4 independent experiments, * $p \leq 0.05$; ** $p \leq 0.01$. (F) *TgFLP2*-HA-mAID 13 C incorporation % in FA from host scavenged lipids, host cells grown in 8 mM 13 C-U-Glucose until full confluency, cultures were infected with parasites for 24 h and treated for an extra 24 h with or without IAA before the harvest, Unpaired t-test, mean \pm SD of 4 independent experiments, **** $p \leq 0.0001$.

P4-ATPases are inserted into the membrane and catalyze the flipping of aminophospholipids, to assess the impact of *TgFLP2* on the phospholipid content of the parasites treated with IAA or not for 12 h, we separated the different lipid classes by two dimensions of high-performance thin-layer chromatography and analyzed them by mass spectrometry. None of the phospholipids were

affected except for the phosphatidylethanolamine (PE), which significantly decreased in the FLP2 over a short period of 12 h (**Figure 5D**) that dropped by almost 10 % compared to -IAA (**Figure Supp 4C**). PC tended to increase as the counterpart of PE decreased and a significant drop in FFA was also observed (**Figure 5D, Figure Supp 4C**).

The impact of the *TgFLP2* deletion on parasite capacities to scavenge lipids from the host and to synthesize *de novo* within the apicoplast were measured. Briefly, to assess the scavenging capacities, parasites were inoculated on HFF prior grown with 8 mM ^{13}C -U-glucose until they reached confluency and the labeled glucose was washed out, parasites were grown for 24 h before the addition of IAA in the +IAA cultures and grown for another 24 h before harvest, lipid extraction and GC-MS analysis (**Figure Supp 4D**). *TgFLP2*-HA-mAID treated with IAA showed a decrease in carbon incorporation in scavenged C14:0, 18:0, and C20:1 indicating a reduction of the scavenging in the mutant (**Figure 5E**). FASII had been shown to work as a balance to the lipid scavenging, and when the scavenging decrease, the FASII activity is upregulated. Here, FASII was assessed after inoculation of parasites on confluent HFF along with 8 mM ^{13}C -U-glucose and grown for 24 h before the addition of IAA in the +IAA cultures and grown for another 24 h before harvest, lipid extraction, and GC-MS analysis (**Figure Supp 4D**). Surprisingly, FASII activity was severely impacted by the repression of *TgFLP2*, as all FA showed a large decrease of ^{13}C carbon incorporation (**Figure 5F**). The mass isotopomer distribution (MID) of the different FA species revealed a normal or higher ^{13}C carbon incorporation until a length of M+8 carbons which then drastically fall in parasites without *TgFLP2* compared to parasites with (**Figure Supp 5**). These unexpected observations combined with the impact on scavenging and PE composition highlight the importance of *TgFLP2* for *Toxoplasma* lipidic homeostasis.

Discussion

P4B-ATPases such as the yeast *ScNeo1p* or the human ATP9A play a critical role in controlling endosomal recycling (Dalton *et al.*, 2017; T *et al.*, 2023), membrane asymmetry (Takar *et al.*, 2016) and endocytosis event (Wicky *et al.*, 2004). The present study highlights the role of P4B-ATPase in *Toxoplasma gondii*, in regulating the parasite vesicular trafficking, controlling the endocytosis as well as the vesicular addressing of secretive apical organelle contents (**Figure 6**).

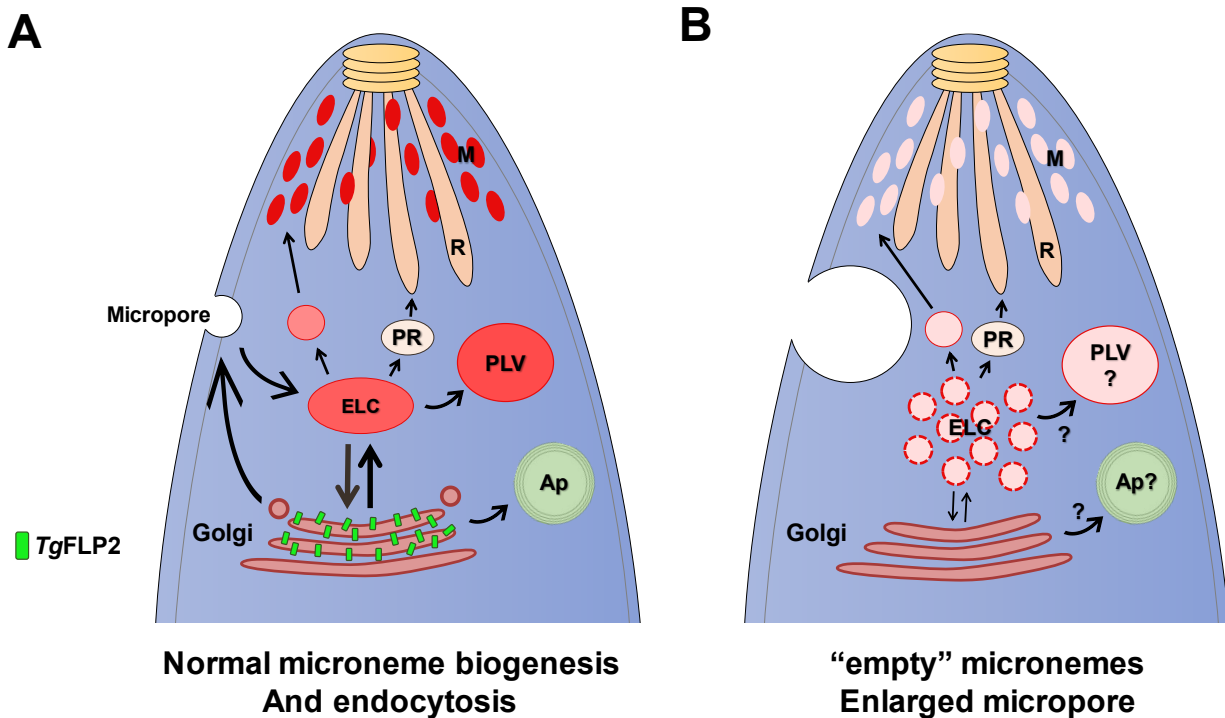


Figure 6: Model to sum up the role of *TgFLP2* as a central element for *Toxoplasma* vesicular trafficking

(A) Correct vesicular trafficking from the trans-Golgi network toward the endosome-like compartments (ELC), for microneme and rhoptry contents addressing to the apical pole. Endocytosis events happening at the level of the micropore are correctly internalized within the parasite allowing the correct entry of scavenged materials from the host and the apicoplast functions/activities are assured in the presence of *TgFLP2*. (B) Absence of *TgFLP2* severely impairs the vesicular trafficking of *Toxoplasma*, ELC appeared affected and microneme contents addressing is dependent on *TgFLP2* as in its absence microneme signals were diffused in the cytosol or stuck in the ER/Golgi compartments. Rhoptries, however, seem to take another path independent from *TgFLP2* as their morphology and localization remained unchanged in the absence of *TgFLP2*. Endocytosis that intercrosses with the micronemes content within the ELC, did not occur properly without *TgFLP2*, and the internalization of the endocytosis vesicles was blocked at the level of the plasma membrane and expanded abnormally. Wan *et al.*, 2023 showed that ER ceramide *de novo* synthesis is essential for endocytosis, *TgFLP2* is probably responsible for sending ceramide-rich vesicles to the plasma membrane for the correct function of the micropore. M = micronemes, R = rhoptries, PR = pre-rhoptries, Ap = apicoplast, ELC = endosome-like compartments, PLV = plant-like vacuolar compartment.

TgFLP2* could act as a PE/PS flippases like *ScNeo1p

TgFLP2 was demonstrated to localize to the Golgi apparatus and its deletion drastically impacts the intracellular development of the parasite, in concordance with the previous study (Chen *et al.*, 2021). *In silico* analysis of *TgFLP2* structure revealed that FLP2 shares critical residues present in the *ScNeo1p* but not *ScDrs2p*, suggesting that *TgFLP2* has the same substrate as Neo1p meaning PE and PS (Bai *et al.*, 2021; Huang *et al.*, 2020; Wu *et al.*, 2016). However, further investigations are required to confirm the substrate affinity.

Analysis of the parasite lipidome revealed that *TgFLP2* is crucial for the parasite's lipidic homeostasis. Indeed, depleted parasites observe a rapid decrease in PE one potential substrate of *TgFLP2*. Precedent works on yeast flippases of the Golgi, aka *Drs2p* and *Neo1p*, have shown the

crucial role of PE in vesicular trafficking (Takar *et al.*, 2016; Takeda *et al.*, 2014). It also has been shown that PS was not important for the vesicular trafficking opposite to PE, for which the over-production can rescue Drs2p deficient yeast (Graham, 2004). In *Toxoplasma*, PE synthesis occurs in the mitochondria where PS decarboxylase 1 (*TgPSD1mt*) converts PS into PE, but *Toxoplasma* also secretes a PSD (*TgPSD1pv*) into the PV and both PSDs can play a redundant role (Hartmann *et al.*, 2014). Decreased PE in our mutant can be explained by default to flip PS/PE at the level of the Golgi apparatus which impairs phospholipids microdomains essential for the recruitment of lipid transfer proteins (Voelker, 2005), and block the addressing of PS to the mitochondria. Another possibility is that PE generated from the secreted *TgPSDpv* from external PS is no longer imported into the parasite as supported by the decrease of lipid scavenging (**Figure 5E**) and the inability of the endocytosis vesicles to detach from the plasma membrane (**Figure 4**). Moreover, these results are supported by the deletion of the Golgi SNARE protein *TgGS27* in which a noticeable decrease in unsaturated PE was observed (Cao *et al.*, 2021), which corroborates the decreased PE and the decrease in unsaturated FA species shown in this study (**Figures 5C and D**).

P4A-ATPases are the alpha subunit of a dimer associated with a beta subunit that belongs to the CDC50/Lem3 family essential for the flipping activity. On the other hand, P4B-ATPases to which belong *ScNeo1p*, *HsATP9A*, and *HsATP9B*, are known to be functional as a monomer independently from CDC50 (Bai *et al.*, 2021; Takatsu *et al.*, 2011) and *TgFLP2* belongs to this sub-family. Despite the predicted structural homology with *ScNeo1p*, the *Toxoplasma* genome encodes for four CDC50 and one has been reported to localize to the Golgi apparatus (Bisio *et al.*, 2021; Chen *et al.*, 2021). The role of this Golgi CDC50 in *Toxoplasma* remains unknown, but the Golgi localization suggests that it could interact with *TgFLP2*. Yeast possesses two Golgi flippases, while in humans, six of the fourteen P4-ATPases have been reported to localize to the Golgi to ensure the PS internalization, the correct membrane asymmetry, and the correct endosomes or plasma membrane to Golgi recycling (Andersen *et al.*, 2016). In contrast, *Toxoplasma* possesses only one, and the presence of the CDC50 could explain the dual role of *TgFLP2* in the regulation of the endo- and the exocytosis in the parasite, the hypothesis is that interaction or not with the CDC50 defines the *TgFLP2* function.

Toxoplasma* vesicular trafficking is dependent on *TgFLP2

TgFLP2 was implicated in the correct trafficking of micronemes content to the apical pole but not directly in the biogenesis of the organelles. Similar observations were made in the mutant *TgStx12*, a SNARE protein located in the ELC and for which the disruption impairs the micronemes contents

but not the morphology of the organelles observed by TEM (Bisio *et al.*, 2020). But in contrast to *TgFLP2*, *TgStx12* also impaired the rhoptry contents. Micronemes and rhoptries paths to the apical pole diverge after their exit of the trans-Golgi, in an unclear manner. McGovern *et al.*, 2018 showed that microneme contents intersect with internalized material from the ingestion pathway, this is not the case for rhoptry proteins, this supports the idea that *TgFLP2* located in the trans-Golgi network regulates both microneme proteins addressing (**Figure 3**) and endocytosis (**Figure 4**) whereas rhoptry proteins traffic through a distinct pathway *TgFLP2*-independent.

The enlarged structures observed attached to the plasma membrane were demonstrated to be endocytosis vesicles (**Figure 4**). Similar structures were reported in the case of the *TgVPS45* mutant, a protein involved in the vesicular trafficking between the plasma membrane of the ELCs and the Golgi, and it was suggested that these structures were enlarged micropores (Bisio *et al.*, 2020). The latest work of Wan *et al.*, 2023, studied the impact of the deletion of different components of the micropore. The deletion of *TgKelch13* led to the formation of similar structures filled with the PV content. The work from Wan *et al.*, 2023 also showed the importance of *de novo* ceramide synthesis in the ER for the endocytosis of host material. *TgFLP2* located in the Golgi probably ensures the transfer of ceramide-rich vesicles to the plasma membrane and the ELCs for correct endocytosis.

One of the most unexpected results was the severe reduction of the FASII activity upon deletion of *TgFLP2* (**Figure 5F**, **Figure Supp 5**), which usually acts as a balance with the host scavenging and upregulates its activity if scavenging decrease (Amiar *et al.*, 2020a; Dass *et al.*, 2021a). In the case of *TgFLP2*, both scavenging and FASII decrease at the same time. We demonstrated the importance of *TgFLP2* for parasite endocytosis which explains the decrease in host scavenging. Concerning the FASII activity, It is known that stromal proteins possess a bipartite signal composed of a transient signal to enter the secretory pathway and a chloroplast addressing sequence recognized by the TIC/TOC complex localized in the two innermost membranes of the apicoplast. But the process by which the apicoplast resident proteins reach the outermost membrane remains unclear. The recent work of Cao *et al.*, 2021 highlighted the importance of the secretion pathway for the correct localization of the apicoplast proteins. Disruption of the SNARE *TgVAMP4-2* present in the apicoplast membranes, impaired the correct localization of apicoplast proteins such as *TgACP* essential for the FASII FA elongation (Mazumdar *et al.*, 2006), showing the importance of the vesicular trafficking for nuclear-encoded apicoplast resident proteins. So the first hypothesis is that, because *TgFLP2* regulates the vesicular trafficking in *Toxoplasma*, its disruption can also affect in

consequence the addressing of apicoplast proteins to their final destination. The second hypothesis, supported by the recent work of Wan *et al.*, 2023, showing the essentiality of the micropore for glucose scavenging and utilization, is that *TgFLP2* is also an essential element for the integrity of the micropore maybe by sending ceramide-rich vesicles to the plasma membrane, and its disruption impairs the micropore and so the entry of external glucose explaining the drastic decrease in FASII carbon labeling.

Plasmodium* homolog *PfATP8* could play a similar role as *TgFLP2

The pleiotropic effects of *TgFLP2* disruption on nutrient acquisition, lipid synthesis, and micronemes show its central role in parasites' tachyzoite survival. *Plasmodium falciparum*, one of the causative agents of human malaria, encodes for one *TgFLP2* homolog named *PfATP8* or *PfFLP2* (**Figures 1A and B**) and is predicted to be essential for the parasite blood stage (Zhang *et al.*, 2018). To characterize its role in *Plasmodium*, an inducible HA-tagged transgenic line was generated using the GlmS system. The sequence coding for the GlmS-HA element was added on the endogenous 3' end of the *PfATP8* coding sequence and correct insertion was confirmed by PCR (**Figures Supp 6A and B**). HA tag was successfully expressed in *PfFLP2* and appeared compartmentalized close to the nucleus (**Figure Supp 6C**), it could be the Golgi/ER of *Plasmodium* but this need to be confirmed. *TgFLP2* plays a critical role in endocytosis and so *PfFLP2* impact on *Plasmodium* uptake from the host was assessed using fluorescent lipids (NBD-PC, NBD-PS, and NBD-PE) and analyzed by flow cytometry. Synchronous parasites were treated or not with N-Acetylglucosamine (GlcNac) for 36 h before being incubated with the different fluorescent lipids or DMSO as control, preliminary data showed that import of both PS and PE were reduced in infected red blood cells compared to PC that remained unchanged after addition of GlcNac (**Figure Supp 6C**). This suggests that *PfFLP2* as *TgFLP2* could play a role in the import of material from the host, probably *via* the cytosome, a structure similar to *Toxoplasma* micropore. Further investigations are required to fully decipher the role of *PfATP8* in *Plasmodium* blood-stage infection.

Altogether, the data presented in this study highlight the importance of a P4B-ATPase as a central element for *Toxoplasma gondii* vesicular trafficking, regulating nutrient acquisition, apical organelle biogenesis, and membrane homeostasis.

Acknowledgments

This work was supported by Agence Nationale de la Recherche, France (Project ApicoLipiAdapt grant ANR-21-CE44-0010), The Fondation pour la Recherche Médicale (FRM EQU202103012700), Laboratoire d'Excellence Parafrap, France (grant ANR-11-LABX-0024), LIA-IRP CNRS Program (Apicolipid project), the Université Grenoble Alpes (IDEX ISP-IRGA Apicolipid), Région Auvergne Rhone-Alpes for the lipidomics analyses platform (Grant IRICE Project GEMELI), the CEFIPRA *via* a Collaborative Research Program Grant (Project 6003-1).

Material and Methods

Toxoplasma gondii strains and cultures:

Human foreskin fibroblasts (HFF) are cultured in Dulbecco's Modified Eagle's Medium (DMEM, Life Technologies) supplemented with 10 % fetal bovine serum (FBS) (Gibco), 2 mM glutamine (Gibco) and 25 µg/mL gentamicin (Gibco) at 37°C and 5% CO₂.

T. gondii tachyzoites (RH-Δku80 osTIR, and inducible knock-down strains) were maintained in human foreskin fibroblasts (HFF) using Dulbecco's Modified Eagle's Medium (DMEM, Life Technologies) supplemented with 1 % fetal bovine serum (FBS) (Gibco), 2 mM glutamine (Gibco) and 25 µg/mL gentamicin (Gibco) at 37°C and 5% CO₂.

Generation of inducible knockdown *TgFLP2* line:

To introduce the endogenous tag (3xHA) along with the mini auxin-inducible degron system, mAID, (Brown *et al.*, 2018) at the 3' end of the genes of interest, the mycophenolic acid resistance cassette, 3xHA, and mAID element were amplified from the plasmid pTUB1:YFP-mAID-3HA HXGPRT using oligos in Table 1. For the transfection, 50 µg of PCR products were co-transfected with 50 µg plasmid Sibley Cas9 coding for the endonuclease CRISPR-Cas9 and the appropriate protospacer (guide RNA) generated on the platform CHOP-CHOP (chopchop.cbu.uib.no). RH-Δku80 osTIR strain was transfected. Electroporations were performed in a 2-mm cuvette in a BTX ECM 630 (Harvard Apparatus, at 1,100 V, 25 Ω, and 25 µF). Stable lines expressing the constructs were selected in media with 25 µg/ml mycophenolic acid and 50 µg/ml xanthine according to the resistance cassette of the insert transfected and cloned by limiting dilution.

Screening of the parasite clones with correct HA-mAID element insertion was done using primers pair in Table 1, Figure supp 2. PCR was performed with TaKara primestar max polymerase.

Immunofluorescence assay:

Primary rabbit anti-CPN60 antibodies were used at a dilution of 1:500, rabbit anti-IMC1 at 1:500, rat anti-HA (Roche) at 1:500, mouse anti-ATRx1 at 1:500, rabbit anti-pro-M2AP 1:500 (Carruthers' lab), mouse anti-SERCA 1:500 (Carruthers' lab), rabbit anti-AMA1 1:500 (Lebrun's lab), mouse anti-RON2-4 1:500 (Lebrun's lab), and mouse anti-MIC3 1:500. Secondary AlexaFluor 488- and 546-conjugated goat anti-rat and anti-rabbit antibodies (Life Technologies) were used at 1:1000 dilutions, respectively. GRASP-RFP is transiently expressed on a transfected plasmid. After 24 h of growth with or without 5 mM IAA, parasites were fixed in PBS containing 4 % paraformaldehyde for 15 min at room temperature. Samples were permeabilized with 0.2 % Triton X-100 in PBS for 10 min at room temperature before blocking in PBS containing 3 % FBS and incubation with primary antibodies then secondary antibodies diluted in the blocking solution. Labeled parasites were stained with Hoechst (1:50,000, Life Technologies) for 20 min and then washed three times in PBS then H₂O. Coverslips were mounted onto slides before observation using a Zeiss epifluorescent microscope.

Prediction of protein structure:

TgFLP2 structure was predicted using the Alphafold2 algorithm (Jumper *et al.*, 2021; Varadi *et al.*, 2022). Alphafold was run through the Colabfold on Google Collaboratory (Mirdita *et al.*, 2022), combining the fast homology search of MMseqs2 with Alphafold2. Molecular graphics and analyses performed with UCSF ChimeraX, developed by the Resource for Biocomputing, Visualization, and Informatics at the University of California, San Francisco, with support from National Institutes of Health R01-GM129325 and the Office of Cyber Infrastructure and Computational Biology, National Institute of Allergy and Infectious Diseases.

Egress assay:

Freshly egressed parasites were added to new HFF and invasion was allowed for 1 h before washes and growth for 30 h. Media were washed out and replaced with either ED1% containing 5 μ M A23187 or DMSO and incubated for 5 min at 37°C. Parasites were fixed after the addition of 2x solution of paraformaldehyde 4 % and glutaraldehyde 0.04 % for 15 min. Samples were processed by IFA using an anti-SAG1 antibody. Vacuoles were counted and the percentage of egressed or non-egressed vacuoles were determined. A minimum of 65 vacuoles were counted per replicate.

Microneme secretion assay:

Freshly egressed parasites were washed and resuspended in an equal volume of intracellular buffer (Dulbecco's Modified Eagle's Medium supplemented with 3 % FBS, 10 mM HEPES, pH 7.5). Treatment with A23187 5 μ M, BIPPO 2.5 μ M, or DMSO was performed for 20 min at 37°C. Parasites were pelleted, at 8000 RPM for 2 min at 4 °C, and supernatant (excreted secreted antigens, ESA) was transferred to new Eppendorf tubes. Pellets were washed with cold PBS and re-pelleted. The excreted secreted antigens and pellet fractions were resuspended in sample buffer (50 mM Tris-HCl, pH 6.8, 10% glycerol, 2 mM EDTA, 2% SDS, 0.05% bromophenol blue, 100 mM dithiothreitol (DTT)) and boiled before analysis by western-blot.

Phylogenetic analysis of P4-ATPases:

P4-ATPase sequences from yeast (*Saccharomyces cerevisiae* and *Schizosaccharomyces pombe*), humans (*Homo sapiens*), plants (*Arabidopsis thaliana*), worms (*Caenorhabditis elegans*) or Apicomplexa parasites (*Toxoplasma gondii* and *Plasmodium falciparum*) have been analyzed and phylogram made on Phylogeny.fr. Alignment was performed with MUSCLE, phylogeny with PhyML v3.0 + Alrt using the WAG model of amino acids substitution with NNI topology search, and the tree was generated with TreeDyn. (Anisimova and Gascuel, 2006; Castresana, 2000; Chevenet *et al.*, 2006; Dereeper *et al.*, 2010, 2008; Edgar, 2004; Guindon and Gascuel, 2003).

Western blot analysis:

Proteins were harvested from scraped, needled (G26 needle), and filtered parasite cultures before counting by hemocytometer. Proteins were normalized and extracted by the addition of sample buffer to the parasite and boiled at 95°C for 5 min. Equal volumes of protein samples were loaded and separated on a 4-12% gradient SDS-polyacrylamide (Life Technologies) and transferred to a nitrocellulose membrane. Incubation of the membrane with primary antibodies rat anti-HA (Roche) and rabbit anti-TOM40 followed by incubation with Horse radish peroxidase (HRP) goat anti-rat and anti-rabbit conjugated antibodies (Thermo Scientific). Revelation was done using the Biorad Chemidoc imager after incubation membrane staining with Luminata Crescendo Western HRP detection kit (Millipore).

Plaque assays in *T. gondii* mutants:

The extracellular parasites were harvested after filtration and counted by a hemocytometer. HFF monolayers were infected with ~1,000 mutant parasites and allowed to develop under normal culture conditions or culture medium supplemented with 5 mM indole-3-acetic acid (IAA) for 8

days untouched before staining with Crystal Violet (Sigma) and cell growth assessment by light microscopy for the presence of intact HFF. The average plaque areas (particles) were analyzed using ImageJ software (at least 45 plaques were counted by replicates)

Replication assay in *T. gondii* mutants:

In 4-well plates (with coverslips) equal numbers of TgFLP2-HA-mAID parasites were allowed to invade confluent HFF cells for 2h. After the invasion, the plates were washed (x3) with ED1 (DMEM, 1% FBS) and parasites were grown for 30 h with or without IAA (5 mM). These coverslips were then processed for IFA and the number of parasites per vacuole was calculated (n = 4 independent experiments).

Electron microscopy:

TgFLP2-HA-mAID parasites were grown 24 h in the presence and absence of IAA, in labteks (Nunk, Thermofisher). The labteks containing parasite infected HFF were fixed in 0.1 M cacodylate buffer with 2.5 % glutaraldehyde for 2 h and kept at 4°C until further processing. During processing, samples were fixed again for 1 h with 1 % osmium tetroxide in cacodylate buffer followed by overnight treatment in 2 % uranyl acetate in distilled water. After dehydration in graded series of acetonitrile, samples were progressively impregnated in Epon812, the wells were then filled with fresh resin and allowed to polymerize for 48 h at 60°C. Ultrathin 70 nm sections were obtained with a Leica UCT Ultramicrotome and collected on copper grids. Grids were poststained with uranyl acetate and lead citrate before their observation on a Jeol1200EXII Transmission Electron Microscope. All chemicals were from Electron Microscopy Sciences.

Lipidomic analysis:

To extract lipids, *T. gondii* tachyzoites were grown on 175 cm² HFF cultures. Freshly egressed parasites (~10⁸ parasites equivalent) were quenched in a bath of pure ethanol/dry ice, then needed, filtered, and counted by hemocytometer before centrifugation. Pellets were washed 3x times in cold PBS to eliminate lipids from the culture media before conservation at -80°C. Internal standard 10 μmol FFA C13:0 and 10 μmol PC C21:0 (Avanti Polar lipids) are added to samples and lipids are extracted following the Bligh and Dyer modified by Folch protocol (Ramakrishnan *et al.*, 2015a), FAs are methanolized by Trimethylsulfonium hydroxide (TMSH) by gas-chromatography coupled with mass-spectrometry (Agilent 5977A-7890B) (GC-MS), fatty acid methyl esters were identified by their mass spectrum and retention time compared to authentic standards.

Phospholipid analyses: The extracted total lipid extracted (as above) was separated by one-dimensional silica gel high-performance thin-layer chromatography (HPTLC, Merck). The 1st and 2nd solvent systems used were chloroform/methanol/water/ acetic acid, 25:15:2:4 (v/v/v/v) and hexane/MTBE/acetic acid, 35:15:0.5 (v/v/v), respectively. The spots correlating to FFA, and PL on the HPTLC plates were scraped off, and lipids were methanolized with 200 μ L 0.5 M methanolic HCl in the presence of 1 nmol pentadecanoic acid (C15:0) as internal standard at 85 °C for 4 h. The resulting FAMES were extracted with hexane and analyzed by GC-MS (Agilent).

Fluoromic analysis:

Lipid scavenging is assessed as described by Dass *et al.*, 2021. T175 are set up with HFF grown for 5 days in D10% (-)Glucose complemented with 500 μ L 800 mM U-¹³C-Glucose. Confluent T175 HFF pre-labeled cultures are set up for scavenging assay, the culture medium is discarded, cells are washed with ED1% (3x) and new ED1% is added. Freshly egressed parasites are loaded on the previous HFF pre-labeled with U-¹³C-Glucose and incubated for 48 h and IAA is added 24 h before parasites harvest and lipid extraction for GC-MS analysis. FASII activity is assessed as follows: confluent T175 HFF cultures are set up for FASII ¹³Carbon labeling, the culture medium is discarded and replaced ED1% (-)Glucose complemented with 500 μ L 800 mM U-¹³C-Glucose. Freshly egressed parasites are loaded on the previous HFF U-¹³C-Glucose and incubated for 48 h and IAA is added 24 h before parasites harvest and lipid extraction for GC-MS analysis.

Generation of inducible knockdown *PfFLP2* line in *Plasmodium falciparum*:

A transgenic *P. falciparum* 3D7 line was generated using riboswitch based GlmS system along with a 3 \times HA tag. The construct used for transfection, pTEX-HA-GlmS, contained 988 bp of homology sequence (3' homology region) immediately upstream of the stop codon of *PfFLP2* (Pf3D7_1223400). The 3' homology flank was PCR amplified from *P. falciparum* 3D7 genomic DNA (gDNA) with the primers pair Table 1 and cloned into the BglII and PstI sites of pTEX-HA-GlmS using neb assembly reaction mix (Counihan *et al.*, 2017). Asexual ring stage 3D7 parasites were transfected with the final construct pTEX-HA-GlmS-*PfFLP2*. Transgenic parasites were selected with 2.5 nM WR99210 (Jacobus).

The positive parasite population was screened using the primer pair Table 1, in the combinations described in Figure Supp 6. PCR was performed using TaKara primestar GXL polymerase.

Fluorescent lipid labeling was performed as described by Patel *et al.*, 2022. Briefly, parasites were tightly synchronized and treated or not with N-Acetylglucosamine (GlcNac) 2.5 mM for 36 h.

Parasites were incubated with the different NBD-lipids for 30 min under agitation, then washed with RPMI 5 % BSA FA-free, fixed, permeabilized, and labeled with propidium iodide (PI, Life Technologies) before analyzing the fluorescence by flow cytometry (BD Accuri C6 Plus flow cytometer).

Statistics and graphs:

Graphs and statistical analysis were made using GraphPad Prism8. Graphs represent means and error bars represent the standard deviation. All data were analyzed with the two-tailed unpaired student's t-test (except when mentioned). All p values are represented by asterisks in figures as follows: ns = $p > 0.05$, * = $p \leq 0.05$, ** = $p < 0.01$, *** = $p < 0.001$, and **** = $p < 0.0001$. We consider all p-values lower than 0.05 to be significant.

Table 1: Oligonucleotide sequences used in this study.

| Oligo ID: | Sequence: |
|----------------------------------|---|
| TgFLP2 mAID Forward | Gaccctccagccgcctcagcatgccaagctcgcgt cgccgGGCAGTGGCGGCgagaagagcgcgtgtcct aaagatccc |
| TgFLP2 mAID Reverse | Caaggcgcctttcctccgggaattccactcgetgt catattggacggattcagcgggtcgc |
| Reverse Cas9 plasmid Sibley | AACTTGACATCCCCATTTAC |
| gRNA Forward Cas9 plasmid | agacaaaggacggttcagtGTTTTAGAGCTAGAA ATAGCAAG |
| <i>Tg</i> FLP2 Forward screen #1 | gctgctgtcaacagaggagg |
| <i>Tg</i> FLP2 Reverse screen #2 | cgaacggcgggtcaaacga |
| <i>Pf</i> FLP2 Forward glmS | acgtaacagacttaggaggaTTTATTTACAGTTAT ATATTTTTTCAGTATAACC |
| <i>Pf</i> FLP2 Reverse glmS | ggacgtcgtacgggtaagctgcaAGCAAGCTTGAA AAACTG |
| <i>Pf</i> FLP2 Forward gRNA | TAAGTATATAATATTattaacggatgcctaaaaca GTTTTAGAGCTAGAA |
| <i>Pf</i> FLP2 Reverse gRNA | TTCTAGCTCTAAAACtgttttaggcatccgtaat AATATTATACTTA |
| <i>Pf</i> FLP2 Forward screen #3 | aataattcagacaatgtcaaatcaag |
| <i>Pf</i> FLP2 Reverse screen #4 | aaaattgctcaaagtattagttaac |

Supplementary figures

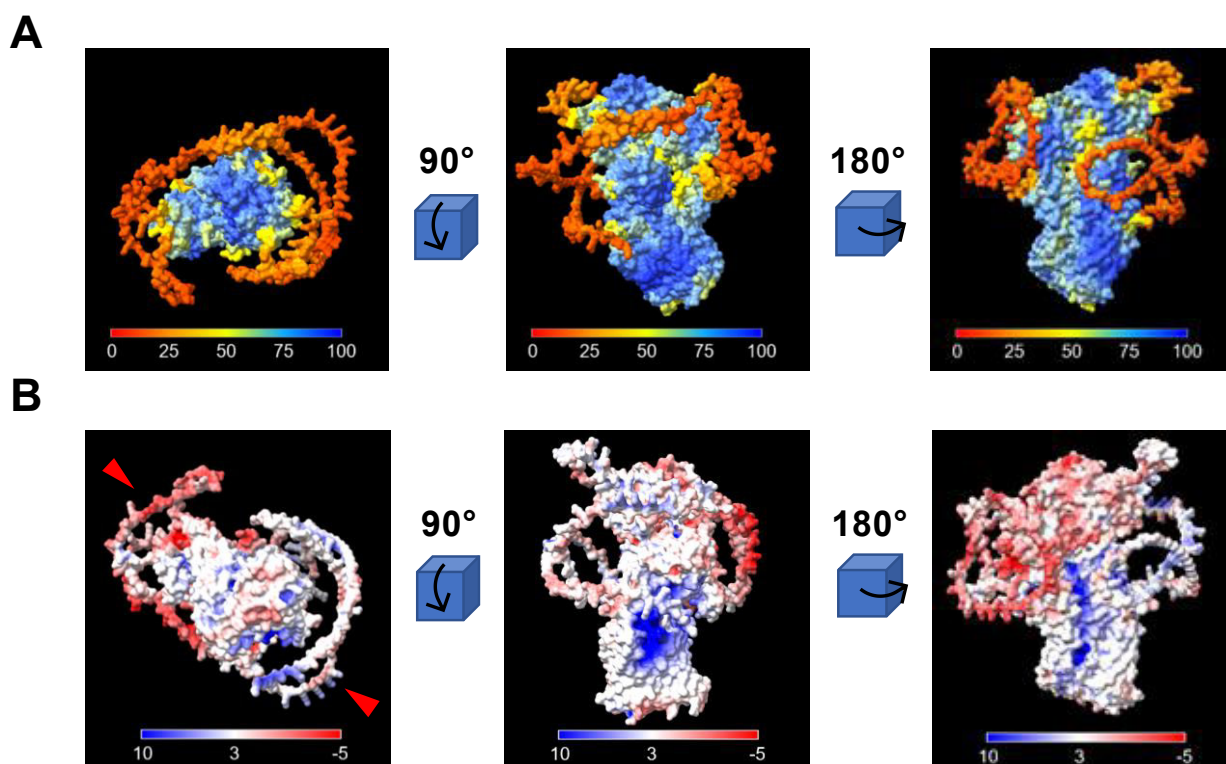


Figure Supp 1: *TgFLP2* predicted structure with Alphafold2

(A) B-factor indicates the confidence of the predicted model, with orange being a very flexible structure, and blue being very well organized. (B) Electrostatic surface potential determines using the Adaptive Poisson-Boltzmann Solver (APBS) software.

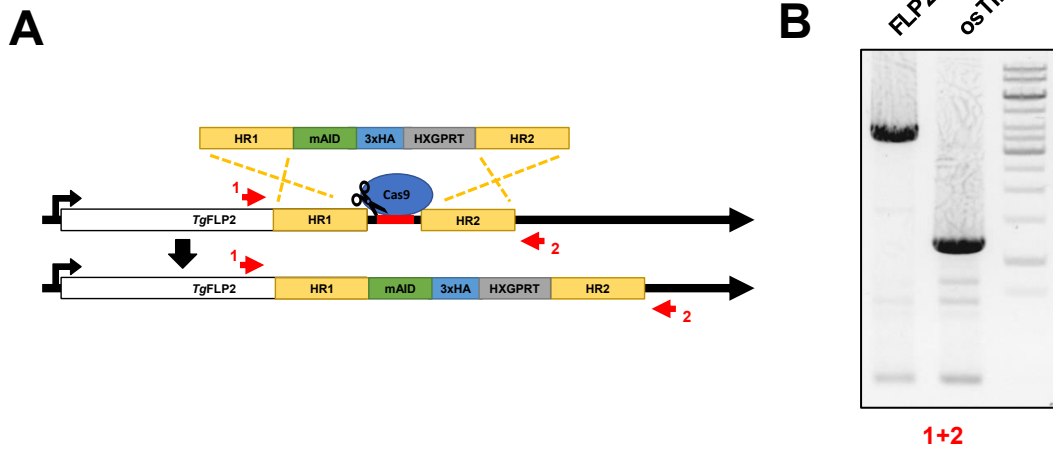


Figure Supp 2: Molecular constructions of *TgFLP2* tagged and inducible knock-down line

(A) mAID-3xHA element integration in 3' of *TgFLP2* coding sequence, CRISPR approach, and homologous recombination. HR = homologous region, HXGPRT = mycophenolic acid resistance cassette. (B) Confirmation by PCR of promoter replacement using pair of primers 1 and 2. Size shift of mAID-3xHA integration is present in the *TgFLP2*-HA-mAID different from the parental strain osTIR.

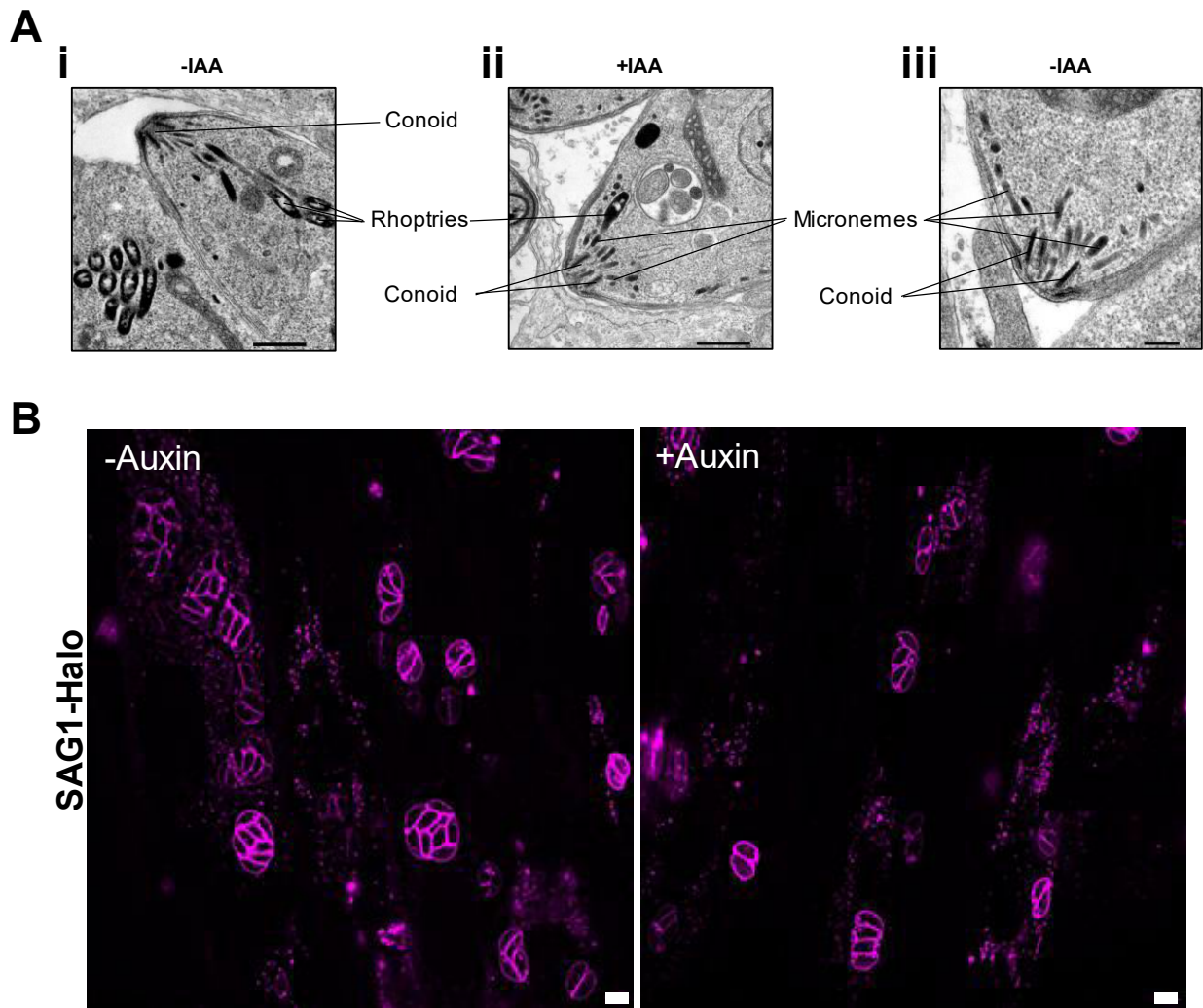


Figure Supp 3: *TgFLP2* is involved in endocytosis

(A) Transmission electron microscopy on *TgFLP2*-HA-mAID treated or not with IAA for 24 h. Scale bar i and ii = 500 nm for; iii = 200 nm. (B) Overall picture of *TgFLP2*-HA-mAID SAG1 Halo parasites with or without auxin treatment (figure 4). Scale bar = 5 μ m.

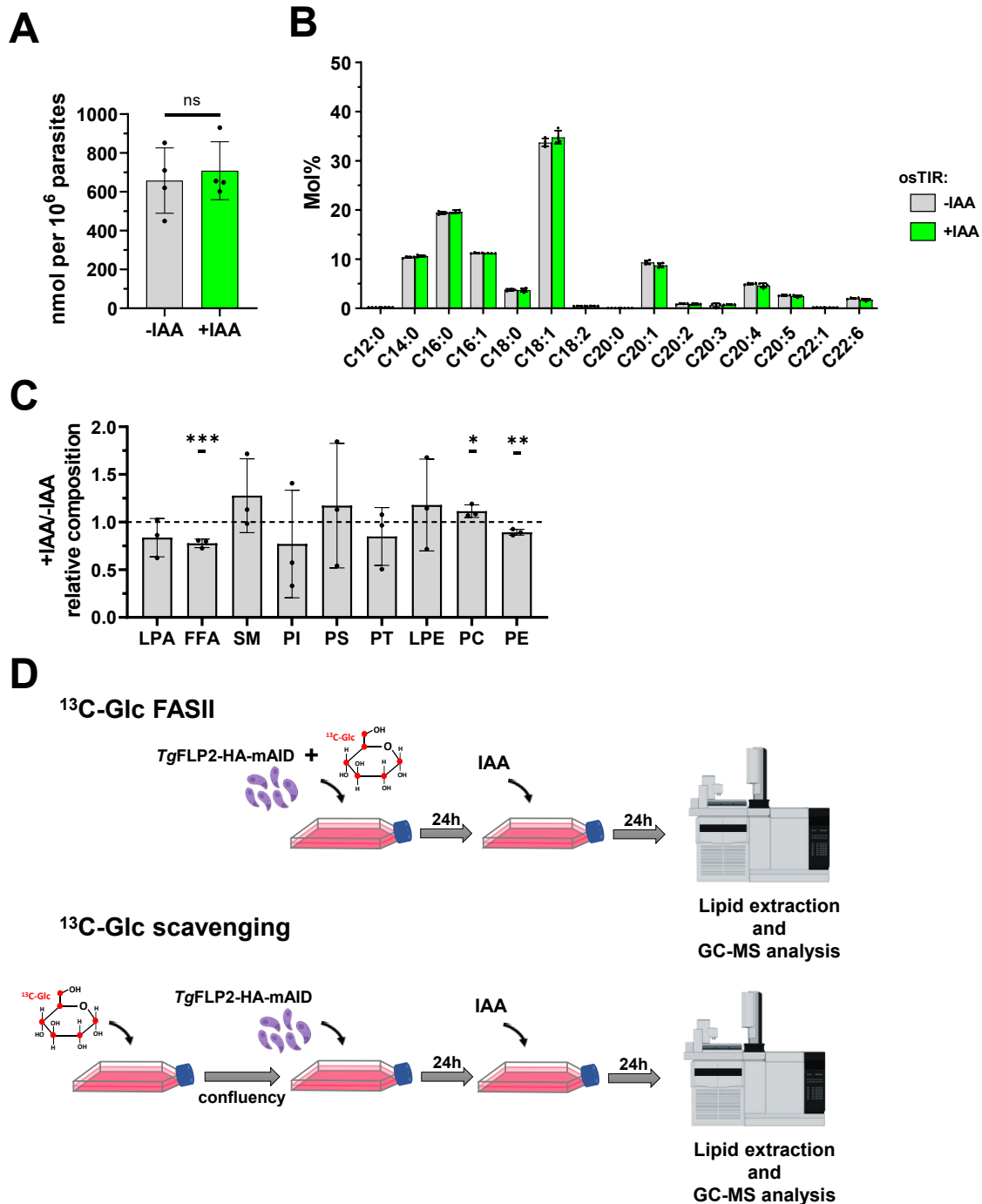
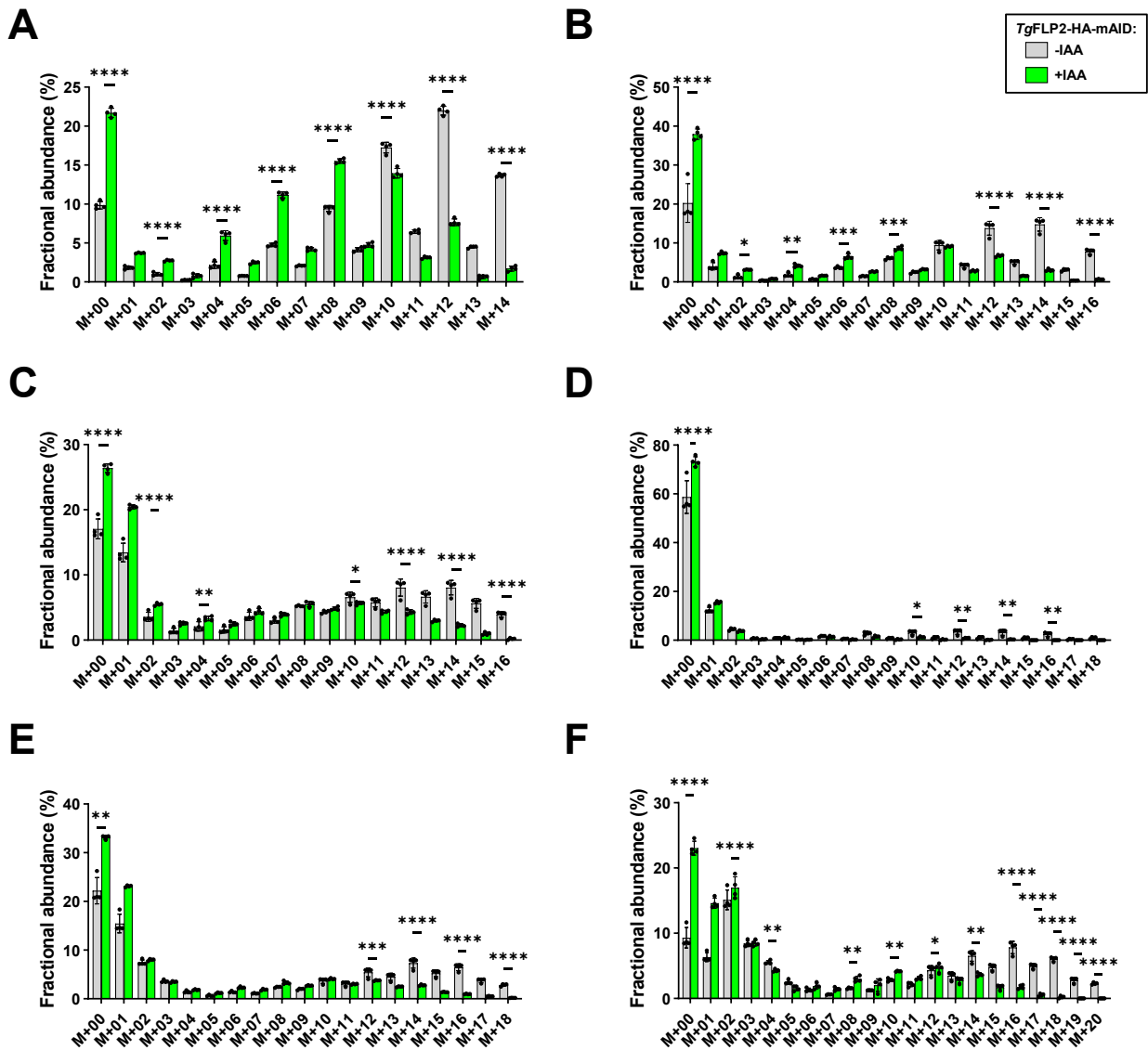


Figure Supp 4: Lipidomic on the parental strain that shows no difference upon IAA treatment

(A) FA total amount, quantified by GC-MS is unchanged after IAA treatment on the parental line Δ Ku80 osTIR, error bars represent +/- SD of 4 independent experiments. (B) FA composition in Mol% of parental line Δ Ku80 osTIR treated with IAA, compared to parasites untreated, error bars represent +/- SD of 4 independent experiments. (C) Lipid classes ratio from *TgFLP2-HA-mAID* treated with IAA for 12 h on parasites untreated, separated by 2D-TLC and analyzed by GC-MS, Unpaired t-test, mean +/- SD of 3 independent experiments. (D) Labeling of FA made by FASII, confluent HFF are infected with *TgFLP2-HA-mAID*, in media glucose-free. Cultures are complemented with 8 mM U-¹³C-Glucose and grown for 24 h before the addition of IAA, then grown for an extra 24 h. Labeling of FA made by the host to measure scavenging capacities, HFF are cultured with media glucose-free and complemented with 8 mM U-¹³C-Glucose until they reached full confluency. Media with labeled glucose is washed out and cells are infected with *TgFLP2-HA-mAID*, in regular media and grown for 24 h before the addition of IAA, then grown for an extra 24 h.



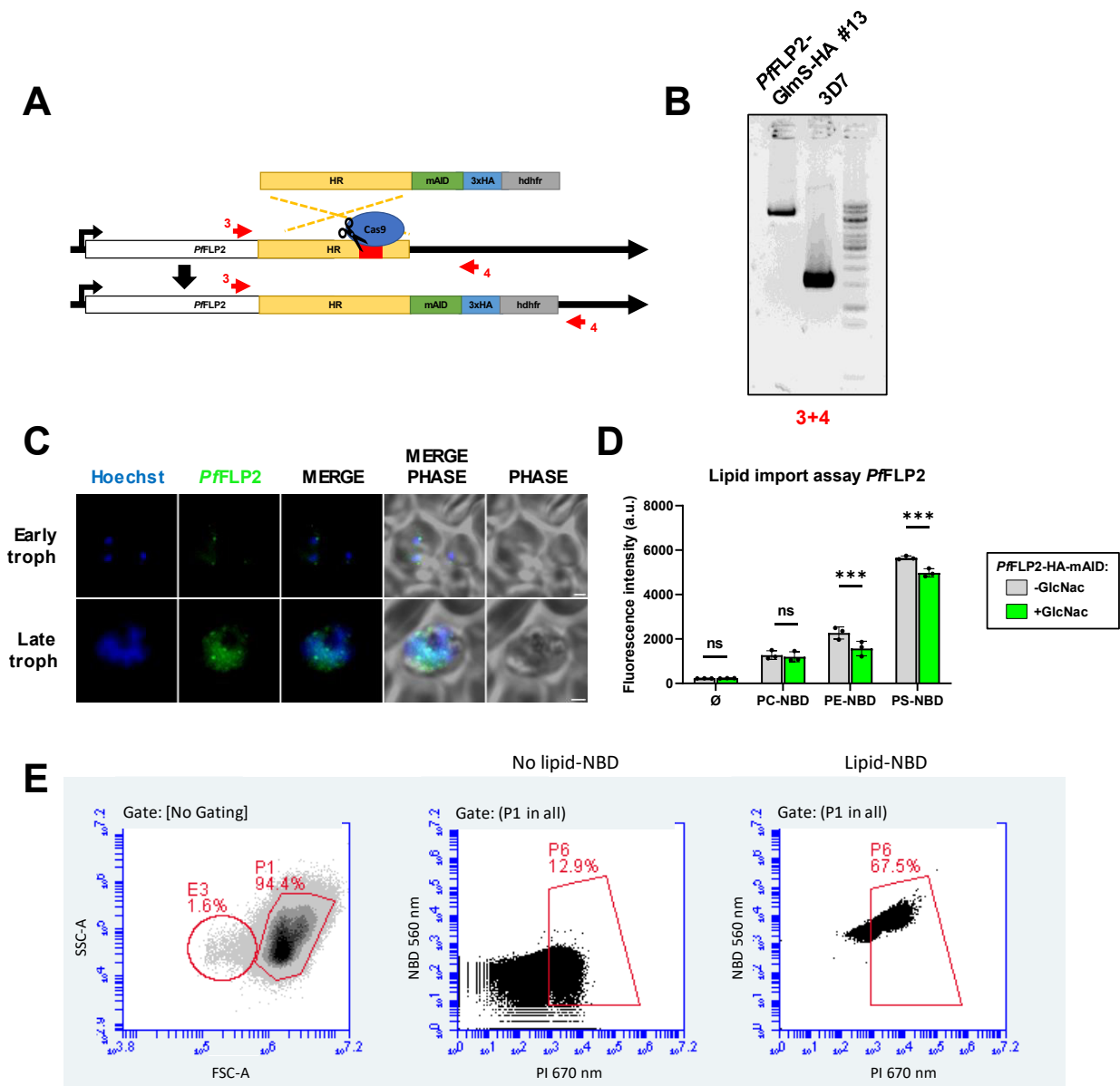


Figure Supp 6: *PfFLP2* could play a similar function as *TgFLP2*

(A) GlmS-3xHA element integration in 3' of *PfFLP2* coding sequence, CRISPR approach, and homologous recombination. HR = homologous region, hdhfr = WR99210 resistance cassette. (B) Confirmation by PCR of promoter replacement using pair of primers 3 and 4. Size shift of GlmS-3xHA integration is present in the *PfFLP2*-GlmS-HA different from the parental strain 3D7. (C) Immunofluorescence assays of *PfFLP2*-HA-GlmS using anti-HA, troph = trophozoite. Scale bar = 3 μ m. (D) Fluorescent lipid import assay on Plasmodium blood stage, parasites tightly synchronized and treated with GlcNac for 36 h. Parasites are incubated with the different NBD-lipids for 30 min under agitation, then washed with RPMI 5 % BSA FA-free, fixed, permeabilized, and labeled with PI before analyzing the fluorescence by flow cytometry. (E) Illustrating of gating for fluorescence signal acquisition by flow cytometry, in P1 are measured infected red blood cells with a positive PI (propidium iodide binds to DNA of parasites), gate P6 = signal at 670 nm emission > 103, and NBD emission signal at 560 nm is measured.

References to chapter V

- Amiar, S., Katris, N.J., Berry, L., Dass, S., Duley, S., Arnold, C.-S., Shears, M.J., Brunet, C., Touquet, B., McFadden, G.I., Yamaro-Botté, Y., Botté, C.Y., 2020. Division and Adaptation to Host Environment of Apicomplexan Parasites Depend on Apicoplast Lipid Metabolic Plasticity and Host Organelle Remodeling. *Cell Reports* 30, 3778-3792.e9. <https://doi.org/10.1016/j.celrep.2020.02.072>
- Amiar, S., MacRae, J.I., Callahan, D.L., Dubois, D., van Dooren, G.G., Shears, M.J., Cesbron-Delauw, M.-F., Maréchal, E., McConville, M.J., McFadden, G.I., Yamaro-Botté, Y., Botté, C.Y., 2016. Apicoplast-Localized Lysophosphatidic Acid Precursor Assembly Is Required for Bulk Phospholipid Synthesis in *Toxoplasma gondii* and Relies on an Algal/Plant-Like Glycerol 3-Phosphate Acyltransferase. *PLoS Pathog* 12, e1005765. <https://doi.org/10.1371/journal.ppat.1005765>
- Andersen, J.P., Vestergaard, A.L., Mikkelsen, S.A., Mogensen, L.S., Chalal, M., Molday, R.S., 2016. P4-ATPases as Phospholipid Flippases—Structure, Function, and Enigmas. *Front. Physiol.* 7. <https://doi.org/10.3389/fphys.2016.00275>
- Anisimova, M., Gascuel, O., 2006. Approximate likelihood-ratio test for branches: A fast, accurate, and powerful alternative. *Syst Biol* 55, 539–552. <https://doi.org/10.1080/10635150600755453>
- Bai, L., Jain, B.K., You, Q., Duan, H.D., Takar, M., Graham, T.R., Li, H., 2021. Structural basis of the P4B ATPase lipid flippase activity. *Nat Commun* 12, 5963. <https://doi.org/10.1038/s41467-021-26273-0>
- Barylyuk, K., Koreny, L., Ke, H., Butterworth, S., Crook, O.M., Lassadi, I., Gupta, V., Tromer, E., Mourier, T., Stevens, T.J., Breckels, L.M., Pain, A., Lilley, K.S., Waller, R.F., 2020. A Comprehensive Subcellular Atlas of the *Toxoplasma* Proteome *via* hyperLOPIT Provides Spatial Context for Protein Functions. *Cell Host Microbe* 28, 752-766.e9. <https://doi.org/10.1016/j.chom.2020.09.011>
- Ben Chaabene, R., Lentini, G., Soldati-Favre, D., 2021. Biogenesis and discharge of the rhoptries: Key organelles for entry and hijack of host cells by the Apicomplexa. *Molecular Microbiology* 115, 453–465. <https://doi.org/10.1111/mmi.14674>
- Bisio, H., Chaabene, R.B., Sabitzki, R., Maco, B., Marq, J.B., Gilberger, T.-W., Spielmann, T., Soldati-Favre, D., 2020. The ZIP Code of Vesicle Trafficking in Apicomplexa: SEC1/Munc18 and SNARE Proteins. *mBio* 11, e02092-20. <https://doi.org/10.1128/mBio.02092-20>
- Bisio, H., Krishnan, A., Marq, J.-B., Soldati-Favre, D., 2021. *Toxoplasma gondii* phosphatidylserine flippase complex ATP2B-CDC50.4 critically participates in microneme exocytosis (preprint). *Cell Biology*. <https://doi.org/10.1101/2021.11.25.470034>
- Bisio, H., Lunghi, M., Brochet, M., Soldati-Favre, D., 2019. Phosphatidic acid governs natural egress in *Toxoplasma gondii* *via* a guanylate cyclase receptor platform. *Nat Microbiol* 4, 420–428. <https://doi.org/10.1038/s41564-018-0339-8>
- Brown, K., Long, S., Sibley, L., 2018. Conditional Knockdown of Proteins Using Auxin-inducible Degron (AID) Fusions in *Toxoplasma gondii*. *BIO-PROTOCOL* 8. <https://doi.org/10.21769/BioProtoc.2728>
- Cao, S., Yang, J., Fu, J., Chen, H., Jia, H., 2021. The Dissection of SNAREs Reveals Key Factors for Vesicular Trafficking to the Endosome-like Compartment and Apicoplast *via* the Secretory System in *Toxoplasma gondii*. *mBio* 12, e01380-21. <https://doi.org/10.1128/mBio.01380-21>

- Castresana, J., 2000. Selection of conserved blocks from multiple alignments for their use in phylogenetic analysis. *Mol Biol Evol* 17, 540–552. <https://doi.org/10.1093/oxfordjournals.molbev.a026334>
- Chen, K., Günay-Esiyok, Ö., Klingeberg, M., Marquardt, S., Pomorski, T.G., Gupta, N., 2021. Aminoglycerophospholipid flipping and P4-ATPases in *Toxoplasma gondii*. *Journal of Biological Chemistry* 296, 100315. <https://doi.org/10.1016/j.jbc.2021.100315>
- Chevenet, F., Brun, C., Bañuls, A.-L., Jacq, B., Christen, R., 2006. TreeDyn: towards dynamic graphics and annotations for analyses of trees. *BMC Bioinformatics* 7, 439. <https://doi.org/10.1186/1471-2105-7-439>
- Daleke, D.L., 2003. Regulation of transbilayer plasma membrane phospholipid asymmetry. *Journal of Lipid Research* 44, 233–242. <https://doi.org/10.1194/jlr.R200019-JLR200>
- Dalton, L.E., Bean, B.D.M., Davey, M., Conibear, E., 2017. Quantitative high-content imaging identifies novel regulators of Neol trafficking at endosomes. *Mol Biol Cell* 28, 1539–1550. <https://doi.org/10.1091/mbc.E16-11-0772>
- Dass, S., Shunmugam, S., Berry, L., Arnold, C.-S., Katris, N.J., Duley, S., Pierrel, F., Cesbron-Delauw, M.-F., Yamaryo-Botté, Y., Botté, C.Y., 2021. *Toxoplasma* LIPIN is essential in channeling host lipid fluxes through membrane biogenesis and lipid storage. *Nat Commun* 12, 2813. <https://doi.org/10.1038/s41467-021-22956-w>
- Dereeper, A., Audic, S., Claverie, J.-M., Blanc, G., 2010. BLAST-EXPLORER helps you building datasets for phylogenetic analysis. *BMC Evol Biol* 10, 8. <https://doi.org/10.1186/1471-2148-10-8>
- Dereeper, A., Guignon, V., Blanc, G., Audic, S., Buffet, S., Chevenet, F., Dufayard, J.-F., Guindon, S., Lefort, V., Lescot, M., Claverie, J.-M., Gascuel, O., 2008. Phylogeny.fr: robust phylogenetic analysis for the non-specialist. *Nucleic Acids Res* 36, W465-469. <https://doi.org/10.1093/nar/gkn180>
- Dubois, D., Fernandes, S., Amiar, S., Dass, S., Katris, N.J., Botté, C.Y., Yamaryo-Botté, Y., 2018. *Toxoplasma gondii* acetyl-CoA synthetase is involved in fatty acid elongation (of long fatty acid chains) during tachyzoite life stages. *J. Lipid Res.* 59, 994–1004. <https://doi.org/10.1194/jlr.M082891>
- Dubois, D.J., Soldati-Favre, D., 2019. Biogenesis and secretion of micronemes in *Toxoplasma gondii*. *Cellular Microbiology* 21, e13018. <https://doi.org/10.1111/cmi.13018>
- Edgar, R.C., 2004. MUSCLE: multiple sequence alignment with high accuracy and high throughput. *Nucleic Acids Res* 32, 1792–1797. <https://doi.org/10.1093/nar/gkh340>
- El Hajj, H., Papoin, J., Cérède, O., Garcia-Réguet, N., Soète, M., Dubremetz, J.-F., Lebrun, M., 2008. Molecular Signals in the Trafficking of *Toxoplasma gondii* Protein MIC3 to the Micronemes. *Eukaryotic Cell* 7, 1019–1028. <https://doi.org/10.1128/EC.00413-07>
- Goddard, T.D., Huang, C.C., Meng, E.C., Pettersen, E.F., Couch, G.S., Morris, J.H., Ferrin, T.E., 2018. UCSF ChimeraX: Meeting modern challenges in visualization and analysis. *Protein Sci* 27, 14–25. <https://doi.org/10.1002/pro.3235>
- Graham, T.R., 2004. Flippases and vesicle-mediated protein transport. *Trends in Cell Biology* 14, 670–677. <https://doi.org/10.1016/j.tcb.2004.10.008>
- Guindon, S., Gascuel, O., 2003. A simple, fast, and accurate algorithm to estimate large phylogenies by maximum likelihood. *Syst Biol* 52, 696–704. <https://doi.org/10.1080/10635150390235520>
- Hartmann, A., Hellmund, M., Lucius, R., Voelker, D.R., Gupta, N., 2014. Phosphatidylethanolamine Synthesis in the Parasite Mitochondrion Is Required for Efficient Growth but Dispensable for Survival of *Toxoplasma gondii*. *J Biol Chem* 289, 6809–6824. <https://doi.org/10.1074/jbc.M113.509406>

- Hua, Z., Fatheddin, P., Graham, T.R., 2002. An Essential Subfamily of Drs2p-related P-Type ATPases Is Required for Protein Trafficking between Golgi Complex and Endosomal/Vacuolar System. *MBoC* 13, 3162–3177. <https://doi.org/10.1091/mbc.e02-03-0172>
- Huang, Y., Takar, M., Best, J.T., Graham, T.R., 2020. Conserved Mechanism of Phospholipid Substrate Recognition by the P4-ATPase Neo1 from *Saccharomyces cerevisiae*. *Biochim Biophys Acta Mol Cell Biol Lipids* 1865, 158581. <https://doi.org/10.1016/j.bbalip.2019.158581>
- Jonscher, E., Flemming, S., Schmitt, M., Sabitzki, R., Reichard, N., Birnbaum, J., Bergmann, B., Höhn, K., Spielmann, T., 2019. PfVPS45 Is Required for Host Cell Cytosol Uptake by Malaria Blood Stage Parasites. *Cell Host & Microbe* 25, 166-173.e5. <https://doi.org/10.1016/j.chom.2018.11.010>
- Jumper, J., Evans, R., Pritzel, A., Green, T., Figurnov, M., Ronneberger, O., Tunyasuvunakool, K., Bates, R., Židek, A., Potapenko, A., Bridgland, A., Meyer, C., Kohli, S.A.A., Ballard, A.J., Cowie, A., Romera-Paredes, B., Nikolov, S., Jain, R., Adler, J., Back, T., Petersen, S., Reiman, D., Clancy, E., Zielinski, M., Steinegger, M., Pacholska, M., Berghammer, T., Bodenstein, S., Silver, D., Vinyals, O., Senior, A.W., Kavukcuoglu, K., Kohli, P., Hassabis, D., 2021. Highly accurate protein structure prediction with AlphaFold. *Nature* 596, 583–589. <https://doi.org/10.1038/s41586-021-03819-2>
- Katris, N.J., Yamaryo-Botte, Y., Janouškovec, J., Shunmugam, S., Arnold, C.-S., Yang, A.S.P., Vardakis, A., Stewart, R.J., Sauerwein, R., McFadden, G.I., Tonkin, C.J., Cesbron-Delauw, M.-F., Waller, Ross.F., Botte, C.Y., 2020. Rapid kinetics of lipid second messengers controlled by a cGMP signalling network coordinates apical complex functions in *Toxoplasma* tachyzoites (preprint). *Microbiology*. <https://doi.org/10.1101/2020.06.19.160341>
- Koreny, L., Mercado-Saavedra, B.N., Klinger, C.M., Barylyuk, K., Butterworth, S., Hirst, J., Rivera-Cuevas, Y., Zaccai, N.R., Holzer, V.J.C., Klingl, A., Dacks, J.B., Carruthers, V.B., Robinson, M.S., Gras, S., Waller, R.F., 2022. Stable and ancient endocytic structures navigate the complex pellicle of apicomplexan parasites. <https://doi.org/10.1101/2022.06.02.494549>
- Koreny, L., Zeeshan, M., Barylyuk, K., Tromer, E.C., van Hooff, J.J.E., Brady, D., Ke, H., Chelaghma, S., Ferguson, D.J.P., Eme, L., Tewari, R., Waller, R.F., 2021. Molecular characterization of the conoid complex in *Toxoplasma* reveals its conservation in all apicomplexans, including *Plasmodium* species. *PLoS Biol* 19, e3001081. <https://doi.org/10.1371/journal.pbio.3001081>
- Liu, K., Surendhran, K., Nothwehr, S.F., Graham, T.R., 2008. P4-ATPase Requirement for AP-1/Clathrin Function in Protein Transport from the *trans* -Golgi Network and Early Endosomes. *MBoC* 19, 3526–3535. <https://doi.org/10.1091/mbc.e08-01-0025>
- Ma, L., Umasankar, P.K., Wrobel, A.G., Lymar, A., McCoy, A.J., Holkar, S.S., Jha, A., Pradhan-Sundd, T., Watkins, S.C., Owen, D.J., Traub, L.M., 2016. Transient Fcho1/2·Eps15/R·AP-2 Nanoclusters Prime the AP-2 Clathrin Adaptor for Cargo Binding. *Dev Cell* 37, 428–443. <https://doi.org/10.1016/j.devcel.2016.05.003>
- Mazumdar, J., H. Wilson, E., Masek, K., A. Hunter, C., Striepen, B., 2006. Apicoplast fatty acid synthesis is essential for organelle biogenesis and parasite survival in *Toxoplasma gondii*. *Proc Natl Acad Sci U S A* 103, 13192–13197. <https://doi.org/10.1073/pnas.0603391103>
- McGovern, O.L., Rivera-Cuevas, Y., Kannan, G., Narwold, A., Carruthers, V.B., 2018. Intersection of Endocytic and Exocytic Systems in *Toxoplasma gondii*. *Traffic* 19, 336–353. <https://doi.org/10.1111/tra.12556>

- McMahon, H.T., Boucrot, E., 2015. Membrane curvature at a glance. *Journal of Cell Science* 128, 1065–1070. <https://doi.org/10.1242/jcs.114454>
- Mirdita, M., Schütze, K., Moriwaki, Y., Heo, L., Ovchinnikov, S., Steinegger, M., 2022. ColabFold: making protein folding accessible to all. *Nat Methods* 19, 679–682. <https://doi.org/10.1038/s41592-022-01488-1>
- Patel, A., Nofal, S.D., Blackman, M.J., Baker, D.A., 2022. CDC50 Orthologues in Plasmodium falciparum Have Distinct Roles in Merozoite Egress and Trophozoite Maturation. *mBio* 13, e01635-22. <https://doi.org/10.1128/mbio.01635-22>
- Pettersen, E.F., Goddard, T.D., Huang, C.C., Meng, E.C., Couch, G.S., Croll, T.I., Morris, J.H., Ferrin, T.E., 2021. UCSF ChimeraX: Structure visualization for researchers, educators, and developers. *Protein Sci* 30, 70–82. <https://doi.org/10.1002/pro.3943>
- Ramakrishnan, S., Docampo, M.D., MacRae, J.I., Pujol, F.M., Brooks, C.F., van Dooren, G.G., Hiltunen, J.K., Kastaniotis, A.J., McConville, M.J., Striepen, B., 2012. Apicoplast and Endoplasmic Reticulum Cooperate in Fatty Acid Biosynthesis in Apicomplexan Parasite *Toxoplasma gondii**. *Journal of Biological Chemistry* 287, 4957–4971. <https://doi.org/10.1074/jbc.M111.310144>
- Ramakrishnan, S., Docampo, M.D., MacRae, J.I., Ralton, J.E., Rupasinghe, T., McConville, M.J., Striepen, B., 2015. The intracellular parasite *Toxoplasma gondii* depends on the synthesis of long-chain and very long-chain unsaturated fatty acids not supplied by the host cell. *Mol Microbiol* 97, 64–76. <https://doi.org/10.1111/mmi.13010>
- Sloves, P.-J., Delhaye, S., Mouveaux, T., Werkmeister, E., Slomianny, C., Hovasse, A., Dilezitoko Alayi, T., Callebaut, I., Gaji, R.Y., Schaeffer-Reiss, C., Van Dorsselear, A., Carruthers, V.B., Tomavo, S., 2012. *Toxoplasma* Sortilin-like Receptor Regulates Protein Transport and Is Essential for Apical Secretory Organelle Biogenesis and Host Infection. *Cell Host & Microbe* 11, 515–527. <https://doi.org/10.1016/j.chom.2012.03.006>
- Spielmann, T., Gras, S., Sabitzki, R., Meissner, M., 2020. Endocytosis in Plasmodium and *Toxoplasma* Parasites. *Trends in Parasitology* 36, 520–532. <https://doi.org/10.1016/j.pt.2020.03.010>
- T, M., X, C., Z, H., H, H., S, L., K, L., G, B., H, L., M, X., H, Z., Y, Z., A, W., Q, L., C, Z., Xd, S., H, H., M, U., Y, Y., D, F., 2023. ATP9A deficiency causes ADHD and aberrant endosomal recycling *via* modulating RAB5 and RAB11 activity. *Molecular psychiatry*. <https://doi.org/10.1038/s41380-022-01940-w>
- Takar, M., Wu, Y., Graham, T.R., 2016. The Essential Neo1 Protein from Budding Yeast Plays a Role in Establishing Aminophospholipid Asymmetry of the Plasma Membrane. *J Biol Chem* 291, 15727–15739. <https://doi.org/10.1074/jbc.M115.686253>
- Takatsu, H., Baba, K., Shima, T., Umino, H., Kato, U., Umeda, M., Nakayama, K., Shin, H.-W., 2011. ATP9B, a P4-ATPase (a Putative Aminophospholipid Translocase), Localizes to the trans-Golgi Network in a CDC50 Protein-independent Manner. *The Journal of Biological Chemistry* 286, 38159. <https://doi.org/10.1074/jbc.M111.281006>
- Takeda, M., Yamagami, K., Tanaka, K., 2014. Role of Phosphatidylserine in Phospholipid Flippase-Mediated Vesicle Transport in *Saccharomyces cerevisiae*. *Eukaryot Cell* 13, 363–375. <https://doi.org/10.1128/EC.00279-13>
- Timcenko, M., Lyons, J.A., Januliene, D., Ulstrup, J.J., Dieudonné, T., Montigny, C., Ash, M.-R., Karlsen, J.L., Boesen, T., Kühlbrandt, W., Lenoir, G., Moeller, A., Nissen, P., 2019. Structure and autoregulation of a P4-ATPase lipid flippase. *Nature* 571, 366–370. <https://doi.org/10.1038/s41586-019-1344-7>
- van Meer, G., 2011. Dynamic transbilayer lipid asymmetry. *Cold Spring Harb Perspect Biol* 3, a004671. <https://doi.org/10.1101/cshperspect.a004671>

- Varadi, M., Anyango, S., Deshpande, M., Nair, S., Natassia, C., Yordanova, G., Yuan, D., Stroe, O., Wood, G., Laydon, A., Židek, A., Green, T., Tunyasuvunakool, K., Petersen, S., Jumper, J., Clancy, E., Green, R., Vora, A., Lutfi, M., Figurnov, M., Cowie, A., Hobbs, N., Kohli, P., Kleywegt, G., Birney, E., Hassabis, D., Velankar, S., 2022. AlphaFold Protein Structure Database: massively expanding the structural coverage of protein-sequence space with high-accuracy models. *Nucleic Acids Research* 50, D439–D444. <https://doi.org/10.1093/nar/gkab1061>
- Venugopal, K., Marion, S., 2018. Secretory organelle trafficking in *Toxoplasma gondii*: A long story for a short travel. *International Journal of Medical Microbiology* 308, 751–760. <https://doi.org/10.1016/j.ijmm.2018.07.007>
- Venugopal, K., Werkmeister, E., Barois, N., Saliou, J.-M., Poncet, A., Huot, L., Sindikubwabo, F., Hakimi, M.A., Langsley, G., Lafont, F., Marion, S., 2017. Dual role of the *Toxoplasma gondii* clathrin adaptor AP1 in the sorting of rhoptry and microneme proteins and in parasite division. *PLoS Pathog* 13, e1006331. <https://doi.org/10.1371/journal.ppat.1006331>
- Voelker, D.R., 2005. Bridging gaps in phospholipid transport. *Trends in Biochemical Sciences* 30, 396–404. <https://doi.org/10.1016/j.tibs.2005.05.008>
- Wan, W., Dong, H., Lai, D.-H., Yang, J., He, K., Tang, X., Liu, Q., Hide, G., Zhu, X.-Q., Sibley, L.D., Lun, Z.-R., Long, S., 2023. The *Toxoplasma* micropore mediates endocytosis for selective nutrient salvage from host cell compartments. *Nat Commun* 14, 977. <https://doi.org/10.1038/s41467-023-36571-4>
- Wehman, A.M., Poggioli, C., Schweinsberg, P., Grant, B.D., Nance, J., 2011. The P4-ATPase TAT-5 inhibits the budding of extracellular vesicles in *C. elegans* embryos. *Curr Biol* 21, 1951–1959. <https://doi.org/10.1016/j.cub.2011.10.040>
- Wicky, S., Schwarz, H., Singer-Krüger, B., 2004. Molecular Interactions of Yeast Neolp, an Essential Member of the Drs2 Family of Aminophospholipid Translocases, and Its Role in Membrane Trafficking within the Endomembrane System. *Mol Cell Biol* 24, 7402–7418. <https://doi.org/10.1128/MCB.24.17.7402-7418.2004>
- Wu, Y., Takar, M., Cuentas-Condori, A.A., Graham, T.R., 2016. Neol and phosphatidylethanolamine contribute to vacuole membrane fusion in *Saccharomyces cerevisiae*. *Cell Logist* 6, e1228791. <https://doi.org/10.1080/21592799.2016.1228791>
- Xu, P., Baldrige, R.D., Chi, R.J., Burd, C.G., Graham, T.R., 2013. Phosphatidylserine flipping enhances membrane curvature and negative charge required for vesicular transport. *Journal of Cell Biology* 202, 875–886. <https://doi.org/10.1083/jcb.201305094>
- Zhang, M., Wang, C., Otto, T.D., Oberstaller, J., Liao, X., Adapa, S.R., Udenze, K., Bronner, I.F., Cassandra, D., Mayho, M., Brown, J., Li, S., Swanson, J., Rayner, J.C., Jiang, R.H.Y., Adams, J.H., 2018. Uncovering the essential genome of the human malaria parasite *Plasmodium falciparum* by saturation mutagenesis. *Science* 360. <https://doi.org/10.1126/science.aap7847>

Chapter VI: General discussion and future perspectives

Lipid metabolism is critical for Apicomplexa parasite development. These parasites rely on massive resource scavenging from the host. However, this scavenging is modulated with their own *de novo* synthesis capacities. Parasites use these lipids to sustain their rapid division rates and generate the material for their plasma membrane and their intracellular organelles. The constant flux of lipids from the host is tightly controlled and oversupply is channeled toward lipid storage by the molecular switch *Tg*LIPIN. The apicoplast is the sole place of the FASII synthesis pathway, producing the short FA chains myristic and palmitic acid (C14:0 and C16:0). These chains can either be exported outside of the plast or directly be used by the plant-like acyl-transferases ATs1 and 2 to produce LPA and PA, which are exported toward the ER to be elongated by the elongases ELO A/B/C (Ramakrishnan *et al.*, 2015b). Parasites and host lipids are then mixed to form a lipidic patchwork essential for the parasite. Lipids, obliged by their physical properties cannot circulate freely within the cell or will cause lipotoxic effects that could be observed after the loss of regulation, *e.g.*, in the *Tg*LIPIN mutant (Dass *et al.*, 2021a) or overfeeding with oleic acid (C18:1) (Nolan *et al.*, 2018). Despite the need for tight control of the lipid flux, general knowledge about metabolites, and specifically lipid transporters in Apicomplexa parasites is limited. To start unravel the mechanism behind lipid flux and transfer in Apicomplexa, my PhD focused on identifying and characterizing two essential transporters putatively involved in lipid metabolism. The first transporter, an unusual P5-ATPase, *Tg*FLP12, was shown to be involved in the exit of FASII lipid products from the apicoplast, and the second transporter, a single Golgi P4-ATPase, *Tg*FLP2, was revealed to be a central element controlling the vesicular transport for parasite endo- and exocytosis.

***Tg*FLP12, a FA exporter of the apicoplast**

Cellular and lipidic characterization of *Tg*FLP12 demonstrated its involvement in the exit of short FA chains of the apicoplast, a plant-relic plastid evolved from an ancestral chloroplast. During its evolution, the apicoplast has lost the photosynthetic capacity and has repurposed the FASII and the plant ATs, initially dedicated to the synthesis of galactoglycerolipids for chloroplast maintenance and function (Amiar *et al.*, 2016a; Botté *et al.*, 2011), for LPA/PA synthesis for bulk phospholipids and membrane biogenesis. Contrary to FASII and ATs, known chloroplast lipid transporters have been lost, such as the FA exporters FAX1 and 2 or PA import TGDs. We identify *Tg*FLP12, a putative transporter that we have shown to localize to the apicoplast membranes. Interestingly, this transporter belongs to the poorly characterized P5-ATPase family closely related to the lipid transporter family, P4-ATPase, which both have macro-molecule substrates (Palmgren and Nissen,

2011b). Lipidomic characterization of *TgFLP12* revealed its role in sorting short FAs made by the FASII out of the apicoplast, and this pathway was revealed to be essential for parasite tachyzoite development.

Apicoplast lipid products have been shown to exit the plast and reach the ER to be elongated and desaturated (Ramakrishnan *et al.*, 2012b). A previous study from our lab on *TgATS1*, responsible for the synthesis of LPA in the apicoplast, revealed that LPA was exported to the ER to be elongated in long FAs (Amiar *et al.*, 2016a). In this thesis, we have shown that disruption of *TgFLP12* did not impact the abundance of ER elongated FAs, but did change the mass isotopomer distribution (MID) with a significant increase of FAs made from C16:0, one of the main products of the FASII pathway, while FAs such as C16:0, C18:1 and C20:1 (product of the ER elongation/desaturation), have a significant decrease in fractional abundance of M+2, M+4, and M+6 respectively, meaning that less C14:0 sourced those lipids. Combined with the stronger growth rescue of FAs supplementation compare to LPA supplementation in parasites depleted for *TgFLP12*, we concluded that *TgFLP12* has a higher specificity for myristic acid and that the exported FAs *via TgFLP12*, are not directly forwarded to the ER contrary to LPA. This pathway certainly participates in fueling the lipidic patchwork previously reported in Amiar *et al.*, 2016, offering short FAs to be used by the cytosolic acyltransferases GPAT, AGPAT (ToxoDB), or DGAT (Quittnat *et al.*, 2004).

***TgFLP2*, a pivotal element of *Toxoplasma* vesicular trafficking**

The Golgi apparatus is an intense place of vesicle budding facilitated by P4-ATPases that play a critical role in eukaryotic vesicular trafficking, generating the membrane asymmetry and the lipid domains necessary for membrane curvatures and thus vesicle budding. Apicomplexa parasites have adapted their secretory pathway for the biogenesis of apical organelles, micronemes, and rhoptries essential for their pathogenicity allowing the entry and the exit of the host. Parasites have conserved essential transport factors known to be involved in the secretion pathway or endocytosis in model organisms, such as Rab-GTPases (Rab5, Rab7), SNAREs (Stx12, Stx16, VAMP4), vacuolar sorting proteins (VPS45), and vesicle coat proteins (clathrin). From the Golgi, microneme, and rhoptry proteins (MICs and ROPs/RONs) are exported to the ELCs thanks to the presence of a sorting motif present in membranous ROPs/RONs or MICs or *via* the association with other MIC or ROP/ROn bearing the motif or with the interaction with SORTLR (Sheiner and Soldati-Favre, 2008; Sloves *et al.*, 2012). The sorting motif in the Golgi participates in the recruitment of the clathrin adaptor complex AP1, interacting with Arf1, Espin-like protein (EspL), and clathrin

mediating vesicular budding (Venugopal *et al.*, 2017). Then ROPs/RONs are sorted to the pre-rhoptry associated with Rab5 to be matured and form the mature rhoptries. MICs are sorted to the ELCs, which are Rab5/Rab7 positive compartments where they are matured, before being addressed to the mature micronemes (Venugopal and Marion, 2018). The work of Venugopal *et al.*, 2017, suggest the existence of two Golgi sorting pathways, one dependent on AP1 and another independent. Regarding our data on the impact of *TgFLP2* deletion on micronemes and ELCs but not rhoptries, we suggest that *TgFLP2* could be involved in MICs sorting independently of AP1. As such *TgFLP2* would thus participate in the discrimination between microneme and rhoptry sortings.

Nutrient acquisition from the environment or the host is crucial for parasites' survival and development. Apicomplexa secrete effectors to control their host immune response, reprogram their metabolic activities, and de-route host organelles, and vesicles to the membrane of the parasitophorous vacuole (PVM). Exogenous material is internalized through the intravacuolar network (IVN), the H.O.S.T. (host organelle–sequestering tubulostructures), or *via* the recruitment of the host ESCRT machinery. Apicomplexa endocytosis remains poorly understood but it occurs in virulent and avirulent *Toxoplasma* strains (Dou *et al.*, 2014; Gras *et al.*, 2019), during the rapid tachyzoite stage and metabolically slow bradyzoite stage (Kannan *et al.*, 2021). In *Plasmodium* blood stages, endocytosis is essential for amino acid acquisition *via* the hemoglobin (Jonscher *et al.*, 2019). Endocytosis seems to happen through the *Toxoplasma* micropore and its *Plasmodium* homolog cytosome. Two recent work by Koreny *et al.*, (2022) and Wan *et al.*, (2023), revealed the importance of the micropore for *Toxoplasma* survival and nutrient acquisition from the host. *TgFLP2* deletion seriously impacted parasite endocytosis, blocking the detachment of vesicles from the plasma membrane. A similar observation was made in the triple knockdown strain of the constitutive elements of the micropore, *TgESP15*, *TgKelch13*, and *TgPPG1* (Wan *et al.*, 2023). The same study also showed the importance of ER *de novo* synthesis of ceramide for host material internalization. *TgFLP2* in the Golgi could be responsible for addressing vesicles rich in ceramide necessary to regulate the vesicle budding at the plasma membrane either directly *via* affecting the membrane curvatures or affecting the recruitment of micropore components. Preliminary data from the *Plasmodium* homolog suggest that *PfFLP2* could also be important for internalization of external material, but this will need further investigation to be confirmed.

Open questions persist regarding the flippase complex β -subunit CDC50/Lem3 present in the *Toxoplasma* Golgi apparatus. Does it interact with *TgFLP2*? Does it define *TgFLP2* specificity? Is

it essential for *TgFLP2* activity or to be addressed to the Golgi? Does its function been repurposed in *Toxoplasma* and in Apicomplexa more generally? Characterizing this potential partner of *TgFLP2* may provide a better understanding of *Toxoplasma* vesicular trafficking regulation. *Toxoplasma* and *Plasmodium* encode respectively 4 and 3 CDC50 orthologs. *TgCDC50.1*, which interacts with *TgGC* localizes at the apical pole (Bisio *et al.*, 2019). It is also the case for *TgCDC50.2*, and *TgCDC50.4*, which both interact with the apical *TgATP2B*. Identification of proteins co-precipitated with *TgCDC50.4* revealed that it mainly interacts with *TgATP2B* and both together are responsible for PS flipping (Bisio *et al.*, 2021). *TgCDC50.3*, the potential *TgFLP2* partner, is important for *Toxoplasma* intercellular development as reported by Chen *et al.*, (2023), but it is not essential as *TgFLP2*, supporting the hypothesis that *TgFLP2* activity could not be entirely dependent on the presence of *TgCDC50.3*. In *Plasmodium*, CDC50A is the partner of GC β . Both partners are essential for the motility of ookinetes in the mosquito's gut (Gao *et al.*, 2018). CDC50B was shown to be required for GC α function (Patel *et al.*, 2022), and CDC50C is the partner of ATP2 (Lamy *et al.*, 2020; Patel *et al.*, 2022). However, none of these three proteins was reported to interact with ATP8, aka FLP2, also supporting the hypothesis that FLP2 as a P4B-ATPase, like *ScNeo1p*, does not require a CDC50 partner.

Apicoplast transporters remain poorly known

The first part of this study allowed the identification of a new sub-family of P5-ATPases, which were previously divided into two sub-families: P5A and P5B. P5A-ATPases localize to the ER and are proposed to transport small peptides as Wnt proteins (T. Li *et al.*, 2021b) or be α -helix dislocases of mistargeted membrane proteins (McKenna *et al.*, 2020). P5B-ATPases localize to the lysosome and the human ATP13A has been shown to transport polyamines (Van Veen *et al.*, 2021). The *Toxoplasma* genome encodes one P5A-ATPase (TGME49_318460) predicted to localize to the ER by the LOPIT and one P5B-ATPase (TGME49_219260) that could play the role of polyamine transporter in the PLVAC. However, *Toxoplasma* and more generally Alveolata, along with some lower plants and fungi, encode P5-ATPases that do not cluster with the two known groups but form a new subgroup that we called P5C-ATPases and which are absent from humans, yeasts, and *Arabidopsis*. Substrate affinity of this new group remains to be determined but the present study suggests that at least one of them, *TgFLP12*, is involved in FA export from the plastidial organelle. Further investigations will be required to confirm the substrate nature, which could be done by structure determination by NMR or cryo-EM tomography similar to what has been done to reveal the *Toxoplasma* ATPase synthase structure (Mühleip *et al.*, 2021).

TgFLP12 starts to unravel the apicoplastic transporters. The apicoplast hosts essential metabolic pathways for the parasite's survival such as the FASII pathway, the isoprenoid DOXP pathway, or the heme synthesis pathway. Nevertheless, the apicoplast also needs resources for housekeeping functions. As summarized in the recent review by Kloehn *et al.*, (2021), little is known about the different importers or exporters, and identifying them could offer a promising drug target in the fight against Apicomplexa. Parasites as such candidate, *TgFLP12* is divergent enough to be absent from the host. It is essential independently of the nutritional status of the host and, as suggested by Kloehn, the rescue observed after exogenous FAs addition, is limited because of the accumulation of the substrate accumulating in the apicoplast and leading to its loss. Exporters for LPA/PA, isoprenoids IPP and DAMPP, or CPO-III remain to be determined. Kloehn *et al.*, (2021) and Sayers *et al.*, (2018) provide an exhaustive list of potential transporters that localize or are predicted to localize to the apicoplast membranes but their roles and substrates are still understudied. Further study of these transporters should reveal efficient drug targets in the fight against Apicomplexa diseases.

Parasite's transportome, the Achille heel of Apicomplexa?

Martin, (2020) nicely illustrated the *Plasmodium* spp membrane transportome and showed the important size reduction of transportome that occurred in *Plasmodium*: ~2.5 % of the genome, compared to the genomes of multi- / unicellular eukaryotes that oscillate between 3 and 5.5 % or prokaryotes that dedicate more than 11 % of their genomes to encode membrane transporters. Parasites, during their evolution and certainly because of their parasitic life, have discarded the unnecessary transporters and *de facto*, the remaining part should be almost all essential for their survival. This review also summed up the findings about the transportome involvement in drug resistance showing that those transporters could indeed be used as targets for drug development as some of them are already the target of some MMV compounds. The limitation of this review is that it does not include cytosolic transporters such as ACBPs, LPTs, etc. We know from PlasmoDB and ToxoDB that *Plasmodium* and *Toxoplasma* also have a reduced number of cytosolic lipid transporters. Their genomes do not code for fatty acid binding proteins (FABP) or plant lipid transfer proteins (PLTP). *Toxoplasma* codes for 2 acyl-CoA binding proteins (ACBP), *Plasmodium* for 4 compared to 6 for *Arabidopsis*. PI and its derivatives are essential in regulating protein functions, signaling events, and membrane identity. Their transport and regulation must be tightly controlled by specific transporters such as ORPs/OSBPs, Sec14/CRAL-TRIO domains, or PITPs. The *Toxoplasma* genome codes for 3 ORPs/OSBPs, 1 PITP, and 4 Sec14. These numbers even

more reduced in *Plasmodium* with only 1 ORP/OSBP, 1 P1TP, and 2 Sec14. None of these transporters has been characterized yet (PlasmoDB and ToxoDB). If their functions are relatively conserved, they could be important for the maintenance of the lipid homeostasis in the different intercellular compartments and the plasma membrane, as well as the maintenance of correct signaling events by controlling the PI, PIPs, and cholesterol distribution in the cell (Lipp *et al.*, 2020).

Membrane contact sites in Apicomplexa

Characterization of the aforementioned lipid transporters will, on a larger scale, increase our knowledge on parasite membrane contact sites (MCSs). MCSs are defined as areas of close apposition between membranes of two or more organelles that are physically connected *via* proteinaceous tethers but do not fuse (Venditti *et al.*, 2021). They are places of active exchanges of metabolites such as lipids or cations. They are also essential for signaling, organelle trafficking, and inheritance. ORPs/OSPBs *via* their FFAT (phenylalanines in an acid tract) motif and pleckstrin homology (PH) domain interact with the ER tether protein VAP and PIPs from the plasma membrane or the Golgi facilitating the formation of MCSs (Prinz, 2014). MCSs in Apicomplexa are poorly investigated and understood but could be involved in major processes such as the exit of LPA from the apicoplast to the ER, or lipid droplet biogenesis and mobilization for energy metabolism (Renne and Hariri, 2021), or autophagy with the recruitment of ATG2 and ATG9 (Zwilling and Reggiori, 2022), or lipid transfer to the mitochondria for PE synthesis from PS (Vance, 2020). My thesis illustrated the role of *TgFLP12* in FA export from the apicoplast and *TgFLP2* in regulating parasite vesicular trafficking. In the bigger perspective, the two transporters could be involved in such MCSs, *TgFLP12* facilitating the transfer of FA to acyl-CoA synthetases, similar to the plant LACS9, which provides activated FA to the ER/cytosolic acyltransferases recruited at the level of the ER membrane and as such, is part of MCSs between the ER and the apicoplast. *TgFLP2* could be the generator of lipid microdomains responsible for the formation of MCSs between the Golgi and the mitochondria, the ELCs, the ER, or the plasma membrane facilitating lipid transfer and controlling lipid homeostasis for correct vesicular budding.

Last word

During my PhD, I had the opportunity to be part of several collaborative work related to the development of anti-malaria compounds targeting the *Plasmodium falciparum* blood stages. I also studied the anti-malaria properties of plant extracts from 1/ *Artemisia annua*, from which

artemisinin is extracted (artemisinin is the current first line treatment against *Plasmodium*) and 2/ *Artemisia afra* that does not contain artemisinin but shows promising results against artemisinin-resistant strains. I was in charge of determining the impact of the different compounds and infusions on *Plasmodium* clinically relevant blood stages and the impact on the apicoplast (see Annex). These collaborative studies have been really important in developing my professional network and enlarging my knowledge and expertise in the field of Apicomplexa. In the same spirit, I also had the chance to participate in several international conferences, where I presented my PhD work and developed collaborative partnerships to achieve the characterization of my protein candidates.

References to chapter VI

- Amiar, S., MacRae, J.I., Callahan, D.L., Dubois, D., van Dooren, G.G., Shears, M.J., Cesbron-Delauw, M.-F., Maréchal, E., McConville, M.J., McFadden, G.I., Yamaro-Botté, Y., Botté, C.Y., 2016. Apicoplast-Localized Lysophosphatidic Acid Precursor Assembly Is Required for Bulk Phospholipid Synthesis in *Toxoplasma gondii* and Relies on an Algal/Plant-Like Glycerol 3-Phosphate Acyltransferase. *PLoS Pathog* 12, e1005765. <https://doi.org/10.1371/journal.ppat.1005765>
- Bisio, H., Krishnan, A., Marq, J.-B., Soldati-Favre, D., 2021. *Toxoplasma gondii* phosphatidylserine flippase complex ATP2B-CDC50.4 critically participates in microneme exocytosis (preprint). *Cell Biology*. <https://doi.org/10.1101/2021.11.25.470034>
- Bisio, H., Lunghi, M., Brochet, M., Soldati-Favre, D., 2019. Phosphatidic acid governs natural egress in *Toxoplasma gondii* via a guanylate cyclase receptor platform. *Nat Microbiol* 4, 420–428. <https://doi.org/10.1038/s41564-018-0339-8>
- Botté, C.Y., Yamaro-Botté, Y., Janouskovec, J., Rupasinghe, T., Keeling, P.J., Crellin, P., Coppel, R.L., Maréchal, E., McConville, M.J., McFadden, G.I., 2011. Identification of plant-like galactolipids in *Chromera velia*, a photosynthetic relative of malaria parasites. *J Biol Chem* 286, 29893–29903. <https://doi.org/10.1074/jbc.M111.254979>
- Chen, K., Huang, X., Distler, U., Tenzer, S., Günay-Esiyok, Ö., Gupta, N., 2023. Apically-located P4-ATPase1-Lem1 complex internalizes phosphatidylserine and regulates motility-dependent invasion and egress in *Toxoplasma gondii*. *Computational and Structural Biotechnology Journal*. <https://doi.org/10.1016/j.csbj.2023.02.032>
- Dass, S., Shunmugam, S., Berry, L., Arnold, C.-S., Katris, N.J., Duley, S., Pierrel, F., Cesbron-Delauw, M.-F., Yamaro-Botté, Y., Botté, C.Y., 2021. *Toxoplasma* LIPIN is essential in channeling host lipid fluxes through membrane biogenesis and lipid storage. *Nat Commun* 12, 2813. <https://doi.org/10.1038/s41467-021-22956-w>
- Dou, Z., McGovern, O.L., Di Cristina, M., Carruthers, V.B., 2014. *Toxoplasma gondii* Ingests and Digests Host Cytosolic Proteins. *mBio* 5, e01188-14. <https://doi.org/10.1128/mBio.01188-14>
- Gras, S., Jimenez-Ruiz, E., Klinger, C.M., Schneider, K., Klingl, A., Lemgruber, L., Meissner, M., 2019. An endocytic-secretory cycle participates in *Toxoplasma gondii* in motility. *PLoS Biol* 17, e3000060. <https://doi.org/10.1371/journal.pbio.3000060>
- Jonscher, E., Flemming, S., Schmitt, M., Sabitzki, R., Reichard, N., Birnbaum, J., Bergmann, B., Höhn, K., Spielmann, T., 2019. PfVPS45 Is Required for Host Cell Cytosol Uptake by Malaria Blood Stage Parasites. *Cell Host & Microbe* 25, 166-173.e5. <https://doi.org/10.1016/j.chom.2018.11.010>
- Kannan, G., Thaprawat, P., Schultz, T.L., Carruthers, V.B., 2021. Acquisition of Host Cytosolic Protein by *Toxoplasma gondii* Bradyzoites. *mSphere* 6, e00934-20. <https://doi.org/10.1128/mSphere.00934-20>
- Kloehn, J., Lacour, C.E., Soldati-Favre, D., 2021. The metabolic pathways and transporters of the plastid organelle in Apicomplexa. *Current Opinion in Microbiology* 63, 250–258. <https://doi.org/10.1016/j.mib.2021.07.016>
- Koreny, L., Mercado-Saavedra, B.N., Klinger, C.M., Barylyuk, K., Butterworth, S., Hirst, J., Rivera-Cuevas, Y., Zaccai, N.R., Holzer, V.J.C., Klingl, A., Dacks, J.B., Carruthers, V.B., Robinson, M.S., Gras, S., Waller, R.F., 2022. Stable and ancient endocytic structures navigate the complex pellicle of apicomplexan parasites. <https://doi.org/10.1101/2022.06.02.494549>

- Lamy, A., Macarini-Bruzaferro, E., Perálvarez-Marín, A., le Maire, M., Vázquez-Ibar, J.L., 2020. ATP2, the essential P4-ATPase of malaria parasites, catalyzes lipid-dependent ATP hydrolysis in complex with a Cdc50 β -subunit (preprint). *Biochemistry*.
<https://doi.org/10.1101/2020.06.08.121152>
- Li, T., Yang, X., Feng, Z., Nie, W., Fang, Z., Zou, Y., 2021. P5A ATPase controls ER translocation of Wnt in neuronal migration. *Cell Rep* 37, 109901.
<https://doi.org/10.1016/j.celrep.2021.109901>
- Lipp, N.-F., Ikhlef, S., Milanini, J., Drin, G., 2020. Lipid Exchangers: Cellular Functions and Mechanistic Links With Phosphoinositide Metabolism. *Front Cell Dev Biol* 8, 663.
<https://doi.org/10.3389/fcell.2020.00663>
- Martin, R.E., 2020. The transportome of the malaria parasite. *Biol Rev* 95, 305–332.
<https://doi.org/10.1111/brv.12565>
- McKenna, M.J., Sim, S.I., Ordureau, A., Wei, L., Harper, J.W., Shao, S., Park, E., 2020. The endoplasmic reticulum P5A-ATPase is a transmembrane helix dislocase. *STRUCTURAL BIOLOGY* 16.
- Mühleip, A., Kock Flygaard, R., Ovcariakova, J., Lacombe, A., Fernandes, P., Sheiner, L., Amunts, A., 2021. ATP synthase hexamer assemblies shape cristae of *Toxoplasma* mitochondria. *Nat Commun* 12, 120. <https://doi.org/10.1038/s41467-020-20381-z>
- Nolan, S.J., Romano, J.D., Kline, J.T., Coppens, I., 2018. Novel Approaches To Kill *Toxoplasma gondii* by Exploiting the Uncontrolled Uptake of Unsaturated Fatty Acids and Vulnerability to Lipid Storage Inhibition of the Parasite. *Antimicrob Agents Chemother* 62, e00347-18, /aac/62/10/e00347-18.atom. <https://doi.org/10.1128/AAC.00347-18>
- Palmgren, M.G., Nissen, P., 2011. P-type ATPases. *Annu Rev Biophys* 40, 243–266.
<https://doi.org/10.1146/annurev.biophys.093008.131331>
- Patel, A., Nofal, S.D., Blackman, M.J., Baker, D.A., 2022. CDC50 Orthologues in *Plasmodium falciparum* Have Distinct Roles in Merozoite Egress and Trophozoite Maturation. *mBio* 13, e01635-22. <https://doi.org/10.1128/mbio.01635-22>
- PlasmoDB [WWW Document], n.d. URL <https://plasmodb.org/plasmo/app/> (accessed 1.26.23).
- Prinz, W.A., 2014. Bridging the gap: Membrane contact sites in signaling, metabolism, and organelle dynamics. *J Cell Biol* 205, 759–769. <https://doi.org/10.1083/jcb.201401126>
- Quittnat, F., Nishikawa, Y., Stedman, T.T., Voelker, D.R., Choi, J.-Y., Zahn, M.M., Murphy, R.C., Barkley, R.M., Pypaert, M., Joiner, K.A., Coppens, I., 2004. On the biogenesis of lipid bodies in ancient eukaryotes: synthesis of triacylglycerols by a *Toxoplasma* DGAT1-related enzyme. *Molecular and Biochemical Parasitology* 138, 107–122.
<https://doi.org/10.1016/j.molbiopara.2004.08.004>
- Ramakrishnan, S., Docampo, M.D., MacRae, J.I., Pujol, F.M., Brooks, C.F., van Dooren, G.G., Hiltunen, J.K., Kastaniotis, A.J., McConville, M.J., Striepen, B., 2012. Apicoplast and Endoplasmic Reticulum Cooperate in Fatty Acid Biosynthesis in Apicomplexan Parasite *Toxoplasma gondii**. *Journal of Biological Chemistry* 287, 4957–4971.
<https://doi.org/10.1074/jbc.M111.310144>
- Ramakrishnan, S., Docampo, M.D., MacRae, J.I., Ralton, J.E., Rupasinghe, T., McConville, M.J., Striepen, B., 2015. The intracellular parasite *Toxoplasma gondii* depends on the synthesis of long chain and very long-chain unsaturated fatty acids not supplied by the host cell. *Mol Microbiol* 97, 64–76. <https://doi.org/10.1111/mmi.13010>
- Renne, M.F., Hariri, H., 2021. Lipid Droplet-Organelle Contact Sites as Hubs for Fatty Acid Metabolism, Trafficking, and Metabolic Channeling. *Front Cell Dev Biol* 9, 726261.
<https://doi.org/10.3389/fcell.2021.726261>

- Sayers, C.P., Mollard, V., Buchanan, H.D., McFadden, G.I., Goodman, C.D., 2018. A genetic screen in rodent malaria parasites identifies five new apicoplast putative membrane transporters, one of which is essential in human malaria parasites. *Cellular Microbiology* 20. <https://doi.org/10.1111/cmi.12789>
- Sheiner, L., Soldati-Favre, D., 2008. Protein Trafficking inside *Toxoplasma gondii*. *Traffic* 9, 636–646. <https://doi.org/10.1111/j.1600-0854.2008.00713.x>
- Sloves, P.-J., Delhaye, S., Mouveaux, T., Werkmeister, E., Slomianny, C., Hovasse, A., Dilezitoko Alayi, T., Callebaut, I., Gaji, R.Y., Schaeffer-Reiss, C., Van Dorsselear, A., Carruthers, V.B., Tomavo, S., 2012. *Toxoplasma* Sortilin-like Receptor Regulates Protein Transport and Is Essential for Apical Secretory Organelle Biogenesis and Host Infection. *Cell Host & Microbe* 11, 515–527. <https://doi.org/10.1016/j.chom.2012.03.006>
- ToxoDB [WWW Document], n.d. URL <https://toxodb.org/toxo/app> (accessed 1.26.23).
- Van Veen, S., Martin, S., Schuermans, M., Vangheluwe, P., 2021. Polyamine Transport Assay Using Reconstituted Yeast Membranes. *Bio Protoc* 11, e3888. <https://doi.org/10.21769/BioProtoc.3888>
- Vance, J.E., 2020. Inter-organelle membrane contact sites: implications for lipid metabolism. *Biology Direct* 15, 24. <https://doi.org/10.1186/s13062-020-00279-y>
- Venditti, R., Wilson, C., De Matteis, M.A., 2021. Regulation and physiology of membrane contact sites. *Current Opinion in Cell Biology, Membrane Trafficking* 71, 148–157. <https://doi.org/10.1016/j.ceb.2021.03.004>
- Venugopal, K., Marion, S., 2018. Secretory organelle trafficking in *Toxoplasma gondii*: A long story for a short travel. *International Journal of Medical Microbiology* 308, 751–760. <https://doi.org/10.1016/j.ijmm.2018.07.007>
- Venugopal, K., Werkmeister, E., Barois, N., Saliou, J.-M., Poncet, A., Huot, L., Sindikubwabo, F., Hakimi, M.A., Langsley, G., Lafont, F., Marion, S., 2017. Dual role of the *Toxoplasma gondii* clathrin adaptor AP1 in the sorting of rhoptry and microneme proteins and in parasite division. *PLoS Pathog* 13, e1006331. <https://doi.org/10.1371/journal.ppat.1006331>
- Wan, W., Dong, H., Lai, D.-H., Yang, J., He, K., Tang, X., Liu, Q., Hide, G., Zhu, X.-Q., Sibley, L.D., Lun, Z.-R., Long, S., 2023. The *Toxoplasma* micropore mediates endocytosis for selective nutrient salvage from host cell compartments. *Nat Commun* 14, 977. <https://doi.org/10.1038/s41467-023-36571-4>
- Zwilling, E., Reggiori, F., 2022. Membrane Contact Sites in Autophagy. *Cells* 11, 3813. <https://doi.org/10.3390/cells11233813>

Annex

In the following section are my *curriculum vitae* as well as all the collaborative works I have been involved in.

First Name: Christophe-Sebastien, **last name:** ARNOLD

Birth date: 18/05/1996

City: Grenoble, FRANCE **Email:** arnoldc@univ-grenoble-alpes.fr, **Phone:** +33 6 17 26 73 24

ORCID: 0000-0002-2392-5837, **Twitter:** @cs_arnold

CURRICULUM VITAE

Current position PhD candidate — Grenoble.

Team ApicoLipid at the Institute for Advanced Biosciences, supervisor: Dr Botté Cyrille, Project: “Study of the lipid trafficking and recycling involved in the membrane biogenesis in Apicomplexa parasites”. **2020-2023:** Elected Student/Post-Doc representative to the IAB Governing Board.

Previous positions

2020-2022: Contractor assistant lecturer — Grenoble. Supervision of 126 h practical work of the BSc 2nd Biotechnology, module: Advanced experimentation, University Grenoble-Alpes. Supervision of 64 h practical work of the MSc 1st Biotechnology, module: Protein engineering, University Grenoble-Alpes.

2019: Institute for Advanced Biosciences, CNRS UMR5309 (M2 Internship) — Grenoble. Team: ApicoLipid, supervisor: Dr Botté Cyrille.

2018: TIMC institute (M1 Internship) — Grenoble. Team: Genetics and Evolution of Microorganisms (GEM), supervisor: Prof Mercier Corinne.

2017: Institut de Biologie Structural (IBS) — Grenoble. Team: Extremophiles and Large Molecular Assemblies (ELMA), supervisor: Dr Madern Dominique. Team: NMR (Nuclear Magnetic Resonance), supervisor: Dr Bersch Beate.

Education

2019: MSc in Immunology, Microbiology and Infectious Diseases (international program): *magna cum laude*, rank 4th/14. University Grenoble-Alpes.

2017: BSc in general biology: *magna cum laude*, rank: 10th/159. University Grenoble-Alpes.

Grants and Awards

2022: ToxoXVI, Best poster award & travel award

2019: MENESR-ED fellowship for PhD, Membrane biogenesis in Apicomplexa parasites: Lipid trafficking proteins of *Toxoplasma* and *Plasmodium* parasites. Supervisor: Dr Botté Cyrille. University Grenoble-Alpes.

Transversal Skills

Languages: French native, English good working knowledge (B2)

Computing: Office pack (C2i), R studio, SnapGene, ImageJ, Icy, Image Lab, Prism8, Agilent mass hunter software.

Communications

Metabolomics2021: Poster (virtual), **Molecular Parasitology Meeting 2021:** Talk (virtual), **ToxoXVI:** Poster (in person), **Molecular Parasitology Meeting 2022:** Talk (in person), **EMBO workshop Paraftrap 2022:** Poster (in person)

Publications

1. Amiar, S., Katris, N.J., Berry, L., Dass, S., Duley, S., **Arnold, C.-S.**, Shears, M.J., Brunet, C., Touquet, B., McFadden, G.I., Yamaro-Botté, Y., Botté, C.Y., 2020. **Division and Adaptation to Host Environment of Apicomplexan Parasites Depend on Apicoplast Lipid Metabolic Plasticity and Host Organelle Remodeling.** Cell Reports 30, 3778-3792.e9. <https://doi.org/10.1016/j.celrep.2020.02.072>

I generated the double knock-out/knockdown line Δ ACBP1/iABC2 and Δ SCP/iACBP1 on analyzed their growth fitness in different host nutrient conditions.

2. Amrane, D., **Arnold, C.-S.**, Hutter, S., Sanz-Serrano, J., Colia, M., Azqueta, A., Paloque, L., Cohen, A., Amanzougaghene, N., Tajeri, S., Franetich, J.-F., Mazier, D., Benoit-Vical, F., Verhaeghe, P., Azas, N., Vanelle, P., Botté, C., Primas, N., 2021a. **2-Phenoxy-3-Trichloromethylquinoxalines Are Antiplasmodial Derivatives with Activity against the Apicoplast of Plasmodium falciparum.** Pharmaceuticals 14, 724. <https://doi.org/10.3390/ph14080724>

I analyzed the impact of different compounds synthesized during the study on *Plasmodium falciparum* blood stage growth, analyzed the impact of the compounds on the apicoplast, and wrote the corresponding section in the manuscript.

3. Amrane, D., Primas, N., **Arnold, C.-S.**, Hutter, S., Louis, B., Sanz-Serrano, J., Azqueta, A., Amanzougaghene, N., Tajeri, S., Mazier, D., Verhaeghe, P., Azas, N., Botté, C., Vanelle, P., 2021b. **Antiplasmodial 2-thiophenoxy-3-trichloromethyl quinoxalines target the apicoplast of Plasmodium falciparum.** European Journal of Medicinal Chemistry 224, 113722. <https://doi.org/10.1016/j.ejmech.2021.113722>

I analyzed the impact of different compounds synthesized during the study on *Plasmodium falciparum* blood stage growth, analyzed the impact of the compounds on the apicoplast, and wrote the corresponding section in the manuscript.

4. Ashraf, K.*, Tajeri, S.*, **Arnold, C.-S.**, Amanzougaghene, N., Franetich, J.-F., Vantaux, A., Soulard, V., Bordessoulles, M., Cazals, G., Bousema, T., Gemert, G.-J., Grand, R., Dereuddre-Bosquet, N., Barale, J.-C., Witkowski, B., Snounou, G., Duval, R., Botté, C., Mazier, D., 2022. **Artemisinin-independent inhibitory activity of Artemisia sp. infusions against different Plasmodium stages including relapse-causing hypnozoites.** Life Science Alliance 5, e202101237. <https://doi.org/10.26508/lsa.202101237>

I analyzed the impact of *Artemisia* infusions on *Plasmodium falciparum* blood stage, studied the impact on the apicoplast on the mitochondria, and wrote the corresponding section in the manuscript.

5. Dass, S.* , Shunmugam, S.* , Berry, L., **Arnold, C.-S.**, Katris, N.J., Duley, S., Pierrel, F., Cesbron-Delauw, M.-F., Yamaro-Botté, Y., Botté, C.Y., 2021. **Toxoplasma LIPIN is essential in channeling host lipid fluxes through membrane biogenesis and lipid storage.** Nat Commun 12, 2813. <https://doi.org/10.1038/s41467-021-22956-w>

I performed IFAs and growth assay on the *Tg*LIPIN mutant.

6. Katris, N.J., Yamaro-Botte, Y., Janouškovec, J., Shunmugam, S., **Arnold, C.-S.**, Yang, A.S.P., Vardakis, A., Stewart, R.J., Sauerwein, R., McFadden, G.I., Tonkin, C.J., Cesbron-Delauw, M.-F., Waller, Ross.F., Botte, C.Y., 2020. **Rapid kinetics of lipid second messengers controlled by a cGMP signalling network coordinates apical complex functions in *Toxoplasma* tachyzoites** (preprint). Microbiology. <https://doi.org/10.1101/2020.06.19.160341>

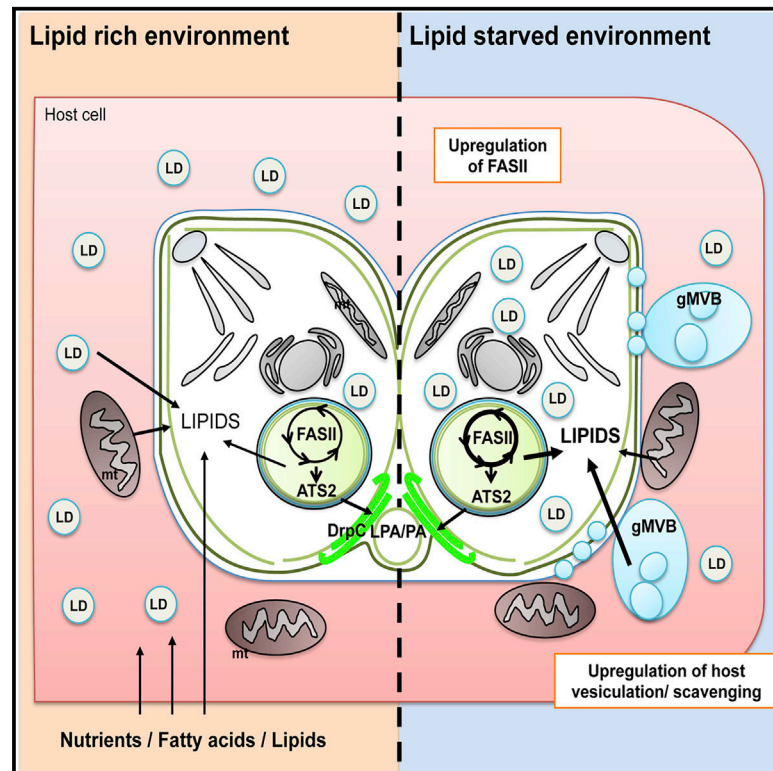
I generated the *Tg*FLP2 and *Tg*FLP5 HA tagged lines and performed the IFAs to determine their localization.

7. Shunmugam, S*., **Arnold, C.-S.***, Dass, S., Katris, N.J., Botté, C.Y., 2022. **The flexibility of Apicomplexa parasites in lipid metabolism.** PLoS Pathog 18, e1010313. <https://doi.org/10.1371/journal.ppat.1010313>

Dr. Serena Shunmugam and I were the co-first authors of this review, the bibliographic research, the redaction, and the corrections have been done equally between us.

Division and Adaptation to Host Environment of Apicomplexan Parasites Depend on Apicoplast Lipid Metabolic Plasticity and Host Organelle Remodeling

Graphical Abstract



Authors

Souad Amiar, Nicholas J. Katris, Laurence Berry, ..., Geoffrey I. McFadden, Yoshiki Yamaro-Botté, Cyrille Y. Botté

Correspondence

yoshiki.yamaro@gmail.com (Y.Y.-B.), cyrille.botte@univ-grenoble-alpes.fr (C.Y.B.)

In Brief

Apicoplast *de novo* lipid synthesis and lipid host scavenging are both critical for apicomplexan intracellular development. Amiar et al. show that the parasite adapts to the fluctuations of host nutritional content to regulate the metabolic activity of both apicoplast and scavenging pathways and maintain parasite development and division.

Highlights

- Knockout of apicoplast *Tg*ATS2 disrupts LPA/PA for DrpC recruitment during cytokinesis
- *T. gondii* can sense host environment and adapt to low host nutritional content
- Under lipid starvation, parasite FASII and other lipid metabolic genes become essential
- Upon nutrient deprivation, *T. gondii* induces host organelle remodeling and vesiculation



Division and Adaptation to Host Environment of Apicomplexan Parasites Depend on Apicoplast Lipid Metabolic Plasticity and Host Organelle Remodeling

Souad Amiar,^{1,5} Nicholas J. Katris,^{1,5} Laurence Berry,² Sheena Dass,¹ Samuel Duley,¹ Christophe-Sebastien Arnold,¹ Melanie J. Shears,³ Camille Brunet,¹ Bastien Touquet,⁴ Geoffrey I. McFadden,³ Yoshiki Yamaro-Botté,^{1,6,*} and Cyrille Y. Botté^{1,6,7,*}

¹ApicoLipid Team, Institute for Advanced Biosciences, CNRS UMR5309, Université Grenoble Alpes, INSERM U1209, Grenoble, France

²Dynamique des interactions Membranaires normales et pathologiques, UMR5235, Université Montpellier II, Montpellier, France

³McFadden Laboratory, School of Biosciences, University of Melbourne, Melbourne, VIC 3010, Australia

⁴Team Cell and Membrane Dynamics of Parasite-Host Interaction, Institute for Advanced Biosciences, INSERM 1209, CNRS UMR5309, Université Grenoble Alpes, Grenoble, France

⁵These authors contributed equally

⁶Senior author

⁷Lead Contact

*Correspondence: yoshiki.yamaro@gmail.com (Y.Y.-B.), cyrille.botte@univ-grenoble-alpes.fr (C.Y.B.)

<https://doi.org/10.1016/j.celrep.2020.02.072>

SUMMARY

Apicomplexan parasites are unicellular eukaryotic pathogens that must obtain and combine lipids from both host cell scavenging and *de novo* synthesis to maintain parasite propagation and survival within their human host. Major questions on the role and regulation of each lipid source upon fluctuating host nutritional conditions remain unanswered. Characterization of an apicoplast acyltransferase, *TgATS2*, shows that the apicoplast provides (lyso) phosphatidic acid, required for the recruitment of a critical dynamin (*TgDrpC*) during parasite cytokinesis. Disruption of *TgATS2* also leads parasites to shift metabolic lipid acquisition from *de novo* synthesis toward host scavenging. We show that both lipid scavenging and *de novo* synthesis pathways in wild-type parasites exhibit major metabolic and cellular plasticity upon sensing host lipid-deprived environments through concomitant (1) upregulation of *de novo* fatty acid synthesis capacities in the apicoplast and (2) parasite-driven host remodeling to generate multi-membrane-bound structures from host organelles that are imported toward the parasite.

INTRODUCTION

Apicomplexa are intracellular protozoan parasites that cause serious infectious diseases in humans, including malaria and toxoplasmosis. Most Apicomplexa harbor a relict non-photosynthetic plastid, the apicoplast, acquired by the secondary endosymbiosis of a red alga (Janouskovec et al., 2010). The apicoplast lost photosynthetic capability during the conversion to a parasitic lifestyle (Botté et al., 2013). However, it still contains plant-like pathways, including a prokaryotic type II fatty acid syn-

thesis pathway (FASII) (Waller et al., 1998). The apicoplast is essential for parasite survival in both *T. gondii* and *P. falciparum* (MacRae et al., 2012).

However, the FASII pathway is thought to be essential only during specific life stages. Indeed, in *Plasmodium*, disruption of FASII was demonstrated to be dispensable in asexual blood stages but essential for late liver stage in rodent malaria parasites and for sporozoite schizogony during mosquito stages (Vaughan et al., 2009). Nevertheless, changes in *P. falciparum* blood stage growth conditions, such as lipid starvation during *in vitro* growth and physiological stress in human patients, induced re-activation of apicoplast FASII (Daily et al., 2007; Botté et al., 2013), suggesting plasticity of FASII in response to nutritional environment. In *T. gondii*, FASII is essential during tachyzoite development (Mazumdar et al., 2006).

Apicomplexan parasite membranes are constituted of up to 80% phospholipid (PL), primarily phosphatidylcholine (PC), phosphatidylethanolamine (PE), phosphatidylserine (PS), and phosphatidylinositol (PI; Welti et al., 2007; Gulati et al., 2015). *T. gondii* can readily scavenge PL and triacylglycerols (TAGs) from the host but is also capable of, and dependent on, *de novo* synthesis of several PL classes (Hu et al., 2017; Amiar et al., 2016; Nolan et al., 2017). Like other eukaryotes, apicomplexan *de novo* PL synthesis is initiated by the assembly of fatty acid (FA) (i.e., esterification onto a glycerol-phosphate backbone) into specific PL precursors. In *T. gondii*, FAs to be used for PLs synthesis derive from three sources: (1) apicoplast FASII generating short FA chains (C12:0, C14:0, and C16:0) (Ramakrishnan et al., 2012), (2) FA elongases located on the parasite endoplasmic reticulum (ER) generating C16:1, C18:1, C20:1, C22:1, and C26:1 (Dubois et al., 2018), and (3) FAs directly scavenged from the host cell (Bisanz et al., 2006). Lipidomics reveals that most *T. gondii* PLs are hybrid/patchwork molecules, comprising one FA moiety from the apicoplast *de novo* synthesis pathway and a second one scavenged from the host (Amiar et al., 2016). Thus, both scavenging and *de novo* synthesis of FA are critical for intracellular development.



Typically, phosphatidic acid (PA) is the central precursor for the *de novo* synthesis of all PL classes by the two-step esterification of FAs onto a glycerol-3-phosphate backbone; first by glycerol-3-phosphate acyltransferases (GPATs) to form lyso-phosphatidic acid (LPA) and then by acyl-glycerol-3-phosphate acyltransferases (AGPATs) to convert LPA to PA. In eukaryotic cells, GPATs and AGPATs of diverse origins work as a set at several locations within the cell. Apicomplexans have two sets of acyltransferases: one plastid-like set putatively in the apicoplast (prokaryotic pathway) (Amiar et al., 2016) and another pair predicted to be in the ER (the so-called eukaryotic pathway). In *T. gondii*, the apicoplast GPAT, *TgATS1* is essential for tachyzoite development, where it generates LPA from apicoplast-FA for the bulk synthesis of PL (Amiar et al., 2016). The role of parasite AGPATs for lipid synthesis is yet to be determined. Beyond their roles as lipid precursors, PA (and LPA) also have important biophysical properties by controlling the formation of positive or negative membrane curvatures, and thereby influence the recruitment of proteins involved in membrane fusion/fission events such as endocytosis in other eukaryotic models (Schmidt et al., 1999; Kooijman et al., 2005; Brown et al., 2008).

Here we characterize *T. gondii* AGPATs, focusing on one localized to the apicoplast, *TgATS2*. We confirm that *TgATS2* is an acyltransferase by heterologous complementation of a bacterial mutant. We then generate a knockout (KO) mutant, which was defective parasite cytokinesis and normal lipid profile. Particularly, the impact of LPA/PA changes on the localization of a dynamin-related protein (Drp), *TgDrpC*, in the *TgATS2* mutant is described and provides a rationale for cytokinesis defects associated with drug inhibition of apicoplast FASII (Martins-Duarte et al., 2015). Finally, changes in parasite lipid composition and lipid fluxes led us to subject parasites to lipid starvation to explore how host nutritional environment affects parasite growth. Analysis of lipid fluxes and growth screening under adverse lipid conditions show that parasites can sense the environment and respond by (1) upregulation of *de novo* lipid synthesis in the apicoplast and (2) manipulation of the human host through vesiculation from host organelles and import of such material to the parasitophorous vacuole (PVM) mediated by export of parasite effectors to improve their lipid scavenging. Our analysis provides unprecedented mechanistic insights into parasite metabolic adaptation under host nutritional challenge, which was poorly understood until now.

RESULTS

Deletion of *Toxoplasma gondii* Apicoplast Acyltransferase *TgATS2* Results in Aberrant Cytokinesis and Residual Body Formation during Replication

To explore *de novo* PA synthesis in *T. gondii*, we searched the genome for AGPATs capable of catalyzing the esterification of an activated FA (i.e., acyl-CoA or acyl-ACP) onto LPA to make PA. We found two AGPAT candidates with conserved motifs: ToxoDB: TGME49_297640 and ToxoDB: TGME49_240860. Phylogenetic analyses reveal that TGME49_297640 clusters with the prokaryotic clade of the pathway with plant and algal sequences and that TGME49_240860 clusters with the eukaryotic

clade of the pathway (Figure S1). We termed these enzymes *TgATS2* and *TgAGPAT* on the basis of the plant and eukaryotic terminology, respectively. We generated parasite lines expressing *TgATS2* and *TgAGPAT* endogenously tagged at the C terminus with a triple HA tag, under control of their respective promoters (Figures S2A–S2C). Immunofluorescence assays (IFAs) confirmed *TgATS2* targets to the apicoplast (Figure 1A), and transient expression of *TgAGPAT*-HA showed a perinuclear structure corresponding to the parasite ER (Figure 1B).

To test if *TgATS2* and *TgAGPAT* are functional AGPAT, we complemented an *E. coli* temperature-sensitive mutant SM2-1 Δ *plsC* lacking AGPAT activity (Coleman, 1990) with recombinant *TgATS2* and *TgAGPAT*. All transformants grew at the permissive temperature of 30°C (Figure 1C). Only those complemented with bacterial *EcPlsC* and *TgATS2* grew at the non-permissive 42°C (Figure 1C). Constructs with *TgAGPAT* including or not its long N-Ter extension did not grow at 42°C, likely because of *TgAGPAT* eukaryotic origin (Figure S1). Indeed, eukaryotic AGPATs favor acyl-CoA substrates over acyl-ACP substrates used in bacterial and plastid systems. Thus, it is unclear if *TgAGPAT* has acyltransferase activity, but *TgATS2* complements defective *E. coli* SM2-1 AGPAT enzymatic activity *in vivo*, confirming LPA-to-PA synthetic capability.

To investigate the importance of apicoplast *TgATS2* during tachyzoite life stages, the *TgATS2* locus was disrupted to generate knock-in (KI) and KO mutants of *TgATS2* using CRISPR-Cas9 strategies (Figures S2D–S2F). Loss of the protein product was confirmed by western blot (Figures 1D and 1E), IFA (Figure 1F), and PCR (Figures S2E and S2F). Both Δ *TgATS2* mutants were viable, but plaque and replication assays revealed that Δ *TgATS2* had a mild yet significant growth defect with significantly more small (two to four parasites) vacuoles and significantly fewer large vacuoles (Figures 1G–1I).

Parasite egress was significantly affected in the Δ *TgATS2* mutant (Figure S2G), but invasion ability showed no difference with the parental line, nor was there a defect in microneme secretion (Figures S2H and S2I). Morphology of different intracellular tachyzoite organelles showed no obvious defects except the apicoplast displaying a mild biogenesis defect (Figures S2J and S2K).

Upon closer inspection of parasite morphology, Δ *TgATS2* parasites appeared fused to each other at their basal poles (Figure 2A), suggesting a cytokinesis defect, which provided a rationale for the egress defect (Figure S2G). Cytokinesis was monitored by localizing MORN1, which curiously displayed no obvious basal mis-localization (Figure 2B). However, Δ *TgATS2* parasites showed important enlargement of the residual body (Figure 2C). Residual body size was quantified by IFA using GAP45 antibody as a marker for the inner membrane complex (IMC). Δ *TgATS2* parasites displayed a significantly larger residual body at the center of big vacuoles (more than four parasites), (Figures 2B and 2C). Accordingly, egressed extracellular parasites often remained tethered at their basal pole via a plasma membrane (PM) structure (Figure 2D). Electron microscopy (EM) of Δ *TgATS2* parasites supported the segregation defects seen by IFA (Figure 2E). In dividing parasites, it is commonly seen that the PM is kept connected between two recently divided cells so that the cells are stuck together and distributed

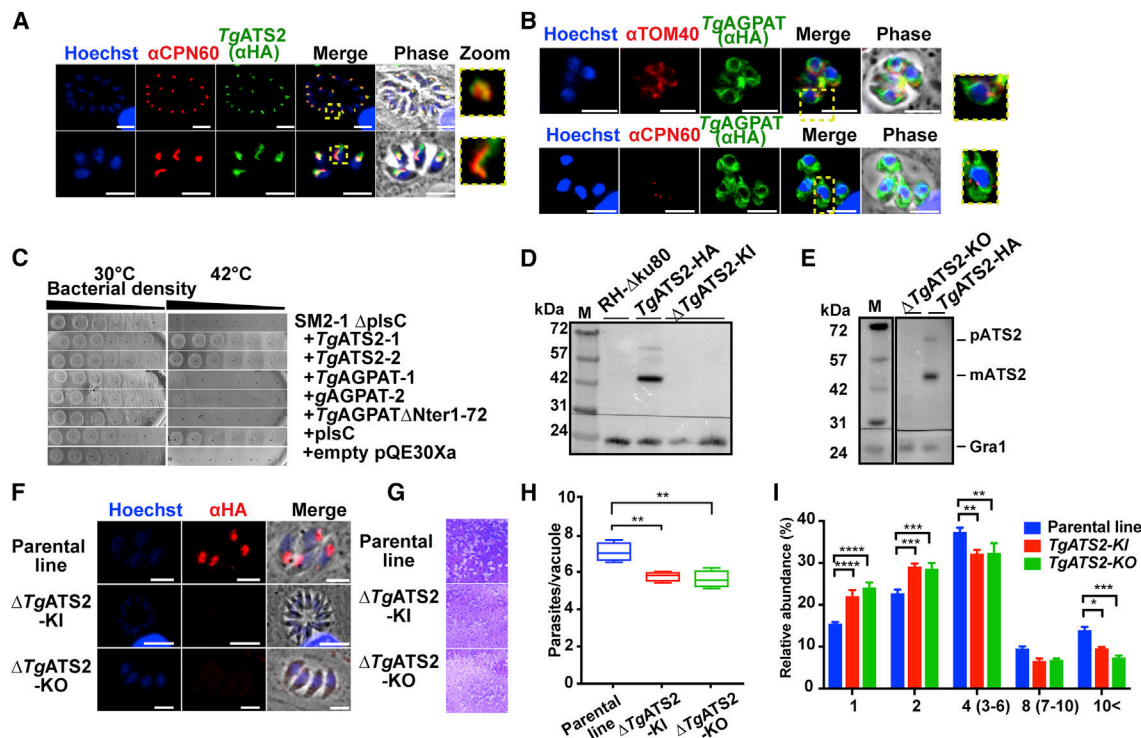


Figure 1. *TgATS2* Is an Apicoplast Lysophosphatidic Acid Acyltransferase Important for Parasite Proliferation

(A and B) IFA of stable *TgATS2*-HA expressing parasites (A) and transient *TgAGPAT*-HA expression (B). CPN60, apicoplast marker; TOM40, mitochondrial marker. Scale bars, 2 μ m.

(C) Expression of *TgATS2* and *TgAGPAT* in LPAAT-deficient *E. coli* strain SM2-1. SM2-1 Δ *plsC* *E. coli* mutant transformed with *TgATS2* (1, 2), *TgAGPAT* (1, 2), *TgAGPAT* $_{\Delta$ Nter1-72}, *EcplsC*, or empty pQE30Xa expression vector were grown at 30°C (permissive) or 42°C (non-permissive) for 20 h (n = 3).

(D and E) Confirmation of *TgATS2*-HA loss by western blot analysis in *TgATS2*-KI (D) and *TgATS2*-KO (E) using anti-HA (anti-Gra1, loading control).

(F) Confirmation of *TgATS2*-HA signal loss in Δ *TgATS2* by IFA using anti-HA. Scale bars, 2 μ m.

(G) Plaque assay showing a mild growth defect in Δ *TgATS2* mutants.

(H) Cell-based growth fitness assay confirmed the growth defect in the Δ *TgATS2* mutants 30 h post-infection (n = 3).

(I) Proliferation assay confirmed a replication defect in Δ *TgATS2* mutants (n = 3).

*p \leq 0.05, **p \leq 0.01, ***p \leq 0.001, and ****p \leq 0.0001.

to daughter cells during cytokinesis. Very little is known on the molecular mechanisms of PM segregation during cytokinesis. In the parental parasites, initial steps of endodyogeny showed the formation of the daughter cell apical pole along with organelle division before the formation of the daughter cells within the mother cell (Figure 2E). Emergence of the daughter cells initiates the apical-to-basal biogenesis of their PM, partly recycled from the mother (Figures 2E1–2E5), and ends by a constriction of both IMC and PM at the basal poles, leaving a small basal residual body (Figure 2E6). In contrast, there were many division and cytokinesis defects in Δ *TgATS2*, which were unable to separate, although a new round of daughter formation could be initiated (Figure 2E1). Furthermore, parasite organelles were frequently found in the residual body as if ejected from improper segregation, likely contributing to the enlarged residual body phenotype (Figure 2E). Affected vacuoles thus displayed enlarged residual bodies that often contained various organelles—including the nucleus, mitochondrion, acidocalcisome vesicles, and other cytosolic material—that appeared to be ejected from the dividing cells because of improper segregation (Figures 2E3 and 2E4).

Pieces of mitochondria were a particular feature within enlarged residual bodies (Figures 2E5 and 2E6).

We attempted to disrupt *TgAGPAT* using CRISPR-Cas9 as per Δ *TgATS2* in wild-type (WT) (Δ *TgAGPAT*) and Δ *TgATS2* (Δ *TgAGPAT*- Δ *TgATS2*) genetic backgrounds, but parasites were not viable (Figures S2L–S2O), suggesting that *TgAGPAT* is indispensable, consistent with its phenotype score (Sidik et al., 2016).

***TgATS2* Disruption Reduces C14:0 FA Incorporation into *T. gondii* Lipids, Skews the LPA/PA Ratio, and Alters PL Abundance and Composition**

To investigate the role of *TgATS2* in lipid metabolism, we performed lipidomic analysis on the Δ *TgATS2* mutant. Disruption of *TgATS2* resulted in a large significant reduction of the relative amount of C14:0, the main product of the apicoplast FASII (Figures 3A and 3B). Significant decreases in C18:1 and C20:1 were also observed (Figures 3A and 3B). In contrast, there were significant increases in the abundance of C18:0, C22:1, C24:1, C20:4, C20:5, and C22:6 (Figures 3A–3C), most of which can be

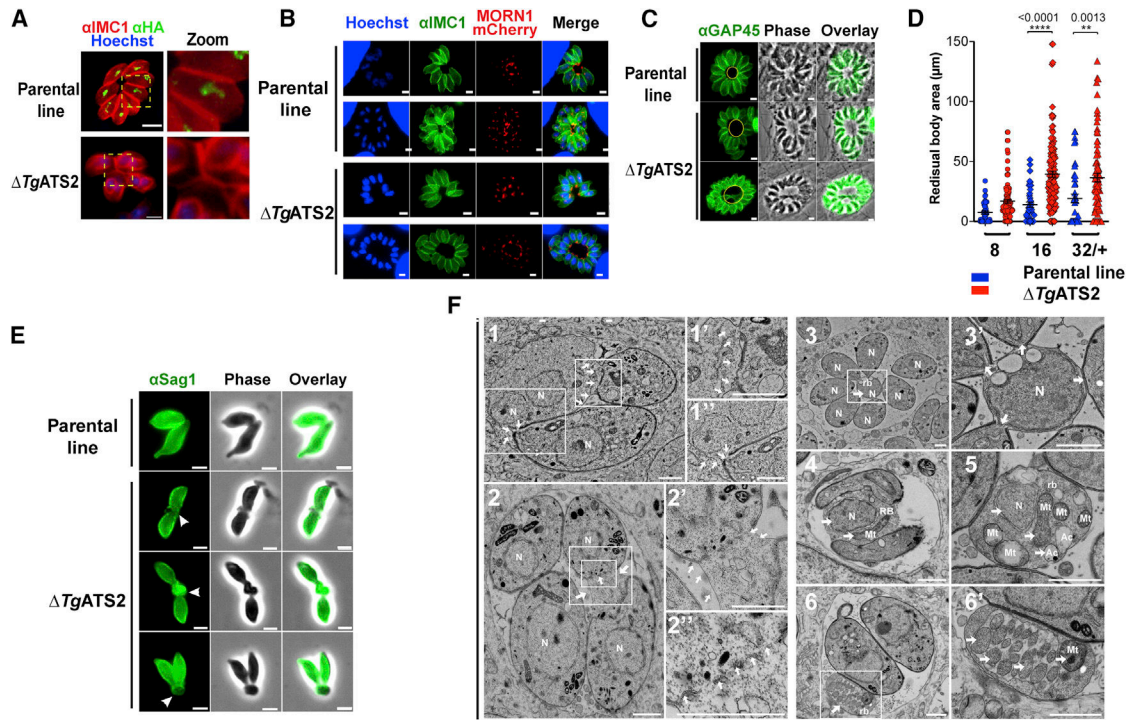


Figure 2. Disruption of *TgATS2* Induces Parasite Cytokinetic Defect, Residual Body Enlargement, and Organelle Segregation Deficiency

(A) IFA of $\Delta TgATS2$ -HA and parental line using anti-HA and anti-IMC1 shows that $\Delta TgATS2$ -HA has a cytokinetic defect phenotype (scale bars, 2 μm). (B) IFA of $\Delta TgATS2$ and parental line transiently expressing MORN1-mCherry (IMC basal tip) and anti-IMC1 (scale bars, 2 μm). (C and D) Confirmation of enlarged residual bodies in $\Delta TgATS2$ by IFA using anti-GAP45 (IMC marker) (C) and by statistical analysis of residual body size (D). Scale bars, 2 μm . (E) IFA observation of extracellular parasites using anti-SAG1 reveals egressed parasites tethered at their basal ends (white arrowhead, PM tether). Scale bars, 2 μm . (F) Electron microscopic image of $\Delta TgATS2$ mutants reveals important cytokinesis defects: major enlargement of the PM, defects in mother cell membrane constriction and cell daughter attachment at the basal pole (F1 and F2; enlarged in F1', F1'', and F2', white arrows), and IMC fragmentation at the separation sites between dividing parasites (F2''). Residual bodies containing unevenly separated nuclei (F1, F3, F3', F4, and F5), mitochondria (F4, F5, F6, and F6'), and acidocalcisomes (F5). N, nucleus; Mt, mitochondria; rb, residual body; Ac, acidocalcisome. Scale bars, 1 μm .

scavenged from the host, such as C20:4 and C20:5 (Welti et al., 2007; Ramakrishnan et al., 2012; Amiar et al., 2016; Figures S3A and S3B). Comparison of the relative FA abundance between $\Delta TgATS2$ and its parental line showed significant decreases of C14:0, C20:0, C20:1, and C22:2 (Figure 3C). These results indicate that in addition to the aforementioned cytokinesis defect, $\Delta TgATS2$ has a highly modified lipid content that relies more on long-chain FAs scavenged from the host (Figures 3A–3C).

To further investigate $\Delta TgATS2$ lipid defects, we analyzed and quantified each PL class and its individual FA content. The $\Delta TgATS2$ mutant accumulates significantly more LPA compared with the control parental line and significantly less PA (Figures 3D and 3E), consistent given that LPA and PA are the likely substrate and product, respectively, of ATS2 (Figure 1C). The slight reduction in PA suggests that *TgATS2* is not responsible for the bulk PA synthesis but rather for a specialist function. Importantly, the LPA/PA ratio was significantly affected in $\Delta TgATS2$ (Figure 3E). We investigated diacylglycerol (DAG) and other related PLs, namely PC, PE, PI, PS, phosphatidylglycerol (PG) and cardiolipin (CL; Figure 3D). The relative abundance of both DAG and PG significantly decreased in $\Delta TgATS2$ (Figure 3D). This is relevant because DAG can be a direct product of PA, and PG is the

sole PL made from PA in plant chloroplasts (Ohlrogge and Browse, 1995). In contrast, the relative abundance of PS, PI, and PE increased in the mutant (Figure 3D).

We then examined the FA profiles of each of these lipid classes. LPA had significant increases in the amounts of C16:0 and C18:0 in $\Delta TgATS2$ parasites, whereas significant decreases in the apicoplast-specific FAs C12:0 and C14:0 were measured in the mutant (Figure 3F). No major difference was observed in PA composition in $\Delta TgATS2$ parasites (Figure 3G). Strikingly, though, DAG, PC, PI, and PE all had significantly reduced C14:0 content (Figures 3D and S3C–S3H), which is the main product of FASII and is used by *TgATS1* for bulk *de novo* synthesis of PC, PI, and PE (Amiar et al., 2016). This indicates that *TgATS2* likely uses apicoplast-generated C14:0 as its major substrate to make these lipids. In contrast, the levels of two long polyunsaturated FAs (PUFAs), C20:4 and C20:5, in all three major PLs (PC, PI, and PE) were significantly increased in $\Delta TgATS2$ (Figures S3C–S3H), which is again consistent with mutant parasites compensating for the lack of *de novo*-made FAs by increasing scavenging long-chain FAs from the host. The FA composition of fetal bovine serum (FBS) and HFF host cells (Figures S3C–S3H) confirmed that C20:4 and C20:5 PUFAs were

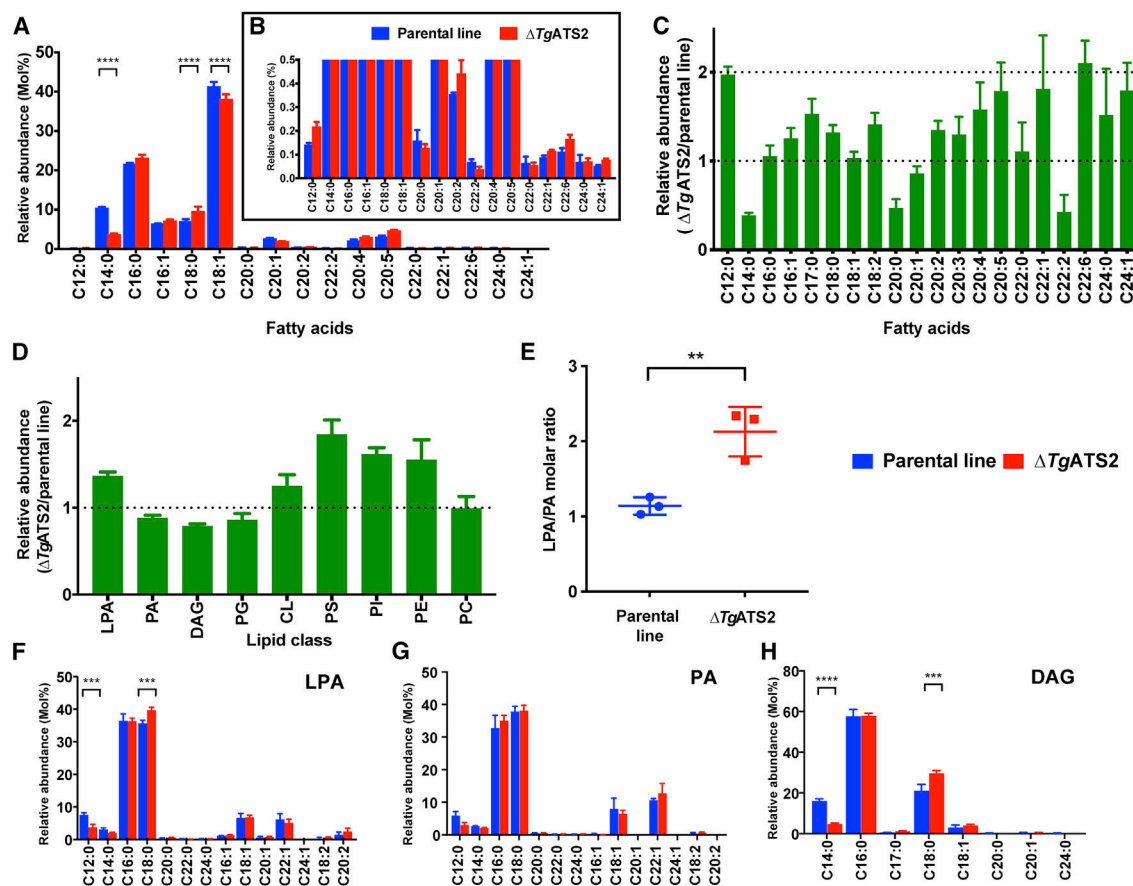


Figure 3. Lipidomic Analysis of $\Delta TgATS2$ Mutant

(A) Fatty acid composition of total lipid extracted 72 h post-infection.

(B) is enlargement of A.

(C) Relative fatty acid abundance of $\Delta TgATS2$ to the parental line.

(D) Relative major phospholipid abundance of $\Delta TgATS2$ to parental line.

(E) LPA/PA ratio.

(F–H) Individual molecular species of LPA (F), PA (G), and DAG (H). Fatty acids are shown as Cx:y, where x is the number of carbons and y is the number of unsaturations.

n = 4; *p ≤ 0.05, **p ≤ 0.01, ***p ≤ 0.001, and ****p ≤ 0.0001.

present from the host environment. This is consistent with the $\Delta TgATS2$ mutants' increasing scavenging of these PUFAs to make PC, PI, and PE. We complemented $\Delta TgATS2$ and WT parasites (Figure S3I) using exogenous PA(14:0;14:0), the putative product of *TgATS2*, and PA(16:0;18:1) as host-derived PAs. Proliferation assays showed that both exogenous PA sources could significantly boost parasite growth (Figures S3I and S3J) but could not rescue $\Delta TgATS2$ growth phenotype. This indicates that the PA source needs to be made *de novo* via *TgATS2* for proper division. Because parasites are capable of scavenging lipids from the host and medium, we determined whether the $\Delta TgATS2$ imported more PA, using PC as a control. $\Delta TgATS2$ imported significantly more PA and PC than the parental control line (Figure S3K). Together these data on extracellular $\Delta TgATS2$ corroborate our lipidomic analyses (Figure 3), indicating that the mutant scavenges more lipids to compensate for reduced *de novo* synthesis.

Disruption of *TgATS2* Induces a Mis-localization of the Parasite DrpC Perturbing Parasite Cytokinesis, IMC Formation, and PM Stability

Lipidomic analyses revealed a drastic LPA/PA imbalance in the $\Delta TgATS2$ mutant (Figure 3E). LPA and PA have important structural influences on membrane architecture and endocytosis by inducing local membrane curvatures, which can affect the recruitment and functions of specific dynamins at precise membrane domains for organelle/vesicle fission (Adachi et al., 2016; Schmidt et al., 1999; Gras et al., 2019). For example, synaptic vesicle transport between neurons requires a protein complex composed of a dynamin and an endophilin that exert acyltransferase activity to create the proper membrane groove where the dynamin can pinch and release the synaptic vesicle, or in human mitochondrial fission by the protein Dynamin-like 1, *HsDrp1*, which requires insertion, recruitment, and regulation through PA. In *T. gondii*, there are three known dynamin-related

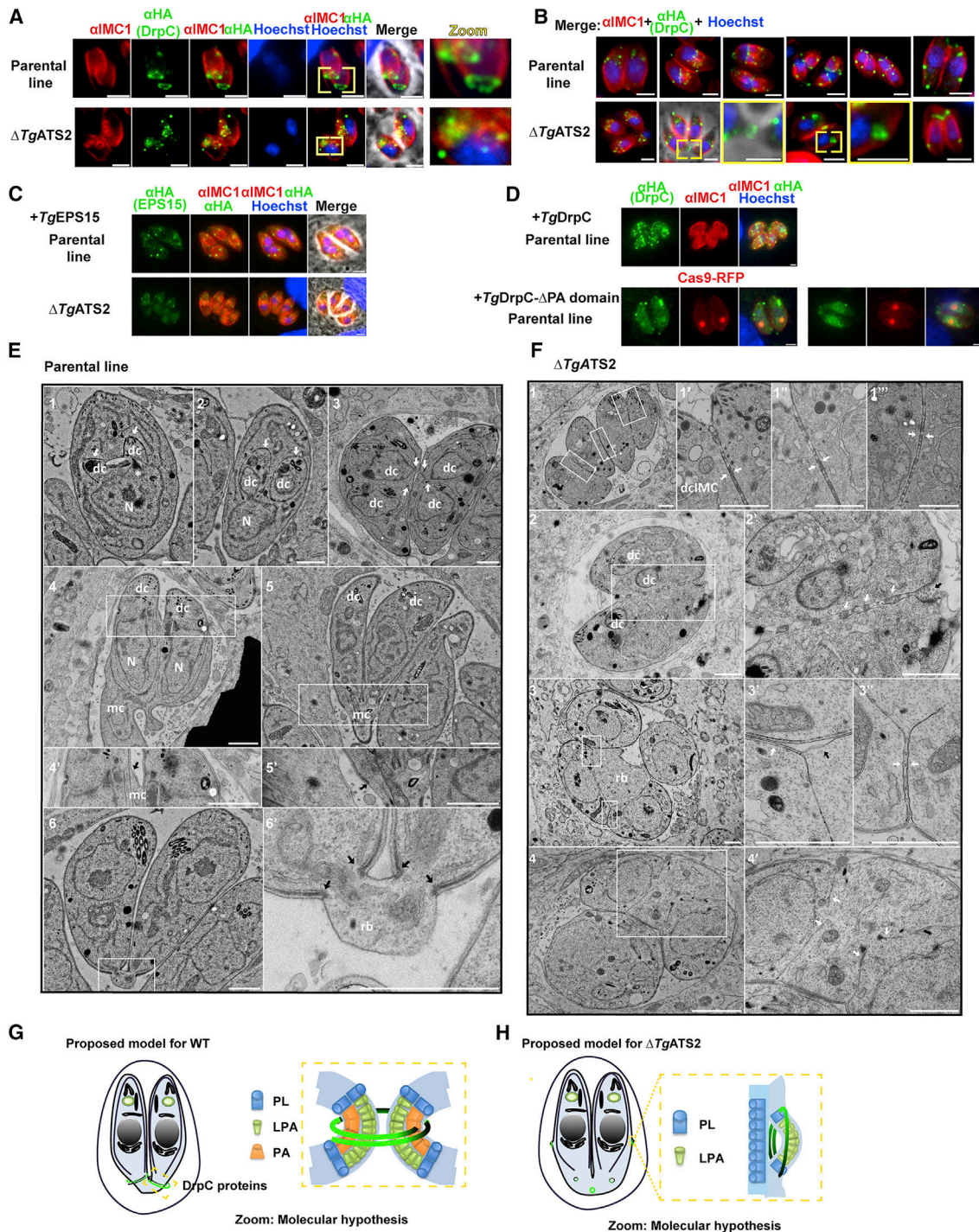


Figure 4. $\Delta TgATS2$ Induces the Specific Mis-localization of *TgDrpC*, a Dynamin-Related Protein Involved in Endodyogeny, Leading to Cytokinetic Defects during Tachyzoite Division

(A) IFA localization of *TgDrpC*-HA expressed in parental line shows ring structures at the growing ends of daughter cells during division (top panel) but fails to do so when expressed in $\Delta TgATS2$ (bottom panel). Scale bars, 2 μ m.

(B) *TgDrpC*-HA localization during tachyzoite division cycle in the parental line (top panel) and its mis-localization in $\Delta TgATS2$ mutant. Scale bars, 2 μ m.

(C) IFA localization of TgEPS15, a known interactor of *TgDrpC*, in $\Delta TgATS2$ and parental line using anti-HA and anti-IMC1. Scale bars, 2 μ m.

(D) IFA localization of *TgDrpC* and *TgDrpC*- Δ PA domain-Cas9-RFP using anti-HA and anti-IMC1 (scale bars, 2 μ m) reveals the mis-localization of *TgDrpC*- Δ PA domain during endodyogeny.

(legend continued on next page)

proteins (Drps): *TgDrpA*, *TgDrpB*, and *TgDrpC*. *TgDrpA* and *TgDrpB* have roles in apicoplast fission and secretory organelle biogenesis, respectively (van Dooren et al., 2009; Breinich et al., 2009). *TgDrpC* was recently localized to the basal poles of dividing daughter cells (Heredero-Bermejo et al., 2019). We generated a parasite line expressing *TgDrpC* fused to a 3xHA tag under the control of its endogenous promoter using CRISPR-Cas9 (Figures S4A and S4B) and localized *TgDrpC*-HA during the tachyzoite intracellular division cycle in $\Delta TgATS2$ and its parental line (Figure 4A). In parental-line parasites, *TgDrpC*-HA clustered in small punctate-like compartments in the apical post-Golgi area during interphase (Figure 4A). During daughter budding, *TgDrpC* re-localized to form two distinct ring-like structures coinciding with the growing ends of the IMC from the budding daughter cells, which constricted at the base of the mother cell during cytokinesis and eventually formed basal caps on the each newly divided parasite (Figures 4A and 4B).

In $\Delta TgATS2$, localization of *TgDrpC*-HA was only mildly affected during interphase but was drastically affected during division (Figures 4A and 4B). Indeed, *TgDrpC*-HA frequently failed to form the typical ring structures at daughter cells (Figures 4A and 4B). Instead, DrpC-HA was scattered in the cytosol, or formed rings pushing on the side of mother IMC, or improperly constricted at the daughter basal pole (Figures 4A and 4B). This contrasted with the normal localization of MORN1, which appears to be a more cytoskeletal component, as its localization remains unaffected during endodyogeny (Figure 2B). We further examined other known interactors of DrpC and thus localized the dynamin-like protein EPS15 (Heredero-Bermejo et al., 2019) by C-terminally tagging by CRISPR-Cas9 (Figures 4C and 4D). In parental strains, EPS15-HA localized to clear punctate dots during interphase similarly to DrpC. During endodyogeny, EPS15 remained as punctate dots and did not re-localize to the daughter rings like DrpC (Figure 4C). In $\Delta TgATS2$ background, EPS15 was unaffected during interphase though more scattered than in the parental line. However, during endodyogeny, EPS15-HA mis-localized in the cytosol of the parasite when expressed in the $\Delta TgATS2$ background (Figure 4C), consistent with its role as a DrpC interactor (Heredero-Bermejo et al., 2019).

In silico sequence alignment showed that (1) *TgDrpC* is the closest *TgDrp* homolog to the *HsDrp1*, which allows mitochondrial fission through its interaction with PA via its Stalk domain including a loop with specific hydrophobic residues (Adachi et al., 2016, 2018), and (2) the Stalk domain and the PA binding loop seem conserved in *TgDrC* (3) but are absent in *TgDrpA*

and *TgDrpB* (Figures S4C–S4E). To confirm this, we tagged and monitored the localization of other *TgDrps* in the $\Delta TgATS2$ background. No obvious change in localization of *TgDrpA* was observed in $\Delta TgATS2$ parasites, even during the fission of the apicoplast (Figure S4B).

On the basis of homology with *HsDrp1*, we disrupted the putative PA-binding region of *TgDrpC*. We expressed this *TgDrpC*- Δ PA version of the protein in the parasite to test the importance of the putative PA-binding domain for the localization of *TgDrpC*. To do so, we transfected a WT *TgDrpC*-HA cell line with a Cas9-RFP and a PCR product targeting the DrpC PA domain. IFAs on parasites with no Cas9-RFP had typical DrpC-HA localization (Figure 4D). However, parasites with positive Cas9-RFP expression showed that DrpC was mis-localized and scattered throughout the cytosol in a similar manner as in *Tg Δ ATS2* parasites. These results are also consistent with the cytosolic mis-localization of truncated *TgDrpC*, excluding the putative PA-binding domain recently reported (Melatti et al., 2019).

Further detailed evidence of improper cytokinesis could be observed under EM. In the parental line, initial steps of endodyogeny showed the formation of the daughter cell apical pole along with organelle division before the formation of the daughter cells within the mother cell (Figure 4E). Emergence of the daughter cells initiates the apical-to-basal biogenesis of their PM, partly recycled from the mother (Figures 4E1–4E5), and ends by a constriction of both IMC and PM at the basal poles, leaving a small basal residual body (Figure 3F6). IMC biogenesis and aberrant endocytosis can be seen in *Tg Δ ATS2* cells upon closer inspection under EM. In contrast $\Delta TgATS2$ were unable to separate, although a new round of daughter formation could be initiated (Figure 4F1). Daughter cells were found tightly apposed at normal emergence sites, and their PMs were often missing between daughter IMCs. Instead, interconnection of PM, vesicles, or cisternae could be observed at these apposition sites and at the basal end of dividing cells (Figures 4F1 and 4F2). Mother cells were frequently observed to be fused to each other, with vesicle fusion frequently occurring between the two at the site of the PM (Figure 4F2). These defects suggested issues at the PM composition and/or problems in membrane fusion/fission sites. Furthermore, there was no constriction of both IMC and PM from daughter cells, resulting in enlarged residual bodies containing organelles and cytosol portions (Figures 4F3 and 4F4). In particular, these membrane invaginations were frequently seen at the junction between two parasites in a process resembling endocytosis.

(E and F) Electron microscopic observation of endodyogenic division in parental line (E) and $\Delta TgATS2$ (F). (E1–E3) Endodyogeny starts with the formation of daughter cells (dc) by growth of IMC (white arrows) and organelle segregation. IMC scaffolding then grows toward the basal pole (white arrows) encompassing divided organelles (e.g., nucleus N). (E4–E5') Recycling and biogenesis of PM (black arrow) ends daughter cell emergence from mother cell (mc). (E6 and E6') Division ends by cytokinesis through constriction of both IMC and PM at basal pole (black arrows) to form a small residual body (rb). (F) $\Delta TgATS2$ shows an incomplete separation of daughter cells during cytokinesis with absence of PM biogenesis between closely apposed IMC (F1 and F3 and insets, white arrows), presence of vesicle/cisternae inside membrane structures at the inter-IMC space (F2', white arrows), absence of mother IMC (F3', black arrow), absence of basal constriction forming large residual bodies leaving floating daughter IMC (F3, F4, and 4', white arrows). Scale bar, 1 μ m.

(G and H) Proposed molecular model for *TgDrpC* function during endodyogeny and cytokinesis in WT parasite (G) and $\Delta TgATS2$ (H). LPA and PA molecules induce positive and negative curvature, creating grooves in membranes for *TgDrpC* to insert at specific sites during division for a pinching function during endodyogeny (G).

Nutrient Starvation Enhances the Synthesis of FA by Apicoplast FASII in *T. gondii* and Blocks Intracellular Proliferation of *P. falciparum* Blood Stages Lacking a Functional FASII

Because TgATS2 has a role in maintaining parasite lipid homeostasis, we set out to determine the balance of *de novo* synthesized versus scavenged lipids in Δ TgATS2 using a stable isotope precursor of apicoplast synthesized FAs, U- ^{13}C -glucose. (Ramakrishnan et al., 2012; Amiar et al., 2016; Dubois et al., 2018). Incorporation of ^{13}C within FA is detected by increase of mass and determined in relation to non-labeled FA. Distribution of ^{13}C incorporation to each FA isotopologue is shown as its own mass (M) plus number of ^{13}C carbon incorporation (i.e., M + x). In both parental and Δ TgATS2 mutant lines, we observed significant differences of ^{13}C incorporation in C14:0, C16:1, C18:0, and C18:1 (Figure 5A). Isotopologue distribution of apicoplast-signature C14:0 showed that Δ TgATS2 had ^{13}C incorporation up to M + 14, but major incorporation occurred at lower masses (M + 8, M + 10) than the parental (M + 12, M + 14; Figure 5B). This indicates that FASII is active in Δ TgATS2 but slowed down in the process of making C14:0, thus explaining the C14:0 reduction previously detected (Figure 3A). Similar significant results were observed for C16:0 isotopologue distribution, although overall incorporation was similar between parental and Δ TgATS2 (Figure 5C). C18:0 in Δ TgATS2 had higher ^{13}C incorporation than the parental, and its isotopologue distribution showed more short FA from the apicoplast (Figure 5D).

Lipidomic analyses thus indicate that both scavenged and *de novo* lipid fluxes are modified in Δ TgATS2. To tease out the impact of host nutritional environment on both pathways, we sought to measure parasite lipid fluxes under adverse host nutritional/lipid conditions, through limitations in FBS concentrations in parasite culture media. Interestingly, gas chromatography-mass spectrometry (GC-MS) analysis revealed that ^{13}C incorporation into all FASII-generated and further ER-elongated FA products (i.e., C14:0, C16:0, C16:1, C18:0, C18:1, and C20:1) was significantly higher by 5%–15% under FBS starvation in the parental line (Figures 5E, 5F, and S5A). In addition, ^{13}C incorporation into most FAs is increased in the WT parental line (Figure 5F). These results suggest that apicoplast *de novo* FA/lipid synthesis can be upregulated during FBS starvation to compensate for the lack of nutrients in the external environment. However, in Δ TgATS2, the ^{13}C incorporation into each FA was decreased by FBS starvation (Figure 5F). No morphological changes could be observed by IFA in the FBS-starved WT or Δ TgATS2 mutant (Figure S5B). Both parental line and Δ TgATS2 mutant showed a significant reduction in the synthesis of C18:0 in FBS-starved conditions, suggesting that C18:0 is obtained predominantly by scavenging from the host cell (Figure 5F). Because the availability of lipids from the environment is limited, the FA abundance in the parental line was decreased (Figure 5G). Interestingly however, the FA abundance in Δ TgATS2 was increased in most of its FA species during FBS starvation (Figure 5G).

Although we observed a defect in the activation of FASII in Δ TgATS2, FASII was nevertheless viable during FBS starvation. This suggests that if FASII is active, regardless of the level of FASII activity, the parasites are viable under FBS starvation,

consistent with its essential role in tachyzoites. However, in *P. falciparum*, FASII is not essential during nutrient-replete blood stage but is activated under lipid starvation, apparently to compensate for reduced availability of scavenge-able lipids (Yu et al., 2008; Botté et al., 2013). Our results in *T. gondii* led us to re-think the current hypothesis regarding the dispensability of the apicoplast FASII in *P. falciparum* blood stages and to test the essentiality of malaria parasite apicoplast FASII under nutrient/lipid-starved conditions. We grew *P. falciparum* FASII KO, Δ PfFabI (Yu et al., 2008), and its parental line (NF54) in either regular (i.e., lipid-rich) culture medium or in “lipid-starved” minimal medium (Mi-ichi et al., 2007; Botté et al., 2013). Both NF54 and Δ PfFabI grew normally in the regular culture medium (Figure 5H). In the lipid-starved medium, NF54 was viable but grew significantly slower than in lipid-replete conditions, as previously reported (Shears et al., 2017). However, Δ PfFabI grew only for the first 2 days in lipid-starved media, but after 4 days, a sharp decrease in growth occurred, and this led to a complete loss of detectable parasites after 8 days and showed no sign of further recovery in the next monitored cycles (Figure 5H). This shows that FASII is required for the malaria parasite blood stages to adapt its lipid metabolism in response to an adverse host lipid environment, a similar situation to that revealed here for *T. gondii*.

Because environmental FBS starvation induces an increase of *de novo* lipid synthesis, we investigated the effect the lipid-nutrient-depleted conditions (i.e., 0%, 1%, and 10% of FBS) on various mutants involved in lipid metabolism in *T. gondii*. We assessed parasite growth by plaque assay and quantified plaque area. The WT and parental parasite lines could grow equally well in DMEM supplemented with 0%, 1%, or 10% FBS (Figures 5I–5R and S5C), without affecting the integrity of HFF host cells. FBS starvation reduced growth of Δ TgATS2 under 0% FBS (Figure 5I). TgATS1-depleted cells grew sharply less in the regular culture conditions (i.e., 1% FBS), but starvation under 0% FBS led to the quasi-absence of plaques, whereas an increase to 10% FBS partially rescued the growth defect seen in 1% FBS (Figure 5J). This suggested that in the absence of the major *de novo* PL precursor synthesis pathway, the parasite could partially compensate the growth defect by accessing more host lipid resources. The acetyl-CoA synthetase TgACS (Dubois et al., 2018) was adequately responsive to FBS starvation (Figure 5K). Interestingly, proteins not involved in bulk membrane/lipid synthesis, such as TgPKA-iKO, could not be rescued by excess nutrients (Figure 5L; Uboldi et al., 2018).

Because host FA binding proteins (FABPs) are upregulated upon tachyzoite invasion (Hu et al., 2017), we searched the genome of *T. gondii* for homologs of FABPs that could be responsible for the transport of FAs in the parasite during starvation but found none. Instead, we found two proteins belonging to the closely related family of acyl-CoA binding protein (ACBP): TgACBP1 and TgACBP2. We found that TgACBP1 and TgACBP2 localized at the parasite cytosol and mitochondrion, respectively (Figures S5D–S5G). We generated mitoch knock-down parasite lines for both (Figures S5D and S5E). However, plaque assays showed that both proteins were dispensable during tachyzoite life stages, and neither was responding to FBS starvation (Figures 5M and 5N), suggesting that neither of the

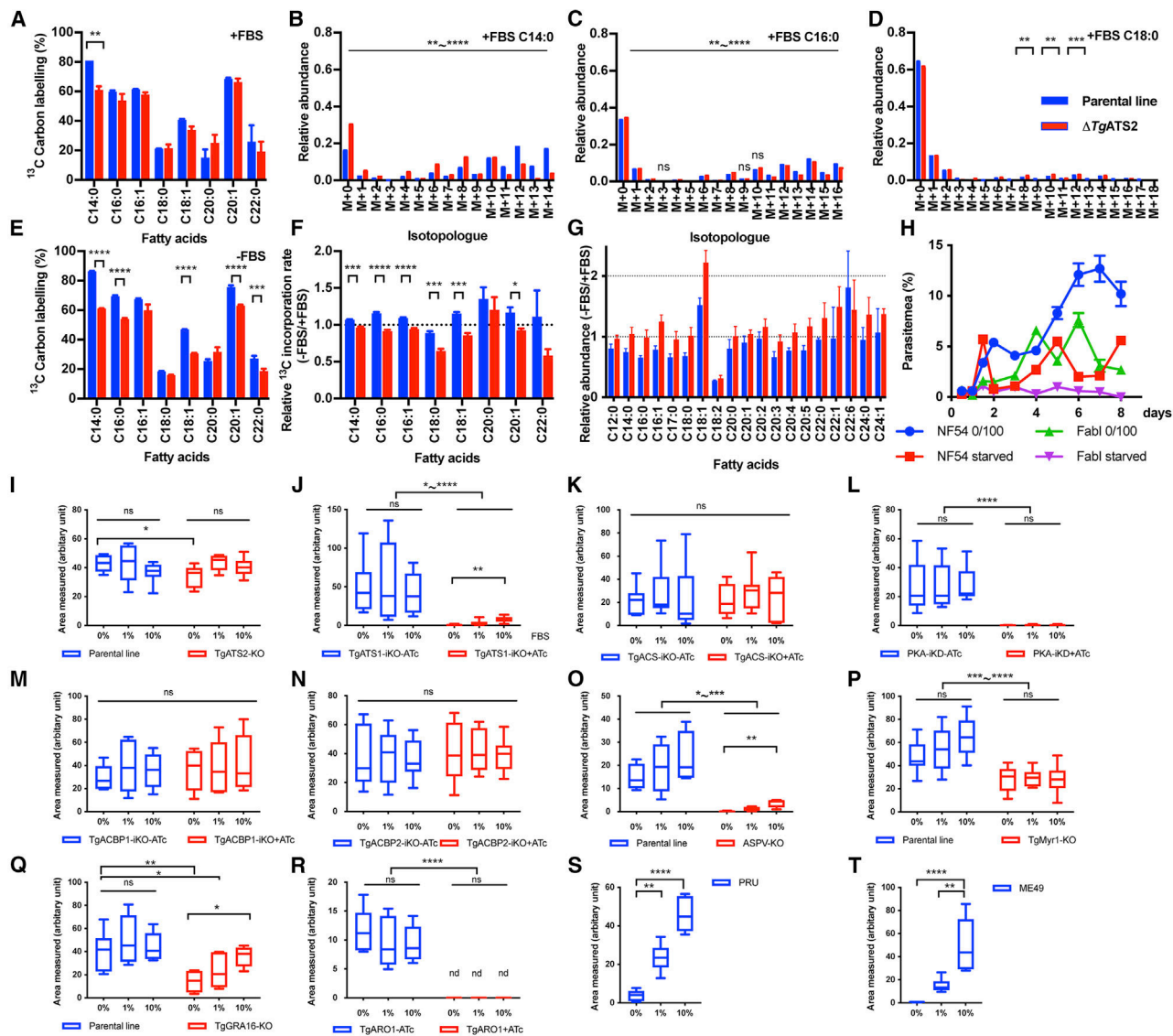


Figure 5. Changes in Host Nutritional Environment Induces an Upregulation of the Apicomplast FASII Metabolic Capacities in *T. gondii* Tachyzoites and *P. falciparum* Blood Stages and Are Pivotal for Enzymes Involved in Metabolic Adaptation

(A–G) U-¹³C-glucose labeling for 72 h to monitor apicomplast FA synthesis by ¹³C incorporation to fatty acids (blue, parental line; red, $\Delta TgATS2$). (A) ¹³C incorporation to each fatty acid in 1% FBS. (B–D) Mass isotopologue distribution in 1% FBS for C14:0 (B), C16:0 (C), and C18:0 (D). The x axis shown as “M + X” represents mass with “X” ¹³C atoms incorporated during the FA synthesis. (E) ¹³C incorporation to each fatty acid in 0.2% FBS. FASII metabolic activity increased upon FBS starvation in the parental line but not in $\Delta TgATS2$. (F) Change in ¹³C incorporation between 0.2% FBS and 1% FBS (–FBS/+FBS). (G) The relative abundance of each FA (–FBS/+FBS).

(H) Asexual blood stage growth assay of *P. falciparum* FabI-KO and its parental line (NF54) in regular (lipid-rich) culture medium and lipid-starved medium reveals that FASII is essential in blood stage in low-lipid environment.

(I–T) Growth assays conducted in 0%, 1%, or 10% FBS in different *T. gondii* mutants and strains: *TgATS2* (I), *TgATS1* (J), *TgACS* (K), *TgPKA* (L), *TgACBP1* (M), *TgACBP2* (N), *TgASP5* (O), *TgMyr1* (P), *TgGRA16* (Q), *TgARO1* (R), type II PRU (S), and type II ME49 (T).

n ≥ 3. ns, not significant; *p ≤ 0.05, **p ≤ 0.01, ***p ≤ 0.001, and ****p ≤ 0.0001.

TgACBPs is involved as an effector for the adaptation to nutritional environment. We generated a *TgACBP1* and *TgACBP2* double KO and a double *ACBP1*KD/sterol carrier protein (*SCP2*) KO cell line, which we also found to be viable and not responsive to starvation (Figures S5H and S5I).

We then hypothesized that parasite effectors putatively exported into the PVM or toward the host cell could be used by

the parasite to collect putative host membrane material generated during FBS starvation. To test this, we investigated *TgASP5*, a Golgi-resident aspartyl protease that controls the non-canonical trafficking pathway of parasite effectors toward the PVM and the host cell, during FBS starvation (Bougdour et al., 2014). Strikingly, FBS starvation significantly exacerbated the growth defect in $\Delta TgASP5$ (Figures 5O and S5). By contrast,

the mutant cell line $\Delta TgMYR1$ (the canonical system to export effectors toward the host; Franco et al., 2016) showed overall less growth than the parental cell line, although $\Delta TgMYR1$ grew equally well among the 0%, 1%, and 10% FBS conditions (Figure 5P). To examine the effects of some specific GRA effectors, we examined a GRA16-KO cell line, which we observed to have a minor but significant growth defect under FBS starvation, suggesting that at least some GRA proteins are important, likely in combination (Figure 5O). We also examined a mutant for rhoptry secretion $TgARO$ -iKO (Mueller et al., 2013) but found that under ATc treatment, the mutant died regardless of FBS concentration (Figure 5R), suggesting a primary role in host invasion prior to host re-wiring.

Last, we explored strain-specific differences between in *Toxoplasma* between the hypervirulent type I RH strain and type II strains (Prugniaud, ME49) capable of forming chronic stages (bradyzoites). Both type II strains showed significantly reduced growth in lipid-depleted medium (Figures 5S and 5T), unlike type I strain.

Together, these data provide evidence that in response to nutrient starvation, parasite effectors can be trafficked to the host cell, primarily via the $TgASP5$ export pathway, likely to enhance the ability to scavenge resources.

Nutrient Starvation Induces the Formation of Multi-membrane-Bound Vesicles in Host Cells that Are Taken up by the Parasite

To investigate potential changes to the host cell and hence host-parasite interactions during lipid starvation, we performed EM on starved (0%, 1%, or 10% FBS) HFF host cells infected with either the parental parasite line or $\Delta TgATS2$. Growth in 10% FBS led to no obvious phenotype changes in the host cells or the parental parasite line or the $\Delta TgATS2$ mutant (Figures 6A and 6B), but reduction to 1% and 0% FBS induced striking changes in the host cells, which became extensively vesiculated irrespective of whether they were infected with the parental line or $\Delta TgATS2$ (Figures 6A and 6B). Such vesiculation was not observed in uninfected HFF host cells put under nutrient starvation. Giant multi-vesicular bodies (gMVBs; i.e., large membrane-bound compartments containing various smaller vesicles) were frequent in 1% FBS-grown cells (Figures 6A and 6B) and very numerous at 0% FBS (Figures 6A and 6B). The gMVBs are distinct from host autophagosome, as they lack the typical double/multiple surrounding membranes and the cytosolic material defining autophagosomes (Ylä-Anttila et al., 2009). This was confirmed by IFA using the typical autophagosome marker anti-LC3, which showed no accumulation of autophagosome under 10%, 1%, or 0% FBS (Figure S6). The gMVBs could arise from the host ER, as the ER could be seen swelling and forming networks containing large lipid bodies (Figure 6B3). gMVBs were also often seen in close apposition or contact with the mitochondria and/or ER network, indicating that material could also be transferred from both (Figures 6B3 and 6B5). However, gMVBs were more often observed arising directly from the host nuclear envelope, potentially a major contributor to their formation (Figures 6B6–6B8). The gMVB accumulated in close vicinity with the PVM, which houses the parasite during its intracellular development and serves as the exchange interphase between the

host and the parasite. The gMVBs were not only close to the PVM but appeared to be interacting with the PVM with host material and vesicles from the gMVB, apparently “percolating” through the PVM (Figure 6B4) or directly from their originating organelles (Figure 6B5) to eventually be found in the PVM (Figures 6A and 6B1). These vesicles appeared in both WT and $\Delta TgATS2$, suggesting that the host cell is responding to the nutrient deficiency in the same way. The $\Delta TgATS2$ parasite cytokinesis phenotype (e.g., Figure 2A) was still observed and apparently exacerbated in 0% and 1% FBS growth medium (Figure 6B). This vesicle/gMVB formation and trafficking to and within the PVM was not apparent in high (10%) FBS medium, suggesting that host gMVBs somehow allow the parasite to increase its lipid scavenging in the absence of nutrient rich serum. Together this indicates that gMVBs contain multiple vesicles that (1) are dependent and induced by nutrient availability and (2) originate directly from diverse host organelles. The gMVBs are distinct from lipid droplets of host cell origin used as a lipid source by *T. gondii* (Nolan et al., 2017; Romano et al., 2017).

However, it is possible that FBS starvation leads to increased host cell lipid droplet import. Nile red staining confirmed that FBS starvation induced a significant increase of the amount of lipid droplets into the parasites and its PVM (Figure 6C). In contrast, low FBS content resulted in a reduced amount of lipid droplets in uninfected host cells, while high FBS content increased their presence in the host cells alone (Figure 6D). This further indicates that increase of import of lipid droplets to the parasite is upregulated by the parasite during FBS starvation.

Because gMVBs also seem to arise from host mitochondria, we used an anti-lyso-bi-PA (LBPA; i.e., a degradation product of mitochondrial CL) antibody (Kobayashi et al., 1998), a lipid that can also be scavenged by intracellular parasites (Romano et al., 2017; Figure 6E). LBPA was found surrounding the PVM in the host cell, within the PV and the parasite, but its localization and intensity remained unchanged in response to reduced FBS content (Figure 6E). Direct salvage of mitochondrial CL per se might not be the primary upregulated scavenging pathway during lipid starvation.

To determine whether host mitochondrial sequestration could affect parasite adaptation to low host nutrient, we measured the levels of mitochondrial sequestration in type I parasites (prone to host mitochondrial sequestration) and type II parasites (not sequestering host mitochondria) (Pernas et al., 2014). Host mitochondria was monitored with MitoTracker. Both RH type I and type II ME49 parasites showed no major difference in host mitochondrial sequestration after FBS starvation (Figure S6).

DISCUSSION

We have shown that $TgATS2$ is an apicoplast acyltransferase able to esterify FAs on LPA to generate PA, a precursor for a wide range of parasite lipids. KO of $TgATS2$ resulted in perturbed lipid fluxes, which affects LPA/PA lipid balance, causing mislocalization of $TgDrpC$ and vesiculation during cytokinesis. Furthermore, changes in lipid profiles of $\Delta TgATS2$ showed the capacity of WT parasites to exhibit considerable metabolic plasticity at both *de novo* FA synthesis in the apicoplast and host modification for organelle membrane scavenging, together

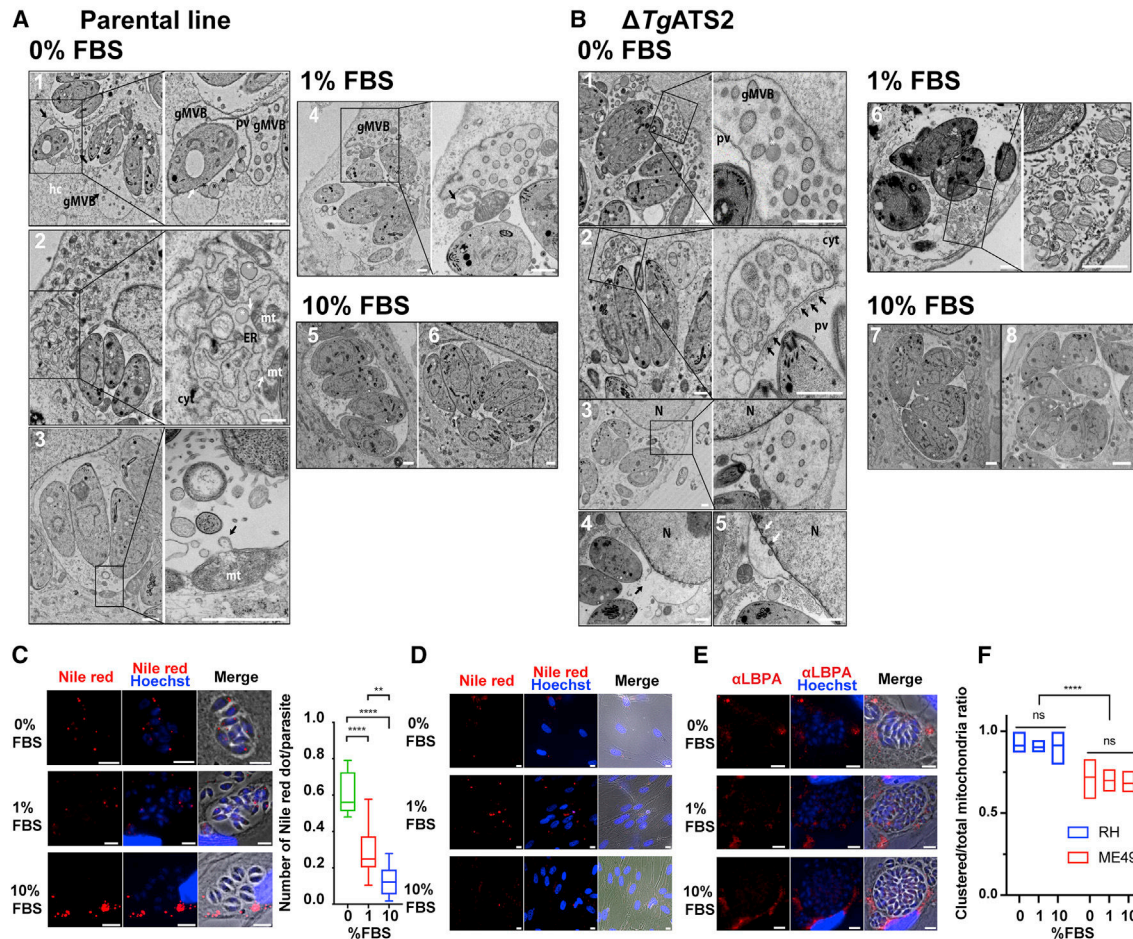


Figure 6. Nutrient Starvation Unveils the Formation of Multi-vesicular Bodies from Host Cell Organelles, Whose Content Is Imported toward Parasites

(A and B) Transmission electron micrographs of intracellular WT tachyzoites (A) and $\Delta TgATS2$ mutant parasites (B) grown in 0%, 1%, and 10% FBS. Nutrient starvation (i.e., 0% and 1% FBS) induces formation of giant multi-vesicular bodies (gMVBs) in the host cell (hc), containing various vesicles, including lipid body-like (white stars). In starvation, gMVBs localized in the cytosol (cyt) in contact with the parasitophorous vacuole (pv) (A1, A2, A4, B1, and B2), and their content was imported through and into the PV (A1, black stars; B2 and B6, black arrows); gMVBs were arising from host endoplasmic reticulum (ER; A2), mitochondria (mt; A2 and A3), and mainly swollen nuclear envelope (N; B3–B5). Ten percent FBS did not induce gMVB formation in both parental and $\Delta TgATS2$. Scale bar, 1 μ m.

(C) Nutrient starvation induces a significant increase of lipid droplets within the parasite and its PV as measured by IFA using Nile red (Nile red dots were counted for 100 or more parasites; n = 3; ns, not significant; *p \leq 0.05, **p \leq 0.01, ***p \leq 0.001, and ****p \leq 0.0001). Scale bar, 2 μ m.

(D) Nutrient starvation induces a decrease of lipid bodies in uninfected HFF host cells as measured by IFA using Nile red. Scale bar, 2 μ m.

(E) IFA shows that import into parasites of LBPA (anti-LBPA) is not affected by nutrient starvation. Scale bar, 2 μ m.

(F) Nutrient starvation induces a significant growth defect in *T. gondii* tachyzoites ME49 type II strain compared with RH type I strain. p values are as mentioned as above.

critical for adaptation to nutrient-limiting conditions in the host (Figure 7; Table S1).

Roles of PA and LPA in Membrane Curvature and Cell Division

Membrane PLs have different physical shapes according to the relative sizes between the polar head and the FA tails. Most PLs are cylindrical, while PA is cone shaped and LPA adopts an inverted cone shape; thus their insertion into membrane bilayers facilitates curvature and in- or evagination (Kooijman et al., 2005).

Furthermore, in human cells, dynamin pinching requires endophilin-1, an ATS2 homolog, as a partner to create LPA/PA curva-

tures (Burger et al., 2000; Shin and Loewen, 2011), improving penetration of a larger part of dynamin into the lipid monolayer (Burger et al., 2000; Shin and Loewen, 2011), similar to the relationship between *TgATS2* and *TgDrcC*. Our results reveal the previously unrecognized importance of the apicoplast in maintaining internal lipid homeostasis. Furthermore, the functional role of *TgATS2* for PA synthesis during division provides a mechanism for the long-standing question of why drugs targeting the apicoplast display a secondary cytokinetic defect (Martins-Duarte et al., 2015).

Our results nicely complement those of a recent study that identified the basal complex as a major site of endocytosis in

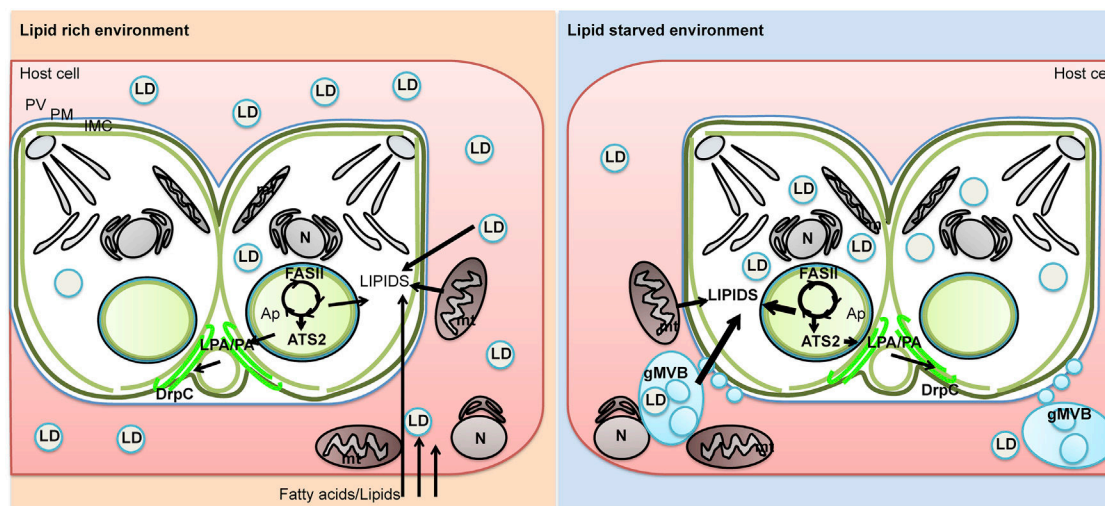


Figure 7. Proposed Model for Cytokinesis, Lipid Acquisition, and Metabolic Adaptation under Adverse Host Lipid Environment in *T. gondii* Left: under lipid-rich environment, *T. gondii* can readily acquire FAs and lipids by *de novo* synthesis (apicoplast) and host cell scavenging. The apicoplast ATS2 generates PA and regulates the balance of LPA/PA, necessary for DrpC. Right: in a host lipid-starved environment, the parasite adapts its metabolism by increasing FASII to produce more fatty acids to compensate their absence from the host cell. Concomitantly, the parasite induces morphological changes in the host to increase scavenged resources, including the nucleus, ER, and gMVBs.

motile tachyzoites, consistent with the basal complex localization of DrpC (Figure 4; (Heredero-Bermejo et al., 2019). Our results show that endocytosis occurs during intracellular stages and that aberrant LPA/PA ratios caused by the loss of ATS2 disrupt this process.

Furthermore, many DrpC-interacting proteins have been identified as part of a larger endocytic protein complex, including EPS15, AP2 adaptins, and, intriguingly, Kelch13 (Heredero-Bermejo et al., 2019). Kelch13 is the infamous protein found mutated in artemisinin-resistant malaria spreading throughout Asia (Mearns and Dondorp, 2017). Kelch13 therefore likely has a role in endocytosis consistent with DrpC and other interacting partners (Heredero-Bermejo et al., 2019). Intriguingly, it has been shown that FASII activity is often increased in artemisinin-resistant parasites (Chen et al., 2014). Our evidence here demonstrates that the upregulation of FASII produces LPA that modulates cytokinesis and endocytosis processes. Again, this highlights the previously unrecognized importance of the apicoplast in maintaining internal lipid homeostasis in parasites.

Environmental and Nutritional Conditions Drive the Adaptation of the Apicoplast Metabolic Capacities as Well as the Scavenging Capacities

Importantly, *Toxoplasma* could increase production of FA in the FASII pathway in nutrient/lipid-deprived medium similarly to *P. falciparum* (Botté et al., 2013). Hence, apicomplexan parasites show high metabolic flexibility to obtain FA for the major membrane building blocks required for growth, as pointed out by recent studies exploring *Plasmodium* survival in nutrient-depleted conditions (Mancio-Silva et al., 2017; Zuzarte-Luís et al., 2017). Importantly, our results demonstrate that *P. falciparum* lacking a FASII and grown in lipid-deprived conditions was unable to properly proliferate, ultimately dying. This

suggests that apicoplast FASII is facultative rather than totally dispensable in malaria parasite blood stage and can be activated during lipid starvation to meet PL needs. This FASII flexibility is consistent with a growing pool of evidence including the upregulation of FASII and the apicoplast acyltransferase PfG3apiGPAT (a homolog of *TgATS1*) transcripts in starved patients (Daily et al., 2007) and the essentiality of most FASII enzymes, including the central acyl-carrier protein ACP in both *T. gondii* and *P. falciparum* (Sidik et al., 2016; Zhang et al., 2018), summarized in Table S1. Therefore, environmental factors could have important consequences in treating patients. Indeed, if patients are under stress, nutrient deprivation, or malnourished conditions, the FASII pathway could become a secondary target of choice to help eradicate the parasites. Altogether these data question whether isopentenyl pyrophosphate (IPP) synthesis is the sole essential function of the apicoplast during *Plasmodium* blood stage (Yeh and DeRisi, 2011). Rather, our data put the parasite back into its physiological context, where nutrient availability and environmental conditions drive the requirement and regulation of a given metabolic pathway. Furthermore, the scavenging of *Toxoplasma* can also be seen to be upregulated through exported effectors by evidence that ASP5 KO is partially rescued by excess host lipids and the induction of host remodeling to make gMVBs, although the identity of these gMVBs warrants further investigation. This redefines what we call an essential gene, where phenotypes might only be seen under starvation conditions.

A major question raised here is the nature the signaling factor(s) responsible for environmental sensing and metabolic adaptation of both apicoplast *de novo* synthesis and scavenging pathways. Both *T. gondii* and *P. falciparum* lack the canonical mTOR-based nutrient-sensing pathways present in other eukaryotes, but a recent study showed that *P. berghei* is capable

of sensing nutrient deprivation by a SNF1-related kinase, KIN1 (Mancio-Silva et al., 2017).

Together, our results reveal the central role of the apicoplast to provide specific precursors for membrane biogenesis during cytokinesis and, most important, to be a central metabolic hub to adapt the parasite metabolic capacities upon nutrient availability and environmental changes. The data also point to major modifications in vesiculation and the use and scavenging of these membrane structures by the parasite upon such environmental changes. The data also corroborate recent results showing that the mosquito lipid environment regulates the metabolic activity of transmissible sporozoites (Costa et al., 2018). The fundamental role of these physiological changes induced by the parasite in response to host environment provides novel insights into parasite biology and offers new avenues to explore in the fight against toxoplasmosis and malaria.

STAR★METHODS

Detailed methods are provided in the online version of this paper and include the following:

- KEY RESOURCES TABLE
- MATERIALS AND METHODS
- LEAD CONTACT AND MATERIALS AVAILABILITY
- EXPERIMENTAL MODEL AND SUBJECT DETAILS
 - *T. gondii* culture
 - *P. falciparum* culture
- METHOD DETAILS
 - Gene identification and sequence analysis
 - *T. gondii* plasmid constructs
 - *T. gondii* transfection
 - *T. gondii* growth assays
 - *T. gondii* Red/Green parasite invasion assay
 - Plasmodium falciparum growth assays
 - Immunofluorescence assay and Microscopy
 - Nile red staining of lipid droplets
 - Activity analysis in LPAAT-deficient *E. coli* strains
 - Transmission electron microscopy
 - Lipidomic analysis by GCMS extraction from *T. gondii* tachyzoites
 - Stable isotope labeling of *T. gondii*
 - Phospholipid import assay
- QUANTIFICATION AND STATISTICAL ANALYSIS
- DATA AND CODE AVAILABILITY

SUPPLEMENTAL INFORMATION

Supplemental Information can be found online at <https://doi.org/10.1016/j.celrep.2020.02.072>.

ACKNOWLEDGMENTS

We would like to thank Prof. Alan Cowman and Dr. Ali Hakimi for sharing parasite strains, reagents, and fruitful advice. This work and C.Y.B., Y.Y.-B., S.A., N.J.K., and C.B. are supported by Agence Nationale de la Recherche, France (grant ANR-12-PDOC-0028, Project Apicolipid), the Atip-Avenir and Finovi programs (CNRS-INSERM-FinoviAtip-AvenirApicolipid projects), and Laboratoire d'Excellence Parafrap, France (grant ANR-11-LABX-0024). C.Y.B. and G.I.M. are supported by the LIA-IRP CNRS Program (Apicolipid project).

AUTHOR CONTRIBUTIONS

S.A. and N.J.K. designed and performed experiments, analyzed and interpreted data, and wrote the manuscript. L.B. performed, analyzed, and interpreted data for EM. S.D. performed Nile red/LBPA and related IFAs. S.D. generated and analyzed the *TgDrpC-ΔPA* mutant. C.S.A. generated and analyzed the double ACBP1-ACBP2- and ACBP1iKD/SCP2-KO mutants. M.J.S. helped perform and analyze the *P. falciparum* lipid starvation growth assay. C.B. helped perform *E. coli* complementation assays. B.T. performed and analyzed *T. gondii* proliferation assays and the related statistical analyses. G.I.M. supervised the *P. falciparum* lipid starvation growth assay. Y.Y.-B. performed, analyzed, interpreted, and supervised lipidomic analyses and wrote the manuscript. C.Y.B. led the project, designed and interpreted data, and wrote the manuscript.

DECLARATION OF INTERESTS

The authors declare no competing interests.

Received: March 22, 2019

Revised: November 12, 2019

Accepted: February 19, 2020

Published: March 17, 2020

REFERENCES

- Adachi, Y., Itoh, K., Yamada, T., Cervený, K.L., Suzuki, T.L., Macdonald, P., Frohman, M.A., Ramachandran, R., Iijima, M., and Sesaki, H. (2016). Coincident phosphatidic acid interaction restrains Drp1 in mitochondrial division. *Mol. Cell* 63, 1034–1043.
- Adachi, Y., Iijima, M., and Sesaki, H. (2018). An unstructured loop that is critical for interactions of the stalk domain of Drp1 with saturated phosphatidic acid. *Small GTPases* 9, 472–479.
- Amiar, S., MacRae, J.I., Callahan, D.L., Dubois, D., van Dooren, G.G., Shears, M.J., Cesbron-Delauw, M.-F., Maréchal, E., McConville, M.J., McFadden, G.I., et al. (2016). Apicoplast-localized lysophosphatidic acid precursor assembly is required for bulk phospholipid synthesis in *Toxoplasma gondii* and relies on an algal/plant-like glycerol 3-phosphate acyltransferase. *PLoS Pathog.* 12, e1005765.
- Bisanz, C., Bastien, O., Grando, D., Jouhet, J., Maréchal, E., and Cesbron-Delauw, M.F. (2006). *Toxoplasma gondii* acyl-lipid metabolism: de novo synthesis from apicoplast-generated fatty acids versus scavenging of host cell precursors. *Biochem. J.* 394, 197–205.
- Botté, C.Y., Yamaro-Botté, Y., Rupasinghe, T.W., Mullin, K.A., MacRae, J.I., Spurck, T.P., Kalanon, M., Shears, M.J., Coppel, R.L., Crellin, P.K., et al. (2013). Atypical lipid composition in the purified relict plastid (apicoplast) of malaria parasites. *Proc. Natl. Acad. Sci. U S A* 110, 7506–7511.
- Bougourd, A., Durandau, E., Brenier-Pinchart, M.-P., Ortet, P., Barakat, M., Kieffer, S., Curt-Varesano, A., Curt-Bertini, R.-L., Bastien, O., Coute, Y., Peloux, H., and Hakimi, M.-A. (2013). Host cell subversion by *Toxoplasma* GRA16, an exported dense granule protein that targets the host cell nucleus and alters gene expression. *Cell Host Microbe* 13, 489–500.
- Bougourd, A., Tardieux, I., and Hakimi, M.A. (2014). *Toxoplasma* exports dense granule proteins beyond the vacuole to the host cell nucleus and rewires the host genome expression. *Cell. Microbiol.* 16, 334–343.
- Braun, L., Brenier-Pinchart, M.-P., Hammoudi, P.-M., Cannella, D., Kieffer-Jacquod, S., Vollaie, J., Josserand, V., Touquet, B., Coute, Y., Tardieux, I., Bougourd, A., and Hakimi, M.-A. (2019). The *Toxoplasma* effector TEEGR promotes parasite persistence by modulating NF- κ B signalling via EZH2. *Nat. Microbiol.* 4, 1208–1220.
- Breinich, M.S., Ferguson, D.J., Foth, B.J., van Dooren, G.G., Lebrun, M., Quon, D.V., Striepen, B., Bradley, P.J., Frischknecht, F., Carruthers, V.B., and Meissner, M. (2009). A dynamin is required for the biogenesis of secretory organelles in *Toxoplasma gondii*. *Curr. Biol.* 19, 277–286.

- Brown, W.J., Plutner, H., Drecktrah, D., Judson, B.L., and Balch, W.E. (2008). The lysophospholipid acyltransferase antagonist CI-976 inhibits a late step in COPII vesicle budding. *Traffic* 9, 786–797.
- Burger, K.N.J., Demel, R.A., Schmid, S.L., and de Kruijff, B. (2000). Dynamin is membrane-active: lipid insertion is induced by phosphoinositides and phosphatidic acid. *Biochemistry* 39, 12485–12493.
- Chen, N., LaCrue, A.N., Teuscher, F., Waters, N.C., Gatton, M.L., Kyle, D.E., and Cheng, Q. (2014). Fatty acid synthesis and pyruvate metabolism pathways remain active in dihydroartemisinin-induced dormant ring stages of *Plasmodium falciparum*. *Antimicrob Agents Chemother* 58, 4773–4781.
- Coleman, J. (1990). Characterization of *Escherichia coli* cells deficient in 1-acyl-sn-glycerol-3-phosphate acyltransferase activity. *J. Biol. Chem.* 265, 17215–17221.
- Costa, G., Gildenhard, M., Eldering, M., Lindquist, R.L., Hauser, A.E., Sauerwein, R., Goosmann, C., Brinkmann, V., Carrillo-Bustamante, P., and Levashina, E.A. (2018). Non-competitive resource exploitation within mosquito shapes within-host malaria infectivity and virulence. *Nat. Commun.* 9, 3474.
- Curt-Varesano, A., Braun, L., Ranquet, C., Hakimi, M.-A., and Bougdour, A. (2016). The aspartyl protease TgASP5 mediates the export of the *Toxoplasma* GRA16 and GRA24 effectors into host cells. *Cell. Microbiol.* 18, 151–167.
- Daily, J.P., Scanzfeld, D., Pochet, N., Le Roch, K., Plouffe, D., Kamal, M., Sarr, O., Mboup, S., Ndir, O., Wypij, D., et al. (2007). Distinct physiological states of *Plasmodium falciparum* in malaria-infected patients. *Nature* 450, 1091–1095.
- Dereeper, A., Guignon, V., Blanc, G., Audic, S., Buffet, S., Chevenet, F., Dufayard, J.-F., Guindon, S., Lefort, V., Lescot, M., et al. (2008). Phylogeny.fr: robust phylogenetic analysis for the non-specialist. *Nucleic Acids Res.* 36, W465–W469.
- Dubois, D., Fernandes, S., Amiar, S., Dass, S., Katris, N.J., Botté, C.Y., and Yarmayo-Botté, Y. (2018). *Toxoplasma gondii* acetyl-CoA synthetase is involved in fatty acid elongation (of long fatty acid chains) during tachyzoite life stages. *J. Lipid Res.* 59, 994–1004.
- Franco, M., Panas, M.W., Marino, N.D., Lee, M.C., Buchholz, K.R., Kelly, F.D., Bednarski, J.J., Sleckman, B.P., Pourmand, N., and Boothroyd, J.C. (2016). A novel secreted protein, MYR1, is central to *Toxoplasma*'s manipulation of host cells. *MBio* 7, e02231-15.
- Gras, S., Jimenez-Ruiz, E., Klinger, C.M., Schneider, K., Klingl, A., Lemgruber, L., and Meissner, M. (2019). An endocytic-secretory cycle participates in *Toxoplasma gondii* in motility. *PLoS Biol.* 17, e3000060.
- Guindon, S., Dufayard, J.F., Lefort, V., Anisimova, M., Hordijk, W., and Gascuel, O. (2010). New algorithms and methods to estimate maximum-likelihood phylogenies: assessing the performance of PhyML 3.0. *Syst. Biol.* 59, 307–321.
- Gulati, S., Eklund, E.H., Ruggles, K.V., Chan, R.B., Jayabalasingham, B., Zhou, B., Mantel, P.Y., Lee, M.C., Spottiswoode, N., Coburn-Flynn, O., et al. (2015). Profiling the Essential nature of lipid metabolism in asexual blood and gametocyte stages of *Plasmodium falciparum*. *Cell Host Microbe* 18, 371–381.
- Herederer-Bermejo, I., Varberg, J.M., Charvat, R., Jacobs, K., Garbuz, T., Sullivan, W.J., Jr., and Arrizabalaga, G. (2019). TgDrpC, an atypical dynamin-related protein in *Toxoplasma gondii*, is associated with vesicular transport factors and parasite division. *Mol. Microbiol.* 111, 46–64.
- Hu, X., Binns, D., and Reese, M.L. (2017). The coccidian parasites *Toxoplasma* and *Neospora* dysregulate mammalian lipid droplet biogenesis. *J. Biol. Chem.* 292, 11009–11020.
- Huynh, M.H., and Caruthers, V.B. (2009). Tagging of endogenous genes in a *Toxoplasma gondii* strain lacking Ku80. *Eukaryot. Cell* 8, 530–539.
- Janouskovec, J., Horák, A., Oborník, M., Lukeš, J., and Keeling, P.J. (2010). A common red algal origin of the apicomplexan, dinoflagellate, and heterokont plastids. *Proc. Natl. Acad. Sci. U S A* 107, 10949–10954.
- Katris, N.J., van Dooren, G.G., McMillan, P.J., Hanssen, E., Tilley, L., and Walker, R.F. (2014). The apical complex provides a regulated gateway for secretion of invasion factors in *Toxoplasma*. *PLoS Pathog.* 10, e1004074.
- Kim, K., Soldati, D., and Boothroyd, J.C. (1993). Gene replacement in *Toxoplasma gondii* with chloramphenicol acetyltransferase as selectable marker. *Science* 262, 911–914.
- Kobayashi, T., Stang, E., Fang, K.S., de Moerloose, P., Parton, R.G., and Gruenberg, J. (1998). A lipid associated with the antiphospholipid syndrome regulates endosome structure and function. *Nature* 392, 193–197.
- Kooijman, E.E., Chupin, V., Fuller, N.L., Kozlov, M.M., de Kruijff, B., Burger, K.N.J., and Rand, P.R. (2005). Spontaneous curvature of phosphatidic acid and lysophosphatidic acid. *Biochemistry* 44, 2097–2102.
- Larkin, M.A., Blackshields, G., Brown, N.P., Chenna, R., McGettigan, P.A., McWilliam, H., Valentin, F., Wallace, I.M., Wilm, A., Lopez, R., et al. (2007). Clustal W and Clustal X version 2.0. *Bioinformatics* 23, 2947–2948.
- Li, W., Cowley, A., Uludag, M., Gur, T., McWilliam, H., Squizzato, S., Park, Y.M., Buso, N., and Lopez, R. (2015). The EMBL-EBI bioinformatics web and programmatic tools framework. *Nucleic Acids Res.* 43 (W1), W580–W584.
- MacRae, J.I., Maréchal, E., Biot, C., and Botté, C.Y. (2012). The apicoplast: a key target to cure malaria. *Curr. Pharm. Des.* 18, 3490–3504.
- Mancio-Silva, L., Slavic, K., Grilo Ruivo, M.T., Grosso, A.R., Modrzynska, K.K., Vera, I.M., Sales-Dias, J., Gomes, A.R., MacPherson, C.R., Crozet, P., et al. (2017). Nutrient sensing modulates malaria parasite virulence. *Nature* 547, 213–216.
- Martins-Duarte, E.S., Dubar, F., Lawton, P., da Silva, C.F., Soeiro, Mde.N., de Souza, W., Biot, C., and Vommaro, R.C. (2015). Ciprofloxacin derivatives affect parasite cell division and increase the survival of mice infected with *Toxoplasma gondii*. *PLoS ONE* 10, e0125705.
- Mazumdar, J., H Wilson, E., Masek, K., A Hunter, C., and Striepen, B. (2006). Apicoplast fatty acid synthesis is essential for organelle biogenesis and parasite survival in *Toxoplasma gondii*. *Proc. Natl. Acad. Sci. U S A* 103, 13192–13197.
- Melatti, C., Pieperhoff, M., Lemgruber, L., Pohl, E., Sheiner, L., and Meissner, M. (2019). A unique dynamin-related protein is essential for mitochondrial fission in *Toxoplasma gondii*. *PLoS Pathog.* 15, e1007512.
- Menard, D., and Dondorp, A. (2017). Antimalarial drug resistance: a threat to malaria elimination. *Cold Spring Harb. Perspect. Med.* 7, a025619.
- Mi-Ichi, F., Kita, K., and Mitamura, T. (2006). Intraerythrocytic *Plasmodium falciparum* utilize a broad range of serum-derived fatty acids with limited modification for their growth. *Parasitology* 133, 399–410.
- Mi-Ichi, F., Kano, S., and Mitamura, T. (2007). Oleic acid is indispensable for intraerythrocytic proliferation of *Plasmodium falciparum*. *Parasitology* 134, 1671–1677.
- Mitamura, T., Hanada, K., Ko-Mitamura, E.P., Nishijima, M., and Horii, T. (2000). Serum factors governing intraerythrocytic development and cell cycle progression of *Plasmodium falciparum*. *Parasitol. Int.* 49, 219–229.
- Mueller, C., Klages, N., Jacot, D., Santos, J.M., Cabrera, A., Gilberger, T.W., Dubremetz, J.-F., and Soldati-Favre, D. (2013). The *Toxoplasma* protein ARO mediates the apical positioning of rhoptry organelles, a prerequisite for host cell invasion. *Cell Host Microbe* 13, 289–301.
- Nolan, S.J., Romano, J.D., and Coppens, I. (2017). Host lipid droplets: an important source of lipids salvaged by the intracellular parasite *Toxoplasma gondii*. *PLoS Pathog.* 13, e1006362.
- Ohlogge, J., and Browse, J. (1995). Lipid biosynthesis. *Plant Cell* 7, 957–970.
- Pernas, L., Adomako-Ankomah, Y., Shastri, A.J., Ewald, S.E., Treeck, M., Boyle, J.P., and Boothroyd, J.C. (2014). *Toxoplasma* effector MAF1 mediates recruitment of host mitochondria and impacts the host response. *PLoS Biol.* 12, e1001845.
- Ramakrishnan, S., Docampo, M.D., Macrae, J.I., Pujol, F.M., Brooks, C.F., van Dooren, G.G., Hiltunen, J.K., Kastaniotis, A.J., McConville, M.J., and Striepen, B. (2012). Apicoplast and endoplasmic reticulum cooperate in fatty acid biosynthesis in apicomplexan parasite *Toxoplasma gondii*. *J. Biol. Chem.* 287, 4957–4971.
- Romano, J.D., Nolan, S.J., Porter, C., Ehrenman, K., Hartman, E.J., Hsia, R.C., and Coppens, I. (2017). The parasite *Toxoplasma* sequesters diverse Rab host vesicles within an intravacuolar network. *J. Cell Biol.* 216, 4235–4254.

- Schmidt, A., Wolde, M., Thiele, C., Fest, W., Kratzin, H., Podtelejnikov, A.V., Witke, W., Huttner, W.B., and Söling, H.D. (1999). Endophilin I mediates synaptic vesicle formation by transfer of arachidonate to lysophosphatidic acid. *Nature* *401*, 133–141.
- Shears, M.J., MacRae, J.I., Mollard, V., Goodman, C.D., Sturm, A., Orchard, L.M., Llinás, M., McConville, M.J., Botté, C.Y., and McFadden, G.I. (2017). Characterization of the *Plasmodium falciparum* and *P. berghei* glycerol 3-phosphate acyltransferase involved in FASII fatty acid utilization in the malaria parasite apicoplast. *Cell. Microbiol.* *19*.
- Sheiner, L., Demerly, J.L., Poulsen, N., Beatty, W.L., Lucas, O., Behnke, M.S., White, M.W., and Striepen, B. (2011). A systematic screen to discover and analyze apicoplast proteins identifies a conserved and essential protein import factor. *PLoS Pathog.* *7*, e1002392.
- Shin, J.J.H., and Loewen, C.J.R. (2011). Putting the pH into phosphatidic acid signaling. *BMC Biol.* *9*, 85.
- Sidik, S.M., Hackett, C.G., Tran, F., Westwood, N.J., and Lourido, S. (2014). Efficient genome engineering of *Toxoplasma gondii* using CRISPR/Cas9. *PLoS ONE* *9*, e100450.
- Sidik, S.M., Huet, D., Ganesan, S.M., Huynh, M.H., Wang, T., Nasamu, A.S., Thiru, P., Saeij, J.P.J., Carruthers, V.B., Niles, J.C., and Lourido, S. (2016). A genome-wide CRISPR screen in *Toxoplasma* identifies essential apicomplexan genes. *Cell* *166*, 1423–1435.e12.
- Trager, W., and Jensen, J.B. (1976). Human malaria parasites in continuous culture. *Science* *196*, 673–675.
- Uboldi, A.D., Wilde, M.-L., McRae, E.A., Stewart, R.J., Dagley, L.F., Yang, L., Katris, N.J., Hapuarachchi, S.V., Coffey, M.J., Lehane, A.M., Botte, C.Y., Waller, R.F., Webb, A.I., McConville, M.J., and Tonkin, C.J. (2018). Protein kinase A negatively regulates Ca²⁺ signalling in *Toxoplasma gondii*. *PLOS Biology* *16*, e2005642.
- van Dooren, G.G., Reiff, S.B., Tomova, C., Meissner, M., Humbel, B.M., and Striepen, B. (2009). A novel dynamin-related protein has been recruited for apicoplast fission in *Toxoplasma gondii*. *Curr. Biol.* *19*, 267–276.
- Vaughan, A.M., O'Neill, M.T., Tarun, A.S., Camargo, N., Phuong, T.M., Aly, A.S., Cowman, A.F., and Kappe, S.H. (2009). Type II fatty acid synthesis is essential only for malaria parasite late liver stage development. *Cell. Microbiol.* *11*, 506–520.
- Waller, R.F., Keeling, P.J., Donald, R.G., Striepen, B., Handman, E., Lang-Unnasch, N., Cowman, A.F., Besra, G.S., Roos, D.S., and McFadden, G.I. (1998). Nuclear-encoded proteins target to the plastid in *Toxoplasma gondii* and *Plasmodium falciparum*. *Proc. Natl. Acad. Sci. U S A* *95*, 12352–12357.
- Welti, R., Mui, E., Sparks, A., Wernimont, S., Isaac, G., Kirisits, M., Roth, M., Roberts, C.W., Botté, C., Maréchal, E., and McLeod, R. (2007). Lipidomic analysis of *Toxoplasma gondii* reveals unusual polar lipids. *Biochemistry* *46*, 13882–13890.
- Yeh, E., and DeRisi, J.L. (2011). Chemical rescue of malaria parasites lacking an apicoplast defines organelle function in blood-stage *Plasmodium falciparum*. *PLoS Biol.* *9*, e1001138.
- Ylä-Anttila, P., Vihinen, H., Jokitalo, E., and Eskelinen, E.L. (2009). Monitoring autophagy by electron microscopy in mammalian cells. *Methods Enzymol.* *452*, 143–164.
- Yu, M., Kumar, T.R., Nkrumah, L.J., Coppi, A., Retzlaff, S., Li, C.D., Kelly, B.J., Moura, P.A., Lakshmanan, V., Freundlich, J.S., et al. (2008). The fatty acid biosynthesis enzyme FabI plays a key role in the development of liver-stage malarial parasites. *Cell Host Microbe* *4*, 567–578.
- Zhang, M., Wang, C., Otto, T.D., Oberstaller, J., Liao, X., Adapa, S.R., Udenze, K., Bronner, I.F., Casandra, D., Mayho, M., et al. (2018). Uncovering the essential genes of the human malaria parasite *Plasmodium falciparum* by saturation mutagenesis. *Science* *360*, eaap7847.
- Zuzarte-Luís, V., Mello-Vieira, J., Marreiros, I.M., Liehl, P., Chora, A.F., Carret, C.K., Carvalho, T., and Mota, M.M. (2017). Dietary alterations modulate susceptibility to *Plasmodium* infection. *Nat. Microbiol.* *2*, 1600–1607.

STAR★METHODS

KEY RESOURCES TABLE

| REAGENT or RESOURCE | SOURCE | IDENTIFIER |
|---|--|--|
| Antibodies | | |
| Mouse anti-HA | Roche | Cat#: 11867423001; RRID:AB_390918 |
| anti-CPN60 | Boris Striepen | N/A |
| anti-LBPA | Echelon Biosciences | Cat#: 117Z-PLBPA-50ug |
| Mouse anti-Sag1 | Abcam | N/A |
| Anti-LC3B antibody produced in rabbit | Sigma | Cat#: L7543; RRID:AB_796155 |
| Rabbit anti-TOM40 | Giel van Dooren | N/A |
| rabbit anti-GAP45 | Dominique Soldati Lab | N/A |
| rabbit polyclonal anti-IMC1 | Gary Ward Lab | N/A |
| Anti-MIC2 | David Sibley | N/A |
| Anti-GRA1 | Cesbron-Delauw Lab | N/A |
| Rabbit anti-ACP | McFadden lab | N/A |
| Rabbit polyclonal anti-MIC4 | Dominique Soldati Lab | N/A |
| rabbit anti-Sumo21 | Hakimi lab | N/A |
| Goat a Mouse Alexa 488 | ThermoFisher Scientific | Cat#: A11001; RRID:AB_2534069 |
| Goat a Rb Alexa 546 | ThermoFisher Scientific | Cat#: A11003; RRID:AB_141370 |
| Goat a Mouse Alexa 546 | ThermoFisher Scientific | Cat#: A11010; RRID:AB_2534077 |
| Goat a Rb Alexa 488 | ThermoFisher Scientific | Cat#: A11008; RRID:AB_143165 |
| Bacterial and Virus Strains | | |
| <i>E. coli</i> SM2-1 Δ plsC | Coleman, 1990 | Coli Genetic Stock Center #7587, Yale University |
| Biological Samples | | |
| Red Blood Cells | Etablissement francais du sang (EFS) | N/A |
| Chemicals, Peptides, and Recombinant Proteins | | |
| DMEM, High Glucose | GIBCO, ThermoFisher Scientific | Cat#: 41965-062 |
| DMEM, no Glucose | GIBCO, ThermoFisher Scientific | Cat#: 11966-025 |
| RPMI 1640 Medium, HEPES | GIBCO, ThermoFisher Scientific | Cat#: 52400-025 |
| Fetal Calf Serum, Sourced from South America (EU Approved). | ThermoFisher Scientific | Cat#: 10270-106 |
| AlbuMAX® II | ThermoFisher Scientific | Cat#: 11021-045 |
| GLUCOSE-D U-13C6 99%13C 10 g | Cambridge Isotope Laboratories (Eurisotop) | Cat#: CLM-1396-10 |
| Sorbitol | Sigma | Cat#: S1876 |
| Giemsa's azur eosin methylene blue solution | Merck | Cat#: MEF1092040500 |
| fatty acid free bovine serum albumin | Sigma | Cat#: A8806 |
| palmitic acid (C16:0) | Sigma | Cat#: P0500-10G |
| oleic acid (C18:1) | Sigma | Cat#: 75090-5ML |
| tridecanoic acid (C13:0) | Sigma | Cat#: 91988-5G |
| pentadecanoic acid C15:0 | Sigma | Cat#: P6125-1G |
| MethPrep II (Alltech) | Alltech | Grace 5122149 |
| HCl | Sigma | Cat#: 258148 |
| 1-butanol | Sigma | N/A |
| Chloroform | Sigma | Cat#: 34854 |
| Hexane | Sigma | Cat#: 34484 |
| Methanol | Sigma | Cat#: 34860 |

(Continued on next page)

Continued

| REAGENT or RESOURCE | SOURCE | IDENTIFIER |
|---|--|---------------------|
| Acetone | Sigma | Cat#: 34850 |
| Ammonium hydroxide | Sigma | Cat#: 221228 |
| Acetic acid | Sigma | Cat#: 27221 |
| Fluorescent NBD PA18:1, 12:0 | Avanti Polar Lipids | Cat#: 810176P-1mg |
| Fluorescent NBD PC 18:1, 12:0 | Avanti Polar Lipids | Cat#: 810133P-1mg |
| PA 18:1, 16:0 | Avanti Polar Lipids | Cat#: 840857 |
| PA 14:0, 14:0 | Avanti Polar Lipids | Cat#: 830845 |
| PA(C17:0/C17:0) | Avanti Polar lipids | Cat#: 830856 |
| HPTLC60 | Merck | Cat#: MEF1056330001 |
| Nile red | Sigma | Cat#: 72485 |
| Chloramphenicol | Sigma | Cat#: C0378-5G |
| Pyrimethamine | Sigma | Cat#: 46706 |
| Mycophenolic acid | Sigma | Cat#: M3536 |
| Xanthine | Sigma | Cat#: X3627 |
| Fluoro-Gel, (with Tris Buffer) | Electron Microscopy Sciences | Cat#: 17985-10 |
| 0.1 M cacodylate buffer | Electron Microscopy Sciences | Cat#: 11650 |
| 25% glutaraldehyde | Electron Microscopy Sciences | Cat#: 16220 |
| 4% osmium tetroxide | Electron Microscopy Sciences | Cat#: 19150? |
| uranyl acetate | Electron Microscopy Sciences | Cat#: 22400 |
| Epon812 | Electron Microscopy Sciences | Cat#: 13940 |
| Crystal Violet | Sigma | Cat#: C0775 |
| Hoechst 33342 | ThermoFisher Scientific | Cat#: 1015-0888 |
| A23187 | Sigma | Cat#: C7522 |
| DIMETHYL SULFOXIDE, | Sigma | Cat#: D2438 |
| 16% Paraformaldehyde | Electron Microscopy Sciences | Cat#: 15710 |
| Triton X-100 | Sigma | Cat#: T9284-100ML |
| K ₂ SO ₄ | Sigma | Cat#: 60528 |
| MgSO ₄ | Sigma | Cat#: M2643 |
| sucrose | Sigma | Cat#: 84100 |
| glucose | Sigma | Cat#: G5400 |
| Tris | Dutscher | Cat#: 091572 |
| BSA | Sigma | Cat#: A9418 |
| HEPES | Sigma | Cat#: H4034 |
| DAPI | Sigma | Cat #: D9542 |
| Critical Commercial Assays | | |
| NucleoSpin Gel and PCR Clean-up | Macherey-Nagel | Cat #: 740609 |
| NucleoSpin Plasmid | Macherey-Nagel | Cat #: 740588 |
| NucleoBond Xtra Midi | Macherey-Nagel | Cat #: 740410 |
| Nucleo spin RNA II | Macherey-Nagel | Cat #: 740955 |
| DNA sequencing | Eurofins Genomics | N/A |
| Oligo nucleotide synthesis | Sigma | N/A |
| Q5® Site-Directed Mutagenesis Kit | NEB | Cat#: E0554S |
| Experimental Models: Cell Lines | | |
| Human Foreskin fibroblasts | ATCC® CCL-171 | N/A |
| Experimental Models: Organisms/Strains | | |
| <i>T. gondii</i> RH TATI1-ΔKu80 | Sheiner et al., 2011 | N/A |
| <i>T. gondii</i> RHΔKu80 | Huynh and Carruthers, 2009 | N/A |
| <i>T. gondii</i> PRU Type II | Marie-France Cesbron Delauw | N/A |

(Continued on next page)

| Continued | | |
|--|--|-------------|
| REAGENT or RESOURCE | SOURCE | IDENTIFIER |
| <i>T. gondii</i> ME49 Type II | Jeroen Saeij | N/A |
| <i>T. gondii</i> ASPV KO | Curt-Varesano et al., 2016 | N/A |
| <i>T. gondii</i> MYR1 KO | Braun et al., 2019 | N/A |
| <i>T. gondii</i> ACASiKD | Dubois et al., 2018 | N/A |
| <i>T. gondii</i> ARO-iKD | Mueller et al., 2013 | N/A |
| <i>T. gondii</i> PKA-iKD | Uboldi et al., 2018 | N/A |
| <i>T. gondii</i> GRA16 | Bougdoor et al., 2013 | N/A |
| <i>T. gondii</i> ATS1 | Amiar et al., 2016 | N/A |
| <i>P. falciparum</i> PfFabI KO | Vaughan et al., 2009 | N/A |
| <i>P. falciparum</i> NF54 | Walter and Eliza Hall Institute | N/A |
| <i>T. gondii</i> ACBP1 iKD | This study | N/A |
| <i>T. gondii</i> ACBP2 iKD | This study | N/A |
| <i>T. gondii</i> ACBP1/ACBP3 double KO | This study | N/A |
| <i>T. gondii</i> ACBP1/SCP2 double KO | This study | N/A |
| <i>T. gondii</i> ATS2-HA | This study | N/A |
| <i>T. gondii</i> ATS2-KI | This study | N/A |
| <i>T. gondii</i> ATS2-KO | This study | N/A |
| Oligonucleotides | | |
| All primers outlined in materials and methods section. | | N/A |
| Recombinant DNA | | |
| U6-Universal Plasmid | Sidik et al., 2014 (Addgene) | N/A |
| Cas9-RFP plasmid | Dominique Soldati | N/A |
| pTOXO_Cas9-CRISPR | Hakimi Lab, Grenoble, France | N/A |
| pTOXO_Cas9-CRISPR::gTgATS2-KI | This study | N/A |
| pTOXO_Cas9-CRISPR::gTgATS2-KO | This study | N/A |
| pTOXO_Cas9-CRISPR::gTgAGPAT-KO | This study | N/A |
| graCAT-sagMcherry | This study | N/A |
| pLIC HA3 DHFR | Huynh and Carruthers, 2009 | N/A |
| pLIC HA3 CAT | Sheiner et al., 2011 | N/A |
| ATS2 KO plasmid MAH | This Study | N/A |
| pPR2 HA3 DHFR | Katriss et al., 2014 | N/A |
| graCAT sagmCherry KO plasmid | This study | N/A |
| Morn1-myc | Marc-Jan Gubbels | N/A |
| pLIC-TgATS2-3HA-DHFR | This study | N/A |
| pLIC-TgAGPAT-3HA-DHFR | This study | N/A |
| pMORN1-CherryRFP-MORN1/SagCAT | This study | N/A |
| pQE30Xa vector | Quiagen | 33203 |
| Software and Algorithms | | |
| Prism software | GraphPad | N/A |
| ImageJ | NIH | N/A |
| Mass Hunter Quantification software | Agilent | N/A |
| Other | | |
| Gas chromatography-mass spectrometry | Agilent | 5977A-7890B |

MATERIALS AND METHODS

See [STAR Methods](#) KEY RESOURCES Table

LEAD CONTACT AND MATERIALS AVAILABILITY

Materials generated in this study are available upon request. Information and requests for resources and reagents should be directed to the Lead Contact, Cyrille Botte (cyrille.botte@univ-grenoble-alpes.fr). Plasmids and parasite lines generated in this study will be made freely available by the Lead Contact upon request which may require the completion of a Material Transfer Agreement.

EXPERIMENTAL MODEL AND SUBJECT DETAILS

T. gondii culture

Toxoplasma gondii parental lines RH TATI1- Δ Ku80 (Sheiner et al., 2011) and RH- Δ Ku80 (Huynh and Carruthers, 2009) and derived transgenic cell lines were grown in confluent human foreskin fibroblasts (HFFs) in high glucose DMEM supplemented with 1% Foetal Bovine Serum, as described (Amiar et al., 2016). ME49 parental cell cultures were additionally supplemented with 10 mM HEPES.

P. falciparum culture

P. falciparum NF54 wild-type parasites were maintained as previously described (Trager and Jensen, 1976). Briefly, *Plasmodium* blood stage parasites were maintained at 2% hematocrit in 1640 RPMI-HEPES supplemented with 10% AlbuMAX II (GIBCO) and 0.25% gentamycin. Parasites were grown sealed Perspex chambers gassed with beta mix gas (1% O₂, 5% CO₂, 94% N₂) at 37°C and maintained on 48-hour cycles.

METHOD DETAILS

Gene identification and sequence analysis

T. gondii plasmid constructs

T. gondii transfection

T. gondii growth assays

T. gondii Red/Green parasite invasion assay:

Plasmodium falciparum growth assays:

Immunofluorescence assay and Microscopy

Nile red staining of lipid droplets

Activity analysis in LPAAT-deficient *E. coli* strains

Transmission electron microscopy:

Lipidomic analysis by GCMS extraction from *T. gondii* tachyzoites

Stable isotope labeling of *T. gondii*

Phospholipid import assay:

Quantification and statistical analysis

Gene identification and sequence analysis

Arabidopsis thaliana sequence of ATS2 (GenBankTM and TAIRTM IDs: NP_194787 and AT4G30580 respectively) was used as a query sequences for BLAST searches against the *Toxoplasma gondii* genome on ToxoDB database (<https://www.toxodb.org/>). Phylogenetic analysis of AGPAT related proteins was performed on the Phylogeny.fr platform (Dereeper et al., 2008). Protein sequences were then aligned by ClustalW software (Larkin et al., 2007) and the maximum likelihood phylogeny was generated using the PhyML (Guindon et al., 2010). We generated multiple sequence alignment using Clustal Omega (Li et al., 2015).

T. gondii plasmid constructs

Plasmid LIC-3HA-DHFR was used to generate a 3' endogenous tagging with 3xHA coding sequence of ToxoDB: TGME49_297640 (*TgATS2*) and ToxoDB: TGME49_240860 (*TgAGPAT*). A 2229 bp fragment corresponding to the 3' of *TgATS2* was amplified from genomic DNA using primer sets 5'-TCCTCCACTTCCAATTTTAGCGTTCGTCTCGGTGGCGGC-3' and 5'-TACTTCCAATC CAATGCTTCAGACACTCGGTGCAAA-3. A 5466 bp fragment corresponding to promoter and gene sequence of *TgAGPAT* was amplified using primer sets 5'-TACTTCCAATCCAATGCAGCCAGCAAAGGACGAAAGG-3' and 5'-TCCTCCACTTCCAATTTTAGC GAGACCGTGGCCTCGGTGGG-3'. These fragments were cloned into pLIC-3HA-DHFR vector as described previously (Huynh and Carruthers, 2009). Vectors LIC-*TgATS2*-3HA-DHFR and LIC-*TgAGPAT*-3HA-DHFR were confirmed by PCR screen using primer sets 5'-GCATAATCGGGCACATCATA-3' and 5'-ATACGCATAATCGGGCACATCATA-3' and by sequencing (Eurofin genomicsTM).

Plasmid pTOXO_Cas9-CRISPR (gift from Hakimi Lab, Grenoble, France) was used to integrate a gRNA within Bsal restriction site as previously described (Sidik et al., 2014). Briefly, Crisp-Fwd and Crisp-Rv primer sets were phosphorylated and annealed: *Tg*ATS2-KI: 5'-AAGTTACGGGTGTGCGCCGCTTGC-3' and 5'-AAAACGCAAGGCGGCGCACACCCGTA-3', *Tg*ATS2-KO: 5'-AAGTTG GAGCGCCGACGGGCGACTGG-3' and 5'-AAAACAGTCGCGCGTGGCGCTCCA-3', *Tg*AGPAT-KO: 5'-AAGTTCTCTGCCGAGT TCCAATCGCG-3' and 5'-AAAACGCGATTGGAAGTCCGCGCAGAGA-3'. The gRNAs were then ligated into pTOXO_Cas9-CRISPR plasmid linearized with Bsal, yielding pTOXO_Cas9-CRISPR::g*Tg*ATS2-KI, pTOXO_Cas9-CRISPR::g*Tg*ATS2-KO and pTOXO_Cas9-CRISPR::g*Tg*AGPAT-KO, respectively.

For *Tg*ATS2 knockout by CRISPR-Cas9, an appropriate HXGPRT cassette amplified by PCR from pMini (kind gift from the Hakimi laboratory) using those primer sets, *Tg*ATS2-KI: 5'-GAGGCCCTGCGTCTCCTCAAGCG- AAAGGCGCCGCCACAGTCGACGGGTGT GCGCC-GCCTCAGCAGCAAACCT-TGCATTCAAACC-3' and 5'-GCTACTCCTTCTCCCTCTCG- CGTTGTGTGTCTCCCGTGTG CGTTCTGCGTCGCCAGCAGTGTCACTGTAGCCTGCCAGAAC-3'; *Tg*ATS2-KO: 5'-GACACACAACGCGAGAGGGGAAGAAGGA GTAGCTCTCG-TCGCCTTTCCAGAAGTACTCCAGCACGAAACCTTGCATTCAAACC-3' and 5'-CTTCG- CTGCTCGTTCGTTCTT C ATGTGGGAAGGAGCAGCACGAAACCTTG- CATTCAAACC-3'.

DrpA and DrpC were localized by CRISPR Cas9 strategy. Guides were inserted into Cas9 U6 universal plasmid (Sidik et al., 2014) by either standard ligation of annealed primers or Q5 mutagenesis. Cells were transfected together with PCR product encoding either HA3-CAT and DrpC homology flanks, for DrpC or GFP sequence without selection and DrpA homology flanks for DrpA.

For DrpC HA3 CAT CRISPR Cas9 tagging, DrpC was tagged at the 3' terminus by CRISPR Cas9 (Sidik et al., 2014). For DrpC, the protospacer gaatggggctgaaactgtg was chosen and primers 5' AAGTTgaatggggctgaaactgtg 3' and 5' AAAACcacagtgttaagccc cattcA 3' were annealed together and ligated into U6 universal plasmid (Sidik et al., 2014). The HA3-CAT cassette was PCR amplified by primers with 50 bp homology flanks (FOR aggaagtccggctcggctcggcaccgtt- gaatggggctAAAATTGGAAGTGGAGGACGGG and REV gttctcccagtgctctggcga- agtgggcccagcacaagccaGTTGTAAAACGACGGCCAGTG) and overhang corresponding to the 3' end of DrpC and in frame with HAX3. 50 μg of both plasmid and PCR product were transfected and placed under chloramphenicol selection (Kim et al., 1993). DrpC was also localized by pLIC-HA3-CAT using primers TACTTCCAATCCAATTTAGCgacaggtctgtgttc tacg and TCCTCCACTTCCAATTTTAGCagccccattcaacgggtg (Sheiner et al., 2011). For DrpA, the protospacer gatggaggagttgattcctg was inserted into the Universal Cas9 Plasmid using the NEB Q5 site directed mutagenesis Kit with the oligos 5' gatggaggagtt gattcctgTTTTAGAGCTAGAAATAGC 3' and 5' AACTTGACATCCCCATTTAC 3'. PCR product was amplified using 5'- gttgccctggctt cctcctcttctcctcctcctcaagATGGCGGTGAGCAAGGGC3' 5'- cgtcctgcagggcagttgacAacaggaatcaactcctccatCCCGGGCTTGTA CAGC 3' using GFP cDNA as a template and co-transfected with U6 guide RNA plasmid described above. Transfected parasites were seeded onto coverslips and then transiently observed after 24 hours growth.

For the DrpC PA domain mutation, a guide was identified within a DrpC exon and the 20 bp protospacer (5' ggcgagctgatcctcgag gt 3') was inserted into a CRISPR Cas9 plasmid using Q5 with primers 5' ggcgagctgatcctcgaggt-GTTTTAGAGCTAGAAATAGCA AG 3' and 5' AACTTGACATCCCCATTTAC 3' (Sidik et al., 2014). The PCR product was amplified with the following primers 5' cgtcgccttgtagcgaagcctt-ggagacgcaaaacggattGCGGTGAGCAAGGGCG 3' and 5' agccccattcaacggtgacggaagccgaccggaacttc tgcCCCGGGCTTGACAGC 3'. The guide and the PCR product were transfected together and parasites were seeded onto HFFs on coverslips and grown for 24 h. Cells were labeled with anti-IMC and anti-HA antibodies and viewed under the microscope. Cas9 expression was visualized by the Cas9-RFP tag to observe parasites with DrpC-HA normally (Cas9-RFP absent) or with the PA binding domain disrupted (Cas9-RFP present).

For *Tg*ACBP1i-HA KD, the 5' UTR flank was PCR amplified using primers ACACGGGCCACGATCAGTTGAGTTCCGAGG and GACACATATGAAGG -TCGAAAGAAGGCTCC and inserted into Apal/NdeI sites of pPR2-HA3 (Katris et al., 2014). The 3' flank was amplified using primers CTTGCCCGGGATGGCCTCGCgtaaggaagg and CAGAGCGGCCGCTGT -GTCGTGAGCGAGTGAC and then inserted in frame with a Tet7O/SAG4 promoter using XmaI/NotI sites. Plasmid was linearized with NotI prior to transfection and selected using pyrimethamine. For ACBP2, flanks were PCR amplified using respective primers below into the plasmid pPR2-GFP or pPR2-mCherry (adapted from pPR2-HA3, (Katris et al., 2014). The 5' UTR flank was amplified using CTGAGGGCCCGC GACGCTCCAGAAGACTCC and GTACCATA -TGTTATTATATGTTGAAAGAAGC inserted first using Apal/NdeI sites. Next, the 3' UTR flank was amplified using GACTGATATCGATT -ACGGCTTCAACTCCGTC and ATTAGCGGCCGCTTCATAGGAC -CAGAGCC and inserted using MscI/NotI sites. ACBP2 cDNA sequence was amplified using GATCAGATCTAAAATGGCGAGGCCTGTA CATCTTGGG and GTACCCTAGGAGTAGCTTTTGGAGCGGTG inserted last into BglII/AvrII sites then selected using pyrimethamine. ACBP1 pLIC was PCR amplified using pLIC primers TACTTCCAATCCAATTTAGCTACAACGGAGCAGACAGAGG and TCCTCCACTTCCAATTTTAGCCGCGCTTTTCTCGCGCC into pLIC-HA3-CAT (Sheiner et al., 2011), and linearized prior to transfection and selection on chloramphenicol.

For ACBP1 KO/ACBP2iKD the following protospacer was selected, 5' GGGGCGTTCCTGAGAGAA 3', inserted into a U6-Cas9 expression construct (Sidik et al., 2014). A PCR product w homology flanks for ACBP1 was made with the following primers 5' ATTTTTTCAAAGTCCATGCTGGGTTTCTCCCTG-TGTCTAGGGAGCCTTAAAACCCTCGAAGGCTGCTAGTAC 3' and 5' AGATGATTTGACGACCGCCTCGGAAGTCGCTCTGTTTACG- CGTTTTTGCCAGAACAATTGTCAACCG3' using a graCAT-sag-mcherry resistance cassette as a template and transfected with U6 construct and selected for with Chloramphenicol. For SCP2 KO/ACBP1iKD, the following protospacer 5' GTACGCTTGCTGTGGAAAAA 3' was inserted into a U6-Cas9 construct and co-transfected with the following primers 5'

gaacaggtgctgacactgtctcgagaatcctgtcgctgcaagttctgagttAAAACCCTCGAAGGCTGCTAGTAC 3' and 5' agggcgagttcacgaaatc
ttcgt -ccaacaaagtgatggtgcagtcgcaTGCCAGAACACTTGTCAACCG 3' using a graCAT-sag-mcherry resistance cassette and
selected for with chloramphenicol.

T. gondii transfection

RH- Δ Ku80 parasite line was transfected with 100 μ g of pLIC-TgATS2-3HA-DHFR linearized with BlnI for stable integration of HA-tag at C terminus of TgATS2. 150 μ g pTOXO_Cas9-CRISPR::gTgATS2-KO and pTOXO_Cas9-CRISPR::gTgAGPAT-KO were transfected in TgATS2-HA line with 10 μ g of appropriate HXGPR cassette for TgATS2-KI and TgATS2-KO, PCR product as described above. Electroporations were performed in a 2-mm cuvette in a BTX ECM 630 (Harvard Apparatus, at 1,100 V, 25 Ω , and 25 μ F. Stable lines expressing the tagged constructs were selected in media with 1 μ M pyrimethamine or 25 μ g/ml mycophenolic acid and 50 μ g/ml xanthine and cloned by limiting dilution.

RH- Δ Ku80 parasites were also transiently transfected with pLIC-TgAGPAT-3HA-DHFR. pTOXO_Cas9-CRISPR::gTgAGPAT-KO was transfected in RH- Δ Ku80 parasites for a simple mutant Δ TgAGPAT and in Δ TgATS2 parasites to obtain a double mutant Δ TgATS2/ Δ TgAGPAT. The plasmid pMORN1-CherryRFP-MORN1/SagCAT were transfected in both RH- Δ Ku80 and Δ TgATS2 parasite lines.

All other transfections were performed with 50 μ g of DNA and electroporation conditions were as described above. Transfected parasites were incubated at different concentration with HFF cell 48 h prior to immunofluorescence assay.

T. gondii growth assays

- Plaque Assay

HFF monolayers were infected with 500 parasites and allowed to develop for 10 days before staining with Crystal Violet (Sigma) and cell growth assessment by light microscopy for the presence of intact HFF. To obtain statistical assessment, each strain was grown in each condition in triplicate and the plaque area in the same square unit ($n = 6$) are measured. Boxplot with whiskers from minimum to maximum with median.

- Cell-based assay

T. gondii growth was determined with an automatic microscope-based screening (Olympus ScanR, Japan). HFFs were seeded at a density of 10,000 cells per well into 96-well plates and were allowed to grow and equilibrate for 48 h at 37°C. Cells were then infected with 4×10^4 parasites/well. Invasion was synchronized by briefly centrifugation of plate at 250 g and placed at 37°C for 2 h. The assay was run for 30 h. Hoechst 33342 (Life technologies) stain was then loaded on live cells/parasites at 5 μ g/ml for 20 min. Infected cells were fixed with PFA (3.7%) for 10 min at 37°C. A mouse anti-GRA1/Alexa488 labeling (dilution 1:500) was used to identify parasitophorous vacuoles. A total of 20 fields per well were taken using the 20X objective. Images were collected for the distinct fluorescence channels (Hoechst 33342: e.g., 360-370 nm, em. 420-460 nm and Alexa488: ex. 460-495, em. 510-550 nm). Images were then analyzed using the ScanR analysis software (Olympus, Tokyo, Japan). For Alexa488 channels images (vacuoles) an intensity algorithm module was used where a fixed threshold was defined with a minimum of 100 pixels size in order to segment the smallest vacuoles (one or two parasite). For Hoechst channel images (parasites nuclei), image process consists to apply a strong background correction and detected parasites with an edge algorithm. A minimum object size of 5 pixels and a maximum object 20 pixels larger one was chosen to discriminate each parasite. ScanR analysis module interface as in flow cytometry allow us to extract and display data as scatterplots and histograms. Using a "gating" procedure we were able to hierarchically filter selected data points with precise boundaries (e.g., number of vacuoles versus number of parasite/vacuoles). The proliferative index was evaluated by parasite/vacuole number ratio. To assess statistically, the samples were prepared in quadruplicate ($n = 4$).

T. gondii egress assay

WT or Δ TgATS2 parasites were incubated on HFF cells for approximately 26 h before aspirating medium and replacing with DMEM containing 2 μ M A23187 or DMSO in quadruplicate ($n = 4$). Parasites were incubated for 3 min before addition of an equivalent volume of 2x fixative containing 5% Paraformaldehyde, 0.05% glutaraldehyde in PBS (final concentration 2.5% Paraformaldehyde, 0.025% glutaraldehyde). Cells were fixed for 15 min before permeabilizing with 0.025% Triton X-100 in PBS for 10 min and then Blocking overnight in blocking solution (2% FBS in PBS). Samples were then probed by immunofluorescence assay and counted manually for egress.

T. gondii Red/Green parasite invasion assay

Experiment was performed as per (Katris et al., 2014). Parasites were grown for 2 days in quadruplicate ($n = 4$). and harvested intracellular after replacing medium with ENDO buffer (44.7 mM K₂SO₄, 10 mM MgSO₄, 106 mM sucrose, 5 mM glucose, 20 mM Tris-H₂SO₄, 3.5 mg/ml BSA, pH 8.2). Cells were scraped, needle passed, filtered and centrifuged at 1800 rpm for 10 min. Cells were resuspended to a concentration of 2.5×10^7 cells ml⁻¹ in ENDO buffer and settled for 20 min onto host cells. Once settled, medium was aspirated and replaced with Invasion buffer (DMEM, 3% FBS and 10 mM HEPES). Parasites were allowed to invade for 15 min before fixation with 2.5% Paraformaldehyde and 0.02% glutaraldehyde. Samples were then blocked in 2% FBS in PBS overnight at 4°C. Samples were probed with mouse anti-SAG1, before washing with PBS, then permeabilized with 0.25% Triton

X-100 in PBS. Cells were then probed with rabbit anti-GAP45 and washed in PBS. Samples were then probed with Alexafluor anti-mouse 546 and anti-rabbit 488 before mounting onto slides. Cells were imaged by microscopy and invasion rate determined using ImageJ.

Plasmodium falciparum growth assays

P. falciparum NF54 wild-type parasites and FabI-KO (Vaughan et al., 2009) were maintained as previously described (Trager and Jensen, 1976) at 2% hematocrit in RPMI-HEPES supplemented with Albumax II (GIBCO). Intra-erythrocytic growth assays in standard media were performed by monitoring the replication of tightly synchronous parasites (5% sorbitol) over four asexual cycles as previously described (Mi-ichi et al., 2006; Mitamura et al., 2000). Media was replaced daily, sub-culturing were performed every 48 h when required, and parasitemia monitored by Giemsa stained blood smears. Growth assays in lipid-depleted media were performed by synchronizing parasites, before transferring trophozoites to lipid-depleted media as previously reported (Botté et al., 2013; Shears et al., 2017). Briefly, lipid-rich Albumax II was replaced by complementing culture media with an equivalent amount of fatty acid free bovine serum albumin (Sigma), 30 μ M palmitic acid (C16:0; Sigma) and 45 μ M oleic acid (C18:1; Sigma). All assays were performed in triplicates on different days.

Immunofluorescence assay and Microscopy

Parasites were infected to HFF cells grown on coverslips as previously mentioned (Amiar et al., 2016). Primary antibodies used: Mouse anti-HA antibody (Roche, 1:1000), anti CPN60 (1:1000), anti GAP45 (1:1000), rabbit anti-ACP (1:2000), rabbit anti-TOM40 (1:3000), polyclonal rabbit anti-IMC1, anti-MIC4 antibodies (1:1000), rabbit anti-Sumo21 at (1:500) and mouse anti-Sag1 (1:500), anti-LBPA (1:500) or anti-LC3 (1:500). Secondary antibodies: anti-mouse Alexa 488 or 546, anti-rabbit Alexa 546- (ThermoFisher Scientific, 1:10000). Mitotracker (1mM) was diluted in DMEM 1:5000 (100–300 nM working concentration).

For the immunofluorescence assay (IFA) parasites were grown on confluent HFF on coverslips and fixed in PBS containing 2.5% paraformaldehyde (PFA) for 15 min at room temperature (RT). Samples were permeabilized with 0.25% Triton X-100 in PBS for 10 min at RT prior to blocking in PBS containing 3% BSA and subsequent incubation with primary antibodies then secondary antibodies diluted in the blocking solution. Labeled parasites were stained with Hoechst (1:10000, ThermoFisher Scientific) for 20 min and then washed three times in PBS before final mounting of the coverslips on a glass slide using Fluoro-Gel (Electron Microscopy Sciences). The fluorescence was visualized using fluorescence microscope (Axio Imager 2_apotome; ZEISS) with 63x objective.

Nile red staining of lipid droplets

The parasites were allowed to infect and growth in confluent monolayer HFF grown on coverslips, in the \pm ATc conditions for x days and then fixed in PBS containing 2.5% paraformaldehyde (PFA) for 15 min at room temperature (RT). Samples were permeabilized with 0.25% Triton X-100 in PBS for 10 min at RT and stained with primary rat anti-HA antibody followed by detection with secondary AlexaFluor 488- conjugated goat anti-rat antibody. Thereafter, the sample coverslips were incubated for 1 h with Nile red in 1X. Lastly, three washing steps with 1X PBS were performed before proceeding to DNA staining with Hoechst. The coverslips were mounted onto a glass slide in fluorogel before proceeding to imaging using fluorescence microscope (Axio Imager 2_apotome; ZEISS). For visualizing Nile red stained droplets yellow-gold fluorescence (excitation, 450–500 nm; emission, greater than 528 nm) was used on the Axio imager. Quantification in \pm ATc condition was done by counting the no. of lipid droplets per parasite.

Activity analysis in LPAAT-deficient *E. coli* strains

Escherichia coli strain deficient in LPAAT/AGPAT activity [SM2-1 Δ plsC, Coli Genetic Stock Center #7587, Yale University] (Coleman, 1990) was used to confirm LPAAT activity in both TgATS2 and TgAGPAT.

Coding sequence of TgATS2 was synthesized (Genscript). TgAGPAT coding sequence was amplified by RT-PCR using primer sets 5'-ATGGCGTCCACGCCGCTGC-3'/5'-TTAGAGACCGTGGCCTCGGTG-3' and TgAGPAT Δ N-ter1-72 coding was amplified by RT-PCR using primer sets 5'-CTCAACCGCCCGCCAGGAATTA-3'/5'-TTAGAGACCGTGGCCTCGGTG-3'. These sequences were digested and ligated into HindIII restriction site on pQE30Xa vector (Quiagen) to generate expression vectors. Additionally, gene coding for *E. coli* LPAAT activity plsC, was amplified from *E. coli* DH5alpha genomic DNA using primer sets 5'-CTATATATCTTTTCGTCTTAT TATTAC-3'/ 5'-AACTTTTCCGCGGCTTC-3' and ligated into pQE30Xa vector. Then these acyltransferase vectors and empty pQE30Xa vector as negative control were transfected to electrocompetent cells of SM2-1 Δ plsC deficient *E. coli*. pREP4 repressor vector to regulate Lac promoter activity. Transformed bacterial populations were grown at 37°C in order to promote growth of all isolates. Two independent clones of each bacterial strain that harbors each plasmid-of-interest were isolated for this study. Rescue of LPAAT activity in SM2-1 Δ plsC mutant was measured by the ability to grow at elevated temperature, 42°C, non-permissive temperature in LB medium as previously described (Coleman, 1990). Bacteria were first grown in LB media at 37°C to stationary phase, then the cultures were diluted to OD600 = 0.04 and finally inoculated with several dilutions (at 10⁻¹ to 10⁻⁶) on LB plates and incubated for 24 h at permissive (30°C) and non-permissive (42°C) temperatures. All experiments were conducted in triplicate with both independent clones.

Transmission electron microscopy

Parasites were grown for 24 h in Labteks (Nunc, Thermofisher) before fixation in 0.1 M cacodylate buffer with 2.5% glutaraldehyde for 2 h. Samples were then kept in fixative at 4°C until further processing. Samples were then post-fixed 1 h with 1% osmium tetroxide in cacodylate buffer followed by overnight in 2% uranyl acetate in distilled water. After dehydration in graded series of acetonitrile, samples were progressively impregnated in Epon812, the wells were then filled with fresh resin and allowed to polymerize 48 h at 60°C. Ultrathin 70 nm sections were obtained with a Leica UCT Ultramicrotome and collected on copper grids. Grids were post-stained with uranyl acetate and lead citrate before their observation on a Jeol1200EXII Transmission Electron Microscope. All chemicals were from Electron Microscopy Sciences.

Lipidomic analysis by GCMS extraction from *T. gondii* tachyzoites

Lipid extraction and analysis of tachyzoites was performed as previously described (Ramakrishnan et al., 2012; Amiar et al., 2016; Dubois et al., 2018). Freshly egressed tachyzoites (1×10^8 cell equivalents) grown in standard culture ($n = 4$) or in starvation culture ($n = 3$), were metabolically quenched by rapid chilling of the cell suspension in a dry ice/ethanol bath and lipids were extracted in chloroform/methanol/water (2:1:0.8, v/v/v containing 25 nmol tridecanoic acid C13:0 as extraction internal standard) for total lipid analysis.

- For lipid quantification

Total lipid extraction was performed as described previously (Amiar et al., 2016). Parasites were prepared as described above except for the addition of 0.1 M HCl to promote PA and LPA extraction. Pooled organic phase was subjected to biphasic separation by adding 0.1 M HCl. In both protocols, the organic phase was dried with speed vacuum and dissolved in 1-butanol.

- Total lipids analysis

An aliquot of the lipid extract was dried in vacuum concentrator with 1 nmol pentadecanoic acid C15:0 as internal standard. Then the dried lipid was dissolved in the chloroform/methanol (2:1, v/v) and derivatised with MethPrep II (Alltech). The resulting fatty acid methyl esters were analyzed by GC-MS as described previously (Amiar et al., 2016). Fatty acid methyl esters were identified by their mass spectrum and retention time compared to authentic standards. Lipid data was analyzed using Agilent® Masshunter software.

- Lipid quantification

Total lipid fraction was separated by 2D-HPTLC (Merck) with 5 μ g PA(C17:0/C17:0) and 5 μ g LPA(C17:0) (Avanti Polar lipids) using chloroform/methanol/28% NH₄OH, 60:35:8 (v/v) as the 1st dimension solvent system and chloroform/acetone/methanol/acetic acid/water, 50:20:10:13:5 (v/v/v/v/v) as the 2nd dimension solvent system (Amiar et al., 2016). For DAG analysis, total lipid fraction was separated by 1D-HPTLC using hexane/diethylether/formic acid, 80:20:2 (v/v/v) as solvent system. The spot on the HPTLC corresponding to each lipid was scrapped off and lipids were directly derivatised with 0.5 M methanoic HCl in the presence of 1 nmol pentadecanoic acid (C15:0) as internal standard. The resulting fatty acid methyl esters were extracted with hexane and analyzed by GC-MS (Amiar et al., 2016). Resulted FAME and cholesterol-TMS was analyzed by GC-MS (5977A-7890B, Agilent). FAME was then quantified using Mass Hunter Quantification software (Agilent). All statistical analyses were conducted using GraphPad Prism software. P values of ≤ 0.05 from statistical analyses (Ttests) were considered statistically significant.

Stable isotope labeling of *T. gondii*

Stable isotope labeling using U-¹³C-glucose (Cambridge Isotope Laboratories, USA), lipid extraction, and GC-MS analysis was performed as previously described in Ramakrishnan et al. (2012) and Amiar et al. (2016). Freshly infected HFF were incubated in glucose-free medium supplemented with 8 mM U-¹³C-glucose. For FBS starvation study, 5% FBS was added to U-¹³C-glucose medium in standard culture conditions and 1% FBS was added to U-¹³C-glucose medium in starvation culture condition. Parasites were harvested 72 h post-infection and metabolites extracted as above.

Phospholipid import assay

Freshly lysed cultures of WT or Δ TgATS2 parasites ($n = 3$) were harvested, filtered and resuspended in DMEM to a concentration of approximately 2×10^8 cells ml⁻¹. Cells were then mixed with a 2x solution containing 10 μ g ml⁻¹ NBD-PA or NBD-PC (5 μ g/mL final) and incubated at 37°C. Parasites were then spun down, resuspended in PBS. PFA was then added to a final concentration of 2.5%, and cells were fixed for 15 min before being spun down again and resuspended in 1xPBS. Parasites were smeared onto polyethyleneimine coated coverslips, and then probed with anti-SAG1 primary (1:1000) and anti-mouse Alexa 546 secondary antibodies (1:10000) by immunofluorescence microscopy, stained with DAPI (1:10000) and mounted onto slides. Samples were imaged by microscopy. SAG1 labeling was used to identify parasites using ImageJ and then estimate the amount of NBD-lipid uptaken by the parasites.

QUANTIFICATION AND STATISTICAL ANALYSIS

Statistical analyses for all experiments were performed with Prism software v7 (GraphPad). In experiments comparing only two groups, t test with Holm-Sidak correction were used to compare the experimental group with the control group. For other experiments including 3 groups, non-parametric ANOVA tests (Sidak correction for multiple tests) were used. Individual p values are indicated in each figure. Each experiment was done in $n = 3$ otherwise mentioned in material methods. For lipidomic analysis,

Agilent® Masshunter software, was used for fatty acid analysis and subjected to statistical analysis as described above. All error bars present standard error of mean, otherwise mentioned individually.

DATA AND CODE AVAILABILITY

No unique code or software was generated in this study. All datasets generated and analyzed during this study are available upon request to the lead contact Cyrille Botte (cyrille.botte@univ-grenoble-alpes.fr).



Article

2-Phenoxy-3-Trichloromethylquinoxalines Are Antiplasmodial Derivatives with Activity against the Apicoplast of *Plasmodium falciparum*

Dyhia Amrane¹, Christophe-Sébastien Arnold² , Sébastien Hutter³, Julen Sanz-Serrano⁴ , Miguel Collia⁴, Amaya Azqueta^{4,5}, Lucie Paloque^{6,7,8} , Anita Cohen³, Nadia Amanzougaghene⁹ , Shahin Tajeri⁹, Jean-François Franetich⁹, Dominique Mazier⁹ , Françoise Benoit-Vical^{6,7,8} , Pierre Verhaeghe^{6,10}, Nadine Azas³ , Patrice Vanelle^{1,11,*}, Cyrille Botté^{2,*} and Nicolas Primas^{1,11,*}



Citation: Amrane, D.; Arnold, C.-S.; Hutter, S.; Sanz-Serrano, J.; Collia, M.; Azqueta, A.; Paloque, L.; Cohen, A.; Amanzougaghene, N.; Tajeri, S.; et al. 2-Phenoxy-3-Trichloromethylquinoxalines Are Antiplasmodial Derivatives with Activity against the Apicoplast of *Plasmodium falciparum*.

Pharmaceuticals **2021**, *14*, 724.
<https://doi.org/10.3390/ph14080724>

Academic Editors: Thierry Besson and Pascal Marchand

Received: 2 July 2021
Accepted: 22 July 2021
Published: 26 July 2021

Publisher's Note: MDPI stays neutral with regard to jurisdictional claims in published maps and institutional affiliations.



Copyright: © 2021 by the authors. Licensee MDPI, Basel, Switzerland. This article is an open access article distributed under the terms and conditions of the Creative Commons Attribution (CC BY) license (<https://creativecommons.org/licenses/by/4.0/>).

- ¹ Aix Marseille Univ, CNRS, ICR UMR 7273, Equipe Pharmaco-Chimie Radicalaire, Faculté de Pharmacie, CEDEX 05, 13385 Marseille, France; dyhia.amrane@etu.univ-amu.fr
- ² ApicoLipid Team, Institute for Advanced Biosciences, Université Grenoble Alpes, 38700 La Tronche, France; arnold.csa@gmail.com
- ³ Aix Marseille Univ, IHU Méditerranée Infection, UMR VITROME, IRD, SSA, Mycology & Tropical Eucaryotic Pathogens, CEDEX 05, 13005 Marseille, France; sebastien.hutter@univ-amu.fr (S.H.); anita.cohen@univ-amu.fr (A.C.); nadine.azas@univ-amu.fr (N.A.)
- ⁴ Department of Pharmacology and Toxicology, Faculty of Pharmacy and Nutrition, University of Navarra, C/Irunlarrea 1, 31008 Pamplona, Spain; jsanz.3@alumni.unav.es (J.S.-S.); mcollia@alumni.unav.es (M.C.); amazqueta@unav.es (A.A.)
- ⁵ Navarra Institute for Health Research, IdiSNA, Irunlarrea 3, 31008 Pamplona, Spain
- ⁶ LCC-CNRS, Université de Toulouse, CNRS UPR8241, UPS, 31400 Toulouse, France; lucie.paloque@lcc-toulouse.fr (L.P.); Francoise.Vical@inserm.fr (F.B.-V.); pierre.verhaeghe@lcc-toulouse.fr (P.V.)
- ⁷ MAAAP, New Antimalarial Molecules and Pharmacological Approaches, MAAAP, Inserm ERL 1289, 31400 Toulouse, France
- ⁸ Institut de Pharmacologie et de Biologie Structurale, IPBS, Université de Toulouse, CNRS, UPS, 31400 Toulouse, France
- ⁹ Sorbonne Université, INSERM, CNRS, Centre d'Immunologie et des Maladies Infectieuses, CIMI, 75013 Paris, France; amanzougaghene_nadia@yahoo.fr (N.A.); tajeri.shahin@inserm.fr (S.T.); jean-francois.franetich@upmc.fr (J.-F.F.); dominique.mazier@sorbonne-universite.fr (D.M.)
- ¹⁰ CHU de Toulouse, Service Pharmacie, 330 Avenue de Grande-Bretagne, CEDEX 9, 31059 Toulouse, France
- ¹¹ APHM, Hôpital Conception, Service Central de la Qualité et de l'Information Pharmaceutiques, 13005 Marseille, France
- * Correspondence: patrice.vanelle@univ-amu.fr (P.V.); cyrille.botte@univ-grenoble-alpes.fr (C.B.); nicolas.primas@univ-amu.fr (N.P.)

Abstract: The malaria parasite harbors a relict plastid called the apicoplast. Although not photosynthetic, the apicoplast retains unusual, non-mammalian metabolic pathways that are essential to the parasite, opening up a new perspective for the development of novel antimalarials which display a new mechanism of action. Based on the previous antiplasmodial hit-molecules identified in the 2-trichloromethylquinoxaline series, we report herein a structure–activity relationship (SAR) study at position two of the quinoxaline ring by synthesizing 20 new compounds. The biological evaluation highlighted a hit compound (**3i**) with a potent *Pf*K1 EC₅₀ value of 0.2 μM and a HepG2 CC₅₀ value of 32 μM (Selectivity index = 160). Nitro-containing (**3i**) was not genotoxic, both in the Ames test and in vitro comet assay. Activity cliffs were observed when the 2-CCl₃ group was replaced, showing that it played a key role in the antiplasmodial activity. Investigation of the mechanism of action showed that **3i** presents a drug response by targeting the apicoplast and a quick-killing mechanism acting on another target site.

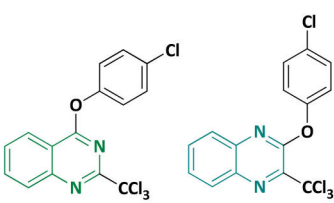
Keywords: quinoxaline; trichloromethyl group; *Plasmodium falciparum*; structure-activity relationships; apicoplast

1. Introduction

Malaria remains the deadliest parasitic disease; according to the World Health Organisation (WHO) [1], malaria caused an estimated 229 million cases leading to 409,000 deaths in 2019 with 94% of malaria cases and deaths occurring in the sub-Saharan Africa region. The most lethal species infecting humans is *Plasmodium falciparum*. The parasite is transmitted to humans by the bite of an infected female *Anopheles* mosquito. Currently, the first-line treatment of malaria caused by *P. falciparum* is based on artemisinin-based combination therapies (ACTs). Unfortunately, despite global efforts, the emergence of parasite resistance to the most effective class of antimalarial drugs, such as artemisinin (ART) [2], has led to treatment failures, particularly in the Greater Mekong Subregion [3]. However, the geographic scope of resistance may be rapidly expanding. Indeed, molecular markers of artemisinin resistance were described in African regions, leading to a significant public health concern [4]. Moreover, there are only six new chemical entities in the Medicines for Malaria Ventures (MMV) clinical pipeline [5].

Therefore, there is an urgent need for new therapies with novel mechanisms of action against *Plasmodium* in order to reduce the risk of emerging resistant parasites and to ensure the sustained efficacy of ACTs.

Focusing on the development of new anti-infective agents, our team has reported the antiplasmodial activities of nitrogenous heterocyclic scaffolds bearing a trichloromethyl (CCl_3) group, including a hit molecule (**A**) in quinazoline series (Figure 1) [6–8]. This hit-compound showed a good antiplasmodial profile (EC_{50} *PfK1* = 1.1 μM and CC_{50} = 50 μM) [9]. Furthermore, replacement of the quinazoline ring by a quinoxaline one (hit **B**, Figure 1), using a scaffold-hopping strategy, improved the antiplasmodial activity and preserved the cytotoxicity profile compared to hit **A**.



| | Hit A | Hit B | Chloroquine | Artesunate | Doxorubicin |
|--|-------|-------|-------------|------------|-------------|
| EC_{50} <i>PfK1</i> (μM) | 1.1 | 0.4 | 0.8 | 0.003 | - |
| CC_{50} HepG2 (μM) | 50 | 50 | 30 | 14.7 | 0.2 |
| Selectivity index (SI) | 40.2 | 100.5 | 37.5 | 4900 | - |

Figure 1. Comparison of biological activities between hit **A**, hit **B** and reference drugs.

Indeed, several quinoxalines have already been described as promising antiplasmodial molecules, including **MMV007224** (Figure 2), which was identified from the Malaria Box [10]. In addition, the 1,4-di-*N*-oxide quinoxaline derivative (**QdNO 19**) showed antiplasmodial activity against both the 3D7 chloroquine-sensitive and FCR-3 multidrug-resistant strains of *P. falciparum* [11].

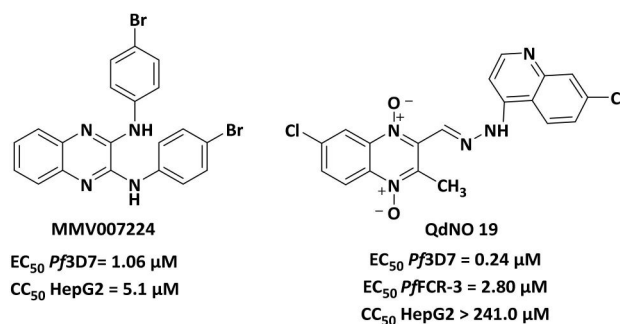


Figure 2. Structures of quinoxalines with antiplasmodial activities.

The MMV has defined requirements for the target candidate profiles (TCP) and target product profiles (TPP) [12]. One way to achieve these goals is to search for compounds with new mechanisms of action. Among antiplasmodial targets identified, the apicoplast, a relic plastid of Apicomplexa, constitutes an interesting target for the development of new antimalarial drugs.

Apicomplexan parasites are responsible for serious infectious diseases, such as malaria. Most apicomplexans have a key organelle called the apicoplast, which is a non-photosynthetic plastid acquired by a secondary endosymbiosis from a plastid-containing red alga [13,14]. This organelle contains the second smallest known circular genome for a plastid (35 kilobases) which encodes for proteins that are targeted to the apicoplast [15]. Although not photosynthetic, the apicoplast performs several essential anabolic functions for the parasite, including isoprenoid precursors biosynthesis, fatty acids biosynthesis, heme biosynthesis, and iron-sulfur cluster assembly [16].

To date, very few molecules targeting the apicoplast have been described, however, some known antibiotics have been studied, such as ciprofloxacin and doxycycline, which target the genetic machinery of *P. falciparum* apicoplast leading to a delayed death drug-response [17]. Clindamycin and azithromycin are other examples of delayed death antibiotics that target *P. falciparum* [18].

The vestigial origin of the apicoplast has paved the way for innovative antimalarial drugs that can be described as herbicidal therapies. Among the biocides targeting the apicoplast, triclosan showed antiparasitic activity against *Plasmodium* through the fatty acid biosynthesis pathway inhibition located in the apicoplast [19], although it was off-target and not active in vivo [20].

It is noteworthy that some trichloromethylated molecules were known as biocides, such as etridiazole (Figure 3) [21] and trichloromethyltriazolothiadiazole, which target pyruvate kinase II located in the apicoplast [22]. In addition, Banach et al. described trichloromethylsulfonylbenzimidazole derivatives with herbicidal activities targeting the apicoplast [23]. Therefore, a possible correlation between the pharmacophore $-CCl_3$ and herbicidal activity could be suggested.

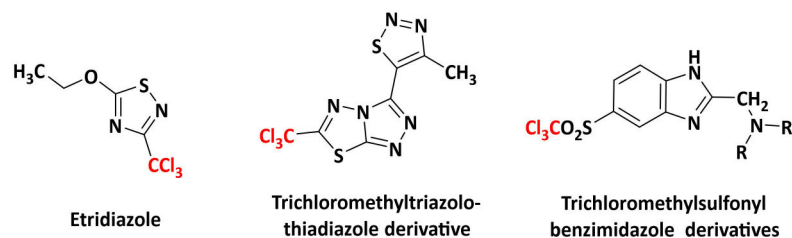


Figure 3. Structures of some trichloromethylated derivatives as biocides.

All these data allowed us to establish a relationship between the biocid effect of the CCl_3 group and the antiplasmodial activities of herbicides that target the apicoplast. In order to decipher the mechanism of action of our trichloromethylated molecules, studies to determine the effect of our molecules on apicoplast biogenesis during the blood and hepatic stages of *Plasmodium falciparum* are discussed here. In parallel, the action against artemisinin-resistant parasites of *P. falciparum* was also studied.

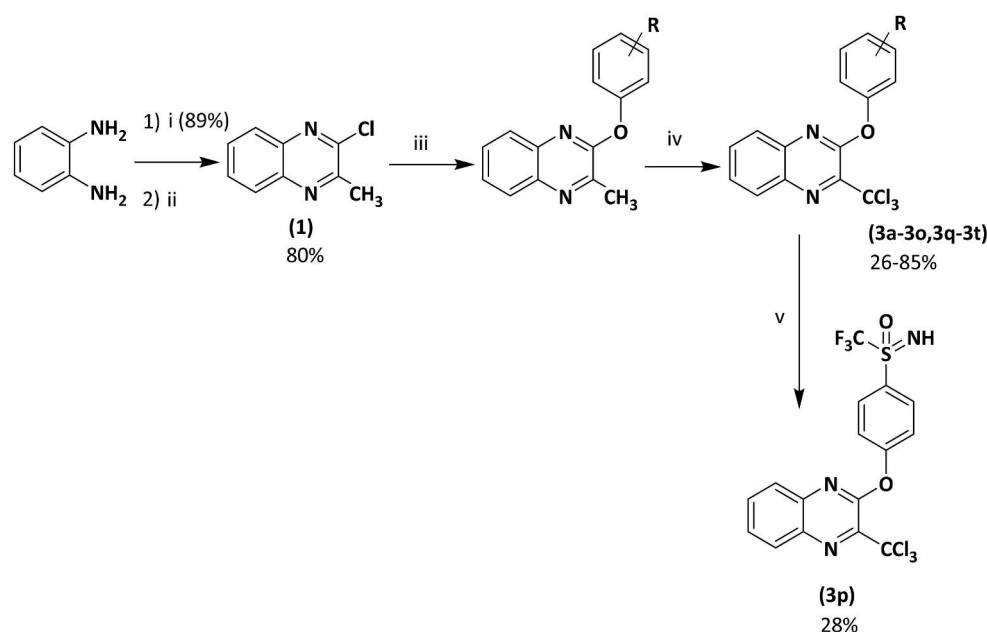
2. Results and Discussion

2.1. Synthesis

We planned to explore the structure–activity relationship by investigating the influence of substituents at position 2 of the 3-trichloromethylquinoxaline scaffold, in a view to identify new optimized hit-compounds.

Key substrate (1) was obtained from a condensation reaction of o-phenylenediamine with ethyl pyruvate to provide the corresponding lactam followed by a chlorination reaction using $POCl_3$ [8] (Scheme 1). Next, chlorimine (1) was reacted by a nucleophilic aromatic

substitution reaction (S_NAr) with various phenol derivatives using cesium carbonate in DMF at 70 °C. The desired intermediates (**2a–2t**) were obtained in moderate to quantitative yields (45 to 99%). Yield variation seems to have no clear correlation with the electron-donating or -withdrawing behavior of the different substituents borne on the phenols. Finally, according to a previously described protocol [24], from the methylated precursors (**2a–2t**), a chlorination reaction using PCl_5 and $POCl_3$ was performed under microwave heating at 100 °C for 30 min, leading to the target analogs of hit **B** (**3a–3t**) in low to very good yields (26–85%). Globally, 20 derivatives (**3a–3t**) were obtained: 16 compounds bearing electro-donating or electro-withdrawing substituents in ortho, meta, and para positions of the phenol moiety, and four cluttered phenol derivatives.

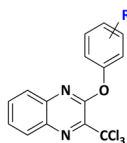


Scheme 1. Preparation of 2-phenoxy-3-trichloromethylquinoxaline derivatives (**3a–3t**). Reagents and conditions: (i) ethyl pyruvate 1 equiv, H_2O , 50 °C, 15 min; (ii) $POCl_3$, reflux, 2 h; (iii) appropriate phenol derivative 1 equiv, Cs_2CO_3 1 equiv, anh. DMF, 70 °C, 12 h, sealed vial, N_2 ; (iv) PCl_5 6 equiv, $POCl_3$ as solvent, 100 °C, MW, 20 min, 800 W; (v) **(3m)** 1 equiv, ammonium carbamate 1.5 equiv, phenyliodine diacetate 2.1 equiv., CF_3CH_2OH , rt, 3 h.

2.2. Biological Results

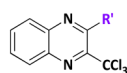
2.2.1. Structure-Activity Relationship (SAR) Study

These new derivatives were evaluated *in vitro* against the K1 chloroquine and pyrimethamine-resistant *P. falciparum* strain by determining their 50% efficacy concentration (EC_{50}), and were compared to three reference antimalarial drugs: chloroquine, artesunate, and doxycycline. The *in vitro* 50% cytotoxic concentrations (CC_{50}) were assessed on the HepG2 human hepatocyte cell line and compared to a cytotoxic reference drug, doxorubicin. For all molecules, the selectivity index was calculated as following $SI = CC_{50}/EC_{50}$. The results are presented in Tables 1 and 2.

Table 1. Reaction yields, antiplasmodial activity, HepG2 cytotoxicity, and clogP of the 3-phenoxy-2-trichloromethylquinoxalines **3a–3p**.

| R | N ^o | Yield Step 2 (%) | EC ₅₀ PfK1 (μM) ± SD | CC ₅₀ HepG2 (μM) ± SD | SI ^d | clogP ^e |
|-----------------------------------|--------------------------|------------------|---------------------------------|----------------------------------|-----------------|--------------------|
| H | 3a | 84 | 0.47 ± 0.10 | 45.3 ± 9.6 | 96.4 | 4.28 |
| 2-Cl | 3b | 67 | 0.55 ± 0.12 | 49.5 ± 10.1 | 90.0 | 4.75 |
| 3-Cl | 3c | 67 | 0.34 ± 0.06 | 37.2 ± 8.1 | 109.4 | 4.77 |
| 2,4-Cl | 3d | 52 | 0.60 ± 0.12 | 37.7 ± 4.7 | 62.8 | 5.28 |
| 2-F | 3e | 43 | 0.64 ± 0.14 | >15.6 ^c | >24.4 | 4.53 |
| 3-F | 3f | 52 | 0.32 ± 0.07 | 33.5 ± 6.3 | 105.0 | 4.54 |
| 4-F | 3g | 58 | 0.42 ± 0.09 | 35.9 ± 7.5 | 85.5 | 4.56 |
| 4-OMe | 3h | 27 | 0.38 ± 0.08 | >7.8 ^c | >20.6 | 4.22 |
| 4-NO ₂ ^f | 3i | 57 | 0.20 ± 0.04 | 32.0 ± 6.1 | 160.0 | 3.53 |
| 4-CF ₃ | 3j | 70 | 0.30 ± 0.06 | 28.3 ± 4.4 | 94.3 | 5.27 |
| 4-OCF ₃ | 3k | 85 | 0.40 ± 0.08 | 27.1 ± 4.7 | 67.8 | 5.15 |
| 4-SF ₅ | 3l | 84 | 0.20 ± 0.03 | 16.6 ± 3.9 | 83.0 | 5.41 |
| 4-SCF ₃ | 3m | 58 | 0.20 ± 0.04 | 25.6 ± 4.6 | 128.0 | 5.70 |
| 4-CN | 3n | 81 | 0.25 ± 0.04 | 15.4 ± 2.1 | 77.0 | 4.06 |
| 4-SO ₂ CF ₃ | 3o | 26 | 0.22 ± 0.07 | 7.2 ± 1.4 | 32.7 | 4.77 |
| 4-SONHCF ₃ | 3p | 28 | 0.21 ± 0.05 | 6.5 ± 1.4 | 31.0 | 5.11 |
| | Chloroquine ^a | | 0.80 | 30.0 | 37.5 | 3.82 |
| | Artesunate ^a | | 0.003 ± 0.0012 | 14.7 ± 1.4 | 4900 | - |
| | Doxycycline ^a | | 6.00 | 20.0 | 3.3 | - |
| | Doxorubicin ^b | | - | 0.2 | - | - |

^a Chloroquine, artesunate, and doxycycline were used as antimalarial reference-drugs; ^b Doxorubicin was used as a cytotoxic reference-drug; ^c Highest concentrations were tested due to a lack of solubility; ^d Selectivity index (SI) was calculated according to the formula: SI = CC₅₀/EC₅₀; ^e Weighted clogP was computed by the SwissADME; ^f The best antiplasmodial hit with the best ratio activity/cytotoxicity.

Table 2. Reaction yields, antiplasmodial activity, HepG2 cytotoxicity, and clogP of the cluttered 3-phenoxy-2-trichloromethylquinoxalines **3q to 3t**.

| R' | N ^o | Yield Step 2 (%) | EC ₅₀ PfK1 (μM) ± SD | CC ₅₀ HepG2 (μM) ± SD | SI ^d | clogP ^e |
|----|--------------------------|------------------|---------------------------------|----------------------------------|-----------------|--------------------|
| | 3q | 43 | 0.60 ± 0.10 | 53.1 ± 7.6 | 88.5 | 5.17 |
| | 3r | 64 | 0.40 ± 0.08 | >31.2 ^c | >78.1 | 5.19 |
| | 3s | 50 | 0.60 ± 0.10 | >62.5 ^c | >104.2 | 5.61 |
| | 3t | 70 | 0.50 ± 0.05 | >31.2 ^c | >62.5 | 5.60 |
| | Chloroquine ^a | | 0.80 | 30.0 | 37.5 | 3.82 |
| | Artesunate ^a | | 0.003 ± 0.0012 | 14.7 ± 1.4 | 4900 | - |
| | Doxycycline ^a | | 6.00 | 20.0 | 3.3 | - |
| | Doxorubicin ^b | | - | 0.2 | - | - |

^a Chloroquine, artesunate and doxycycline were used as antimalarial reference-drugs; ^b Doxorubicin was used as a cytotoxic reference-drug; ^c Highest concentration tested due to a lack of solubility; ^d Selectivity index (SI) was calculated according to the formula: SI = CC₅₀/EC₅₀; ^e Weighted clogP was computed by the SwissADME.

Out of the 20 tested molecules, five showed poor aqueous solubility in the cell culture medium (**3e**, **3h**, **3r**, **3s**, **3t**), limiting their in vitro cytotoxicity evaluation. Regarding the effect on cell viability of the HepG2 human cells, except for two compounds (**3o** and **3p**), all derivatives showed good cytotoxicity values ranging from 15.4 to 53.1 μM in comparison with reference drug doxorubicin (CC_{50} HepG2 = 0.20 μM). It appeared that the cluttered derivatives (**3q**, **3s**) and the 2-chlorophenoxy derivative (**3b**) were the less cytotoxic compounds. The electron-withdrawing groups (EWG) (**3l**, **3n**) at *para* position of 3-phenoxy moiety led to slightly more cytotoxic compounds (CC_{50} HepG2 = 15.4 and 16.6 μM , respectively).

The *meta*-halogenated (chloro or fluoro) phenoxy group (**3c** and **3f**) gave the best antiplasmodial activities with quite similar activities (EC_{50} Pf K1 = 0.34 and 0.32 μM , respectively) compared to the ortho (**3b**, **3e**) and para (**3g**) positions.

The *para*-EWG as 4-OCF₃ (**3k**) and the *para*-electro-donating group (EDG) as OMe (**3h**) remained active as the halogenated phenoxy moieties (EC_{50} Pf K1 = 0.40 and 0.38 μM , respectively). The unsubstituted phenoxy group (**3a**) also showed good antiplasmodial activity. Among the cluttered analogs, the 2-(naphthalen-2-yloxy) was slightly better than the 2-(naphthalen-1-yloxy) compound (EC_{50} Pf K1 = 0.40 vs. 0.60 μM). Strong EWG such as 4-SF₅, 4-SCF₃, and 4-CN (**3l**, **3m**, **3n**) afforded the best antiplasmodial activities (EC_{50} Pf K1 = 0.20 μM for each molecule).

From the trifluoromethylthio derivative (**3m**), in order to add H-bond donor and decrease clogP, an analog bearing a trifluoromethylsulfoximine at *para* position was synthesized. Moreover, to anticipate the potential in vivo sulfur oxidation of (**3m**), the sulfonyl **3o** was prepared. These two analogs (**3o**, **3p**) showed both good antiplasmodial activity. However, these were the most cytotoxic derivatives.

Finally, the best compound in this series is the 4-NO₂-substituted phenoxy group (**3i**) which showed both good EC_{50} and CC_{50} values, leading to the highest selectivity index in the series (SI = 160.0) (Tables 1 and 2). It is also notable that the best compound has also the lowest clogP.

2.2.2. In Vitro Toxicity Data

Toxicity concerns related to nitro-containing drugs emerged a long time ago [25], particularly due to the mutagenic potential of these compounds [26]. Most of molecules bearing a nitro group are well known for their mutagenicity against the *Salmonella typhimurium* strain used in the Ames test [27].

Nevertheless, the evaluation of the mutagenicity of compound (**3i**) was carried out using the Ames test on four *S. typhimurium* strains at 5 mM and 25 mM (four doses per concentrations: 2, 3, 4, 5 μL /plate for assay without S9 mix and 4, 6, 8, 10 μL /plate for assay with S9 mix). After 48 h of exposition of (**3i**), no significant number of revertants was observed compared to the positive control, indicating that this nitro-containing trichloromethylated molecule is not mutagenic in vitro (see Supplementary Materials).

To complete the mutagenic Ames test, in vitro comet assay was performed on the HepG2 cell line at the concentration of 3.2 and 16 μM (CC_{50} (**3i**)/2 and CC_{50} (**3i**)/10, 72 h) (Table 3). Compound **3i** did not induce DNA strand breaks or alkali labile sites after either short (2 h) or long (72 h) exposition at two concentrations tested (Supplementary Materials) Methyl methanesulphonate (MMS), the positive control used in the comet assay, gave the expected results.

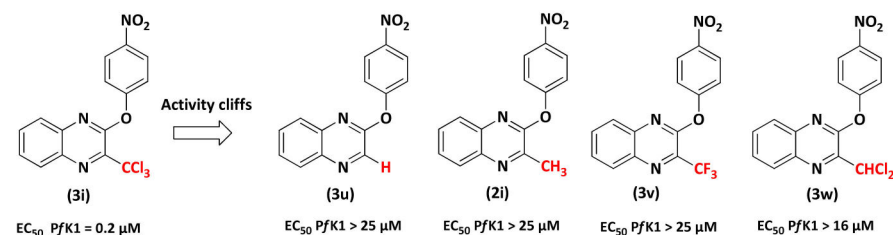
Table 3. Ames test and in vitro comet assay data regarding hit compound **3i**.

| | Time (h) | [3i] Concentration | Result |
|-----------------------------------|----------|--------------------|----------|
| Ames test ^a | 48 | 5 mM (w/o S9 mix) | negative |
| | | 25 mM (w/o S9mix) | |
| | | 5 mM (w/S9 mix) | |
| | | 25 mM (w/S9mix) | |
| In vitro comet assay ^b | 2 | 3.2 μM | negative |
| | 2 | 16 μM | |
| | 72 | 3.2 μM | |
| | 72 | 16 μM | |

^a Ames test: each concentration of [3i] tested at 2, 3, 4 at 5 μL/plate (w/o S9 mix assay) or 4, 6, 8, 10 μL/plate (w/S9 mix assay). ^b In vitro comet assay was performed on HepG2 cell line.

2.2.3. Role of the 3-CCl₃ Group

Previously, we have shown that the CCl₃ group is mandatory to provide antiplasmodial activity [28–30]. To confirm the key role played by the 3-CCl₃ group of the most potent compound (**3i**) in phenoxyquinoxaline series, the CCl₃ group was replaced by a proton (**3u**), a CH₃ group (**2i**), a CF₃ group (**3v**), and a CHCl₂ group (**3w**). All these analogs without the CCl₃ group lost their activity against *P. falciparum* (EC₅₀ PfK1 > 16 μM). Once again, the CCl₃ group appeared essential for antiplasmodial activity (Figure 4) [31].

**Figure 4.** Comparison of the in vitro antiplasmodial activities of hit molecule **3i** with analogs **3u**, **3v**, **3w**, **3x**.

2.2.4. Evaluation on *P. falciparum* Apicoplast

To determine the impact of (**3i**) on apicoplast biogenesis, parasites were treated for 48 h with 0.2 μM of (**3i**) or 0.2 μM of (**2i**) (a control of (**3i**) for which the active CCl₃ was replaced by a methyl CH₃ group) and compared to untreated parasites by immunofluorescence assay. In the untreated culture, parasites presented normal apicoplast biogenesis depending on the life stage (elongated for trophozoite stage and individualized for schizont) while treated culture with (**3i**) showed a dotted single non-elongated apicoplast at the mid-trophozoite life stage and apicoplast, which seems to diffuse into the cytosol and form vesicles for advance life stages (i.e., late trophozoite) (Figure 5A). This result is similar to what was previously reported after parasite chemical rescue after apicoplast loss [32]. We confirmed the absence of effect of molecule (**2i**) on the apicoplast biogenesis and *Plasmodium* growth, correlated to the replacement of the CCl₃ group of (**3i**) by CH₃ (Figure 5B,C). In order to determine if the apicoplast is the main target of (**3i**), we performed a growth assay over three life cycles to assess a potential delayed death effect, one of the major signature for compounds affecting apicoplast. The results show a drastic reduction in the parasite growth within the first life cycle in the cultures treated with 0.2 μM of (**3i**) (Figure 5C), which can be interpreted in two ways: the first is that the primary target is outside of the apicoplast and the impact on apicoplast biogenesis is a collateral effect. The second interpretation could be that, unlike chloramphenicol or doxycycline, which cause a delayed death phenotype on *Plasmodium*, (**3i**) could act like fosmidomycin or actinonin and cause a rapid death phenotype [31]. Hence, although, we cannot exclude an indirect effect on the apicoplast, (**3i**) affects its presence and morphology.

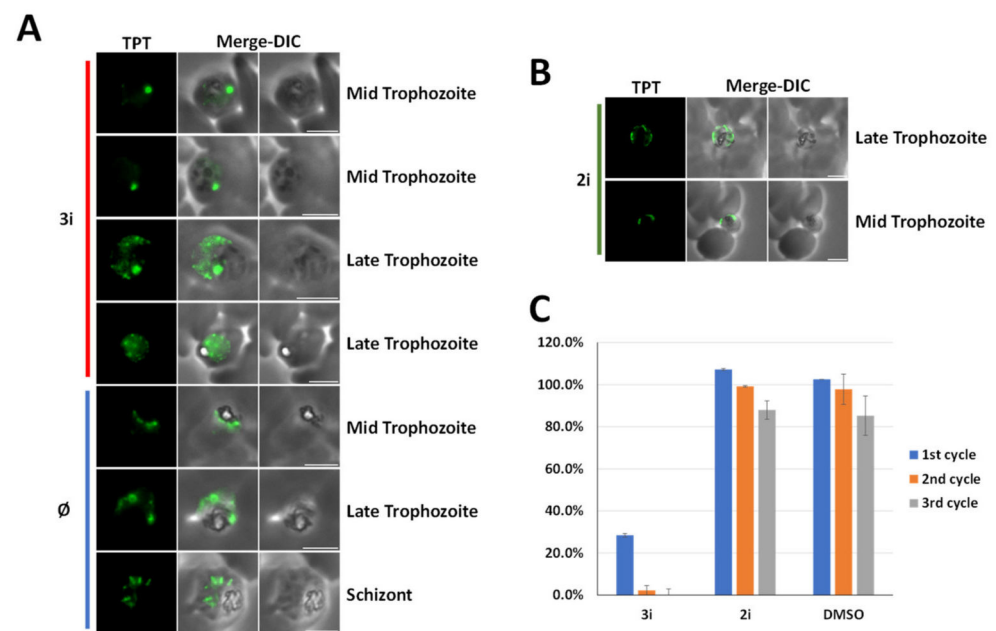


Figure 5. (3i) treatment affects apicoplast biogenesis. (A,B) A triose phosphate transporter (TPT) fluorescent signal is shown in green (TPT labeled with an 3 × HA tag). Apicoplasts of treated parasites with 0.2 μM of (3i) molecule or 0.2 μM of (2i) are compared to normal plastid visualized in ∅ untreated control. Microscopic images were obtained by an epifluorescence microscope. DIC, differential interference contrast. (C) Growth assay over three life cycles (48 h), bars represent the ratio treated parasites on untreated. ($n = 3$, error bar = standard deviation, SD).

2.2.5. Evaluation on Artemisinin-Resistant and Artemisinin-Sensitive Parasites

It is essential to assess the efficacy of new antimalarial compounds against ART-resistance, as its worldwide spreading threatens malaria control [1]. In this context, the ART-resistant strain F32-ART5 and its tween ART-sensitive strain F32-TEM were used [33,34]. Compound (3i) showed similar antiplasmodial activity on both strains F32-ART5 and F32-TEM with mean EC_{50} values of 400 nM and 392 nM, respectively (Mann–Whitney test p -value = 0.8). However, despite ART-resistant genotype of F32-ART5, EC_{50} values of ART were also similar for both strains (ranging from 11 to 19 nM, Mann–Whitney test p -value = 0.267) (Table 4), due to the specific *P. falciparum* quiescence-based mechanism of ART-resistance leading to parasite cell cycle arrest during drug exposure. Therefore, evaluation of (3i) with specific assays of artemisinin-resistance [33–35] was conducted and evidenced that this compound was active against the artemisinin-resistant parasites at the proliferative state but not at the quiescent state (see Supplementary Materials Figure S49).

Table 4. Evaluation of chemo-sensitivity, by standard assay, of *P. falciparum* strains F32-ART5 (ART-resistant) and F32-TEM (ART-sensitive) to (3i). Artemisinin was used as drug control.

| | Mean ± SEM EC_{50} values | | |
|-------------|-----------------------------|----------------------|--------------|
| | F32-ART5 $n = 4$ * | F32-TEM $n = 2$ * | p -value § |
| 3i | 400 ± 105 nM | 392 ± 34 nM | 0.8 |
| Artemisinin | 11 ± 3 nM | 19 ± 3 nM | 0.267 |

* Results represent the mean of four and two independent experiments for F32-ART5 and F32-TEM, respectively.

§ Mann–Whitney test. A p -value < 0.05 was considered as statistically significant.

2.2.6. Studying the Effect of (3i) on the Liver Stage Development of *P. falciparum*

The effect of (3i) on the hepatic stage of *P. falciparum* was next studied in order to know if (3i) was active against another stage of *P. falciparum* cycle. Cryopreserved primary

human hepatocytes were infected with 30,000 freshly extracted *P. falciparum* sporozoites and simultaneously treated with a dose range (0.9–30 μM) of (**3i**). Atovaquone (ATQ) was used as a positive parasite-killing control at 25 nM. Treatment with (**3i**) had no effect on exoerythrocytic forms (EEF or schizont) size and numbers at 6 or 12 days post-infection, while ATQ could completely clear all parasites from the culture (see Supplementary Materials Figures S50 and S51). The apicoplast in the hepatic stage was quite not affected by (**3i**) even at high concentrations (up to 30 μM) (see Supplementary Materials Figure S52).

Finally, we studied the hepatotoxicity of (**3i**). This was carried out by quantification of DAPI-stained hepatocyte nuclei in culture wells. Generally, if a drug is hepatotoxic, it causes death and detachment of hepatocytes leading to less hepatocyte nuclei counts. The nuclei numbers in control and **3i**-treated wells are comparable and no reduction in hepatocyte numbers could be detected under the dose range tested (Figure 6). Interestingly, no cytotoxicity was observed on human hepatocytes up to 30 μM of (**3i**).

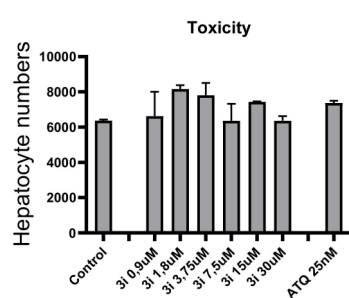


Figure 6. Toxicity of (**3i**) on human hepatocytes.

3. Materials and Methods

3.1. Chemistry

3.1.1. Generality

Melting points were determined on a Köfler melting point apparatus (Wagner & Munz GmbH, München, Germany) and were uncorrected. Elemental analyses were carried out at the Spectropole, Faculté des Sciences de Saint-Jérôme (Marseille) with a Thermo Finnigan EA1112 analyzer (Thermo Finnigan, San Jose, CA, USA). NMR spectra were recorded on a Bruker AV (Billerica, MA, USA) 200 or AV 250 spectrometers or a Bruker Avance NEO 400MHz NanoBay spectrometer at the Faculté de Pharmacie of Marseille or on a Bruker Avance III nanobay 400 MHz spectrometer at the Spectropole, Faculté des Sciences de Saint-Jérôme (Marseille). (^1H NMR: reference CHCl_3 $\delta = 7.26$ ppm, reference DMSO-d_6 $\delta = 2.50$ ppm and ^{13}C NMR: reference CHCl_3 $\delta = 76.9$ ppm, reference DMSO-d_6 $\delta = 39.52$ ppm). The following adsorbent was used for column chromatography: silica gel 60 (Merck KGaA, Darmstadt, Germany, particle size 0.063–0.200 mm, 70–230 mesh ASTM). TLC was performed on 5 cm \times 10 cm aluminum plates coated with silica gel 60F-254 (Merck) in an appropriate eluent. Visualization was performed with ultraviolet light (234 nm). Purity of synthesized compounds was checked by LC/MS analyses, which were realized at the Faculté de Pharmacie of Marseille with a Thermo Scientific Accela High Speed LC System[®] (Waltham, MA, USA) coupled using a single quadrupole mass spectrometer Thermo MSQ Plus[®]. The RP-HPLC column is a Thermo Hypersil Gold[®] 50 \times 2.1 mm (C18 bounded), with particles of a diameter of 1.9 mm. The volume of sample injected on the column was 1 μL . Chromatographic analysis, total duration of 8 min, was on the gradient of the following solvents: $t = 0$ min, methanol/water 50:50; $0 < t < 4$ min, linear increase in the proportion of methanol to a methanol/water ratio of 95:5; $4 < t < 6$ min, methanol/water 95:5; $6 < t < 7$ min, linear decrease in the proportion of methanol to return to a methanol/water ratio of 50:50; $6 < t < 7$ min, methanol/water 50:50. The water used was buffered with ammonium acetate 5 mM. The flow rate of the mobile phase was 0.3 mL/min. The retention times (t_R) of the molecules analyzed were indicated in min. The microwave reactions were performed using multimode reactors: ETHOS Synth

Lab station and MicroSYNTH[®] Lab terminal 1024 (Ethos start, MLS GmbH, Leutkirch, Germany); or monomode reactors: Biotage Initiator[®] classic in sealed vials with a power output of 0 to 400 W. Reagents were purchased and used without further purifications from Sigma-Aldrich or Fluorochem.

3.1.2. General Procedure for 2-chloro-3-methyl Substituted Quinoxaline (2a–2p)

To a solution of 2-chloro-3-methylquinoxaline (1) (500 mg, 2.8 mmol) and the appropriate phenol (2.8 mmol, 1.0 equiv) in anhydrous DMF (10 mL), Cs₂CO₃ (912 mg, 2.8 mmol, 1.0 equiv) was added under inert atmosphere. The mixture was stirred at 70 °C overnight. After completion of the reaction, water was added, leading to a precipitate which was separated by filtration. The resulting precipitate was then thoroughly washed with water. The precipitate was dissolved in CH₂Cl₂ and dried with Na₂SO₄. After filtration and evaporation, the resulting solid was purified by silica gel column chromatography (using the appropriate eluant) to afford the desired compound.

2-Methyl-3-phenoxyquinoxaline (2a)

Yield 79% (523 mg). White solid. Mp 90 °C. ¹H NMR (250 MHz, CDCl₃) δ 8.02–7.96 (m, 1H), 7.74–7.67 (m, 1H), 7.60–7.54 (m, 2H), 7.51–7.43 (m, 2H), 7.32–7.19 (m, 3H), 2.84 (s, 3H). ¹³C NMR (63 MHz, CDCl₃) δ 156.2, 153.0, 148.2, 139.6, 139.2, 129.7 (2C), 129.3, 127.9, 127.5, 125.4, 121.8 (2C), 115.5, 20.7. LC-MS (ESI+) t_R 6.01 min, *m/z* [M + H]⁺ 237.27. MW: 236.27 g.mol⁻¹. HRMS (ESI): *m/z* [M + H]⁺ calcd for C₁₅H₁₂N₂O: 237.1022, Found: 237.1022.

2-(2-Chlorophenoxy)-3-methylquinoxaline (2b)

Yield 73% (553 mg). Brown solid. Mp 140 °C. ¹H NMR (250 MHz, CDCl₃) δ 8.04–7.97 (m, 1H), 7.69–7.63 (m, 1H), 7.61–7.55 (m, 2H), 7.54–7.49 (m, 1H), 7.40–7.35 (m, 2H), 7.30–7.23 (m, 2H), 2.88 (s, 2H). ¹³C NMR (63 MHz, CDCl₃) δ 155.5, 149.2, 147.7, 139.5, 139.4, 130.7, 129.3, 128.0, 127.9, 127.6, 127.5, 127.2, 126.7, 124.4, 20.7. LC-MS (ESI+) t_R 3.77 min, *m/z* [M + H]⁺ 271.15/273.19. MW: 270.71 g.mol⁻¹. HRMS (ESI): *m/z* [M + H]⁺ calcd for C₁₅H₁₀ClN₂O: 271.0633, Found: 271.0632.

2-(3-Chlorophenoxy)-3-methylquinoxaline (2c)

Yield 90% (682 mg). Red-brown solid. Mp 108 °C. ¹H NMR (250 MHz, CDCl₃) δ 8.02–7.95 (m, 1H), 7.76–7.69 (m, 1H), 7.62–7.56 (m, 2H), 7.42–7.24 (m, 2H), 7.21–7.16 (m, 1H), 2.81 (s, 3H). ¹³C NMR (63 MHz, CDCl₃) δ 155.7, 153.5, 147.9, 139.5, 139.3, 134.9, 130.4, 129.4, 128.0, 127.7, 127.5, 125.7, 122.4, 120.2, 20.6. LC-MS (ESI+) t_R 4.13 min, *m/z* [M + H]⁺ 271.09/273.18. MW: 270.71 g.mol⁻¹. HRMS (ESI): *m/z* [M + H]⁺ calcd for C₁₅H₁₀ClN₂O: 271.0633, Found: 271.0634.

2-(2,4-Dichlorophenoxy)-3-methylquinoxaline (2d)

Yield 83% (709 mg). Yellow solid. Mp 110 °C. ¹H NMR (250 MHz, CDCl₃) δ 7.95–7.91 (m, 1H), 7.63–7.59 (m, 1H), 7.53–7.45 (m, 2H), 7.45 (d, *J* = 1.9 Hz, 1H), 7.32–7.20 (m, 2H), 2.82 (s, 3H). ¹³C NMR (63 MHz, CDCl₃) δ 155.2, 147.9, 147.5, 139.7, 139.3, 131.4, 130.4, 129.4, 128.1, 128.1, 127.7, 127.4, 125.3, 20.6. (a quaternary carbon was visible in these conditions). LC-MS (ESI+) t_R 4.61 min, *m/z* [M + H]⁺ 304.92/306.97/309.10. MW: 305.16 g.mol⁻¹. HRMS (ESI): *m/z* calcd. For C₁₅H₁₀Cl₂N₂O [M + H]⁺ 305.0243. Found: 305.0244.

2-(2-Fluorophenoxy)-3-methylquinoxaline (2e)

Yield 53% (377 mg). Brown solid. Mp 149 °C. ¹H NMR (250 MHz, CDCl₃) δ 8.04–7.96 (m, 1H), 7.71–7.65 (m, 1H), 7.60–7.53 (m, 2H), 7.37–7.19 (m, 3H), 2.86 (s, 3H). ¹³C NMR (63 MHz, CDCl₃) δ 156.7 (d, *J* = 250.2 Hz), 155.4, 152.7, 147.4, 140.4, 140.2, 139.5, 129.3, 128.0, 127.5 (d, *J* = 4.6 Hz), 126.8 (d, *J* = 7.2 Hz), 124.7 (d, *J* = 3.8 Hz), 124.3, 117.0 (d, *J* = 18.4 Hz), 94.8. LC-MS: t_R = 3.48 min; *m/z* [M + H]⁺ 255.19. MW: 254.26 g.mol⁻¹. HRMS (ESI): *m/z* calcd. For C₁₅H₁₀FN₂O [M + H]⁺ 255.0928. Found: 255.0928.

2-(3-Fluorophenoxy)-3-methylquinoxaline (2f)

Yield 92% (655 mg). Brown solid. Mp 83 °C. ¹H NMR (250 MHz, CDCl₃) δ 8.01–7.95 (m, 1H), 7.75–7.69 (m, 1H), 7.62–7.55 (m, 2H), 7.47–7.36 (m, 1H), 7.09–6.95 (m, 2H), 2.81 (s, 3H). ¹³C NMR (63 MHz, CDCl₃) δ 163.2 (d, J = 247.0 Hz), 155.7, 153.9 (d, J = 10.9 Hz), 147.9, 139.4, 139.4, 130.4 (d, J = 9.5 Hz), 129.4, 128.02, 127.7, 127.5, 117.5 (d, J = 3.3 Hz), 112.5 (d, J = 21.1 Hz), 109.8 (d, J = 24.4 Hz), 20.6. LC-MS (ESI+) t_R 3.69 min, *m/z* [M + H]⁺ 255.27. MW: 254.26 g.mol⁻¹. HRMS (ESI): *m/z* calcd. For C₁₅H₁₀FN₂O [M + H]⁺ 255.0928. Found: 255.0928.

2-(4-Fluorophenoxy)-3-methylquinoxaline (2g)

Yield 91% (648 mg). Brown solid. Mp 86 °C. ¹H NMR (250 MHz, CDCl₃) δ 8.05–7.95 (m, 1H), 7.73–7.64 (m, 1H), 7.63–7.53 (m, 2H), 7.25–7.09 (m, 3H), 2.83 (s, 3H). ¹³C NMR (63 MHz, CDCl₃) δ 160.1 (d, J = 243.6 Hz), 156.1, 148.6 (d, J = 2.9 Hz), 147.9, 139.3 (d, J = 21.0 Hz, 2C), 129.4, 127.9, 127.6, 127.4, 123.3 (d, J = 8.4 Hz, 2C), 116.5, 116.1, 20.6. LC-MS (ESI+) t_R 3.63 min, *m/z* [M + H]⁺ 255.18. MW: 254.26 g.mol⁻¹. HRMS (ESI): *m/z* calcd. For C₁₅H₁₀FN₂O [M + H]⁺ 255.0928. Found: 255.0928.

2-(4-Methoxyphenoxy)-3-methylquinoxaline (2h)

Yield 97% (723 mg). White solid. Mp 144 °C. ¹H NMR (250 MHz, CDCl₃) δ 7.98–7.95 (m, 1H), 7.72–7.68 (m, 1H), 7.57–7.53 (m, 2H), 7.19 (d, J = 9.0 Hz, 2H), 6.97 (d, J = 9.0 Hz, 2H), 3.85 (s, 3H), 2.81 (s, 3H). ¹³C NMR (63 MHz, CDCl₃) δ 157.0, 156.5, 148.1, 146.3, 139.6, 139.2, 129.1, 128.0, 127.4, 127.2, 122.7(2C), 114.6(2C), 55.7, 20.7. LC-MS (ESI+) t_R 6.00 min; *m/z* [M + H]⁺ 267.22. MW: 266.29 g.mol⁻¹. HRMS (ESI): *m/z* calcd. For C₁₆H₁₄N₂O₂ [M + H]⁺ 267.1128. Found: 267.1128.

2-Methyl-3-(4-nitrophenoxy)quinoxaline (2i)

Yield 86% (677 mg). Brown powder. Mp 163 °C. ¹H NMR (250 MHz, CDCl₃) δ 8.35–8.25 (m, 2H), 8.00–7.93 (m, 1H), 7.84–7.76 (m, 2H), 7.75–7.70 (m, 1H), 7.68–7.59 (m, 2H), 2.80 (s, 3H). ¹³C NMR (101 MHz, CDCl₃) δ 153.5, 151.7, 148.0, 141.2, 140.4, 138.2, 134.9 (2C), 129.6, 129.3, 128.5, 128.1, 124.0 (2C), 22.5. LC-MS (ESI+) t_R 4.26 min, no ionization. MW: 281.27 g.mol⁻¹. HRMS (ESI): *m/z* calcd. For C₁₅H₁₁N₃O₂S [M + H]⁺ 282.0873. Found: 282.0869.

2-Methyl-3-(4-trifluoromethylphenoxy)quinoxaline (2j)

Yield 90% (767 mg). Pink solid. Mp 95 °C. ¹H NMR (250 MHz, CDCl₃) δ 8.06–7.93 (m, 1H), 7.77–7.67 (m, 3H), 7.66–7.55 (m, 2H), 7.41 (d, J = 8.3 Hz, 2H), 2.83 (s, 3H). ¹³C NMR (63 MHz, CDCl₃) δ 155.6 (q, J = 1.4 Hz), 155.5, 147.9, 139.8, 139.2, 129.5, 128.2, 127.8, 127.5 (q, J = 32.8 Hz), 127.4, 127.0 (q, J = 3.7 Hz), 124.2 (q, J = 271.9 Hz), 122.1, 20.7. LC-MS (ESI+) t_R 4.99 min, *m/z* [M + H]⁺ 304.44. MW: 304.28 g.mol⁻¹. HRMS (ESI): *m/z* calcd. For C₁₆H₁₁F₃N₂O [M + H]⁺ 305.0896. Found: 305.0894.

2-Methyl-3-(4-trifluoromethoxyphenoxy)quinoxaline (2k)

Yield 86% (771 mg). Beige solid. Mp 86 °C. ¹H NMR (250 MHz, CDCl₃) δ 8.01–7.77 (m, 2H), 7.72–7.59 (m, 2H), 7.59–7.45 (m, 4H), 2.77 (s, 3H). ¹³C NMR (101 MHz, CDCl₃) δ 155.8, 151.2, 147.9, 146.3 (q, J = 1.9 Hz), 139.6, 139.4, 129.4, 128.1, 127.7, 127.4, 123.1 (2C), 122.3, 120.7 (q, J = 257.1 Hz), 20.7. LC-MS (ESI+) t_R 4.70 min, *m/z* [M + H]⁺ 321.22. MW: 320.27 g.mol⁻¹. HRMS (ESI): *m/z* calcd. For C₁₆H₁₁F₃N₂O₂ [M + H]⁺ 321.0845. Found: 321.0842.

2-Methyl-3-[4-(pentafluorosulfanyl)phenoxy]quinoxaline (2l)

Yield 90% (914 mg). Beige solid. Mp 154 °C. ¹H NMR (250 MHz, CDCl₃) δ 8.07–7.94 (m, 1H), 7.93–7.77 (m, 2H), 7.78–7.66 (m, 1H), 7.67–7.55 (m, 2H), 7.46–7.33 (m, 2H), 2.83 (s, 3H). ¹³C NMR (101 MHz, CDCl₃) δ 155.2, 155.0, 150.5 (t, J = 17.9 Hz), 147.8, 139.8, 139.2, 129.6, 128.2, 128.0, 127.8 (p, J = 4.6 Hz), 127.4, 121.8, 20.6. LC-MS (ESI+) t_R 4.58 min, *m/z* [M

+ H]⁺ 362.90. MW: 362.32 g.mol⁻¹. HRMS (ESI): *m/z* calcd. For C₁₅H₁₁F₅N₂OS [M + H]⁺ 363.0585. Found: 363.0584.

2-Methyl-3-[4-(trifluoromethylthio)phenoxy]quinoxaline (2m)

Yield 87% (819 mg). Pink powder. Mp 85 °C. ¹H NMR (250 MHz, CDCl₃) δ 8.04–7.95 (m, 1H), 7.79–7.68 (m, 3H), 7.65–7.56 (m, 2H), 7.40–7.33 (m, 2H), 2.82 (s, 3H). ¹³C NMR (101 MHz, CDCl₃) δ 155.4, 148.0, 139.8, 139.3, 138.1 (2C), 129.7 (q, J = 308.2 Hz), 129.5, 128.2, 127.9, 127.5, 122.8 (2C), 120.6, 120.6 (q, J = 2.2 Hz), 20.7. LC-MS (ESI+) t_R 4.93 min, *m/z* [M + H]⁺ 336.61. MW: 336.33 g.mol⁻¹. HRMS (ESI): *m/z* calcd. For C₁₆H₁₁F₃N₂OS [M + H]⁺ 337.0617. Found: 337.0615.

4-[(3-Methylquinoxalin-2-yl)oxy]benzotrile (2n)

Yield 72% (527 mg). Pink powder. Mp 188 °C. ¹H NMR (250 MHz, CDCl₃) δ 8.04–7.96 (m, 1H), 7.81–7.74 (m, 2H), 7.72–7.66 (m, 1H), 7.66–7.59 (m, 2H), 7.46–7.39 (m, 2H), 2.82 (s, 3H). ¹³C NMR (63 MHz, CDCl₃) δ 156.5, 155.1, 147.8, 139.9, 139.1, 134.0 (2C), 129.6, 128.3, 128.1, 127.4, 122.7 (2C), 118.7, 109.1, 20.7. LC-MS (ESI+) t_R 3.01 min, *m/z* [M + H]⁺ 262.03. MW: 261.28 g.mol⁻¹. HRMS (ESI): *m/z* calcd. For C₁₆H₁₁N₃O [M + H]⁺ 262.0975. Found: 262.0975.

2-Methyl-3-[4-(trifluoromethylsulfonyl)phenoxy]quinoxaline (2o)

Yield 45% (464 mg). White solid. Mp 156 °C. ¹H NMR (400 MHz, CDCl₃) δ 8.14 (d, J = 8.8 Hz, 2H), 8.06–7.99 (m, 1H), 7.79–7.72 (m, 1H), 7.68–7.61 (m, 4H), 2.84 (s, 3H). ¹³C NMR (101 MHz, CDCl₃) δ 159.9, 154.6, 147.7, 140.2, 138.9, 133.0, 129.9, 128.5, 128.4, 127.5, 127.1, 122.8, 119.9 (d, J = 325.7 Hz), 20.7. LC-MS (ESI+) t_R 4.02 min, *m/z* [M + H]⁺ 368.51. MW: 368.33 g.mol⁻¹. HRMS (ESI): *m/z* calcd. For C₁₆H₁₁F₃N₂O₃S [M + H]⁺ 369.0515. Found: 369.0513.

2-Methyl-3-(naphthalen-1-yloxy)quinoxaline (2q)

Yield 94% (754 mg). Beige solid. Mp 169 °C. ¹H NMR (400 MHz, CDCl₃) δ 8.04–7.97 (m, 1H), 7.96–7.90 (m, 2H), 7.81 (d, J = 8.2 Hz, 1H), 7.62–7.50 (m, 5H), 7.49–7.41 (m, 2H), 2.98 (s, 3H). ¹³C NMR (101 MHz, CDCl₃) δ 156.5, 149.0, 147.9, 139.7, 139.4, 135.1, 129.2, 128.2, 128.0, 127.6, 127.5, 127.3, 126.5, 126.4, 125.7, 125.6, 121.8, 118.0, 20.9. LC-MS (ESI+) t_R 4.24 min, *m/z* [M + H]⁺ 287.05. MW: 286.33 g.mol⁻¹. HRMS (ESI): *m/z* calcd. For C₁₉H₁₄N₂O [M + H]⁺ 287.1179. Found: 287.1180.

2-Methyl-3-(naphthalen-2-yloxy)quinoxaline (2r)

Yield 90% (721 mg). Beige solid. Mp 149 °C. ¹H NMR (250 MHz, CDCl₃) δ 7.97–7.89 (m, 1H), 7.89–7.79 (m, 2H), 7.78–7.72 (m, 1H), 7.64 (t, J = 3.3 Hz, 1H), 7.59 (m, 1H), 7.54–7.46 (m, 2H), 7.46–7.39 (m, 2H), 7.37–7.29 (m, 1H), 2.89–2.72 (m, 3H). ¹³C NMR (101 MHz, CDCl₃) δ 156.5, 149.0, 147.9, 139.7, 139.5, 135.1, 129.2, 128.2, 128.0, 127.6, 127.5, 127.3, 126.5, 126.4, 125.7, 125.6, 121.8, 118.0, 20.9. LC-MS (ESI+) t_R 4.45 min, *m/z* [M + H]⁺ 287.02. MW: 286.33 g.mol⁻¹. HRMS (ESI): *m/z* calcd. For C₁₉H₁₄N₂O [M + H]⁺ 287.1179. Found: 287.1180.

2-([1,1'-Biphenyl]-4-yloxy)-3-methylquinoxaline (2s)

Yield 99% (866 mg). White solid. Mp 158 °C. ¹H NMR (250 MHz, CDCl₃) δ 8.03–7.94 (m, 1H), 7.78–7.68 (m, 2H), 7.68–7.61 (m, 3H), 7.60–7.55 (m, 2H), 7.52–7.42 (m, 2H), 7.41–7.31 (m, 3H), 2.85 (s, 3H). ¹³C NMR (63 MHz, CDCl₃) δ 156.1, 152.6, 148.2, 140.7, 139.6 (2C), 138.5, 129.2, 129.0 (2C), 128.4 (2C), 128.2, 127.5, 127.4 (2C), 127.3 (2C), 122.0 (2C), 20.8. LC-MS (ESI+) t_R 4.81 min, *m/z* [M + H]⁺ 313.08. MW: 312.36 g.mol⁻¹. HRMS (ESI): *m/z* calcd. For C₂₁H₁₆N₂O [M + H]⁺ 313.1335. Found: 313.1331.

2-([1,1'-Biphenyl]-3-yloxy)-3-methylquinoxaline (2t)

Yield 99% (866 mg). White solid. Mp 109 °C. ¹H NMR (250 MHz, CDCl₃) δ 8.05–7.95 (m, 1H), 7.79–7.69 (m, 1H), 7.67–7.55 (m, 4H), 7.55–7.50 (m, 3H), 7.49–7.41 (m, 2H), 7.40–7.34 (m, 1H), 7.31–7.25 (m, 1H), 2.85 (s, 3H). ¹³C NMR (63 MHz, CDCl₃) δ 156.1, 153.5, 148.2, 143.1, 140.5, 139.6 (2C), 129.9, 129.2, 129.0 (2C), 128.2, 127.8, 127.5, 127.4, 127.3 (2C), 124.1, 120.5 (2C), 20.8. LC-MS (ESI+) t_R 4.82 min, *m/z* [M + H]⁺ 313.09. MW: 312.36 g.mol⁻¹. HRMS (ESI): *m/z* calcd. For C₂₁H₁₆N₂O [M + H]⁺ 313.1335. Found: 313.1332.

3.1.3. General Procedure for Preparation of 3-thiophenoxy-2-trichloromethylquinoxaline Derivatives

To a solution of 2-chloro-3-methyl substituted quinoxaline (2a–2p) (624 mg, 2.8 mmol) and PCl₅ (2.88 g, 16.8 mmol), POCl₃ was added to make a slurry (ca 5 mL). The mixture was then heated in a multimode microwave oven at 100 °C, 800 W for 20–30 min. After completion of the reaction, the mixture was poured into ice and was then neutralized with Na₂CO₃. The resulting solution was extracted with CH₂Cl₂ and dried with Na₂SO₄. After filtration and evaporation, the resulting solid was purified by silica gel column chromatography (eluent: Petroleum Ether/CH₂Cl₂, 9:1) to afford the desired compound.

2-Phenoxy-3-trichloromethylquinoxaline (3a)

Yield 84% (799 mg). White solid. Mp 59 °C. ¹H NMR (250 MHz, CDCl₃) δ 8.14–8.06 (m, 1H), 7.72–7.56 (m, 3H), 7.43–7.37 (m, 2H), 7.26–7.16 (m, 3H). ¹³C NMR (63 MHz, CDCl₃) δ 152.8, 152.7, 142.5, 141.3, 136.9, 132.2, 129.8, 129.8 (2C), 128.5, 127.1, 125.8, 121.8 (2C), 95.0. LC-MS (ESI+) t_R 5.0 min, *m/z* [M + H]⁺ no ionization. MW: 339.6 g.mol⁻¹. HRMS (ESI): *m/z* [M + H]⁺ calcd for: C₁₅H₉Cl₃N₂O: 338.9853. Found: 338.9854.

2-(2-Chlorophenoxy)-3-trichloromethylquinoxaline (3b)

Yield 67% (702 mg). White solid. Mp 99 °C. ¹H NMR (250 MHz, CDCl₃) δ 8.19–8.15 (m, 1H), 7.77–7.66 (m, 3H), 7.58–7.52 (m, 1H), 7.42–7.36 (m, 1H), 7.32–7.27 (m, 2H). ¹³C NMR (63 MHz, CDCl₃) δ 151.9, 148.8, 141.9, 141.3, 137.1, 132.2, 130.8, 129.9, 128.6, 128.1, 127.6, 127.2, 127.1, 124.0, 94.8. LC-MS (ESI+) t_R 5.11 min, *m/z* [M + H]⁺ no ionization. MW: 374.05 g.mol⁻¹. HRMS (ESI): *m/z* calcd. for C₁₅H₈Cl₄N₂O [M + H]⁺ 372.9464. Found: 372.9464.

2-(3-Chlorophenoxy)-3-(trichloromethylquinoxaline (3c)

Yield 67% (702 mg). White solid. Mp 58 °C. ¹H NMR (250 MHz, CDCl₃) δ 8.08–8.04 (m, 1H), 7.72–7.56 (m, 3H), 7.32–7.10 (m, 4H). ¹³C NMR (63 MHz, CDCl₃) δ 153.1, 152.3, 142.3, 141.1, 137.1, 135.0, 132.4, 130.5, 129.9, 128.9, 127.1, 126.1, 122.4, 120.1, 94.8. LC-MS (ESI+) t_R 5.74 min, *m/z* [M + H]⁺ no ionization. MW: 374.05 g.mol⁻¹. HRMS (ESI): *m/z* calcd. for C₁₅H₈Cl₄N₂O [M + H]⁺ 372.9464. Found: 372.9463.

2-(2,4-Dichlorophenoxy)-3-trichloromethylquinoxaline (3d)

Yield 52% (595 mg). White solid. Mp 120 °C. ¹H NMR (250 MHz, CDCl₃) δ 8.22–8.13 (m, 1H), 7.78–7.66 (m, 3H), 7.56 (d, *J* = 2.4 Hz, 1H), 7.36 (dd, *J* = 8.7 Hz, 2.4 Hz, 1H), 7.26–7.21 (m, 1H). ¹³C NMR (63 MHz, CDCl₃) δ 151.7, 147.6, 141.8, 141.1, 137.2, 132.4, 132.0, 130.6, 129.9, 128.9, 128.6, 128.3, 127.1, 124.9, 94.7. LC-MS (ESI+) t_R 5.5 min, *m/z* [M + H]⁺ no ionization. MW: 408.49 g.mol⁻¹. HRMS (ESI): *m/z* calcd. for C₁₅H₇Cl₅N₂O [M + H]⁺ 406.9074. Found: 406.9074.

2-(2-Fluorophenoxy)-3-trichloromethylquinoxaline (3e)

Yield 43% (430 mg). White solid. Mp 138 °C. ¹H NMR (250 MHz, CDCl₃) δ 8.19–8.15 (m, 1H), 7.78–7.66 (m, 3H), 7.40–7.21 (m, 4H). ¹³C NMR (63 MHz, CDCl₃) δ 154.6 (d, *J* = 250.2 Hz), 151.9, 141.9, 141.3, 139.9, 139.7, 137.2, 132.3, 129.9, 128.7, 127.2 (d, *J* = 7.0 Hz), 124.8 (d, *J* = 3.9 Hz), 124.1, 117.1 (d, *J* = 18.3 Hz), 94.8. LC-MS (ESI+) t_R 4.9 min, *m/z* [M

+ H]⁺ no ionization. MW: 357.59 g.mol⁻¹. HRMS (ESI): *m/z* calcd. for C₁₅H₈Cl₃FN₂O [M + H]⁺ 356.9759. Found: 356.9762.

2-(3-Fluorophenoxy)-3-trichloromethylquinoxaline (3f)

Yield 52% (521 mg). White solid. Mp 101 °C. ¹H NMR (250 MHz, CDCl₃) δ 8.22–8.13 (m, 1H), 7.84–7.68 (m, 3H), 7.49–7.39 (m, 1H), 7.16–7.00 (m, 3H). ¹³C NMR (63 MHz, CDCl₃) δ 163.2 (d, J = 247.5 Hz), 153.5 (d, J = 11.0 Hz), 152.3, 142.4, 141.2, 137.1, 132.4, 130.5 (d, J = 9.4 Hz), 129.9, 128.9, 127.1, 117.5 (d, J = 3.3 Hz), 112.8 (d, J = 21.0 Hz), 109.9 (d, J = 24.5 Hz), 94.8. LC-MS (ESI+) t_R 5.1 min, *m/z* [M + H]⁺ no ionization. MW: 357.59 g.mol⁻¹. HRMS (ESI): *m/z* calcd. for C₁₅H₈Cl₃FN₂O [M + H]⁺ 356.9759. Found: 356.9761.

2-(4-Fluorophenoxy)-3-trichloromethylquinoxaline (3g)

Yield 58% (581 mg). White solid. Mp 56 °C. ¹H NMR (250 MHz, CDCl₃) δ 8.17–8.13 (m, 1H), 7.79–7.63 (m, 3H), 7.33–7.24 (m, 2H), 7.20–7.10 (m, 2H). ¹³C NMR (63 MHz, CDCl₃) δ 160.3 (d, J = 244.2 Hz), 152.7, 148.4 (d, J = 2.9 Hz), 142.3, 141.2, 136.9, 132.3, 129.9, 128.6, 127.0, 123.3 (d, J = 8.5 Hz, 2C), 116.4 (d, J = 23.5 Hz, 2C), 94.9. LC-MS (ESI+) t_R 4.9 min, *m/z* [M + H]⁺ no ionization. MW: 357.59 g.mol⁻¹. HRMS (ESI): *m/z* calcd. for C₁₅H₈Cl₃FN₂O [M + H]⁺ 356.9759. Found: 356.9754.

2-(4-Methoxyphenoxy)-3-trichloromethylquinoxaline (3h)

Yield 27% (270 mg). White solid. Mp 171 °C. ¹H NMR (250 MHz, CDCl₃) δ 8.17–8.13 (m, 1H), 7.81–7.64 (m, 3H), 7.26–7.23 (m, 2H), 7.01–6.97 (m, 2H), 3.86 (s, 3H). ¹³C NMR (63 MHz, CDCl₃) δ 157.3, 153.1, 146.1, 142.4, 141.4, 136.9, 132.1, 129.8, 128.4, 127.1, 122.6 (2C), 114.7 (2C), 95.0, 55.8. LC-MS (ESI+) t_R 4.9 min, *m/z* [M + H]⁺ no ionization. MW: 357.59 g.mol⁻¹. HRMS (ESI): *m/z* calcd. for C₁₆H₁₁Cl₃N₂O₂ [M + H]⁺ 368.9959. Found: 368.9957.

2-(4-Nitrophenoxy)-3-trichloromethylquinoxaline (3i)

Yield 57% (614 mg). Yellow solid. Mp 178 °C. ¹H NMR (250 MHz, CDCl₃) δ 8.41–8.35 (m, 2H), 8.23–8.19 (m, 1H), 7.82–7.73 (m, 3H), 7.54–7.48 (m, 2H). ¹³C NMR (63 MHz, CDCl₃) δ 157.6, 151.7, 145.2, 142.4, 140.9, 137.4, 132.7, 130.0, 129.4, 127.1, 125.7 (2C), 122.3 (2C), 94.6. LC-MS (ESI+) t_R 4.12 min; *m/z* [M + H]⁺ no ionization. MW: 384.60 g.mol⁻¹. HRMS (ESI): *m/z* calcd. for: C₁₅H₈Cl₃N₃O₃ [M + H]⁺ 383.9704. Found: 383.9704.

2-Trichloromethyl-3-[4-(trifluoromethyl)phenoxy]quinoxaline (3j)

Yield 70% (799 mg). White powder. Mp 129 °C. ¹H NMR (250 MHz, CDCl₃) δ 8.30–8.08 (m, 1H), 7.93–7.62 (m, 5H), 7.60–7.36 (m, 2H). ¹³C NMR (63 MHz, CDCl₃) δ 155.3, 152.1, 142.5, 141.1, 137.2, 132.5, 130.0, 129.0, 127.9 (q, J = 32.8 Hz), 127.2 (q, J = 3.7 Hz), 127.1 (2C), 124.1 (q, J = 272.0 Hz), 122.1 (2C), 94.8. LC-MS (ESI+) t_R 6.62 min, *m/z* [M + H]⁺ don't ionise. MW: 407.60 g.mol⁻¹. HRMS (ESI): *m/z* calcd. for C₁₆H₈Cl₃F₃N₂O: 406.9727, Found: 406.9722.

2-Trichloromethyl-3-[4-(trifluoromethoxy)phenoxy]quinoxaline (3k)

Yield 85% (1008 mg). White solid. Mp 66 °C. ¹H NMR (250 MHz, CDCl₃) δ 8.22–8.14 (m, 1H), 7.84–7.69 (m, 3H), 7.44–7.30 (m, 4H). ¹³C NMR (63 MHz, CDCl₃) δ 152.4, 150.9, 146.6 (q, J = 1.9 Hz), 142.4, 141.1, 137.1, 132.4, 129.9, 128.9, 127.1, 123.1, 122.5, 120.6 (q, J = 257.3 Hz), 94.9. LC-MS (ESI+) t_R 5.72 min, *m/z* [M + H]⁺ Don't ionise. MW: 423.60 g.mol⁻¹. HRMS (ESI): *m/z* calcd. for C₁₆H₈Cl₃F₃N₂O₂: 422.9676, Found: 422.9675.

2-Trichloromethyl-3-[4-(pentafluorosulfonyl)phenoxy]quinoxaline (3l)

Yield 84% (1095 mg). Green crystal. Mp 99 °C. ¹H NMR (250 MHz, CDCl₃) δ 8.29–8.13 (m, 1H), 7.93–7.71 (m, 5H), 7.44 (d, J = 8.8 Hz, 2H). ¹³C NMR (63 MHz, CDCl₃) δ 154.6, 151.9, 150.8 (p, J = 17.2 Hz), 142.4, 141.0, 137.3, 132.6 (2C), 130.0, 129.2, 127.9 (p, J = 4.6 Hz), 127.1, 121.7 (2C), 94.7. LC-MS (ESI+) t_R 5.70 min, *m/z* [M + H]⁺ 468.77. MW: 465.65 g.mol⁻¹. HRMS (ESI): *m/z* calcd. for C₁₅H₈Cl₃F₅N₂OS: 466.9387, Found: 466.9315.

2-Trichloromethyl-3-[4-(trifluoromethylthio)phenoxy]quinoxaline (3m)

Yield 58% (714 mg). White crystal. Mp 94 °C. ¹H NMR (250 MHz, CDCl₃) δ 8.24–8.14 (m, 1H), 7.86–7.69 (m, 5H), 7.46–7.38 (m, 2H). ¹³C NMR (63 MHz, CDCl₃) δ 155.0, 152.1, 142.5, 141.1, 138.2, 137.2, 132.5, 130.0, 129.6 (q, J = 307.7 Hz), 129.0, 127.1, 122.8, 121.2 (q, J = 2.1 Hz), 94.8. LC-MS (ESI+) t_R 5.8 min, m/z [M + H]⁺ no ionization. MW: 439.67 g.mol⁻¹. HRMS (ESI): m/z calcd. for C₁₆H₈Cl₃F₃N₂O_S: 440.9419, Found: 440.9419.

4-[(3-Trichloromethylquinoxalin-2-yl)oxy]benzonitrile (3n)

Yield 81% (827 mg). White solid. Mp 194 °C. ¹H NMR (250 MHz, CDCl₃) δ 8.23–8.14 (m, 1H), 7.86–7.71 (m, 5H), 7.51–7.42 (m, 2H). ¹³C NMR (63 MHz, CDCl₃) δ 156.1, 151.8, 142.4, 140.9, 137.3, 134.1 (2C), 132.6, 130.0, 129.3, 127.1, 122.6 (2C), 118.5, 109.5, 94.6. LC-MS (ESI+) t_R 4.62 min, m/z [M + H]⁺ no ionization. MW: 364.61 g.mol⁻¹. HRMS (ESI): m/z calcd. for C₁₆H₈Cl₃N₃O: 363.9806, Found: 363.9806.

2-Trichloromethyl-3-[4-(trifluoromethylsulfonyl)phenoxy]quinoxaline (3o)

Yield 26% (343 mg). White solid. Mp 107 °C. ¹H NMR (400 MHz, CDCl₃) δ 8.25–8.20 (m, 1H), 8.19–8.13 (m, 2H), 7.88–7.83 (m, 2H), 7.82–7.76 (m, 1H), 7.69–7.62 (m, 2H). ¹³C NMR (101 MHz, CDCl₃) δ 159.4, 151.3, 142.6, 140.8, 137.6, 133.1, 132.9, 130.1, 129.7, 127.8, 127.2, 122.8, 120.0 (q, J = 325.6 Hz), 94.5. LC-MS (ESI+) t_R 5.08 min, m/z [M + H]⁺ no ionization. MW: 471.67 g.mol⁻¹. HRMS (ESI): m/z calcd. for C₁₆H₈Cl₃F₃N₂O₃S: 472.9318, Found: 472.9319.

2-(Naphthalen-2-yloxy)-3-trichloromethylquinoxaline (3q)

Yield 64% (698 mg). White solid. Mp 143 °C, (isopropanol). ¹H NMR (250 MHz, CDCl₃) δ 8.24–8.13 (m, 1H), 8.00–7.83 (m, 3H), 7.83–7.78 (m, 1H), 7.78–7.65 (m, 3H), 7.57–7.49 (m, 2H), 7.49–7.41 (m, 1H). ¹³C NMR (63 MHz, CDCl₃) δ 153.0, 150.5, 142.6, 141.4, 137.1, 134.2, 132.2, 131.6, 129.9, 129.7, 128.6, 128.0, 127.8, 127.1, 126.8, 125.8, 121.5, 118.5, 95.1. LC-MS (ESI+) t_R 5.66 min, m/z [M + H]⁺ 390.89/392.31/393.07. MW: 389.66 g.mol⁻¹. HRMS (ESI): m/z calcd for C₁₉H₁₁Cl₃N₂O: 389.0010, Found: 389.0004.

2-(Naphthalen-1-yloxy)-3-trichloromethylquinoxaline (3r)

Yield 26% (284 mg). Yellow solid. Mp 124 °C, (isopropanol). ¹H NMR (250 MHz, CDCl₃) δ 8.23–8.12 (m, 1H), 8.11–8.00 (m, 1H), 7.97–7.85 (m, 1H), 7.85–7.74 (m, 1H), 7.68–7.57 (m, 3H), 7.57–7.42 (m, 3H), 7.41–7.31 (m, 1H). ¹³C NMR (63 MHz, CDCl₃) δ 153.3, 149.0, 142.3, 141.6, 137.1, 135.1, 132.2, 129.9, 128.6, 128.2, 127.5, 127.2, 126.7, 126.6, 126.0, 125.7, 122.2, 117.6, 95.2. LC-MS (ESI+) t_R 5.41 min, m/z [M + H]⁺ 388.93/390.95/392.94. MW: 389.66 g.mol⁻¹. HRMS (ESI): m/z calcd for C₁₉H₁₁Cl₃N₂O: 389.0010, Found: 389.0004.

2-([1,1'-Biphenyl]-4-yloxy)-3-trichloromethylquinoxaline (3s)

Yield 50% (582 mg). White solid. Mp 160 °C, (isopropanol). ¹H NMR (250 MHz, CDCl₃) δ 8.22–8.14 (m, 1H), 7.86–7.78 (m, 1H), 7.78–7.72 (m, 1H), 7.72–7.67 (m, 2H), 7.67–7.61 (m, 2H), 7.52–7.46 (m, 2H), 7.46–7.33 (m, 4H). ¹³C NMR (63 MHz, CDCl₃) δ 152.8, 152.2, 142.6, 141.4, 140.6, 138.9, 137.1, 132.2, 129.9, 129.0 (2C), 128.6, 128.5 (2C), 127.5, 127.3 (2C), 127.2, 121.9 (2C), 95.0. LC-MS (ESI+) t_R 5.88 min, m/z [M + H]⁺ no ionization. MW: 415.70 g.mol⁻¹. HRMS (ESI): m/z calcd for C₂₁H₁₃Cl₃N₂O: 415.0166, Found: 415.0164.

2-([1,1'-Biphenyl]-3-yloxy)-3-trichloromethylquinoxaline (3t)

Yield 70% (815 mg). White oil. ¹H NMR (250 MHz, CDCl₃) δ 8.21–8.00 (m, 1H), 7.85–7.77 (m, 1H), 7.76–7.68 (m, 2H), 7.66–7.61 (m, 2H), 7.58–7.52 (m, 3H), 7.49–7.41 (m, 2H), 7.38 (m, 1H), 7.35–7.28 (m, 1H). ¹³C NMR (63 MHz, CDCl₃) δ 153.2, 152.8, 143.3, 142.6, 141.4, 140.4, 137.1, 132.2, 130.0, 129.9, 129.0 (2C), 128.6, 127.9, 127.4, 127.3 (2C), 124.5, 120.5, 120.4, 95.1. LC-MS (ESI+) t_R 5.89 min, m/z [M + H]⁺ no ionization. MW: 415.70 g.mol⁻¹. HRMS (ESI): m/z calcd for C₂₁H₁₃Cl₃N₂O: 415.0166, Found: 415.0164.

2-Trichloromethyl-3-[4-(S-trifluoromethylsulfonimidoyl)phenoxy]quinoxaline (3p)

2-trichloromethyl-3-[4-(trifluoromethylthio)phenoxy]quinoxaline 3m (1.23 g, 2.8 mmol, 1 equiv.), trifluoroethanol (TFE, 0.4 M), ammonium carbamate (328 mg, 4.2 mmol, 1.5 equiv.), and phenyliodine (III) diacetate (PIDA) (1.9 g, 5.88 mmol, 2.1 equiv.) were successively added to a round bottom flask in one portion. The reaction mixture was stirred at room temperature for 3 h. After completion, trifluoroethanol was removed under reduced pressure. The crude mixture was diluted in an aqueous solution of HCl (6 M, 1 mL/mmol) and CH₃CN (2 mL/mmol), and the reaction was stirred overnight at room temperature. The pH of the aqueous phase was adjusted to 7 with NaHCO₃ (10% aqueous solution); then, the crude mixture was extracted with CH₂Cl₂ (3 × 10 mL). The organic layer was dried with MgSO₄, concentrated under reduced pressure, and purified by column chromatography on silica gel.

Yield 28% (369 mg). White solid. Mp 127 °C. ¹H NMR (400 MHz, CDCl₃) δ 8.26 (d, J = 8.8 Hz, 2H), 8.23–8.17 (m, 1H), 7.86–7.81 (m, 2H), 7.78 (m, 1H), 7.65–7.58 (m, 2H), 3.65 (br, 1H). ¹³C NMR (101 MHz, CDCl₃) δ 158.6, 151.6, 142.5, 140.9, 137.5, 132.9 (2C), 132.8, 130.1, 129.5, 128.1, 127.2, 122.5 (2C), 121.1 (q, J = 332.1 Hz), 94.6. LC-MS (ESI+) t_R 4.74 min, m/z [M + H]⁺ 469.61/471.50. MW: 470.68 g.mol⁻¹. HRMS (ESI): m/z calcd. for C₁₆H₉Cl₃F₃N₃O₂S: 471.9478, Found: 471.9477.

3.1.4. General Procedure for Compounds 3u–3v

Preparation of 2-chloro-3-trifluoromethylquinoxaline

Step 1: To a solution of *o*-phenylenediamine (2 g, 18.5 mmol, 1.0 equiv) in H₂O, ethyl trifluoropyruvate was added (3g 146, 18.5 mmol, 1.0 equiv) and dissolved in H₂O (30 mL). The reaction mixture was heated at 50 °C for 15 min. After cooling, the precipitate was filtered off and washed with H₂O. 3-Trifluoromethylquinoxalin-2(1H)-one was recrystallized from ethanol, precipitating as a white solid, and engaged directly in step 2. Yield 93%.

Step 2: 3-Trifluoromethylquinoxalin-2-ol (3.5 g, 16.8 mmol, 1.0 equiv) was heated to reflux in phosphorus oxychloride (30 mL) for 2 h. After the starting material was consumed, the reaction mixture was cooled to r.t. and then quenched with ice at 0 °C. The precipitate was purified by flash chromatography to afford 2-chloro-3-trifluoromethylquinoxaline as a white solid. Yield 96%. Mp 140 °C. ¹H NMR (400 MHz, CDCl₃) δ 8.25–8.20 (m, 1H), 8.15–8.09 (m, 1H), 7.99–7.86 (m, 2H). NMR was consistent with the description provided in [36].

Preparation of compounds (3u, 3v)

To a solution of 2-chloroquinoxaline or 2-chloro-3-trifluoromethylquinoxaline [37] (300 mg, 1.3 mmol, 1.0 equiv.) and thiophenol reagent (143 mg, 1.3 mmol, 1.0 equiv.) in anhydrous DMF (5 mL), Cs₂CO₃ (1.0 equiv.) was added under inert atmosphere. The mixture was stirred at 70 °C overnight. After completion of the reaction, water was added, leading to a precipitate which was separated by filtration. The resulting precipitate was then thoroughly washed with water. The resulting solid was purified by silica gel column chromatography (eluent: Cyclohexane/CH₂Cl₂, 4:6) to afford the desired compound.

2-(4-Nitrophenoxy)quinoxaline (3u)

Yield 73% (254 mg). Red solid. Mp 156 °C, (isopropanol). ¹H NMR (400 MHz, CDCl₃) δ 8.76 (s, 1H), 8.41–8.29 (m, 2H), 8.15–8.05 (m, 1H), 7.83–7.76 (m, 1H), 7.76–7.62 (m, 2H), 7.54–7.45 (m, 2H). ¹³C NMR (101 MHz, CDCl₃) δ 157.9, 155.9, 144.9, 140.3, 139.6, 139.0, 131.0, 129.3, 128.4, 127.8, 125.7 (2C), 121.9 (2C). LC-MS (ESI+) t_R 3.14 min, m/z [M + H]⁺ 267.84. MW: 267,24 g.mol⁻¹. HRMS (ESI): m/z calcd. for C₁₄H₉N₃O₃: 268.0717, Found: 268.0716.

2-(4-Nitrophenoxy)-3-trifluoromethylquinoxaline (3v)

Yield 72% (314 mg). White solid. Mp 125 °C, (isopropanol). ¹H NMR (400 MHz, CDCl₃) δ 8.44–8.30 (m, 2H), 8.21 (d, J = 8.3 Hz, 1H), 7.90–7.68 (m, 3H), 7.57–7.40 (m, 2H). ¹³C

NMR (101 MHz, CDCl₃) δ 157.2, 152.9, 145.4, 141.1, 138.2, 134.8 (q, J = 36.8 Hz), 133.3, 130.0, 129.6, 127.6, 125.7 (2C), 122.5 (2C), 120.6 (q, J = 275.3 Hz). LC-MS (ESI+) t_R 4.14 min, m/z [M + H]⁺ No ionization. MW: 335.24 g.mol⁻¹. HRMS (ESI): m/z calcd. for C₁₅H₈F₃N₃O₃: 336.059, Found: 336.0585.

2-Dichloromethyl-3-(4-nitrophenoxy)quinoxaline (3w)

Yield 20% (91 mg). White solid. Mp 112 °C, (isopropanol). ¹H NMR (400 MHz, CDCl₃) δ 8.43–8.32 (m, 2H), 8.20–8.12 (m, 1H), 7.80–7.76 (m, 2H), 7.76–7.70 (m, 1H), 7.55–7.47 (m, 2H), 7.24 (s, 1H). ¹³C NMR (101 MHz, CDCl₃) δ 157.5, 152.4, 145.4, 143.4, 140.5, 139.0, 132.2, 129.6, 129.2, 127.5, 125.7 (2C), 122.5 (2C), 67.2. LC-MS (ESI+) t_R 4.1 min, m/z [M + H]⁺ No ionization. MW: 350.16 g.mol⁻¹. HRMS (ESI): m/z calcd. for C₁₅H₉Cl₂N₃O₃: 350.0094, Found: 350.0092.

3.2. Biology

3.2.1. In Vitro Cytotoxicity Evaluation HepG2

The HepG2 cell line was maintained at 37 °C, 5% CO₂, at 90% humidity in MEM supplemented with 10% fetal bovine serum, 1% L-glutamine (200 mM), and penicillin (100 U/mL)/streptomycin (100 µg/mL) (complete RPMI medium). The cytotoxicity of the tested molecules on the HepG2 (hepatocarcinoma cell line purchased from ATCC, ref HB-8065) cell line was assessed according to the method of Mosmann [37] with slight modifications. Briefly, 5.10³ cells in 100 µL of complete medium were inoculated into each well of 96-well plates and incubated at 37 °C in humidified 5% CO₂. After 24 h incubation, 100 µL of medium with various product concentrations dissolved in DMSO (final concentration less than 0.5% v/v) were added and the plates were incubated for 72 h at 37 °C. Triplicate assays were performed for each sample. Each plate-well was then microscopically examined for possible precipitate formation before the medium was aspirated from the wells. Next, 100 µL of MTT (3-(4,5-dimethyl-2-thiazolyl)-2,5-diphenyl-2H-tetrazolium bromide) solution (0.5 mg/mL in medium without FBS) was added to each well. Cells were incubated for 2 h at 37 °C. After this time, the MTT solution was removed and DMSO (100 µL) was added to dissolve the resulting blue formazan crystals. Plates were shaken vigorously (700 rpm) for 10 min. The absorbance was measured at 570 nm with 630 nm as reference wavelength using a BIO-TEK ELx808 Absorbance Microplate Reader (LabX, Midland, ON, Canada). DMSO was used as blank and doxorubicin (purchased from Sigma Aldrich) as positive control. Cell viability was calculated as a percentage of control (cells incubated without compound). The 50% cytotoxic concentration (CC₅₀) was determined from the dose–response curve, using TableCurve software 2D v.5.0. CC₅₀ values to represent the mean value calculated from three independent experiments.

3.2.2. In Vitro Antiplasmodial Evaluation

In this study, a K1 culture-adapted *P. falciparum* strain resistant to chloroquine, pyrimethamine, and proguanil was used in an in vitro culture. It was maintained in continuous culture, as described previously by Trager and Jensen [38]. Cultures were maintained in fresh A+ human erythrocytes at 2.5% hematocrit in complete medium (RPMI 1640 with 25 mM HEPES, 25 mM NaHCO₃, 10% of A+ human serum) at 37 °C under reduced O₂ atmosphere (gas mixture 10% O₂, 5% CO₂, and 85% N₂). Parasitemia was maintained daily between 1 and 3%. The *P. falciparum* drug susceptibility test was carried out by comparing quantities of DNA in treated and control cultures of parasite in human erythrocytes according to an SYBR Green I fluorescence-based method [39] using a 96-well fluorescence plate reader. Compounds, previously dissolved in DMSO (final concentration less than 0.5% v/v), were incubated in a total assay volume of 200 µL (RPMI, 2% hematocrit and 0.4% parasitemia) for 72 h in a humidified atmosphere (10% O₂ and 5% CO₂) at 37 °C, in 96-well flat bottom plates. Duplicate assays were performed for each sample. After incubation, plates were frozen at 20 °C for 24 h. Then, the frozen plates were thawed for 1 h at 37 °C. Fifteen µL of each sample were transferred to 96-well flat bottom non-sterile black plates

(Greiner Bio-one, Kremsmünster, Austria), already containing 15 µL of the SYBR Green I lysis buffer (2X SYBR Green I, 20 mM Tris base pH 7.5, 20 mM EDTA, 0.008% *w/v* saponin, 0.08% *w/v* Triton X-100). Negative control treated by solvents (DMSO or H₂O) and positive controls (chloroquine and doxycycline) were added to each set of experiments. Plates were incubated for 15 min at 37 °C and then read on a TECAN Infinite F-200 spectrophotometer with excitation and emission wavelengths at 485 and 535 nm, respectively. The concentrations of compounds required to induce a 50% decrease in parasite growth (EC₅₀ K1) were calculated from three independent experiments.

3.2.3. Ames Test

Compounds were assessed for mutagenicity by a modified version of the liquid incubation assay of the classical Ames test at five concentrations (25–125 nM) [40]. *Salmonella* tester strains (TA97a: Acridine ICR191, TA98: 2,4,7 trinitrofluorenone, TA100: Sodium Azide and TA102: Mitomycin C) as positive control w/o S9 mix and benzo[alpha]pyrene as positive control w/S9 mix) were grown overnight in a nutrient broth n_2 (Oxoid, Dardilly, France). After this period, products dissolved in DMSO (Sigma) were added to 0.1 mL of culture and incubated for 1 h at 37 °C with shaking. Each sample was assayed in duplicate. After incubation, 2 mL of molten top agar were mixed gently with the pre-incubated solution and poured onto Vogel–Bonner minimal agar plates. After 48 h at 37 °C, the number of spontaneous and drug-induced revertants per plate was determined for each dose with a laser bacterial colony counter (laser bacterial colony counter 500A, Interscience). A product was considered mutagenic when it induced a two-fold increase in the number of revertants, compared with the spontaneous frequency (negative control). For each *Salmonella* strain, a specific positive- and solvent-control were performed.

3.2.4. Comet Assay

Cell Culture and Treatment

The human hepatocarcinoma cell line HepG2 was obtained from the American Type Culture Collection (ATCC, ref. HB-8065). Cells were cultured in Eagle's minimum essential medium (EMEM, ref. ATCC[®] 30-2003TM) and supplemented with 10% heat-inactivated foetal bovine serum, 100 U/mL penicillin, and 0.1 mg/mL streptomycin (all from Gibco). Cells were maintained at 37 °C in a humidified atmosphere with 5% CO₂ and used in passage number 11 to 15. Two concentrations of the compound 3i (3.2 and 16 µM) were tested at 2 different times of incubation (2 and 72 h). Briefly, HepG2 cells were seeded at 1.13×10^5 cells/mL in 6-well plates (3 mL of cell suspension per well) and incubated at 37 °C in a humidified atmosphere with 5% CO₂. After 24 and 94 h of incubation, cells were treated with different concentrations of the compound or the vehicle (0.5% dimethylsulfoxide, DMSO) for 72 and 2 h, respectively. Additionally, in the 2 h treatment plate, cells in an additional well were treated with 1 mM MMS as positive control for the comet assay. After treatment, medium was removed from the wells and cells were washed with phosphate buffered saline (PBS). Finally, cells were trypsinized and trypsin was neutralized with fresh medium. From this point, cells were kept ice-cold to avoid DNA repair.

Comet Assay

The standard alkaline comet assay was employed for the detection of DNA strand breaks (SBs) and alkali-labile sites (ALS) in cells treated with molecule 3i. Trypsinized HepG2 cells were centrifuged at $125 \times g$ for 5 min at 4 °C and resuspended in cold PBS at 1×10^6 cells/mL. For the preparation of the agarose gels, 30 µL of cell suspension were mixed with 140 µL of 1% low melting point agarose in PBS at 37 °C and 2 aliquots of 70 µL of cell/agarose mixture were placed on agarose-precoated microscope slides. Each droplet was covered with a 20 × 20 mm coverslip and, after 2–3 min on a cold metal plate, the coverslips were removed. Then, slides were immersed in lysis solution (2.5 M NaCl, 0.1 M Na₂EDTA, 0.01 M Tris base, pH 10, and 1% Triton X-100) at 4 °C for 1 h. After lysis,

slides were transferred to the electrophoresis tank and incubated for 40 min at 4 °C in the electrophoresis solution (0.3 M NaOH, 1 mM Na₂EDTA, pH > 13) to allow DNA unwinding. After that, electrophoresis was carried out at 1 V/cm for 20 min (4 °C). Then, gels were neutralized and washed by immersing the slides in PBS for 10 min and distilled water for another 10 min (both at 4 °C). Gels were then air-dried at room temperature. Comets were stained by adding 30 µL of 1 mg/mL of 4,6-diamidino-2-phenylindole (DAPI) on top of each gel and placing 22 × 22 mm coverslips on top. Slides were incubated with DAPI at room temperature for 30 min before the analysis. The semi-automated image analysis system Comet Assay IV (Instem, Stone, UK) was used to evaluate 50 comets per gel (i.e., 100 comets/condition). The percentage of DNA in tail was the descriptor used for each comet.

Statistics

The median percentage of DNA in tail for 50 comets was calculated for each of the duplicate gels in each experiment, and the mean of the two medians were then calculated. The mean percentage of DNA in tail of 3 independent experiments and the standard deviation (SD) were calculated.

3.2.5. Evaluation against ART-Resistant Strain

Parasite Culture

The *Plasmodium falciparum* ART-resistant strain F32-ART5 and its tween ART-sensitive strain F32-TEM [33,41] were cultivated at 37 °C with 5% CO₂ in human red blood cells (EFS, French Blood Bank) diluted to 2% hematocrit in RPMI-1640 medium (Biowest, Nuaillé, France) supplemented with 5% human serum (EFS, French Blood Bank), as previously reported [41].

Standard In Vitro Chemo-Sensitivity Assay

The chemosensitivity assay was carried out in 96-well culture plates on synchronized ring-stage parasites at 1% parasitemia obtained after D-sorbitol treatment. The antiplasmodial activities were evaluated using the SYBR Green I method [42]. Parasites were exposed for 48 h to a range of concentrations of the different tested compounds. Each drug concentration was tested in triplicates. Parasite pellets were then washed in 1 × PBS prior to lysing red blood cells at −20 °C overnight. Then, the plates were thawed and 100 µL of each well were transferred into a black 96-well plate. Next, 100 µL per well of SYBR Green I (Thermo Fisher) diluted at a final concentration of 2 × in lysis buffer (20 mM Tris base pH 7.5, 5 mM EDTA, 0.008% w/v saponin, 0.08% w/v Triton X-100) were added and left to incubate for 1 h at room temperature prior to reading the plates on BioTek FLx800 Microplate Fluorescence Reader (λ_{excitation} = 485 nm, λ_{emission} = 528 nm). Relative EC₅₀ values were determined using GraphPad Prism software.

Recrudescence Assay

Recrudescence assay was performed to evaluate the ability of the F32-ART5 parasites to survive drug exposure comparatively to the F32-TEM parasites [33,34]. D-sorbitol synchronized ring-stages at 3% parasitemia (2% hematocrit) were exposed to drug for 48 h. After drug exposure, parasite cultures were washed with RPMI-1640 medium and replaced in normal drug-free culture conditions. The time to parasite recrudescence was determined as the time required to reach the 3% initial parasitemia. If no parasites were observed in the following 30 days, the culture was considered “not recrudescence”. Each experiment was performed for F32-ART5 and F32-TEM and cultivated in parallel in the same conditions to generate paired results. This was carried out at least three times independently. A statistical analysis (log-rank Mantel–Cox test) was carried out on data thanks to a Kaplan–Meier survival analysis (using GraphPad Prism software) considering censored data.

Quiescent-Stage Survival Assay

Chemosensitivity evaluation of ART-resistant parasites at the quiescent stage was performed on the strain F32-ART5 thanks to the quiescent-stage survival assay (QSA) [35]. D-sorbitol synchronized ring-stages parasites at 3% parasitemia (2% hematocrit) were first exposed to 700 nM of dihydroartemisinin (DHA) for 6 h to induce quiescence of artemisinin-resistant parasites. Then, quiescent parasites were exposed or not (as control condition) to the drug to be tested for 48 h. After drug exposure, parasite cultures were washed with RPMI-1640 medium and replaced in normal drug-free culture conditions. The time to parasite recrudescence was determined as the time required to reach the 3% initial parasitemia. If no parasites were observed in the following 30 days, the culture was considered “not recrudescence”. In each experiment, results obtained with the condition “DHA 6 h/DHA 48 h” were compared to those obtained with the condition “DHA 6 h/(DHA + drug to be tested) 48 h” in order to determine the delay in recrudescence time. This delay is representative of the capacity of the tested compound to be active on quiescent parasites and it is assumed that a 6-day threshold is necessary to classify a compound as active on quiescent parasites [35].

3.2.6. Apicoplast Studies

Culturing Plasmodium-Infected Red Blood Cells

Plasmodium falciparum blood stage parasites were maintained at 2% hematocrit in 1640 RPMI-HEPES, supplemented with 5% AlbuMAX II (GIBCO) and 0.25% gentamycin. Parasites were grown sealed Perspex chambers gassed with beta mix gas (1% O₂, 5% CO₂ and 94% N₂) at 37 °C and maintained on 48-h cycles. Cultures were tightly synchronized at ring stage using sorbitol treatment (5% *v/v*) as previously described [43].

IFA on Treated Parasites

Prior to the treatment, parasites were synchronized using 5% sorbitol. After 48 h treatment (0.3 μM of (3i) molecule, 0.3 μM of (2i) molecule or DMSO) parasites were fixed using 4% paraformaldehyde (PFA) and 0.0075% glutaraldehyde for 30 min at room temperature. Fixing solution was washed 3x times with PBS and cells were permeabilized with 0.1% TX-100 for 10 min at room temperature. The permeabilization solution was washed 3x times with PBS and cells were blocked with 3% fetal bovine serum (FBS) for 1 h. Primary antibody (Rat IgG anti-HA, Roche, 1/500 in 3% FBS) was incubated for 1 h at room temperature. The primary antibody was washed out 3x times with PBS and cells were incubated with secondary antibody (Alexa Fluor 488 goat anti-mouse IgG, Invitrogen, 1/1000 in 3% FBS) for 1 h at room temperature. The secondary antibody was washed out 3x times with PBS and cells are incubated with DAPI, 1/25000 in PBS. The samples were fixed between a slide and a coverslip with fluorogel and observed by epi-fluorescent microscopy.

Growth Assay

To observe a potential effect of delayed death of the molecule on the parasite, *Plasmodium* was maintained on three life cycles (48 h). At 48 h, 96 h, and 144 h, 100 μL of cultures were transferred into a 96-wells black wall flat bottom plate and mixed with 100 μL SYBR Green lysis buffer (20 mM Tris, pH 7.5; 5 mM EDTA; 0.008% (*w/v*) saponin; 0.08% (*v/v*) Triton X-100) with freshly added SYBR Green I (10000x), and incubated for 1 h at room temperature protected from the light. Fluorescence from each well was measured with TECAN infinite M200 plate reader (excitation: 485 nm, emission: 538 nm and integration time: 1000 μs). The rest of the cultures were diluted 1/10 as the untreated cultures. A graph was obtained by performing the ration of the treated culture fluorescence intensity on the untreated culture fluorescence intensity ($n = 3$).

3.2.7. Study on the Liver Stage

P. falciparum Sporozoite Isolation

P. falciparum (NF135 strain) sporozoites were isolated by dissection of the salivary glands of infected *A. stephensi* 14–21 days after an infective blood meal (Department of medical microbiology, University Medical Centre, St Radboud, Nijmegen Netherland). All infected salivary glands were removed by hand dissection, crushed in a potter for sporozoites isolation, and filtrated through a 40 µm filter to remove mosquito debris (Cell Strainer, BD BioSciences, Franklin Lakes, NJ, USA). The sporozoites were counted using a disposable Glasstic microscope slide (KOVA, Garden Grove, CA, USA).

Hepatocyte Culture and In Vitro Infection with Plasmodium Sporozoites

One day before hepatocyte thawing, 96-well plates were coated by a Corning® collagen solution (50 µg/mL rat tail type I collagen in 0.02N acid acetic) over night at room temperature. The next day, the wells were washed twice by PBS solution. Cryopreserved primary human hepatocytes (LONZA, Basel, Swiss) were seeded in 96-well plates with a pre-determined seeding dose that gave a single dense layer of attached hepatocytes. Four days post-seeding, each plate well was infected with 30,000 freshly extracted *Plasmodium falciparum* sporozoites. The culture plates were kept at 37 °C with 5% CO₂ and the Williams E medium (Gibco) containing usual supplements were used to feed the cells. [44]

Immunostaining and Confocal Microscopy of Infected Hepatocyte Cultures

Hepatocyte cultures were fixed with 4% paraformaldehyde solution (PFA, Invitrogen) for 10 min. To visualize intracellular *Plasmodium* schizonts anti-serum raised in mice against recombinant *P. falciparum* heat-shock protein 70 (PfHSP70) (1:1000 dilution in PBS-1% BSA-0.3% Triton) and to visualize parasite apicoplast, an antibody against *Plasmodium yoelli* acyl carrier protein (PyACP) (1:250 dilution in PBS-BSA-Triton) was used. Host and parasite nuclei were stained by DAPI. Fixed and immunostained hepatocyte cultures were studied by a confocal (Leica SP8 white laser) microscope located at the ICM Quant microscopy platform (Institut du Cerveau et de la Moelle, ICM) in Paris, France. Images were analyzed and prepared with ImageJ software. Apicoplast morphology was observed and quantified by eye under a confocal microscope.

Quantification of Parasite Size and Numbers in Treated Versus Control Wells

Upon immunostaining of parasites, the study plates were scanned using a CellInsight high-content screening platform equipped with the Studio HCS software (Thermo Fisher Scientific, Waltham, MA, USA). The details of analysis is provided elsewhere [45]. The number of host hepatocyte nuclei per well was counted by the system as a measure of toxicity of 3i towards the liver cells.

4. Conclusions

An antiplasmodial SAR study, against the asexual erythrocytic stage, was conducted through the synthesis and evaluation of 20 original 3-trichloromethylquinoxaline derivatives. All the molecules showed good in vitro antiplasmodial activity. Among them, compound (3i) had the best EC₅₀ values against the K1 *P. falciparum* strain along with a low cytotoxicity on the HepG2 cell line (SI = 160) and no cytotoxicity on human hepatocytes. Nitro-containing (3i) was not mutagenic in the Ames test or genotoxic in the in vitro comet assay. The CCl₃ group was found to be essential for antiplasmodial activity. Moreover, (3i) showed an effect on the apicoplast biogenesis, inducing a quick-killing mechanism. A parasite chemical rescue strategy could address the question of whether (3i) targets the apicoplast as a primary target or an off-target. The essential metabolic pathways that reside in the apicoplast are attractive targets for the development of new antimalarial drugs with novel mechanisms of action.

Supplementary Materials: The following are available online at <https://www.mdpi.com/article/10.3390/ph14080724/s1>, Figures S1–S48: ¹H and ¹³C NMR spectra, Figure S49: Evaluation of (3i) on the ART-resistant strain F32-ART5, Figure S50: Quantification of *P. falciparum* hepatic exo-erythrocytic forms (EEFs) number (A) and size (B) in hepatocyte culture plate fixed at day 6 post-infection, Figure S51: Quantification of *P. falciparum* hepatic exo-erythrocytic forms (EEFs) number (A) and size (B) in hepatocyte culture plate fixed at day 12 post-infection, Figure S52: The effect of (3i) on apicoplast in liver stage development of *P. falciparum*.

Author Contributions: Conceptualization, N.P., C.B. and P.V. (Pierre Verhaeghe); methodology, N.P., C.B., P.V. (Pierre Verhaeghe), N.A. (Nadine Azas), A.A. and F.B.-V.; validation, N.P., C.B., P.V. (Pierre Verhaeghe), N.A. (Nadine Azas), D.M., J.-F.F., A.A. and F.B.-V.; formal analysis, D.A., C.-S.A., S.H., J.S.-S., M.C., A.C., L.P., N.A. (Nadia Amanzougaghene), J.-F.F. and S.T.; writing—original draft preparation, D.A., C.-S.A., A.A., L.P., N.A. (Nadia Amanzougaghene) and S.T.; writing—review and editing, N.P., C.B., P.V. (Pierre Verhaeghe), D.M., N.A. (Nadia Amanzougaghene), P.V. (Patrice Vanelle), A.A., F.B.-V.; supervision, N.P., P.V. (Patrice Vanelle), C.B., D.M., N.A. (Nadine Azas), F.B.-V., P.V. (Pierre Verhaeghe); project administration, N.P. and P.V. (Patrice Vanelle); funding acquisition, N.P. and D.M. All authors have read and agreed to the published version of the manuscript.

Funding: This research was funded by “Agence Nationale de la Recherche (ANR)”, Project-ANR-17-CE11-0017 and by “Fondation pour la recherche médicale (FRM)”, project code DCM20181039565.

Institutional Review Board Statement: Not applicable.

Informed Consent Statement: Not applicable.

Data Availability Statement: Data sharing not applicable.

Acknowledgments: This work benefited from equipment and services from the CELIS cell culture core facility (Paris Brain Institute), a platform supported through the ANR grants, ANR-10-455 IAIHU-06 and ANR-11-INBS-0011-NeurATRIS. Part of this work was carried out on the icm.Quant core facility of ICM (Institut du Cerveau et de la Moelle, Paris). We gratefully acknowledge David Akbar, Claire Lovo and Aymeric Millécamps for their kind technical advice.

Conflicts of Interest: The authors declare no conflict of interest. The funders had no role in the design of the study; in the collection, analyses, or interpretation of data; in the writing of the manuscript, or in the decision to publish the results.

References

1. World Health Organization (WHO), World Malaria Report 2020. Available online: <https://www.who.int/publications-detail-redirect/world-malaria-report-2020> (accessed on 6 April 2021).
2. Talman, A.M.; Clain, J.; Duval, R.; Ménard, R.; Ariey, F. Artemisinin Bioactivity and Resistance in Malaria Parasites. *Trends Parasitol.* **2019**, *35*, 953–963. [[CrossRef](#)] [[PubMed](#)]
3. Menard, D.; Dondorp, A. Antimalarial Drug Resistance: A Threat to Malaria Elimination. *Cold Spring Harb. Perspect. Med.* **2017**, *7*, a025619. [[CrossRef](#)] [[PubMed](#)]
4. Rosenthal, P.J. Has Artemisinin Resistance Emerged in Africa? *Lancet Infect. Dis.* **2021**. [[CrossRef](#)]
5. MMV-Supported Projects | Medicines for Malaria Venture. Available online: <https://www.mmv.org/research-development/mmv-supported-projects> (accessed on 6 April 2021).
6. Verhaeghe, P.; Rathelot, P.; Rault, S.; Vanelle, P. Convenient Preparation of Original Vinylic Chlorides with Antiparasitic Potential in Quinoline Series. *Lett. Org. Chem.* **2006**, *3*, 891–897. [[CrossRef](#)]
7. Primas, N.; Verhaeghe, P.; Cohen, A.; Kieffer, C.; Dumètre, A.; Hutter, S.; Rault, S.; Rathelot, P.; Azas, N.; Vanelle, P. A New Synthetic Route to Original Sulfonamide Derivatives in 2-Trichloromethylquinazoline Series: A Structure-Activity Relationship Study of Antiplasmodial Activity. *Molecules* **2012**, *17*, 8105–8117. [[CrossRef](#)] [[PubMed](#)]
8. Gellis, A.; Kieffer, C.; Primas, N.; Lanzada, G.; Giorgi, M.; Verhaeghe, P.; Vanelle, P. A New DMAP-Catalyzed and Microwave-Assisted Approach for Introducing Heteroaryl amino Substituents at Position 4 of the Quinazoline Ring. *Tetrahedron* **2014**, *78*, 8257–8266. [[CrossRef](#)]
9. Castera-Ducros, C.; Azas, N.; Verhaeghe, P.; Hutter, S.; Garrigue, P.; Dumètre, A.; Mbatchi, L.; Laget, M.; Remusat, V.; Sifredi, F.; et al. Targeting the Human Malaria Parasite Plasmodium Falciparum: In Vitro Identification of a New Antiplasmodial Hit in 4-Phenoxy-2-Trichloromethylquinazoline Series. *Eur. J. Med. Chem.* **2011**, *46*, 4184–4191. [[CrossRef](#)]
10. De Souza, G.E.; Bueno, R.V.; de Souza, J.O.; Zanini, C.L.; Cruz, F.C.; Oliva, G.; Guido, R.V.C.; Aguiar, A.C.C. Antiplasmodial Profile of Selected Compounds from Malaria Box: In Vitro Evaluation, Speed of Action and Drug Combination Studies. *Malar. J.* **2019**, *18*, 447. [[CrossRef](#)]

11. Quiliano, M.; Pabón, A.; Ramirez-Calderon, G.; Barea, C.; Deharo, E.; Galiano, S.; Aldana, I. New Hydrazine and Hydrazide Quinoxaline 1,4-Di-N-Oxide Derivatives: In Silico ADMET, Antiplasmodial and Antileishmanial Activity. *Bioorg. Med. Chem. Lett.* **2017**, *27*, 1820–1825. [[CrossRef](#)]
12. Burrows, J.N.; Duparc, S.; Gutteridge, W.E.; Van Huijsduijnen, R.H.; Kaszubska, W.; Macintyre, F.; Mazzuri, S.; Möhrle, J.J.; Wells, T.N.C. New Developments in Anti-Malarial Target Candidate and Product Profiles. *Malar. J.* **2017**, *16*, 26. [[CrossRef](#)]
13. McFadden, G.I.; Yeh, E. The Apicoplast: Now You See It, Now You Don't. *Int. J. Parasitol.* **2017**, *47*, 137–144. [[CrossRef](#)]
14. Weatherby, K.; Carter, D. Chromera velia: The Missing Link in the Evolution of Parasitism. *Adv. Appl. Microbiol.* **2013**, *85*, 119–144. [[CrossRef](#)] [[PubMed](#)]
15. Janouskovec, J.; Horák, A.; Oborník, M.; Lukes, J.; Keeling, P.J. A Common Red Algal Origin of the Apicomplexan, Dinoflagellate, and Heterokont Plastids. *Proc. Natl. Acad. Sci. USA* **2010**, *107*, 10949–10954. [[CrossRef](#)] [[PubMed](#)]
16. Mukherjee, A.; Sadhukhan, G.C. Anti-Malarial Drug Design by Targeting Apicoplasts: New Perspectives. *J. Pharmacopunct.* **2016**, *19*, 7–15. [[CrossRef](#)]
17. Botté, C.Y.; Dubar, F.; McFadden, G.I.; Maréchal, E.; Biot, C. Plasmodium falciparum Apicoplast Drugs: Targets or off-Targets? *Chem. Rev.* **2012**, *112*, 1269–1283. [[CrossRef](#)]
18. Corral, M.G.; Leroux, J.; Stubbs, K.A.; Mylne, J.S. Herbicidal Properties of Antimalarial Drugs. *Sci. Rep.* **2017**, *7*, 45871. [[CrossRef](#)]
19. Saïdani, N.; Botté, C.Y.; Deligny, M.; Bonneau, A.-L.; Reader, J.; Lasselin, R.; Merer, G.; Niepceon, A.; Brossier, F.; Cintrat, J.-C.; et al. Discovery of Compounds Blocking the Proliferation of Toxoplasma Gondii and Plasmodium Falciparum in a Chemical Space Based on Piperidiny-Benzimidazolone Analogs. *Antimicrob. Agents Chemother.* **2014**, *58*, 2586–2597. [[CrossRef](#)]
20. Baschong, W.; Wittlin, S.; Inglis, K.A.; Fairlamb, A.H.; Croft, S.L.; Kumar, T.R.S.; Fidock, D.A.; Brun, R. Triclosan Is Minimally Effective in Rodent Malaria Models. *Nat. Med.* **2011**, *17*, 33–34. [[CrossRef](#)] [[PubMed](#)]
21. Dalvi, R.R.; Howell, C.D. Toxic Effects of a Fungicide, 5-Ethoxy-3-(Trichloromethyl)-1,2,4-thiadiazole (Terrazole), on the Hepatic Drug Metabolizing Enzyme System in Mice. *Bull. Environ. Contam. Toxicol.* **1977**, *17*, 225–232. [[CrossRef](#)] [[PubMed](#)]
22. Zhao, B.; Fan, S.; Fan, Z.; Wang, H.; Zhang, N.; Guo, X.; Yang, D.; Wu, Q.; Yu, B.; Zhou, S. Discovery of Pyruvate Kinase as a Novel Target of New Fungicide Candidate 3-(4-Methyl-1,2,3-Thiadiazolyl)-6-Trichloromethyl-[1,2,4]-Triazol-3,4-b[1,3,4]-Thiadiazole. *J. Agric. Food. Chem.* **2018**, *66*, 12439–12452. [[CrossRef](#)]
23. Ochal, Z.; Ochal, I.; Banach, Ł. Transformations of Trichloromethyl-4-Chlorophenyl Sulfone into New Compounds with Potential Pesticidal Activity. *Pol. J. Appl. Chem.* **2010**, *54*, 49–61.
24. Verhaeghe, P.; Rathelot, P.; Gellis, A.; Vanelle, P. Highly Efficient Microwave Assisted α -Trichlorination Reaction of a -Methylated Nitrogen Containing Heterocycles. *Tetrahedron* **2006**, *62*, 8173–8176. [[CrossRef](#)]
25. Strauss, M.J. The Nitroaromatic Group in Drug Design. Pharmacology and Toxicology (for Nonpharmacologists). *Ind. Eng. Chem. Prod. Res. Dev.* **1979**, *18*, 158–166. [[CrossRef](#)]
26. McCann, J.; Spingarn, N.E.; Kobori, J.; Ames, B.N. Detection of carcinogens as mutagens: Bacterial tester strains with R factor plasmids. *Proc. Natl. Acad. Sci. USA* **1975**, *72*, 979–983. [[CrossRef](#)]
27. Primas, N.; Suzanne, P.; Verhaeghe, P.; Cohen, A.; Broggi, J.; Lancelot, J.; Kieffer, C.; Vanelle, P.; Azas, N. Synthesis and in Vitro Evaluation of 4-Trichloromethylpyrrolo [1,2-a]Quinoxalines as New Antiplasmodial Agents. *Eur. J. Med. Chem.* **2014**, *83*, 26–35. [[CrossRef](#)] [[PubMed](#)]
28. Desroches, J.; Kieffer, C.; Primas, N.; Hutter, S.; Gellis, A.; El-Kashef, H.; Rathelot, P.; Verhaeghe, P.; Azas, N.; Vanelle, P. Discovery of New Hit-Molecules Targeting Plasmodium Falciparum through a Global SAR Study of the 4-Substituted-2-Trichloromethylquinazoline Antiplasmodial Scaffold. *Eur. J. Med. Chem.* **2017**, *125*, 68–86. [[CrossRef](#)] [[PubMed](#)]
29. Amrane, D.; Gellis, A.; Hutter, S.; Prieri, M.; Verhaeghe, P.; Azas, N.; Vanelle, P.; Primas, N. Synthesis and Antiplasmodial Evaluation of 4-Carboxamido- and 4-Alkoxy-2-Trichloromethyl Quinazolines. *Molecules* **2020**, *25*, 3929. [[CrossRef](#)]
30. Stumpfe, D.; Bajorath, J. Exploring Activity Cliffs in Medicinal Chemistry. *J. Med. Chem.* **2012**, *55*, 2932–2942. [[CrossRef](#)]
31. Yeh, E.; DeRisi, J.L. Chemical Rescue of Malaria Parasites Lacking an Apicoplast Defines Organelle Function in Blood-Stage Plasmodium falciparum. *PLoS Biol.* **2011**, *9*, e1001138. [[CrossRef](#)]
32. Uddin, T.; McFadden, G.I.; Goodman, C.D. Validation of Putative Apicoplast-Targeting Drugs Using a Chemical Supplementation Assay in Cultured Human Malaria Parasites. *Antimicrob. Agents Chemother.* **2017**, *62*, e01161-17. [[CrossRef](#)]
33. Witkowski, B.; Lelièvre, J.; Barragán, M.J.L.; Laurent, V.; Su, X.; Berry, A.; Benoit-Vical, F. Increased Tolerance to Artemisinin in Plasmodium Falciparum Is Mediated by a Quiescence Mechanism. *Antimicrob. Agents Chemother.* **2010**, *54*, 1872–1877. [[CrossRef](#)] [[PubMed](#)]
34. Ménard, S.; Ben Haddou, T.; Ramadani, A.P.; Ariey, F.; Iriart, X.; Beghain, J.; Bouchier, C.; Witkowski, B.; Berry, A.; Mercereau-Puijalon, O.; et al. Induction of Multidrug Tolerance in Plasmodium Falciparum by Extended Artemisinin Pressure. *Emerg. Infect. Dis.* **2015**, *21*, 1733–1741. [[CrossRef](#)] [[PubMed](#)]
35. Reyser, T.; Paloque, L.; Oujj, M.; Nguyen, M.; Ménard, S.; Witkowski, B.; Augereau, J.-M.; Benoit-Vical, F. Identification of Compounds Active against Quiescent Artemisinin-Resistant Plasmodium Falciparum Parasites via the Quiescent-Stage Survival Assay (QSA). *J. Antimicrob. Chemother.* **2020**, *75*, 2826–2834. [[CrossRef](#)] [[PubMed](#)]
36. Wei, Z.; Qi, S.; Xu, Y.; Liu, H.; Wu, J.; Li, H.; Xia, C.; Duan, G. Visible Light-Induced Photocatalytic C–H Perfluoroalkylation of Quinoxalinones under Aerobic Oxidation Condition. *Adv. Synth. Catal.* **2019**, *361*, 5490–5498. [[CrossRef](#)]
37. Mosmann, T. Rapid Colorimetric Assay for Cellular Growth and Survival: Application to Proliferation and Cytotoxicity Assays. *J. Immunol. Methods* **1983**, *65*, 55–63. [[CrossRef](#)]

38. Trager, W.; Jensen, J.B. Human Malaria Parasites in Continuous Culture. *Science* **1976**, *193*, 673–675. [[CrossRef](#)] [[PubMed](#)]
39. Guiguemde, W.A.; Shelat, A.A.; Bouck, D.; Duffy, S.; Crowther, G.J.; Davis, P.H.; Smithson, D.C.; Connelly, M.; Clark, J.; Zhu, F.; et al. Chemical Genetics of *Plasmodium falciparum*. *Nature* **2010**, *465*, 311–315. [[CrossRef](#)]
40. De Méo, M.; Laget, M.; Di Giorgio, C.; Guiraud, H.; Botta, A.; Castegnaro, M.; Duménil, G. Optimization of the Salmonella/Mammalian Microsome Assay for Urine Mutagenesis by Experimental Designs. *Mutat. Res.* **1996**, *340*, 51–65. [[CrossRef](#)]
41. Benoit-Vical, F.; Lelièvre, J.; Berry, A.; Deymier, C.; Dechy-Cabaret, O.; Cazelles, J.; Loup, C.; Robert, A.; Magnaval, J.-F.; Meunier, B. Trioxaquines Are New Antimalarial Agents Active on All Erythrocytic Forms, Including Gametocytes. *Antimicrob. Agents Chemother.* **2007**, *51*, 1463–1472. [[CrossRef](#)]
42. Smilkstein, M.; Sriwilaijaroen, N.; Kelly, J.X.; Wilairat, P.; Riscoe, M. Simple and Inexpensive Fluorescence-Based Technique for High-Throughput Antimalarial Drug Screening. *Antimicrob. Agents Chemother.* **2004**, *48*, 1803–1806. [[CrossRef](#)]
43. Amiar, S.; Katris, N.J.; Berry, L.; Dass, S.; Duley, S.; Arnold, C.-S.; Shears, M.J.; Brunet, C.; Touquet, B.; McFadden, G.I.; et al. Division and Adaptation to Host Environment of Apicomplexan Parasites Depend on Apicoplast Lipid Metabolic Plasticity and Host Organelle Remodeling. *Cell Rep.* **2020**, *30*, 3778–3792. [[CrossRef](#)] [[PubMed](#)]
44. Dembélé, L.; Franetich, J.-F.; Lorthiois, A.; Gego, A.; Zeeman, A.-M.; Kocken, C.H.M.; Le Grand, R.; Dereuddre-Bosquet, N.; van Gemert, G.-J.; Sauerwein, R.; et al. Persistence and activation of malaria hypnozoites in long-term primary hepatocyte cultures. *Nat. Med.* **2014**, *20*, 307–312. [[CrossRef](#)] [[PubMed](#)]
45. Bosson-Vanga, H.; Franetich, J.-F.; Soulard, V.; Sossau, D.; Tefit, M.; Kane, B.; Vaillant, J.-C.; Borrmann, S.; Müller, O.; Dereuddre-Bosquet, N.; et al. Differential activity of methylene blue against erythrocytic and hepatic stages of *Plasmodium*. *Malar. J.* **2018**, *17*, 143. [[CrossRef](#)] [[PubMed](#)]



Antiplasmodial 2-thiophenoxy-3-trichloromethyl quinoxalines target the apicoplast of *Plasmodium falciparum*



Dyhia Amrane^a, Nicolas Primas^{a, b, *}, Christophe-Sébastien Arnold^c, Sébastien Hutter^d, Béatrice Louis^a, Julen Sanz-Serrano^e, Amaya Azqueta^{e, f}, Nadia Amanzougaghene^g, Shahin Tajeri^g, Dominique Mazier^g, Pierre Verhaeghe^{h, i}, Nadine Azas^d, Cyrille Botté^{c, **}, Patrice Vanelle^{a, b, ***}

^a Aix Marseille Univ, CNRS, ICR UMR 7273, Equipe Pharmaco-Chimie Radicale, Faculté de Pharmacie, 13385, Marseille Cedex 05, France

^b APHM, Hôpital Conception, Service Central de la Qualité et de l'Information Pharmaceutiques, 13005, Marseille, France

^c ApicoLipid Team, Institute for Advanced Biosciences, Université Grenoble Alpes, La Tronche, France

^d Aix Marseille Univ, IHU Méditerranée Infection, UMR VITROME, IRD, SSA, Mycology & Tropical Eucaryotic Pathogens, 13005, Marseille Cedex 05, France

^e Department of Pharmacology and Toxicology, Faculty of Pharmacy and Nutrition, University of Navarra, C/ Irunlarrea 1, CP 31008, Pamplona, Navarra, Spain

^f Navarra Institute for Health Research, IdISNA, Irunlarrea 3, 31008, Pamplona, Spain

^g Sorbonne Université, INSERM, CNRS, Centre d'Immunologie et des Maladies Infectieuses, CIMI, 75013, Paris, France

^h LCC-CNRS Université de Toulouse, CNRS, UPS, 31400, Toulouse, France

ⁱ CHU de Toulouse, Service Pharmacie, 330 Avenue de Grande-Bretagne, 31059, Toulouse Cedex 9, France

ARTICLE INFO

Article history:

Received 16 June 2021

Received in revised form

22 July 2021

Accepted 25 July 2021

Available online 29 July 2021

Dedicated to the memory of Professor José Maldonado, PharmD-PhD (1940–2020).

Keywords:

Quinoxaline

Trichloromethyl group

Plasmodium falciparum

In vitro antiplasmodial Activity

Structure-activity relationships

Apicoplast

ABSTRACT

The identification of a plant-like Achilles' Heel relict, i.e. the apicoplast, that is essential for *Plasmodium* spp., the causative agent of malaria lead to an attractive drug target for new antimalarials with original mechanism of action. Although it is not photosynthetic, the apicoplast retains several anabolic pathways that are indispensable for the parasite. Based on previously identified antiplasmodial hit-molecules belonging to the 2-trichloromethylquinazoline and 3-trichloromethylquinoxaline series, we report herein an antiplasmodial Structure-Activity Relationships (SAR) study at position two of the quinoxaline ring of 16 newly synthesized compounds. Evaluation of their activity toward the multi-resistant K1 *Plasmodium falciparum* strain and cytotoxicity on the human hepatocyte HepG2 cell line revealed a hit compound (**3k**) with a *Pf*K1 EC₅₀ value of 0.3 μM and a HepG2 CC₅₀ value of 56.0 μM (selectivity index = 175). Moreover, hit-compound **3k** was not cytotoxic on VERO or CHO cell lines and was not genotoxic in the *in vitro* comet assay. Activity cliffs were observed when the trichloromethyl group was replaced by CH₃, CF₃ or H, showing that this group played a key role in the antiplasmodial activity. Biological investigations performed to determine the target and mechanism of action of the compound **3k** strongly suggest that the apicoplast is the putative target as showed by severe alteration of apicoplast biogenesis and delayed death response. Considering that there are very few molecules that affect the *Plasmodium* apicoplast, our work provides, for the first time, evidence of the biological target of trichloromethylated derivatives.

© 2021 Elsevier Masson SAS. All rights reserved.

* Corresponding author. Aix Marseille Univ, CNRS, ICR UMR 7273, Equipe Pharmaco-Chimie Radicale, Faculté de Pharmacie, 13385, Marseille Cedex 05, France.

** Corresponding author.

*** Corresponding author. Aix Marseille Univ, CNRS, ICR UMR 7273, Equipe Pharmaco-Chimie Radicale, Faculté de Pharmacie, 13385, Marseille Cedex 05, France.

E-mail addresses: nicolas.primas@univ-amu.fr (N. Primas), cyrille.botte@univ-grenoble-alpes.fr (C. Botté), Patrice.vanelle@univ-amu.fr (P. Vanelle).

1. Introduction

Malaria remains the leading cause of death among parasitic infections worldwide, mainly affecting children under the age of 8, the elderly and pregnant women. According to the World Malaria Report 2020 [1], malaria caused an estimated 229 million clinical cases leading to 409 000 deaths. Eighty nine countries from the sub-tropical zone are endemic, where the mosquito vectors are

present. Most cases and deaths occur in sub-Saharan Africa and South-East Asia. Malaria is caused by a unicellular eukaryote, i.e. protist, of the Apicomplexa phylum and the *Plasmodium* genus, among which the species *falciparum* is responsible for most fatal malaria cases, including cerebral malaria. The parasite is transmitted to humans by a bite of an infected female *Anopheles* mosquito during a blood meal. Despite numerous and ambitious malaria control efforts, *Plasmodium* strains that resist commercial anti-malarial drugs such as chloroquine [2], quinine [3], atovaquone [4], mefloquine [5], piperazine [6] and associations of pyrimethamine-cycloguanil [7] or sulfadoxine-pyrimethamine [8] are spreading worldwide. In addition, the emergence of resistances toward the first line treatments against severe *P. falciparum* infections, Artemisinin-based Combination Therapies (ACTs), is now threatening the efficacy of malaria treatment particularly in the Greater Mekong Subregion [9], Africa [10,11] and India [12]. Therefore, new chemotypes with original modes of action, for use in combination therapies, are urgently needed to overcome these resistances and move towards malaria eradication.

Working on the synthesis and reactivity of new heterocycles bearing a trichloromethyl group as potential antiparasitic agents [13–15], our research group has previously reported an antiplasmodial 2-trichloromethylquinazoline derivative (Hit A, Table 1) bearing a thiophenoxy group at position 4 [16]. From this initial compound, a quinoxaline position isomer (Hit B, Table 1) was prepared and evaluated, showing an improved antiplasmodial profile [17]. Based on this encouraging result, we decided to synthesize a series of original quinoxaline derivatives bearing a thiophenoxy moiety at the 2-position of the quinoxaline ring, with the aim of identifying a new optimized hit-compound and investigating the antiplasmodial structure-activity relationships.

Indeed, several quinoxalines have already been identified as promising antiplasmodial molecules, including BQR695 (Fig. 1), identified from a phenotypic screening of the Novartis chemical library, exerting antiplasmodial activity through inhibition of the plasmodial protein kinase PfPK1 [18]. Guillon et al. [19] previously described a series of bis- and tris-pyrrolo [1,2-*a*]quinoxaline derivatives (C, Fig. 1) showing good antiplasmodial activity during the intraerythrocytic stage of *P. falciparum* W2 and 3D7 with EC₅₀ in the micromolar range. In addition, (*R*)-enantiomers of pyrrolo [1,2-*a*]quinoxalines (D) showed good

antiplasmodial activities [20]. In addition, our lab has previously described 2-trichloromethylpyrroloquinoxaline derivatives (E) which also show selective antiplasmodial activity [21], illustrating the potential of quinoxaline ring in antiplasmodial drug-design.

With the aim of discovering and developing new antimalarial compounds, Medicines for Malaria Ventures (MMV) defined target candidates (TCPs) and target product profiles (TPPs) for the treatment and chemoprevention of malaria [22]. MMV currently lists four molecules in pre-clinical trials and 14 compounds in clinical trials [23]. Therefore, new compounds with novel mechanisms of action are urgently required to overcome the resistance of *Plasmodium* against commercial drugs. In this context, apicoplast, a plant plastid-like organelle that is essential for parasite survival provide potentially an interesting antimalarial target.

The discovery in Australian corals of a photosynthetic apicomplexan *Chromera velia* confirmed the common plant and photosynthetic evolutionary origin of *P. falciparum* and its peculiar organelle, the apicoplast [24]. Indeed, the apicoplast is a non-photosynthetic plastid acquired by secondary endosymbiosis from a plastid-containing red algal ancestor [25]. As a consequence of this secondary endosymbiotic origin, the apicoplast is delimited by four membranes [26]. This *P. falciparum* organelle possesses a housekeeping machinery maintained in its small 35 kb circular genome, which encodes for tRNAs, ribosomal proteins and a handful of proteins that are targeted to the apicoplast [27]. Despite being non photosynthetic, the apicoplast retains several anabolic pathways that are essential for parasite survival. These pathways include fatty acids biosynthesis, isoprenoid biosynthesis precursors, iron-sulfur cluster assembly and heme biosynthesis [27]. These metabolic pathways have no equivalent in the human host. Isoprenoid precursors such as isopentenyl pyrophosphate (IPP) have previously been described as the only required function of the apicoplast in the asexual blood stage of malaria parasite *in vitro* under rich culture conditions [28]. Thus, it was confirmed that IPP inhibitors, such as fosmidomycin, mainly target the apicoplast. On the other hand, the apicoplast fatty acid biosynthesis plays a vital role during the *in vitro* liver stage [29], and can be reactivated during the blood stages and become critical in a low host nutritional/lipid environment [30,31]. Furthermore, even if disrupted and absent in blood stage parasites by anti-plastidial treatment (azythromycin, doxycycline, fosmidomycin), the apicoplast remains

Table 1
Comparison between antiplasmodial Hit A and position isomer Hit B.

| | Hit A | Hit B |
|-----------------------------|-------|-------|
| EC ₅₀ PfPK1 (μM) | 0.9 | 0.5 |
| CC ₅₀ HepG2 (μM) | >25 | 38.6 |
| Selectivity index (SI) | >28 | 77.2 |

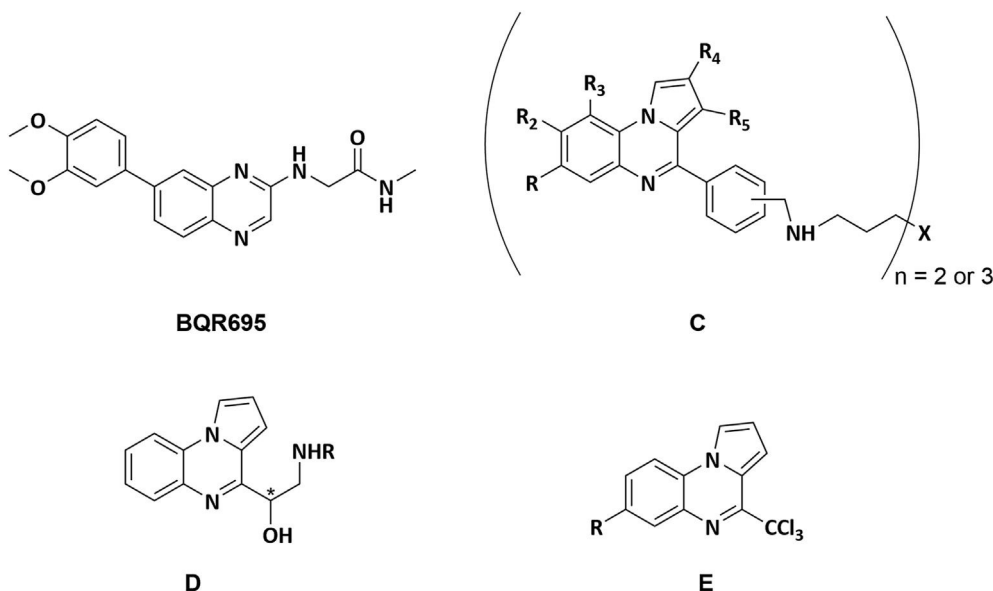


Fig. 1. Structures of some previously described antiplasmodial derivatives containing a quinoxaline moiety.

metabolically active in the form of vesicles, showing once again that the IPP pathway is not the only essential pathway of the apicoplast [32]. Moreover, Prigge et al. [33] have recently demonstrated the importance of carbon metabolism in the apicoplast of the malaria parasite. Indeed, a loss of pyruvate kinase II activity which is an essential *Plasmodium* enzyme providing the pyruvate necessary for the generation of essential isoprenoid precursors, leads to a reduction of apicoplast RNA, following by apicoplast disruption and parasite death. Seven enzymes of the isoprenoid precursors pathway are drug-target in the apicoplast, which are DOXP synthase, IspC, IspD, IspE, IspF, IspG and IspH. Knowing that the isoprenoid precursors biosynthesis is localized only to apicoplast, chemical rescue by adding IPP to the growth medium identified **MMV-08138** as a potent IspD inhibitor during the blood stage of *P. falciparum* with an EC₅₀ of 110 nM (Fig. 2) [34].

Currently very few molecules targeting the apicoplast have been reported, but some known antibiotics have been studied, such as ciprofloxacin and doxycycline belonging to the fluoroquinolone and tetracycline classes respectively, which target DNA replication and rRNA translation respectively in *P. falciparum* apicoplast, leading to a delayed death drug-response [26].

The delayed death phenomenon in the apicomplexan parasite is well studied and its molecular mechanism appears to be related to the inhibition of functions in the apicoplast that induce death of daughter cell after one life cycle. It is related to apicoplast house-keeping processes such as DNA replication, transcription and translation mechanisms [27].

In addition to these antibiotics, several biocides such as triclosan (Fig. 3) are reported to be active against *Plasmodium* through the metabolic pathway of fatty acid synthesis located in the apicoplast [26] although it was further proved that the apicoplast is not the main target [35]. As *P. falciparum* apicoplast is an essential chloroplast-like organelle, studies have demonstrated that herbicides active against plants are also active against *P. falciparum* and therefore could act as antimalarials [36,37]. Indeed, clomazone [38] and fluridone [39] affect DOXP synthase and block plastidial abscisic acid synthesized by the plastid DOXP pathway respectively, localized in the apicoplast (Fig. 3).

After working for 15 years on the development of trichloromethylated heterocycles without identifying their mechanism of action, we decided herein to evaluate the effect of our

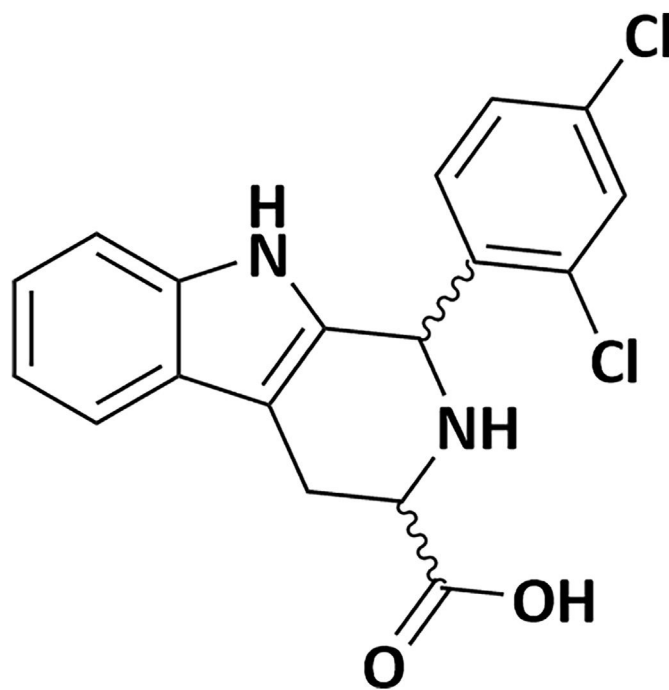


Fig. 2. MMV-08138 acting at the level of the *Plasmodium* apicoplast.

molecules toward this vital organelle in *P. falciparum* in order to look for the mechanism of action of such trichloromethyl derivatives.

2. Results

2.1. Synthesis

As shown in Scheme 1, the key substrate (**1**) was easily obtained by reacting *o*-phenylenediamine with ethyl pyruvate to provide the corresponding lactam which was then chlorinated using POCl₃ (Scheme 1) [15]. Next, chlorimine (**1**) was reacted through a nucleophilic aromatic substitution reaction (S_NAr) with various thiophenol derivatives in the presence of cesium carbonate in DMF

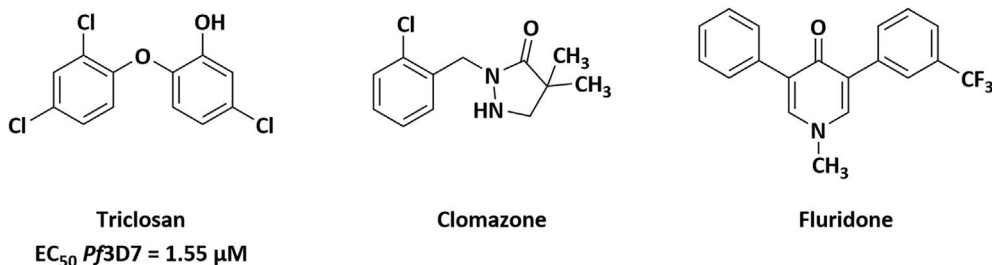
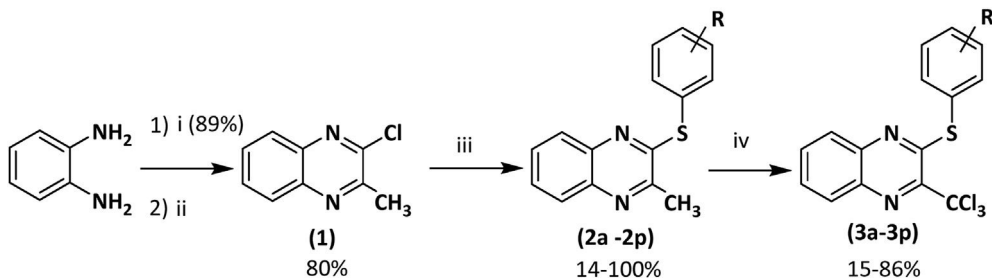


Fig. 3. Chemical structures of antiapicomplex biocids.



Scheme 1. Preparation of 2-thiophenoxy-3-trichloromethylquinoxaline derivatives (**3a-3p**). Reagents and conditions: (i) ethyl pyruvate 1 equiv, H₂O, 50 °C, 15 min; (ii) POCl₃, reflux, 2 h; (iii) appropriate thiophenol derivative 1 equiv, Cs₂CO₃ 1 equiv, anh. DMF, 70 °C, 12 h, sealed vial, N₂; (iv) PCl₅ 6 equiv, POCl₃ as solvent, 100 °C, MW, 20 min, 800 W.

at 70 °C. The desired intermediates (**2a-2p**) were obtained in low to quantitative yields (14–100%). Yield variation does not seem to be correlated with the electron-donating or -withdrawing behavior of the different thiophenol substituents. Finally, from the methylated precursors (**2a-2p**), a chlorination reaction using PCl₅ and POCl₃ was performed under microwave heating at 100 °C for 30 min, according to a previously reported method [40], leading to the target compounds (**3a-3p**) in low to very good yields (15–86%). A series of 16 original derivatives (**3a-3p**) was then prepared, bearing electron-donating or electron-withdrawing substituents in *ortho*, *meta* and *para* positions of the thiophenol moiety. It is to note that attempt to chlorinate the intermediate (**2i**), bearing a 3'-OMe substituent on the thiophenoxy group, led to the only the unexpected 2'-chlorinated product.

2.2. Biological results

2.2.1. Structure-activity relationship (SAR) study

These new derivatives were evaluated *in vitro* against the K1 multidrug-resistant *P. falciparum* strain, by determining their 50% efficacy concentration (EC₅₀), and compared with three reference antimalarial drugs: chloroquine, atovaquone and doxycycline. The *in vitro* 50% cytotoxic concentrations (CC₅₀) were assessed on the HepG2 human hepatocyte cell line and compared with >cytotoxic reference drug: doxorubicin. Selectivity indexes were calculated: SI = CC₅₀/EC₅₀. The results are presented in Table 2.

All the 16 newly synthesized compounds showed good aqueous solubility except for compound (**3j**), which precipitated above 1.9 μM in the cell viability assay. The derivatives showed cytotoxicity values ranging from 19.9 to 69.7 μM, comparable or better than chloroquine (30 μM) or doxycyclin (20 μM). It appears that strong electron-withdrawing groups (EWG) (**3m-3o**) at 4-position of 2-thiophenoxy group led to slightly more cytotoxic compounds (19.9–29.9 μM), contrary to electron-donating groups (EDG) (**3p**) or the unsubstituted thiophenoxy moiety (**3k**) (69.7–56.0 μM, respectively).

With regard to the antiplasmodial activity, all derivatives showed submicromolar activity except for (**3p**) bearing a 4-Me group (1.5 μM). A strong EWG such as 4-NO₂ group (**3o**) gave the best antiplasmodial

activity with only 0.2 μM. The 2, 3 or 4 fluoro-substituted thiophenoxy moiety (**3e-3g**) led to quite similar activities (0.32, 0.31, 0.36 μM respectively). Other 4-EWG such as 4-CF₃ (**3m**) and 4-OCF₃ (**3n**) gave quite similar activities to the fluoro-substituted thiophenoxy group (0.40 and 0.30 μM respectively). Substitution by a methoxy group was slightly detrimental to the activity, especially for the 2-OMe compound (**3h**) (0.74 μM). The disubstituted 2-chloro-3-methoxy-thiophenoxy moiety (**3i**) led to a better antiplasmodial activity than only 2- or 4-methoxy substitution (**3h**, **3j**). For the dichloro-containing molecules (**3c**, **3d**), 2–3 substitutions were better than the 2–4 substitutions (0.31 vs 0.90 μM).

Finally, the best compound in this series was the unsubstituted thiophenoxy group (**3k**) which combined both good antiplasmodial activity and low cytotoxicity, leading to the highest selectivity index in series (175) (Table 2). It is to note that there is no correlation between the calculated logP and activity.

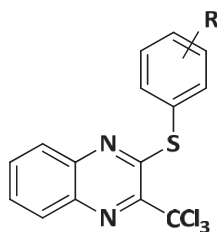
2.2.2. Toxicity data

In order to complete the cytotoxicity data of the best molecule (**3k**) in this series, we tested it on CHO Chinese Hamster Ovary cells and Vero cells (Table 3). After 72 h of treatment, low cytotoxicities was observed both on cell lines (58.5 μM and 63.5 μM respectively), similar to that measured on HepG2 cell line (56.0 μM).

To complete the *in vitro* toxicological evaluation of compound (**3k**), its genotoxic potential was studied, using the comet assay on the HepG2 cell line (Table 3). Compound (**3k**) did not induce DNA strand breaks or alkali labile sites after either short (2 h) or long (72 h) exposure at two concentrations (5.6 and 28 μM; CC₅₀/2 and CC₅₀/10 after 72 h of treatment) (see supplementary material). The positive control (i.e., cells treated with 1 mM Methyl MethaneSulphonate, MMS) showed the expected results.

2.2.3. Role of the 2-CCl₃ group

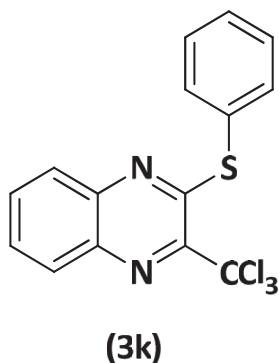
We have previously shown that the -CCl₃ group is mandatory to provide antiplasmodial activity [17,21,41]. To confirm the key role of the CCl₃ group in the activity of **3k**, we compared the antiplasmodial activity of (**3k**) with that of three analogs bearing a proton (**3r**), a methyl group (**2k**) or a trifluoromethyl group (**3s**) at position 3 of the

Table 2
Antiplasmodial activity, cLogP and human cell toxicity on HepG2 cell line of the 2-phenoxy-3-trichloro-methylquinoxaline compounds (**3a-3p**).

| R | N° | Yields (%) | EC ₅₀ PfK1 (μM) | CC ₅₀ HepG2 (μM) | SI ^d | cLogP ^e |
|--------------------------|-----------|------------|----------------------------|-----------------------------|-----------------|--------------------|
| 2-Cl | 3a | 62 | 0.50 ± 0.10 | 36.9 ± 8.1 | 73.8 | 5.15 |
| 3-Cl | 3b | 74 | 0.41 ± 0.08 | 38.3 ± 8.1 | 93.4 | 5.16 |
| 2,3-Cl | 3c | 61 | 0.31 ± 0.06 | 34.6 ± 7.1 | 111.6 | 5.68 |
| 2,4-Cl | 3d | 46 | 0.90 ± 0.10 | >31.2 ^c | >34.7 | 5.69 |
| 2-F | 3e | 56 | 0.32 ± 0.07 | 40.5 ± 8.1 | 126.6 | 4.94 |
| 3-F | 3f | 63 | 0.31 ± 0.07 | 35.9 ± 7.9 | 115.8 | 4.94 |
| 4-F | 3g | 51 | 0.36 ± 0.08 | 30.8 ± 7.0 | 85.6 | 4.95 |
| 2-OMe | 3h | 64 | 0.74 ± 0.16 | 42.6 ± 5.2 | 56.8 | 4.63 |
| 2-Cl-3-OMe | 3i | 15 | 0.46 ± 0.15 | 58.4 ± 5.8 | 126.9 | 5.14 |
| 4-OMe | 3j | 59 | 0.65 ± 0.15 | >1.9 ^c | >3.0 | 4.61 |
| H ^f | 3k | 71 | 0.32 ± 0.07 | 56.0 ± 11.0 | 175.0 | 4.68 |
| 4-Br | 3l | 44 | 0.46 ± 0.10 | 42.2 ± 8.6 | 93.0 | 5.25 |
| 4-CF ₃ | 3m | 80 | 0.50 ± 0.10 | 29.9 ± 5.1 | 59.8 | 5.68 |
| 4-OCF ₃ | 3n | 68 | 0.36 ± 0.10 | 21.0 ± 3.1 | 58.3 | 5.55 |
| 4-NO ₂ | 3° | 64 | 0.25 ± 0.05 | 19.9 ± 3.0 | 79.6 | 3.92 |
| 4-CH ₃ | 3p | 40 | 1.50 ± 0.20 | 69.7 ± 14.6 | 46.5 | 5.01 |
| Hit B | | | 0.50 | 38.6 | 77.2 | 5.17 |
| Chloroquine ^a | | | 0.80 | 30.0 | 37.5 | 3.82 |
| Atovaquone ^a | | | 0.001 | >15.6 | 15600 | 4.23 |
| Doxycycline ^a | | | 6.00 | 20.0 | 3.3 | – |
| Doxorubicin ^b | | | – | 0.20 | – | – |

^a Chloroquine, Atovaquone and doxycycline were used as antimalarial reference-drugs;^b Doxorubicin was used as a cytotoxic reference-drug;^c Highest concentration tested due to a lack of solubility;^d Selectivity index (SI) was calculated according to the formula: SI = CC₅₀/EC₅₀.^e Weighted clogP was computed by swissADME;^f The best antiplasmodial molecule.**Table 3**
Cytotoxic and genotoxic data for hit compound (**3k**).

| Entry | CC ₅₀ HepG2 (μM) | CC ₅₀ CHO (μM) | CC ₅₀ Vero (μM) | Comet assay ^a |
|-------|-----------------------------|---------------------------|----------------------------|--------------------------|
| | 56.0 ± 11.0 | 58.5 ± 3.9 | 63.5 ± 8.6 | Negative |

^a Comet assay was performed on HepG2 cell line at 5.6 and 28 μM for 2 or 72 h.

quinoxaline ring respectively. None of these analogs lacking a CCl_3 group was active against *P. falciparum* (EC_{50} $\text{PfK1} > 50 \mu\text{M}$). These activity cliffs revealed once again the key role of the CCl_3 group in antiplasmodial activity in the studied series (Fig. 4) [42].

2.2.4. Evaluation on *P. falciparum* apicoplast

- Treatment with molecule **3k** affects parasites growth and apicoplast development

Using an epifluorescence microscope, we monitored the effect of molecule (**3k**) on different intraerythrocytic stages of *P. falciparum* parasite in order to identify the mechanism by which the molecule could affect parasite survival and whether this was directed against the apicoplast. The loss of apicoplast by molecule (**3k**)-treatment can then be visualized via fluorescence microscopy. The EC_{50} treatment was performed on synchronized cultures of *P. falciparum* 3D7 strain during a 48-h parasite life cycle (Fig. 5A).

Parasites treated with $0.3 \mu\text{M}$ of molecule (**3k**) shows a severe defect in apicoplast biogenesis when compared to the DMSO control. The apicoplast development, elongation and branching typically happening during asexual blood stage intracellular development is highly affected by the treatment and strongly suggest a direct effect on *Plasmodium* apicoplast (Fig. 5A). Furthermore, overall parasite development is also slightly reduced, as the nucleus staining shows a defect in replication and the culture is enriched in mid trophozoite parasites (Fig. 5A), suggesting either that apicoplast disruption induces parasite death or that the drug could have some sort of off target mechanism. If the apicoplast is the primary target of the (**3k**) molecule, one could expect a so-called delayed death phenotype, which is characteristic of some apicoplast targeting drugs such as chloramphenicol, doxycycline or ciprofloxacin. To confirm this, we performed a growth assay on three life cycles ($3 \times 48 \text{ h}$) by measuring the development of treated parasite with $0.3 \mu\text{M}$ of (**3k**) and $0.3 \mu\text{M}$ of (**2k**). The replacement of CCl_3 by a methyl group in (**2k**) analog shows to have no effect on the apicoplast development (Fig. 5B) compared to untreated parasites (DMSO control). Results show a slight reduction of the parasites development at the first cycle (48 h), and a drastic reduction of the growth at the second and third cycles, confirming the delayed effect of apicoplast targeting drugs, compared to inactive (**2k**) molecule, which has no significant difference with DMSO (Fig. 5C). Nevertheless, the slight decrease of the growth at the first cycle confirms the potential off target of (**3k**) molecule, outside of the apicoplast, coherent with the reduction of nucleus replication shown by IFA at 48 h treatment (Fig. 5A).

It should be noted out that all derivatives (**3a-p**) including (**3k**) have a high lipophilicity ($3.92 < \log P < 5.69$). This may be necessary property to cross the four membranes that envelop the apicoplast.

2.2.5. Evaluation on human hepatocyte infection

In order to further explore the potency of molecule (**3k**), an evaluation was made on the hepatic stage of *P. falciparum* infection. Cryopreserved primary human hepatocyte cultures were infected with *P. falciparum* NF135 strain. Treatment with (**3k**) at various doses was applied simultaneously with the sporozoites addition to hepatocytes and contact was maintained until post-infection day 6 (pi). (**3k**) treatment significantly reduced parasite size without affecting parasite numbers in a dose-dependent manner. Atovaquone (ATQ), a potent hepatic schizonticide was used as positive control.

We then tried to understand if apicoplast of *P. falciparum* schizonts was targeted by (**3k**). In untreated control wells fixed at day 6 pi, the parasitic apicoplast has a uniform appearance. The apicoplast is in its terminal stage of development (considering the 5–6 days schizogony of *P. falciparum*) and the Apicoplast protein acyl Carrier Protein (ACP) signal looks like small dots densely decorating the periphery of the organelle. In (**3k**) treated cultures, the integrity of small dots shown in the control parasites appears to be affected and the ACP signal is condensed leading to the appearance of larger aggregates. At the high dose of $30 \mu\text{M}$ approximately 93% of *P. falciparum* schizonts showed partial or complete alteration of the apicoplast signal (Fig. 6). Interestingly, no cytotoxicity was observed on human hepatocytes up to $30 \mu\text{M}$ (Fig. 7).

3. Conclusion

An antiplasmodial SAR study was conducted through the synthesis and evaluation of 16 original thiophenoxyquinoxaline derivatives. All of these molecules displayed good *in vitro* antiplasmodial activity. Among these compounds, (**3k**) showed the best antiplasmodial activity ($\text{EC}_{50} = 0.32 \mu\text{M}$) and low cytotoxicity towards three cell-lines and no cytotoxicity on human hepatocytes. Moreover, compound (**3k**) presented no genotoxic effect in the comet assay. The activity cliffs showed that the CCl_3 group was essential to provide antiplasmodial activity. Although no effect was demonstrated on hepatic stage, at high concentration, the size of parasite was affected. Interestingly, the molecule (**3k**) shows a delayed death inhibition and apicoplast biogenesis branching defect, confirming that it affects growth of *P. falciparum* by targeting the apicoplast, and probably another target outside of the apicoplast which affects the cell division. Essential metabolic pathways reside within the apicoplast which provide promising new drug targets for the development of new antimalarials, with a novel mechanism of action. Further investigations will be necessary in order to decipher the action of trichloromethylquinoxaline derivatives on the apicoplast.

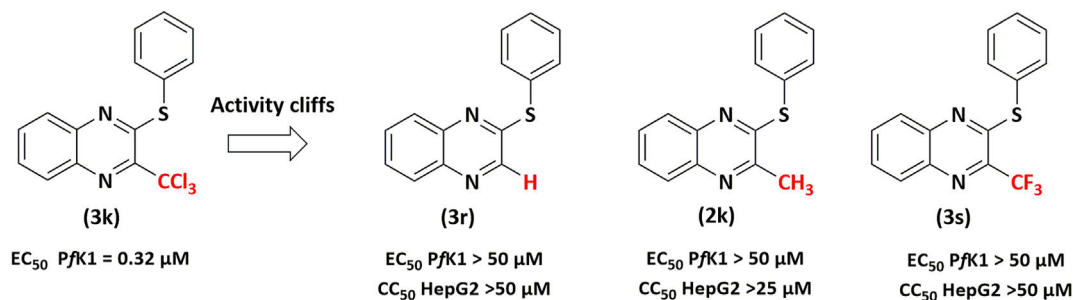


Fig. 4. Comparison of the *in vitro* antiplasmodial activities of hit molecule **3k** with analogs **3r**, **2k** and **3s**.

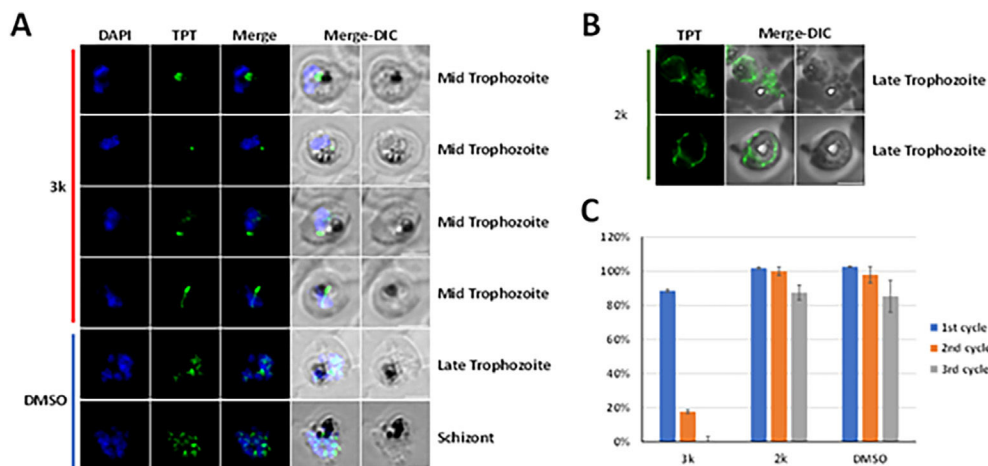


Fig. 5. (3k) molecule treatment affects apicoplast biogenesis. (A, B) Triose Phosphate Transporter (TPT) fluorescent signal is shown in green (TPT labelled with an 3xHA tag). DAPI, as a marker for the nucleus, is shown in blue. Apicoplasts of treated parasites with 0.3 μM of (3k) molecule or 0.3 μM of (2k) molecule are compared to normal plastid visualized in DMSO-treated control. The microscopic images were obtained by epifluorescence microscope. DIC, differential interference contrast. (C) Plastid associated with the delayed death of *P. falciparum* trophozoite was observed after treatment with molecule (3k) on three life cycles ($n = 3$, error bar = standard deviation, SD).

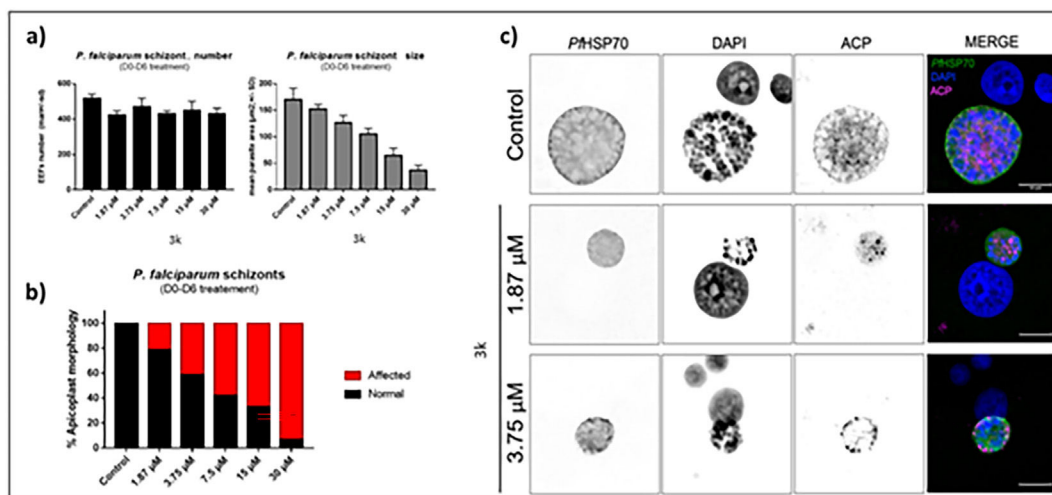


Fig. 6. The effect of (3k) on liver stage *P. falciparum* growth. a) D0 pi-D6 (3k) exposure of human hepatocytes infected with *P. falciparum* and its impact on parasite numbers expressed as mean \pm SD and parasite size expressed as surface area expressed as μm^2 mean \pm SD. Parasites were immunostained with anti-HSP70 antibody and plates were scanned. b) Quantification of different apicoplast morphologies (normal and affected) in 100 parasites with percentage distribution of each defined category. c) Confocal microscopic images of control and treated *P. falciparum* schizonts. The schizonts were immunolabelled with anti-HSP70 antibody. Host and parasite DNA were visualized by 4',6-diamidino-2-phenylindole (DAPI) dye. The apicoplast was labelled by Anti-PyACP (Scale bar = 10 μm).

4. Experimental section

4.1. Chemistry

4.1.1. Generality

Melting points were determined on a Kofler melting point apparatus (Wagner & Munz GmbH, München, Germany) and are uncorrected. Elemental analyses were carried out at the Spectropole, Faculté des Sciences de Saint-Jérôme (Marseille) with a Thermo Finnigan EA1112 analyzer (Thermo Finnigan, San Jose, CA, USA). NMR spectra were recorded on a Bruker AV (Billerica, MA, USA) 200 or AV 250 spectrometers or on a Bruker Avance NEO 400 MHz NanoBay spectrometer at the Faculté de Pharmacie de Marseille or on a Bruker Avance III nanobay 400 MHz spectrometer at the Spectropole, Faculté des Sciences de Saint-Jérôme (Marseille). (^1H NMR: reference CDCl_3 $\delta = 7.26$ ppm, reference $\text{DMSO}-d_6$ $\delta = 2.50$ ppm and ^{13}C NMR: reference CHCl_3 $\delta = 76.9$ ppm, reference

$\text{DMSO}-d_6$ $\delta = 39.52$ ppm). The following adsorbent was used for column chromatography: silica gel 60 (Merck KGaA, Darmstadt, Germany, particle size 0.063–0.200 mm, 70–230 mesh ASTM). TLC was performed on 5 cm \times 10 cm aluminum plates coated with silica gel 60F-254 (Merck) in an appropriate eluent. Visualization was performed with ultraviolet light (234 nm). The purity of synthesized compounds was checked by LC/MS analyses, which were performed at the Faculté de Pharmacie of Marseille with a Thermo Scientific Accela High Speed LC System® (Waltham, MA, USA) coupled to a single quadrupole mass spectrometer Thermo MSQ Plus®. The RP-HPLC column is a Thermo Hypersil Gold® 50 \times 2.1 mm (C18 bounded), with particles of a diameter of 1.9 μm . The volume of sample injected on the column is 1 μL . The chromatographic analysis with a total duration of 8 min, is performed on the following solvents gradient: $t = 0$ min, methanol/water 50:50; $0 < t < 4$ min, linear increase in the proportion of methanol to a methanol/water ratio of 95:5; $4 < t < 6$ min, methanol/water

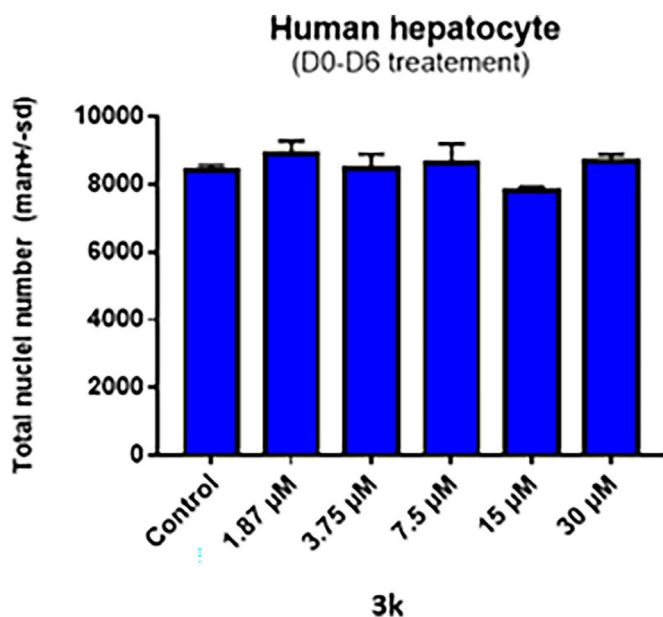


Fig. 7. Toxicity of (3k) on primary human hepatocytes. The number of hepatocyte nuclei quantified from a certain number of microscopic scanning fields from control and (3k) treated groups.

95:5; $6 < t < 7$ min, linear decrease in the proportion of methanol to return to a methanol/water ratio of 50:50; $6 < t < 7$ min, methanol/water 50:50. The water used was buffered with ammonium acetate 5 mM. The flow rate of the mobile phase was 0.3 mL/min. The retention times (t_R) of the molecules analyzed are indicated in min. The microwave reactions were performed using multimode reactors: ETHOS Synth Lab station and MicroSYNTH® Lab terminal 1024 (Ethos start, MLS GmbH, Leutkirch, Germany.); or monomode reactors: Biotage Initiator® classic in sealed vials with a power output of 0–400 W. Reagents were purchased and used without further purifications from Sigma-Aldrich or Fluorochem.

4.1.2. 2-Chloro-3-methylquinoxaline (1)

Step 1 To a solution of *o*-phenylenediamine (6 g, 1.0 equiv) in H₂O was added ethyl pyruvate (1.0 equiv) dissolved in H₂O (80 mL). The reaction mixture was heated at 50 °C for 15–30 min. After cooling, the precipitate product of 3-methylquinoxalin-2(1*H*)-one was recrystallized from ethanol as a white solid, 7.92 g, yield 89%. This was used directly in step 2.

Step 2 To a solution of 3-methyl-2(1*H*)-quinoxalinone (12.5 g, 121.8 mmol, 1.0 equiv) was added cold POCl₃ (65 mL) in portions to get a slurry. The mixture was refluxed for 2 h. Then, the reaction was added to ice cold water (500 mL) and basified slowly under cooling with Na₂CO₃ to pH 8. The organic phase was separated and washed with brine, dried over anhydrous MgSO₄, filtered, and concentrated in vacuum to afford the crude product, which was purified by silica gel flash chromatography (using dichloromethane) to afford (1) as an off-white solid, yield 80% (7 g). Mp 84 °C. ¹H NMR (250 MHz, CDCl₃) δ 8.08–7.84 (m, 2H), 7.79–7.62 (m, 2H), 2.82 (s, 3H). ¹³C NMR (63 MHz, CDCl₃) δ 152.9, 147.9, 141.0, 141.0, 130.2, 130.1, 128.5, 128.2, 23.4. Spectral data matched with literature [43].

4.1.3. General procedure for 3-methyl-2-substituted-quinoxaline (2a–2p)

To a solution of 2-chloro-3-methylquinoxaline (1) (500 mg, 2.8 mmol) and the appropriate thiophenol (2.8 mmol, 1.0 equiv) in anhydrous DMF (10 mL), Cs₂CO₃ (912 mg, 2.8 mmol, 1.0 equiv) was added under inert atmosphere. The mixture was stirred at 70 °C overnight. After completion of the reaction, water was added, leading to a precipitate which was separated by filtration. The resulting precipitate was then thoroughly washed with water. The precipitate was dissolved in CH₂Cl₂ and dried with Na₂SO₄. After filtration and evaporation, the resulting solid was purified by silica gel column chromatography (using the appropriate eluant) to afford the desired compound.

4.1.3.1. 2-(2-Chlorophenylthio)-3-methylquinoxaline (2a). Yield 100% (803 mg). White solid. Mp 155 °C. ¹H NMR (250 MHz, CDCl₃) δ 7.97–7.93 (m, 1H), 7.70–7.51 (m, 5H), 7.46–7.31 (m, 2H), 2.82 (s, 3H). ¹³C NMR (63 MHz, CDCl₃) δ 154.6, 151.5, 141.6, 139.6, 139.6, 137.6, 131.0, 130.4, 129.2, 128.7, 128.3, 128.2, 128.1, 127.5, 22.4. **LC-MS** (ESI+) t_R 6.54 min; m/z [M+H]⁺ 286.36/289.00. MW: 286.78 g mol⁻¹. **HRMS (ESI):** m/z calcd. for C₁₅H₁₁ClN₂S [M+H]⁺ 287.0404. Found: 287.0402.

4.1.3.2. 2-(3-Chlorophenylthio)-3-methylquinoxaline (2b). Yield 94% (755 mg). White solid. Mp 97 °C. ¹H NMR (250 MHz, CDCl₃) δ 7.98–7.94 (m, 1H), 7.74–7.69 (m, 1H), 7.65–7.55 (m, 3H), 7.52–7.33 (m, 3H), 2.78 (s, 3H). ¹³C NMR (63 MHz, CDCl₃) δ 155.0, 151.4, 141.4, 139.8, 134.9, 134.8, 133.3, 130.5, 130.3, 130.2, 129.5, 129.3, 128.8, 128.2, 22.4. **LC-MS** (ESI+) t_R 6.83 min; m/z [M+H]⁺ 286.36/289.04. MW: 286.78 g mol⁻¹. **HRMS (ESI):** m/z calcd. for C₁₅H₁₁ClN₂S [M+H]⁺ 287.0404. Found: 287.0402.

4.1.3.3. 2-(2,3-Dichlorophenylthio)-3-methylquinoxaline (2c). Yield 100% (899 mg). Brown solid. Mp 142 °C. ¹H NMR (250 MHz, CDCl₃) δ 7.92–7.88 (m, 1H), 7.65–7.49 (m, 5H), 7.23–7.20 (m, 1H), 2.76 (s, 3H). ¹³C NMR (63 MHz, CDCl₃) δ 154.0, 151.5, 141.4, 140.0, 137.7, 135.6, 134.1, 131.7, 130.9, 129.2, 128.9, 128.3, 128.2, 127.6, 22.5. **LC-MS** (ESI+) t_R 4.69 min; m/z [M+H]⁺ 319.75/322.54. MW: 321.22 g mol⁻¹. **HRMS (ESI):** m/z [M+H]⁺ calcd for C₁₅H₁₀Cl₂N₂S; 321.0015 Found: 321.0013.

4.1.3.4. 2-(2,4-Dichlorophenylthio)-3-methylquinoxaline (2d). Yield 80% (719 mg). Brown solid. Mp 116 °C. ¹H NMR (400 MHz, CDCl₃) δ 7.97–7.91 (m, 1H), 7.70–7.66 (m, 1H), 7.65–7.54 (m, 4H), 7.34 (dd, $J = 8.3, 2.2$ Hz, 1H), 2.80 (s, 3H). ¹³C NMR (101 MHz, CDCl₃) δ 154.0, 151.4, 141.5, 140.5, 140.0, 138.4, 136.5, 130.3, 129.2, 128.8, 128.4, 128.2, 127.8, 127.0, 22.5. **LC-MS** (ESI+) t_R 0.74 min; m/z [M+H]⁺ 320.94/322.85/325.10. MW: 321.22 g mol⁻¹. **HRMS (ESI):** m/z [M+H]⁺ calcd for C₁₅H₁₀Cl₂N₂S; 321.0015, Found: 321.0013.

4.1.3.5. 2-(2-Fluorophenylthio)-3-methylquinoxaline (2e). Yield 78% (590 mg). Brown solid. Mp 159 °C. ¹H NMR (250 MHz, CDCl₃) δ 8.03–7.85 (m, 1H), 7.69–7.47 (m, 4H), 7.28–7.20 (m, $J = 19.4$ Hz, 3H), 2.82 (s, 3H). ¹³C NMR (63 MHz, CDCl₃) δ 163.3 (d, $J = 249.6$ Hz), 154.3, 151.3, 141.5, 139.9, 137.3, 132.01 (d, $J = 8.2$ Hz), 129.1, 128.6, 128.3, 128.2, 124.8 (d, $J = 3.8$ Hz), 116.3 (d, $J = 22.9$ Hz), 115.8, 22.5. **LC-MS** (ESI+) t_R 3.90 min; m/z [M+H]⁺ 271.10. MW: 270.32 g mol⁻¹. **HRMS (ESI):** m/z [M+H]⁺ calcd for C₁₅H₁₁FN₂S; 271.0700, Found: 271.0699.

4.1.3.6. 2-(3-Fluorophenylthio)-3-methylquinoxaline (2f). Yield 95% (719 mg). Brown solid. Mp 92 °C. ¹H NMR (250 MHz, CDCl₃) δ 7.92–7.89 (m, 1H), 7.74–7.70 (m, 1H), 7.63–7.53 (m, 2H), 7.48–7.36 (m, 3H), 7.20–7.12 (m, 1H), 2.77 (s, 3H). ¹³C NMR (63 MHz, CDCl₃) δ 162.8 (d, $J = 248.5$ Hz), 155.0, 151.5, 141.4, 139.9, 130.8, 130.7 (d,

$J = 3.2$ Hz), 130.4 (d, $J = 8.3$ Hz), 129.3, 128.8, 128.3, 128.2, 122.1 (d, $J = 22.6$ Hz), 116.4 (d, $J = 21.1$ Hz), 22.5. **LC-MS** (ESI+) t_R 4.24 min; m/z [M+H]⁺ 271.26. MW: 270.32 g mol⁻¹. **HRMS** (ESI): m/z [M+H]⁺ calcd for C₁₅H₁₁FN₂S: 271.0700, Found: 271.0698.

4.1.3.7. 2-(4-Fluorophenylthio)-3-methylquinoxaline (2 g). Yield 98% (742 mg). orange solid. Mp 115 °C. **¹H NMR** (250 MHz, CDCl₃) δ 7.93 (dd, $J = 6.5, 3.2$ Hz, 1H), 7.69–7.52 (m, 5H), 7.17 (t, $J = 8.7$ Hz, 2H), 2.77 (s, 3H). **¹³C NMR** (63 MHz, CDCl₃) δ 163.6 (d, $J = 249.5$ Hz), 155.8, 151.3, 141.4, 139.8, 137.7 (d, $J = 8.5$ Hz), 129.2, 128.6, 128.2, 128.1, 123.7 (d, $J = 3.4$ Hz), 116.5 (d, $J = 22.1$ Hz), 22.4. **LC-MS** (ESI+) t_R 4.20 min; m/z [M+H]⁺ 271.24. MW: 270.32 g mol⁻¹. **HRMS** (ESI): m/z [M+H]⁺ calcd for C₁₅H₁₁FN₂S: 271.0700, Found: 271.0699.

4.1.3.8. 2-(2-Methoxyphenylthio)-3-methylquinoxaline (2h). Yield 72% (569 mg). Brown solid. Mp 138 °C. **¹H NMR** (400 MHz, CDCl₃) δ 7.93 (dd, $J = 8.1, 1.5$ Hz, 1H), 7.67–7.62 (m, 1H), 7.58 (dd, $J = 7.5, 1.6$ Hz, 1H), 7.56–7.50 (m, 2H), 7.51–7.43 (m, 1H), 7.08–6.99 (m, 2H), 3.76 (s, 3H), 2.81 (s, 3H). **¹³C NMR** (101 MHz, CDCl₃) δ 160.3, 155.3, 151.9, 141.6, 139.9, 137.0, 131.4, 128.8, 128.3, 128.1, 128.1, 121.3, 116.9, 111.8, 56.2, 22.6. **LC-MS** (ESI+) t_R 3.61 min; m/z [M+H]⁺ 283.19. MW: 282.36 g mol⁻¹. **HRMS** (ESI): m/z [M+H]⁺ calcd for C₁₆H₁₄N₂OS: 283.0900, Found: 283.0899.

4.1.3.9. 2-(3-Methoxyphenylthio)-3-methylquinoxaline (2i). Yield 100% (791 mg). orange solid. Mp 103 °C. **¹H NMR** (400 MHz, CDCl₃) δ 7.95–7.91 (m, 1H), 7.74–7.72 (m, 1H), 7.61–7.53 (m, 2H), 7.38–7.34 (m, 1H), 7.21–7.19 (m, 2H), 7.00 (m, 1H), 3.83 (s, 3H), 2.77 (s, 3H). **¹³C NMR** (101 MHz, CDCl₃) δ 160.0, 155.7, 151.8, 141.5, 139.9, 130.0, 129.8, 129.1, 128.6, 128.2, 128.2, 127.2, 120.0, 115.5, 55.6, 22.6. **LC-MS** (ESI+) t_R 4.12 min; m/z [M+H]⁺ 283.28. MW: 282.36 g mol⁻¹. **HRMS** (ESI): m/z [M+H]⁺ calcd for C₁₆H₁₄N₂OS: 283.0900, Found: 283.0898.

4.1.3.10. 2-(4-Methoxyphenylthio)-3-methylquinoxaline (2j). Yield 39% (308 mg). White solid. Mp 113 °C. **¹H NMR** (250 MHz, CDCl₃) δ 7.96–7.88 (m, 1H), 7.71–7.65 (m, 1H), 7.60–7.50 (m, 4H), 7.03–6.97 (m, 2H), 3.88 (s, 3H), 2.77 (s, 3H). **¹³C NMR** (63 MHz, CDCl₃) δ 160.7, 156.7, 151.5, 141.5, 139.8, 137.2 (2C), 129.0, 128.3, 128.2, 128.1, 119.0, 114.9 (2C), 55.5, 22.5. **LC-MS** (ESI+) t_R 4.12 min; m/z [M+H]⁺ 283.20. MW: 282.36 g mol⁻¹. **HRMS** (ESI): m/z [M+H]⁺ calcd for C₁₆H₁₄N₂OS: 283.0900, Found: 283.0901.

4.1.3.11. 2-Methyl-3-(phenylthio)quinoxaline (2k). Yield 87% (615 mg). Red solid. Mp 134 °C. **¹H NMR** (400 MHz, CDCl₃) δ 7.95–7.89 (m, 1H), 7.71–7.66 (m, 1H), 7.65–7.60 (m, 2H), 7.60–7.51 (m, 2H), 7.49–7.04 (m, 3H), 2.78 (s, 3H). **¹³C NMR** (101 MHz, CDCl₃) δ 155.8, 151.7, 141.5, 140.1, 135.3 (2C), 129.3 (2C), 129.2, 129.0, 128.9, 128.4, 128.3, 128.2, 22.6. **LC-MS** (ESI+) t_R 4.05 min; m/z [M+H]⁺ 253.28. MW: 252.33 g mol⁻¹. **Chemical Formula**: C₁₅H₁₂N₂S. **HRMS** (ESI): m/z [M+H]⁺ calcd for C₁₅H₁₂N₂S: 253.0794, Found: 253.0789.

4.1.3.12. 2-(4-Bromophenylthio)-3-methylquinoxaline (2l). Yield 99% (918 mg). White solid. Mp 121 °C. **¹H NMR** (250 MHz, CDCl₃) δ 7.95–7.91 (m, 1H), 7.72–7.68 (m, 1H), 7.61–7.54 (m, 4H), 7.49–7.46 (m, 2H), 2.77 (s, 3H). **¹³C NMR** (63 MHz, CDCl₃) δ 155.1, 151.5, 141.4, 140.1, 136.9 (2C), 132.4 (2C), 129.2, 128.6, 128.3, 128.1, 127.8, 123.8, 22.5. **LC-MS** (ESI+) t_R 4.81 min; m/z [M+H]⁺ 331.00/333.08/334.19. MW: 331.23 g mol⁻¹. **HRMS** (ESI): m/z [M+H]⁺ calcd for C₁₅H₁₁BrN₂S: 332.9879, Found: 332.9879.

4.1.3.13. 2-Methyl-3-(4-trifluoromethylphenylthio)quinoxaline (2 m). Yield 87% (780 mg). Beige solid. Mp 99 °C. **¹H NMR** (250 MHz, CDCl₃) δ 7.98–7.94 (m, 1H), 7.77–7.69 (m, 5H), 7.66–7.54 (m, 2H), 2.79 (s, 3H). **¹³C NMR** (63 MHz, CDCl₃) δ 154.5, 151.6, 141.3, 140.1,

135.1, 133.8 (q, $J = 1.5$), 131.1 (q, $J = 32.7$ Hz), 130.8, 129.3, 128.9, 128.4, 128.1, 126.2, 126.0 (q, $J = 3.7$ Hz), 124.2 (q, $J = 272.36$ Hz), 22.5. **LC-MS** (ESI+) t_R 4.70 min; m/z [M+H]⁺ 319.78. MW: 320.33 g mol⁻¹. **HRMS** (ESI): m/z [M+H]⁺ calcd for C₁₆H₁₁F₃N₂S: 321.0668, Found: 321.0663.

4.1.3.14. 2-Methyl-3-(4-trifluoromethoxyphenylthio)quinoxaline (2n). Yield 89% (838 mg). Yellow solid. Mp 81 °C. **¹H NMR** (250 MHz, CDCl₃) δ 7.94 (m, 1H), 7.71–7.62 (m, 3H), 7.62–7.54 (m, 2H), 7.31 (d, $J = 8.0$ Hz, 2H), 2.78 (s, 3H). **¹³C NMR** (63 MHz, CDCl₃) δ 155.2, 151.4, 150.0 (q, $J = 1.8$ Hz), 141.4, 140.1, 137.0 (2C), 129.2, 128.7, 128.4, 128.1, 127.2, 121.5 (2C), 120.6 (q, $J = 257.9$ Hz), 22.5. **LC-MS** (ESI+) t_R 4.97 min; m/z [M+H]⁺ no ionization. MW: 336.33 g mol⁻¹. **HRMS** (ESI): m/z [M+H]⁺ calcd for C₁₆H₁₁F₃N₂OS: 337.0617, Found: 337.0615.

4.1.3.15. 2-Methyl-3-(4-nitrophenylthio)quinoxaline (2°). Yield 86% (716 mg). Brown solid. Mp 163 °C. **¹H NMR** (250 MHz, CDCl₃) δ 8.35–8.25 (m, 2H), 8.00–7.93 (m, 1H), 7.84–7.76 (m, 2H), 7.75–7.70 (m, 1H), 7.68–7.59 (m, 2H), 2.80 (s, 3H). **¹³C NMR** (101 MHz, CDCl₃) δ 153.5, 151.7, 148.0, 141.2, 140.4, 138.2, 134.9 (2C), 129.6, 129.3, 128.5, 128.1, 124.0 (2C), 22.5. **LC-MS** (ESI+) t_R 4.26 min; m/z [M+H]⁺ 298.16. MW: 297.33 g mol⁻¹. **HRMS** (ESI): m/z [M+H]⁺ calcd for C₁₅H₁₁N₃O₂S: 298.0645, Found: 298.0645.

4.1.3.16. 2-Methyl-3-(4-tolylthio)quinoxaline (2p). Yield 74% (552 mg). Brown solid. Mp 92 °C. **¹H NMR** (400 MHz, CDCl₃) δ 7.96–7.89 (m, 1H), 7.73–7.67 (m, 1H), 7.59–7.52 (m, 2H), 7.52–7.47 (m, 2H), 7.30–7.26 (m, 2H), 2.77 (s, 3H), 2.43 (s, 3H). **¹³C NMR** (101 MHz, CDCl₃) δ 156.2, 151.7, 141.5, 139.9, 139.5, 135.3 (2C), 130.1 (2C), 128.9, 128.3, 128.3, 128.2, 125.1, 22.5, 21.5. **LC-MS** (ESI+) t_R 0.71 min; m/z [M+H]⁺ 266.66. MW: 266.36 g mol⁻¹. **HRMS** (ESI): m/z [M+H]⁺ calcd for C₁₆H₁₄N₂S: 267.0950, Found: 267.0948.

4.1.4. General procedure for the preparation of 2-thiophenoxy-3-trichloromethylquinoxaline derivatives

To a solution of 2-methyl-3-substituted quinoxaline (2a–2p) (624 mg, 2.8 mmol) and PCl₅ (2.88 g, 16.8 mmol, 1.0 equiv), POCl₃ was added to make a slurry (ca.5 mL). The mixture was then heated in a multimode microwave oven at 100 °C, 800 W for 20–30 min. After completion of the reaction, the mixture was poured into ice and was then neutralized with Na₂CO₃. The resulting solution was extracted with CH₂Cl₂ and dried with Na₂SO₄. After filtration and evaporation, the resulting solid was purified by silica gel column chromatography (eluent: Petroleum Ether/CH₂Cl₂, 9:1) to afford the desired compound.

4.1.4.1. 2-(2-Chlorophenylthio)-3-trichloromethylquinoxaline (3a). Yield 62% (675 mg). White solid. Mp 127 °C (isopropanol). **¹H NMR** (250 MHz, CDCl₃) δ 8.14–8.07 (m, 1H), 7.75–7.62 (m, 4H), 7.59–7.55 (m, 1H), 7.44 (dt, $J = 7.6, 1.9$ Hz, 1H), 7.33 (dt, $J = 7.4, 1.6$ Hz, 1H). **¹³C NMR** (63 MHz, CDCl₃) δ = 152.1, 147.4, 141.9, 139.9, 138.1, 136.8, 132.0, 131.2, 130.4, 129.8, 129.7, 129.5, 127.9, 127.5, 96.5. **LC-MS** (ESI+) t_R 5.4 min, m/z [M+H]⁺ no ionization, purity 99%. MW: 390.11 g mol⁻¹. **HRMS** m/z [M+H]⁺ calcd for C₁₅H₈Cl₄N₂S: 388.9235, Found: 388.9240.

4.1.4.2. 2-(3-Chlorophenylthio)-3-trichloromethylquinoxaline (3b). Yield 74% (437 mg). White solid. Mp 81 °C (isopropanol). **¹H NMR** (250 MHz, CDCl₃) δ 8.13–8.07 (m, 1H), 7.73–7.65 (m, 4H), 7.52 (dt, $J = 7.2, 1.6$ Hz, 1H), 7.47–7.36 (m, 2H). **¹³C NMR** (63 MHz, CDCl₃) δ = 152.4, 147.3, 141.8, 136.8, 135.4, 134.7, 133.8, 132.1, 131.6, 130.2, 129.9, 129.7, 129.6, 127.8, 96.5. **LC-MS** (ESI+) t_R 5.7 min, m/z [M+H]⁺ 378.96/380.90/386.38, purity 99%. MW: 390.11 g mol⁻¹. **HRMS** m/z [M+H]⁺ calcd for C₁₅H₈Cl₄N₂S: 388.9235, Found: 388.9235.

4.1.4.3. *2-(2,3-Dichlorophenylthio)-3-(trichloromethyl)quinoxaline (3c)*. Yield 61% (725 mg). Beige solid. Mp 91 °C (isopropanol). $^1\text{H NMR}$ (400 MHz, CDCl_3) δ 8.13–8.09 (m, 1H), 7.74–7.62 (m, 4H), 7.60 (dd, $J = 8.1, 1.5$ Hz, 1H), 7.30 (t, $J = 7.9$ Hz, 1H). $^{13}\text{C NMR}$ (101 MHz, CDCl_3) $\delta = 151.5, 147.4, 141.9, 138.1, 136.8, 136.2, 134.2, 132.2, 132.0, 131.9, 130.0, 129.8, 127.9, 127.6, 96.4$. **LC-MS** (ESI+) t_R 5.7 min, m/z $[\text{M}+\text{H}]^+$ no ionization, purity 99%. MW: 424.56 g mol $^{-1}$. HRMS m/z $[\text{M}+\text{H}]^+$ calcd for $\text{C}_{15}\text{H}_7\text{N}_2\text{SCl}_5$: 424.8816, Found: 424.8808.

4.1.4.4. *2-(2,4-Dichlorophenylthio)-3-trichloromethylquinoxaline (3d)*. Yield 46% (547 mg). Yellow solid. Mp 97 °C (isopropanol). $^1\text{H NMR}$ (400 MHz, DMSO) δ 8.13–8.04 (m, 1H), 7.77–7.63 (m, 4H), 7.58 (d, $J = 2.2$ Hz, 1H), 7.40–7.32 (m, 1H). $^{13}\text{C NMR}$ (101 MHz, DMSO) δ 151.8, 147.7, 142.1, 141.2, 139.1, 137.1, 137.0, 132.5, 130.6, 130.3, 130.1, 128.4, 128.1 (2C), 96.7. **LC-MS** (ESI+) t_R 6.07 min, m/z $[\text{M}+\text{H}]^+$ no ionization, purity 98%. MW: 424.56 g mol $^{-1}$. HRMS m/z $[\text{M}+\text{H}]^+$ calcd $\text{C}_{15}\text{H}_7\text{N}_2\text{SCl}_5$: 424.8816, Found: 424.8808.

4.1.4.5. *2-(2-Fluorophenylthio)-3-trichloromethylquinoxaline (3e)*. Yield 56% (555 mg). Beige solid. Mp 104 °C (isopropanol). $^1\text{H NMR}$ (400 MHz, CDCl_3) δ 8.11–8.06 (m, 1H), 7.70–7.61 (m, 4H), 7.53–7.47 (m, 1H), 7.26–7.19 (m, 2H). $^{13}\text{C NMR}$ (101 MHz, CDCl_3) $\delta = 163.3$ (d, $J = 250.0$ Hz), 151.7, 147.3, 141.9, 137.4, 136.8, 132.2 (d, $J = 8.2$ Hz), 132.0, 129.8, 129.7, 127.8, 124.8 (d, $J = 3.8$ Hz), 117.3 (d, $J = 18.8$ Hz), 116.2 (d, $J = 22.8$ Hz), 96.5. **LC-MS** (ESI+) t_R 5.2 min, m/z $[\text{M}+\text{H}]^+$ no ionization, purity 99%. MW: 353.66 g mol $^{-1}$. HRMS m/z $[\text{M}+\text{H}]^+$ calcd for $\text{C}_{15}\text{H}_8\text{N}_2\text{FSCl}_3$: 374.9502, Found: 374.9492.

4.1.4.6. *2-(3-Fluorophenylthio)-3-trichloromethylquinoxaline (3f)*. Yield 63% (659 mg). Beige solid. Mp 57 °C (isopropanol). $^1\text{H NMR}$ (400 MHz, CDCl_3) δ 8.12–8.06 (m, 1H), 7.73–7.64 (m, 3H), 7.45–7.40 (m, 3H), 7.22–7.15 (m, 1H). $^{13}\text{C NMR}$ (101 MHz, CDCl_3) $\delta = 162.6$ (d, $J = 248.9$ Hz), 152.3, 147.2, 141.6, 136.6, 131.9, 131.7 (d, $J = 8.0$ Hz), 131.2 (d, $J = 3.0$ Hz), 130.3 (d, $J = 8.1$ Hz), 129.8, 129.6, 127.65, 122.5 (d, $J = 22.3$ Hz), 116.5 (d, $J = 21.0$ Hz), 96.5. **LC-MS** (ESI+) t_R 5.4 min, m/z $[\text{M}+\text{H}]^+$ no ionization, purity 99%. MW: 373.66 g mol $^{-1}$. HRMS m/z $[\text{M}+\text{H}]^+$ calcd for $\text{C}_{15}\text{H}_8\text{N}_2\text{SFCl}_3$: 374.9502, Found: 374.9495.

4.1.4.7. *2-(4-Fluorophenylthio)-3-trichloromethylquinoxaline (3g)*. Yield 51% (534 mg). Yellow solid. Mp 76 °C (isopropanol). $^1\text{H NMR}$ (400 MHz, CDCl_3) δ 8.09–8.08 (m, 1H), 7.69–7.61 (m, 5H), 7.18 (t, $J = 8.6$ Hz, 2H). $^{13}\text{C NMR}$ (101 MHz, CDCl_3) $\delta = 163.6$ (d, $J = 250.0$ Hz), 153.1, 147.1, 141.7, 138.1 (d, $J = 8.6$ Hz) (2C), 136.6, 131.9, 129.6, 127.6, 124.8 (d, $J = 3.4$ Hz), 116.4 (d, $J = 22.0$ Hz) (2C), 96.6. **LC-MS** (ESI+) t_R 5.4 min, m/z $[\text{M}+\text{H}]^+$ no ionization, purity 99%. MW: 373.66 g mol $^{-1}$. HRMS m/z $[\text{M}+\text{H}]^+$ calcd for $\text{C}_{15}\text{H}_8\text{N}_2\text{SFCl}_3$: 374.9502, Found: 374.9494.

4.1.4.8. *2-(2-Methoxyphenylthio)-3-trichloromethylquinoxaline (3h)*. Yield 64% (691 mg). Yellow solid. Mp 96 °C (isopropanol). $^1\text{H NMR}$ (400 MHz, CDCl_3) δ 8.10–8.06 (m, 1H), 7.65–7.61 (m, 4H), 7.48 (td, $J = 8.2, 1.6$ Hz, 1H), 7.05 (td, $J = 7.5, 0.9$ Hz, 1H), 7.00 (d, $J = 8.2$ Hz, 1H), 3.69 (s, 3H). $^{13}\text{C NMR}$ (101 MHz, CDCl_3) $\delta = 160.1, 152.9, 147.6, 142.0, 137.1, 136.6, 131.8, 131.6, 129.7, 129.4, 127.7, 121.2, 118.4, 111.6, 96.7, 56.1$. **LC-MS** (ESI+) t_R 5.1 min, m/z $[\text{M}+\text{H}]^+$ no ionization, purity 99%. MW: 385.70 g mol $^{-1}$. HRMS m/z $[\text{M}+\text{H}]^+$ calcd for $\text{C}_{16}\text{H}_{11}\text{N}_2\text{OSCl}_3$: 386.9702, Found: 386.9698.

4.1.4.9. *2-(2-Chloro-5-methoxyphenylthio)-3-trichloromethylquinoxaline (3i)*. Yield 15% (176 mg). Yellow solid. Mp 144 °C (isopropanol). $^1\text{H NMR}$ (250 MHz, CDCl_3) δ 8.16–8.06 (m, 1H), 7.77–7.63 (m, 3H), 7.51–7.40 (m, 1H), 7.27 (d, $J = 3.0$ Hz, 1H), 6.98 (dd, $J = 8.8, 3.0$ Hz, 1H), 3.84 (s, 3H). $^{13}\text{C NMR}$ (63 MHz, CDCl_3) $\delta = 158.51, 151.94, 147.40, 141.97, 136.80, 132.06, 131.06, 130.74, 130.07, 129.84, 129.77, 127.93, 122.66, 117.23, 96.54, 55.89$. **LC-MS**

(ESI+) t_R 7.4 min, m/z $[\text{M}+\text{H}]^+$ no ionization, purity = 99%. MW: 420.14 g mol $^{-1}$. HRMS m/z $[\text{M}+\text{H}]^+$ calcd for $\text{C}_{16}\text{H}_{10}\text{Cl}_4\text{N}_2\text{OS}$: 420.9312, Found: 420.9312.

4.1.4.10. *2-(4-Methoxyphenylthio)-3-trichloromethylquinoxaline (3j)*. Yield 59% (637 mg). Yellow solid. Mp 149 °C (isopropanol). $^1\text{H NMR}$ (250 MHz, CDCl_3) δ 8.10–8.05 (m, 1H), 7.72–7.63 (m, 3H), 7.55 (dt, $J = 2.5; 9.0$ Hz, 2H), 6.99 (dt, $J = 2.6; 8.8$ Hz, 2H), 3.89 (s, 3H). $^{13}\text{C NMR}$ (63 MHz, CDCl_3) $\delta = 160.8, 154.1, 147.2, 141.9, 137.7$ (2 C), 136.7, 131.9, 129.7, 129.5, 127.8, 120.2, 114.9 (2 C), 96.7, 55.5. **LC-MS** (ESI+) t_R 5.4 min, m/z $[\text{M}+\text{H}]^+$ no ionization, purity = 99%. MW: 385.70 g mol $^{-1}$. HRMS m/z $[\text{M}+\text{H}]^+$ calcd for $\text{C}_{16}\text{H}_{11}\text{N}_2\text{OSCl}_3$: 386.9702, Found: 386.9699.

4.1.4.11. *2-(Phenylthio)-3-trichloromethylquinoxaline (3k)*. Yield 71% (707 mg). Beige solid. Mp 66 °C (isopropanol). $^1\text{H NMR}$ (400 MHz, CDCl_3) δ 8.12–8.07 (m, 1H), 7.72–7.67 (m, 3H), 7.66–7.62 (m, 2H), 7.48–7.46 (m, 3H). $^{13}\text{C NMR}$ (101 MHz, CDCl_3) $\delta = 153.4, 147.4, 141.9, 136.8, 135.8$ (3 C), 131.9, 129.9, 129.7, 129.4, 129.3 (2 C), 127.8, 96.7. **LC-MS** (ESI+) t_R 5.3 min, m/z $[\text{M}+\text{H}]^+$ no ionization, purity 98%. MW: 355.67 g mol $^{-1}$. HRMS m/z $[\text{M}+\text{H}]^+$ calcd for $\text{C}_{15}\text{H}_9\text{N}_2\text{SCl}_3$: 356.9596, Found: 356.9594.

4.1.4.12. *2-(4-Bromophenylthio)-3-trichloromethylquinoxaline (3l)*. Yield 44% (535 mg). Beige solid. Mp 96 °C (isopropanol). $^1\text{H NMR}$ (250 MHz, CDCl_3) δ 8.14–8.06 (m, 1H), 7.74–7.66 (m, 3H), 7.62–7.56 (m, 2H), 7.51–7.46 (m, 2H). $^{13}\text{C NMR}$ (101 MHz, CDCl_3) $\delta = 152.6, 147.3, 141.8, 137.4$ (2 C), 136.8, 132.4 (2 C), 132.1, 129.9, 129.7, 128.9, 127.8, 124.1, 96.5. **LC-MS** (ESI+) t_R 5.8 min, m/z $[\text{M}+\text{H}]^+$ no ionization, purity 99%. MW: 434.57 g mol $^{-1}$. HRMS m/z $[\text{M}+\text{H}]^+$ calcd for $\text{C}_{15}\text{H}_8\text{N}_2\text{SCl}_3\text{Br}$: 434.8705, Found: 434.8701.

4.1.4.13. *2-Trichloromethyl-3-(4-trifluoromethylphenylthio)quinoxaline (3m)*. Yield 80% (949 mg). Yellow solid. Mp 102 °C (isopropanol). $^1\text{H NMR}$ (250 MHz, CDCl_3) δ 8.23–7.96 (m, 1H), 7.86–7.54 (m, 7H). $^{13}\text{C NMR}$ (63 MHz, CDCl_3) $\delta = 152.0, 147.5, 141.8, 136.9, 135.6, 134.9$ (d, $J = 1.4$ Hz), 132.3, 131.3 (q, $J = 32.7$ Hz), 130.2, 129.8, 127.8, 126.0 (q, $J = 3.7$ Hz), 124.1 (q, $J = 27.2$ Hz), 96.5. **LC-MS** (ESI+) t_R 5.38 min, m/z $[\text{M}+\text{H}]^+$ no ionization. MW: 423.67 g mol $^{-1}$, purity 99%. HRMS m/z $[\text{M}+\text{H}]^+$ calcd for $\text{C}_{16}\text{H}_8\text{Cl}_3\text{F}_3\text{N}_2\text{S}$: 424.9470, Found: 424.9468.

4.1.4.14. *2-Trichloromethyl-3-(4-trifluoromethoxyphenylthio)quinoxaline (3n)*. Yield 68% (837 mg). Yellow oil. $^1\text{H NMR}$ (250 MHz, CDCl_3) δ 8.16–8.06 (m, 1H), 7.76–7.62 (m, 5H), 7.36–7.28 (m, 2H). $^{13}\text{C NMR}$ (63 MHz, CDCl_3) $\delta = 152.7, 150.2$ (q, $J = 1.7$ Hz), 147.4, 141.8, 137.5 (2C), 136.8, 132.2, 129.9, 129.8, 128.3, 127.8, 121.5 (2C), 120.6 (q, $J = 258.0$ Hz), 96.5. **LC-MS** (ESI+) t_R 6.1 min, m/z $[\text{M}+\text{H}]^+$ no ionization. MW: 439.67 g mol $^{-1}$, purity 99%. HRMS m/z $[\text{M}+\text{H}]^+$ calcd for $\text{C}_{16}\text{H}_8\text{Cl}_3\text{F}_3\text{N}_2\text{OS}$: 438.9448, Found: 438.9447.

4.1.4.15. *2-(4-Nitrophenylthio)-3-trichloromethylquinoxaline (3°)*. Yield 64% (718 mg). White solid. Mp 161 °C (isopropanol). $^1\text{H NMR}$ (250 MHz, CDCl_3) δ 8.34–8.23 (m, 2H), 8.20–8.10 (m, 1H), 7.88–7.67 (m, 5H). $^{13}\text{C NMR}$ (63 MHz, CDCl_3) $\delta = 151.1, 148.1, 147.7, 141.8, 139.2, 137.1, 135.4$ (2C), 132.6, 130.6, 129.9, 127.7, 124.1 (2C), 96.3. **LC-MS** (ESI+) t_R 4.9 min, m/z $[\text{M}+\text{H}]^+$ no ionization. MW: 400.67 g mol $^{-1}$, purity 99%. HRMS m/z $[\text{M}+\text{H}]^+$ calcd for $\text{C}_{15}\text{H}_8\text{Cl}_3\text{N}_3\text{O}_2\text{S}$: 401.9447, Found: 401.9447.

4.1.4.16. *2-(4-Tolylthio)-3-trichloromethylquinoxaline (3p)*. Yield 40% (414 mg). Yellow solid. Mp 99 °C (isopropanol). $^1\text{H NMR}$ (400 MHz, CDCl_3) δ 8.13–8.04 (m, 1H), 7.76–7.64 (m, 3H), 7.56–7.46 (m, 2H), 7.30–7.23 (m, 2H), 2.44 (s, 3H). $^{13}\text{C NMR}$ (101 MHz, CDCl_3) $\delta = 153.7, 147.4, 142.0, 139.7, 136.7, 135.8$ (2C), 131.9, 130.1 (2C),

129.7, 129.6, 127.8, 126.2, 96.7, 21.6. **LC-MS** (ESI+) t_R 5.67 min, m/z [M+H]⁺+368.18/371.01/373.05. MW: 369.70 g mol⁻¹, purity 99%. **HRMS** m/z [M+H]⁺ calcd for C₁₆H₁₁Cl₃N₂S: 370.9753, Found: 370.9752.

4.1.5. General procedure for compounds 3q–3s

4.1.5.1. Preparation of 2-chloro-3-(trifluoromethyl)quinoxaline (3q)

Step 1 To a solution of *o*-phenylenediamine (2 g, 18.5 mmol, 1.0 equiv) in H₂O was added ethyl trifluoropyruvate (3 g 146, 18.5 mmol, 1.0 equiv) dissolved in H₂O (30 mL). The reaction mixture was heated at 50 °C for 15 min. After cooling, the precipitate was filtered off and washed with H₂O. 3-(Trifluoromethyl)quinoxalin-2(1H)-one was recrystallized from ethanol, precipitating as a white solid and engaged directly in step 2. Yield 93%.

Step 2 3-(Trifluoromethyl)quinoxalin-2-ol (3.5 g, 16.8 mmol, 1.0 equiv) was heated to reflux in phosphorus oxychloride (30 mL) for 2 h. After the starting material was consumed, the reaction mixture was cooled to r.t. and then quenched with ice at 0 °C. The precipitate was purified by flash chromatography, to afford 2-chloro-3-(trifluoromethyl)quinoxaline (3q) as a white solid, yield 96%. Mp 140 °C. **¹H NMR (400 MHz, CDCl₃)** δ 8.25–8.20 (m, 1H), 8.15–8.09 (m, 1H), 7.99–7.86 (m, 2H). NMR was consistent with description [44].

4.1.5.2. Preparation of compounds (3r, 3s). To a solution of 2-chloroquinoxaline or 2-chloro-3-(trifluoromethyl)quinoxaline (300 mg, 1.3 mmol, 1.0 equiv.) and thiophenol reagent (143 mg, 1.3 mmol, 1.0 equiv.) in anhydrous DMF (5 mL), Cs₂CO₃ (1.0 equiv.) was added under inert atmosphere. The mixture was stirred at 70 °C overnight. After completion of the reaction, water was added, leading to a precipitate which was separated by filtration. The resulting precipitate was then thoroughly washed with water. The resulting solid was purified by silica gel column chromatography (eluent: Cyclohexane/CH₂Cl₂, 4:6) to afford the desired compound.

4.1.5.2.1. 2-(Phenylthio)quinoxaline (3r). Yield 90% (279 mg). orange solid. Mp 88 °C (isopropanol). **¹H NMR (400 MHz, CDCl₃)** δ 8.44 (s, 1H), 7.99 (dd, *J* = 8.2, 1.4 Hz, 1H), 7.90 (dd, *J* = 8.3, 1.3 Hz, 1H), 7.73–7.60 (m, 4H), 7.50–7.44 (m, 3H). **¹³C NMR (101 MHz, CDCl₃)** δ = 157.3, 143.6, 142.3, 140.0, 135.1 (2C), 130.6, 129.9 (2C), 129.8, 129.3, 129.1, 128.9, 128.4. **LC-MS** (ESI+) t_R 3.4 min, m/z [M+H]⁺ 239.16. MW: 238.31 g mol⁻¹, purity 99%. **HRMS** m/z [M+H]⁺ calcd for C₁₄H₁₀N₂S: 239.0637, Found: 239.0638.

4.1.5.2.2. 2-(Phenylthio)-3-(trifluoromethyl)quinoxaline (3s). Yield 89% (354 mg). white solid. Mp 93 °C (isopropanol). **¹H NMR (400 MHz, CDCl₃)** δ 8.14–8.07 (m, 1H), 7.75–7.67 (m, 3H), 7.66–7.61 (m, 2H), 7.51–7.45 (m, 3H). **¹³C NMR (101 MHz, CDCl₃)** δ = 153.5, 143.0, 139.8 (q, *J* = 35.8 Hz), 137.9, 136.0 (2C), 132.5, 129.8, 129.4 (2C), 129.2, 128.3, 127.9 (d, *J* = 1.9 Hz), 121.2 (q, *J* = 276.0 Hz). **LC-MS** (ESI+) t_R 6.8 min, m/z [M+H]⁺ 307.07. MW: 306.31 g mol⁻¹, purity 99%. **HRMS** m/z [M+H]⁺ calcd for C₁₅H₉F₃N₂S: 307.0511, Found: 307.0511.

4.2. Biology

4.2.1. In vitro cytotoxicity evaluation HepG2

HepG2 cell line was maintained at 37 °C, 5% CO₂, at 90% humidity in MEM supplemented with 10% fetal bovine serum, 1% L-glutamine (200 mM) and penicillin (100 U/mL)/streptomycin (100 µg/mL) (complete RPMI medium). The cytotoxicity of the

tested molecules on the HepG2 (hepatocarcinoma cell line purchased from ATCC, ref HB-8065) cell line was assessed according to the method of Mosmann [45] with slight modifications. Briefly, 5.103 cells in 100 µL of complete medium were inoculated into each well of 96-well plates and incubated at 37 °C in humidified 5% CO₂. After 24 h incubation, 100 µL of medium with various product concentrations dissolved in DMSO (final concentration less than 0.5% v/v) were added and the plates were incubated for 72 h at 37 °C. Triplicate assays were performed for each sample. Each plate-well was then microscope examined for possible precipitate formation before the medium was aspirated from the wells. 100 µL of MTT (3-(4,5-dimethyl-2-thiazolyl)-2,5-diphenyl-2H-tetrazolium bromide) solution (0.5 mg/mL in medium without FBS) were then added to each well. Cells were incubated for 2 h at 37 °C. After this time, the MTT solution was removed and DMSO (100 µL) was added to dissolve the resulting blue formazan crystals. Plates were shaken vigorously (700 rpm) for 10 min. The absorbance was measured at 570 nm with 630 nm as reference wavelength using a BIO-TEK ELx808 Absorbance Microplate Reader (LabX, Midland, ON, Canada). DMSO was used as blank and doxorubicin (purchased from Sigma Aldrich) as positive control. Cell viability was calculated as percentage of control (cells incubated without compound). The 50% cytotoxic concentration (CC₅₀) was determined from the dose–response curve, using TableCurve software 2D v.5.0. CC₅₀ values represent the mean value calculated from three independent experiments.

4.2.2. In vitro cytotoxicity evaluation CHO

CHO cell line was maintained at 37 °C, 5% CO₂ with 90% humidity in RPMI supplemented with 10% foetal bovine serum, 1% L-glutamine (200 mM) and penicillin (100 U/mL)/streptomycin (100 µg/mL) (complete RPMI medium). The evaluation of the tested molecules cytotoxicity on the CHO cell line (purchased from ATCC, ref CCL-61) was performed according to the method of Mosmann with slight modifications. Briefly, 5.10³ cells in 100 µL of complete medium were inoculated into each well of 96-well plates and incubated at 37 °C in a humidified 5% CO₂. After 24 h incubation, 100 µL of medium with various product concentrations dissolved in DMSO (final concentration less than 0.5% v/v) were added and the plates were incubated for 24 h at 37 °C. Triplicate assays were performed for each sample. Each plate-well was then microscope-examined for detecting possible precipitate formation before the medium was aspirated from the wells. 100 µL of MTT (3-(4,5-dimethyl-2-thiazolyl)-2,5-diphenyl-2H-tetrazolium bromide) solution (0.5 mg/mL in medium without FCS) were then added to each well. Cells were incubated for 2 h at 37 °C. After this time, the MTT solution was removed and DMSO (100 µL) was added to dissolve the resulting blue formazan crystals. Plates were shaken vigorously (700 rpm) for 10 min. The absorbance was measured at 570 nm with 630 nm as reference wavelength using a BIO-TEK ELx808 Absorbance Microplate Reader. DMSO was used as blank and doxorubicin (purchased from Sigma Aldrich) as positive control. Cell viability was calculated as percentage of control (cells incubated without compound). The 50% cytotoxic concentration (CC₅₀) was determined from the dose–response curve by using the TableCurve software 2D v.5.0. CC₅₀ values represent the mean value calculated from three independent experiments.

4.2.3. In vitro cytotoxicity evaluation VERO

VERO cell line was maintained at 37 °C, 5% CO₂ with 90% humidity in MEM supplemented with 10% foetal bovine serum, 1% L-glutamine (200 mM) and penicillin (100 U/mL)/streptomycin (100 µg/mL) (complete MEM medium). The evaluation of the tested molecules cytotoxicity on the VERO cell line (purchased from ATCC, ref CRL-1586) was performed according to the method of Mosmann

with slight modifications. Briefly, 5.10^3 cells in 100 μL of complete medium were inoculated into each well of 96-well plates and incubated at 37 °C in a humidified 5% CO_2 . After 24 h incubation, 100 μL of medium with various product concentrations dissolved in DMSO (final concentration less than 0.5% v/v) were added and the plates were incubated for 48 h at 37 °C. Triplicate assays were performed for each sample. Each plate-well was then microscope-examined for detecting possible precipitate formation before the medium was aspirated from the wells. 100 μL of MTT (3-(4,5-dimethyl-2-thiazolyl)-2,5-diphenyl-2H-tetrazolium bromide) solution (0.5 mg/mL in medium without FCS) were then added to each well. Cells were incubated for 2 h at 37 °C. After this time, the MTT solution was removed and DMSO (100 μL) was added to dissolve the resulting blue formazan crystals. Plates were shaken vigorously (700 rpm) for 10 min. The absorbance was measured at 570 nm with 630 nm as reference wavelength using a BIO-TEK ELx808 Absorbance Microplate Reader. DMSO was used as blank and doxorubicin (purchased from Sigma Aldrich) as positive control. Cell viability was calculated as percentage of control (cells incubated without compound). The 50% cytotoxic concentration (CC_{50}) was determined from the dose–response curve by using the TableCurve software 2D v.5.0. CC_{50} values represent the mean value calculated from three independent experiments.

4.2.4. In vitro antiplasmodial evaluation

In this study, a K1 culture-adapted *P. falciparum* strain resistant to chloroquine, pyrimethamine, and proguanil was used in an *in vitro* culture. It was maintained in continuous culture as described previously by Trager and Jensen [46]. Cultures were maintained in fresh A+ human erythrocytes at 2.5% hematocrit in complete medium (RPMI 1640 with 25 mM HEPES, 25 mM NaHCO_3 , 10% of A+ human serum) at 37 °C under reduced O_2 atmosphere (gas mixture 10% O_2 , 5% CO_2 , and 85% N_2). Parasitemia was maintained daily at between 1 and 3%. The *P. falciparum* drug susceptibility test was carried out by comparing quantities of DNA in treated and control cultures of parasite in human erythrocytes according to an SYBR Green I fluorescence-based method [47] using a 96-well fluorescence plate reader. Compounds, previously dissolved in DMSO (final concentration less than 0.5% v/v), were incubated in a total assay volume of 200 μL (RPMI, 2% hematocrit and 0.4% parasitemia) for 72 h in a humidified atmosphere (10% O_2 and 5% CO_2) at 37 °C, in 96-well flat bottom plates. Duplicate assays were performed for each sample. After incubation, plates were frozen at -20 °C for 24 h. Then, the frozen plates were thawed for 1 h at 37 °C. Fifteen μL of each sample were transferred to 96-well flat bottom non-sterile black plates (Greiner Bio-one) already containing 15 μL of the SYBR Green I lysis buffer (2X SYBR Green I, 20 mM Tris base pH 7.5, 20 mM EDTA, 0.008% w/v saponin, 0.08% w/v Triton X-100). Negative control treated by solvents (DMSO or H_2O) and positive controls (chloroquine and doxycycline) were added to each set of experiments. Plates were incubated for 15 min at 37 °C and then read on a TECAN Infinite F-200 spectrophotometer with excitation and emission wavelengths at 485 and 535 nm, respectively. The concentrations of compounds required to induce a 50% decrease of parasite growth (EC_{50} K1) were calculated from three independent experiments.

4.2.5. Comet assay

4.2.5.1. Cell culture and treatment. The human hepatocarcinoma cell line HepG2 was obtained from the American Type Culture Collection (ATCC, ref. HB-8065). Cells were cultured in Eagle's Minimum Essential Medium (EMEM, ref. ATCC® 30-2003TM) supplemented with 10% heat-inactivated foetal bovine serum, 100 U/mL penicillin and 0.1 mg/mL streptomycin (all from Gibco). Cells were maintained at 37 °C in a humidified atmosphere with 5% CO_2 .

Cells were used in passage number 11 to 15. Two concentrations of the compound **3k** (5.6 and 28 μM) were tested for 2 different times of incubation (2 and 72 h). Briefly, HepG2 cells were seeded at 1.13×10^5 cells/mL in 6-well plates (3 mL of cell suspension per well) and incubated at 37 °C in a humidified atmosphere with 5% CO_2 . After 24 and 94 h of incubation, cells were treated with different concentrations of the compound or the vehicle (0.5% dimethylsulfoxide, DMSO) for 72 and 2 h, respectively. Additionally, in the 2 h treatment plate, cells in an additional well were treated with 1 mM MMS as positive control for the comet assay. After treatment, medium was removed from the wells and cells were washed with phosphate buffered saline (PBS). Finally, cells were trypsinized and trypsin was neutralized with fresh medium. From this point, cells were kept ice-cold to avoid DNA repair.

4.2.5.2. Comet assay. The standard alkaline comet assay was employed for the detection of DNA strand breaks (SBs) and alkali-labile sites (ALS) in cells treated with molecule **3k**. Trypsinized HepG2 cells were centrifuged at 125 g for 5 min at 4 °C and resuspended in cold PBS at 1×10^6 cells/mL. For the preparation of the agarose gels, 30 μL of cell suspension were mixed with 140 μL of 1% low melting point agarose in PBS at 37 °C and 2 aliquots of 70 μL of cell/agarose mixture were placed on agarose-precoated microscope slides. Each droplet was covered with a 20×20 mm coverslip and after 2–3 min on a cold metal plate, the coverslips were removed. Then, slides were immersed in lysis solution (2.5 M NaCl, 0.1 M Na_2EDTA , 0.01 M Tris base, pH 10, and 1% Triton X-100) at 4 °C for 1 h. After lysis, slides were transferred to the electrophoresis tank and incubated for 40 min at 4 °C in the electrophoresis solution (0.3 M NaOH, 1 mM Na_2EDTA , pH>13) to allow DNA unwinding. After that, electrophoresis was carried out at 1 V/cm for 20 min (4 °C). Then, gels were neutralized and washed by immersing the slides in PBS for 10 min and distilled water for another 10 min (both at 4 °C). Gels were then air dried at room temperature. Comets were stained by adding 30 μL of 1 mg/mL of 4,6-diamidino-2-phenylindole (DAPI) on top of each gel and placing 22×22 mm coverslips on top. Slides were incubated with DAPI at room temperature for 30 min before the analysis. The semiautomated image analysis system Comet Assay IV (Instem) was used to evaluate 50 comets per gel (i.e., 100/condition). The percentage of DNA in tail was the descriptor used for each comet.

4.2.5.3. Statistics. The median percentage of DNA in tail for 50 comets was calculated for each of the duplicate gels in each experiment, and the mean of the two medians was then calculated. The mean percentage of DNA in tail of 3 independent experiments and the standard deviation (SD) were calculated.

4.2.6. Apicoplast

4.2.6.1. Culturing Plasmodium-infected red blood cells. *Plasmodium falciparum* blood stage parasites were maintained at 2% hematocrit in 1640 RPMI-HEPES supplemented with 5% AlbuMAX II (GIBCO) and 0.25% gentamycin. Parasites were grown sealed Perspex chambers gassed with beta mix gas (1% O_2 , 5% CO_2 and 94% N_2) at 37 °C and maintained on 48-h cycles. Cultures were tightly synchronized at ring stage using sorbitol treatment (5% v/v) as previously described [31].

4.2.6.2. IFA on treated parasites. Prior to the treatment parasites are synchronized using 5% sorbitol. After 48h treatment (0.3 μM of (**3k**) molecule, 0.3 μM of (**2a**) molecule or DMSO) parasites are fixed using 4% paraformaldehyde (PFA) and 0.0075% glutaraldehyde for 30 min at room temperature. Fixing solution is washed 3x times with PBS and cells are permeabilized with 0.1% TX-100 for 10 min at room temperature. Permeabilization solution is washed 3x times

with PBS and cells are blocked with 3% fetal bovine serum (FBS) for 1 h. Primary antibody (Rat IgG anti-HA, Roche, 1/500 in 3% FBS) is incubated 1h at room temperature. Primary antibody is washed out 3x times with PBS and cells are incubated with secondary antibody (Alexa Fluor 488 goat anti-mouse IgG, Invitrogen, 1/1000 in 3% FBS) for 1h at room temperature. Secondary antibody is washed out 3x times with PBS and cells are incubated with DAPI, 1/25000 in PBS. Samples are fixed between a slide and a coverslip with fluorogel and observed by epi-fluorescent microscopy.

4.2.6.3. Growth assay. To observe a potential effect of delayed death of the molecule on the parasite, *Plasmodium* is maintained on Three life cycles (48h). At 48 h, 96 h and 144 h, 100 μ L of cultures are transferred into a 96 wells black wall flat bottom plate and mixed with 100 μ L SYBR Green lysis buffer (20 mM Tris, pH 7.5; 5 mM EDTA; 0.008% (w/v) saponin; 0.08% (v/v) Triton X-100) with freshly added SYBR Green I (10000X), and incubated 1h at room temperature protected from the light. Fluorescence from each well is measured with TECAN infinite M200 plate reader (excitation: 485 nm, emission: 538 nm and integration time: 1000 μ s). The rest of the cultures are diluted 1/10 as the untreated cultures. Graph is obtain by doing the ration the treated culture fluorescence intensity on the untreated culture fluorescence intensity (n = 3).

4.2.7. Study on the liver stage

4.2.7.1. Parasite strain and sporozoites isolation. *P. falciparum* (NF135 strain) sporozoites were isolated by dissection of the salivary glands of infected *A. stephensi* 14–21 days after an infective blood meal (Department of medical microbiology, University Medical Centre, St Radboud, Nijmegen Netherland). All infected salivary glands were removed by hand dissection and crushed in a potter for sporozoites isolation and filtrated through a 40 μ m filter to remove mosquito debris (Cell Strainer, BD BioSciences, USA). The sporozoites were counted using a disposable Glasstic microscope slide (KOVA, USA).

4.2.7.2. Primary hepatocytes culture. Conserved primary human hepatocytes were purchased from Biopredic International (France). Cells were seeded in 96-well plates (Falcon by Becton Dickinson Labware Europe, France) coated with collagen I (BD Bioscience, USA), at a density of 80 000 cells per well. They are cultured at 37 °C in 5% CO₂ in William's E medium (Gibco, Life Technologies, Saint Aubin, France) supplemented with 10% of Foetal Bovine Serum FCIII, 5 \times 10⁻⁵ M hydrocortisone hemisuccinate (Upjohn Laboratoires SERB, France), 5 μ g per ml Insulin (Sigma Aldrich, USA), 2 mM L-glutamine, and 0.02 U per ml – 0.02 μ g per ml penicillin – streptomycin (Life Technologies) until infection with sporozoites.

4.2.7.3. In vitro infection and drug assays. *P. falciparum* sporozoites were re-suspended in the above complete medium used for hepatocytes culture. Cultured human hepatocytes were inoculated with *P. falciparum* sporozoites (30,000 sporozoites/well of 96 well plates each) in 50 μ L of complete media. The infected culture plate was centrifuged 10 min at 2000 rpm to allow fast parasite sedimentation onto the target cells and further incubated with serial dilution of drugs that were prepared in advance. After 3 h incubation, cultures were washed and further incubated in fresh medium containing the appropriate drug concentration which were changed daily until cells fixation at day 6 post infection with 4%PFA for 20 min at room temperature.

The exo-erythrocytic forms (EEFs) were stained using the anti-HSP70 serum for *P. falciparum* and revealed with an Alexa 488-conjugated goat anti-mouse immunoglobulin (Molecular Probes). Host cell and parasite nuclei were labelled with 4',6-diamidino-2-phenylindole (DAPI). The EEFs were counted under a fluorescence

microscope (Leica DMI4000B) or by using a CellInsight High Content Screening platform equipped with the Studio HCS software (Thermo Fisher, Scientific). To investigate the effect of drugs inhibition on the apicoplast maturation during liver-stage development, the EEFs were stained using Acyl carrier protein (ACP) antibody and revealed with an Alexa Fluor 680-conjugated goat anti-rabbit immunoglobulin (Molecular Probes), and then imaged using a confocal microscope (Olympus FV1200). The images were analyzed using ImageJ software.

4.2.7.4. Data analysis. GraphPad Prism 7 statistical Software (GraphPad. Software, San Diego, CA, USA) were used for data analysis and graphing. All values were expressed as means and standard deviations (SD).

Funding

Work was supported by the French Agence Nationale de la Recherche [grant number ANR-17-CE11-0017]; the Fondation pour la Recherche Médicale [grant number DCM20181039565].

Declaration of competing interest

The authors declare that they have no known competing financial interests or personal relationships that could have appeared to influence the work reported in this paper.

Appendix A. Supplementary data

Supplementary data to this article can be found online at <https://doi.org/10.1016/j.ejmech.2021.113722>.






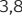

References

- [1] World Health Organization (WHO), World Malaria Report, 2020. <https://www.who.int/publications-detail-redirect/world-malaria-report-2020>. (Accessed 8 January 2021).
- [2] J.F. Trape, The public health impact of chloroquine resistance in Africa, *Am. J. Trop. Med. Hyg.* 64 (2001) 12–17, <https://doi.org/10.4269/ajtmh.2001.64.12>.
- [3] M.I. Veiga, S.K. Dhingra, P.P. Henrich, J. Straimer, Gna' dig, N., A.-C. Uhlemann, R.E. Martin, A.M. Lehane, D.A. Fidock, Globally prevalent PfMDR1 mutations modulate *Plasmodium falciparum* susceptibility to artemisinin-based combination therapies, *Nat. Commun.* 7 (2016) 11553, <https://doi.org/10.1038/ncomms11553>.
- [4] A.B. Vaidya, M.W. Mather, Atovaquone resistance in malaria parasites, *Drug Resist. Updates* 3 (2000) 283–287, <https://doi.org/10.1054/drup.2000.0157>.
- [5] A.C. Uhlemann, S. Krishna, Antimalarial multi-drug resistance in Asia: mechanisms and assessment, *Curr. Top. Microbiol. Immunol.* 295 (2005) 39–53, https://doi.org/10.1007/3-540-29088-5_2.
- [6] R.T. Eastman, N.V. Dharia, E.A. Winzeler, D.A. Fidock, Piperaquine resistance is associated with a copy number variation on chromosome 5 in drug-pressured *Plasmodium falciparum* parasites, *Antimicrob. Agents Chemother.* 55 (2011) 3908–3916, <https://doi.org/10.1128/AAC.01793-10>.
- [7] C.V. Plowe, Monitoring antimalarial drug resistance: making the most of the tools at hand, *J. Exp. Biol.* 206 (2003) 3745–3752, <https://doi.org/10.1242/jeb.00658>.
- [8] C.H. Sibley, J.E. Hyde, P.F. Sims, C.V. Plowe, J.G. Kublin, E.K. Mberu, A.F. Cowman, P.A. Winstanley, W.M. Watkins, A.M. Nzila, Pyrimethamine-sulfadoxine resistance in *Plasmodium falciparum*: what next? *Trends Parasitol.* 17 (2001) 582–588, [https://doi.org/10.1016/s1471-4922\(01\)02085-2](https://doi.org/10.1016/s1471-4922(01)02085-2).
- [9] D. Menard, A. Dondorp, Antimalarial drug resistance: a threat to malaria elimination, *Cold. Spring. Harb. Perspect. Med.* (2017), <https://doi.org/10.1101/cshperspect.a025619>, 7:a025619.
- [10] F. Lu, R. Culleton, M. Zhang, A. Ramaprasad, L. von Seidlein, H. Zhou, G. Zhu, J. Tang, Y. Liu, W. Wang, Y. Cao, S. Xu, Y. Gu, J. Li, C. Zhang, Q. Gao, D. Menard, A. Pain, H. Yang, Q. Zhang, J. Cao, Emergence of indigenous artemisinin-resistant *Plasmodium falciparum* in Africa, *N. Engl. J. Med.* 376 (2017) 991–993, <https://doi.org/10.1056/NEJMc1612765>.
- [11] A. Uwimana, E. Legrand, B.H. Stokes, J.-L.M. Ndikumana, M. Warsame, N. Umulisa, D. Ngamije, T. Munyaneza, J.-B. Mazarati, K. Munguti, P. Campagne, A. Criscuolo, F. Ariey, M. Murindahabi, P. Ringwald, D.A. Fidock, A. Mbituyumuremyi, D. Menard, Emergence and clonal expansion of in vitro artemisinin-resistant *Plasmodium falciparum* Kelch13 R561H mutant parasites in Rwanda, *Nat. Med.* 26 (2020) 1602–1608, <https://doi.org/10.1038/>

- s41591-020-1005-2.
- [12] P.J. Rosenthal, Artemisinin resistance in eastern India, *Clin. Infect. Dis.* 69 (2019) 1153–1155, <https://doi.org/10.1093/cid/ciy1043>.
- [13] P. Verhaeghe, P. Rathelot, S. Rault, P. Vanelle, Convenient preparation of original vinylic chlorides with antiparasitic potential in quinoline series, *Lett. Org. Chem.* 3 (2006) 891–897, <https://doi.org/10.2174/157017806779467997>.
- [14] N. Primas, P. Verhaeghe, A. Cohen, C. Kieffer, A. Dumètre, S. Hutter, S. Rault, P. Rathelot, N. Azas, P. Vanelle, A new synthetic route to original sulfonamide derivatives in 2-trichloromethylquinazoline series: a structure-activity relationship study of antiplasmodial activity, *Molecules* 17 (2012) 8105–8117, <https://doi.org/10.3390/molecules17078105>.
- [15] A. Gellis, C. Kieffer, N. Primas, G. Lanzada, M. Giorgi, P. Verhaeghe, P. Vanelle, A new DMAP-catalyzed and microwave-assisted approach for introducing heteroaryl amino substituents at position 4 of the quinazoline ring, *Tetrahedron* 78 (2014) 8257–8266, <https://doi.org/10.1016/j.tet.2014.09.024>.
- [16] P. Verhaeghe, A. Dumètre, C. Castera-ducros, S. Hutter, M. Laget, C. Fersing, M. Prieri, J. Yzombard, F. Sifredi, S. Rault, P. Rathelot, P. Vanelle, N. Azas, 4-Thiophenoxy-2-Trichloromethylquinazolines display in vitro selective antiplasmodial activity against the human malaria parasite, *Plasmodium falciparum*. *Bioorg. Med. Chem. Lett.* 21 (2011) 6003–6006, <https://doi.org/10.1016/j.bmcl.2011.06.113>.
- [17] J. Desroches, C. Kieffer, N. Primas, S. Hutter, A. Gellis, H. El-Kashef, P. Rathelot, P. Verhaeghe, N. Azas, P. Vanelle, Discovery of new hit-molecules targeting *Plasmodium falciparum* through a global SAR study of the 4-substituted-2-trichloromethylquinazoline antiplasmodial scaffold, *Eur. J. Med. Chem.* 125 (2017) 68–86, <https://doi.org/10.1016/j.ejmech.2016.09.029>.
- [18] C.W. McNamara, M.C.S. Lee, C.S. Lim, S.H. Lim, J. Roland, A. Nagle, O. Simon, B.K.S. Yeung, A.K. Chatterjee, S.L. McCormack, M.J. Manary, A.-M. Zeeman, K.J. Decheney, T.R.S. Kumar, P.P. Henrich, K. Gagaring, M. Ibanez, N. Kato, K.L. Kuhlen, C. Fischli, M. Rottmann, D.M. Plouffe, B. Bursulaya, S. Meister, L. Rameh, J. Trappe, D. Haasen, M. Timmerman, R.W. Sauerwein, R. Suwanarusk, B. Russell, L. Renia, F. Nosten, D.C. Tully, C.H.M. Kocken, R.J. Glynn, C. Bodenreider, D.A. Fidock, T.T. Diagana, E.A. Wenzler, Targeting *Plasmodium* Pf(4)K to eliminate malaria, *Nature* 504 (2013) 248–253, <https://doi.org/10.1038/nature12782>.
- [19] Guillon, J., A. Cohen, N.M. Gueddouda, R.N. Das, S. Moreau, L. Ronga, S. Savrimoutou, L. Basmaciyan, A. Monnier, M. Monget, S. Rubio, T. Garnerin, N. Azas, J.-L. Mergny, C. Mullié, P. Sonnet, Design, synthesis and antimalarial activity of novel bis *N*-[(*Pyrr*olo[1,2-*a*]Quinoxalin-4-*Y*l)Benzyl]-3-Aminopropylamine derivatives, *J. Enzym. Inhib. Med. Chem.* 32 (2017) 547–563, <https://doi.org/10.1080/14756366.2016.1268608>.
- [20] A. Jonet, J. Guillon, J.; Mullié, C., A. Cohen, G. Bentzinger, J. Schneider, N. Taudon, S. Hutter, N. Azas, S. Moreau, S. Savrimoutou, P. Agnamey, A. Dassonville-Klimpt, P. Sonnet, Synthesis and antimalarial activity of new enantiopure aminoalcoholpyrrolo[1,2-*a*]quinoxalines, *Med. Chem.* 14 (2018) 293–303, <https://doi.org/10.2174/1573406413666170726123938>.
- [21] N. Primas, P. Suzanne, P. Verhaeghe, A. Cohen, J. Broggi, J. Lancelot, C. Kieffer, P. Vanelle, N. Azas, Synthesis and in vitro evaluation of 4-trichloromethylpyrrolo [1,2-*a*] quinoxalines as new antiplasmodial agents, *Eur. J. Med. Chem.* 83 (2014) 26–35, <https://doi.org/10.1016/j.ejmech.2014.06.014>.
- [22] J.N. Burrows, S. Duparc, W.E. Gutteridge, R.H. Van Huijsduijnen, W. Kaszubski, F. Macintyre, S. Mazzuri, J.J. Möhrle, T.N.C. Wells, New developments in anti-malarial target candidate and product profiles, *Malar. J.* 16 (2017) 26, <https://doi.org/10.1186/s12936-016-1675-x>.
- [23] MMV-supported projects | Medicines for Malaria Venture. <https://www.mmv.org/research-development/mmv-supported-projects>. (Accessed 21 February 2021).
- [24] K. Weatherby, D. Carter, *Chromera velia*: the missing link in the evolution of parasitism, *Adv. Appl. Microbiol.* 85 (2013) 119–144, <https://doi.org/10.1016/B978-0-12-407672-3.00004-6>.
- [25] G.I. McFadden, E. Yeh, The apicoplast: now you see it, now you don't, *Int. J. Parasitol.* 47 (2017) 137–144, <https://doi.org/10.1016/j.ijpara.2016.08.005>.
- [26] C.Y. Botté, F. Dubar, G.I. McFadden, E. Maréchal, C. Biot, *Plasmodium falciparum* apicoplast drugs: targets or off-targets? *Chem. Rev.* 112 (2012) 1269–1283, <https://doi.org/10.1021/cr200258w>.
- [27] A. Mukherjee, G.C. Sadhukhan, Anti-malarial drug design by targeting apicoplasts: new perspectives, *J. Pharmacopuncture* 19 (2016) 7–15, <https://doi.org/10.3831/KPL2016.19.001>.
- [28] T. Uddin, G.I. McFadden, C.D. Goodman, Validation of putative apicoplast-targeting drugs using a chemical supplementation assay in cultured human malaria parasites, *Antimicrob. Agents Chemother.* 62 (2018), <https://doi.org/10.1128/AAC.01161-17> e01161-17.
- [29] A.M. Vaughan, M.T. O'Neill, A.S. Tarun, N. Camargo, T.M. Phuong, A.S.I. Aly, A.F. Cowman, S.H.I. Kappe, Type II fatty acid synthesis is essential only for malaria parasite late liver stage development, *Cell Microbiol.* 11 (2009) 506–520, <https://doi.org/10.1111/j.1462-5822.2008.01270.x>.
- [30] C.Y. Botté, Y. Yamaryo-Botté, T.W.T. Rupasinghe, K.A. Mullin, J.I. MacRae, T.P. Spurck, M. Kalanon, M.J. Shears, R.L. Coppel, P.K. Crellin, E. Maréchal, M.J. McConville, G.I. McFadden, Atypical lipid composition in the purified relict plastid (apicoplast) of malaria parasites, *Proc. Natl. Acad. Sci. Unit. States Am.* 110 (2013) 7506–7511, <https://doi.org/10.1073/pnas.1301251110>.
- [31] S. Amiar, N.J. Katris, L. Berry, S. Dass, S. Duley, C.-S. Arnold, M.J. Shears, C. Brunet, B. Touquet, G.I. McFadden, Y. Yamaryo-Botté, C.Y. Botté, Division and adaptation to host environment of apicomplexan parasites depend on apicoplast lipid metabolic plasticity and host organelle remodeling, *Cell Rep.* 30 (2020) 3778–3792, <https://doi.org/10.1016/j.celrep.2020.02.072>.
- [32] R.P. Swift, K. Rajaram, H.B. Liu, S.T. Prigge, Dephospho-CoA kinase, a nuclear-encoded apicoplast protein, remains active and essential after *Plasmodium falciparum* apicoplast disruption, *EMBO J.* (2021) e107247, <https://doi.org/10.15252/emboj.2020107247>.
- [33] R.P. Swift, K. Rajaram, C. Keutcha, H.B. Liu, B. Kwan, A. Dziejdz, A.E. Jedlicka, S.T. Prigge, The NTP generating activity of pyruvate kinase II is critical for apicoplast maintenance in *Plasmodium falciparum*, *eLife* 9 (2020) e50807, <https://doi.org/10.7554/eLife.50807>.
- [34] M. Ghavami, E.F. Merino, Z.-K. Yao, R. Elahi, M.E. Simpson, M.L. Fernández-Murga, J.H. Butler, M.A. Casasanta, P.M. Krai, M.M. Totrov, D.J. Slade, P.R. Carlier, M.B. Cassera, Biological studies and target engagement of the 2-C-Methyl-d-Erythritol 4-phosphate cytidyltransferase (IspD)-Targeting anti-malarial agent (1R,3S)-MMV008138 and analogs, *ACS Infect. Dis.* 4 (2018) 549–559, <https://doi.org/10.1021/acscinfed.7b00159>.
- [35] W. Baschong, S. Wittlin, K.A. Inglis, A.H. Fairlamb, S.L. Croft, T.R.S. Kumar, D.A. Fidock, R. Brun, Triclosan is minimally effective in rodent malaria models, *Nat. Med.* 17 (2011) 33–34, <https://doi.org/10.1038/nm1111-33>.
- [36] M. Witschel, M. Rottmann, M. Kaiser, R. Brun, Agrochemicals against malaria, sleeping sickness, leishmaniasis and chagas disease, *PLoS Neglected Trop. Dis.* 6 (2012) e1805, <https://doi.org/10.1371/journal.pntd.0001805>.
- [37] M.G. Corral, J. Leroux, K.A. Stubbs, J.S. Mylne, Herbicidal properties of anti-malarial drugs, *Sci. Rep.* 7 (2017) 45871, <https://doi.org/10.1038/srep45871>.
- [38] M. Clastre, A. Goubard, A. Prel, Z. Mincheva, M.-C. Viaud-Massart, D. Bout, M. Rideau, F. Velge-Roussel, F. Laurent, The methylerythritol phosphate pathway for isoprenoid biosynthesis in coccidia: presence and sensitivity to fosmidomycin, *Exp. Parasitol.* 116 (2007) 375–384, <https://doi.org/10.1016/j.exppara.2007.02.002>.
- [39] K. Nagamune, L.M. Hicks, B. Fux, F. Brossier, E.N. Chini, L.D. Sibley, Abscisic acid controls calcium-dependent egress and development in, *Toxoplasma Gondii*. *Nature* 451 (2008) 207–210, <https://doi.org/10.1038/nature06478>.
- [40] P. Verhaeghe, P. Rathelot, A. Gellis, P. Vanelle, Highly efficient microwave assisted a -trichlorination reaction of a -methylated nitrogen containing heterocycles, *Tetrahedron* 62 (2006) 8173–8176, <https://doi.org/10.1016/j.tet.2006.05.081>.
- [41] D. Amrane, A. Gellis, S. Hutter, M. Prieri, P. Verhaeghe, N. Azas, P. Vanelle, N. Primas, Synthesis and antiplasmodial evaluation of 4-carboxamido- and 4-alkoxy-2-trichloromethyl quinazolines, *Molecules* 25 (2020) 3929, <https://doi.org/10.3390/molecules25173929>.
- [42] D. Stumpfe, J. Bajorath, Exploring activity cliffs in medicinal chemistry, *J. Med. Chem.* 55 (2012) 2932–2942, <https://doi.org/10.1021/jm201706b>.
- [43] S. Wagie, A.V. Adhikari, N.S. Kumari, Synthesis of some new 4-Styryltetrazolo [1,5-*a*]Quinoxaline and 1-Substituted-4-Styryl[1,2,4]Triazololo[4,3-*a*]Quinoxaline derivatives as potent anticonvulsants, *Eur. J. Med. Chem.* 44 (2009) 1135–1143, <https://doi.org/10.1016/j.ejmech.2008.06.006>.
- [44] Z. Wei, S. Qi, Y. Xu, H. Liu, J. Wu, H. Li, C. Xia, G. Duan, Visible light-induced photocatalytic C–H perfluoroalkylation of quinoxalinones under aerobic oxidation condition, *Adv. Synth. Catal.* 361 (2019) 5490–5498, <https://doi.org/10.1002/adsc.201900885>.
- [45] T. Mosmann, Rapid colorimetric assay for cellular growth and survival: application to proliferation and cytotoxicity assays, *J. Immunol. Methods* 65 (1983) 55–63, [https://doi.org/10.1016/0022-1759\(83\)90303-4](https://doi.org/10.1016/0022-1759(83)90303-4).
- [46] W. Trager, J.B. Jensen, Human malaria parasites in continuous culture, *Science* 193 (1976) 673–675, <https://doi.org/10.1126/science.781840>.
- [47] W.A. Guiguemde, A.A. Shelat, D. Bouck, S. Duffy, G.J. Crowther, P.H. Davis, D.C. Smithson, M. Connelly, J. Clark, F. Zhu, M.B. Jiménez-Díaz, M.S. Martínez, E.B. Wilson, A.K. Tripathi, J. Gut, E.R. Sharlow, I. Bathurst, F. El Mazouni, J.W. Fowble, I. Forquer, P.L. McGinley, S. Castro, I. Angulo-Barturen, S. Ferrer, P.J. Rosenthal, J.L. Derisi, D.J. Sullivan, J.S. Lazo, D.S. Roos, M.K. Riscoe, M.A. Phillips, P.K. Rathod, W.C. Van Voorhis, V.M. Avery, R.K. Guy, Chemical genetics of *Plasmodium falciparum*, *Nature* 465 (2010) 311–315, <https://doi.org/10.1038/nature09099>.



Artemisinin-independent inhibitory activity of *Artemisia* sp. infusions against different *Plasmodium* stages including relapse-causing hypnozoites

Kutub Ashraf^{1,2,3,*} , Shahin Tajeri^{1,*} , Christophe-Sébastien Arnold⁴ , Nadia Amanzougaghene¹, Jean-François Franetich¹, Amélie Vantaux^{2,3} , Valérie Soulard¹, Mallaury Bordessoulles¹, Guillaume Cazals⁵, Teun Bousema⁶, Geert-Jan van Gemert⁶ , Roger Le Grand⁷, Nathalie Dereuddre-Bosquet⁷, Jean-Christophe Barale^{3,8} , Benoit Witkowski^{2,3}, Georges Snounou⁷, Romain Duval⁹, Cyrille Y Botté⁴ , Dominique Mazier¹

Artemisinin-based combination therapies (ACT) are the frontline treatments against malaria worldwide. Recently the use of traditional infusions from *Artemisia annua* (from which artemisinin is obtained) or *Artemisia afra* (lacking artemisinin) has been controversially advocated. Such unregulated plant-based remedies are strongly discouraged as they might constitute sub-optimal therapies and promote drug resistance. Here, we conducted the first comparative study of the anti-malarial effects of both plant infusions *in vitro* against the asexual erythrocytic stages of *Plasmodium falciparum* and the pre-erythrocytic (i.e., liver) stages of various *Plasmodium* species. Low concentrations of either infusion accounted for significant inhibitory activities across every parasite species and stage studied. We show that these antiplasmodial effects were essentially artemisinin-independent and were additionally monitored by observations of the parasite apicoplast and mitochondrion. In particular, the infusions significantly incapacitated sporozoites, and for *Plasmodium vivax* and *P. cynomolgi*, disrupted the hypnozoites. This provides the first indication that compounds other than 8-aminoquinolines could be effective antimalarials against relapsing parasites. These observations advocate for further screening to uncover urgently needed novel antimalarial lead compounds.

DOI [10.26508/lsa.202101237](https://doi.org/10.26508/lsa.202101237) | Received 20 September 2021 | Revised 18 November 2021 | Accepted 19 November 2021 | Published online 2 December 2021

Introduction

Sustainable control and elimination of malaria mainly relies on effective treatment, as well as on the ability to eliminate the dormant forms (hypnozoites) responsible for the relapses of the widely distributed *Plasmodium vivax* (Mazier et al, 2009). Artemisinin-based combination therapies (ACT) are the frontline treatments against malaria worldwide (WHO, 2019b). The recent emergence and spread of ACT-resistant *Plasmodium falciparum* strains in South-East Asia, is of major concern, and a similar emergence in Africa will have catastrophic consequences (Imwong et al, 2017; Lu et al, 2017; Uwimana et al, 2020). Elimination of hypnozoites, the dormant hepatic forms responsible for *P. vivax* relapses, can only be achieved at present using 8-aminoquinoline drugs (primaquine or tafenoquine), but their use is restricted by their deleterious effects in persons with glucose-6-phosphate dehydrogenase deficiency (Mazier et al, 2009). Thus, novel antimalarials are urgently needed.

Artemisinin present in *Artemisia annua* (sweet wormwood) is considered to be solely responsible for the plant's potent activity against the parasite's blood stages. Recently, decoctions of *Artemisia*-dried leaves have been controversially advocated as cheaper traditional plant-based treatments for malaria. Such self-administered and unregulated treatments are strongly discouraged because of variable and potentially sub-optimal artemisinin content not least as they would promote the emergence of drug resistance (WHO, 2019a). It has been suggested that the efficacy of

¹Sorbonne Université, Institut National de la Santé et de la Recherche Médicale (INSERM), Centre National pour la Recherche Scientifique (CNRS), Centre d'Immunologie et des Maladies Infectieuses, CIMI, Paris, France ²Unité d'Epidémiologie Moléculaire du Paludisme, Institut Pasteur du Cambodge, Phnom Penh, Cambodia ³Institut Pasteur, Pasteur International Network, Malaria Translational Research Pasteur International Unit, Phnom Penh, Cambodia and Paris, Paris, France ⁴ApicoLipid Team, Institute for Advanced Biosciences, Centre National pour la Recherche Scientifique (CNRS) UMR5309, Université Grenoble Alpes, Institut National de la Santé et de la Recherche Médicale (INSERM) U1209, La Tronche, France ⁵Institut des Biomolécules Max Mousseron, UMR 5247, Université de Montpellier, Montpellier, France ⁶Department of Medical Microbiology, Radboud University Nijmegen Medical Center, Nijmegen, Netherlands ⁷Commissariat à l'Energie Atomique et aux Energies Alternatives (CEA)-Université Paris Sud 11-INSERM U1184, Immunology of Viral Infections and Autoimmune Diseases (IMVA-HB), Infectious Disease Models and Innovative Therapies (IDMIT) Department, Institut de Biologie François Jacob (IBFJ), Direction de la Recherche Fondamentale (DRF), Fontenay-aux-Roses, France ⁸Institut Pasteur, Université de Paris, CNRS UMR 3528, Structural Microbiology Unit, Paris, France ⁹Université de Paris, Institut de Recherche pour le Développement (IRD), UMR 261 MERIT, Paris, France

Correspondence: romain.duval@ird.fr; cyrille.botte@univ-grenoble-alpes.fr; dominique.mazier@sorbonne-universite.fr

*†Kutub Ashraf and Shahin Tajeri contributed equally to this work

such remedies also rests with additional plant compounds that can synergize to enhance parasite killing. This claim is supported by the purported anti-malarial traditional herbal teas based on the African wormwood *Artemisia afra*, a species devoid of artemisinin (du Toit & van der Kooy, 2019). We have exploited this difference to explore this issue through comparative and extensive in vitro assessment of the inhibitory activity of infusions from both plants on *Plasmodium*.

Results

Exposure of *P. falciparum* rings (double synchronized with 5% sorbitol at 8 h interval) to infusions from either plant for 72 h inhibited their growth in a dose-dependent manner (Fig 1A), with that of *A. annua* active at slightly lower doses. The maturation of the exposed parasites appeared to have been affected by the infusions (Fig S1). We opted to examine the biogenesis of the apicoplast and the mitochondrion as surrogates for the viability of the exposed parasites. Thus, detailed morphological examination revealed that apicoplast biogenesis was

disrupted in both *A. annua*- or *A. afra*-exposed parasites where apicoplasts failed to elongate and divide at the schizont stage as they normally do in unexposed parasites (Fig 1B). The parasite's mitochondria were also affected by both infusions (Fig 1C). These observations do not imply that the artemisinin-independent inhibitory activity is directly due to an effect on the biogenesis of these organelles. Nonetheless, preliminary data (Figs S2A–E and S3A–C) suggest that this process is affected to some extent for both organelles.

We then assessed the infusions against the pre-erythrocytic (hepatic) stages of diverse *Plasmodium* species, where part of the apicoplast metabolism (e.g., FASII activity) is indispensable (Yu et al, 2008; Vaughan et al, 2009). Exposure of primary simian hepatocytes to the infusions from the time of *Plasmodium berghei* sporozoites inoculation and for a further 48 h (spanning the time for full maturation), led to a significant dose-dependent reduction in the size and number of hepatic schizonts, with that of *A. afra* exerting its inhibitory effect at a slightly lower concentration (Fig 2A and B). Similar observations were obtained with *P. falciparum*-infected human primary hepatocytes (Fig 2C and D), a parasite with a longer hepatic development (5–6 d). Neither infusion had a cytotoxic effect

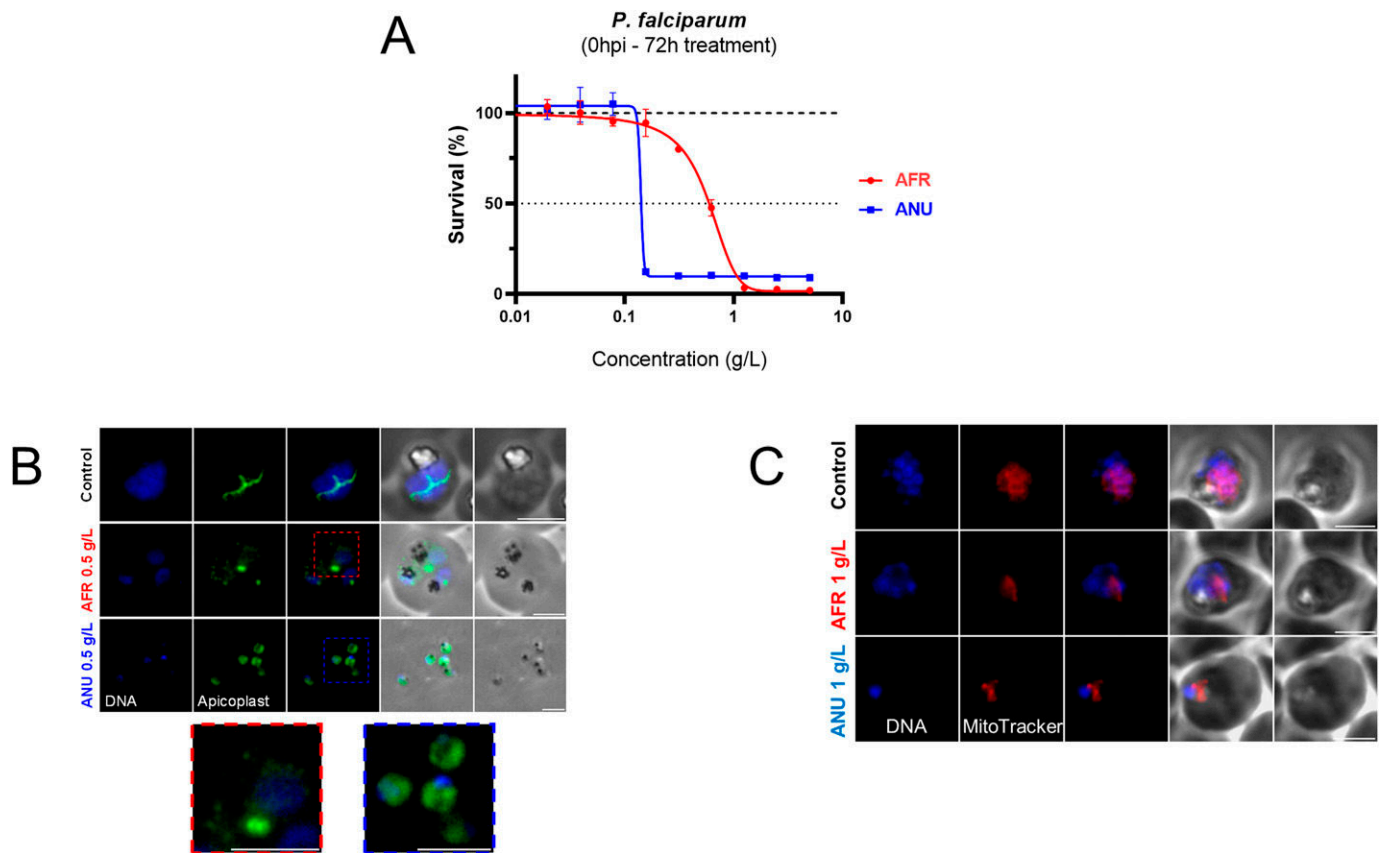


Figure 1. Activity of *Artemisia* infusions on the *Plasmodium falciparum* asexual blood stages.

(A) Survival of synchronous ring-stage parasites cultivated for 72 h in the presence of increasing concentrations of *Artemisia afra* (“AFR”) or *Artemisia annua* (“ANU”) infusions. Results are representative of three independent experiments. (B) Visualisation of apicoplasts by immunofluorescence in untreated control parasites (trophozoite stage) or those grown in the presence of the infusions (*A. afra*, trophozoite stage, red inset; *A. annua*, ring stage, blue inset). An anti-HA antibody was used to localize apicoplasts in a *P. falciparum* cell line expressing a C-terminally HA tagged version of the outer membrane triose phosphate transporter (*PfoTPT*), a protein known to be located on the outer membrane of the apicoplast (Botté et al, 2013). Parasite nuclei were detected by Hoechst 33342 staining. Scale bar is 3 μ m. (C) Visualisation of parasite mitochondria with Mitotracker Red in infusion-exposed and control cultures. Scale bar is 3 μ m. Concentrations of infusions are provided as dry weight of leaves prepared in water and presented as gram per litre (g/l) (see the Materials and Methods section).

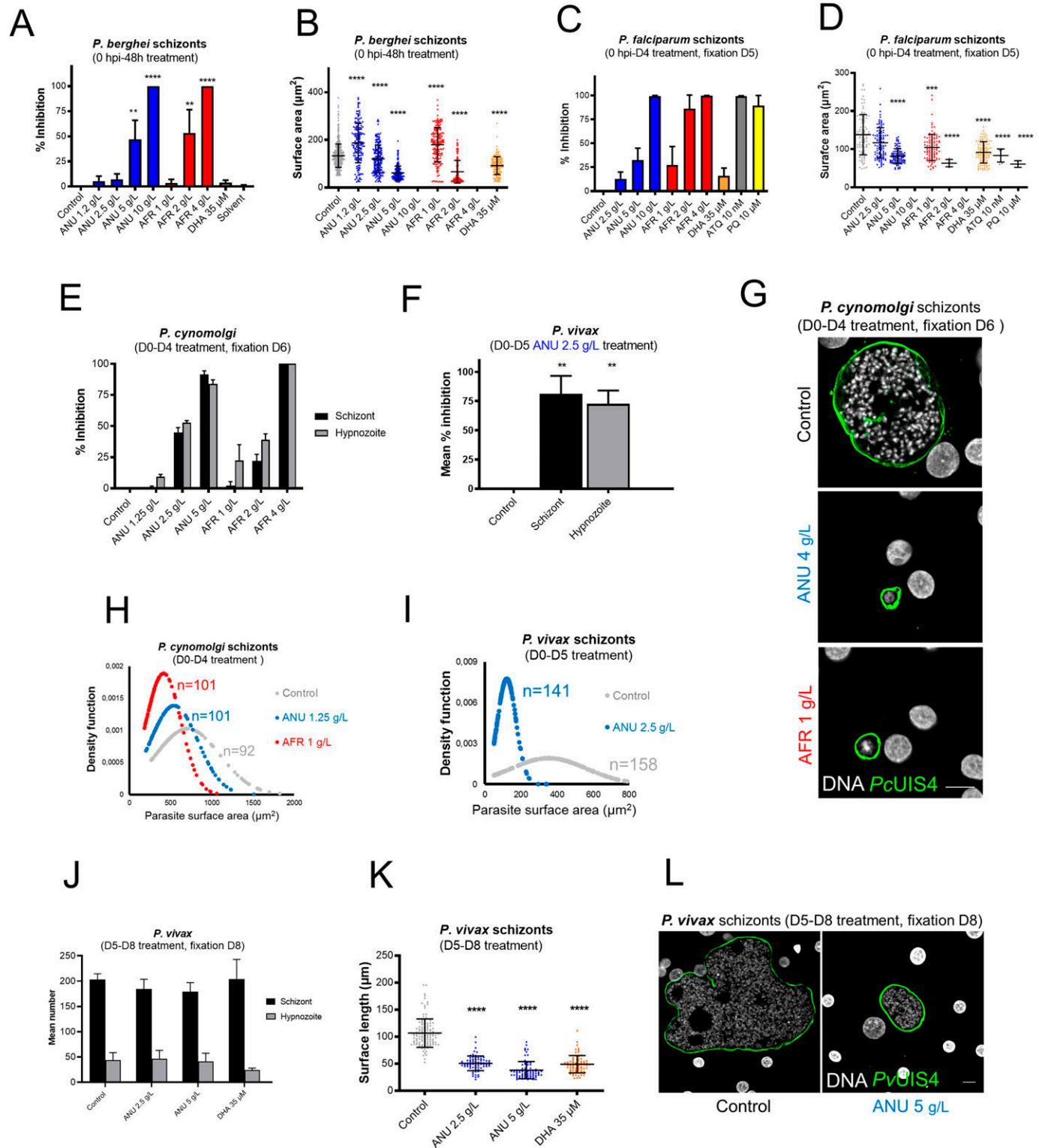


Figure 2. Activity of Artemisia infusions on the pre-erythrocytic Plasmodium parasites.

(A, B) Quantification of intracellular *P. berghei*-GFP schizont numbers expressed as % of the mean numbers (536 per well) observed in control wells (A), and size distribution of these schizonts treated with *Artemisia* infusion and DHA (B). 10 g/l *Artemisia annua* and 4 g/l *Artemisia afra* completely cleared parasites from the cultures. (C, D) Impact of the exposure (D0-D4) of *Plasmodium falciparum*-infected human primary hepatocytes on parasite numbers expressed as % inhibition compared with controls (mean of 732 per well) (C), and size expressed as surface area (μm²) (D); 10 g/l *A. annua* and 4 g/l *A. afra* cleared all *P. falciparum* schizonts from the cultures. Results are representative of three independent experiments. (E, F) Effect of exposure to infusions on the schizont and hypnozoite numbers in primary hepatocytes cultures of *Plasmodium cynomolgi* (E) or *Plasmodium vivax* (F) expressed as mean % inhibition. Control cultures had 120 (51 schizonts/69 hypnozoites) and 317

on the hepatocytes, nor did dihydroartemisinin (DHA, used as negative control) affect hepatic schizont numbers though their size was reduced (Fig S4A–D). We further demonstrated that exposure of sporozoites to the infusions for 1 h before their addition to the hepatocyte cultures, also led to a significant reduction in the number of hepatic schizonts for both parasite species (Fig S5A and B). Nonetheless, the viability of such exposed sporozoites, as assessed by vital staining and by their motility, was not altered (Fig S6A–D).

The assays were then extended to two parasite species, *P. vivax* and *Plasmodium cynomolgi* that produce hypnozoites. Prophylactic treatment from inoculation and for a further 4 d (D0–D4 post-inoculation) of *P. cynomolgi*-infected primary simian hepatocytes cultured in the presence of infusions significantly reduced the number of both schizonts and hypnozoites in a dose-dependent manner, by 85% for *A. annua*, and completely for *A. afra* at the highest concentrations (Fig 2E). Because of restricted number of *P. vivax* sporozoites, only the 2.5 g/l *A. annua* infusion could be tested and this had a slightly higher inhibitory effect on both schizonts and hypnozoites than that on those of *P. cynomolgi* (Fig 2F). For both *P. vivax* and *P. cynomolgi*, the remaining surviving hepatic schizonts were significantly smaller than those in control cultures (Fig 2G–I). However, exposure of *P. vivax* in human hepatocytes on days 5–8 post-infection (D5–D8 pi) to the infusions did not lead to a significant reduction in the number of schizonts or hypnozoites (Fig 2J), the schizonts showed a significant size reduction (Fig 2K and L) that was similar to that observed in parasites treated with DHA (Fig 2J and K).

The apicoplasts in the exposed sporozoites were affected in that most of the parasites displayed the dot form and some lacked an apicoplast (“void” category, Fig 3A), in contrast to those in control sporozoites where only 19% presented as a single dot with the others showing the mature elongated form (probably reflecting the presence in the salivary gland (SG) of sporozoites of different ages). For both *A. annua* and *A. afra* infusions, the shift to a high proportion of sporozoites with affected apicoplasts was dose-dependent (Fig 3A), with no concomitant change to the size, shape, or morphology of the parasite nuclei. The biogenesis of the apicoplast was also disrupted by the infusions in the hepatic stages of *P. falciparum* and *P. cynomolgi*, where an increasing fraction of parasites with “affected” apicoplasts was observed as infusion concentrations increased (Fig 3B and C). For these observations, analysis of the organellar genomes was also consistent with some inhibitory action directed against the apicoplast and the mitochondrion (Fig S2F–H). The development of apicoplasts in relapsing parasite species has been rarely recorded (Mikolajczak et al, 2015; Gural et al, 2018; Pewkliang et al, 2018), and only once for the *P. vivax* putative hypnozoite in a chimeric mouse, where it was found to consist of a single organelle elongating and then branching to form new discrete organelles that appear as a

punctate pattern. We observed a similar pattern in the hypnozoites in the *P. cynomolgi* control cultures, whereas in those exposed to the infusions (D0–D4), we noted apicoplasts with a diffuse staining pattern, implying a disrupted biogenesis (Fig 4A). Similar infusion-affected hypnozoites were also observed on D10 in *P. vivax* hepatic cultures exposed on D4–D10, although their proportion was less than that for *P. cynomolgi* (Fig 4B).

The inhibitory activity of the infusions is not primarily due to loss of the 1-deoxy-D-xylulose 5-phosphate (DOXP) pathway (demonstrated to be the only apicoplast function essential for in vitro growth of the erythrocytic parasites in lipid-rich medium) (Yeh & DeRisi, 2011; McFadden & Yeh, 2017) because similar inhibition by the infusions was observed in apicoplast-negative parasites generated via chloramphenicol (Cm) treatment that were grown in media supplemented or not with isopentenyl pyrophosphate (Yeh & DeRisi, 2011; Amiar et al, 2020) (IPP) (Fig S2A for the study design). It also appears that both infusions exhibit a strong growth inhibition at low exposition time (6 h), not rescued by the IPP addition (Fig S2B–E). The observed apicoplast loss is supported by a rapid loss overtime of the apicoplast genome in infusion-treated cultures, which parallels that of doxycycline-treated positive control cultures (Yeh & DeRisi, 2011; Uddin et al, 2018) (Fig S2F). Furthermore, quantification of mitochondrial DNA (Fig S2G) during the 48-h *P. berghei* hepatic cycle along with the microscopic imaging (Fig 2D) also revealed disruption of this organelle (Yeh & DeRisi, 2011; Uddin et al, 2018). In both control and treated conditions, parasites continued to augment their DNA and replicated during the 48-h intracellular development, but this increase in DNA was less obvious in doxycycline and infusion exposed groups (Fig 2H).

To further assess whether infusion treatments exert organelle-specific inhibition, synchronized rings were exposed to 0.5 g/l *A. annua* or *A. afra* for 24 and 48 h and apicoplast development was assessed and compared to those treated or not with 0.8 nM atovaquone (ATQ). Indeed, ATQ is a drug that is currently in use to treat human malaria, and which kills the parasite by targeting its mitochondrion, thus not directly affecting the apicoplast biogenesis. Results at 24 h show a slight but not significant effect of the ATQ treatment on apicoplast biogenesis compared to control or DMSO but both infusion treatments significantly increase the percentage of affected apicoplast with a stronger effect for *annua*-exposed parasites (Fig S3A). Apicoplast elongation and branching seemed blocked, unlike ATQ treatment, with unelongated apicoplast after *afra* treatment and apicoplast signal is diffused in the parasite cytosol with vesicles for *annua* (Fig S3A). After 48 h of treatment (Fig S3B), the percentage of parasite with affected apicoplast was even higher for the two infusions but also for ATQ, which in this case was similar to *afra* treatment. Microscopic imaging of these *P. berghei* hepatic cultures also indicated a disruption of this organelle (Fig

(205 schizonts/112 hypnozoites) hepatic parasites per well of a 96-well plate for *P. cynomolgi* and *P. vivax*, respectively. (G) Confocal microscopy images of exposed *P. cynomolgi* schizonts. The parasitophorous vacuole of fixed parasites were immunolabeled with anti-PcUIS4 antibody. Host and parasite DNA were visualized by 4',6-diamidino-2-phenylindole (DAPI) dye (Scale bar = 10 μ m). (H, I) Density function plots of *P. cynomolgi* (H) and *P. vivax* (I) schizonts size distribution (“n” represents the number of schizonts for which the size was measured); the peaks show where most of the population is concentrated. (J, K) Quantification of *P. vivax* parasite numbers (J) and size (K) in human primary hepatocytes treated on D5–D8 pi with *A. annua* infusion. (L) Confocal microscopic images of treated *P. vivax* schizonts fixed at D8 pi, using an anti-PvUIS4 antibody as a parasite PVM marker and DAPI for the DNA marker (scale bar = 10 μ m). ANU, *A. annua* and AFR, *A. afra*. Statistical significance was determined using a one-way ANOVA followed by Kruskal–Wallis test (Dunn’s multiple comparisons to control) where significance is determined by $P < 0.0001$ (****), $P < 0.0011$ (**) and $P < 0.05$ (*).

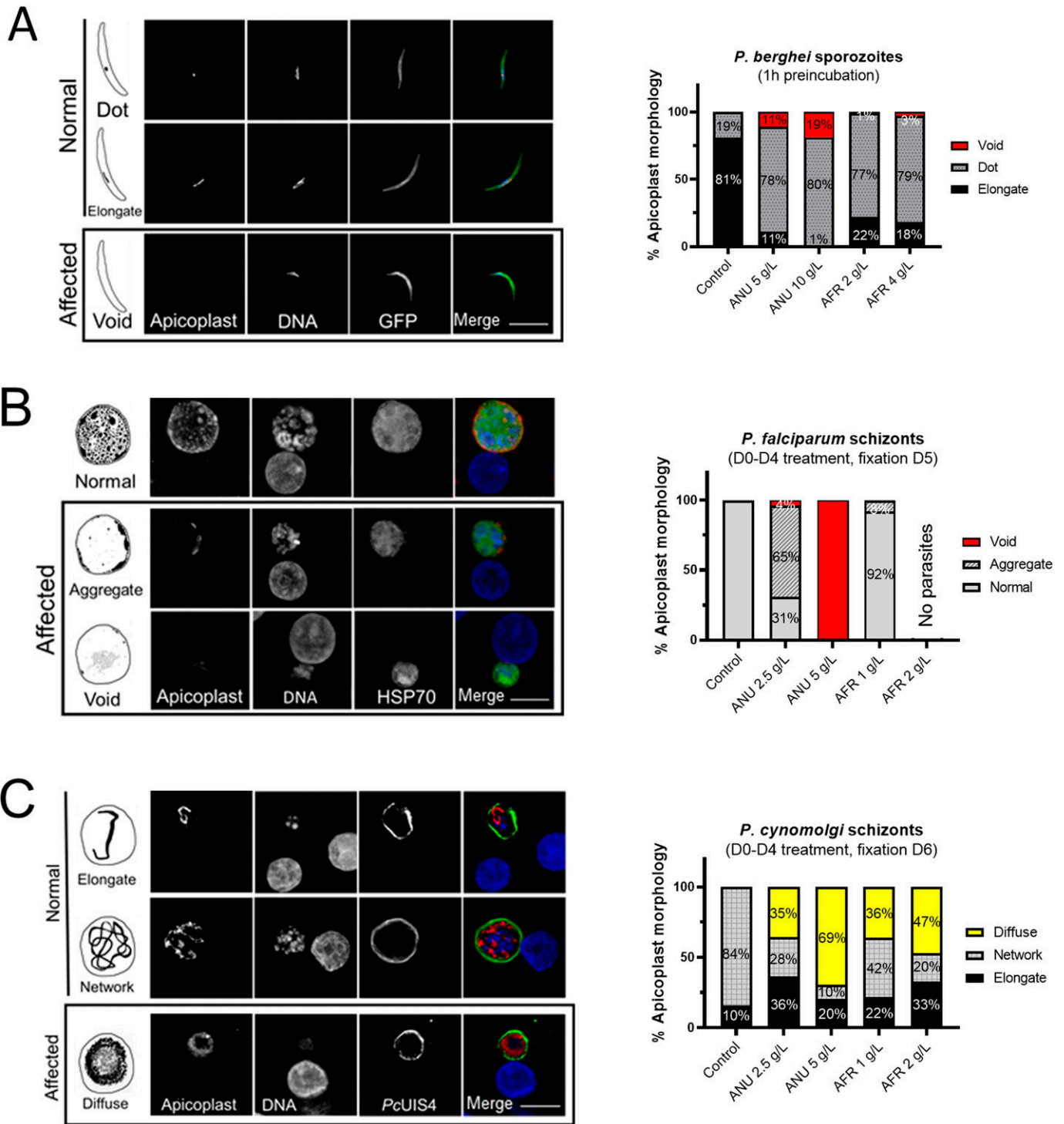


Figure 3. Disruption of apicoplast and mitochondrial integrity in *Plasmodium* pre-erythrocytic stages by *Artemisia* infusions. (A, B, C) Schematic and confocal images of *P. berghei* sporozoites (A), *Plasmodium falciparum* schizonts (B), and *Plasmodium cynomolgi* schizonts (C) in control and treated groups. (B) For *P. falciparum*, the 2 g/l treatment cleared all schizonts (i.e., no parasites in panel B). The apicoplast morphologies presented in the "Affected" panels have only been observed in exposed parasites. The frequencies of the various morphologies are presented in the associated graphs. *P. falciparum* and *P. cynomolgi* parasites were detected by anti-HSP70 and *PcUIS4* antibodies, respectively. Apicoplasts were labelled by anti-PyACP antibody (scale bar = 10 μ m).

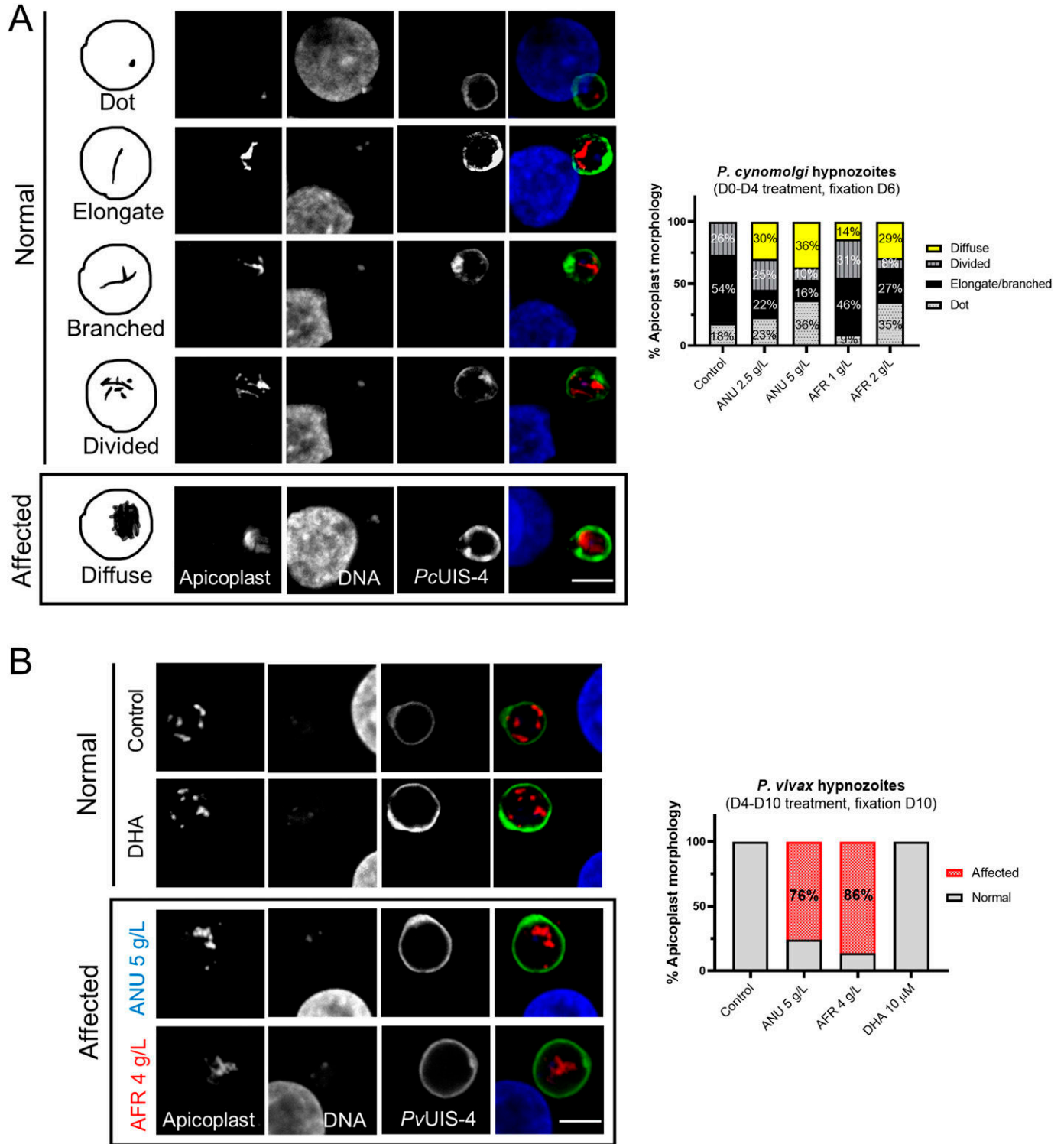


Figure 4. Disruption of hypnozoites' apicoplast by Artemisia infusions.

(A) Schematic (left panels) and confocal images of *Plasmodium cynomolgi* hypnozoites on D6 in cultures exposed to infusion during the early hepatic phase. In control cultures, three apicoplast morphologies could be observed, a dot-shaped apicoplast in younger hypnozoites that evolves into an elongate organelle that then branches to show a divided morphology as the hypnozoites mature. In infusion-treated cultures (D0-D4), hypnozoites with a diffuse apicoplast signal were additionally observed. (B) Apicoplast morphology of *Plasmodium vivax* hypnozoites exposed to infusions from D4-D10 pi. The apicoplast morphologies presented in the "Affected" panels have only been observed in exposed parasites. (A, B) Quantification of the various apicoplast morphologies in 100 and 50 parasites for (A) and (B), respectively, are presented. *P. cynomolgi* and *P. vivax* were visualized by using an anti-PcUIS4 and anti-PvUIS4 antibodies, respectively (scale bar = 5 μm).

S3C). Together, this strongly suggests that apicoplast biogenesis might be indirectly affected by the overall death of the parasite after a longer exposure to the different treatments (*afra* or ATQ). But the stronger effect of *afra* at early stage (24 h) indicates a possible direct impact on the apicoplast. Hence, *annua* also highly affect the general development of the parasites, by blocking them at the late ring/early trophozoite stage upon 24 h. However, a high around 60% of the parasites harbour a single punctate apicoplast while ~40% harbour a disrupted/diffused apicoplast, which could also indicate an impact on the apicoplast but also and meanly a stronger impact on an apicoplast off-target that block the parasite development after short exposition to the infusion (concomitant with Fig S2D, which shown a drastic negative impact of *annua* after only 6 h of exposure).

Discussion

The discovery of artemisinin from Chinese traditional medicine has revived interest in *Artemisia* plants as a source of treatments for diverse infectious and non-infectious pathologies beyond than malaria (de Ridder et al, 2008; Liu et al, 2009; du Toit & van der Kooy, 2019). The investigations of the in vitro anti-malarial efficacy of *Artemisia* infusions have been essentially conducted with the species *A. annua* or *A. afra*, and this exclusively on the erythrocytic stages (asexual and sexual) of *P. falciparum* parasites (Silva et al, 2012; Suberu et al, 2013; Elfawal et al, 2015). Their results are inconsistent and difficult to interpret. Data from our extensive comparative assays clearly demonstrate that infusions from either plant species can fully inhibit the multiplication and the development of both erythrocytic and pre-erythrocytic stages of various *Plasmodium sp.* in vitro. Importantly, this inhibition is independent of their artemisinin content (see Table S1 for measurement of artemisinin in both infusions), with maximal activity occurring at broadly similar infusion concentrations, without observable cytotoxic effects against the host cells. Our observations are supported by a recent study investigating the effect of these *Artemisia* infusions on asexual and gametocyte *P. falciparum* erythrocytic stages (Snider & Weathers, 2021), which shows an inhibition of the asexual growth after 48 h exposure to both infusions with a significant stronger effect for that of *A. annua*. The higher inhibition levels we observed are probably because we assessed parasite survival 72 h post-exposure (as compared to 48 h). However, we also observed a strong inhibition effect at 24 and 48 h of culture exposed to *A. annua* or *A. afra* 0.5 g/l. Of note, the inhibition of the hepatic stages appears to be mainly due to a detrimental effect on the ability of the sporozoite to achieve a productive hepatocyte infection, which also significantly led to a substantial reduction in hypnozoite numbers in the case of *P. cynomolgi* and *P. vivax*. It is likely that the detrimental effects also observed on the apicoplast in developing *P. vivax* hypnozoite will adversely affect its capacity to reactivate, although this would require further in vivo testing. It is important to note that the infusion concentrations at which we observed significant inhibition of the pre-erythrocytic stages (both sporozoites and hepatic parasites) were significantly higher (10- to 20-fold) than those needed for the *P. falciparum* erythrocytic parasites. The reason for this differential susceptibility is not known and requires further investigation.

Our in vitro observations are clearly insufficient to support claims of in vivo curative efficacy and much less for a prophylactic use for any traditional remedy from the two plants. They do however suggest the presence of hitherto unknown plant components with potent inhibitory activity. Mechanistically, PCR analysis show that some compounds present in the *Artemisia* infusions quickly and directly affect the replication of the parasite's apicoplast and mitochondria, consistent with some disruption of their biogenesis as observed by immunofluorescence imaging of these organelles in the assays conducted with several parasite species. It thus appears that one or a combination of the myriad of compounds present in the infusion might target the mitochondrion or the apicoplast directly. The direct correlation between organelle disruption or impaired development and parasite inhibition and death remains to be established.

Ultimately, the relatively similar pan-species and cross-life cycle inhibitory effects resulting from exposure to the two infusions demonstrates the presence of one or more potential lead compounds unrelated to artemisinin. This warrants systematic bio-guided screening to identify them. This is of particular interest because this might lead to a novel antimalarial class of compound that could effectively and safely prevent *P. vivax* relapses. Indeed, any drugs that could supplant 8-aminoquinolines, the only drugs currently capable of exerting hypnozoitocidal activity (Mazier et al, 2009), would greatly enhance the prospect of global malaria elimination.

Materials and Methods

Primary cryopreserved hepatocytes maintenance and infection

In this study, human and simian primary hepatocytes were used. Simian (*Macaca fascicularis*) hepatocytes were isolated from the liver of healthy animals using collagenase perfusion as previously described (Dembélé et al, 2011). The use of hepatocytes was approved by the Ethical Animal Committee of the Primate center, Commissariat à l'Energie Atomique et aux Energies Alternatives (permit number A 92-032-02). Cryopreserved human primary hepatocyte vials were purchased from Biopredic (Lot no. LHuf17905A) or Lonza (Lot no. HUM182641). Cells were seeded in 96-well plates (Falcon by Becton–Dickinson Labware Europe) coated with collagen I (BD Bioscience), such that a single cell layer homogenously covers each well. Cryopreserved primary human hepatocytes (Biopredic International and Lonza) were seeded generally 4 d before infection. Both human and simian hepatocytes were maintained at 37°C in 5% CO₂ in William's E medium (Gibco) supplemented with 10% fetal clone III serum (FCS, Hyclone), 1% penicillin–streptomycin (Gibco), 5 × 10⁻³ g/l human insulin (Sigma-Aldrich), 5 × 10⁻⁵ M hydrocortisone (Upjohn Laboratories SERB), and Matrigel (Ref. 354234; Corning). The sporozoites used to infect the cultures were purified from dissected SGs of infected mosquito (Dembélé et al, 2011). During the infection Matrigel cover was removed carefully before adding the sporozoite inoculum. The plates were then centrifuged at 900g for 6 min at room temperature before incubation at 37°C for 3 h. After a wash, Matrigel was added to the culture and allowed to solidify at 37°C for 45 min. The cell culture medium was changed thereafter every 24 h until cell fixation.

List of different *Plasmodium* species used for infection of hepatocytes.

| Parasites | Strains | Source |
|----------------------|--------------|--|
| <i>P. berghei</i> | GFP ANKA | Centre d'Immunologie et des Maladies Infectieuses (CIMI), Paris, France |
| <i>P. falciparum</i> | NF54 | Department of Medical Microbiology, University Medical Centre, St Radboud, Nijmegen, The Netherlands |
| <i>P. cynomolgi</i> | M | Primate center, Commissariat à l'Énergie Atomique et aux Énergies Alternatives (CEA), Fontenay aux Roses, France |
| <i>P. vivax</i> | Unidentified | Symptomatic Patients, Pasteur Institute of Phnom Penh, Cambodia |

Culturing *Plasmodium*-infected red blood cells

P. falciparum blood stage parasites were maintained at 2% hematocrit in 1640 RPMI-HEPES supplemented with 5% AlbuMAX II (GIBCO) and 0.25% gentamycin. Parasites were grown in sealed Perspex chambers gassed with β mix gas (1% O₂, 5% CO₂, and 94% N₂) at 37°C and maintained on 48-h cycles. Cultures were tightly synchronized at ring stage using sorbitol treatment (%5 vol/vol) as previously described (Amiar et al, 2020).

Production of *P. vivax* sporozoites

Sporozoites were obtained from mosquitoes infected by feeding on symptomatic patients presenting with *P. vivax* in Monduliri Province (eastern Cambodia) after obtaining their consent. The patients were managed by the medical staff based at these health facilities. Heparinized blood samples were collected by venepuncture before the initiation of treatment, and a diagnostic PCR assay was used to confirm that *P. vivax* was the only *Plasmodium* species present. The blood was centrifuged at 1,174g at 37°C for 5 min, and the plasma was replaced by heat-inactivated naïve human AB serum. Batches of 300–600 5–7-d-old adult female mosquitoes (*Anopheles dirus*) that were starved overnight were fed via an artificial membrane attached to a water-jacketed glass feeder maintained at 37°C. Engorged mosquitoes were maintained at 26°C and 80% relative humidity, and provided with a 10% sucrose plus 0.05% para-amino-benzoic acid solution on cotton pads. SGs of mosquitoes were dissected 14–20 d post-blood meal in L15 medium supplemented with antibiotics and Amphotericin B (Gibco).

Production of sporozoites (other species than *P. vivax*)

P. falciparum was transmitted to *Anopheles stephensi* mosquitoes using an artificial membrane feeding on in vitro cultivated gametocytes, in Department of Medical Microbiology, Radboud University Medical Center, Nijmegen, The Netherlands. *P. berghei* and *P. cynomolgi* infections of *An. stephensi* mosquitoes were performed in Paris, respectively, by direct mosquito feeding on anesthetized Pb-GFP (Manzoni et al, 2014) infected mice, or by artificial membrane feeding on *P. cynomolgi* (strain M) infected blood from *Macaca fascicularis*. All simian procedures (infection, monitoring, and blood sampling) were performed in CEA, Fontenay aux Rose before the infected blood samples were transferred to CIMI-Paris

for mosquito infection. 2–3 wk post blood meal, *Plasmodium*-infected mosquitoes were killed with 70% ethanol. They were then washed once in Leibovitz's L-15 medium (Gibco) containing 5% fetal calf serum, 100 UI penicillin, 100 µg/ml streptomycin, and 0.5 µg/ml amphotericin B, followed by another two washes in the same medium, this time lacking serum. The mosquitos were then hand dissected under stereomicroscope and the SGs were crushed in a 1.5-ml Eppendorf tube and passed through a 40-µm filter (Cell Strainer; BD Biosciences). Sporozoites were finally counted and after dilution adjustment, directly inoculated to the cultures.

Preparation of *Artemisia* infusion

A. afra (PAR, voucher ID: LG0019528 Université de Liège) and *A. annua* (LUX, voucher ID: MNHNL17733 Herbarium Luxembourg) were collected as leaves and twigs and were preserved at room temperature. Both products were protected from sunlight until infusion preparation.

The stock infusion was prepared as follows: 2.5 g *Artemisia* dried leaves and twigs were added to 25 ml of pre-boiled 25 ml commercial drinkable water (Crystalline Company) and the mixture was then boiled while being stirred for 5 min. After cooling over 10 min, the infusion was passed through a 40-µm cell strainer (Falcon, Corning Brand) to remove plant debris, and then centrifuged at 1,600g for 10 min to pellet any remaining fine solids, with a final filtration step over a 0.20-µm membrane filter (CA-Membrane) to obtain a fully clear solution. Filtration was done to eliminate debris produced during plant boiling. During in vitro use, debris accumulated on top of hepatocyte culture layer and made parasite quantification difficult. To our knowledge, filtration of *Artemisia* infusions is not performed by patients in endemic areas. The stock infusion (100 g/l) was stored at 4°C (short term storage) or at -20°C (long term storage). For the in vitro drug assay, the decoction was diluted to the appropriate concentration (g/l) with William's E medium (along with supplements). Frozen and freshly prepared *Artemisia* decoction samples were subjected to chemical analyses including artemisinin content quantification.

Quantification of artemisinin in infusion: UHPLC analysis

The chromatographic apparatus consisted of Nexera X2 UHPLC system (Shimadzu) equipped with a binary pump, solvent degasser, and thermostatted column compartment. A reversed-phase

column was used for separation: Kinetex C18 (2.1 × 100 mm 1.7 μm from Phenomenex). Mobile phase A and B consisted of water (0.1% formic acid) and acetonitrile (0.1% formic acid), respectively. The 10-min linear gradient program used was 10–100% B over 5 min, a plateau at 100% B for 2 min was used to wash the column, decreasing from 100–10% B in 0.1 min, followed by a 2.9 min post-run isocratic step at 10% B to re-equilibrate the column. The flow rate was constant at 0.5 ml/min at 25°C.

Quantification of artemisinin in infusion: MS/MS detection

MS/MS experiments were carried out using the Shimadzu UHPLC system described above coupled to a Shimadzu LCMS-8050 triple quadrupole mass spectrometer using the multiple reaction monitoring technique operating in positive ion mode. The following parameters were used for all experiments: electrospray interface voltage was 3 kV; heat block temperature of 350°C; desolvation line temperature of 300°C; interface temperature of 300°C; drying gas flow gas was set at 5 liters/min; and nebulizing gas flow at 3 liters/min, heating gas flow rates were set at 15 liters/min. Q1 and Q3 were set to unit resolution. The dwell time was set at 1 ms for each multiple reaction monitoring transition; optimal CE values were chosen to obtain the most characteristic fragments (see below table).

Drugs

Drugs were dissolved in different solvents according to the manufacturer's instructions which are enlisted below: atovaquone (A7986; Sigma-Aldrich), primaquine biphosphate (160393; Sigma-Aldrich), DHA (1200520; Sigma-Aldrich), isopentenyl pyrophosphate NH₄⁺ salt (Isoprenoids), chloramphenicol (C0378-5G; Sigma-Aldrich), and doxycycline (D9891; Sigma-Aldrich). Media with drugs were changed every 24 h during the assays.

Immunostaining

Cultured hepatocytes were fixed using 4% PFA for 10–15 min at room temperature. The fixed samples were subjected to immune labelling. The primary antibodies (see below table) were diluted in dilution buffer (1% wt/vol Bovine Serum Albumin and 0.3% vol/vol Triton X-100 in PBS) and incubated at room temperature. Primary antibody-stained cultures were washed thrice with PBS 1X and were incubated with secondary antibody (below table) along with DAPI (1:1,000) to visualize the nuclei at room temperature for 1 h. Mitotracker (Thermo Fisher Scientific) was used to visualize parasite mitochondria.

Quantification of Artemisinin in *A. annua* and *A. afra* infusions by UHPLC-LCMS

| Precursor (m/z) | Fragment ion (m/z) | Collision energy (eV) |
|-----------------|--------------------|-----------------------|
| 283.10 | 247.15 | 9 |
| 283.10 | 265.15 | 8 |
| 283.10 | 219.10 | 12 |

Confocal microscopy and image analysis

Confocal images of immunostained cultures were taken by Leica SP8 white laser microscope controlled by the Leica Application Suite AF software at the QUANT microscopy platform (Institut du Cerveau et de la Moelle épinière, ICM) in Paris, France. Z-stack images were constructed and analyzed by Fiji package of ImageJ software. Final images were made by Microsoft Powerpoint. Schematic figures of Plasmodium apicoplast were designed by Procreate application in Apple iPad pro.

Quantification of apicoplast morphologies

Pre-erythrocytic and hypnozoite stages: ACP-immunolabeled parasites were quantified considering the distinguishable morphology in drug-treated versus control by an individual with the aid of confocal (Leica SP8 white laser microscope) at 63X magnification. For each condition, 100 parasites were observed. Erythrocytic stage: TPT-HA-immunolabeled parasites were quantified considering the distinguishable morphology in drug-treated versus control by an individual with the aid of fluorescence microscope (Axio Imager 2_apotome; ZEISS, ×100 magnification). For each condition, between 54 and 116 parasites were observed.

Parasite enumeration and toxicity assessment using high-content imaging

Upon fixation and immunostaining, cell culture plates were analyzed to determine the number and size of the parasites using a CellInsight High Content Screening platform equipped with the Studio HCS software (Thermo Fisher Scientific). Uninuclear hepatic parasite forms observed beyond D4 were considered to be putative hypnozoites, whereas multinucleate forms were classed as schizonts. The parasite size reduction was calculated on the average object area using the total surface area of each selected object (μm²). The high-content imaging approach has been described previously (Bosson-Vanga et al, 2018). To assess cell toxicity of infusion for hepatic cultures, fixed plates were further scanned for the DAPI signal representing host nuclei. The analysis was based on counting of total cell nuclei.

qPCR to quantify apicoplast and mitochondrion

To perform relative quantification of apicoplast, mitochondrial and nuclear genomes we extracted genomic DNA from *Pb*-GFP infected hepatocytes treated or not with infusion using a NucoelSpin Tissue kit (Macherey-Nagel) according to manufacturer's manual. The amount and the purity of the extracted DNA were checked by a NanoDrop ND 1000 machine (Thermo Fischer Scientific). The following gene-specific primers were designed to target genes found in each organelle or nuclear genomes:

*tufa*_PBANKA_API00280 (apicoplast) 5'-GATATTGATTCATCTCCA-GAAGAAA-3'/5'-ATATCCATTTGTGTAGCACCAATAA-3',

Cytb3_PBANKA_MIT01900 (mitochondrion) 5'-AGATATATGCATGCTACTGG-3'/5'-TCATTTGTCCCAAGGTAATAA-3'

List of primary and secondary antibodies used in the study.

| Antibody | Source | Working dilution |
|--|---|------------------|
| Recombinant mouse anti-PvUIS4 | Noah Sather (Centre for Infectious Disease Research, Seattle, USA) | 1:20,000 |
| Mouse anti-PcUIS4, polyclonal | Laurent Rénia (Singapore Immunology Network, Agency for Science, Technology, and Research, Singapore) | 1:500 |
| Recombinant rabbit monoclonal antibody against PyACP | Scot E. Lindner (Huck Centre for Malaria Research, Penn State, USA) | 1:250 |
| Mouse polyclonal serum raised against PfHSP70 | Centre d'Immunologie et des Maladies Infectieuses (CIMI), Paris | 1:1,500 |
| Mouse polyclonal anti-PfHSP60 | Philippe Grellier (Muséum National d'Histoire Naturelle, Paris) | 1:500 |
| Rat IgG anti-HA | Roche | 1:500 |
| Alexa Fluor 488 goat anti-mouse IgG | Invitrogen | 1:500 |
| Alexa Fluor 594 goat anti-rabbit IgG | Life Technologies | 1:500 |
| Alexa Fluor 488 goat anti-Rat IgG | Life Technologies | 1:1,000 |

GFP 5'-GATGGAAGCGTTCAACTAGCAGACC-3'/5'-AGCTGTACAACT-CAAGAAGGACC-3', and *CHT1_PBanka_0800500* (nuclear) 5'-AACA-AAATAGAGGTGGATTT-3'/5'-AATTCCTACACCATCGGCTC-3'.

The quantification of each target gene was normalized to GFP, expressed as a transgene under the *P. berghei* elongation factor 1 α promoter (Janse et al, 2006). All reactions were performed on an Applied Biosystems 7300 Real-Time PCR System using the Power SYBR Green PCR Master Mix kit (Applied Biosystems), according to the manufacturer's instructions. The cycling conditions were as follows: initial denaturation at 95°C for 5 min, followed by 40 cycles at 94°C for 30 s, 56°C for 30 s, and 72°C for 30 s. The experiments were performed in triplicate. Relative quantification of target genes was calculated according to the 2^{- $\Delta\Delta C_t$} method (Schmittgen & Livak, 2008).

Sporozoite viability assay

Freshly dissected *P. berghei*-GFP sporozoites were incubated with varying concentrations of *Artemisia* infusion for 1 h. Then the infusion was removed by centrifugation and sporozoites resuspended in culture medium. 1 μ L of propidium iodide (Gibco) was added to 15,000 cells and incubated for 2–3 min. A 15- μ L aliquot of sporozoite suspension was put on a KOVA Glasstic microscopic slide (KOVA International) and visualized under a microscope. Finally, dead and viable sporozoites were quantified under epifluorescence microscope.

In vitro screening assay for sporozoite motility inhibition via video microscopy

SGs from infected mosquitoes (17–24 d post infectious blood) feeding on Swiss mice infected with *P. berghei*-GFP were isolated by hand dissection and placed into Leibovitz L15 media (11415049; Gibco) supplemented with 20,000 units penicillin–streptomycin (15140122; Gibco) and amphotericin B. Sporozoites were then released by SG mechanical disruption, filtered through a 40- μ m mesh (Cell Strainer, Falcon) to remove SG debris and diluted in activation medium

(William's E medium supplemented with 10% of fetal clone III serum, 1% penicillin–streptomycin, 5 \times 10⁻³ g/l human insulin, and 5 \times 10⁻⁵ M hydrocortisone) to a final concentration of 400,000 sporozoites/ml and kept on ice. Aliquots of 50 μ L were inoculated into wells of a 96-well plate (final amount of ~20,000 sporozoites per well). An equal volume of *Artemisia* infusion dilutions was added to the sporozoites to give a final concentration of (*A. annua* 5%, *A. annua* 10% and *A. afra* 5%) and mixed by gentle pipetting. The plate was centrifuged for 6 min at 900g to maximize the sporozoite settlement and immediately placed at RT for 30 min. Then, the motility of sporozoites was recorded under video microscopy Zeiss Axio Observer 7 at 40X objectives with the GFP excitation/emission filter and pictures were recorded under a frame rate of 1 frame per second with a Hamamatsu Orca Flash 4.0 V3 camera and Zen software for 3 min. Notably, the experiments were performed at 37°C. Finally, the tracking of sporozoites was further analyzed with Fiji ImageJ and the moving patterns characterized on maximum intensity z-projections. Thereby, sporozoites were classed as gliding if they moved with a circular pattern describing at least one complete circle loop during the 3 min acquisition. The percentage residual motile population was then calculated and compared with uninhibited controls (media containing an equivalent amount of water).

SYBR Green-I-based cell proliferation assay

Plasmodium blood stage parasites (regular or apicoplast-free lines) are incubated in 96 well flat bottom plates, 2% hematocrit in 1640 RPMI-HEPES supplemented with 5% AlbuMAX II (GIBCO) and 0.25% gentamycin complemented with appropriate *Artemisia* infusion dilutions and with or with IPP and Cm. Parasites were grown sealed Perspex chambers gassed with β mix gas (1% O₂ 5% CO₂, 94% N₂) at 37°C for 72 h. New 96-well black wall flat-bottom plates are set up with 100 μ L SYBR Green lysis buffer (20 mM Tris, pH 7.5; 5 mM EDTA; 0.008% [wt/vol] saponin; and 0.08% [vol/vol] Triton X-100) with freshly added SYBR Green I (1000X), and 100 μ L from the cultures was transferred and mixed with the SYBR Green lysis buffer and incubated

1 h at room temperature, protected from the light. Fluorescence from each well is measured with TECAN infinite M200 plate reader (excitation: 485 nm, emission: 538 nm and integration time: 1,000 μ s).

Statistical analysis

GraphPad Prism 5 (GraphPad. Software) and Excel 2016 (Microsoft Office) were used in this study for the data analysis. All graph values are represented by means with s.d.

Data Availability

All data are available within the manuscript.

Supplementary Information

Supplementary Information is available at <https://doi.org/10.26508/lsa.202101237>.

Acknowledgements

K Ashraf was supported by Labex ParaFrap-IRD PhD South program (ANR-11-LABX-0024). S Tajeri acknowledges postdoctoral funding support from Fondation pour la Recherche Médicale (FRM) for the PALUKILL project. N Amanzougaghene was supported by Agence nationale de la recherche, project Plasmodrug, and Fondation Sorbonne Université. The work performed by CY Botté and C-S Arnold are supported by Fondation pour la Recherche Médicale (FRM, EQU202103012700), Agence Nationale de la Recherche, France (grant ANR-21-CE44-0010-01, Project ApicoLipidAdapt), Région Auvergne Rhône Alpes (Grant AuRA IRICE GEMELI), Finovi program (Apicolipid project), Laboratoire d'Excellence Parafrap, France (grant ANR-11-LABX-0024), LIA-IRP CNRS Program (Apicolipid project), CEFIPRA-MESRI (Project 6003-1), IDEX Université Grenoble-Alpes and MESRI PhD program fellowship. The investigations on *P. cynomolgi* were funded through a grant from the Agence Nationale de la Recherche, France (ANR-17-CE13-0025-01); IDMIT infrastructure is supported by the French government "Programme d'Investissements d'Avenir" (PIA), under grants ANR-11-INBS-0008 (INBS IDMIT). This work benefited from the support of Maison de l'Artemisia, ITMO I3M, as well as equipment and services from the CELIS cell culture core facility (Paris Brain Institute), a platform supported through the ANR grants, ANR-10-IAIHU-06 and ANR-11-INBS-0011-NeurATRIS. We would like to acknowledge the help of QUANT microscopy platform of the Paris Brain Institute specially David Akbar, Claire Lovo, and Aymeric Millécamps for their help in analysis of microscopic images and sporozoite motility videos. We thank Laurent Rénia, Noah Sather, Philippe Grellier, and Scott Lindner for the kind gift of anti-*Plasmodium* antibodies listed in the Materials and Methods section. The kind help of Sivchheng Phal and Chansopheha Chhin (Institut Pasteur du Cambodge, Phnom Penh, Cambodia) with *P. vivax* experiments is sincerely thanked. We are grateful to Lucile Cornet-Vernet and Pierre Lutgen for providing us *Artemisia* plants.

Author Contributions

K Ashraf: data curation, formal analysis, investigation, methodology, and writing—original draft, review, and editing.

S Tajeri: conceptualization, data curation, formal analysis, supervision, validation, methodology, and writing—original draft, review, and editing.

C-S Arnold: data curation, formal analysis, investigation, methodology, and writing—original draft, review, and editing.

N Amanzougaghene: data curation, formal analysis, and writing—original draft.

J-F Franetich: conceptualization, resources, supervision, investigation, visualization, methodology, and project administration.

A Vantaux: formal analysis.

V Soulard: formal analysis.

M Bordessoulles: formal analysis.

G Cazals: data curation and formal analysis.

T Bousema: formal analysis.

G-J van Gemert: formal analysis.

R Le Grand: formal analysis.

N Dereuddre-Bosquet: formal analysis.

J-C Barale: resources.

B Witkowski: supervision, funding acquisition, validation, and investigation.

G Snounou: data curation, investigation, methodology, project administration, and writing—original draft, review, and editing.

R Duval: conceptualization, data curation, formal analysis, supervision, validation, project administration, and writing—original draft, review, and editing.

CY Botté: conceptualization, data curation, formal analysis, supervision, funding acquisition, validation, investigation, visualization, methodology, project administration, and writing—original draft, review, and editing.

D Mazier: conceptualization, data curation, supervision, funding acquisition, investigation, visualization, methodology, project administration, and writing—original draft, review, and editing.

Conflict of Interest Statement

The authors declare that they have no conflict of interest.

References





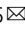
- Amiar S, Katris NJ, Berry L, Dass S, Duley S, Arnold CS, Shears MJ, Brunet C, Touquet B, McFadden GI, et al (2020) Division and adaptation to host environment of apicomplexan parasites depend on apicoplast lipid metabolic plasticity and host organelle remodeling. *Cell Rep* 30: 3778–3792.e9. doi:[10.1016/j.celrep.2020.02.072](https://doi.org/10.1016/j.celrep.2020.02.072)
- Bosson-Vanga H, Franetich JF, Soulard V, Sossau D, Tefit M, Kane B, Vaillant JC, Borrmann S, Müller O, Dereuddre-Bosquet N, et al (2018) Differential activity of methylene blue against erythrocytic and hepatic stages of *plasmodium*. *Malar J* 17: 143. doi:[10.1186/s12936-018-2300-y](https://doi.org/10.1186/s12936-018-2300-y)
- Botte CY, Yamaryo-Botte Y, Rupasinghe TWT, Mullin KA, MacRae JI, Spurck TP, Kalanon M, Shears MJ, Coppel RL, Crellin PK, et al (2013) Atypical lipid composition in the purified relict plastid (apicoplast) of malaria parasites. *Proc Natl Acad Sci U S A* 110: 7506–7511. doi:[10.1073/pnas.1301251110](https://doi.org/10.1073/pnas.1301251110)
- de Korne CM, Lageschaar LT, van Oosterom MN, Baalbergen E, Winkel BMF, Chevalley-Maurel SC, Velders AH, Franke-Fayard BMD, van Leeuwen FWB, Roestenberg M (2019) Regulation of *plasmodium* sporozoite motility by formulation components. *Malar J* 18: 155. doi:[10.1186/s12936-019-2794-y](https://doi.org/10.1186/s12936-019-2794-y)
- de Ridder S, van der Kooy F, Verpoorte R (2008) *Artemisia annua* as a self-reliant treatment for malaria in developing countries. *J Ethnopharmacol* 120: 302–314. doi:[10.1016/j.jep.2008.09.017](https://doi.org/10.1016/j.jep.2008.09.017)

- Dembele L, Gego A, Zeeman AM, Franetich JF, Silvie O, Rametti A, Le Grand R, Dereuddre-Bosquet N, Sauerwein R, van Gemert GJ, et al (2011) Towards an *in vitro* model of *plasmodium* hypnozoites suitable for drug discovery. *PLoS One* 6: e18162. doi:10.1371/journal.pone.0018162
- du Toit A, van der Kooy F (2019) *Artemisia afra*, a controversial herbal remedy or a treasure trove of new drugs? *J Ethnopharmacol* 244: 112127. doi:10.1016/j.jep.2019.112127
- Elfawal MA, Towler MJ, Reich NG, Weathers PJ, Rich SM (2015) Dried whole-plant *artemisia annua* slows evolution of malaria drug resistance and overcomes resistance to artemisinin. *Proc Natl Acad Sci U S A* 112: 821–826. doi:10.1073/pnas.1413127112
- Gural N, Mancio-Silva L, Miller AB, Galstian A, Butty VL, Levine SS, Patrapuvich R, Desai SP, Mikolajczak SA, Kappe SHI, et al (2018) *In vitro* culture, drug sensitivity, and transcriptome of *plasmodium vivax* hypnozoites. *Cell Host Microbe* 23: 395–406.e4. doi:10.1016/j.chom.2018.01.002
- Imwong M, Suwannasin K, Kunasol C, Sutawong K, Mayxay M, Rekol H, Smithuis FM, Hlaing TM, Tun KM, van der Pluijm RW, et al (2017) The spread of artemisinin-resistant *plasmodium falciparum* in the greater mekong subregion: A molecular epidemiology observational study. *Lancet Infect Dis* 17: 491–497. doi:10.1016/S1473-3099(17)30048-8
- Janse CJ, Franke-Fayard B, Mair GR, Ramesar J, Thiel C, Engelmann S, Matuschewski K, van Gemert GJ, Sauerwein RW, Waters AP (2006) High efficiency transfection of *plasmodium berghei* facilitates novel selection procedures. *Mol Biochem Parasitol* 145: 60–70. doi:10.1016/j.molbiopara.2005.09.007
- Liu NQ, Van der Kooy F, Verpoorte R (2009) *Artemisia afra*: A potential flagship for african medicinal plants? *South Afr J Bot* 75: 185–195. doi:10.1016/j.sajb.2008.11.001
- Lu F, Culleton R, Zhang M, Ramaprasad A, von Seidlein L, Zhou H, Zhu G, Tang J, Liu Y, Wang W, et al (2017) Emergence of indigenous artemisinin-resistant *plasmodium falciparum* in africa. *N Engl J Med* 376: 991–993. doi:10.1056/NEJMc1612765
- Manzoni G, Briquet S, Risco-Castillo V, Gaultier C, Topçu S, Ivănescu ML, Franetich JF, Hoareau-Coudert B, Mazier D, Silvie O (2014) A rapid and robust selection procedure for generating drug-selectable marker-free recombinant malaria parasites. *Sci Rep* 4: 4760. doi:10.1038/srep04760
- Mazier D, Rénia L, Snounou G (2009) A pre-emptive strike against malaria's stealthy hepatic forms. *Nat Rev Drug Discov* 8: 854–864. doi:10.1038/nrd2960
- McFadden GI, Yeh E (2017) The apicoplast: Now you see it, now you don't. *Int J Parasitol* 47: 137–144. doi:10.1016/j.ijpara.2016.08.005
- Mikolajczak SA, Vaughan AM, Kangwanrangsang N, Roobsoong W, Fishbaugh M, Yimamnuaychok N, Rezakhani N, Lakshmanan V, Singh N, Kaushansky A, et al (2015) *Plasmodium vivax* liver stage development and hypnozoite persistence in human liver-chimeric mice. *Cell Host Microbe* 17: 526–535. doi:10.1016/j.chom.2015.02.011
- Pewkliang Y, Rungin S, Lerdpanyangam K, Duangmanee A, Kanjanasirirat P, Suthivanich P, Sa-ngiamsuntorn K, Borwornpinoy S, Sattabongkot J, Patrapuvich R, et al (2018) A novel immortalized hepatocyte-like cell line (imhc) supports *in vitro* liver stage development of the human malarial parasite *plasmodium vivax*. *Malar J* 17: 50. doi:10.1186/s12936-018-2198-4
- Schmittgen TD, Livak KJ (2008) Analyzing real-time PCR data by the comparative C(T) method. *Nat Protoc* 3: 1101–1108. doi:10.1038/nprot.2008.73
- e Silva LFR, de Magalhães PM, Costa MRF, Alecrim MdGC, Chaves FCM, Hidalgo AdF, Pohlit AM, Vieira PPR (2012) *In vitro* susceptibility of *plasmodium falciparum* welch field isolates to infusions prepared from *artemisia annua* L. Cultivated in the brazilian amazon. *Mem Inst Oswaldo Cruz* 107: 859–866. doi:10.1590/s0074-02762012000700004
- Snider D, Weathers PJ (2021) *In vitro* reduction of *plasmodium falciparum* gametocytes: *Artemisia* spp. Tea infusions vs. Artemisinin. *J Ethnopharmacol* 268: 113638. doi:10.1016/j.jep.2020.113638
- Suberu JO, Gorka AP, Jacobs L, Roepe PD, Sullivan N, Barker GC, Lapkin AA (2013) Anti-plasmodial polyvalent interactions in *Artemisia annua* L. aqueous extract—possible synergistic and resistance mechanisms. *PLoS One* 8: e80790. doi:10.1371/journal.pone.0080790
- Uddin T, McFadden GI, Goodman CD (2018) Validation of putative apicoplast-targeting drugs using a chemical supplementation assay in cultured human malaria parasites. *Antimicrob Agents Chemother* 62: e01161–e01167. doi:10.1128/aac.01161-17
- Uwimana A, Legrand E, Stokes BH, Ndikumana JM, Warsame M, Umulisa N, Ngamije D, Munyaneza T, Mazarati JB, Munguti K, et al (2020) Emergence and clonal expansion of *in vitro* artemisinin-resistant *plasmodium falciparum* kelch13 r561h mutant parasites in Rwanda. *Nat Med* 26: 1602–1608. doi:10.1038/s41591-020-1005-2
- Vaughan AM, O'Neill MT, Tarun AS, Camargo N, Phuong TM, Aly AS, Cowman AF, Kappe SH (2009) Type ii fatty acid synthesis is essential only for malaria parasite late liver stage development. *Cell Microbiol* 11: 506–520. doi:10.1111/j.1462-5822.2008.01270.x
- WHO (2019a) Who technical document of the use of non-pharmaceutical forms of artemisia.
- WHO (2019b) World malaria report.
- Yeh E, DeRisi JL (2011) Chemical rescue of malaria parasites lacking an apicoplast defines organelle function in blood-stage *plasmodium falciparum*. *PLoS Biol* 9: e1001138. doi:10.1371/journal.pbio.1001138
- Yu M, Kumar TR, Nkrumah LJ, Coppi A, Retzlaff S, Li CD, Kelly BJ, Moura PA, Lakshmanan V, Freundlich JS, et al (2008) The fatty acid biosynthesis enzyme fabi plays a key role in the development of liver-stage malarial parasites. *Cell Host Microbe* 4: 567–578. doi:10.1016/j.chom.2008.11.001



License: This article is available under a Creative Commons License (Attribution 4.0 International, as described at <https://creativecommons.org/licenses/by/4.0/>).

Toxoplasma LIPIN is essential in channeling host lipid fluxes through membrane biogenesis and lipid storage

Sheena Dass^{1,4}, Serena Shunmugam ^{1,4}, Laurence Berry², Christophe-Sebastien Arnold¹, Nicholas J. Katris¹, Samuel Duley¹, Fabien Pierrel ³, Marie-France Cesbron-Delauw¹, Yoshiki Yamaro-Botté^{1,5}  & Cyrille Y. Botté ^{1,5} 

Apicomplexa are obligate intracellular parasites responsible for major human diseases. Their intracellular survival relies on intense lipid synthesis, which fuels membrane biogenesis. Parasite lipids are generated as an essential combination of fatty acids scavenged from the host and de novo synthesized within the parasite apicoplast. The molecular and metabolic mechanisms allowing regulation and channeling of these fatty acid fluxes for intracellular parasite survival are currently unknown. Here, we identify an essential phosphatidic acid phosphatase in *Toxoplasma gondii*, TgLIPIN, as the central metabolic nexus responsible for controlled lipid synthesis sustaining parasite development. Lipidomics reveal that TgLIPIN controls the synthesis of diacylglycerol and levels of phosphatidic acid that regulates the fine balance of lipids between storage and membrane biogenesis. Using fluxomic approaches, we uncover the first parasite host-scavenged lipidome and show that TgLIPIN prevents parasite death by 'lipotoxicity' through effective channeling of host-scavenged fatty acids to storage triacylglycerols and membrane phospholipids.

¹ Apicolipid Team, Institute for Advanced Biosciences, CNRS UMR5309, Université Grenoble Alpes, INSERM U1209, Grenoble, France. ² Laboratory of Pathogen Host Interactions, UMR 5235, Université de Montpellier, Montpellier, France. ³ Université Grenoble Alpes, CNRS, Grenoble INP, TIMC-IMAG, Grenoble, France. ⁴ These authors contributed equally: Sheena Dass, Serena Shunmugam. ⁵ These authors jointly supervised this work: Yoshiki Yamaro-Botté, Cyrille Y. Botté.  email: yoshiki.botte-yamaro@univ-grenoble-alpes.fr; cyrille.botte@univ-grenoble-alpes.fr

Apicomplexa includes several pathogenic protists that are responsible for major chronic and infectious diseases with a massive social and economic burden. *Toxoplasma gondii* and *Plasmodium falciparum* parasites are responsible for toxoplasmosis and malaria, respectively. These obligate intracellular parasites have an enormous demand for lipids in maintaining their survival within their human host cells. The utilization of fatty acids (FA) to synthesize complex lipids is an essential determinant for successful host adaptation by these parasites. Apicomplexa meet their high need for lipids through de novo synthesis via type II fatty acid synthesis (FASII) within the apicoplast and via copious salvage directly from the host and extracellular environment^{1–6}. Recent data suggest that the tight regulation of FA flux between host, parasite, and its metabolic organelles is particularly vital for intracellular development of these apicomplexa pathogens^{4,7}. Metabolic adaptation of the parasite toward host nutritional environment is also important for parasite propagation⁴. For instance, in low nutrient environments, the parasite is able to form giant multivesicular bodies (gMVBs) in the host, which somehow facilitates the parasite's ability to scavenge lipids in suboptimal nutritional conditions⁴. However, the molecular and metabolic pathways controlling the lipid flux toward parasite membrane biogenesis and storage remain largely unknown.

Phosphatidic acid (PA), the simplest glycerophospholipid, contributes to the regulation of FA flux in apicomplexa, as it is the key intermediate balancing the biosynthesis of both glycerophospholipids and triacylglycerols (TAGs) toward membrane biogenesis and lipid storage in eukaryotes⁸. PA has pleiotropic roles within the parasite: (i) as a signal transducer modulating parasite invasion, motility, and egress, produced by the action of diacylglycerol kinases (DGK1 and DGK2)^{9–12}, (ii) as a regulator of lysoPA (LPA)/PA levels for modulating membrane curvature for cytokinesis and endocytosis, formed by acyltransferase ATS2⁴, and (iii) as the central precursor for bulk phospholipid synthesis and membrane biogenesis, made de novo from FA and a glycerol-3-phosphate backbone by the sequential acylation catalyzed by acyltransferases, in the apicoplast/ER pathways formed by ATS1/GPAT and ATS2/AGPAT^{4,13}. Further, PA can be catabolized to a key lipid class, diacylglycerol (DAG) by phosphatidic acid phosphatases (PAP), which play vital metabolic functions in eukaryotes¹⁴. Together, PA and DAG are central lipid precursors from which most lipid classes can be generated de novo. This includes all phospholipids made from PA and DAG via the CDP-DAG from PA and the Kennedy pathway from DAG, respectively^{15,16}. DAG is also the precursor for the synthesis of the major storage lipids, TAG.

Since PA is pivotal for parasite lipid metabolism, the enzymes involved in PA metabolism are critical for understanding parasite pathogenesis. One such critical enzyme class is PAP, as it allows to fine-tune the balance between PA and DAG. Apicomplexa parasites possess three putative PAPs, none of which have been characterized to date.

Here, we determined that *Toxoplasma gondii* LIPIN; TgLIPIN is a PAP that localizes to the cytosolic-ER interface and is essential for the intracellular survival of tachyzoites. Its inducible disruption quickly leads to aberrant membrane anomalies, mostly at the IMC and the endomembrane system, causing division defects and parasite death. Lipidomics of the mutant reveals a time-dependent accumulation of PA and free FA (FFA), concomitant with the reduction of DAG, lipid droplets, and storage, TAG. Both lipidomic and cellular membrane phenotypes are aggravated in a high host nutrient environment. The mutant dies from a lipotoxic accumulation of FFA and major membrane phospholipids, specifically PA. Further, we conducted novel fluxomic experiments using U-¹³C glucose-labeled host cells to

monitor the host FA scavenging capacity of the parasite, providing the first host-scavenged lipidome of *Toxoplasma*. This approach showed that TgLIPIN channels host FA to maintain an appropriate PA/DAG synthesis ratio. TgLIPIN acts as a metabolic checkpoint, tightly regulating membrane biogenesis versus lipid storage, which is essential for proper intracellular growth division and survival.

Results

***Toxoplasma gondii* genome encodes a single lipin, TgLIPIN, which has functional phosphatidate phosphatase activity.** Bioinformatics analysis revealed that *T. gondii* parasites possess a single lipin homolog, much larger than other phosphatidate phosphatases encoded by the genome of *T. gondii*, and which we named TgLIPIN (TGGT1_230690). TgLIPIN possesses the two typical and highly conserved domains of eukaryotic lipins, the amino-terminal N-LIP domain, and the carboxy-terminal C-LIP domain harboring its functional PA phosphatase catalytic motif DXDXT/V (HAD-like domain, Fig. 1a)¹⁷. Phylogenetic analysis confirms that the enzyme is highly conserved as a single lipin within phylum Apicomplexa, cladding specifically within a coccidian subgroup (Supplementary Fig. 1a).

To confirm the predicted phosphatidic acid phosphatase activity of TgLIPIN (Fig. 1b), we performed heterologous complementation using a *Saccharomyces cerevisiae* triple mutant, $\Delta dpp1\Delta lpp1\Delta pah1$, that is deficient in PAP activity with a temperature-sensitive phenotype (low growth at 37 °C)^{18,19}. We attempted to generate the full TgLIPIN sequence and the corresponding recombinant protein but were not able to do so, due to limitations posed by the large size of the protein. Instead, we successfully generated TgLIPIN C-LIP domain, containing the putative catalytic (HAD-like) domain of the protein, and expressed it in the yeast mutant. We thus conducted lipidomic analyses on the yeast mutant, complemented or not with TgLIPIN C-LIP domain. The yeast mutant displayed a severe and significant accumulation of PA and a significant reduction of DAG compared to the wild-type yeast strain, corresponding to the loss of PA phosphatase activity (Fig. 1c). Complementation of the yeast mutant with the C-LIP domain of TgLIPIN fully restored the levels of PA and DAG to those of the wild type, thus confirming its predicted PAP activity (Fig. 1b, c).

To determine its cellular localization, TgLIPIN was endogenously tagged with 3×HA at its C-terminal end²⁰. Immunofluorescence assay (IFA) and colocalization with known organelle markers revealed a broad cytosolic and perinuclear localization (Supplementary Fig. 1b). Interestingly TgLIPIN lacks an apparent nuclear localization signal (NLS), possessed by most eukaryotic LIPINs^{8,21}. To further resolve its localization, we conducted IFAs of TgLIPIN-HA with a known *Toxoplasma* ER marker, DER-1-GFP²² an episomally expressing plasmid, which confirmed proximity to the endomembrane system with partial ER colocalization (Fig. 1d). TgLIPIN was not further detected outside the parasite or in the host cell (Supplementary Fig. 1b).

TgLIPIN disruption induces rapid membrane malformation, division, and replication defects leading to parasite death, all aggravated under a high host nutrient environment.

To understand the importance of TgLIPIN in parasite growth, we generated an N-terminal HA-tagged inducible knockdown parasite line based on the Tet-off system, TgLIPIN-ikD^{23,24} (Supplementary Fig. 2a, b). Downregulation of TgLIPIN-ikD showed no detectable protein by western blot after 48 h of anhydrotetracycline (ATc) treatment (Fig. 2a). Cytoplasmic localization of the protein in the same manner as C-terminally tagged strains and its downregulation were both confirmed by IFA (Fig. 2b). This result

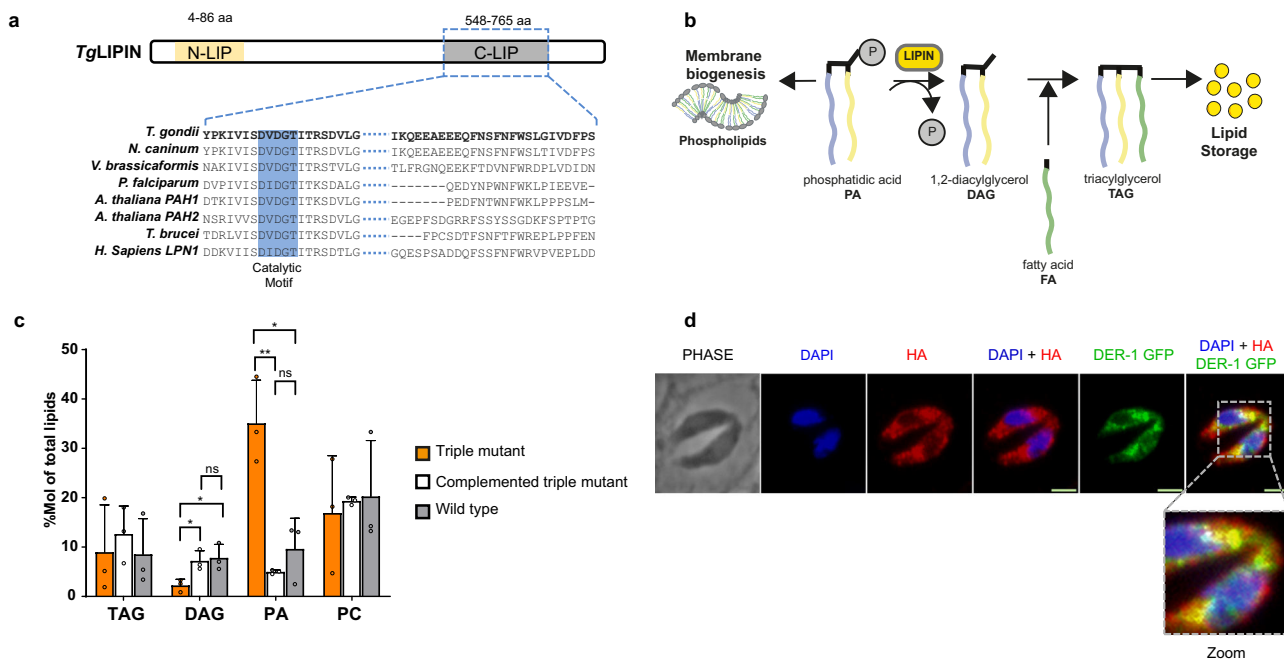


Fig. 1 | *T. gondii* LIPIN (*TgLIPIN*) is a phosphatidate phosphatase localized to parasite cytoplasm and endoplasmic reticulum. **a The C-LIP domain of *TgLIPIN* is evolutionarily conserved among eukaryotic orthologs and harbors the catalytic motif DVDGT known to be central to PA phosphatase activity. **b** Graphical scheme of the biochemical function of LIPIN in the glycerolipid biosynthesis pathway in eukaryotes. **c** The complementation of the yeast triple KO mutant ($\Delta dpp1\Delta lpp1\Delta pah1$), lacking phosphatidic acid phosphatase activity, with the C-LIP domain of *TgLIPIN* restores PA and DAG ($n = 3$, unpaired t test P values where $*P = 0.024$ DAG triple mutant vs DAG complemented triple mutant, $*P = 0.032$ DAG triple mutant vs DAG wild-type, $**P = 0.0039$ PA triple mutant vs PA complemented triple mutant, $*P = 0.039$ PA triple mutant vs PA wild type). Data are presented as mean values \pm SEM. **d** IFA of *TgLIPIN*-HA (endogenous C-terminal tag) with anti-HA, DAPI, and a transiently expressed DER-1-GFP plasmid shows co-localization of *TgLIPIN* to the ER of the parasite. Scale bar: 2.0 μ m.**

suggests that *TgLIPIN* disruption dramatically impacts parasite intracellular growth and development *TgLIPIN* disruption caused a severe intracellular replication defect in *TgLIPIN*-ikD with a significant increase of small vacuoles containing 1–2 parasite vacuoles (15–20%) and vacuoles containing morphologically abnormal parasites (15–20%), alongside with a concomitant significant decrease of larger vacuoles (25–30%) containing 4–10 parasites (Fig. 2c). To further assess the effect of *TgLIPIN* on parasite intracellular growth, plaque assays were performed investigating the mutant’s capacity to maintain proper growth with fluctuating levels of host nutrients. When cultured in regular growth conditions with 1% FBS, *TgLIPIN*-ikD (+ATc) exhibited a severe growth defect with few plaques (Fig. 2d, e) as expected from IFA results (Fig. 2b, f). To rescue this defect, the parasites were grown in high nutrient content with 10% FBS⁴. However, surprisingly, *TgLIPIN*-ikD (+ATc) showed a more significant decline in growth in 10% than with 1% FBS containing culture medium, as marked by the complete absence of plaques (Fig. 2d, e). Contrastingly, a decrease in the host nutritional environment with 0% FBS slightly but significantly enhanced the growth of *TgLIPIN*-ikD (+ATc) (Fig. 2d, e) suggesting that exogenous lipid-nutrient source of FFA or PL are somehow toxic to parasites lacking *TgLIPIN*. To further delineate the division defect phenotype of *TgLIPIN* downregulation, we performed IFAs to probe the morphology of the inner membrane complex (IMC) as a marker of parasite shape and division. IFAs were conducted prior to and after complete protein loss, at 24 h (Fig. 2f and Supplementary Fig. 2c) and 48 h (Fig. 2g) of ATc treatment, respectively, under low, normal, and high host nutrient contents. Severe membrane anomalies and division defects were observed even as early as 24-h ATc treatment. Such membrane defects were

strongly increased at 48-h ATc treatment, with membrane extrusion, loss of parasite integrity, and division arrest. Importantly, IMC and division defect were more evident when host nutrient content increased.

Electron microscopy reveals gross membrane anomalies as an early impact of *TgLIPIN* downregulation. To further resolve the cellular phenotype marked by *TgLIPIN* downregulation, *TgLIPIN*-ikD (+ATc) parasites were examined by transmission electron microscopy (TEM) at 12, 24, and 48 h post ATc treatment under low, normal, and high host nutrient content (0%, 1%, and 10% FBS, respectively). Interestingly, as early as 12 h of treatment with ATc, when *TgLIPIN* levels are only slightly reduced, both parasite IMC and plasma membrane displayed gross abnormalities in forming evaginations or lateral interruptions, without affecting the parasite size (Fig. 3a–c). Concordantly, IFA data of *TgLIPIN*-ikD (+ATc) also hinted at aberrant IMC (Fig. 2f, g). The morphology of the nuclear envelope (NE) started to adopt tubular or multilobed shapes (Fig. 3d–d¹ and Supplementary Fig. 3). Extensions of the NE seemed to expand in the cytoplasm in connection with the ER (Supplementary Fig. 3a) making tubular whorls in the cytoplasm (Fig. 3e–e¹). At 48-h treatment, tubular or multilamellar membrane accumulation could entirely fill the cytoplasm of the parasites (Fig. 3f–f¹). Local fusion of the outer membrane of different nuclear lobes could be observed (Supplementary Fig. 3b). The NE tended to adopt hairpin shapes where the inner membrane from two different regions was seen closely apposed, separated by electron-dense material (Supplementary Fig. 3c, e). Local detachment and fusion of the inner membranes could be also observed (Supplementary Fig. 3e, red arrow). Interestingly, similar expansions affecting the NE are also

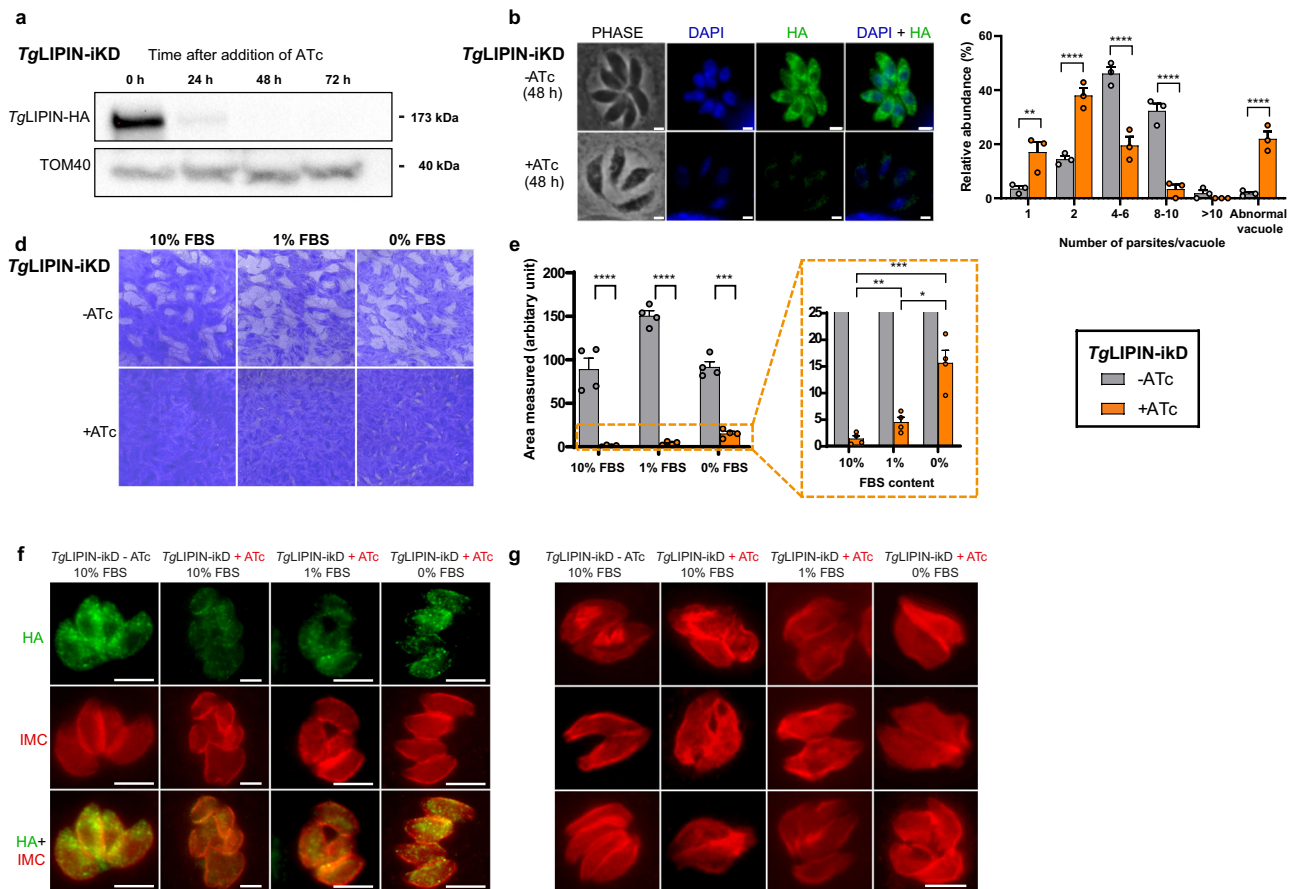


Fig. 2 TgLIPIN is indispensable for parasite replication and growth within its host. **a** Western blot shows *TgLIPIN* downregulation, 48 h + ATc (0.5 μ g/ml), *TgLIPIN* (anti-HA), and TOM40 (control). **b** IFA of *TgLIPIN-ikD*, indicating loss of protein using anti-HA antibody at 48 h + ATc. Scale bar: 2.0 μ m. **c** Replication rate of *TgLIPIN* parasites grown with (+) or without (–) ATc measured by parasite number per parasitophorous vacuole after 24 h of growth post infection (>100 vacuoles were counted per biological replicate; $n = 3$, unpaired t test P values where $**P = 0.002$ –ATc vs +ATc 1 parasite/vacuole, $****P < 0.000001$ –ATc vs +ATc 2/4-6/8-10 and abnormal parasite/vacuole). Data are presented as mean values \pm SEM. **d** *TgLIPIN-ikD* plaque assays measuring parasite growth over 8–10 days (+/–ATc) in different FBS conditions. **e** shown as a bar graph (10%, 1% and 0%; $n = 4$, unpaired t test P values where $****P < 0.000001$ –ATc vs +ATc 10/1/0% FBS, $**P = 0.026$ +ATc 10% FBS vs +ATc 1% FBS, $***P = 0.0001$ +ATc 10%FBS vs +ATc 0% FBS, $**P = 0.0047$ +ATc 1% FBS vs +ATc 0% FBS). Data are presented as mean values \pm SEM. **f** IFA illustrating early phenotypic effects of *TgLIPIN* depletion (24 h+ ATc) showing the presence of residual protein (HA-green). Inner membrane complex antibody (IMC- red) clearly shows aberrant IMC membrane biogenesis. **g** IFA illustrating the phenotypic effects of *TgLIPIN* depletion after 48 h (+ATc) using anti-IMC antibody in *TgLIPIN-ikD*. Scale bar: 5.0 μ m.

observed in the yeast LIPIN mutant coupling phospholipid biosynthesis to the nuclear membrane^{25,26}.

Both parasite IMC and plasma membrane (PM) also displayed abnormalities in forming bumps (Fig. 3d, red arrow) or lateral evaginations (Fig. 3g–g²). Large inclusions could be observed in the vacuolar space that could correspond to such abnormal parasite evagination depending on the cutting plane. Complex structures were also observed in the cytoplasm, showing lasso-like structures formed by zippered membrane tubules (Supplementary Fig. 3f, g). It is not clear whether this type of structure originated from the ER, the nuclear membrane, or even IMC.

At 48 h, the ultrastructure of the vacuole appeared dramatically altered. Endodyogeny was strongly affected in *TgLIPIN-ikD* parasites, showing incomplete sister cells separation (Fig. 3e¹–f¹), cytokinesis failure harboring multiple daughter cells (Fig. 3h–i², red asterisk). Local fusion of the parasitophorous membrane (PVM) with the PM of the parasite was also observed (Fig. 3f). Some vacuoles showed signs of parasite PM rupture, with cytoplasmic material reminiscent of parasite cytoplasm filling the vacuolar space (Fig. 3g², h², i¹). Large autophagosomes with

unidentified content were also frequently observed in infected host cells suggesting that the parasites died and were eliminated by the host cell (Supplementary Fig. 3h–k). Large giant multivesicular bodies (gMVBs) and swelling of the host NE, previously described as enhanced under starvation conditions⁴ were abundant in *TgLIPIN-ikD* parasites, even in the presence of 10% FBS. In some cases, the outer membrane of the NE had fused with the PVM (Supplementary Fig. 3c), occasionally leading to its rupture (Supplementary Fig. 3d).

In agreement with the replication assay data (Fig. 2c), TEM images showed that dynamics of parasite membranes was profoundly affected by the absence of appropriate levels of *TgLIPIN*, which seemed to start at the NE level as soon as 12 h of treatment. Further loss of *TgLIPIN* then induced strong aberrant membrane abnormalities mostly affecting the endomembrane system (NE, ER, IMC, and PM). This resulted in endodyogeny failure, anarchic membrane proliferation, and unexpected membrane fusion events, leading to parasite growth arrest and death. These membrane abnormalities and division phenotypes were observed in all host nutrient contents, but were always

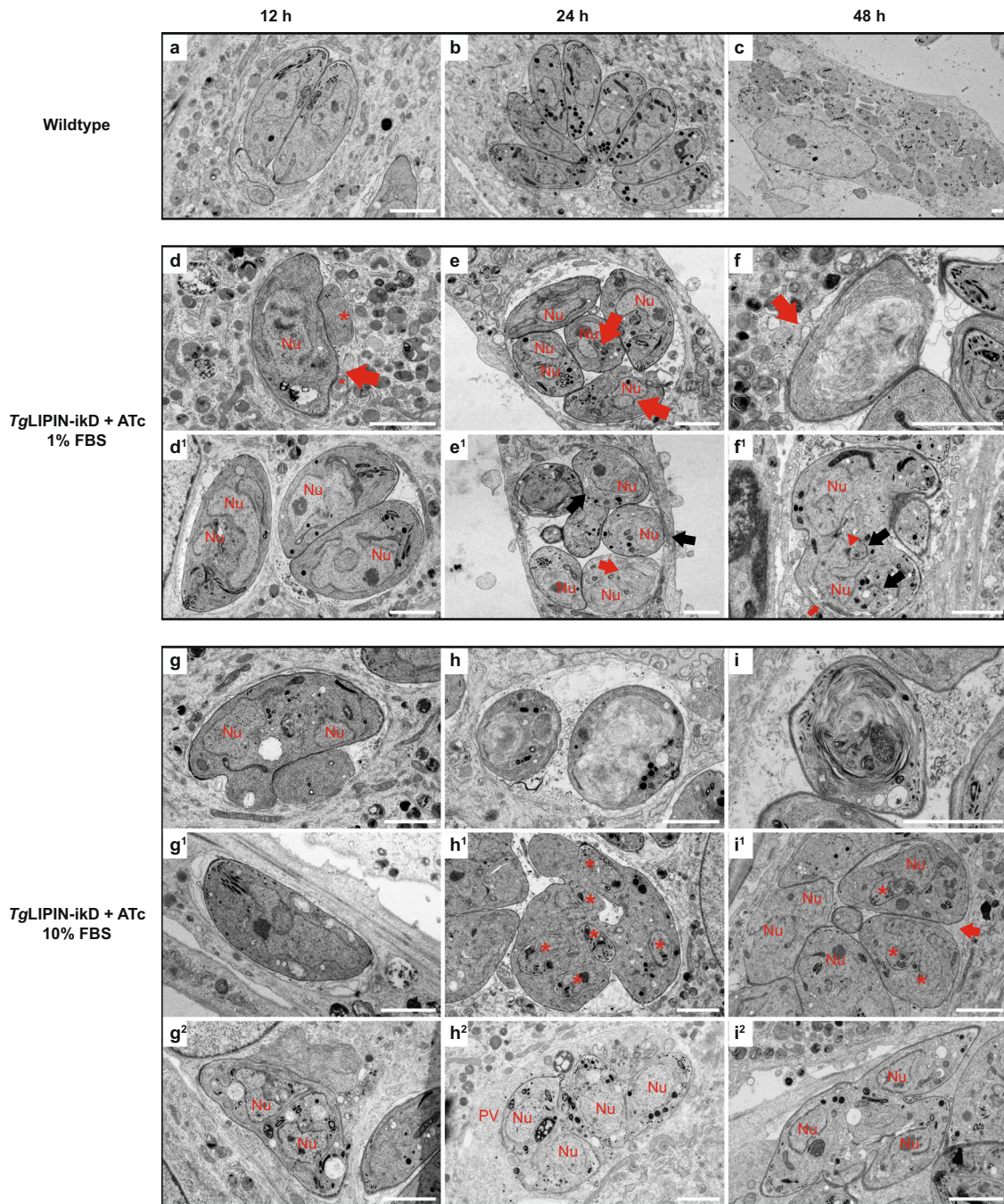


Fig. 3 TgLIPIN depletion results in gross membrane anomalies early in the process of ATc downregulation. Transmission electron micrographs showing wild-type (a–c) and *TgLIPIN-ikD* parasites at 1% (d–f) or 10% FBS (g–i), after 12, 24, and 48 h of ATc treatment. After 12 h of growth, wild-type parasites showed vacuoles containing (a) 2–4 parasites, (b) 8–16 parasites at 24 h, and (c) after 48 h, the first round of egress/reinvasion has occurred showing cells with multiple small vacuoles showing regular nuclei and organelles. **d–f** *TgLIPIN-ikD* parasites show membrane anomalies as early as **d–d'** 12 h of induction. Vacuoles showed large inclusions in the parasitophorous vacuole, red asterisks. **d'** Nuclei showed a multilobed shape even in the absence of early signs of mitosis. **e–e'** At 24 h, nuclear envelope showed pronounced anomalies with elongations connected with rough ER tubules, red arrows. **e'** The ER showed exaggerated proliferation generating big membrane whorls. Incomplete cytokinesis was observed, black arrow. **f** Forty-eight hours after induction, parasites were full of ER-derived membranes and there was the fusion of the parasitophorous membrane (PVM) and parasite plasma membrane (PM), red arrow. **f'** Endodogony defect: a new round of mitosis started, shown by the presence of IMC buds (black arrows) and centrosome (red arrowhead), while two sister cells from the previous generation have not separated. **g–i** All membrane defects were present and enhanced in 10% FBS. **g–g'** At 12 h, nucleus elongation and cytoplasmic evaginations were observed. **g''** Cytokinesis failure was observed. **h–h'** At 24 h, ER proliferation and cytokinesis defect were observed. Vacuoles showed signs of necrosis with PM rupture and cytoplasmic leakage in the vacuolar space. **i** At 48 h, *TgLIPIN-ikD* did not reinvade, the remaining vacuoles showed profoundly abnormal parasites, **i'** PVM or **i''** PM rupture/cytokinesis failure. Nu nucleus. Scale bar: 2 μm, *n* = 3.

stronger and aggravated under high host nutrient content (10% FBS). This suggests that the essential role of TgLIPIN for membrane biogenesis and parasite survival is directly linked to the nutritional status of the host.

TgLIPIN regulates lipid homeostasis. To determine the functional role of TgLIPIN in parasite PA synthesis and membrane biogenesis, we conducted comprehensive lipidomic analyses. To precisely assess the timely impact of TgLIPIN-ikD disruption on lipid synthesis, parasites were grown for 24 or 48 h with and without ATc. Total lipids were separated by high-performance thin-layer chromatography (HPTLC) and quantified by gas chromatography–mass spectrometry (GC–MS). Relative abundance of PA was unchanged at 24 h of +ATc (Fig. 4a). After 48 h +ATc, there was a large significant increase of PA, confirming its role for PA synthesis and our WB results for the loss of TgLipin (Fig. 4a). FA composition of PA showed an increase in the level of myristic (C14:0) and palmitic (C16:0) acids along with a decline in the levels of stearate (C18:0) (Fig. 4b). Concomitantly to PA increase, the relative abundance of DAG was decreased after 48 h of TgLIPIN downregulation by ATc (Fig. 4c) showing that TgLIPIN is an active phosphatidic acid phosphatase, controlling the levels of PA and DAG, as confirmed by our yeast heterologous complementation (Fig. 1c). Despite a strong replication defect and reduction in parasite number, the total amount of phospholipids was increased up to 1.5-fold in the TgLIPIN-ikD (+ATc) in comparison to the control (–ATc) (Supplementary Fig. 4a). Accordingly, most PL classes were further increased by TgLIPIN disruption such as the ones usually made from PA via the CDP–DAG pathway²⁵ i.e., cardiolipin (CL), PS, and PC (Supplementary Fig. 4b). This suggests that TgLIPIN controls PL homeostasis likely through PA synthesis.

In eukaryotes, TAG biosynthesis occurs at the last step of the glycerol-3-phosphate pathway through the *sn*-3 acylation of DAG catalyzed by a diacylglycerol-acyltransferase (DGAT) that uses FFA^{7,26,27}. However, the key and limiting step of TAG synthesis is the formation of its precursor, DAG, the production of which depends on the action of a PAP/LIPIN. TAG is not a membrane but a storage lipid that accumulates within lipid droplets together with other neutral lipids such as cholesteryl esters (CE). We thus investigated the putative role of TgLIPIN in lipid-storage formation by comparing the number of parasite lipid droplets using Nile red staining²⁸ in the TgLIPIN-ikD parasites (+ATc and –ATc). This showed that the number of lipid droplets per parasite vacuole in the presence of ATc was reduced to almost 60% in comparison to the control in both normal (1% FBS) and furthermore in high host nutrient content (10% FBS) (Fig. 4d, e), suggesting that TgLIPIN is involved in the synthesis of storage lipids. According to this hypothesis, the relative abundance of TAGs was significantly reduced after 48 h of ATc treatment (Fig. 4f). Other neutral lipids making the bulk of lipid droplets, CE levels were also significantly decreased (Supplementary Fig. 4d).

TAGs and CEs are neutral storage lipids potentially implicit in the parasite's ability to cope with the excess FA⁷. The synthesis of TAG via enzyme DGAT requires two substrates, DAG and FFA. We, therefore, determined the FFA content of the TgLIPIN-ikD. Lipidomics revealed slight increases in total FFA levels in the TgLIPIN-ikD (+ATc/–ATc) (Fig. 4g). Interestingly, C18:1 (oleate) was the only FA found significantly increased in the parasite-free FA (FFA) pool (Supplementary Fig. 4c), suggesting C18:1 may be an important intermediate in the pathways regulated by TgLIPIN, as previously hinted^{7,29,30}. In a high host environment (10% FBS), lipidomic analyses revealed that only TAG levels decreased under these conditions (Fig. 4h), explaining the reduction of lipid droplets. This impairment in TAG

biosynthesis is consistent with the reduction in parasite viability seen under high FBS conditions (Fig. 2d, e).

TgLIPIN channels the flux of host fatty acids to prevent the accumulation of free fatty acids levels and promotes TAG synthesis. Our data reveal the essential role for TgLIPIN in regulating PA and DAG synthesis to control lipid homeostasis, especially the level of storage lipid molecule, TAG. TgLIPIN function seems directly connected to host nutritional status and the origin of lipid precursors used (FASII, host cell, and external environment) to maintain parasite survival.

Fatty acids required for lipid synthesis in *T. gondii* parasites are obtained from the host and/or host environment (i.e., medium)^{1,2,4,26,29} and/or synthesized de novo via the apicoplast FASII pathway^{12,30,31}. To identify the source of increased FA and phospholipids detected upon TgLIPIN depletion, we set up fluxomics approaches where we grew parasites and/or host cells using different stable isotope substrates-containing media (¹³C-U-glucose, ³¹d-C16:0) and performed lipidomic analyses for each experimental setup (Fig. 5a–c).

To monitor apicoplast FASII activity, parasites were labeled with U-¹³C-glucose, which was added to a glucose-free medium, to confluent host cells together with parasites with or without ATc (Fig. 5a), as previously reported¹³. Total lipid content, PL, and neutral lipids were extracted to determine the ratio of ¹³C incorporation of each FA as a measure of FASII activity. In TgLIPIN-ikD (+ATc), the amount of labeled FA made by FASII (i.e., FASII activity) decreased under the suppression of TgLIPIN (+ATc) in terms of total lipid content (Fig. 5d) as well as the pools of FFA/PL/TAG (Fig. 5e, f and Supplementary Fig. 5a, b). Interestingly, there was a significant decrease in all the signature FA from FASII (i.e., C14:0) but also in FASII-derived FA, i.e., oleic acid C18:1, reduced in total lipids, FFA, PL and TAG made from FASII (Fig. 5d, e, f and Supplementary Fig. 5a, b). There was an overall decrease in FASII-derived C18:1 in FFA (Fig. 5e) and TAG (Fig. 5f, supporting the lipid droplet analyses) and an increase in PC16:0 (Supplementary Fig. 5b). This suggests that with the loss of TgLIPIN, the increased overall PA levels with FASII-derived FAs, can be directed towards the production of excess PC. The distribution of ¹³C incorporation to each isotopologue of FASII FA product confirmed that the pathway was nevertheless functional (Supplementary Fig. 5c–g). To monitor the FAs sourced from the external environment/culture medium, we grew parasites and confluent host cells in a medium supplemented with deuterated palmitic acid (³¹d-C16:0) (Fig. 5b). Parasites were harvested and total lipids were extracted to determine the incorporation of ³¹d-C16:0 in parasite lipids. In the total lipid content, ³¹d-C16:0 and its elongation/desaturation products ³¹d-C18:0 and ²⁹d-C18:1 were detected in lower amounts in the TgLIPIN-ikD parasites with ATc (Fig. 5g). In addition, a drastic reduction in the incorporation of all three (³¹d-C16:0, ³¹d-C18:0, ²⁹d-C18:1) to FFA species within TgLIPIN-ikD (+ATc) in comparison to the control (–ATc), further suggesting that the host external environment is not the source of increased lipids within the mutant (Fig. 5h).

To monitor the fatty acids directly scavenged from the host, we designed a novel assay using U-¹³C-glucose to label host lipids (Fig. 5c). Nonconfluent host cells were grown in the presence of medium containing U-¹³C-glucose which would theoretically fuel any of the active FA synthesis pathways within the host (FASII, elongases) via the synthesis of their substrates, acetyl-CoA, thereby generating ¹³C-pre-labeled host metabolites including lipids and fatty acids³². These ¹³C-pre-labeled host cells were then infected with parasites in the presence of a normal culture medium, which contains regular ¹²C-glucose. Total lipid was

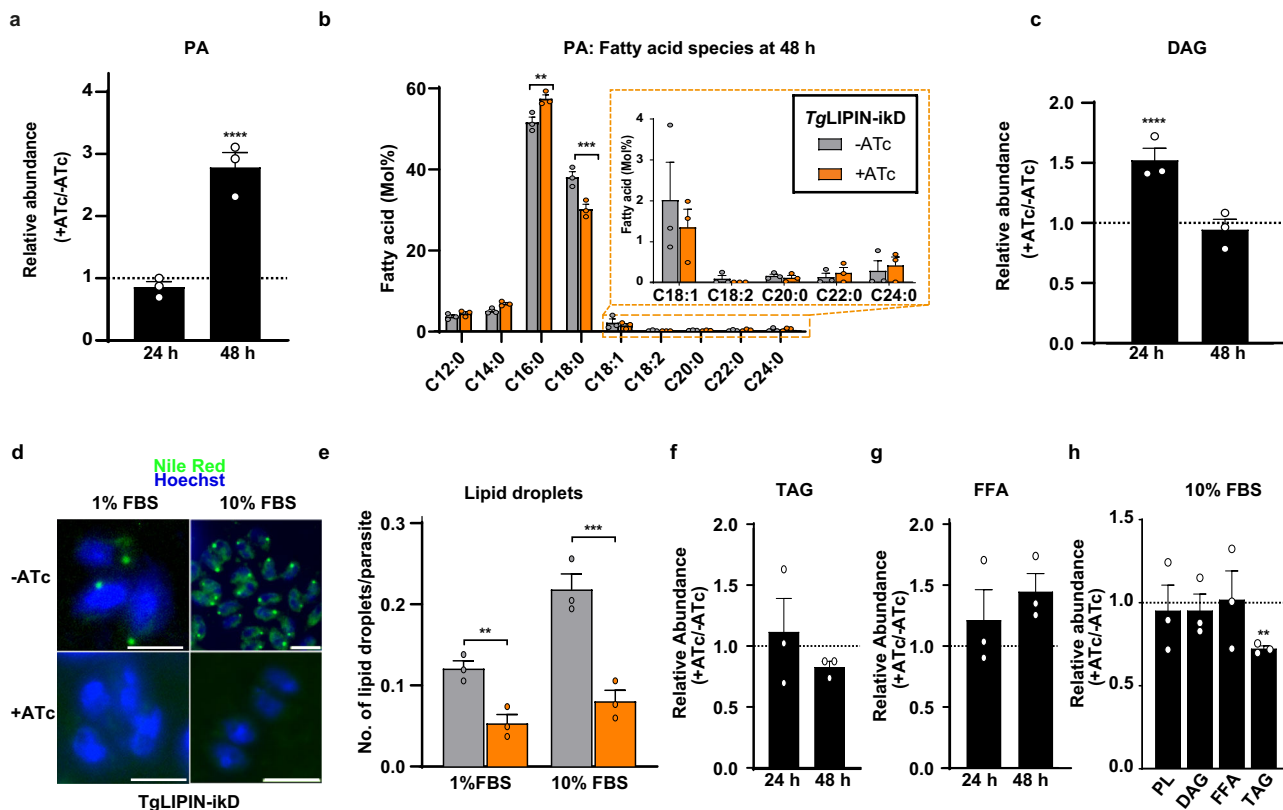


Fig. 4 *TgLIPIN* regulates critical levels of PA and other major phospholipids while generating DAG that is directed toward neutral lipid storage. **a** Relative abundance of PA in *TgLIPIN*-ikD (nmol/parasites number, +ATc/-ATc; %; $n = 3$, unpaired t test P values where **** $P < 0.00001$ relative PA abundance ratio nmol/parasites number +ATc/-ATc at 48 h vs +ATc/-ATc = 1). **b** Fatty acid composition of PA in *TgLIPIN*-ikD (+/-ATc) in Mol%; $n = 3$, unpaired t test P values where ** $P < 0.0021$ PA C16:0 -ATc vs +ATc, *** $P < 0.0002$ PA C18:0 -ATc vs +ATc. **c** Relative abundance of DAG (+ATc/-ATc) is reduced by *TgLIPIN* depletion after 48 h + ATc ($n = 3$, unpaired t test P values where **** $P < 0.00001$ relative DAG abundance ratio nmol/parasites number +ATc/-ATc at 24 h vs +ATc/-ATc = 1). **d** Nile red staining showed the number of lipid droplet within the parasites after 24 h of +/-ATc (scale bar = 5.0 μm) with (e) a representative bar graph ($n = 3$, unpaired t test P values where ** $P < 0.0093$ number of lipid droplets per parasite +ATc/-ATc at 1% FBS, *** $P < 0.0003$ at 10% FBS). **f** Relative abundance of TAGs in *TgLIPIN*-ikD (+ATc/-ATc) showing that TAG levels were relatively reduced in the *TgLIPIN*-ikD (48 h + ATc). **g** Relative abundance of free fatty acids (FFA, +ATc/-ATc in the *TgLIPIN*-ikD). **h** Relative abundance of PLs, DAG, FFA and TAG in the *TgLIPIN*-ikD +ATc to -ATc at 10% FBS ($n = 3$, unpaired t test P values where ** $P < 0.004$ relative TAG abundance ratio nmol/parasites number +ATc/-ATc at 10% FBS vs +ATc/-ATc = 1). Data are presented as mean values +/- SEM.

extracted from the parasites to determine the ratio of ^{13}C incorporation to each fatty acid and determine the origin from the host or not. Using this novel approach, we were able to determine (i) the FA biosynthetic capacities of the host cells (Fig. 5i), and more importantly (ii) the first scavenged FA lipidome of the parasite (Fig. 5j-m), the scavenger. Host cells, human foreskin fibroblast (HFF), are capable of synthesizing FA ranging from C14:0 to C20:1, with the most abundant FA species being C18:1 (Fig. 5i). The wild type (*TgLIPIN*-ikD -ATc) parasites are capable of scavenging all these FA species made by the host cell with a major preference again for C18:1 (Fig. 5j). Importantly, in *TgLIPIN* mutant (+ATc), ^{13}C -labeled C16:0, C18:0 and C18:1 from host cells were significantly increased in the FFAs (Fig. 5k), together with a significant increase of host-derived C18:0 in both parasite total lipids and PL (Fig. 5j, l). Therefore, since FA from both FASII and the external environment decrease in the absence of *TgLIPIN*, whilst FAs from host cell are found increasing, our data strongly suggest that the major origin of excess lipids in the *TgLIPIN* mutant is from the host cell. Correlating with the lipid droplet analyses, there was a significant decrease in the ^{13}C labeled FA, specifically C16:1 and C18:1, in TAG (Fig. 5m). The distribution of ^{13}C incorporation to each isotopologue of host-derived FAs was also determined

(Supplementary Fig. 5h-m). Together these data show that the disruption of *TgLIPIN* induced the massive accumulation of host cell-scavenged FA, specifically including C18:1, that cannot be used for TAG synthesis.

Hence, *TgLIPIN* regulates parasite membrane biogenesis by controlling the synthesis and content of PA and DAG, and by channeling the constant flux of host cell scavenged FA for TAG. Without *TgLIPIN*, the parasite accumulates toxic levels of PA, FFA, and PL that eventually cause massive membrane malformations, cytokinesis defect, and parasite death.

Discussion

TgLIPIN plays a pivotal role in the synthesis of central lipid precursors, PA and DAG while regulating the flux of host lipids thereby controlling the equilibrium between membrane biogenesis and lipid storage. Collectively this controls intracellular development and the propagation of the parasite (Fig. 6a).

Our data here show that *TgLIPIN* is an essential PAP controlling the PA/DAG equilibrium along with the level of FFAs. Disruption of this equilibrium together with impairment of storage capacity has multiple phenotypic consequences within the parasite (Fig. 6b). In mammalian cells, LIPIN is encoded by three

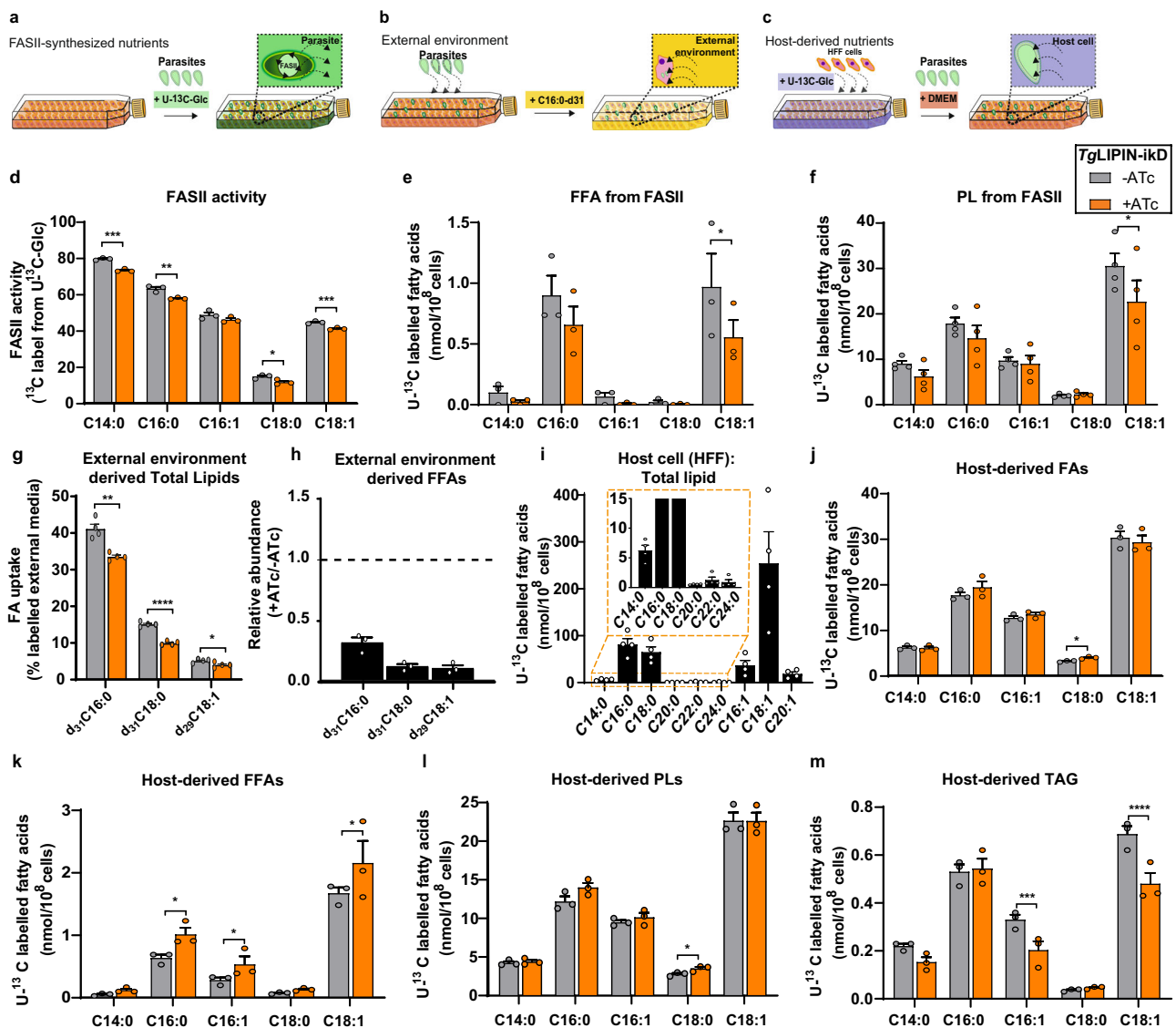


Fig. 5 Monitoring the source of fatty acids in *TgLIPIN-iKD*. **a–c** Schematic for the experimental procedure of stable isotope labeling to determine the origin of fatty acids in *TgLIPIN-iKD*; **a** Parasite FASII derived FAs were determined by the addition of $U-^{13}C$ -glucose (Glc) to the culture medium (1% FBS, no glucose, +/-ATc) at the time of parasite infection to the host. **b** FAs scavenged from the external environment (medium) was determined by the addition of ^{31}d -palmitic acid (^{31}d -C16:0) to the parasite culture medium (high glucose, 1% FBS). **c** Host cell-derived FAs were determined by growing host cells in the presence of $U-^{13}C$ -glucose (no glucose, 10% FBS) to confluent in prior to the infection parasites with normal medium (glucose, 1% FBS, +/-ATc). **d** FASII activity in *TgLIPIN-iKD* as measured as % ^{13}C -incorporation ($n = 3$, unpaired t test P values; *** $P < 0.0005$ % FASII derived C14:0/C16:0/C18:0/C18:1 -ATc vs +ATc, ** $P < 0.007$ /* $P < 0.04$ /** $P < 0.0003$). **e** Abundance of apicoplast FASII derived ^{13}C labeled FFAs ($n = 3$, unpaired t test P values; * $P < 0.02$ of FASII derived FFA C18:1-ATc vs +ATc). **f** Abundance of apicoplast FASII derived ^{13}C -labeled phospholipids (PLs, $n = 4$, unpaired t test P values; * $P < 0.03$ of FASII derived PL C18:0-ATc vs +ATc). **g** FA uptake of deuterated external environment-derived FAs ($n = 4$, unpaired t test P values; ** $P = 0.0034$ /** $P < 0.00001$ /* $P = 0.01$ FA uptake from the external environment as $d_{31}C16:0/d_{31}C18:0/d_{29}C18:1$ -ATc vs +ATc). **h** Relative abundance of deuterated external environment-derived (+ATc/-ATc) ($n = 3$). **i** The abundance of ^{13}C -labeled fatty acids in the host cells ($n = 4$). **j** Host derived FFAs measured as % ^{13}C -incorporation ($n = 3$, unpaired t test P values; * $P < 0.02$ Host derived FA C18:1-ATc vs +ATc). **k** Abundance of host-derived ^{13}C -labeled FFAs ($n = 3$, unpaired t test P values; * $P < 0.05$ Host derived FA C16:0/16:1/18:1-ATc vs +ATc). **l** Abundance of host-derived ^{13}C labeled PL ($n = 3$, unpaired t test P values; * $P < 0.023$ Host derived PL C18:0-ATc vs +ATc) and **m** TAG levels ($n = 3$, unpaired t test P values; **** $P < 0.0001$ Host-derived TAG C16:0/18:1-ATc vs +ATc). Data are all presented as mean values +/- SEM.

independent genes *lipin1*, 2, 3; all of which have PAP activity modulating the levels of TAGs and phospholipids²¹. Genetic mutation within these LIPINs causes severe metabolic disorders, including rhabdomyolysis (*lipin1*), obesity (*lipin1*), autoimmune-inflammatory disease (*lipin2*), and impaired lipoprotein assembly in the intestines (*lipin2* and 3)³³. The essentiality of LIPIN for *T. gondii* growth also suggests distinct functionality from the two

other parasite PAPs. Neither *Toxoplasma* PAPs appeared to compensate for the loss of *TgLIPIN*, unlike in yeast whereby deletion of genes encoding LIPIN can be partly compensated by other PAPs¹⁹. The absence of a NLS (nuclear localization signal) in the *TgLIPIN* sequence is consistent with a cytosolic localization, colocalization specifically with the NE membrane, ER, and other endomembrane. The localization and catalytic activity of

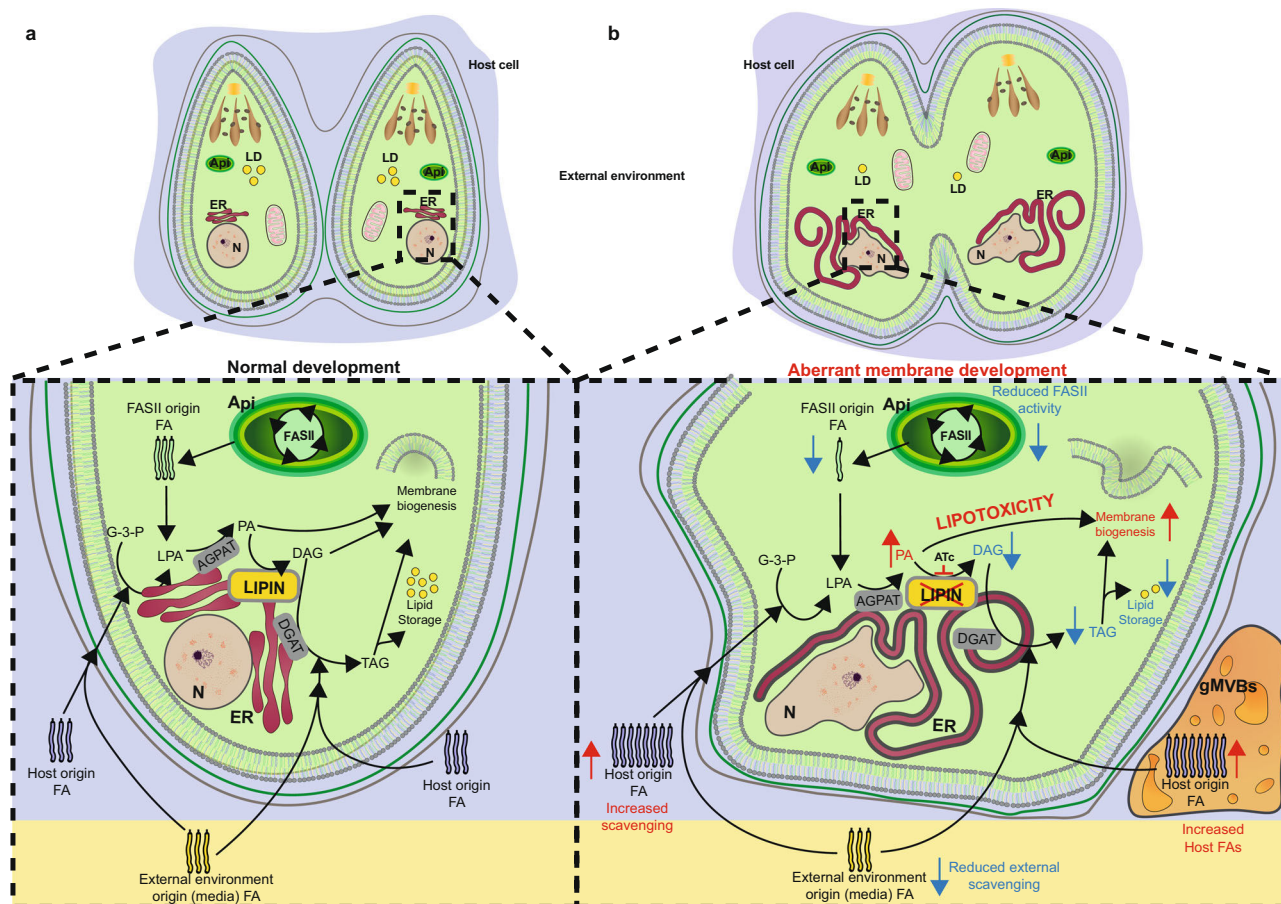


Fig. 6 Proposed role of LIPIN in *Toxoplasma* lipid metabolism. Schematic representation of the dual essential role of *TgLIPIN* in parasite lipid metabolism, including, membrane biogenesis, and lipid storage. **a** The parasite utilizes, and glycerol-3-phosphate (G-3-P) and fatty acid (FA)s derived from both apicoplast (Api) FASII and host to synthesize major lipids by forming lysophosphatidic acid (LPA) followed by phosphatidic acid (PA). PA is hydrolyzed by *TgLIPIN* to generate diacylglycerol (DAG), which is further acylated to generate triacylglycerol (TAG). The other branch of this pathway redirects PA toward the generation of major membrane phospholipids. The FA homeostasis between membrane biogenesis and storage essential for normal parasite development within its host is maintained by the PA phosphatase *TgLIPIN*. **b** Genetic ablation of *TgLIPIN* in *TgLIPIN*-iKΔ parasites in the presence of anhydrotetracycline (ATc) caused the PA/DAG imbalance. The increased PA is channeled towards PL synthesis resulting in excess PLS and consequent gross membrane anomalies within the parasite IMC, nucleus, and ER, while forming giant multivesicular bodies (gMVBs). Simultaneously, the reduction in DAG affected TAG biogenesis and hence the lipid storage capacity, marked by decreased lipid droplets (LD), within the parasite lacking *TgLIPIN*. The impairment of TAG biosynthesis, resulted in excess fatty acids derived from the host, within *TgLIPIN* mutant, causing lipotoxicity.

LIPIN proteins in humans and yeast are regulated by a phosphatase bearing the HAD domain as its substrate^{34–36}.

Therefore, it is conceivable that *TgLIPIN* is quite dynamic and can be recruited on endosomal membranes to regulate the PA/DAG equilibrium, depending on metabolic demand, cell cycle, or coupled to membrane trafficking events. This hints at a probable link between metabolism and the nucleus of the parasite, however contrary to yeast and mammals, there is no evidence of a direct effect of *TgLIPIN* on gene regulation, which could explain the absence of nuclear localization.

One of the early phenotypic stresses evoked in the *TgLIPIN*-deficient mutant was the impact on major membranes including the nuclear envelope complexed with the ER and the parasite IMC. There is evidence that suggests that nuclear membrane biogenesis is linked to PA metabolism^{37,38}. In Δ *pah1* yeast, mutations in upstream biosynthetic steps of the glycerolipid pathway that lower PA levels also reduced the aberrant expansion of nuclear membrane³⁷. Effects of *pah1* deletion could be phenocopied by overexpression of Dgk1p, a nuclear/ER membrane DAG kinase that generates PA³⁷.

A recent study demonstrated that the use of DGAT inhibitor-T863, inhibiting DAG to TAG synthetic reaction in *T. gondii* parasites resulted in rapid accumulation of membranous structures accompanied by rapid parasite death due to strong replication defect⁶. This cytopathy was restricted mainly to the ER and the associated nuclear envelope, similarly as in the case of *TgLIPIN* depletion. The electron micrographs of the *TgLIPIN* mutant (+ATc) clearly suggest that the replication arrest was initially due to profound modifications of the nuclear membrane resulting in aberrant membrane proliferation, cytokinesis defect, and parasite death.

In the absence of *TgLIPIN*, we observed an overall increase in the major membrane phospholipids, including CL, PS, and PC which is a derivative of the CDP-DAG pathway in other eukaryotes³⁹. In absence of DAG, PL biosynthesis was expected to be reduced. Instead, an increase in both PL and FFA is observed, which is likely due to excessive host lipid scavenging. The TAG content in *TgLIPIN* mutant decreases only 48 h post protein downregulation with ATc suggesting that due to a decrease in the substrate-specific DAG species because of *TgLIPIN* unavailability,

the parasite is unable to acylate the free fatty acids to generate its subsequent product TAG. This is supported by the drop in lipid droplet numbers in 1% and 10% FBS when *Tg*LIPIN is suppressed and the exaggerated effect in a high host nutrient environment (Fig. 4d, e). In mammalian cells the inhibition of TAG synthesis leads to oleic acid (C18:1) induced lipotoxicity³⁹. Thus, lipid droplets act as more than just cellular energy reserves by protecting the cells from deleterious effects of toxic excess FFAs by their incorporation into TAGs.

The prelabeling of host fibroblast cells with U-¹³C-Glucose, allowed us to track the source of excess fatty acid and phospholipid content in the *Tg*LIPIN mutant. In keeping with previously reported data, using ¹³C-fluxomics we observed that the parasite has a specific preference for scavenging oleate (C18:1) directly from host⁴⁰. Existing literature provides strong evidence of the involvement of C18:1 in TAG biosynthesis and subsequent lipid droplet formation in mammals³⁹ as well as parasites⁷. Thus, the excess oleate in the form of FFAs within the parasite sourced directly from the host has a strong correlation to the lipid storage defect in *Tg*LIPIN mutant (Fig. 5k). The role of *Tg*LIPIN in the production of TAG was further strengthened by the decrease of host-derived C18:1 in TAG (Fig. 5m). In *T. gondii* parasites, excessive scavenging of C18:1 results in lipotoxicity and parasite death⁷. We show in the absence of *Tg*LIPIN, C18:1 accumulates as FFA and cannot be incorporated into TAG. A significant decrease of C18:1 derived from FASII in the form of FFA is also observed. By sensing this change in nutrients, the parasite attempts to compensate by arresting FASII activity. C18:1 is likely a major FA that is typically scavenged and cannot be stored to avoid lipotoxicity in the absence of *Tg*LIPIN. Taken together, this correlates to previous findings⁴ showing that the parasite is capable of sensing host conditions and metabolically adapt. Similar observations on metabolic plasticity show that there is a reduction in the growth of *P. falciparum* FASII KO mutant in the presence of nutrient-deprived culture conditions⁴. Another study in bacteria shows that the FASII pathway is repressed in a negative feedback loop mediated by acyl-CoA⁴¹. The mechanisms of metabolic adaptation in Apicomplexa still need to be uncovered. In this study, we were able to reveal the first parasite lipid scavengome, which shows that *Tg*LIPIN prevents parasite 'lipotoxicity' in high nutrient environments through effective channeling of host-scavenged fatty acids while maintaining parasite membrane integrity.

Methods

Sequence analysis. *Tg*LIPIN (TGGT1_230690) was identified using EuPathDB web sources ToxoDB (<http://toxodb.org/toxo/>). A phylogenetic tree of LIPIN proteins in several eukaryotes was created using the online platform Phylogeny.fr. The organisms used for LIPIN protein sequences for generation of the phylogenetic tree include *Toxoplasma gondii* (TGGT1_230690), *Plasmodium falciparum* (PF3D7_0303200), *P. berghei* (PBANKA_040180), *Homo sapiens* (NX_Q14693), *H. sapiens* (NX_Q92539), *H. sapiens* (NX_Q9BQK8), *Saccharomyces cerevisiae* _PAH1 (PAP1, SMP2, YMR165C, YM8520.14C), *Cryptosporidium parvum* (cgd3_3210), *Cyanidioschyzon merolae* (CYME_CMN061C), *Neospora caninum* (BN1204), *Hammondia hammondi* (HHA_230690), *Chlamydomonas reinhardtii* (CHLRE_12g506600v5), *Arabidopsis thaliana* _AtPAH1 (At3g09560), *Arabidopsis thaliana* _AtPAH2 (At5g42870), *Leishmania major* (LMJF_06_0830), *Trypanosoma brucei* (Tb927.7.5450), *Chromera velia* (Cvel_24403). The first step involved the curation of these protein sequences. The protein sequences were aligned (ClustalW) and then gaps were removed from the alignment. Finally, the phylogenetic tree was constructed using the maximum likelihood method in the PhyML program (3.1/3.0 aLRT). The default substitution model (WAG) was selected. Graphical representation and edition of the phylogenetic tree were performed with Cladogram.

***T. gondii* strains and cultures.** The parasite host cells human foreskin fibroblasts (HFF) were cultured using Dulbecco's Modified Eagle's Medium (DMEM, Gibco) supplemented with 10% fetal bovine serum (FBS, Gibco), 2 mM glutamine (Gibco), and 25 µg/mL gentamicin (Gibco) at 37 °C and 5% CO₂.

T. gondii tachyzoite parental strains RH-ΔKu80 TATI, RH-ΔKu80 as well as mutant strains *Tg*LIPIN-ikD, *Tg*LIPIN-3XHA were propagated by serial passage within their host HFF using DMEM supplemented with 1% fetal bovine serum (FBS, Gibco), 2 mM glutamine (Gibco), and 25 µg/mL gentamicin (Gibco) at 37 °C and 5% CO₂.

Generation of HA-tagged and inducible knockdown line for *Tg*LIPIN. A C-terminally tagged HA line was generated expressing from the gene's endogenous locus using the classical pLIC strategy using homologous recombination in a RH-ΔKu80 strain. For the same, a 1677-bp homology region of *Tg*LIPIN located toward to C-terminus excluding the stop codon, was amplified from the parasite genomic DNA using the primers forward 5'-TACTTCCAATCCAATTTAATGCACGGCAGATTTCTCTACTGG-3' and reverse 5'-TCCTCCACTTCCAATTTAGCCAAATTAAGTGCATTGCGTTCAC-3'. The homology region was assembled into *PacI* digested pLIC-HA-DHFR plasmid using ligation-independent cloning protocol¹⁷. The assembled plasmid with linearized with single-enzyme site specific to the parasite DNA sequence within the plasmid-*NsiI* just before transfection. Parasites were selected with the drug pyrimethamine and cloned by limiting dilution.

For generation of inducible knockdown plasmid pPR2-DHFR⁴², two separate homology flanks were chosen. The 5' flank was amplified 1637 bp upstream of the *Tg*LIPIN start codon using the primers F1-3' and R1. The PCR product was ligated to *PacI* and *NdeI* digested vector pPR2 using NEB assembly reaction. Next, the 3' flank was amplified as a 1739-bp fragment beginning at the start codon of *Tg*LIPIN with the primers F2 and reverse R2. The 3' homology flank was annealed to *XmaI* and *NotI* digested pPR-HA3-DHFR vector that already contained the *Tg*LIPIN 5' flank. The final cloned vector positions the start codon of *Tg*LIPIN downstream of the ATc-regulatable *t*s4 promoter and a 3xHA tag. The resulting vector with *NotI* and transfected this into TATIΔku80 parasites. Parasites were selected with the drug pyrimethamine and cloned by limiting dilution.

Screening of parasite clones where the *t*s4 promoter had successfully replaced the native *Tg*LIPIN promoter, was done using the screen primers 1–6 in the combinations described in Supplementary Fig. S2. All PCRs were performed with TaKara primaster max polymerase. The knockdown of *Tg*LIPIN was induced with 0.5 µg ml⁻¹ of anhydrotetracycline (ATc). Primer list can be found in Supplementary Table 1.

Immunofluorescence assay. Primary antibodies anti-HA (Rat, Roche 1:500), anti-IMC1 (mouse, 1:1000), anti-SAG1 (mouse, 1:1000), anti-MIC2 (rabbit, 1:1000), anti-CPN60 (rabbit, 1:1000), and anti-TOM40 (rabbit, 1:1000) were used at dilutions their respective dilutions. Secondary AlexaFluor 488- and 546-conjugated anti-rat, anti-mouse, and anti-rabbit antibodies (Life Technologies) were used at 1/2500. For the immunofluorescence assay (IFA), parasites were grown on confluent HFF on coverslips and fixed in PBS containing 2.5% paraformaldehyde (PFA) for 15 min at room temperature (RT). Samples were permeabilized with 0.25% Triton X-100 in PBS for 10 min at RT prior to blocking in PBS containing 3% BSA and subsequent incubation with primary antibodies then secondary antibodies diluted in the blocking solution. Labeled parasites were stained with Hoechst 33342 (1:10000, Life Technologies) for 20 min and then washed three times in PBS before final mounting of the coverslips on a glass slide using fluorogel. The IFA slides were visualized using fluorescence microscope (Axio Imager 2_apotome; ZEISS, ×60–100 magnification).

Western blot analysis. Parasites were harvested for western blot analyses after complete egress from their host. To remove any host cell debris, the parasites were passed through a 3-µm filter, then counted by haemocytometer and solubilized in SDS buffer at equivalent cell densities. Equal amount of protein was separated on a 4–12% gradient SDS-polyacrylamide (Life Technologies) and transferred to a nitrocellulose membrane using the XCellII Blot Module (Invitrogen). Primary antibodies anti-HA (rat, Roche) and anti-TOM40⁴³ (rabbit) were used at a dilution of 1:500 and 1:1000, respectively. Secondary goat anti-mouse and anti-rabbit horseradish peroxidase (HRP) conjugated antibodies (Thermo Scientific) were used at 1:2000. Protein signal was detected by chemiluminescence after membrane staining with luminata crescendo western HRP detection kit (Millipore). The signal strength of protein was quantified using a BioRad chemidoc imager (BioRad).

Phenotypic analysis. Plaque assay: The extracellular parasites were harvested after filtration and counted by haemocytometer. Then ~500 parasites were inoculated to a confluent HFF flask (25 cm²). *Tg*LIPIN-ikD was grown for plaque assay in the presence or absence of Anhydrotetracycline (ATc) (0.5 µg ml⁻¹) for 7–10 days. Plaque sizes were visualized by crystal violet staining (30–60 min) after aspiration of culture media, and cells fixation with 100% ethanol (5 min) followed by phosphate-buffered saline (PBS) wash. The plaque area was calculated (*n* = 3) using Image J which calculated an arbitrary unit value assessing the viability of the parasite with and without the protein.

Replication assay: The parasites were grown for two days with or without ATc (0.5 µg ml⁻¹), harvested and filtered. Equal number of parasites were allowed to invade confluent HFF grown on coverslips. Following 2 h of invasion, the coverslips were washed thrice with ED1 (1% FBS containing DMEM), to remove

extracellular parasites and promote synchronized replication. ATc (0.5 $\mu\text{g ml}^{-1}$) was added at the start of the experiment, allowing the treatment for 24 h, alongside control parasites without ATc. These coverslips were then fixed and processed for IFA using anti-HA, anti-SAG1 antibodies wherein the parasite number per parasitophorous vacuole was analyzed.

Electron microscopy. The TgLIPIN-ikD parasites were grown for 12, 24 and 48 h in the presence and absence of ATc, in labteks (Nunk, Thermofisher). The parental ΔKu80 strain treated with ATc was used as the wild-type control. The labteks containing parasite-infected HFF were fixed in 0.1 M cacodylate buffer with 2.5% glutaraldehyde for 2 h and kept at 4 °C until further processing. During processing, the sample were fixed again for 1 h with 1% osmium tetroxide in cacodylate buffer followed by overnight treatment in 2% uranyl acetate in distilled water. After dehydration in graded series of acetonitrile, samples were progressively impregnated in Epon812, the wells were then filled with fresh resin and allowed to polymerize 48 h at 60 °C. Ultrathin 70-nm sections were obtained with a Leica UC7 ultramicrotome and collected on copper grids. Grids were post-stained with uranyl acetate and lead citrate before their observation on a Jeol1200 EXII Transmission Electron Microscope on the Electron microscopy facility of the University of Montpellier (MEA). Chemicals and consumables were from Electron Microscopy Sciences.

Nile red staining of lipid droplets. The TgLIPIN-ikD parasites were allowed to infect and grow in confluent monolayer HFF grown on coverslips in 1% and 10% FBS, in the +/− ATc conditions for 24 h and 48 h. Similar to IFA, these coverslips were fixed using 2.5% PFA, permeabilized with 0.25% Triton X-100 and then stained with primary rat anti-HA antibody followed by detection with secondary AlexaFluor 488-conjugated goat anti-rat antibody. Thereafter, the sample coverslips were incubated for 1 h with Nile red (1:2000) in 1× PBS before proceeding to DNA staining with Hoechst. The coverslips were mounted onto a glass slide in fluorogel prior to imaging using a fluorescence microscope (Axio Imager 2, apotome; ZEISS). For visualizing Nile red-stained droplets yellow-gold fluorescence (excitation, 450–500 nm; emission, greater than 528 nm³⁰) was used on the axio-imager. Quantification in +/− ATc condition was done by counting the number of lipid droplets per parasite vacuole.

Heterologous complementation. The codon-optimized carboxy terminal sequence of TgLIPIN (548–765 a.a., C-LIP) harboring the catalytic HAD domain (DVDGT), obtained from GenScript, was ligated to *NotI/MluI* digested pD0170 yeast expression vector (obtained from Carman's lab) to yield pD0170-CLIP. This plasmid was transformed into yeast strain $\Delta\text{dpp1}\Delta\text{lpp1}\Delta\text{pah1}$ (*pah1::URA3 dpp1::TRP1/Kanr lpp1::HIS3/Kanr*, triple mutant) or $\Delta\text{dpp1}\Delta\text{lpp1}\Delta\text{pah1}\Delta\text{app1}$ (*app1::natMX4 pah1::URA3 dpp1::TRP1/Kanr lpp1::HIS3*, quadruple mutant) (gifts from Dr. George Carman's lab, Rutgers Center for Lipid Research, New Jersey), and transformants were selected on solid SD medium (YNB, 2% glucose, agar) lacking leucine¹⁹.

Lipidomic analysis

Saccharomyces cerevisiae. The triple mutant strain was transformed with vector pD0170-CLIP or pD01050 (lacking the HAD domain) and the cells were grown in YNB glucose medium at 30 °C until OD₆₀₀ reached 1–3. Cultures were centrifuged for 5 min at 1000 × g, washed with PBS thrice, and normalized by cell weight.

Total lipid analysis: Total lipids were extracted in chloroform/methanol/water (1:3:1, v/v/v) containing FFA (free fatty acids C13:0, 10 nmol) and PC (21:0/21:0, 10 nmol) as internal standards for extraction. Next, the polar and apolar metabolites were separated by phase partitioning by adding chloroform and water to give the ratio of chloroform/methanol/water as 2:1:0.8 (v/v/v). For lipid analysis, 50 μl of the extract was directly dried and dissolved in 2:1 chloroform:methanol and trimethylsulfonium hydroxide (TMSH, Machenery Nagel) for total fatty acid content. Resultant FAMES were then analyzed by GC-MS as previously described⁴⁴. All FAMES were identified by comparison of retention time and mass spectra from GC-MS with authentic chemical standards. The concentration of FAMES was quantified after initial normalization to different internal standards.

Phospholipid, DAG/TAG analyses: The extracted total lipid extracted (as above) was separated with 5 nmol DAG/PA(C16:0/C18:1) (Avanti Polar lipids) by one-dimensional silica gel high-performance thin-layer chromatography (HPTLC, Merck). The 1st and 2nd solvent system used were chloroform/methanol/water/acetic acid, 25:15:2:4 (v/v/v/v) and hexane/MTBE/acetic acid, 35:15:0.5 (v/v/v), respectively. For DAG, TAG, FFA, and CE analysis, total lipid fraction was separated by 1D-HPTLC using hexane/diethyl ether/formic acid, 80:20:2 (v/v/v) as solvent system. The spots correlating to TAG, DAG, PA, and PC on the HPTLC plate were scraped off, and lipids were methanolyzed with 200 μl 0.5 M methanolic HCl in the presence of 1 nmol pentadecanoic acid (C15:0) as internal standard at 85 °C for 4 h. The resulting FAMES were extracted with hexane and analyzed by GC-MS (Agilent).

Toxoplasma gondii. The parasites were grown for 24 h and 48 h in +/− ATc conditions within a confluent monolayer of HFF in flasks (175 cm²). At each time point, parasites were harvested as intracellular tachyzoites (1 × 10⁷ cell equivalents

per replicate) after syringe filtration with 3- μm pore size membrane. These parasites were metabolically quenched by rapid chilling in a dry ice-ethanol slurry bath and then centrifuged down at 4 °C. The parasite pellet was washed with ice-cold PBS thrice, before transferring the final pellet to a microcentrifuge tube. Then total lipids were extracted in chloroform/methanol/water (1:3:1, v/v/v) containing PC (C13:0/C13:0), 10 nmol and C21:0 (10 nmol) as internal standards for extraction. Polar and apolar metabolites were separated by phase partitioning by adding chloroform and water to give the ratio of chloroform/methanol/water as 2:1:0.8 (v/v/v). For lipid analysis, the organic phase was dried under N₂ gas and dissolved in 1-butanol to obtain 1 μl butanol/10⁷ parasites.

Total lipid analysis: The extracted total lipid sample was then added with 1 nmol pentadecanoic acid (C15:0) as an internal standard as stated before using TMSH for total fatty acid content. Resultant FAMES were analyzed by GC-MS as previously described⁴⁴. All FAMES were identified by comparison of retention time and mass spectra from GC-MS with authentic chemical standards. The concentration of FAMES was quantified after initial normalization to different internal standards and finally to parasite number.

Free fatty acid and cholesterol analysis: Total lipid samples were dried and derivatized with BSTFA + TMCS, 99:1 (Sigma) to generate trimethylsilyl (TMS-) fatty acids and TMS-cholesterol. These TMS derivatives were analyzed by GCMS as described above.

Phospholipid and neutral lipid analysis: For phospholipid analysis, the extracted total lipid extracted (as above) was separated with 1 nmol PA(C17:0/C17:0) (Avanti Polar lipids) by two-dimensional silica gel high-performance thin-layer chromatography (HPTLC, Merck). The solvent system used for the 1st and 2nd dimension was chloroform/methanol/28% ammonium hydroxide, 12:7:1.6 (v/v) and chloroform/acetone/methanol/acetic acid/water, 10:4:2:2.6:1 (v/v/v/v/v), respectively. For DAG, TAG, Free fatty acids (FFA) and cholesteryl ester (CE) analysis, total lipid fraction was separated by 1D-HPTLC using hexane/diethyl ether/formic acid, 80:20:2 (v/v/v) as solvent system. Then each lipid spot on the HPTLC plate was scraped off, and lipids were methanolyzed with 200 μl 0.5 M methanolic HCl in the presence of 1 nmol pentadecanoic acid (C15:0) as internal standard at 85 °C for 3 h. The resulting FAMES were extracted with hexane and analyzed by GC-MS (Agilent).

Stable isotope metabolic labeling experiment

Tracking FASII origin fatty acids (monitoring de novo FA synthesis by the parasite apicoplast FASII). The TgLIPIN parasites were infected to a confluent monolayer of HFF in glucose-free-DMEM (1% FBS) supplemented with U-¹³C-glucose or U-¹²C-glucose at a final concentration of 800 μM , with or without ATc (0.5 $\mu\text{g ml}^{-1}$). The parasites were harvested up to 48 h post depletion of TgLIPIN and metabolically quenched in a dry ice and ethanol slurry in a tube until the sample reached 4 °C. Lipids were extracted, derivatized using TMSH (Machenery-Nagel) and analyzed by GC-MS as described above. ¹³C incorporation to each fatty acid was calculated as the percent of the metabolite pool containing one or more ¹³C atoms after correction for natural abundance and the amount of ¹³C-carbon source in the culture medium. The degree of the incorporation of ¹³C into fatty acids (% carbon incorporation) was determined by the mass isotopomer distribution (MID) of each FAMES. MID was obtained from the shift in isotopic mass dependent on the amount of ¹²C carbons compared to the integration of ¹³C carbon atoms. The total abundance of ¹³C-labeled fatty acids was obtained by calculating the concentration of all isotopomers of ¹³C-labeled FAMES and finally normalizing to authentic internal standards and parasite number.

Tracking host-derived fatty acids (monitoring parasite scavenging capacities). The HFF cells were grown (1 × 10⁸ cell equivalents per replicate) to confluency in the presence of stable isotope U-¹³C-glucose at a final concentration of 800 μM added to a glucose-free DMEM. These ¹³C-pre-labeled HFF were then infected with TgLIPIN-ikD parasites in the presence of normal-glucose containing DMEM under +/− ATc (0.5 $\mu\text{g/ml}$). The host HFF and parasites were metabolically quenched separately, and their lipid content was quantified by GC-MS as described above. As described previously, the degree of the incorporation of ¹³C into fatty acids (%carbon incorporation) is determined by the mass isotopomer distribution (MID) of each FAMES. The total abundance of ¹³C-labeled fatty acids was analyzed initially for HFF to check labeling of the metabolites (described previously). Later, the same was calculated for parasites to confirm direct uptake of ¹³C-labeled fatty acids from the host.

Tracking uptake of deuterated fatty acid from medium (monitoring extracellular host environment). Deuterated palmitic acid (³¹d-C16:0) was dissolved in 10 mM in fatty acid-free bovine serum albumin/PBS solution by sonication in a water bath for 30 min followed by incubation at 55 °C for 30 min. Freshly egressed TgLIPIN parasites were allowed to invade a confluent monolayer of HFF for at least 2 h under conditions of +/− ATc. Following the invasion, the uninvaded parasites were washed off with DMEM and further allowed to grow in the normal culture medium-DMEM (1% FBS) containing ³¹d-C16:0 at a final concentration of 0.1 mM in +/− ATc until 24 and 48 h of growth. The parasites were harvested by metabolic quenching as described previously. Lipids were extracted, derivatized using TMSH as well as TMS, and further analyzed by GC-MS. All raw data were quantitatively and qualitatively analyzed using Agilent MassHunter Software: MS B.07.00.

Statistics and reproducibility. The graphical data for this study was generated using GraphPad Prism software. Three biological replicates were used per experiment ($n = 3$, unless stated otherwise). The error bars are representative of the standard error of mean (SEM) for each study. Statistical significance was determined for each experiment by unpaired t tests using GraphPad Prism. The range of statistical significance was signified as per the P value, where $0.01-0.05 = *$, $0.01-0.001 = **$, $<0.001 = ***$, and $<0.0001 = ****$.

Reporting summary. Further information on research design is available in the Nature Research Reporting Summary linked to this article.

Data availability

Authors can confirm that all relevant data are included in the paper and/or its Supplementary/Source data files. Protein and gene sequences were acquired from EuPathDB web sources ToxoDB (<http://toxodb.org/toxo/>). Source data are provided with this paper.

Code availability

No codes were used to analyze the data in this study.

Received: 19 February 2020; Accepted: 24 March 2021;

Published online: 17 May 2021

References

- Ramakrishnan, S., Serricchio, M., Striepen, B. & Bütikofer, P. Lipid synthesis in protozoan parasites: a comparison between kinetoplastids and apicomplexans. <https://doi.org/10.1016/j.plipres.2013.06.003> (2013).
- Ramakrishnan, S. et al. The intracellular parasite *Toxoplasma gondii* depends on the synthesis of long chain and very long-chain unsaturated fatty acids not supplied by the host cell HHS public access. *Mol. Microbiol.* **97**, 64–76 (2015).
- Coppens, I. Targeting lipid biosynthesis and salvage in apicomplexan parasites for improved chemotherapies. *Nat. Rev. Microbiol.* **11**, 823–835 (2013).
- Amiar, S. et al. Division and adaptation to host environment of apicomplexan parasites depend on apicoplast lipid metabolic plasticity and host organelle remodeling. *Cell Rep.* **30**, 3778–3792 (2020).
- Di Genova, B. M., Wilson, S. K., Dubey, J. P. & Knoll, L. J. Intestinal delta-6-desaturase activity determines host range for *Toxoplasma* sexual reproduction. *PLoS Biol.* **17**, 1–19 (2019).
- Mazumdar, J. & Striepen, B. Make it or take it: fatty acid metabolism of apicomplexan parasites. *Eukaryot. Cell* **6**, 1727–1735 (2007).
- Nolan, S. J., Romano, J. D., Kline, J. T. & Coppens, I. Novel approaches to kill *Toxoplasma gondii* by exploiting the uncontrolled uptake of unsaturated fatty acids and vulnerability to lipid storage inhibition of the parasite. *Antimicrob. Agents Chemother.* **62**, e00347–18 (2018).
- Csaki, L. S. & Reue, K. Lipins: multifunctional lipid metabolism proteins. *Annu. Rev. Nutr.* **30**, 257–272 (2010).
- Bullen, H. E. et al. Phosphatidic acid-mediated signaling regulates microneme secretion in toxoplasma. *Cell Host Microbe* **19**, 349–360 (2016).
- Jacot, D. et al. An apicomplexan actin-binding protein serves as a connector and lipid sensor to coordinate motility and invasion. *Cell Host Microbe* **20**, 731–743 (2016).
- Bisio, H., Lunghi, M., Brochet, M. & Soldati-Favre, D. Phosphatidic acid governs natural egress in *Toxoplasma gondii* via a guanylate cyclase receptor platform. *Nat. Microbiol.* <https://doi.org/10.1038/s41564-018-0339-8> (2019).
- Jimah, J. R. et al. Malaria parasite CelTOS targets the inner leaflet of cell membranes for pore-dependent disruption. *eLife* <https://doi.org/10.7554/eLife.20621> (2016).
- Amiar, S. et al. Apicoplast-localized lysophosphatidic acid precursor assembly is required for bulk phospholipid synthesis in *Toxoplasma gondii* and relies on an algal/plant-like glycerol 3-phosphate acyltransferase. *PLoS Pathog.* **12**, 1–30 (2016).
- Carman, G. M. & Han, G. S. Fat-regulating phosphatidic acid phosphatase: a review of its roles and regulation in lipid homeostasis. *J. Lipid Res.* **60**, 2–6 (2019).
- Gupta, N., Zahn, M. M., Coppens, I., Joiner, K. A. & Voelker, D. R. Selective disruption of phosphatidylcholine metabolism of the intracellular parasite *Toxoplasma gondii* arrests its growth. *J. Biol. Chem.* **280**, 16345–16353 (2005).
- Déchamps, S., Shastri, S., Wengelnik, K. & Vial, H. J. Glycerophospholipid acquisition in Plasmodium—A puzzling assembly of biosynthetic pathways. *Int. J. Parasitol.* **40**, 1347–1365 (2010).
- Carman, G. M. & Han, G. S. Phosphatidic acid phosphatase, a key enzyme in the regulation of lipid synthesis. *J. Biol. Chem.* <https://doi.org/10.1074/jbc.R800059200> (2009).
- Nakamura, Y. et al. Arabidopsis lipins mediate eukaryotic pathway of lipid metabolism and cope critically with phosphate starvation. *Proc. Natl Acad. Sci. USA* **106**, 20978–20983 (2009).
- Chae, M., Han, G. S. & Carman, G. M. The *Saccharomyces cerevisiae* actin patch protein app1p is a phosphatidate phosphatase enzyme. *J. Biol. Chem.* **287**, 40186–40196 (2012).
- Huynh, M. H. & Carruthers, V. B. Tagging of endogenous genes in a *Toxoplasma gondii* strain lacking Ku80. *Eukaryot. Cell* **8**, 530–539 (2009).
- Zhang, P. & Reue, K. Lipin proteins and glycerolipid metabolism: roles at the ER membrane and beyond. *Biochimica et Biophysica Acta - Biomembranes* <https://doi.org/10.1016/j.bbmem.2017.04.007> (2017).
- Agrawal, S., Dooren, G. G. Van, Beatty, W. L. & Striepen, B. Genetic evidence that an endosymbiont-derived endoplasmic reticulum-associated protein degradation (ERAD) system functions in import of apicoplast proteins. *J. Biol. Chem.* **284**, 33683–33691 (2009).
- Sheiner, L. et al. A systematic screen to discover and analyze apicoplast proteins identifies a conserved and essential protein import factor. *PLoS Pathog.* **7**, e1002392 (2011).
- Soldati, D., Meissner, M. & Schluter, D. Role of *Toxoplasma gondii* myosin A in powering parasite gliding and host cell invasion. *Science* **298**, 837–840 (2002).
- Santos-Rosa, H., Leung, J., Grimsey, N., Peak-Chew, S. & Siniosoglou, S. The yeast lipin Smp2 couples phospholipid biosynthesis to nuclear membrane growth. *EMBO J.* <https://doi.org/10.1038/sj.emboj.7600672> (2005).
- Siniosoglou, S. Lipins, lipids and nuclear envelope structure. *Traffic* <https://doi.org/10.1111/j.1600-0854.2009.00923.x> (2009).
- Kong, P. et al. Two phylogenetically and compartmentally distinct CDP-diacylglycerol synthases cooperate for lipid biogenesis in *Toxoplasma gondii*. *J. Biol. Chem.* <https://doi.org/10.1074/jbc.M116.765487> (2017).
- Cases, S. et al. Identification of a gene encoding an acyl CoA:diacylglycerol acyltransferase, a key enzyme in triacylglycerol synthesis. *Proc. Natl Acad. Sci. USA* <https://doi.org/10.1073/pnas.95.22.13018> (1998).
- Nolan, S. J., Romano, J. D. & Coppens, I. Host lipid droplets: an important source of lipids salvaged by the intracellular parasite *Toxoplasma gondii*. *PLoS Pathogens* **13**, e1006362 (2017).
- Greenspan, P., Mayer, E. P. & Fowler, S. D. Nile red: a selective fluorescent stain for intracellular lipid droplets. *J. Cell Biol.* **100**, 965–973 (1985).
- Hu, X., Binns, D. & Reese, M. L. The coccidian parasites *Toxoplasma* and *Neospora* dysregulate mammalian lipid droplet biogenesis. *J. Biol. Chem.* **292**, 11009–11020 (2017).
- Mashima, T., Seimiya, H. & Tsuruo, T. De novo fatty-acid synthesis and related pathways as molecular targets for cancer therapy. *Br. J. Cancer* <https://doi.org/10.1038/sj.bjc.6605007> (2009).
- Reue, K. & Wang, H. Mammalian lipin phosphatidic acid phosphatases in lipid synthesis and beyond: Metabolic and inflammatory disorders. *J. Lipid Res.* <https://doi.org/10.1194/jlr.S091769> (2019).
- Karanasios, E., Han, G. S., Xu, Z., Carman, G. M. & Siniosoglou, S. A phosphorylation-regulated amphipathic helix controls the membrane translocation and function of the yeast phosphatidate phosphatase. *Proc. Natl Acad. Sci. USA* <https://doi.org/10.1073/pnas.1007974107> (2010).
- Kim, Y. et al. A conserved phosphatase cascade that regulates nuclear membrane biogenesis. *Proc. Natl. Acad. Sci. USA* <https://doi.org/10.1073/pnas.0702099104> (2007).
- Pascual, F. & Carman, G. M. Phosphatidate phosphatase, a key regulator of lipid homeostasis. *Biochim. Biophys. Acta* **1831**, 514–522 (2013).
- Han, G. S., O'Hara, L., Carman, G. M. & Siniosoglou, S. An unconventional diacylglycerol kinase that regulates phospholipid synthesis and nuclear membrane growth. *J. Biol. Chem.* **283**, 20433–20442 (2008).
- Barbosa, A. D. et al. Lipid partitioning at the nuclear envelope controls membrane biogenesis. *Mol. Biol. Cell* <https://doi.org/10.1091/mbc.E15-03-0173> (2015).
- Listenberger, L. L. et al. Triglyceride accumulation protects against fatty acid-induced lipotoxicity. *Proc. Natl Acad. Sci. USA* <https://doi.org/10.1073/pnas.0630588100> (2003).
- Pernas, L., Bean, C., Boothroyd, J. C. & Scorrano, L. Mitochondria restrict growth of the intracellular parasite *Toxoplasma gondii* by limiting its uptake of fatty acids. *Cell Metab.* **27**, 886–897.e4 (2018).
- Fujita, Y., Matsuoka, H. & Hirooka, K. Regulation of fatty acid metabolism in bacteria. *Mol. Microbiol.* <https://doi.org/10.1111/j.1365-2958.2007.05947.x> (2007).
- Katris, N. J. et al. The apical complex provides a regulated gateway for secretion of invasion factors in toxoplasma. *PLoS Pathog.* **10**, e1004074 (2014).
- Van Dooren, G. G., Yeoh, L. M., Striepen, B. & McFadden, G. I. The import of proteins into the mitochondrion of *Toxoplasma gondii*. *J. Biol. Chem.* **291**, 19335–19350 (2016).
- Dubois, D. et al. *Toxoplasma gondii* acetyl-CoA synthetase is involved in fatty acid elongation (of long fatty acid chains) during tachyzoite life stages. *J. Lipid Res.* **59**, 994–1004 (2018).

Acknowledgements

We would like to thank Prof George M. Carman for providing us the yeast mutant with corresponding plasmids. This work and C.Y.B., Y.Y.B., S.D., S.S., C.S.A., and N.J.K. are supported by Agence Nationale de la Recherche, France (Grant ANR-12-PDOC-0028-Project Apicolipid), the Atip-Avenir and Finovi programs (CNRS-INSERM-FinoviAtip-Avenir Apicolipid projects), CEFIPRA (Indo-French Centre for the Promotion of Advanced Research), IDEX-Université Grenoble Alpes, Region Auvergne Rhone-Alpes (IRICE Grant, Project GEMELI) and the Laboratoire d'Excellence ParaFrap, France (Grant number ANR-11-LABX-0024).

Author contributions

C.Y.B., Y.Y.B., and S.D. contributed to the design of the work. C.Y.B., Y.Y.B., L.B., S.S., F.B., M.F.C., and S.Da. contributed to the interpretation of data. S.Da., S.S., S.Du., F.B., C.S.A., N.J.K., L.B., Y.Y.B., and C.Y.B. contributed the acquisition and analysis of data. M.F.C. and C.Y.B. financed the project.

Competing interests

The authors declare no competing interests.

Additional information

Supplementary information The online version contains supplementary material available at <https://doi.org/10.1038/s41467-021-22956-w>.

Correspondence and requests for materials should be addressed to Y.Y.-B. or C.Y.B.

Peer review information *Nature Communications* thanks Laura Knoll, Rachel Zufferey, and the other, anonymous reviewer(s) for their contribution to the peer review of this work.

Reprints and permission information is available at <http://www.nature.com/reprints>

Publisher's note Springer Nature remains neutral with regard to jurisdictional claims in published maps and institutional affiliations.



Open Access This article is licensed under a Creative Commons Attribution 4.0 International License, which permits use, sharing, adaptation, distribution and reproduction in any medium or format, as long as you give appropriate credit to the original author(s) and the source, provide a link to the Creative Commons license, and indicate if changes were made. The images or other third party material in this article are included in the article's Creative Commons license, unless indicated otherwise in a credit line to the material. If material is not included in the article's Creative Commons license and your intended use is not permitted by statutory regulation or exceeds the permitted use, you will need to obtain permission directly from the copyright holder. To view a copy of this license, visit <http://creativecommons.org/licenses/by/4.0/>.

© The Author(s) 2021

Rapid kinetics of lipid second messengers controlled by a cGMP signalling network coordinates apical complex functions in *Toxoplasma* tachyzoites.

Nicholas J. Katris^{*1}, Yoshiki Yamaro-Botte¹, Jan Janouškovec², Serena Shunmugam¹, Christophe-Sebastien Arnold¹, Annie S. P. Yang³, Alexandros Vardakis⁴, Rebecca J. Stewart⁵, Robert Sauerwein³, Geoffrey I. McFadden⁶, Christopher J. Tonkin^{5,7}, Marie-France Cesbron-Delauw¹, Ross. F. Waller⁴, Cyrille Y. Botte^{@*1}.

1. ApicoLipid Team, Institute for Advanced Biosciences, CNRS UMR5309, Université Grenoble Alpes, INSERM U1209, Grenoble, France; **2.** Department of Pharmacy, University of Oslo Norway; **3.** Radboud University Medical Center, PO Box 9101, 6500 HB Nijmegen, The Netherlands; **4.** Department of Biochemistry, University of Cambridge, Cambridge, UK; **5.** The Walter and Eliza Hall Institute of Medical Research, Parkville, Melbourne, Victoria, Australia; **6.** McFadden Laboratory, School of Biosciences, University of Melbourne, Melbourne, VIC 3010, Australia; **7** Department of Medical Biology, The University of Melbourne, Melbourne, Victoria, Australia

*corresponding authors nicholas.katris@univ-grenoble-alpes.fr, cyrille.botte@univ-grenoble-alpes.fr.

ABSTRACT:

Host cell invasion and subsequent egress by *Toxoplasma* parasites is regulated by a network of cGMP, cAMP, and calcium signalling proteins. Such eukaryotic signalling networks typically involve lipid second messengers including phosphatidylinositol phosphates (PIPs), diacylglycerol (DAG) and phosphatidic acid (PA). However, the lipid signalling network in *Toxoplasma* is poorly defined. Here we present lipidomic analysis of a mutant of central flippase/guanylate cyclase TgGC in *Toxoplasma*, which we show has disrupted turnover of signalling lipids impacting phospholipid metabolism and membrane stability. The turnover of signalling lipids is extremely rapid in extracellular parasites and we track changes in PA and DAG to within 5 seconds, which are variably defective upon disruption of TgGC and other signalling proteins. We then identify the position of each protein in the signal chain relative to the central cGMP signalling protein TgGC and map the lipid signal network coordinating conoid extrusion and microneme secretion for egress and invasion.

Abbreviations:

FA-Fatty Acid

FFAs-Free Fatty Acids

PA- Phosphatidic acid

PI (P)- Phosphatidylinositol (Phosphate)

PS-Phosphatidylserine

PT-Phosphatidylthreonine

ATc-Anhydrotetracycline

GC-Guanylate cyclase

DAG-Diacylglycerol

IP3-Inositol triphosphate

TLCs-Thin Layer Chromatography

GCMS-Gas Chromatography Mass Spectrometry.

cGMP-Cyclic guanosine monophosphate

cAMP-Cyclic adenosine monophosphate

OSBP-Oxysterol Binding Protein

Introduction:

The phylum Apicomplexa includes infectious agents of major human and animal diseases such as malaria and toxoplasmosis, which create a massive global burden for human health (World Health Organization, 2018). These parasitic protists are obligate intracellular parasites of human cells, which means that they must invade a human cell in order to divide, persist and cause disease. Central to this process of host cell invasion is a unique structure at the apex of the parasite cell termed the apical complex, which also defines the name of the Apicomplexa phylum. The core of the apical complex is made up of tubulin based cytoskeletal components forming a circular apical polar ring, to which are connected a series of sub-pellicular microtubules which cascade down the length of the parasite body. Apicomplexan parasites also bear an arsenal of secretion factors including microneme and rhoptry proteins, which are secreted through the apical complex to allow invasion and subsequent egress. Interestingly, the apical complex bears an additional tight-knit cytoskeletal structure, the conoid, best studied in *Toxoplasma*. This conoid is connected to the apical polar ring and can extrude and retract from as part of the apical complex (Grainger et al. 2016). However, the conoid is less conspicuous, or even proposed to be absent from *Plasmodium* species (Wall et al. 2016). The apical complex (bearing or not the conoid) is also present in some photosynthetic relatives of Apicomplexa, such as *Chromera velia* (Obornik et al. 2012; 2011). The conoid is presumed to have a function in parasite invasion as it is typically extruded in extracellular stages, and retracted during intracellular replication (Grainger et al. 2016; Katris et al. 2014), although its precise function is not fully resolved.

Parasite invasion of a host cell requires the release of secretion factors such as micronemes and rhoptries, both of which are well characterized. Micronemes are essential for attachment to the host surface and required for active motility in both host cell invasion and egress (Bullen et al. 2016). Similarly, rhoptries are required to form the junction between the parasite and host cell during the host entry, an invasion-specific event which is dispensable for egress (Mueller et al. 2013). The signalling mechanism behind microneme secretion is well documented and is regulated by the highly conserved eukaryotic Protein Kinase G (PKG) in both *Plasmodium* zoite stages and *Toxoplasma* tachyzoites (Brochet et al. 2014; Wiersma et al. 2004). PKG has been shown to be essential both in every stage of the *Plasmodium* life cycle including blood, mosquito and liver stages, and in *Toxoplasma* asexual tachyzoites, and is critical for microneme secretion to facilitate invasion and egress in both parasite species (Brochet et al. 2014). PKG is a highly conserved signalling protein, which is typically present in flagellated eukaryotes, where it organizes flagellar movements (e.g., in ciliated mammalian cells and the free-swimming alga *Chlamydomonas reinhardtii*), and typically absent in non-flagellated eukaryotes such as higher plants and fungi (Johnson and Leroux 2010). Therefore, the finding that PKG regulates apical complex secretion is consistent with the association of the apical complex with proteins homologous to algal flagellar root components (Francia et al. 2012).

In metazoans such as human cells and *C. elegans*, calcium signalling is regulated by the well characterized G-Protein Coupled Receptors (GPCRs), GPCR activation triggers cAMP production and calcium release which activates Protein Kinase C (PKC) (Xu and Jin 2015). In particular, GPCRs trigger the highly conserved signalling cascade to breakdown lipid second messengers phosphatidylinositol-biphosphate (PIP2) into diacylglycerol (DAG) and inositol triphosphate (IP3), a fundamental eukaryotic signalling process, wherein the cytosolic IP3 activates ER-resident calcium channels to initiate a stress response (Bahar, Kim, and Yoon 2016). However, canonical metazoan GPCRs are absent in Apicomplexa which instead rely on activation of guanylate cyclase and cGMP signalling to activate intracellular calcium release (Stewart et al. 2017; Brochet et al. 2014) for invasion and egress processes. Furthermore, apicomplexan parasites possess a set of plant-like CDPKs which regulate secretion and motility in response to IP3-dependent calcium release for life-stage specific functions (Brochet et al. 2014; McCoy et al. 2012), some of which have roles at intersections with the cGMP pathway (Brochet et al. 2014; McCoy et al. 2012). Other core eukaryotic signalling elements in the

cGMP pathway are absent in Apicomplexa including calcium-gated ion channels and soluble and membrane forms of guanylate cyclase. Instead, apicomplexans possess an unusual alveolate-specific dual-domain phospholipid transporter/cGMP cyclase protein (TgGC) fusion protein (Johnson and Leroux 2010; Yang et al. 2019). Recently in *Toxoplasma*, TgGC has been shown to be critical for activation of TgPKG to trigger microneme secretion (Brown and Sibley 2018; Yang et al. 2019; Bisio et al. 2019). Similarly, *Plasmodium* species possess two GCs, type a and type b (GCa + GCb), and the *Plasmodium yoelli* protein PyGCb has been shown to have an apical localization in sporozoites, critical for ookinete traversal of the mosquito midgut (Gao et al. 2018). PyGCa however has a role in blood stage gametocytogenesis and its roles in intraerythrocytic blood stage and mosquito stage have yet to be determined (Jiang et al. 2020).

The function of the P-Type ATPase domain of TgGC is poorly understood but is predicted to have a role in lipid trafficking across membranes, or possibly of ion transport such as K^+ or Ca^{2+} (Yang et al. 2019; Bisio et al. 2019). However, several studies have concluded that both domains are essential for TgGC function and that the ATPase domain likely links a metabolic function to a signalling response (Brown and Sibley 2018; Yang et al. 2019), although extensive lipidomic analysis in TgGC-depleted cells is lacking. Exactly what the substrate of the ATPase domain might be is uncertain although it has been shown that cells with disrupted TgGC are less responsive to changes in pH while disruption of cofactors of TgGC, including TgCDC50, leads to parasites that can still egress in response to changes in pH (Bisio et al. 2019), suggesting that TgGC is the primary responder to external pH signals. This change in pH is thought to be mediated at least in part by phosphatidic acid (Bisio et al. 2019), which due to its sole phosphate headgroup can bear variable charge through variable binding of hydrogen groups from the external environment (Abramson et al. 1964; van Paridon et al. 1986).

Despite evidence of TgGC being involved in PA signalling, there is no evidence yet for any phosphatidylinositol (PI) during signalling in *Toxoplasma* invasion or egress. This is of particular importance as PI has also been shown to act as a pH biosensor in the Golgi of fibroblasts (Shin et al. 2020). Moreover, despite the existence of a putative PI-PLC in *Toxoplasma* (Bullen et al. 2016), diacylglycerol is still a poorly understood second messenger in *Toxoplasma*. Here we extend on the cGMP signalling model to map out the lipid signalling network. We perform exhaustive lipidomic analysis of TgGC-depleted parasites and establish TgGC as the central regulator of lipid signalling controlling rapid egress and invasion of tachyzoites. Loss of TgGC impacts conoid extrusion, the regulation of which is tightly integrated into the cGMP signalling network controlling apical secretion of micronemes. We further show that TgCDPK1, TgPKG, and TgRNG2 are some of the key proteins involved in this cGMP-dependent lipid signalling network. Crucially, we identify putative homologues of proteins involved in the phosphatidylinositol cycle including a set of putative phospholipid transporters with putative phosphatidic acid binding (PH domain) and oxysterol binding proteins domains (OSBPs), to maintain phospholipid homeostasis (Kim et al. 2015; Shin et al. 2020) and that this is likely regulated by the cGMP signalling network controlled by TgGC.

Results:

TgGC has a dynamic localization.

TgGC is the only flippase, (lipid transporters that flip lipids across membranes) and an unusual Alveolate-specific dual domain flippase-guanylate cyclase fusion protein (**Figure S1**). Previous studies all showed that TgGC is primarily found at the apical cap (Yang et al. 2019; Brown and Sibley 2018; Bisio et al. 2019), but it is also present in other secondary locations including an ER-like compartment (Brown and Sibley 2018), and the residual body (Bisio et al. 2019). This mixed distribution is consistent with a recent hyperLOPIT (Localization of Organellar Proteins by Isotopic Tagging) study that did not assign TgGC to any one location although did indicate a dynamic distribution including the Golgi (Barylyuk et al., n.d.) (www.toxodb.org). After imaging HA-tagged parasites, we found TgGC was localized primarily to the apical cap but we also saw TgGC at what appears to be a Golgi/ER-like compartment just anterior to the nucleus (**Figure 1A**), consistent with the hyperLOPIT signal. Our data supports that TgGC has a very dynamic localization in tachyzoites, with the apical cap as the primary localization, but also with prominent secondary localizations at Golgi/ER-like compartments.

TgGC-depleted cells were found to have a severe growth defect caused by an inability to secrete micronemes and egress from the host cell (Bisio et al. 2019; Yang et al. 2019). However, the effects of variable serum concentration were not explored. The presence of a phospholipid transporter ATPase domain in TgGC is still ambiguous and we hypothesized that TgGC might have roles in lipid uptake, possibly via the host cell. To test whether TgGC has a role in nutrient (specifically lipid) uptake, we grew an ATc regulated TgGC inducible knockdown mutant (Yang et al. 2019) with and without ATc in variable serum conditions to see if TgGC-depleted parasites could be rescued in a lipid rich environment, as has been shown in other mutants involved in phospholipid metabolism (Amiar et al. 2020). Interestingly, we found that this growth defect could not be rescued by growing parasites in excess serum (**Figure 1B**).

The cGMP signal chain regulates conoid extrusion

Microneme secretion and conoid extrusion are both critical processes that are known to occur in extracellular parasite when searching for a new host cell and subsequent invasion of that host (Katris et al. 2014). The cGMP signal pathway is well established as having a crucial role in activating microneme secretion for subsequent egress and invasion of host cells (Wiersma et al. 2004). However, any effects on the conoid upon inhibition of the cGMP signal pathway have been overlooked (Wiersma et al. 2004; Brown and Sibley 2018; Yang et al. 2019; Bisio et al. 2019). Given the apical localization of TgGC, we hypothesized that the cGMP signal network might have a role in triggering conoid extrusion in *Toxoplasma* tachyzoites. To test this, we harvested extracellular tachyzoites and stimulated them with cGMP phosphodiesterase (PDE) inhibitors Zaprinast and BIPPO, which are known to stimulate the cGMP pathway (Howard et al. 2015). We found that both Zaprinast and BIPPO were very efficient agonists of conoid extrusion (**Figure 1Ci**).

Toxoplasma mutants of proteins in the cGMP signal chain are defective in conoid extrusion.

Having established that the cGMP contributes to the regulation of conoid extrusion, we next asked if TgGC mutant parasites could still efficiently extrude their conoids in response to a stimulus. To test this, we treated WT and TgGC-depleted cells with either A23187 or BIPPO as before. TgGC-depleted cells extruded their conoids less efficiently in response to a stimulus, although they were relatively slightly less responsive to BIPPO than A23187 at the indicated concentrations (**Figure 1Cii**). We then observed that many proteins important for microneme secretion and invasion have yet to be investigated for defects in conoid extrusion (Brown, Long, and Sibley 2017; Lourido et al. 2010) and

hypothesized that at least some known mutants might have additional conoid extrusion defects. So, we performed conoid extrusion assays using multiple parasite mutants and inhibitors and then stimulated these cells with both BIPPO and A23817. We found TgRNG2-depleted cells showed significantly less conoid extrusion upon BIPPO treatment but were mostly responsive to A23817 stimulus (**Figure 1Ciii**) similar to the response of for microneme exocytosis (Katris et al. 2014).

We next examined the involvement of Protein Kinase G, TgPKG, the primary kinase which is activated by cGMP produced by TgGC (Brown, Long, and Sibley 2017). After treatment of extracellular tachyzoites with the PKG inhibitor Compound 1, we found Compound 1-treated parasites were less able to extrude their conoids in response to either BIPPO or A23187 stimulus (**Figure 1Civ**). The same defects in both BIPPO and A23187 mediated conoid extrusion were also seen when cells were pre-treated with Compound 2, another inhibitor of TgPKG (**Figure S2A**) (Donald et al. 2006). Calcium signalling is also a well-known signalling factor responsible for conoid extrusion and microneme secretion, with a well-established model where cGMP signalling proteins TgGC and TgPKG trigger downstream intracellular calcium release to activate TgCDPK1 and TgCDPK3 for microneme secretion (Stewart et al. 2017). We thus next tested known mutants of calcium-dependent kinases involved in egress and invasion. We found that a tetracycline-inducible KO mutant of TgCDPK1 (Lourido et al. 2010) was less able to extrude its conoid in response to either BIPPO or A23187 treatment (**Figure 1Cv**). Conversely, when we examined TgCDPK3 KO cells (McCoy et al. 2012) they were able to efficiently extrude their conoids in response to both BIPPO and A23187 treatment (**Figure 1Cvi**). Taken together, these results support a previously overlooked role for cGMP signalling in conoid extrusion and that conoid extrusion is wired into the same calcium signal network regulating microneme secretion facilitating their concomitant activation for egress and invasion.

Of the proteins investigated thus far, TgRNG2 is the only protein which has not yet been investigated for calcium signalling dynamics. To examine its role, we generated a TgRNG2iKD cell line with a genetically encoded GCaMP6 calcium biosensor and tracked changes in calcium indirectly via GCaMP6 fluorescence (**Figure S2B**). TgRNG2iKD+GCaMP6 cells were pre-treated with or without ATc, stimulated with BIPPO and tracked over 60 seconds. We found that TgRNG2 depleted cells showed less BIPPO-triggered calcium release (**Figure S2B**), suggesting that TgRNG2 interacts in some way in the cGMP signal pathway controlled by TgGC. Furthermore, we found that TgRNG2 depleted cells were slower to respond to BIPPO-triggered egress (**Figure S2C**) but were responsive to A23187 (**Figure S2D**), broadly consistent with a defect in the cGMP signal pathway that can be rescued by a downstream calcium signal (Katris et al. 2014). Taken together, TgRNG2 acts within the cGMP signalling pathway and is apparently implicated in signal amplification through calcium release, although the mechanism of this role is not fully clear.

TgGC-depleted parasites display both disrupted phospholipid metabolism and signalling.

In diverse eukaryotes, both phospholipid transporter and cGMP cyclase proteins are well known to be important for lipid trafficking and lipid signalling respectively. So, we thought that the Alveolate specific GC would represent a unique opportunity to examine a novel biological example of a protein responsible for regulating lipids for both these processes simultaneously. We therefore examined changes in lipids involved in trafficking and/or signalling upon TgGC knockout by performing an exhaustive fatty acid and phospholipid analysis by Gas Chromatography Mass Spectrometry (GC-MS). The fatty acid composition of TgGC-depleted cells showed key differences in major fatty acid species (**Figure 2A**). First, there was a notable increase in the remnant plastid (apicoplast) derived C14:0, and ER derived C20:1 (Ramakrishnan et al. 2012) in TgGC-depleted cells pre-treated with ATc (**Figure 2A**). Both the apicoplast and ER are major metabolic hubs for phospholipid production (Amiar et al. 2016), suggesting that the parasites might be adapting by upregulating phospholipid production when TgGC is knocked out. There was also a notable decrease in oleic acid 18:1 in TgGC-depleted cells (**Figure 2A**).

Unsaturated fatty acids are important for increasing membrane fluidity during movement and it is possible that the reduction in 18:1 represents a decrease in membrane fluidity during extracellular motility. Additionally, C20:4 (arachidonic acid) is significantly reduced in cells with TgGC-depleted after ATc treatment (**Figure 2A**), which is interesting as lipid intermediates of the PI cycle are commonly enriched in C20:4 (Epanand 2017).

When we examined individual lipid classes, we observed that TgGC-depleted cells have broadly similar levels of lyso-phosphoinositol (LPI), lyso-phosphatidylcholine (LPC), inositol phospho-ceramide (IPC), cardiolipin (CL) and free fatty acids (FAs) (**Figure 2B**). Parasites with TgGC-depleted after ATc treatment exhibited slightly reduced levels of phosphatidylserine (PS), phosphatidic acid (PA), phosphatidylethanolamine (PE) and sphingomyelin (**Figure 2B**). However, by far the most significantly reduced lipid in TgGC-depleted cells was phosphatidylinositol (**Figure 2B, S3**), which has known roles in both lipid trafficking and signalling (Shin et al. 2020). TgGC-depleted cells showed a mild increase in phosphatidylcholine (PC) abundance but the apicomplexan specific lipid phosphatidylthreonine (PT) was rather unexpectedly by far the most significantly increased phospholipid in TgGC-depleted cells (**Figure 2B**).

Despite their levels being reduced in TgGC-depleted cells, the fatty acid profile of PA, PS and PI was broadly similar, although PA and PS showed slight decreases in oleic acid 18:1, and slight concomitant increases in unsaturated C16:0 and C18:0 (**Figure 2C**). In TgGC-depleted cells PT showed an overall normal FA profile but with slightly increased levels of the signature 20:1 and 20:4 FA chains for which PT is known (**Figure 2C**) (Arroyo-Olarte et al. 2015). Interestingly, the FA profile of PC showed a large increase in 18:1 suggesting that the TgGC-depleted cells are either synthesising or scavenging more of this specific PC (**Figure 2C**). We also saw a large increase in 18:1 in the profile of SM upon TgGC depletion (**Figure S3**), so that PC and SM were the only lipids to have a large increase in 18:1 (**Figure S3**). This may reflect differences in outer and inner leaflet lipid composition of PC and SM (Lorent et al. 2020). The FA profile of PE was largely similar between TgGC-depleted and non-depleted cells, however there was an increase in C20:1 and a decrease in C20:4 consistent with the total FA analysis (**Figure 2A, C**). Taken together, in TgGC-depleted cells, there are conspicuous changes in phospholipid metabolism, particularly phosphatidylinositol and phosphatidylthreonine, and to some extent in oleic acid 18:1.

Both TgGC and TgRNG2 are involved in the apical DAG-PA signalling events

The phospholipid PA is well known to be involved in signalling events that control microneme secretion in *Toxoplasma* tachyzoites. Given changes in PA levels detected in the TgGC-depleted cells (**Figure 2B**), and the known function of PA interchanged with DAG in controlling microneme secretion (Bullen et al. 2016), we wondered whether TgGC plays a role in PA metabolism during the signalling events of invasion and egress? Particularly, we wondered what the behaviour of signalling lipids such as PA might look like in real time, over the course of activation of egress and/or subsequent invasion of a host cell which occurs in a matter of minutes. To test this, we examined levels of PA over time in response to a cGMP stimulus, BIPPO, to determine whether PA-mediated events are controlled by the cGMP signal path. Given that conoid extrusion occurs within a very rapid time frame of 30 seconds (**Figure 1C**), we considered that a time frame of up to one minute would be appropriate to examine lipid kinetics in extracellular tachyzoites. TgGCiKD cells without ATc pre-treatment were stimulated by BIPPO and a rapid increase in PA was detected within an astonishing 5 seconds of stimulus with PA levels returning to near pre-treatment levels within 60 seconds (**Figure 3A**). Cells depleted of TgGC, however, showed no significant increase in PA levels after BIPPO treatment (**Figure 3A**). This suggested that cGMP generated by TgGC is required for this fast response of PA production. We then hypothesized that other proteins known to be involved in the cGMP signal path might also show abnormal PA production with these proteins inhibited or depleted. So, we investigated cells with

disrupted TgPKG and TgRNG2 to see if they produce less PA upon BIPPO stimulation. Having established that 5 seconds is enough to observe a rapid change in PA, we then focused on this time point and measured PA production in parasites within 5 seconds of BIPPO stimulus in WT cells with or without pre-treatment with PKG inhibitor Compound 2 (Donald et al. 2006). We found that Compound 2 inhibited cells had lower levels of PA at 5 seconds of BIPPO stimulation (**Figure 3B**). Similarly, we quantified PA in TgRNG2iKD cells pre-treated with or without ATc, stimulated with BIPPO, and RNG2-depleted cells showed lower levels of PA within 5 seconds of stimulus also (**Figure 3C**). These data confirm that PA is a rapidly produced product of the cGMP signal chain and that TgRNG2 and TgPKG are part of the is signal network controlled by TgGC.

In the known signalling events of microneme secretion DAG sits in a central location. DAG can form PA via DGK and also be restored by PA conversion back to DAG by PAP (Phosphatidic Acid Phosphatase) (Bullen et al. 2016). Furthermore, IP3 is a common signalling product of PI-PLC signalling activity. Specifically, PI-PLC dependent cleavage of PIP2, produces DAG and IP3. IP3 signal release is a common activator of Ca²⁺ store release, and in *Plasmodium* it is known to occur downstream of PKG activation (Brochet et al. 2014; Stewart et al. 2017). Therefore, DAG is at a crucial intersection, interchanging with multiple second messengers, making DAG kinetics a potentially useful readout of invasion-related signalling events. Given the fast response of PA to BIPPO-stimulation (**Figure 3A**) we sought to test if DAG changes in the same manner over time. To test this, we measured DAG kinetics over the same times as for PA. No significant change in DAG levels were seen throughout the events following BIPPO stimulus in TgGCiKD cells regardless of ATc pre-treatment (**Figure 3D**). Similarly, pre-treatment with PKG inhibitor Compound 2 also resulted in no change of DAG, nor was a change seen in parasites treated with DMSO instead of BIPPO. (**Figure 3E**). However, in TgRNG2 depleted parasites a sharp, short-lived DAG increase was seen following BIPPO stimulus (**Figure 3F**) This implies that the cGMP signal pathway initiated by TgGC is still active in TgRNG2 depleted cells and that loss of TgRNG2 is preventing the conversion of DAG to PA during microneme secretion.

TgGC has been shown to be involved in microneme secretion in *Toxoplasma* tachyzoites (Brown and Sibley 2018; Yang et al. 2019; Bisio et al. 2019). We repeated these experiments and we found that TgGC-depleted cells were unable to secrete in response to BIPPO stimulus and only partially by A23187 stimulus similar to previous reports (**Figure 3G**) (Yang et al. 2019; Bisio et al. 2019). Additionally, we tested for secretion of dense granule proteins by examining secretion of GRA1, which we found to be secreted in broadly similar amounts in both WT and TgGC-depleted cells (**Figure 3G**). Dense granule proteins are secreted independently of micronemes and therefore serve as a good indicator of both the specificity of a process and also parasite viability. Viability is also supported by the lack of CAT release into the supernatant showing that parasites are likely intact and not lysed (**Figure 3H**). Taken together, these experiments place TgGC upstream in the lipid signal chain, likely as the master regulator of lipid signalling controlling both conoid extrusion and microneme secretion in *Toxoplasma* tachyzoites (**Figure 3H**).

Extracellular Toxoplasma tachyzoites readily take up exogenous PA as part of normal membrane remodelling processes.

The P-type ATPase domain function of GC is hotly debated in both *Plasmodium* and *Toxoplasma* parasites. The ATPase domain is a predicted phospholipid transporter/flippase with some proposing that it may possibly transport calcium or K⁺ ions (Yang et al. 2019), and others even showing a role for responding to changes in plasma membrane lipid composition caused by excess phosphatidic acid (Bisio et al. 2019). We also can see from *in silico* analysis, contrary to previous reports (Gao et al. 2018), that the ATPase domain of TgGC is predicted fully functional with all conserved residues intact for activity of the flippase domain (**Figure S1C**), although *in vitro* experimental evidence for phospholipid transport is currently lacking.

Recently a novel class of transporters has emerged which include HsNir2 and Oxysterol Binding Proteins (OSBPs) which are important for maintaining ER-PM contact sites (Kim et al. 2015; Shin et al. 2020; Peretti et al. 2008). Notably, at least one of these transporters, HsNir2 has been shown to be important for importing PA from the outer leaflet of the plasma membrane towards the ER to fuel phospholipid synthesis. This is the important final step of the phosphatidylinositol cycle in which PA is recycled from the outer membrane to maintain phospholipid homeostasis during PIP signalling after vesicle secretion. (Kim et al. 2016; 2015). In *Toxoplasma* the closest homologue to HsNir2 is TGGT1_289570, which bears the putative phospholipid transfer domain, phosphatidic acid-binding PH domain, and additionally, an OSBP domain which in mammalian cells acts both as a lipid transporter and as a tether for ER organelle localization with proteins like HsNir2 and the cofactor HsVAPB (Mesmin et al. 2013). Many Oxysterol-related Proteins also bind lipids such as PI4P (Antonny, Bigay, and Mesmin 2018; Mesmin et al. 2013). In the *Toxoplasma* genome we can find a full set of proteins necessary to complete the recycling step of the phosphatidylinositol cycle (Figure S6). Therefore, given the existence of a complete set of putative PA transporters in *Toxoplasma*, we consider it unlikely that the ATPase domain of TgGC is dedicated to importing PA from the outer plasma membrane leaflet, although we cannot rule out the possibility that TgGC transports phosphatidic acid (and maybe even additional phospholipids) from the outer membrane.

Given the existence of a complete phosphatidylinositol cycle for recycling PA from the outer leaflet, we first wanted to test if phosphatidic acid could be internalized by extracellular parasites as part of the PI cycle. To test if PA can be imported, we exposed extracellular parasites to PA18:1, PA16:0 and control PC18:1, and measured their uptake to gauge which lipids are imported as part of membrane remodelling during extracellular stages. Given the extremely rapid time with which parasites extrude their conoids and turnover lipid second messengers, we chose 30 seconds as an incubation time for exposure to exogenous PA, before placing on ice to stop the lipid uptake. In this short time we found that PA is taken up extremely rapidly and localizes primarily to the peripheral plasma membrane and a cytosolic/endomembrane-like compartment that avoided the nucleus, occasionally localizing at internal puncta (**Figure 4A, S4A**). The localization of PA appeared to be broadly similar in parasites exposed to both exogenous PA16:0 and PA18:1. PC18:1 was taken up less readily over a short time scale, but after an hour of incubation, there was more intense fluorescence in what appeared to be the cytosol and at internal dots/puncta, likely endomembrane compartments (**Figure 4A**). Interestingly, when quantified by FACS, PA 18:1 was taken up more readily than PA16:0 suggesting that the unsaturated double bond in 18:1 was better at disrupting the plasma membrane to increase fluidity to then become internalized as part of normal membrane remodelling (**Figure 4Bi**). However, PA 16:0 was taken up more than PC18:1 suggesting a primarily head-group-dependent selection process for lipid internalization/membrane remodelling (**Figure 4Bii**). As an independent control, we also tested PA and PC uptake using a microscopy based method similar to published microscopy based quantification (Gras et al. 2019) in which parasites incubated with NBD-PA or NBD-PC were smeared onto coverslips coated with PEI and blocked overnight (**Figure S4**). An Immunofluorescence assay was then performed to label parasites with anti-SAG. The SAG1 provided an unbiased overlay to identify parasites and then parasites were measured for 488 fluorescence, indicative of NBD-lipid uptake. Using this method, we found broadly similar results to the FACS methods (**Figure S4B, C, D**). These results show that parasites actively take up phosphatidic acid as part of membrane remodelling during extracellular events.

We also tested phospholipid uptake in intracellular tachyzoites and we found that neither PA 16:0 or PA 18:1 could be taken up by the parasites during intracellular stages but PC18:1 clustered around the parasite vacuole and in between the parasites suggesting that PC, but not PA, could readily be taken up during intracellular host scavenging, consistent with previous reports (**Figure S4F**) (Charron and Sibley 2002). To test if similar phospholipid uptake occurs in other apicomplexan parasites, we

examined the closely related apicomplexan parasite *Plasmodium falciparum*. We incubated blood stage *P. falciparum* with either PA 16:0, PA 18:1 or PC 18:1 for 48 hours to see which lipids could be imported during replication. We found that neither PA16:0 nor PA 18:1 was taken up by the *Plasmodium* parasites during blood-stage replication (**Figure S5**), similar to *Toxoplasma*. When we exposed blood stage *Plasmodium* parasites to growth with PC 18:1 we found that fluorescent PC was readily up-taken and co-localized with DAPI indicative of dividing *P. falciparum* parasites (**Figure S5**) which is consistent with previous reports that PC is readily up-taken during blood stage growth (Grellier et al. 1991). This is in contrast to recent reports that PC cannot be scavenged by blood stage *Plasmodium* (Brancucci et al. 2017) suggesting a primarily 18:1 fatty acid chain dependent uptake compared to the PC 16:0 used in other studies (Brancucci et al. 2017). *Plasmodium falciparum* blood stage PC uptake is also consistent with what was seen here in *Toxoplasma*. We also incubated mosquito-stage sporozoites with NBD-PA and NBD-PC and found that sporozoites readily took up both PA 16:0, PA 18:1 and PC18:1 (**Figure S5**). These experiments show that phospholipid uptake as part of membrane remodelling is also important in *Plasmodium* parasite development.

To get further insight into the PA transporter family, we attempted to tag the identified family of proteins. The *Toxoplasma* genome encodes for three putative OSBPs; TgOSBP1 (TGGT1_289750), TgOSBP2 (TGGT1_264670) and TgOSBP3 (TGGT1_294740) (**Figure S6**). Both TgOSBP1 (closest homologue to PA transporter HsNir2 (Kim et al. 2015)) and TgOSBP2 (ScOsh1 homologue (Shin et al. 2020)) have putative PH domains which are known to bind PA, in support of their putative roles as PA importers, while TgOSBP3 has no predicted PH domain suggesting some other function (www.toxodb.org) (**Figure S6**). Both TgOSBP1 and TgOSBP2 have additional OSBP domains, which have known roles in ER lipid homeostasis hence our arbitrary naming of these *Toxoplasma* genes in this study. TGGT1_289570 also bears the putative phosphatidylinositol transfer domain present in HsNir2, while TGGT1_264670 lacks the PI transfer domain, and appears more like yeast ScOsh1 (Shin et al. 2020). Furthermore, the *Toxoplasma* genome also encodes for a putative cofactor TgVAP (TGGT1_318160), a homologue of HsVAP which assists HsNir1 (Kim et al. 2015), OSBPs and Ceramide Transfer proteins (CERTs) to localize at the ER (Peretti et al. 2008). We were unable to tag any of the TgOSBPs, but we could generate an N-terminally HA-tagged mutant of the HsNir2 cofactor, TgVAP. We found that HA-TgVAP was localized to the periphery of the nucleus consistent with an ER-like localization (**Figure 4C**). This is consistent with experimental evidence by hyperLOPIT in which TgVAP is assigned to the ER (Barylyuk et al. 2020), and we speculate that it could be involved in ER-PM contact sites. TgOSBP1 and TgOSBP3 are predicted to be non-essential according to a recent genome wide KO screen while TgVAPB and TgOSBP2 are have strong mutant phenotypes (Sidik et al. 2016)(www.toxodb.org) and will be the subject of future research. Taken together, these data show support the existence of a complete PI cycle in *Toxoplasma* based in the ER and PM contact sites.

Recently, TgGC was shown to be essential for secreting micronemes in response to exogenous PA. It is presumed that the exogenous PA generated instability in the plasma membrane which was then detected by the ATPase domain of TgGC and transmitted via the cyclase domain to activate motility. Furthermore, it was shown that TgGC-depleted cells were unable to egress in response to change in pH. It was thought that the phosphate headgroup of PA, with its variable charge state acts as a pH sensor by accepting protons or not depending on the extracellular pH (Young et al. 2010). However, recently PI4P has been proposed to act as a pH biosensor owing to its variable pH-dependent protonation state (Shin et al. 2020). Therefore, much of the inability of TgGC-depleted cells to respond to changes in pH could equally be attributed to PI4P or PIP2 instead of PA. Nevertheless, given that TgGC was shown to be important cells to respond to changes in PA at the plasma membrane either by membrane curvature or pH changes (Bullen and Soldati-Favre 2016), we sought to examine PA uptake in TgGC-depleted cells. We pre-treated TgGCiKD cells with or without ATc and exposed them to exogenous phospholipids and analysed by FACS. We found that TgGC-depleted cells showed reduced PA18:1 uptake over 30 seconds (**Figure 4E**). However, there was no difference in uptake of PA16:0

suggesting a chain length preference for PA uptake (**Figure 4E**). Interestingly, PC uptake was unchanged in TgGC-depleted cells over 30 seconds, but after 1 hour of incubation, TgGC-depleted cells imported slightly more PC18:1 (**Figure 4E**). Given the close proximity of TgRNG2 to TgGC, we tested phospholipid import in TgRNG2iKD cells with the hypothesis that we might see altered uptake in TgRNG2-depleted cells, which might interfere indirectly with TgGC function (**Figure 4F**). Interestingly, we found that TgRNG2 depleted cells imported more PA over 30 seconds (**Figure 4F**). Import of PA16:0 was largely unaffected after loss of TgRNG2 (**Figure 4F**). PC import was also unaffected in TgRNG2-depleted cells over 30 seconds, although there appeared to be a slight increase in PC18:1 after a 1-hour incubation, similar to TgGC (**Figure 4F**). Similar results were observed when quantified by microscopy methods (**Figure S4B,C,D,E**) Despite this apparent reduction in PA uptake, it is highly likely that TgGC is not importing PA, but rather regulating PA turnover as part of membrane remodelling via the TgOSBP/TgVAP complex in the PI cycle during extracellular stages, although we cannot rule out the possibility that TgGC does indeed import one or more phospholipids from the outer leaflet such as phosphatidic acid.

Evolution of phospholipid trafficking proteins in apicomplexans and other eukaryotes.

Studies on *Toxoplasma* have revealed the important role of phosphatidic acid signalling in invasion and egress. Due to its excellent genetic tractability, *Toxoplasma* has emerged in recent years as the best-studied alveolate and a model organism for investigation of the alveolate cytoskeleton. Proteins of the cytoskeleton are relatively fast evolving and therefore poorly conserved with only a handful of conserved domains identified such as alveolins (Gould et al. 2008). The emergence of phosphatidic acid as a crucial signalling lipid regulating conoid extrusion and microneme secretion at the apical complex suggest that PA regulating enzymes such as GC and DGKs could provide a framework for interpreting aspects of the evolution of parasite invasion machinery.

To illuminate the distribution and functional conservation of membrane remodelling proteins involved in PA signalling, we sought to understand their global evolution by the means of phylogenetic inference. Because the bimodular nature of apicomplexan GCs is uncommon in other eukaryotes the phylogenies of the P-type ATPase (GC:ATPase) and cyclase domains (GC:cyclase) were inferred independently (Methods). The N- and C-terminal domains in 2-domain GC:cyclase were also split and subsequently aligned together in a one-domain alignment to test whether they have co-evolved as a single evolutionary unit. Phylogenetic matrices including a broad sampling of eukaryotes were compiled by extracting homologous sequences primarily from GenBank nr and EuPathDb databases. Processed matrices were analysed by maximum likelihood tree inference.

In the Maximum Likelihood tree of 223 GC:cyclases (**Figure 5; Figure S7 S8**), the N- and C-terminal domain form two independent clades. Both clades have almost identical species presence and similar branching patterns despite the relatively short domain length (148 informative sites). Apart from the alveolates, the 2-domain GC:cyclase is present in some stramenopiles (oomycetes and a thraustochytrid) and amoebozoans. Although the N- and C-terminal GC:cyclase clades do not branch strictly as sister groups in the tree, their deep relationships are weakly resolved and their otherwise congruent evolutionary histories suggest that they once originated by tandem duplication (**Figure 5A**). The 2-domain GC:cyclase are most closely related to 1-domain GC:cyclases from eukaryotes such as humans (pdb: 4NI2_A) and further to various other proteins including the adenylyl cyclase of *Mycobacterium tuberculosis* (Guo et al. 2001). The characteristic arrangement of *Plasmodium* GC:cyclase, in which a P-type ATPase domain is fused to the N-terminus, is found in a specific subset of 2-domain GC:cyclase in alveolates and oomycetes (**Figure 5A; Figure S7 and S8**). We thus propose that the unique apicomplexan GC:cyclase architecture was present at least in the alveolate ancestor,

and possibly earlier in their common ancestor with the stramenopiles (**Fig. 5C**), and originated by a single evolutionary fusion of a P-type ATPase and 2-domain GC:cyclase.

The phylogeny of the GC:ATPase (**Figure 5B and S9**) is more difficult to interpret, in part because many paralogs are present and evolutionary rates of individual sequences are highly variable (over 10-fold difference in branch length). The backbone of the tree is nevertheless broadly congruent with the GC:cyclase tree - all alveolate GC:ATPases group together and are placed among diverse eukaryotic ATPases that lack the GC:cyclase fusion (**Figure 5B**). The fast-evolving apicomplexan and ciliate sequences group together, in contrast to the GC:cyclase phylogeny, but this might be a long branch attraction artefact caused by strong substitutional bias. The alveolate GC:ATPase contain several paralogs (**Figure. S9**). Their relationships are not well resolved but because two variants are present in most apicomplexans (haemosporidians, *Gregarina*, and eimeriid coccidians), we conclude that an early apicomplexan underwent a GC duplication (**Figure 5C**).

Curiously, several variants of GC proteins have one of the domains either absent or substituted with another protein. The ATPase domain appears to be absent in the GCb protein of some coccidians including *Toxoplasma*, suggesting that their second copy of GC has been lost secondarily. This may be true of *Cryptosporidium* also which has only one GC variant. Notable domain substitutions include *Chromera*, which has the GC: ATPase domain fused to a domain with homology to the *Drosophila* Patched protein (Cvel_16197), and *Symbiodinium* which has GC-like proteins with an ATPase fused to a CDC50 domain, a well-known flippase co-factor (Bai et al. 2019, 50) (SmATP2-OLQ09111.1, SmATP3-OLP97098.1). Considering that these variants do not bear cyclase domains, they may not represent true GCs and may be involved in processes other than signalling. However, an assignment to GCs may be warranted by their bi-modular structure, which bears similarity to canonical GCs, and because at least the Patched domain has been shown to be involved indirectly in cAMP signalling (Lepage et al. 1995). Possibly, these alternative GCs have evolved to activate a signalling response via an atypical pathway, although it is unclear whether they remain active.

In summary, we propose that the early alveolate ancestor first fused a cyclase domain to a phospholipid transporter to couple cGMP signalling with lipid homeostasis. This dual domain GC then duplicated into at least 2x copies as can be seen in *Plasmodium*, and most other apicomplexans. The second copy of GC was then likely lost in some species such as *Toxoplasma* and *Cryptosporidium*, and is possibly in the process of loss in other coccidians such as *Eimeria* (**Figure 5C S11**).

DGKs are another group of membrane remodelling proteins known to be involved in microneme secretion and integral to the PA signalling cascade. Specifically, a parasitophorous vacuole resident protein DGK2 produces PA to activate egress via TgGC. We hypothesized that the evolutionary history of DGK2 or other DGKs might reflect changes in the evolution of GC in Alveolata. To test this, we performed a phylogenetic analysis of DGKs in alveolates to see if its evolutionary behaviour is coordinated with that of GCs. The phylogeny of DGKs (**Figure S10**) reveals a deep evolutionary divergence between the apicomplexan DGK1 and 2, and DGK3 forms. Apicomplexan DGK1 and DGK2 are each related to sequences from other alveolates and eukaryotes and were both likely present in the alveolate ancestor, having originated by an earlier duplication (**Figure S10**). Chromerids and *Cryptosporidium* contain divergent forms related to DGK1 and 2, which we call "DGK2-like"; *Chromera* also contains a distinct DGK4 form (**Figure S10**). More detailed evolution of DGK is difficult to interpret due to the low resolution of the tree, presence of paralogs, and the loss of redundant forms: for example, DGK2 is present in coccidians but no other apicomplexans. Since DGK2 is exported to the parasitophorous vacuole in *Toxoplasma* (Bisio et al. 2019) we searched for N-terminal signal peptides in all identified DGKs by using SignalP. Although the sensitivity of this approach is limited and some DGKs have incorrectly predicted N-termini, nine sequences contained strongly predicted signal

peptides. Seven of these include the DGK2 proteins in coccidians, *Perkinsus* and *Symbiodinium*, and the DGK2-like proteins in *Chromera* and *Vitrella* (**Figure S10**). It is thus possible that the chromerid DGK2-like is exported extracellularly like the coccidian DGK2 and shares similar functional aspects.

Discussion:

Conoid extrusion is wired into the same signal network regulating microneme secretion.

In summary we define the lipid signalling network controlling conoid extrusion and microneme secretion for invasion and subsequent egress in *Toxoplasma* tachyzoites and establish that it is regulated by TgGC. Conoid extrusion is a Ca^{2+} driven process and CDPK1 plays a central role in its control, but cGMP and PKG are also required for the full conoid extrusion response. Furthermore, blocking conoid extrusion by depletion of TgRNG2 reduces the efficiency of cGMP to be able to stimulate turnover of lipid second messenger DAG and downstream calcium release. This shows that conoid extrusion is wired into the cGMP and Ca^{2+} signalling pathways which also regulate microneme secretion. One possible theory is that conoid extrusion is necessary to facilitate microneme release (the retracted conoid might prevent microneme release during intracellular replication) and so their concomitant activation is coordinated by cGMP and Ca^{2+} for this reason. Recent research has found that the loss of the conoid caused by KO of TgAC9 and TgAC10 resulted in a defect in microneme secretion (Tosetti et al. 2020), consistent with the notion that conoid extrusion facilitates microneme release. While the full extent of conoid function is not known we can see that facilitating microneme release is at least one major function of the conoid and that the behaviour of conoid extrusion in *Toxoplasma* is intimately wired into the other signalling networks that are known to be important for microneme secretion and parasite motility and are therefore part of the coordinated behaviour of invasion and egress regulated by TgGC.

TgGC shows defects in lipids required for both signalling and membrane fluidity.

The behaviour of PA and DAG has important implications for both signalling and the biophysical properties of the parasite membrane. Firstly, the increase in overall PA is consistent with previous research that PA production is important for activation of microneme secretion (Bullen et al. 2016). We would also point out that a general increase in PA would serve to destabilize the plasma membrane more and thus increase fluidity for extracellular motility (Bullen and Soldati-Favre 2016), and the lack of an increase in TgGC-depleted cells shows that this is a cGMP dependent process. The lack of 18:1 in TgGC-depleted cells would also decrease membrane fluidity with increased tight inflexible packing of the bilayer, preventing proper membrane bending during motility. However, in TgGC-depleted cells by far the biggest lipid disruptions were the reduction of phosphatidylinositol for signalling and the concomitant increase in PT (**Figure 2**). We also saw a smaller decrease in PS which is consistent with previous research which showed an inverse relationship between PT and PS (Arroyo-Olarte et al. 2015). Smaller reductions could also be seen in sphingomyelin (SM) and phosphoethanolamine (PE) (**Figure 2**).

DAG shows unusual kinetics in both wild type and mutant parasites.

In kinetics experiments during activation of the early events of invasion, WT cells showed no increase in DAG, which could be because DAG is used in many other compartments of the parasite such as storage lipids and that the relative amount used for signalling purposes are small (**Figure 3**) and difficult to detect. Alternatively, it could be that DAG is maintained at steady levels and turned over very rapidly. Indeed, this would appear to be the case as we saw a 30% increase in DAG in TgRNG2 depleted cells stimulated with BIPPO, before DAG dropped back down to basal levels within 10 seconds (**Figure 3**). This has several interesting implications. Firstly, given this behaviour with BIPPO stimulus, this suggests that the 30% increase in DAG is made exclusively by TgPLC for the purposes of microneme secretion (**Figure 3**), and the activity of TgPLC is extremely high and supports the idea that DAG is being turned over into PA as part of phospholipid metabolism. Secondly, this suggests that even though DAG levels remains flat in all the mutants, it is very likely that the DAG in WT cells is being turned over into PA at a consistent rate while in the TgRNG2 and TgGC mutants, and TgPKG inhibited cells (by treatment with Compound 2), DAG is not being turned over. Yet it is interesting that DAG is not accumulating excessively in TgRNG2iKD (**Figure 3E**), suggesting the presence of yet more

phospholipid homeostasis mechanisms to prevent excess accumulation of DAG. It would be interesting then to find out what DAG is being turned into when it drops back to basal levels in the TgRNG2 depleted cells; back into CDP-DAG? cut up by a phospholipase? Thirdly, the fact that we see a large spike in DAG suggests that TgGC (**Figure 3E**) is active in TgRNG2-depleted cells and confirms that TgGC is the upstream regulator of the cGMP and calcium signal network, and that TgRNG2 is downstream in this process likely at the point of PA synthesis by one of the TgDGKs during microneme secretion, which is possibly blocked by improper conoid extrusion in the absence of TgRNG2. Similarly, the increase in PA import in TgRNG2 depleted cells can be seen as due to TgGC being active in TgRNG2 depleted cells and attempting to increase membrane remodelling for secretion and motility. More precise details on the interaction of TgRNG2 and TgGC are presently unknown, however we can clearly see that TgRNG2 is in the pathway downstream of TgGC and that the extrusion of the conoid facilitated by TgRNG2 is part of the cGMP signal chain of events.

The function of the ATPase domain of GC is still unknown.

An unusual feature of TgGC is the presence of a P-type ATPase, phospholipid import domain, aka flippase domain, at its N-terminus. This type of accessory domain is a common feature of guanylyl cyclases in protists, whereas the mammalian GC homologue does not bear an ATPase domain. Instead there exists two isoforms of GC encoded by two separate genes; one membrane bound and one soluble/cytosolic (Johnson and Leroux 2010). Recently exogenous PA was shown to be a very potent agonist of *Toxoplasma* microneme secretion, presumably because it disrupts the plasma membrane, which triggered a secretion response regulated by TgGC. This exogenous PA mimicked an external PA source which was shown to be provided by an exported effector, TgDGK2, which was shown to be necessary for egress of *Toxoplasma* tachyzoites from the parasitophorous vacuole. However, the role of the ATPase in this PA signalling cascade was still rather mysterious and P-Type ATPase activity has yet to be shown, although predicted (**Figure S1**). Despite ours and others' efforts, the exact function of the ATPase domain and its relationship to PA at the plasma membrane remains elusive.

TgGC likely regulates the PI cycle

The import of PA from the outer leaflet of the PM was an important subject of research for the phosphoinositide cycle in wider eukaryotes for many years as it was unknown how end-products of phosphatidylinositol signalling were recycled to complete the PI cycle. Recently, a novel PA transporter was discovered localized to ER-PM contact sites to import PA from the external leaflet to be recycled back into CDP-DAG (Kim et al. 2015). HsNir2 is a putative PA transporter which appears to be conserved in *Toxoplasma* and curiously has additional OSBP domains which also functions in phospholipid trafficking to and from the ER in other eukaryotes (hence our naming system of these *Toxoplasma* genes) (Shin et al. 2020; Mesmin et al. 2013) (**Figure S6**) (www.toxodb.org). Both TgOSBP1 and TgOSBP2 bear a conserved PH domain which is predicted to bind PA, but not TgOSBP3 (Kim et al. 2015; Shin et al. 2020) (**Figure S6**). Additionally, a conserved transporter cofactor homologue of HsVAPB (Kim et al. 2015) can be found in the *Toxoplasma* genome, TgVAP (**Figure 4C**), which in fibroblasts was shown to assist HsNir1 localization (Kim et al. 2015). This PA transporter HsNir2 (closest TgOSBP1 homologue), and the co-factor HsVAPB (TgVAP homologue) answered a long-standing question in wider eukaryotes regarding how PI homeostasis is maintained and how end products like PA are recycled to prevent build-up of PA at the plasma membrane and maintain phospholipid homeostasis (Kim et al. 2015). However, we cannot rule out the possibility that the ATPase domain of TgGC does indeed import PA or other phospholipids based on the limited experimental evidence presented here. Perhaps TgGC transports PI or PIPs to and from the apical cap? Although given the existence of conserved PA transporters in *Toxoplasma*, we consider it unlikely that the ATPase domain of TgGC would also specifically import PA because there already exists a conserved mechanism to recycle PA.

Interestingly, previous proteomics studies on a rodent malaria PbGCb KO cell line and Compound 2-treated cells showed that the PA transporter PbOSBP1 shows significantly altered phosphorylation of at least some sites upon disruption of the cGMP signal pathway (Brochet et al. 2014). Additionally, the putative cofactor PbVAP shows significantly reduced expression in the PbGCb KO background (Brochet et al. 2014). This evidence in *Plasmodium* suggests that the putative conserved phosphatidylinositol recycling system in *Toxoplasma* is regulated by TgGC. Given the well-established role of cGMP signalling upstream of other major calcium signalling pathways in apicomplexan parasites (Yang et al. 2019; Brochet et al. 2014), this strongly suggests that TgGC acts on TgVAP and TgOSBPs to regulate PA import as is the case for PbGCb on PbOSBPs and PbVAP. This also means that the reduced PA import seen in TgGC KO cells is much more likely to be an indirect effect of TgGC regulating membrane remodelling during active motility instead of directly importing PA which according to our proposed model, would be likely to be imported by TgOSBP1 and TgVAPB after secretion of micronemes. Similar research has shown that inhibition of endocytosis blocks motility in extracellular *Toxoplasma* tachyzoites (Gras et al. 2019). This was linked to the turnover of lipids as part of membrane remodelling through endocytosis, and that the concave lipid lysophosphatidic acid (LPA) was a key mediator of endocytosis (Gras et al. 2019). It would be interesting to examine proteomics and transcriptomics of TgOSBP or TgVAP mutants to see if a reciprocal result can be seen with expression/phosphorylation of TgGC, and this requires further research.

Altered phosphorylation of PIP kinases was a key result of cGMP signal pathway inhibition in *Plasmodium berghei* (Brochet et al. 2014), but the most striking changes were reduced expression of PbPIS, PbVAPB and PbDGK3 in the PbGCb KO, which are all proteins related to the trafficking specifically of PI or PA (Brochet et al. 2014). There was no significantly altered expression or phosphorylation of enzymes regulating DAG or CDP-DAG (Brochet et al. 2014), suggesting that regulation of phospholipids in trafficking and membrane remodelling particularly PI and PA are key features of the cGMP signal path. Interestingly, both PI and PA have variable charge state depending on the pH of the medium (van Paridon et al. 1986; Abramson et al. 1964), and have been shown to act indirectly as pH biosensors (Young et al. 2010; Shin et al. 2020), which gives some physiological understanding of why TgGC might prefer to act on these lipids and is consistent with previous observations linking pH to the role of TgGC (Bisio et al. 2019). Surprisingly, the major DAG-kinase found to be dis-regulated upon cGMP pathway ablation was PbDGK3 (PBANKA_083120) (Brochet et al. 2014), the homologue to the *Toxoplasma* TgDGK3 found in the micronemes (Bullen et al. 2016). TgDGK1 has been well-studied and found to be essential for vesicle fusion in *Toxoplasma* (Bullen et al. 2016), but the study of PbGCb KO suggests that microneme-resident DGK3, not the shorter canonical PbDGK1 homologue (PBANKA_133460), is the major DAG-Kinase responsible for microneme secretion during egress and invasion in Apicomplexa in the cGMP regulated pathway (Brochet et al. 2014). While we are still uncertain about what exactly the ATPase domain of GC does, it is clear that it is involved in regulating the PI cycle as part of a signalling process linked to sensing changes in pH. TgGC likely responds to changes in PA at the plasma membrane (Bisio et al. 2019), but based on our research it is equally likely that TgGC responds to the protonation state of PI4P or PIP2 in response to pH and the ATPase domain may even traffic PIPs to the between the apical cap and the Golgi/ER, although this theory is speculative. Taken together, according to ours and previous data, apicomplexan GC is responsible for regulating PI and PA trafficking as part of membrane turnover in the phosphoinositide cycle during extracellular motility which is likely linked to the ability of PI and PA to act as pH biosensors.

The cGMP signal network regulates oleic acid 18:1 for membrane fluidity.

Interestingly, in our results, TgGC-depletion only affected import of PA 18:1 and there was no difference seen in import of PA16:0 (Figure 4E,F). A recent study was able to differentiate the FA chain profiles of the lipids comprising the outer and inner leaflets of the plasma membrane and showed that the outer leaflet had more saturated fatty acids, while the inner membrane lipids had more

unsaturated fatty acids (Lorent et al. 2020). Likely the unsaturated fatty acids incorporate into the outer leaflet and stay there, but the 18:1 is unstable in the outer layer and is transported more rapidly inside the parasite. This is probably because the 18:1 chain is less flexible and disrupts the bilayer so the parasite needs to clear this excess PA to prevent destabilizing the outer leaflet (**Figure 4B**) (Lorent et al. 2020). This shows an unexpected role for oleic acid 18:1 in increasing membrane fluidity as part of normal biophysical processes as part of extracellular motility regulated by TgGC. However, lipid uptake is seemingly largely headgroup-dependent as even PA 16:0 was imported more readily than weakly charged cylindrical PC18:1, even with an 18:1 fatty acid chain (**Figure 4**). It is presently unclear however if TgGC binds any lipids and if so, whether it has a preference for oleic acid and future research will focus on answering this question. Perhaps TgGC is able to move lipids between the apical cap and the Golgi, maybe in trafficking/signalling of phosphatidylinositol/PIPs? Interestingly, the PA examined in this study has a much higher presence of PA 18:1 than previous studies (Amiar et al. 2020) and it might be because the parasites examined here are extracellular. The increase in PA might therefore have more 18:1 in extracellular parasites and more 18:0 in intracellular parasites, and this will be an interesting topic for future research.

Implications for conserved PA trafficking proteins in the evolution of parasitic modes of living.

The identification of the dual domain Alveolate GC protein has important implications for understanding eukaryotic evolution (**Figure 5, S7-S9**), and particularly the importance of the appearance of the second copy of GC in some organisms has been under-appreciated. To our surprise, the fact that the apicomplexan ancestor had two canonical variants of GC suggests that the *P. falciparum* signal network with two GCs probably more closely resembles the apicomplexan ancestor than *Toxoplasma*, which only has one copy of GC (**Figure 5C**). Interestingly, *Eimeria falciformis* and some other coccidians have a second copy of GC which seemingly has a defunct ATPase domain, suggesting that these coccidians may be in the process of losing their second GC variant (**Figure S11**). It is interesting that GC would serve to regulate secretion of micronemes in both *Toxoplasma* and *Plasmodium*, but that *Plasmodium* would require an additional variant compared to *Toxoplasma*. Some have suggested a stage specific function for PfGCa and PfGCb, but this is still not clear since there is no experimental evidence for *Plasmodium* GCa in mosquito stages and *Plasmodium* GCb KO mutants have not been fully characterized in the blood stage in which they are apparently not essential (Jiang et al. 2020; Moon et al. 2009). However, given the highly conserved nature of these genes, we argue that the difference in variant number probably reflects different cellular architectures (such as apical complex differences, modes of egress etc.) and host environments in the two species (fibroblasts vs. red blood cells, etc.). It will be interesting to see how the difference in GC variant number reflects differences in coccidian and haemosporidian egress and invasion biology which could be indicative of their evolution infecting different host cells.

The phylogeny of other conserved phosphatidic acid signalling DGK proteins has also given us interesting evolutionary insights into the alveolates (**Figure S10, S11**). We find conserved TgDGK2-like homologues with signal peptides in *Vitrella* and *Chromera*. This is exciting because, to our knowledge, this is the first known effector protein exported outside of the *Toxoplasma* parasite cell which appears to have a homologue in alveolate algae. Parasite host effectors are generally poorly conserved due to the highly specific molecular nature of the parasitized host cell in question. However, it is clear that there is at least one highly conserved *Toxoplasma* dense granule protein in *Vitrella* and *Chromera* (**Figure S10, S11**), which suggests that there are probably more exported effectors that are yet to be discovered. It is presently unclear if the chromerid DGK2 is also exported, but if so it might be used to manipulate their host (e.g., if some of them exist in symbiotic fashion as suggested (Oborník et al. 2011)) or possibly to regulate their egress from a cyst stage similar to a parasitophorous vacuole (Bisio et al. 2019). Curiously, DGK2 is absent in *Plasmodium*, and this may indicate differences in its egress regulation compared to *Toxoplasma* (**Figure S11**). The major difference between the acute asexual stages of the two parasites is that *Plasmodium* asexual blood stages must undergo a developmental

change into a motile zoite prior to egress in order to escape (Wang et al. 2020; Absalon et al. 2018; Rudlaff et al. 2020). It might be that *Plasmodium* has lost DGK2 because there is no requirement to signal to rings or trophozoites that have not yet developed into invasion-ready merozoites so instead *Plasmodium* possibly relies on internal metabolic cues for egress. By that same logic, perhaps elements of the conoid has also been lost or reduced in *Plasmodium* (Wall et al. 2016) because activation of egress and invasion events are more tightly linked to developmental maturation of the zoite form. In asexual *Toxoplasma* tachyzoites, there is no such delayed formation of zoites and so the tachyzoites are always invasion-ready. Thus, it is important that they have a well-regulated switch and the mobile conoid (at least in part) might control these events such as release of micronemes (Tosetti et al. 2020). Further research is needed on the full set of phosphatidic acid signalling proteins in both parasites and algae to distinguish between these speculative models.

Toxoplasma is an outstanding genetic model alveolate and the central role phosphatidic acid and associated proteins play in its biology has helped us identify crucial regulatory components of the alveolate cytoskeleton necessary for egress and host cell invasion. Until other genetic systems become established, *Toxoplasma* will continue to serve as a model for understudied alveolate algae and the phylum of apicomplexan parasites, which are the causative agents of numerous global diseases.

Methods:

Parasite Culture and Transfection:

T. gondii tachyzoites were grown by serial passage in human foreskin fibroblast (HFF) cells in DMEM supplemented with 1% Foetal Bovine Serum (FBS) as previously described (Striepen B, 2007).

Plasmids and cloning:

TgGCiKD was obtained from Yang et al. 2019 and used primarily throughout this study. TgGCiKD was also independently constructed using primers in Table S1 and inserted into equivalent cut sites of plasmid pPR2-HA3 (Katris et al. 2014). To localize TGGT1_224190 (TgFLP2), the following primers **TACTTCCAATCCAATTTAGCCTCGAGTA-CTCGGTCTTGACTACG** and **TCCTCCACTTCCAATTTAGCCGGCGACGCGAGCT** were used to amplify the gDNA. For TGGT1_245510 (TgFLP5) primers **TACTTCCAATCCAATTTAGCCAACCGGAAGGTCGTCAAGG** and **TCCTCCACTTCCAATTTAGCCGCATCGTTGGCTGCGTTC** were used to amplify the gDNA. Both PCR products were inserted into plasmid pLIC-HA-tubCAT. The plasmids for TgFLP2 and TgFLP5 were linearized with BglII and PstI respectively as previously described (Sheiner et al. 2011).

| Primer/Plasmid | Sequence |
|-----------------------------------|--|
| TgGC iHA KD 3' flank FOR XmaI | GACTCCC GGATGAAGAAGACGCGAAG |
| TgGC iHA KD 3' flank REV NotI | GACTGCGGCCGCAACGACTGACGACATTGC |
| TgGC iHA KD 5' flank FOR ApaI | GTATGGGCCCTCTGCCTGACTCGCTTGG |
| TgGC iHA KD 5' flank REV PacI | CAGATTAATTAAGACAGAGACAAGATGCG |
| TgFLP2 HA pLIC CAT FOR | <u>TACTTCCAATCCAATTTAGCCTCGAGTACTCGGTCTTGACTACG</u> |
| TgFLP2 HA pLIC CAT REV | <u>TCCTCCACTTCCAATTTAGCCGGCGACGCGAGCT</u> |
| TgFLP5 HA pLIC CAT FOR | <u>TACTTCCAATCCAATTTAGCCAACCGGAAGGTCGTCAAGG</u> |
| TgFLP5 HA pLIC CAT REV | <u>TCCTCCACTTCCAATTTAGCCGCATCGTTGGCTGCGTTC</u> |
| TgVAP Cas9 guide FOR | <u>AAGTTgcatgattgaaacgcgaaaaG</u> |
| TgVAP Cas9 guide REV | <u>AAAACttttcgcgtttcaatcatgcA</u> |
| TgVAP PR2-HA3-CAT CRISPR PCR FOR | tcacgtgcgcccgctcgtctcgaaggtgatgtacagctgacgctctCCTGTGTGTCATTCGTTGTCG |
| TgVAP pPR2-HA3-CAT CRISPR PCR FOR | aaactcgatcaccttctcgggagttatccgcagcaacgggtcccgccatGATATCGACGTCCCCGGGTAA |

Conoid extrusion assays:

Extracellular parasites were filtered, counted and spun at 1000 xg for 10 minutes. Parasites were resuspended in DMEM (without additional supplements), to a concentration of approximately 5.0x10⁷ parasites/ml. 100 microliters of parasites were then mixed with equivalent volumes of solutions containing double concentrations of 10 μM calcium ionophore A23187 or 5μM BIPPO to make a 200 μl solution (final concentration 5μM A23187 and 2.5μM BIPPO), or equivalent concentration of DMSO control. Parasites with agonist or DMSO were allowed to extrude conoids by shifting to a 37 °C water bath. Cells were incubated for 30 seconds and then fixed by addition of 10 μl of 25% glutaraldehyde (final concentration 1.25%), for 30 minutes. Parasites were spun at 800 rpm for 2 minutes, and resuspended in 200 μl 1xPBS. 50 microliters of parasites was then smeared onto Polyethylenimine(PEI)-coated coverslips and parasites were allowed to settle for 20 minutes, before being rinsed in deionized water and mounted onto microscope slides using 10 microliters of Fluorogel®. Parasite conoids were scored blindly by phase contrast on a 63x or 100x objective.

DAG Pulse /Lipid kinetics:

Parasites were grown for three days with or without ATc and harvested fresh on day of egress. Fully lysed cultures were filtered through a 3.0um polycarbonate filter and spun down at 1800rpm for 10 minutes. Parasites were aspirated, washed with DMEM and flasks of each treatment were pooled together, and spun down as before. Parasites were aspirated and resuspended to a concentration of 4×10^8 cells per ml and 0.5ml was each aliquoted into 1.5ml tubes and maintained at room temperature prior to treatment (Where appropriate, Compound 2 was added at this point and allowed to equilibrate for 5 minutes prior to stimulus.). Pairs of tubes with or without ATC/Compound 2 treatment were shifted to a 37°C heat block and allowed to equilibrate for 60 seconds before addition of 0.5ml of preheated 2x DMEM solution with 5uM of BIPPO (2.5uM final) or DMSO (0 seconds). Cells were incubated for the indicated time points before quenching immediately on dry ice/ethanol for 5 seconds and placed on ice. Parasites were then spun down at 8000 rpm for 2 minutes at 4 °C, aspirated, washed with 1ml of ice cold 1xPBS, and spun down as before. Cells were washed with 1xPBS once more and spun down as before. Pellets were then placed at -80 for storage prior to lipid extraction and GC-MS analysis.

Lipid analysis and PA quantification:

Total lipids were extracted using chloroform:methanol, 1:2 (v/v) and chloroform:methanol, 2:1 (v/v) in the presence of 0.1MHCl with periodic sonication. Pooled organic phase was subjected to biphasic separation by adding 0.1 MHCl. The organic phase was dried under N2 gas and dissolved in 1-butanol. Total lipid was then separated by 2D-HPTLC spiked with 1 µg PA(C17:0/C17:0) (Avanti Polar lipids) using chloroform/methanol/28% NH4OH, 60:35:8 (v/v) as the 1st dimension solvent system and chloroform/acetone/methanol/acetic acid/water, 50:20:10:13:5 (v/v) as the 2nd dimension solvent system [72]. All spots including PA were visualized with primulin and scraped. Lipids were then prepared for GC-MS analysis in hexane (Agilent 5977A- 7890B) after derivatization by methanolysis using 0.5M HCl in methanol incubated at 85°C for 3.5 hrs. Fatty acid methyl esters were identified by their mass spectrum and retention time compared to authentic standards. Individual lipid classes were normalized according to the parasite cell number and internal standard.

Fluorescent Lipid import assay:

Extracellular parasites were filtered, counted and spun at 1800rpm for 10 minutes. Parasites were washed once with DMEM and spun down as before. Parasites were resuspended in DMEM w 10mM HEPES (which we found crucial for the experiment), to a concentration of approximately 5×10^7 parasites/ml. 100 µl of parasites were then shifted to 37°C for 1 minute to equilibrate. Parasites were then mixed with 100 µl of pre-warmed serum free DMEM w 10mM HEPES containing double concentrations of NBD-PA and NBD PC ($10 \mu\text{M}^{-1}$) to make a final reaction volume of 200µl ($5 \mu\text{M}$ final concentration of NBD-PA or NBD-PC) Parasites were incubated for a further 30 seconds for NBD-PA, NBD-PC or 60 minutes for NBD-PC. Parasites were then quenched on ice for 2 minutes, spun down 8000rpm for 2 minutes at 4°C and aspirated. Cell pellets were resuspended in 150µL 1xPBS and fixed by addition of 80 µL of 10% Paraformaldehyde (approximately 3% final PFA) for 15 minutes at room temperature. Cells were spun down as before and resuspended in 200µl 1xPBS before smearing onto PEI coated coverslips and blocked in 2% FBS overnight at 4°C. Parasites were then probed by IFA using mouse anti-SAG1 (Abcam) and Alexafluor goat anti-mouse-546 and stained with DAPI. Slides were imaged on a Zeiss Apotome epifluorescence microscope. Phospholipid uptake was quantified with ImageJ, where the SAG1 signal was used to identify and label parasites creating an unbiased overlay. Identified parasites were then measured for fluorescent lipid uptake in the 488 channel. Alternatively, after fixation, parasites were resuspended in 1xPBS, diluted, and analysed directly by FACS for intensity of NBD uptake under 488 wavelength (Stocks of PA or PC were made up in DMSO to a concentration of 1mM, and stored at -20°C in aliquots).

Intracellular lipid uptake:

For intracellular parasites, host cells were inoculated with tachyzoites in growth medium containing NBD-PA or NBD-PC and grown for a further 24 hours before fixation with 2.5% PFA in 1xPBS. Samples were mounted directly onto slides with fluorogel.

GCaMP6 experiments:

A construct containing the GCaMP6 plasmid was transfected into the TgRNG2iKD cell line using FUDR/UPRT selection as previously described (Stewart et al. 2017). TgRNG2iKD cells were then pre-treated with or without ATc as previously described (Yang et al. 2019). Briefly, upon harvest, TgRNG2iKD cells with or without ATc pre-treatment were filtered, spun down and resuspended in phenol-red free DMEM. Parasites were allowed to equilibrate at room temperature before being fed into a FACS and imaged in real time. Incremental concentrations of BIPPO were added to the parasites and the GCaMP6 fluorescence was detected over time. Microscopy of RNG2iKD cells was performed as previously described (Stewart et al. 2017).

***Plasmodium falciparum* IFAs:**

Plasmodium falciparum was cultured as previously described (Botte et al., 2013). Briefly, cultures were grown in 2% haematocrit with RPMI supplemented with 10% Albumax, hypoxanthine and gentamicin. Cultures in airtight Perspex boxes were gassed with Beta-Mix gas. Parasites were grown for 24 hours in normal conditions before addition of 5 $\mu\text{g ml}^{-1}$ fluorescent 16:0 PA, 18:1 PA or 18:1 PC into the culture and grown for a further 24 hours. Parasites were then harvested and smeared onto PEI coated coverslips before staining with DAPI and mounting onto slides with fluorogel.

Mosquito stage IFAs:

Live *P. falciparum* sporozoites were incubated at room temperature using the indicated concentrations of fluorescent lipids and then mounted on coverslips and observed by confocal microscopy.

Phylogenetic analysis:

Assembly of phylogenetic datasets:

Plasmodium and *Toxoplasma* GC and DGK proteins were used to identify a small set of homologous sequences in other alveolates. Of these, the proteins in *Chromera velia* (2 GCs and 4 DGKs) had the slowest evolutionary rates (as evaluated by branch lengths in preliminary trees) and were used as representative queries in BLASTP searches against sequence databases. Sequences were retrieved from GenBank nr (a minimum of 250 closest hits for each query with an additional retrieval of selected species), GenBank pdb (all closest relevant hits; highlighted in tree figures), EuPathDb (proteins predicted from representative apicomplexan genomes) and the Marine Microbial Eukaryote Transcriptome Sequencing Project (proteins predicted from representative dinoflagellate transcriptomes). The GC was aligned in MAFFT v7.402 (Katoh and Standley, 2013) by using the --linsi algorithm and the N-terminal ATPase domain was separated (where present) from the cyclase domain region in the intervening spacer. Domains in all proteins were identified by NCBI Batch CD-search. The two cyclase domains of the *Chromera* GCa were then used as queries for another round of BLASTP searches in sequence databases as above. This was to ensure that all proteins related to the comparatively more divergent cyclase region are retrieved (if missed in the first round of searches). The cyclase dataset, combining specific hits to "CHD", "CYC" or "GC" domains and generic hits to "NCS" superfamily (as determined by CD Search), was then realigned in MAFFT --linsi. The N- and C-terminal domains in 2-domain cyclases were split in the spacer region and combined together with 1-domain cyclases into a single alignment. Redundant sequences and other domain types if present (rare) were removed from all three datasets, which were then subjected to progressive rounds of streamlining. In each round, a quick Maximum Likelihood phylogeny was built in FastTree v2.1.10 (Price et al., 2010) and sequences that either belonged to distantly related protein families, were too

fast-evolving, were heavily fragmented or belonged to closely related species or strains were removed.

Phylogenetic inference and signal peptide prediction:

The three completed datasets were realigned by using the --linsi algorithm in MAFFT. Hypervariable sequence regions were trimmed in BMGE v1.1 (Criscuolo and Gribaldo, 2010) by using the -b 3 and -g 0.4 parameters. The final phylogenetic matrices of GC:cyclase (233 sequences, 148 sites), GC:ATPase (191 sequences, 569 sites) and DGK (149 sequences, 169 sites) were analyzed in IQ-TREE v1.6.5 (Nguyen et al., 2015). IQ-TREE was run by using the LG+F+I+G4 model and 1000 ultrafast bootstrap replicates to compute the branch supports (we avoided using standard non-parametric bootstraps, which are no suitable because of the short lengths of the GC:cyclase and DGK matrices). The presence of putative signal peptides in DGKs was predicted in all sequences in SignalP v4.1 by using the -euk model and default settings (Petersen et al., 2011).

Author Contributions:

Conceptualization: NJK, RFW, CYB,

Data curation: NJK, YYB, JJ, CYB,

Formal analysis: NJK, YYB, JJ, CYB,

Funding acquisition: GIM, RFW, MFCD, CYB

Investigation: NJK, YYB, JJ, CSA, ASPY, AV, RJS, CJT

Methodology: NJK, YYB, JJ, RFW, CYB.

Project administration: NJK, RFW, MFCD, CYB,

Resources: RFW, MFCD, CYB,

Supervision: NJK, RS, GIM, CJT, RFW, CYB,

Validation: NJK, YYB, JJ, CSA, ASPY, AV, RJS

Visualization: NJK, RFW, CYB

Writing – original draft: NJK

Writing – review & editing: NJK, JJ, RFW, MFCD, CYB

Acknowledgements:

We would like to thank David Sibley, Sebastian Lourido and Dominique Soldati-Favre for gifting antibodies and cell lines used in this study. We thank Oliver Billker for gifting Compound 2.

This work and N.J.K, C.Y.B., Y.Y.-B, M.F.C.D are supported by Agence Nationale de la Recherche, France (grant ANR-12-PDOC-0028, Project Apicolipid), the Atip-Avenir and Finovi programs (CNRS-INSERM-Finovi Atip-Avenir Apicolipid projects), and Laboratoire d'Excellence Parafrap, France (grant ANR-11-LABX-0024). C.Y.B, C.J.T and G.I.M. are supported by the LIA-IRP CNRS Program (Apicolipid project). Lipidomic and fluxomic analysis was conducted in our GEMELI Lipidomics platform, which is supported by Region Auvergne Rhone-Alpes (IRICE GEMELI Grant) and Universite Grenoble Alpes.

References:

- Abramson, M. B., R. Katzman, C. E. Wilson, and H. P. Gregor. 1964. "IONIC PROPERTIES OF AQUEOUS DISPERSIONS OF PHOSPHATIDIC ACID." *The Journal of Biological Chemistry* 239 (December): 4066–72.
- Absalon, Sabrina, Karin Blomqvist, Rachel M. Rudlaff, Travis J. DeLano, Michael P. Pollastri, and Jeffrey D. Dvorin. 2018. "Calcium-Dependent Protein Kinase 5 Is Required for Release of Egress-Specific Organelles in Plasmodium Falciparum." *MBio* 9 (1). <https://doi.org/10.1128/mBio.00130-18>.
- Amiar, Souad, Nicholas J. Katris, Laurence Berry, Sheena Dass, Samuel Duley, Christophe-Sebastien Arnold, Melanie J. Shears, et al. 2020. "Division and Adaptation to Host Environment of Apicomplexan Parasites Depend on Apicoplast Lipid Metabolic Plasticity and Host Organelle Remodeling." *Cell Reports* 30 (11): 3778-3792.e9. <https://doi.org/10.1016/j.celrep.2020.02.072>.
- Amiar, Souad, James I. MacRae, Damien L. Callahan, David Dubois, Giel G. van Dooren, Melanie J. Shears, Marie-France Cesbron-Delauw, et al. 2016. "Apicoplast-Localized Lysophosphatidic Acid Precursor Assembly Is Required for Bulk Phospholipid Synthesis in Toxoplasma Gondii and Relies on an Algal/Plant-Like Glycerol 3-Phosphate Acyltransferase." *PLoS Pathogens* 12 (8): e1005765. <https://doi.org/10.1371/journal.ppat.1005765>.
- Antonny, Bruno, Joëlle Bigay, and Bruno Mesmin. 2018. "The Oxysterol-Binding Protein Cycle: Burning Off PI(4)P to Transport Cholesterol." *Annual Review of Biochemistry* 87: 809–37. <https://doi.org/10.1146/annurev-biochem-061516-044924>.
- Arroyo-Olarte, Ruben D., Jos F. Brouwers, Arunakar Kuchipudi, J. Bernd Helms, Aindrila Biswas, Ildiko R. Dunay, Richard Lucius, and Nishith Gupta. 2015. "Phosphatidylthreonine and Lipid-Mediated Control of Parasite Virulence." *PLoS Biology* 13 (11): e1002288. <https://doi.org/10.1371/journal.pbio.1002288>.
- Bahar, Entaz, Hyongsuk Kim, and Hyonok Yoon. 2016. "ER Stress-Mediated Signaling: Action Potential and Ca(2+) as Key Players." *International Journal of Molecular Sciences* 17 (9). <https://doi.org/10.3390/ijms17091558>.
- Bai, Lin, Amanda Kovach, Qinglong You, Hao-Chi Hsu, Gongpu Zhao, and Huilin Li. 2019. "Autoinhibition and Activation Mechanisms of the Eukaryotic Lipid Flippase Drs2p-Cdc50p." *Nature Communications* 10 (1): 4142. <https://doi.org/10.1038/s41467-019-12191-9>.
- Barylyuk, Konstantin, Koreny, Ludek, Ke, Huiling, Butterworth, Simon, Crook, Oliver M., Lassadi, Imen, Gupta, Vipul, et al. n.d. "A Subcellular Atlas of Toxoplasma Reveals the Functional Context of the Proteome." *Biorxiv*. <https://doi.org/10.1101/2020.04.23.057125>.
- Bisio, Hugo, Matteo Lunghi, Mathieu Brochet, and Dominique Soldati-Favre. 2019. "Phosphatidic Acid Governs Natural Egress in Toxoplasma Gondii via a Guanylate Cyclase Receptor Platform." *Nature Microbiology* 4 (3): 420–28. <https://doi.org/10.1038/s41564-018-0339-8>.
- Brancucci, Nicolas M. B., Joseph P. Gerdt, ChengQi Wang, Mariana De Niz, Nisha Philip, Swamy R. Adapa, Min Zhang, et al. 2017. "Lysophosphatidylcholine Regulates Sexual Stage Differentiation in the Human Malaria Parasite Plasmodium Falciparum." *Cell* 171 (7): 1532-1544.e15. <https://doi.org/10.1016/j.cell.2017.10.020>.
- Brochet, Mathieu, Mark O. Collins, Terry K. Smith, Eloise Thompson, Sarah Sebastian, Katrin Volkmann, Frank Schwach, et al. 2014. "Phosphoinositide Metabolism Links CGMP-

- Dependent Protein Kinase G to Essential Ca²⁺ Signals at Key Decision Points in the Life Cycle of Malaria Parasites." *PLoS Biology* 12 (3): e1001806. <https://doi.org/10.1371/journal.pbio.1001806>.
- Brown, Kevin M., Shaojun Long, and L. David Sibley. 2017. "Plasma Membrane Association by N-Acylation Governs PKG Function in Toxoplasma Gondii." *MBio* 8 (3). <https://doi.org/10.1128/mBio.00375-17>.
- Brown, Kevin M., and L. David Sibley. 2018. "Essential CGMP Signaling in Toxoplasma Is Initiated by a Hybrid P-Type ATPase-Guanylate Cyclase." *Cell Host & Microbe* 24 (6): 804–816.e6. <https://doi.org/10.1016/j.chom.2018.10.015>.
- Bullen, Hayley E., Yonggen Jia, Yoshiki Yamaro-Botté, Hugo Bisio, Ou Zhang, Natacha Klages Jemelin, Jean-Baptiste Marq, Vern Carruthers, Cyrille Y. Botté, and Dominique Soldati-Favre. 2016. "Phosphatidic Acid-Mediated Signaling Regulates Microneme Secretion in Toxoplasma." *Cell Host & Microbe* 19 (3): 349–60. <https://doi.org/10.1016/j.chom.2016.02.006>.
- Bullen, Hayley E., and Dominique Soldati-Favre. 2016. "A Central Role for Phosphatidic Acid as a Lipid Mediator of Regulated Exocytosis in Apicomplexa." *FEBS Letters* 590 (15): 2469–81. <https://doi.org/10.1002/1873-3468.12296>.
- Charron, Audra J., and L. David Sibley. 2002. "Host Cells: Mobilizable Lipid Resources for the Intracellular Parasite Toxoplasma Gondii." *Journal of Cell Science* 115 (Pt 15): 3049–59.
- Donald, Robert G. K., Tanya Zhong, Helen Wiersma, Bakela Nare, Dan Yao, Anita Lee, John Allocco, and Paul A. Liberator. 2006. "Anticoccidial Kinase Inhibitors: Identification of Protein Kinase Targets Secondary to CGMP-Dependent Protein Kinase." *Molecular and Biochemical Parasitology* 149 (1): 86–98. <https://doi.org/10.1016/j.molbiopara.2006.05.003>.
- Epanand, Richard M. 2017. "Features of the Phosphatidylinositol Cycle and Its Role in Signal Transduction." *The Journal of Membrane Biology* 250 (4): 353–66. <https://doi.org/10.1007/s00232-016-9909-y>.
- Francia, Maria E., Carly N. Jordan, Jay D. Patel, Lilach Sheiner, Jessica L. Demerly, Justin D. Fellows, Jessica Cruz de Leon, Naomi S. Morrissette, Jean-François Dubremetz, and Boris Striepen. 2012. "Cell Division in Apicomplexan Parasites Is Organized by a Homolog of the Striated Rootlet Fiber of Algal Flagella." *PLoS Biology* 10 (12): e1001444. <https://doi.org/10.1371/journal.pbio.1001444>.
- Gao, Han, Zhenke Yang, Xu Wang, Pengge Qian, Renjie Hong, Xin Chen, Xin-Zhuan Su, Huiting Cui, and Jing Yuan. 2018. "ISP1-Anchored Polarization of GCβ/CDC50A Complex Initiates Malaria Ookinete Gliding Motility." *Current Biology: CB* 28 (17): 2763–2776.e6. <https://doi.org/10.1016/j.cub.2018.06.069>.
- Gould, Sven B., Wai-Hong Tham, Alan F. Cowman, Geoffrey I. McFadden, and Ross F. Waller. 2008. "Alveolins, a New Family of Cortical Proteins That Define the Protist Infrakingdom Alveolata." *Molecular Biology and Evolution* 25 (6): 1219–30. <https://doi.org/10.1093/molbev/msn070>.
- Graindorge, Arnault, Karine Fréchal, Damien Jacot, Julien Salamun, Jean Baptiste Marq, and Dominique Soldati-Favre. 2016. "The Conoid Associated Motor MyoH Is Indispensable for Toxoplasma Gondii Entry and Exit from Host Cells." *PLoS Pathogens* 12 (1): e1005388. <https://doi.org/10.1371/journal.ppat.1005388>.
- Gras, Simon, Elena Jimenez-Ruiz, Christen M. Klinger, Katja Schneider, Andreas Klingl, Leandro Lemgruber, and Markus Meissner. 2019. "An Endocytic-Secretory Cycle

- Participates in *Toxoplasma Gondii* in Motility." *PLoS Biology* 17 (6): e3000060.
<https://doi.org/10.1371/journal.pbio.3000060>.
- Grellier, P., D. Rigomier, V. Clavey, J. C. Fruchart, and J. Schrevel. 1991. "Lipid Traffic between High Density Lipoproteins and Plasmodium Falciparum-Infected Red Blood Cells." *The Journal of Cell Biology* 112 (2): 267–77.
<https://doi.org/10.1083/jcb.112.2.267>.
- Guo, Y. L., T. Seebacher, U. Kurz, J. U. Linder, and J. E. Schultz. 2001. "Adenylyl Cyclase Rv1625c of Mycobacterium Tuberculosis: A Progenitor of Mammalian Adenylyl Cyclases." *The EMBO Journal* 20 (14): 3667–75.
<https://doi.org/10.1093/emboj/20.14.3667>.
- Howard, Brittany L., Katherine L. Harvey, Rebecca J. Stewart, Mauro F. Azevedo, Brendan S. Crabb, Ian G. Jennings, Paul R. Sanders, et al. 2015. "Identification of Potent Phosphodiesterase Inhibitors That Demonstrate Cyclic Nucleotide-Dependent Functions in Apicomplexan Parasites." *ACS Chemical Biology* 10 (4): 1145–54.
<https://doi.org/10.1021/cb501004q>.
- Jiang, Yuanyuan, Jun Wei, Huiting Cui, Chuanyuan Liu, Yuan Zhi, ZhengZheng Jiang, Zhenkui Li, et al. 2020. "An Intracellular Membrane Protein GEP1 Regulates Xanthurenic Acid Induced Gametogenesis of Malaria Parasites." *Nature Communications* 11 (1): 1764.
<https://doi.org/10.1038/s41467-020-15479-3>.
- Johnson, Jacque-Lynne F., and Michel R. Leroux. 2010. "CAMP and CGMP Signaling: Sensory Systems with Prokaryotic Roots Adopted by Eukaryotic Cilia." *Trends in Cell Biology* 20 (8): 435–44. <https://doi.org/10.1016/j.tcb.2010.05.005>.
- Katris, Nicholas J., Giel G. van Dooren, Paul J. McMillan, Eric Hanssen, Leann Tilley, and Ross F. Waller. 2014. "The Apical Complex Provides a Regulated Gateway for Secretion of Invasion Factors in *Toxoplasma*." *PLoS Pathogens* 10 (4): e1004074.
<https://doi.org/10.1371/journal.ppat.1004074>.
- Kim, Yeun Ju, Maria Luisa Guzman-Hernandez, Eva Wisniewski, Nicolas Echeverria, and Tamas Balla. 2016. "Phosphatidylinositol and Phosphatidic Acid Transport between the ER and Plasma Membrane during PLC Activation Requires the Nir2 Protein." *Biochemical Society Transactions* 44 (1): 197–201.
<https://doi.org/10.1042/BST20150187>.
- Kim, Yeun Ju, Maria-Luisa Guzman-Hernandez, Eva Wisniewski, and Tamas Balla. 2015. "Phosphatidylinositol-Phosphatidic Acid Exchange by Nir2 at ER-PM Contact Sites Maintains Phosphoinositide Signaling Competence." *Developmental Cell* 33 (5): 549–61. <https://doi.org/10.1016/j.devcel.2015.04.028>.
- Lepage, T., S. M. Cohen, F. J. Diaz-Benjumea, and S. M. Parkhurst. 1995. "Signal Transduction by CAMP-Dependent Protein Kinase A in *Drosophila* Limb Patterning." *Nature* 373 (6516): 711–15. <https://doi.org/10.1038/373711a0>.
- Lorent, J. H., K. R. Levental, L. Ganesan, G. Rivera-Longworth, E. Sezgin, M. Doktorova, E. Lyman, and I. Levental. 2020. "Plasma Membranes Are Asymmetric in Lipid Unsaturation, Packing and Protein Shape." *Nature Chemical Biology* 16 (6): 644–52.
<https://doi.org/10.1038/s41589-020-0529-6>.
- Lourido, Sebastian, Joel Shuman, Chao Zhang, Kevan M. Shokat, Raymond Hui, and L. David Sibley. 2010. "Calcium-Dependent Protein Kinase 1 Is an Essential Regulator of Exocytosis in *Toxoplasma*." *Nature* 465 (7296): 359–62.
<https://doi.org/10.1038/nature09022>.

- McCoy, James M., Lachlan Whitehead, Giel G. van Dooren, and Christopher J. Tonkin. 2012. "TgCDPK3 Regulates Calcium-Dependent Egress of *Toxoplasma Gondii* from Host Cells." *PLoS Pathogens* 8 (12): e1003066. <https://doi.org/10.1371/journal.ppat.1003066>.
- Mesmin, Bruno, Joëlle Bigay, Joachim Moser von Filseck, Sandra Lacas-Gervais, Guillaume Drin, and Bruno Antonny. 2013. "A Four-Step Cycle Driven by PI(4)P Hydrolysis Directs Sterol/PI(4)P Exchange by the ER-Golgi Tether OSBP." *Cell* 155 (4): 830–43. <https://doi.org/10.1016/j.cell.2013.09.056>.
- Moon, Robert W., Cathy J. Taylor, Claudia Bex, Rebecca Schepers, David Goulding, Chris J. Janse, Andrew P. Waters, David A. Baker, and Oliver Billker. 2009. "A Cyclic GMP Signalling Module That Regulates Gliding Motility in a Malaria Parasite." *PLoS Pathogens* 5 (9): e1000599. <https://doi.org/10.1371/journal.ppat.1000599>.
- Mueller, Christina, Natacha Klages, Damien Jacot, Joana M. Santos, Ana Cabrera, Tim W. Gilberger, Jean-François Dubremetz, and Dominique Soldati-Favre. 2013. "The *Toxoplasma* Protein ARO Mediates the Apical Positioning of Rhoptry Organelles, a Prerequisite for Host Cell Invasion." *Cell Host & Microbe* 13 (3): 289–301. <https://doi.org/10.1016/j.chom.2013.02.001>.
- Oborník, Miroslav, David Modrý, Martin Lukeš, Eva Cernotíková-Stříbrná, Jaromír Cihlár, Martina Tesařová, Eva Kotabová, Marie Vancová, Ondřej Prášil, and Julius Lukeš. 2012. "Morphology, Ultrastructure and Life Cycle of *Vitrella Brassicaformis* n. Sp., n. Gen., a Novel Chromerid from the Great Barrier Reef." *Protist* 163 (2): 306–23. <https://doi.org/10.1016/j.protis.2011.09.001>.
- Oborník, Miroslav, Marie Vancová, De-Hua Lai, Jan Janouškovec, Patrick J. Keeling, and Julius Lukeš. 2011. "Morphology and Ultrastructure of Multiple Life Cycle Stages of the Photosynthetic Relative of Apicomplexa, *Chromera Velia*." *Protist* 162 (1): 115–30. <https://doi.org/10.1016/j.protis.2010.02.004>.
- Paridon, P. A. van, B. de Kruijff, R. Ouwerkerk, and K. W. Wirtz. 1986. "Polyphosphoinositides Undergo Charge Neutralization in the Physiological PH Range: A 31P-NMR Study." *Biochimica Et Biophysica Acta* 877 (1): 216–19. [https://doi.org/10.1016/0005-2760\(86\)90137-2](https://doi.org/10.1016/0005-2760(86)90137-2).
- Peretti, Diego, Nili Dahan, Eyal Shimoni, Koret Hirschberg, and Sima Lev. 2008. "Coordinated Lipid Transfer between the Endoplasmic Reticulum and the Golgi Complex Requires the VAP Proteins and Is Essential for Golgi-Mediated Transport." *Molecular Biology of the Cell* 19 (9): 3871–84. <https://doi.org/10.1091/mbc.e08-05-0498>.
- Ramakrishnan, Srinivasan, Melissa D. Docampo, James I. Macrae, François M. Pujol, Carrie F. Brooks, Giel G. van Dooren, J. Kalervo Hiltunen, Alexander J. Kastaniotis, Malcolm J. McConville, and Boris Striepen. 2012. "Apicoplast and Endoplasmic Reticulum Cooperate in Fatty Acid Biosynthesis in Apicomplexan Parasite *Toxoplasma Gondii*." *The Journal of Biological Chemistry* 287 (7): 4957–71. <https://doi.org/10.1074/jbc.M111.310144>.
- Rudlaff, Rachel M., Stephan Kraemer, Jeffrey Marshman, and Jeffrey D. Dvorin. 2020. "Three-Dimensional Ultrastructure of *Plasmodium Falciparum* throughout Cytokinesis." *PLoS Pathogens* 16 (6): e1008587. <https://doi.org/10.1371/journal.ppat.1008587>.
- Sheiner, Lilach, Jessica L. Demerly, Nicole Poulsen, Wandy L. Beatty, Olivier Lucas, Michael S. Behnke, Michael W. White, and Boris Striepen. 2011. "A Systematic Screen to Discover and Analyze Apicoplast Proteins Identifies a Conserved and Essential

- Protein Import Factor." *PLoS Pathogens* 7 (12): e1002392.
<https://doi.org/10.1371/journal.ppat.1002392>.
- Shin, John J. H., Peter Liu, Leslie J. Chan, Azmat Ullah, Jingxi Pan, Christoph H. Borchers, John E. Burke, Christopher Stefan, Gertien J. Smits, and Christopher J. R. Loewen. 2020. "PH Biosensing by PI4P Regulates Cargo Sorting at the TGN." *Developmental Cell* 52 (4): 461-476.e4. <https://doi.org/10.1016/j.devcel.2019.12.010>.
- Sidik, Saima M., Diego Huet, Suresh M. Ganesan, My-Hang Huynh, Tim Wang, Armiyaw S. Nasamu, Prathapan Thiru, et al. 2016. "A Genome-Wide CRISPR Screen in *Toxoplasma* Identifies Essential Apicomplexan Genes." *Cell* 166 (6): 1423-1435.e12. <https://doi.org/10.1016/j.cell.2016.08.019>.
- Stewart, Rebecca J., Lachlan Whitehead, Brunda Nijagal, Brad E. Sleebs, Guillaume Lessene, Malcolm J. McConville, Kelly L. Rogers, and Christopher J. Tonkin. 2017. "Analysis of Ca²⁺ Mediated Signaling Regulating *Toxoplasma* Infectivity Reveals Complex Relationships between Key Molecules." *Cellular Microbiology* 19 (4). <https://doi.org/10.1111/cmi.12685>.
- Tosetti, Nicolò, Nicolas Dos Santos Pacheco, Eloïse Bertiaux, Bohumil Maco, Lorène Bournonville, Virginie Hamel, Paul Guichard, and Dominique Soldati-Favre. 2020. "Essential Function of the Alveolin Network in the Subpellicular Microtubules and Conoid Assembly in *Toxoplasma Gondii*." *ELife* 9 (May). <https://doi.org/10.7554/eLife.56635>.
- Wall, Richard J., Magali Roques, Nicholas J. Katris, Ludek Koreny, Rebecca R. Stanway, Declan Brady, Ross F. Waller, and Rita Tewari. 2016. "SAS6-like Protein in Plasmodium Indicates That Conoid-Associated Apical Complex Proteins Persist in Invasive Stages within the Mosquito Vector." *Scientific Reports* 6: 28604. <https://doi.org/10.1038/srep28604>.
- Wang, Xu, Pengge Qian, Huiting Cui, Luming Yao, and Jing Yuan. 2020. "A Protein Palmitoylation Cascade Regulates Microtubule Cytoskeleton Integrity in Plasmodium." *The EMBO Journal*, May, e104168. <https://doi.org/10.15252/embj.2019104168>.
- Wiersma, Helen I., Stefan E. Galuska, Fiona M. Tomley, L. David Sibley, Paul A. Liberator, and Robert G. K. Donald. 2004. "A Role for Coccidian CGMP-Dependent Protein Kinase in Motility and Invasion." *International Journal for Parasitology* 34 (3): 369–80. <https://doi.org/10.1016/j.ijpara.2003.11.019>.
- Xu, Xuehua, and Tian Jin. 2015. "The Novel Functions of the PLC/PKC/PKD Signaling Axis in G Protein-Coupled Receptor-Mediated Chemotaxis of Neutrophils." *Journal of Immunology Research* 2015: 817604. <https://doi.org/10.1155/2015/817604>.
- Yang, Luning, Alessandro D. Ubaldi, Simona Seizova, Mary-Louise Wilde, Michael J. Coffey, Nicholas J. Katris, Yoshiki Yamaryo-Botté, et al. 2019. "An Apically Located Hybrid Guanylate Cyclase-ATPase Is Critical for the Initiation of Ca²⁺ Signaling and Motility in *Toxoplasma Gondii*." *The Journal of Biological Chemistry* 294 (22): 8959–72. <https://doi.org/10.1074/jbc.RA118.005491>.
- Young, Barry P., John J. H. Shin, Rick Orij, Jesse T. Chao, Shu Chen Li, Xue Li Guan, Anthony Khong, et al. 2010. "Phosphatidic Acid Is a PH Biosensor That Links Membrane Biogenesis to Metabolism." *Science (New York, N.Y.)* 329 (5995): 1085–88. <https://doi.org/10.1126/science.1191026>.

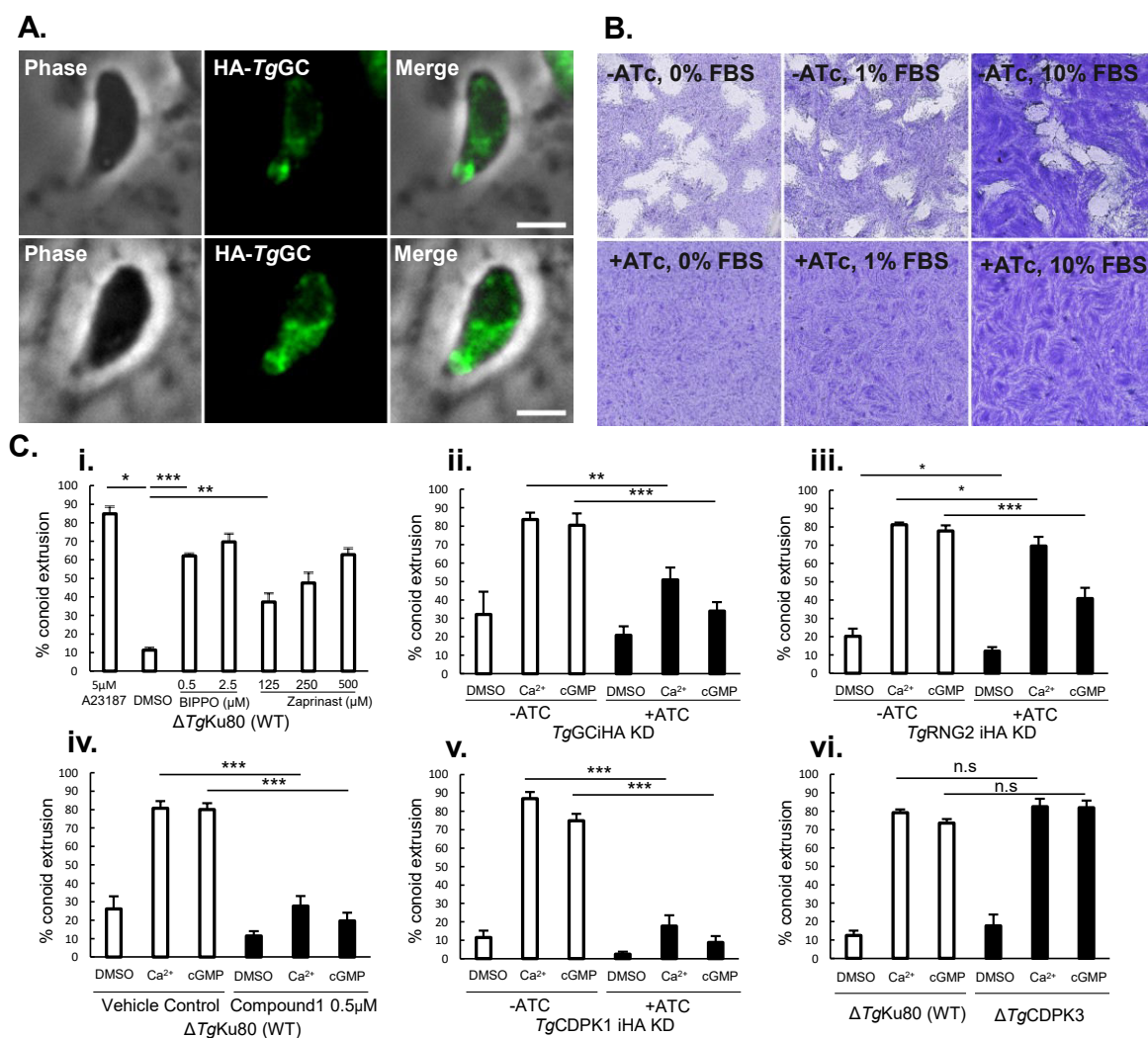


Figure 1: cGMP signalling regulates conoid extrusion.

A Localization of TgGC (TGGT1_254370) to the apical cap and an ER-like compartment **B.** Growth assay of TgGC iKD cells under 0,1,10%FBS shows TgGC cannot be rescued by excess serum. **C i.** Conoid extrusion assays using phosphodiesterase inhibitors Zaprinast and BIPPO at indicated concentrations on WT tachyzoites with 5µM A2387 as a positive control. n=8 Biological replicates, error bars represent SEM. **C ii-vi.** Conoid extrusion on various mutant cell lines and 0.5 µM Compound 1. A final concentration of 5µM final A23187 (Ca²⁺) or 2.5µM BIPPO (cGMP) was used for experiments on mutant cells unless otherwise indicated. For TgGC n=4, TgRNG2 n=8, TgCDPK1 n=4, C1 n=6, CDPK3 n=4 biological replicates. For all graphs, error bars represent SEM. P<0.05, * χ <0.05, ** χ <0.01, *** χ <0.005, **** χ <0.001.

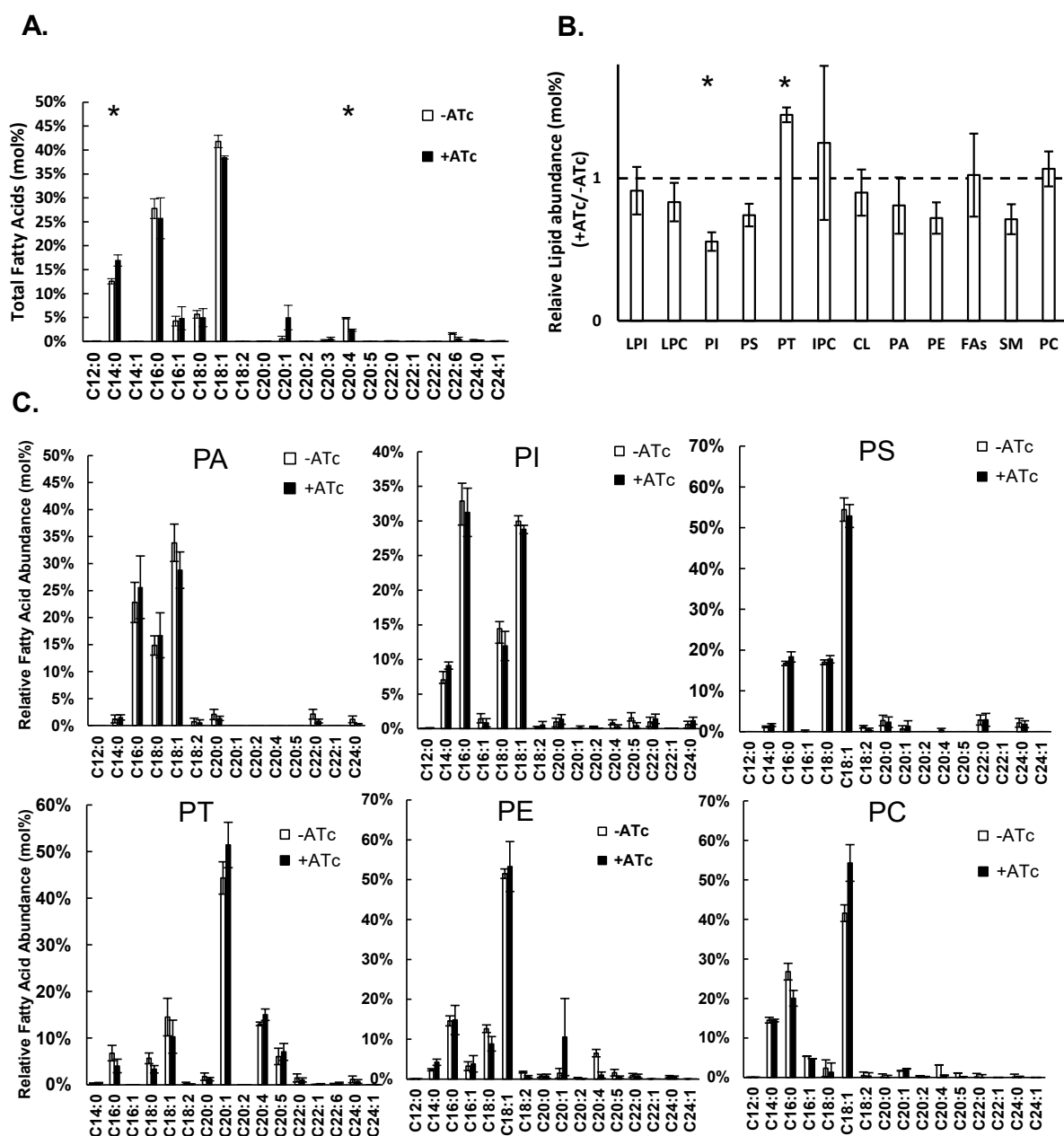


Figure 2: Lipidomic analysis of TgGCiKD suggests a role for TgGC in Phosphatidylinositol signalling.

A. Fatty acid profile(mol%) of TgGCiKD cells treated with or without Atc **B.** GC-MS analysis of lipids extracted by TLC, expressed as a ratio +ATc/-ATc **C-H.** Fatty acid profiles of PA, PI, PS, PT, PE and PC of TgGC with and without ATc pre-treatment. For all graphs, TgGC: n=3 biological replicates. P<0.05, *x <0.05. All error bars represent SEM.

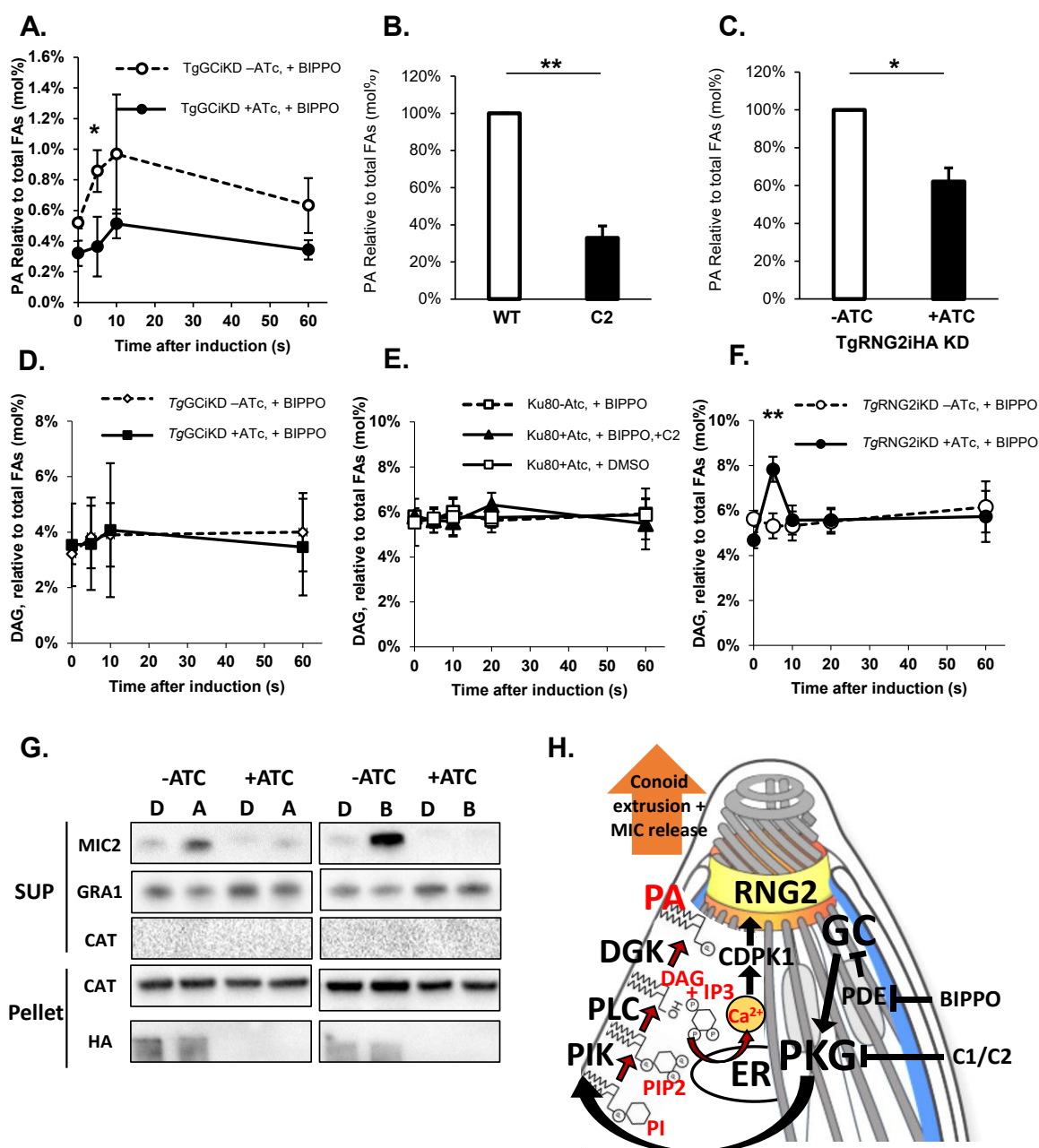


Figure 3: Rapid kinetics of DAG and PA are altered in TgGC and TgRNG2 mutants.

A. Pulse experiment to analyse PA kinetics over time. TgGCiKD cells pre-treated with or without ATc were stimulated with 2 μ M BIPPO over 60 seconds, and PA levels (mol%) analysed at each time point. n=3 biological replicates **B.** WT tachyzoites were treated with TgPKG inhibitor Compound 2 (C2, 0.5 μ M) before being stimulated with BIPPO, and quenched within 5 seconds, and PA was quantified. n=3 biological replicates **C.** PA quantification in TgRNG2 cells pre-treated with ATc after being stimulated with BIPPO and quenched within 5 seconds. n=5 biological replicates **D,E,F.** Graphs showing kinetics of lipid second messenger DAG in TgGC, TgPKG and TgRNG2 inhibited cells. For TgGC and TgPKG n=3, for TgRNG2iKD n=4 biological replicates. P<0.05, *x <0.05, ** x <0.01, *** x <0.005, **** x <0.001. All error bars represent SEM. **G.** Secretion assay of TgGCiKD cells pretreated with or without ATc, and stimulated for 20 minutes with A23187 (A) or BIPPO (B). **H.** Model for lipid second messenger turnover in *Toxoplasma* during concomitant activation of conoid extrusion and microneme secretion, beginning clockwise from TgGC.

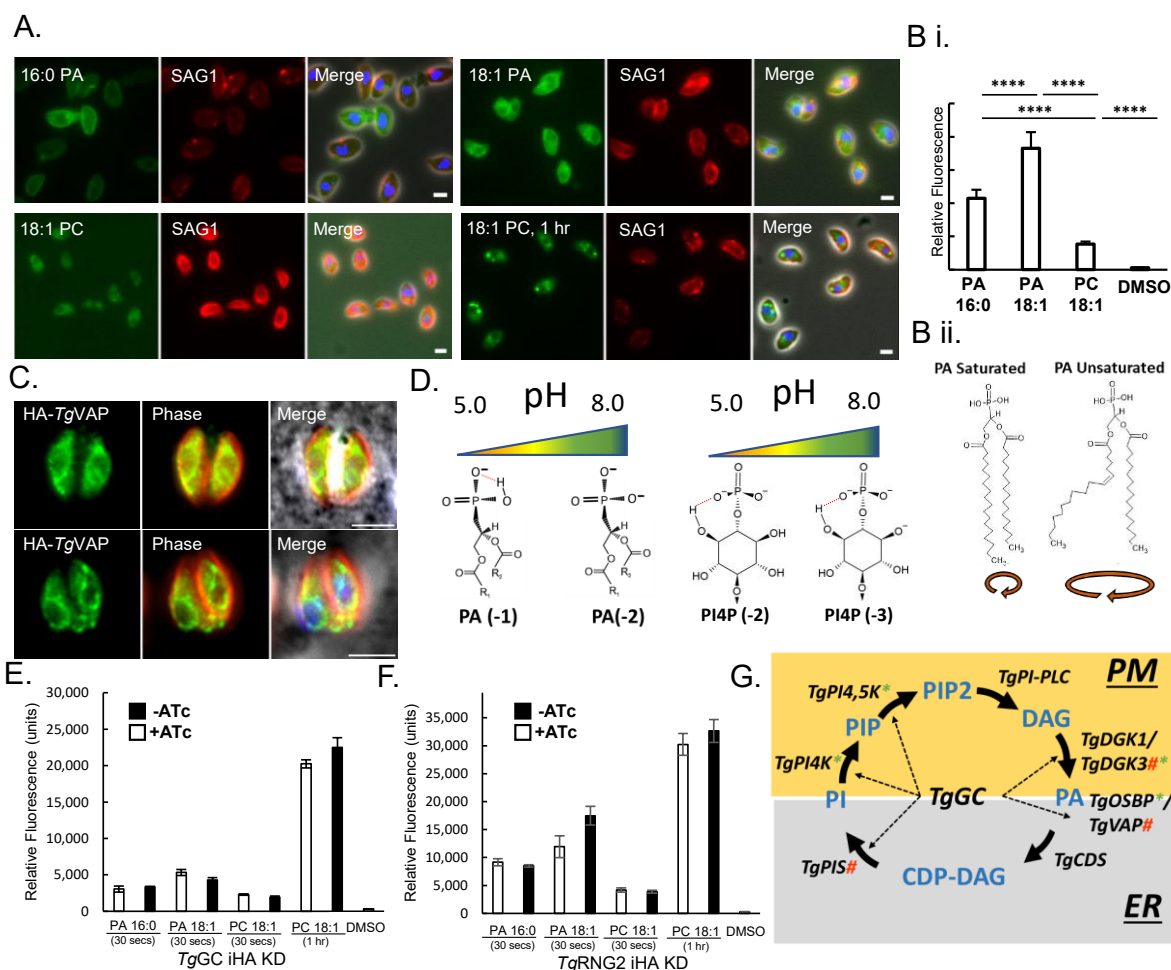
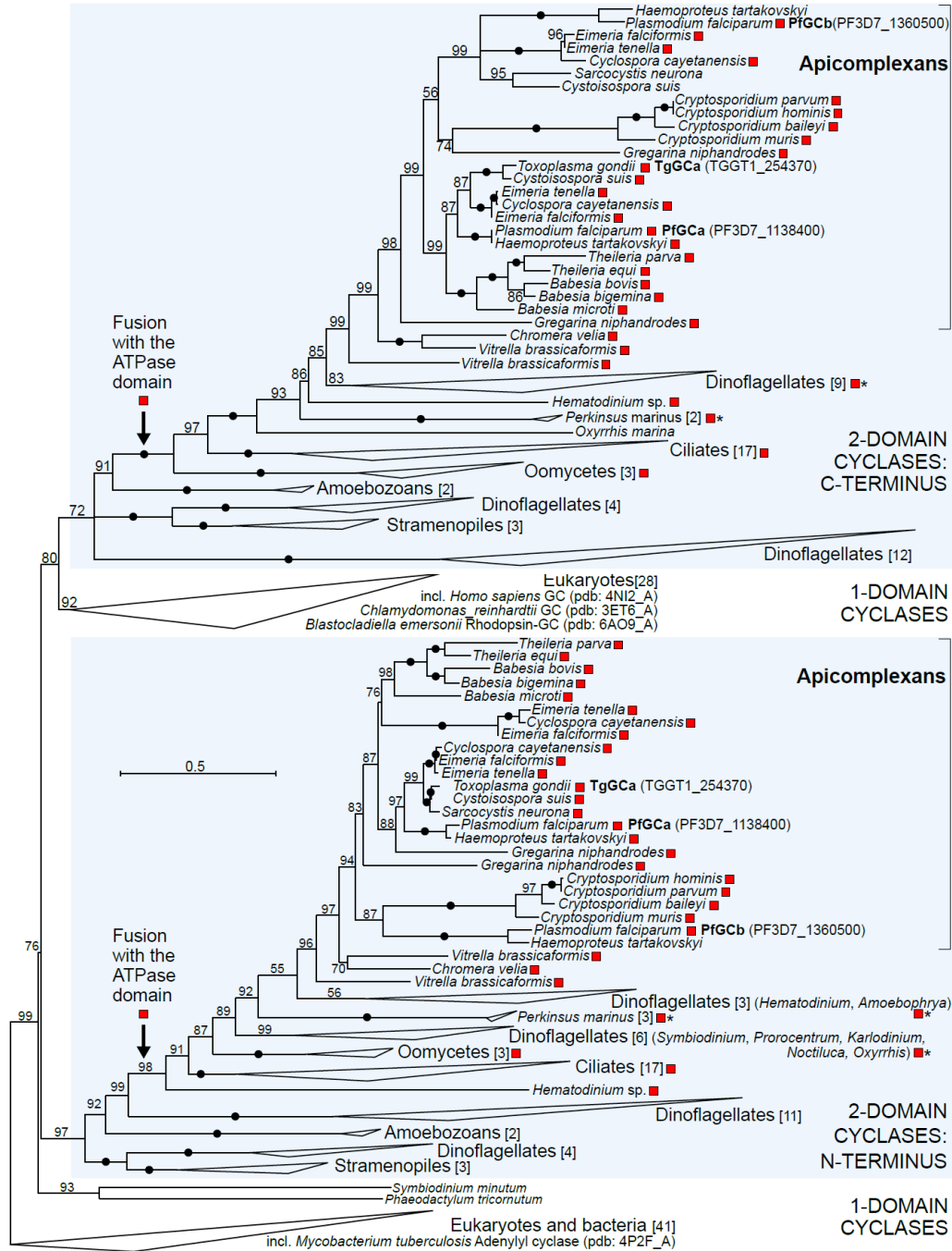


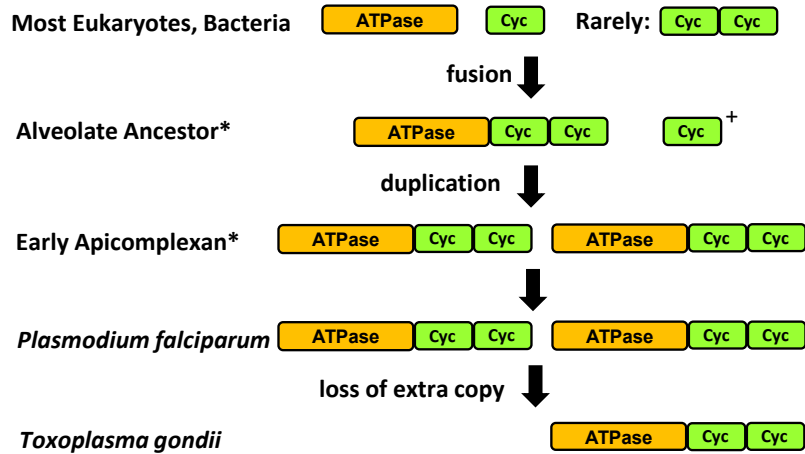
Figure 4: Extracellular *Toxoplasma* tachyzoites readily take up PA as part of membrane remodelling to balance the phosphatidylinositol cycle.

A. Lipid uptake assay in extracellular *Toxoplasma* tachyzoites analysed by fluorescence microscopy. Extracellular parasites were incubated in DAG buffer with 5 μ M of indicated fluorescent NBD-lipid over 30 seconds (or 1hr where indicated). **B. i** Quantification of lipid uptake in extracellular *Toxoplasma* tachyzoites analysed by FACS comparing uptake of 5 μ M NBD-PA16:0, NBD-PA18:1, NBPC18:1 or equivalent DMSO control. n=24 biological replicates. **ii.** Structural model of saturated and unsaturated PA and the effect on lipi dbilayer fluidity due to packing of lipids. (image adapted from Avanit Polar Lipids, www.avantilipids.com) **C.** Immunofluorescence of TgVAPB by 3xHA tag. TgVAPB localizes to an ER-like localization at the periphery of the nucleus. **D.** Chemical structure indicating the variable charge state of PA and PI4P with increasing or decreasing pH ([van Paridon et al. 1986](#), [Abramson et al. 1964](#)). **E, F.** FACS analysis of uptake of indicated NBD fluorescent lipids at indicated time points in TgGCiHA KD and TgRNG2iHA KD pre-treated with or without ATc. For TgRNG2iKD, n=4 biological replicates, and TgGCiKD n=3 biological replicates. For All graphs, error bars represent SEM. **G.** Complete model of the PI-Cycle in *Toxoplasma gondii*. Green Asterisk (*) represents protein which shows at least one altered phosphorylation site in a homologous protein in either PbGCb KO or Compound 2 treated cells in a previous Plasmodium bergehi study ([Brochet et al. 2014](#)). Red Hashtag (#) represents gene which shows significantly altered transcription in a homologous protein of a PbGCb KO cell line in a previous Plasmodium study ([Brochet et al. 2014](#)).





Guanylate Cyclase (GC) Evolution



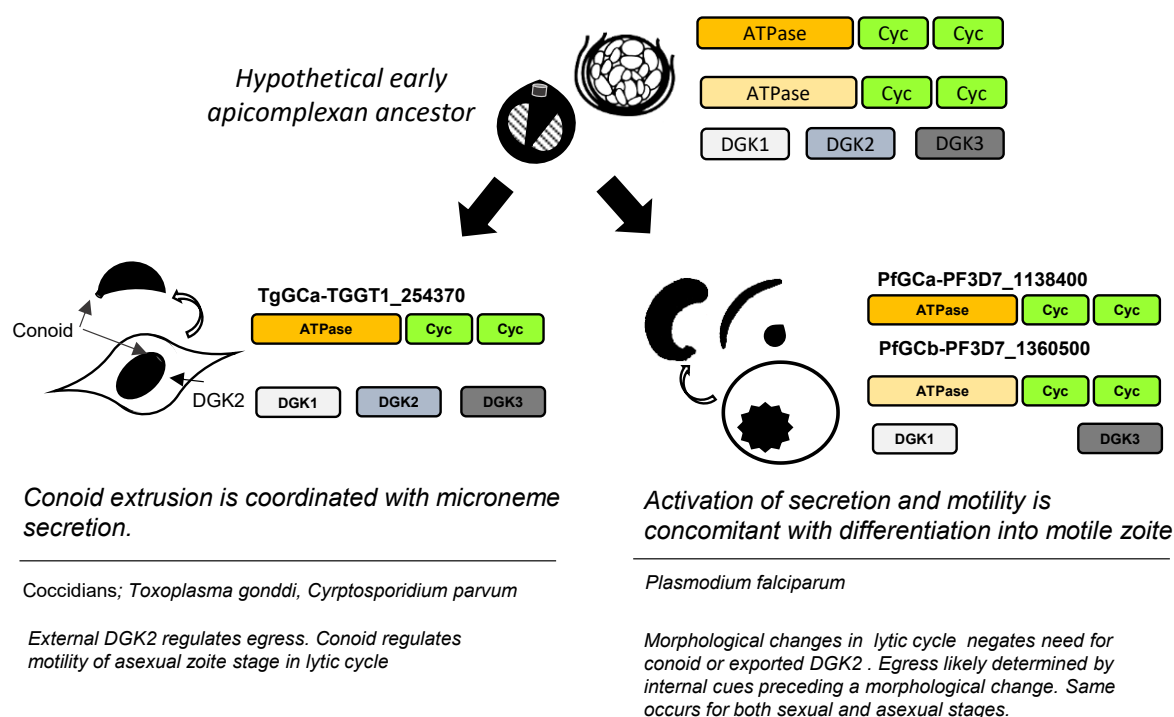


Figure 5: Phylogenetic analysis of phosphatidic acid signalling and trafficking proteins.

Phylogenetic analysis of phosphatidic acid signalling and trafficking proteins. Phylogenetic analysis of GC in Alveolata using only the CHD cyclase domain (A) and ATPase domain (B) separately. Evolutionary scheme depicting changes in domain arrangement in GC and DGK proteins. Ancestral states represent latest predicted acquisitions of the given domain arrangement (*). Additional unfused ATPases and 1- or 2-domain cyclases were likely present in the alveolate ancestor (+). (C) Schematic of evolution of the GC protein in apicomplexan parasites. The cyclase and ATPase domains fused in the alveolate ancestor before the whole GC protein was duplicated in apicomplexans. The second GC copy was lost in coccidia, but retained in Plasmodium. Toxoplasma lost the second copy of GC, but retained DGK2. Plasmodium has kept both copies of GC but lost an exported DGK2.

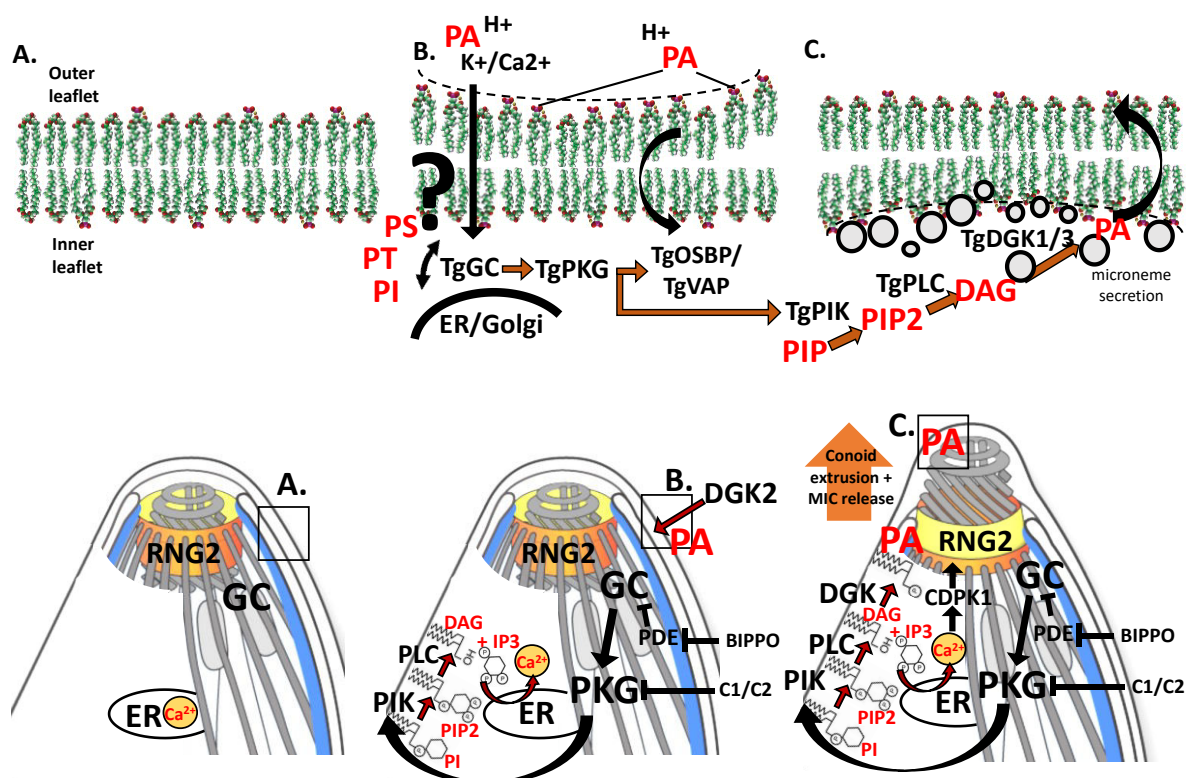


Figure 6: Model for PA production during cGMP and calcium signalling in *Toxoplasma*.

A. Tachyzoite at rest during intracellular stage with stable plasma membrane **(B)** Extracellular conditions to egress result in a drop in pH at least partly attributed to exported TgDGK2 which produces PA to signal egress. Changes in the plasma membrane composition and/or pH trigger TgGC to activate PI cycle. TgGC activates TgPKG to phosphorylate PI kinase to produce PIP2 which ultimately gets cleaved to produce DAG and IP3. IP3 activates calcium release and DAG is used to produce PA at the apical complex as part of microneme secretion **(C)**. Simultaneously TgGC regulates the import of excess PA via activation of the TgOSBP/VAP complex to maintain phospholipid homeostasis **(B)**.

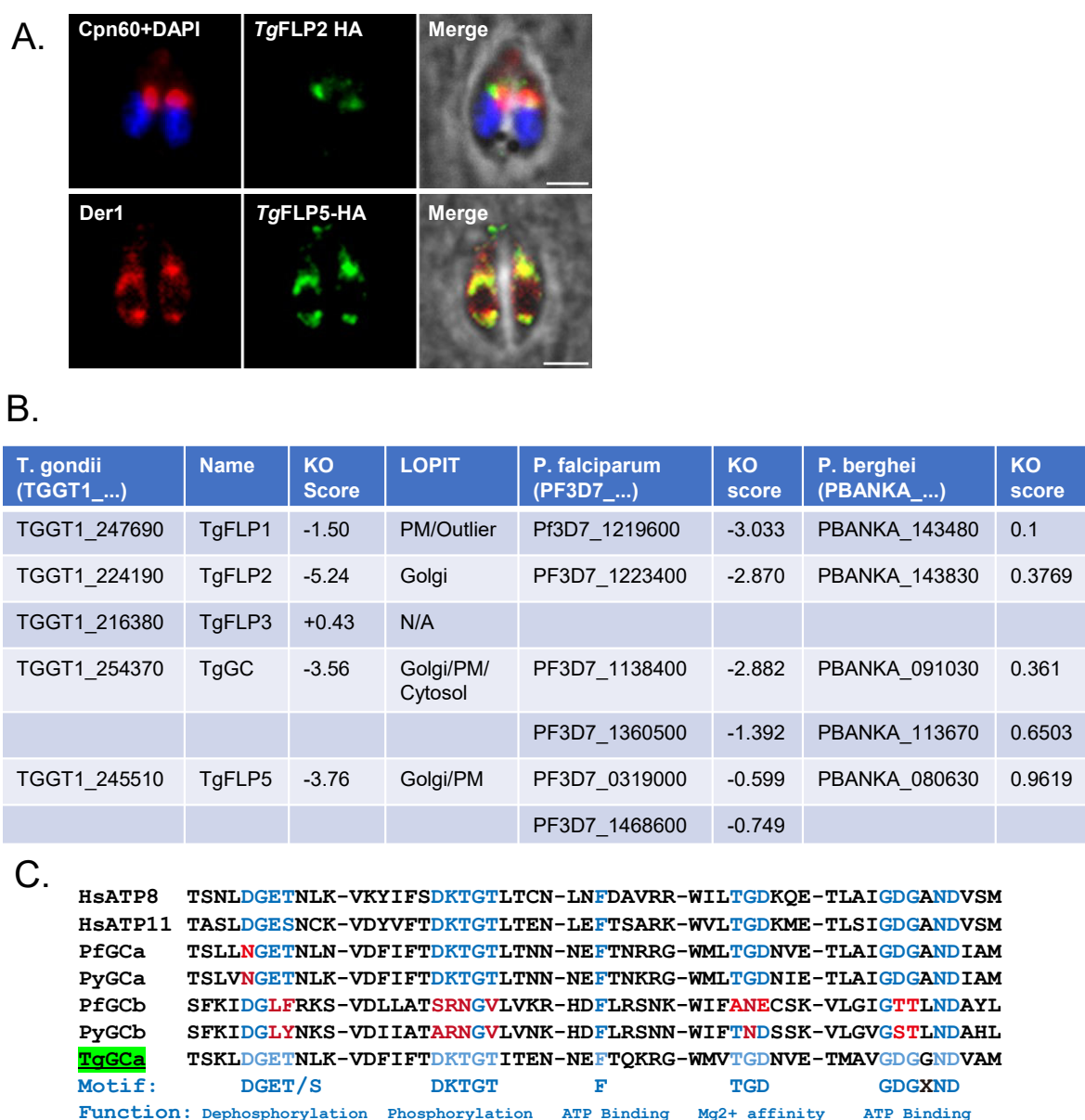


Figure S1: Phylogeny of phospholipid flippases in *Toxoplasma* and *Plasmodium*..

A. Localization of TgFLP2 (TGGT1_224190) to a Golgi-like compartment that does not co-localize with the apicoplast anti-Cpn60. Localization of TgFLP5 (TGGT1_245510) to the ER (Der1). Scale bars represent 2 μ m. **B.** Table of known flippases in *Toxoplasma* and *Plasmodium* with predicted localization by Hyper-LOPIT and predicted essentiality. **C.** MUSCLE Alignment of the key residues of the Human flippase ATP8 and ATP11 with the ATPase domain of Apicomplexan dual domain GCs.

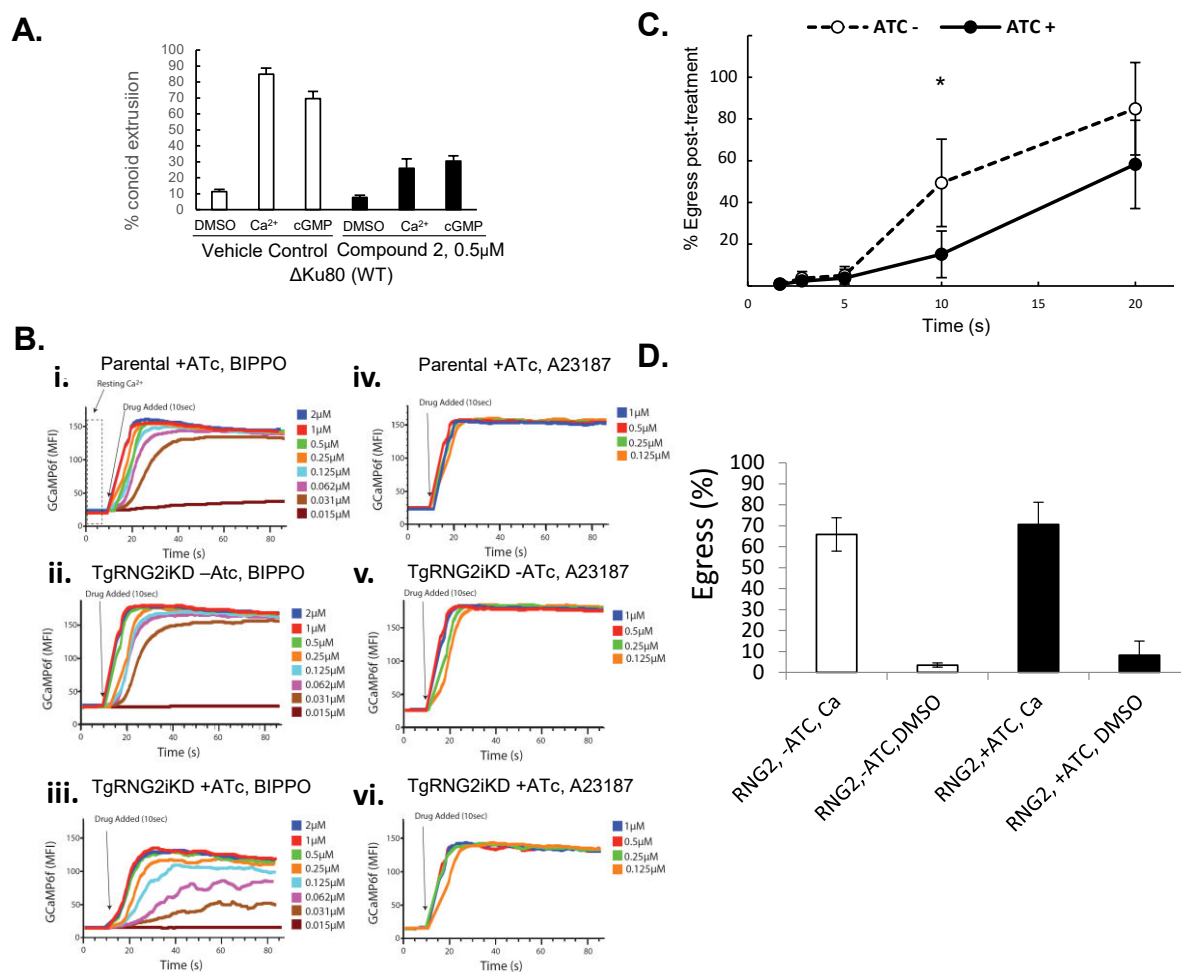


Figure S2: the role of cGMP signalling in conoid extrusion.

A i. Conoid extrusion assay with WT cells and cells pre-treated with the PKG inhibitor Compound 2 (0.5 μ M). $n=4$. **B.** FACS analysis of Calcium flux in TgRNG2iKD cells expressing the calcium biosensor GCaMP6 after stimulus with either A23187 or BIPPO over time at indicated concentrations. **C.** Egress assay of TgRNG2iKD cells with or without ATc pre-treatment following stimulus with 10 μ M BIPPO over time. $n=3$ biological replicates. **D.** Egress assay of TgRNG2iKD cells with or without ATc pre-treatment following stimulus with 5 μ M A23187 after 5 minutes. $n=4$. For all graphs, error bars represent SEM. For all graphs $P < 0.05$, * $x < 0.05$, ** $x < 0.01$, *** $x < 0.005$, **** $x < 0.001$.

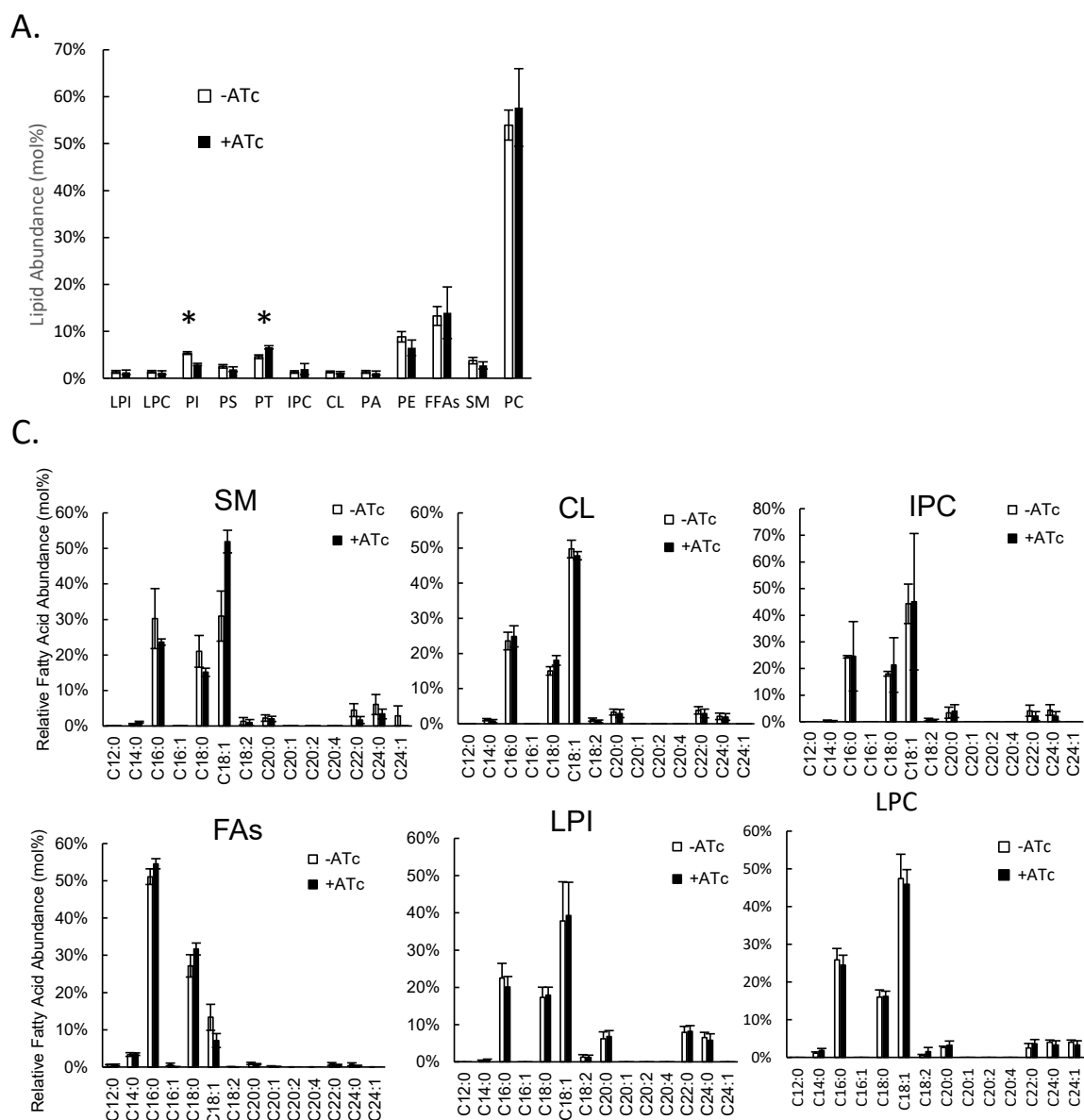


Figure S3:

A. Global phospholipid analysis of all phospholipid species. Total lipids expressed as mol%, normalized to total fatty acids. B. Fatty acids profile of Sphingomyelin (SM), Cardiolipin (CL), Inositol Phosphoceramide (IPC) Free Fatty acids (FAs), Lysophosphoinositol (LPI) and Lysophosphocholine (LPC). For all graphs, n=3 biological replicates, error bars represent SEM.

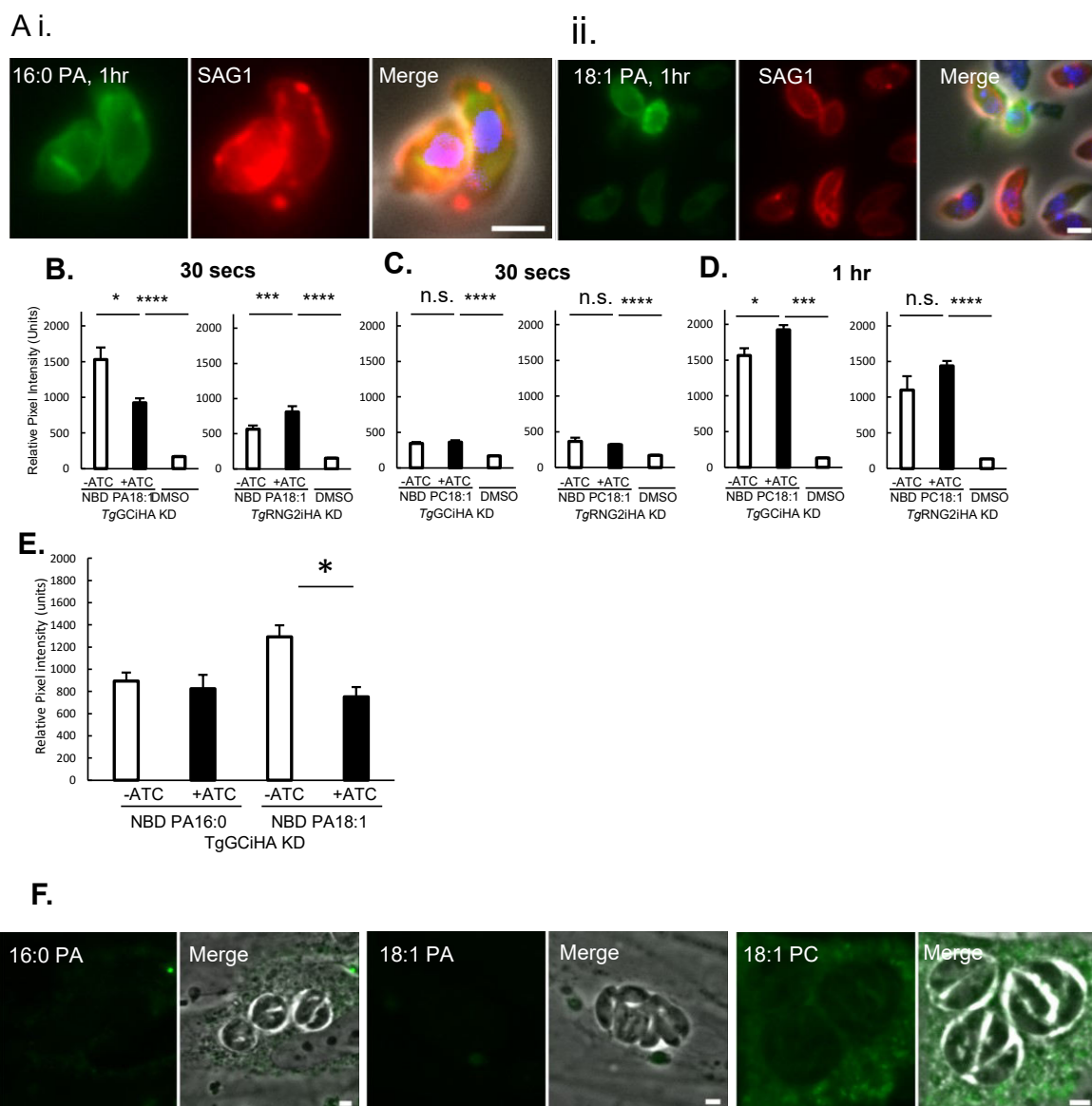


Figure S4: Extracellular *Toxoplasma* tachyzoites readily take up PA

A. Lipid uptake assay in extracellular *Toxoplasma* tachyzoites analysed by fluorescence microscopy. Extracellular parasites were incubated in DAG buffer with 5 μ M of indicated fluorescent NBD-lipid over 1 hour. **B.** Quantification of fluorescent NBD-PA18:1 uptake by microscopy in TgGCiKD and TgRNG2iKD mutants pre-treated with or without ATc over 30 seconds. n=12 biological replicates **C.** Quantification of fluorescent NBD-PC18:1 uptake by microscopy in TgGCiKD and TgRNG2iKD mutants pre-treated with or without ATc over 30 seconds. n=6 biological replicates **D.** Quantification of fluorescent NBD-PC18:1 uptake by microscopy in TgGCiKD and TgRNG2iKD mutants pre-treated with or without ATc over 1 hour. n=6 biological replicates **E.** Comparison of uptake of fluorescent NBD-PA18:1 and NBD-PA 16:0 by microscopy. n=3 biological replicates **F.** Lipid uptake of intracellular tachyzoites with 5 μ M of fluorescent NBD-lipids over 24 hours For all graphs, * $x < 0.05$, ** $x < 0.01$, *** $x < 0.005$, **** $x < 0.001$. All error bars represent SEM. Scale bars represent 2 μ m

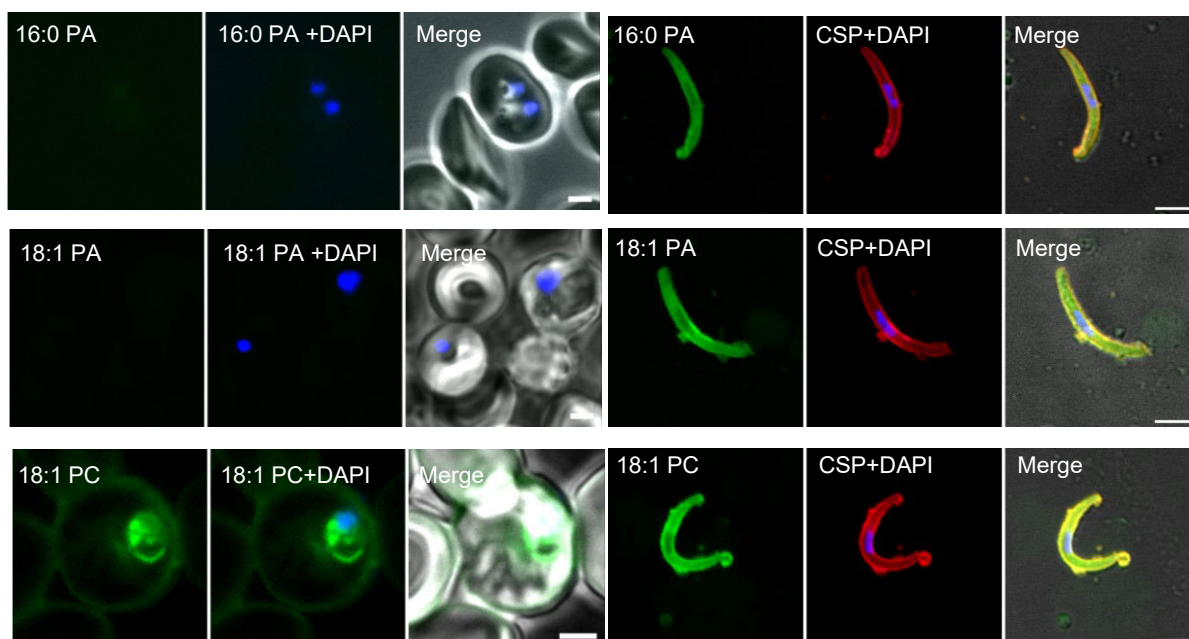


Figure S5: Phospholipid uptake in *Plasmodium falciparum* parasites.

A. Fluorescent lipid uptake in blood stage *P. falciparum* incubated with $5\mu\text{M}$ of NBD-PA16:0, NBD-PA18:1, or NBD-PC18:1 for 24 hours. Scale bars represent $2\mu\text{m}$ **B.** Fluorescent lipid uptake in extracellular sporozoites incubated with $5\mu\text{M}$ of NBD-PA16:0, NBD-PA18:1, or NBD-PC18:1 for 10 minutes. Scale bars represent $5\mu\text{m}$.

| T. gondii (TGGT1_...) | Name | KO Score | LOPIT | P. falciparum (PF3D7_...) | KO score | P. berghei (PBANKA_...) | KO score |
|-----------------------|---------|----------|--------------------|---------------------------|----------|-------------------------|----------|
| TGGT1_289570 | TgOSBP1 | -1.70 | ER | PF3D7_1351000 | -1.852 | PBANKA_1363800 | N/A |
| TGGT1_264760 | TgOSBP2 | -6.07 | Nucleolus /Nucleus | PF3D7_1131800 | -0.001 | PBANKA_0916600 | 0.8692 |
| TGGT1_294320 | TgOSBP3 | 0.88 | N/A | | | | |
| TGGT1_318160 | TGVAPB | -3.54 | ER | PF3D7_1439800 | -3.157 | PBANKA_1303700 | 0.0737 |
| | | | | | | | |

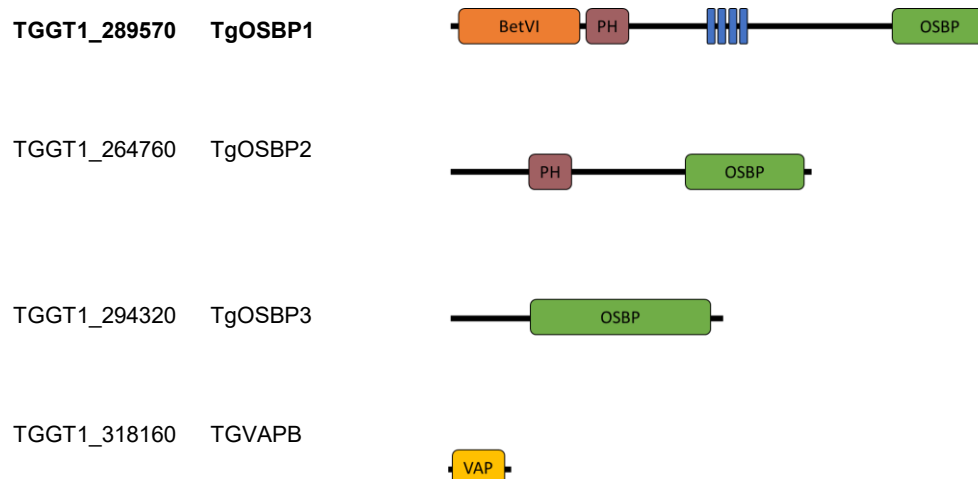


Figure S6: Phylogenetic analysis of genes in the Phosphatidylinositol cycle.

A. Table of putative OSBPs and VAP cofactors in *Toxoplasma* and *Plasmodium* with predicted hyper-LOPIT localization and essentiality prediction. **B.** Conserved domains of putative OSBP proteins in *Toxoplasma* and VAP cofactor.

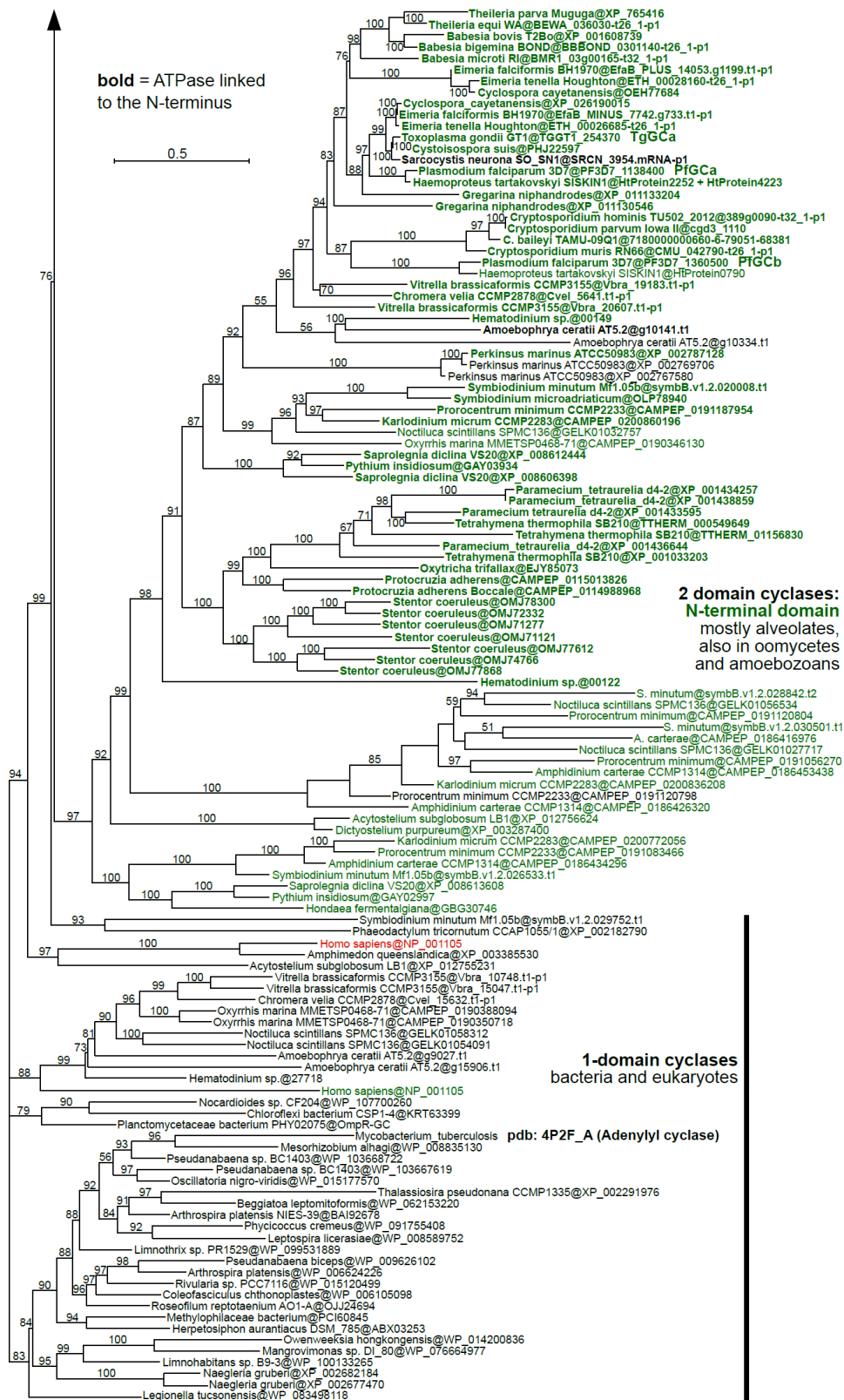


Figure S7: Phylogenetic analysis of N-terminal portion of double cyclase domain of GC. Phylogeny of the cyclase domain (233 protein sequences). Best Maximum Likelihood tree (IQ-TREE) is shown with ultrafast bootstraps at branches. Two-domain cyclase were split in between the N-terminal (in green) and C-terminal somain (in red) and both regions were

included in the final alignment. Sequences containing an upstream ATPase domain are shown in bold. Species names are followed by sequence accessions after the @ sign (see Materials and Methods for sequence database sources).

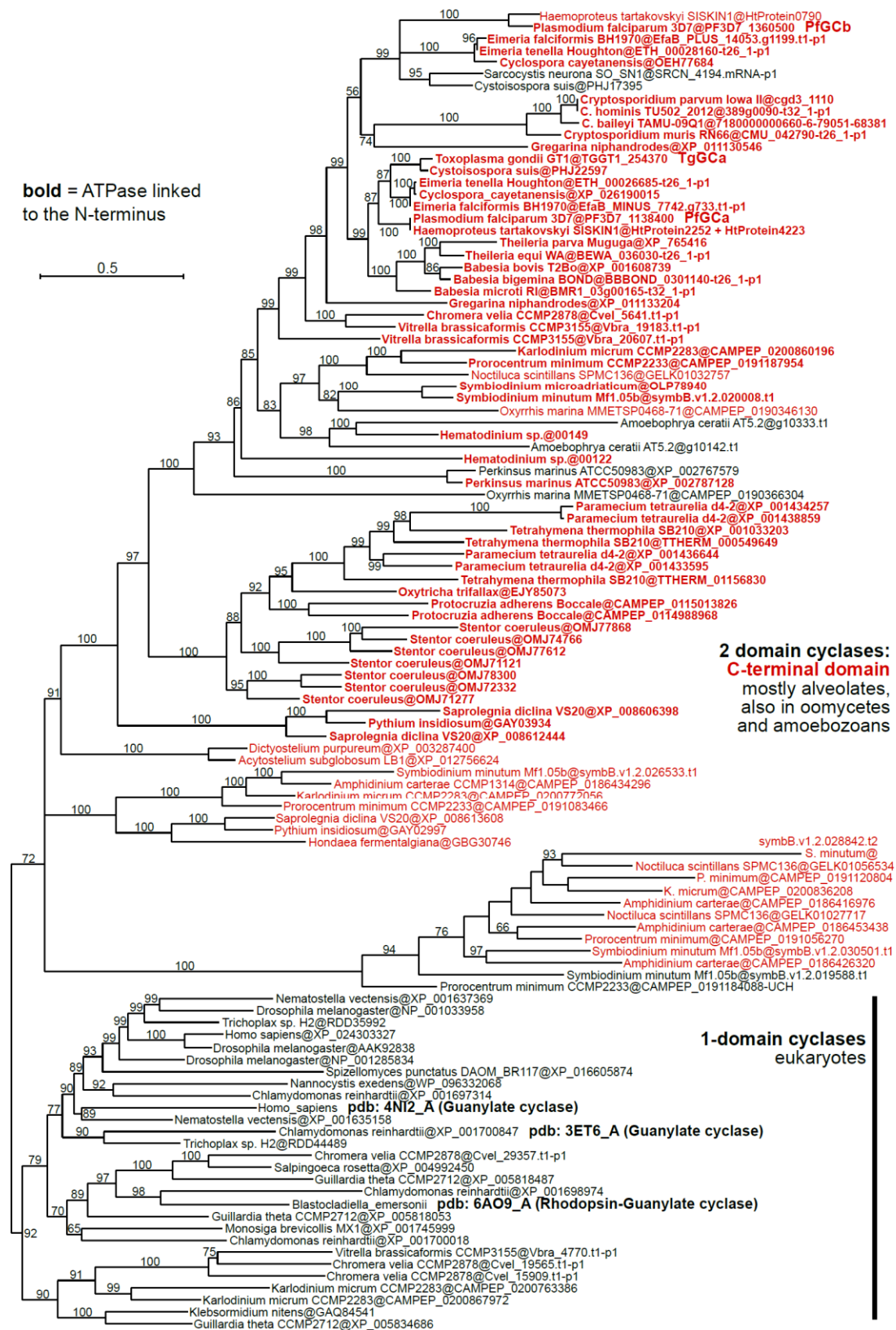


Figure S8: Phylogenetic analysis of C-terminal portion of double cyclase domain of GC.

Phylogeny of the cyclase domain (233 protein sequences). Best Maximum Likelihood tree (IQ-TREE) is shown with ultrafast bootstraps at branches. Two-domain cyclase were split in between the N-terminal (in green) and C-terminal somain (in red) and both regions were included in the final alignment. Sequences containing an upstream ATPase domain are shown in bold. Species names are followed by sequence accessions after the @ sign (see Materials and Methods for sequence database sources).

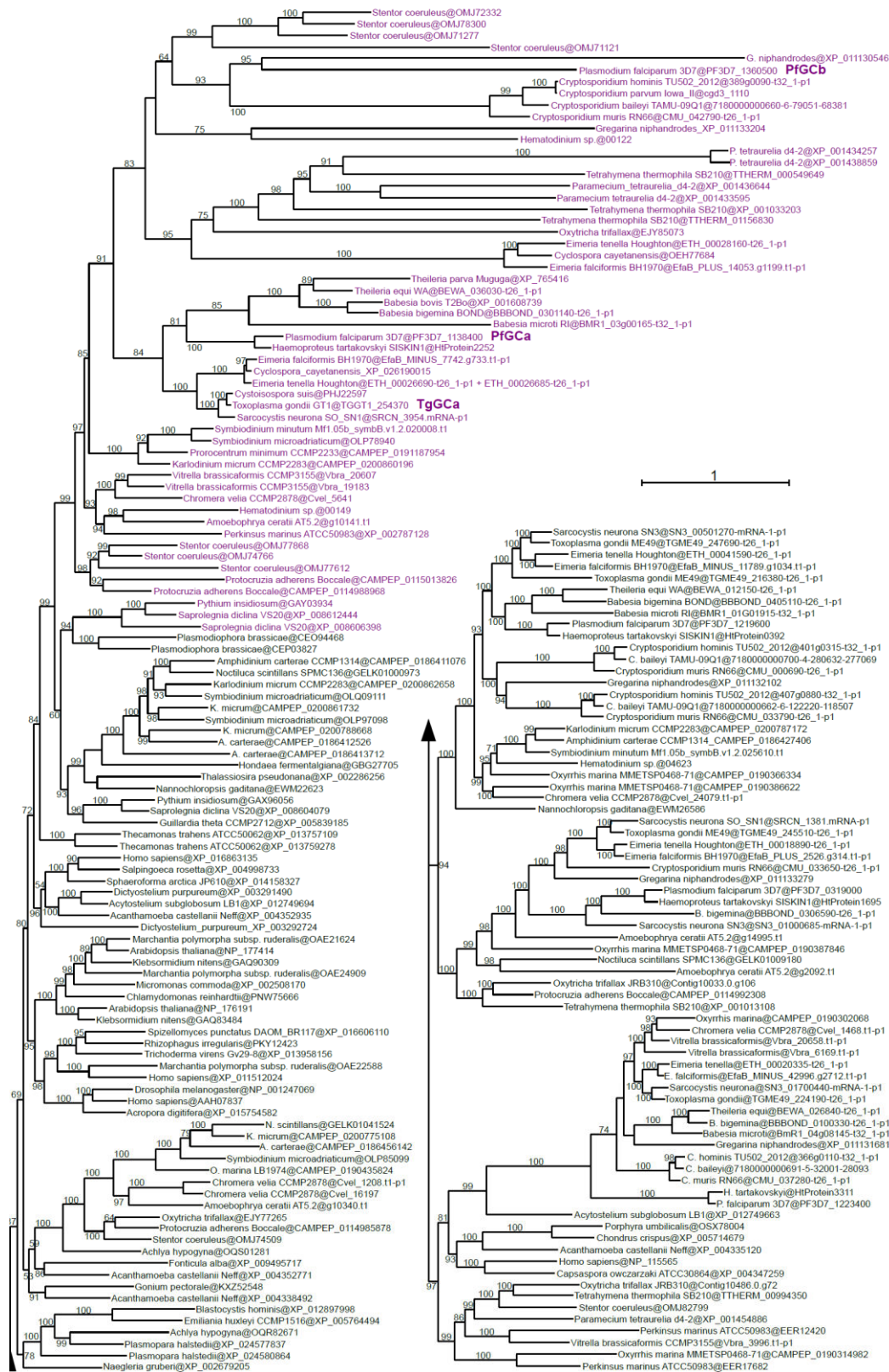


Figure S9: Phylogenetic analysis of putative phospholipid flippases in Alveolates.

Phylogeny of DAG kinases (DGKs; 149 protein sequences). Best Maximum Likelihood tree (IQ-TREE) is shown with ultrafast bootstraps at branches. The presence of positively predicted signal peptides is shown by “SP” letters. Species names are followed by sequence accessions after the @ sign (see Materials and Methods for sequence database sources).

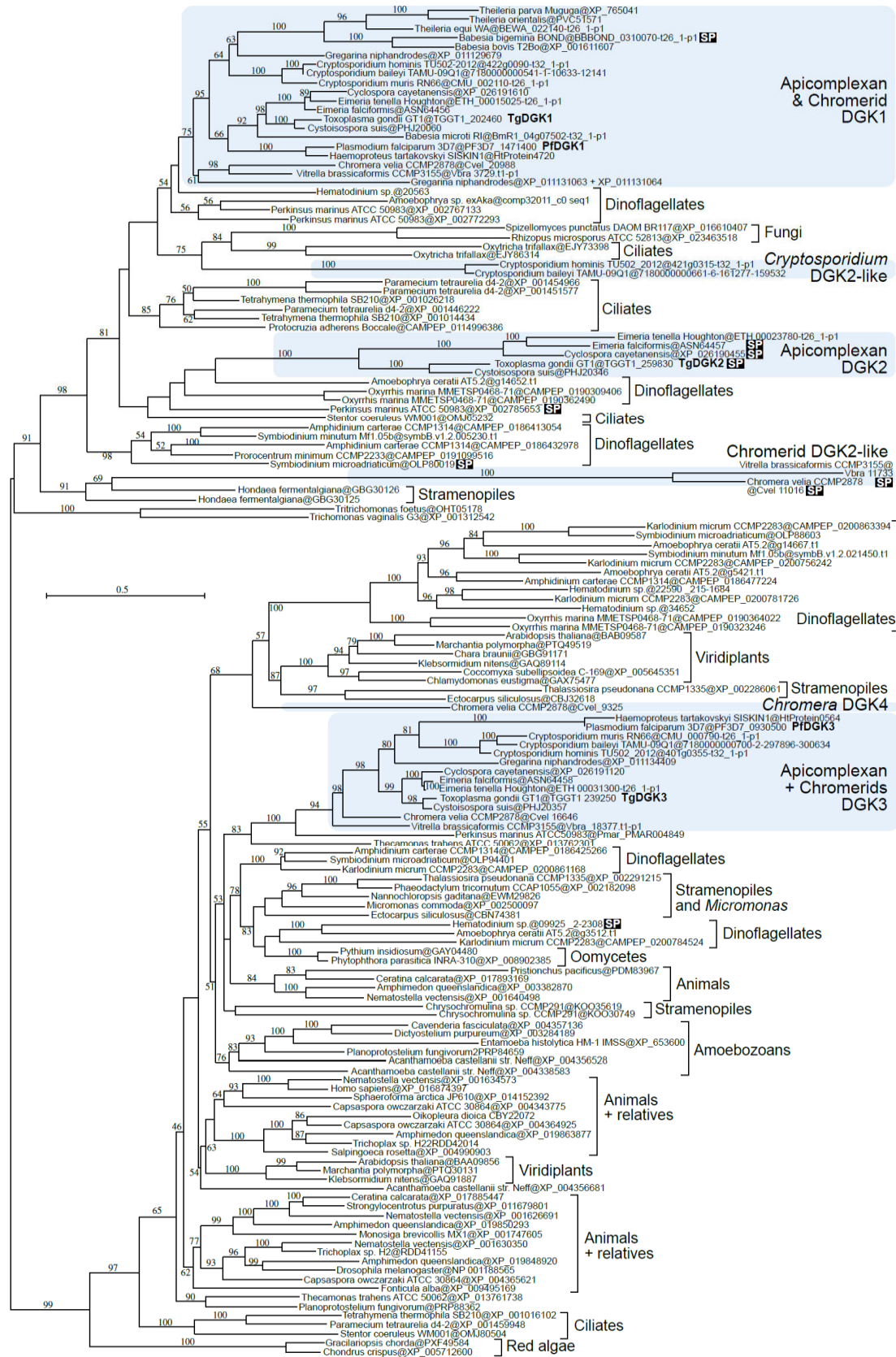


Figure S10: Phylogenetic analysis of DAG Kinases in Alveolates.

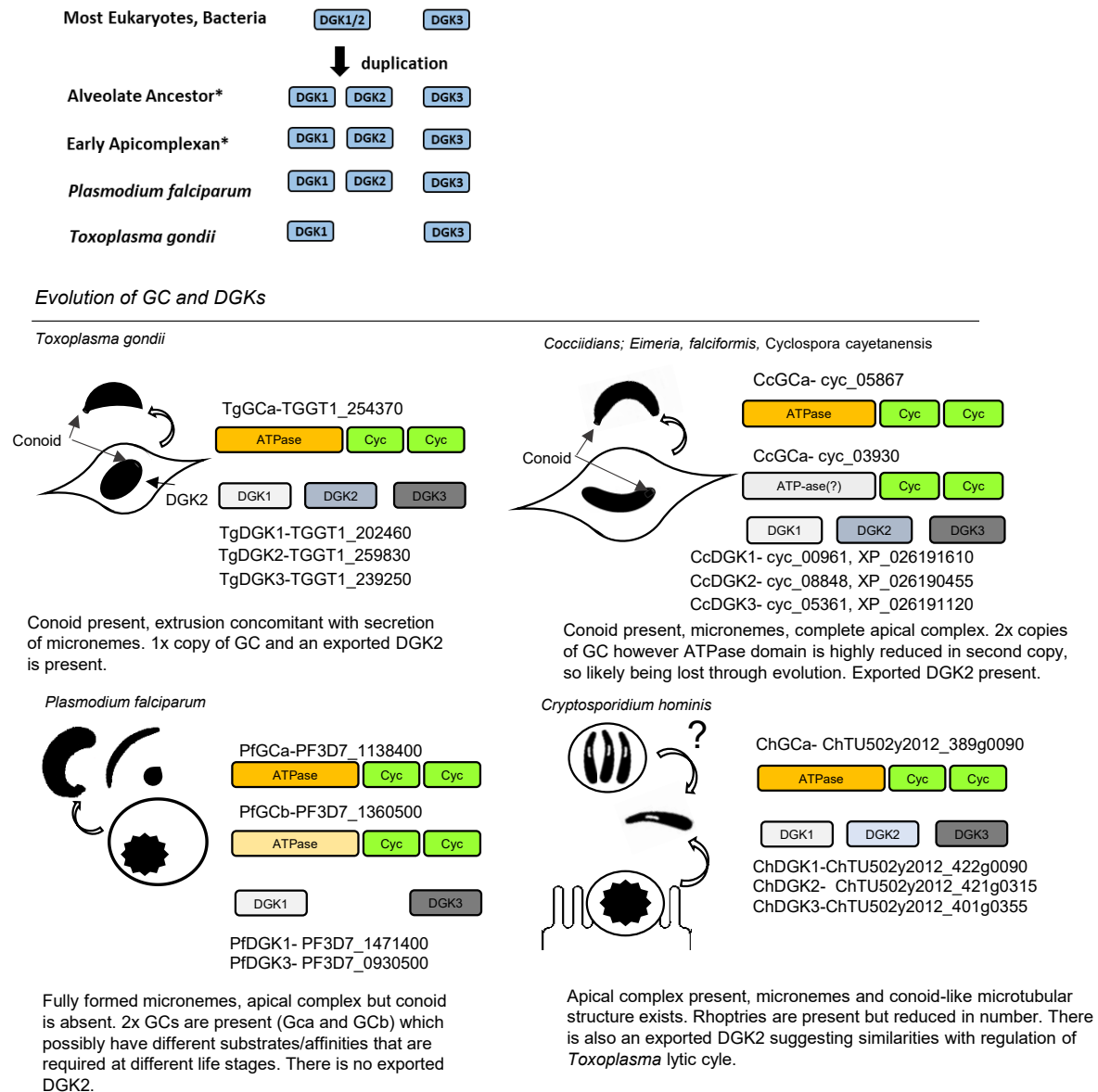


Figure S11:

A. Evolution of DGK in *Toxoplasma* and *Plasmodium* parasites.

B. Evolution of GCs and DGKs in Apicomplexan parasites. Coccidia appear to be losing the second copy of GC present in other Apicomplexa. *Plasmodium* is only species listed here which has lost exported DGK2,

REVIEW

The flexibility of Apicomplexa parasites in lipid metabolism

Serena Shunmugam¹, Christophe-Sébastien Arnold¹, Sheena Dass, Nicholas J. Katris, Cyrille Y. Botté^{1*}

Apicolipid Team, Institute for Advanced Biosciences, CNRS UMR5309, Université Grenoble Alpes, INSERM U1209, Grenoble, France

* These authors contributed equally to this work.

* cyrille.botte@univ-grenoble-alpes.fr, cyrille.botte@gmail.com

OPEN ACCESS

Citation: Shunmugam S, Arnold C-S, Dass S, Katris NJ, Botté CY (2022) The flexibility of Apicomplexa parasites in lipid metabolism. *PLoS Pathog* 18(3): e1010313. <https://doi.org/10.1371/journal.ppat.1010313>

Editor: Bjorn F.C. Kafsack, Joan and Sanford I. Weill Medical College of Cornell University, UNITED STATES

Published: March 17, 2022

Copyright: © 2022 Shunmugam et al. This is an open access article distributed under the terms of the [Creative Commons Attribution License](https://creativecommons.org/licenses/by/4.0/), which permits unrestricted use, distribution, and reproduction in any medium, provided the original author and source are credited.

Funding: This work and the authors are supported by Agence Nationale de la Recherche, France (Grant ApicolipidAdapt ANR-21-CE44-0010 and ANR-12-PDOC-0028), the Atip-Avenir and Finovi programme (CNRS-INSERM-Finovi Atip Avenir Apicolipid projects), CEFIPRA (Indo-French Centre for the Promotion of Advanced Research, project 6003-1), IDEX-Université Grenoble Alpes (ISP programme), Region Auvergne Rhone-Alpes (IRICE Grant, Project GEMELI), The Fondation pour la Recherche Médicale (TEAM FRMEQU202103012700), Project LIA-IRP CNRS programme (Apicolipid Project) and the Laboratoire d'Excellence ParaFrap, France (Grant number ANR-11-LABX-0024) to CYB. The funders

Abstract

Apicomplexa are obligate intracellular parasites responsible for major human infectious diseases such as toxoplasmosis and malaria, which pose social and economic burdens around the world. To survive and propagate, these parasites need to acquire a significant number of essential biomolecules from their hosts. Among these biomolecules, lipids are a key metabolite required for parasite membrane biogenesis, signaling events, and energy storage. Parasites can either scavenge lipids from their host or synthesize them de novo in a relict plastid, the apicoplast. During their complex life cycle (sexual/asexual/dormant), Apicomplexa infect a large variety of cells and their metabolic flexibility allows them to adapt to different host environments such as low/high fat content or low/high sugar levels. In this review, we discuss the role of lipids in Apicomplexa parasites and summarize recent findings on the metabolic mechanisms in host nutrient adaptation.

Introduction

Lipids are one of the most predominant constituents of any living organism and are crucial for cell development and division. They serve as the building blocks of biological membranes, such as those from intracellular organelles. Lipids are also major signaling molecules and serve a central storage moiety for the generation of energy and new membranes. Lipids are therefore essential in the pathogenesis of infectious diseases [1]. Apicomplexa parasites, which are responsible for major social and economic burdens, are no different in this need for substantial amounts of lipids for survival. *Plasmodium* sp. and *Toxoplasma gondii* both belong to this phylum and are the infectious causative agents of malaria and toxoplasmosis, respectively [2,3]. These obligate intracellular parasites have 2 distinct life cycles, either alternating between asexual and sexual life stages, and/or replicative versus low replicative life stages (more particularly for *T. gondii*: highly replicative in any nucleated cells from warm-blooded animals versus chronic stages nondividing cells), with distinct organism/cellular requirements, as well as specific replicative and metabolic profiles.

All these life stages are highly dependent on large and specific amounts of lipids, as well as maintaining a specific lipid homeostasis to sustain intracellular development, membrane/organelle biogenesis, and parasite survival and propagation. Parasites also require lipids as

had no role in study design, data collection and analysis, decision to publish, or preparation of the manuscript.

Competing interests: The authors have declared that no competing interests exist.

signaling molecules, notably to regulate and control the timely release of the secretory organelles called micronemes, which trigger active invasion and egress mechanisms of the parasite in and from their host cell. Importantly, these parasites can metabolically adapt to changing host nutrient environments, setting up a unique metabolic program upon the host nutritional status and, hence, continue to optimally propagate. The unique lipid metabolism of these parasites has been thoroughly characterized by a so-called “make and take” paradigm, where lipid acquisition is met by a combination of de novo–made lipids (“make lipids”) and scavenged lipids from the host (“take lipids”) [4] (Fig 1). Furthermore, recent studies uncovered that the parasites’ survival is governed by their ability to salvage and synthesize simple fatty acyl chains and carry out an obligate “patchwork” assembly with lipids originating from both sources to generate most lipid species and thus maintain the essential parasite lipid homeostasis [5]. Importantly, recent work revealed that the parasite metabolic ability to scavenge, make de novo and reassemble lipids, are regulated, and controlled via sensing and metabolic adaptation of the parasite toward the nutritional status of the host and nutrient availability [6]. Changes in the host nutrient induces a metabolic reprogramming of the parasite where different sets of genes and proteins and not a unique one are responsible for parasite adaptation and survival.

This review will primarily cover recent developments in lipid synthesis/salvage in *Toxoplasma* with reference to other apicomplexan parasite for comparison.

Lipids are essential in Apicomplexa parasites

Originally, these parasites were thought to solely rely on scavenging from the host for lipids, and not to being able to synthesize their own. Instead cellular investigations, genome mining, and biochemical investigations revealed the presence of a nonphotosynthetic plastid, the apicoplast, harboring a prokaryotic type II fatty acid (FA) synthesis pathway, which is essential during tachyzoite and becomes dispensable during bradyzoite development [7–11]. The pathway in sexual stages (oocyst formation in cats) remains mainly understudied, and its

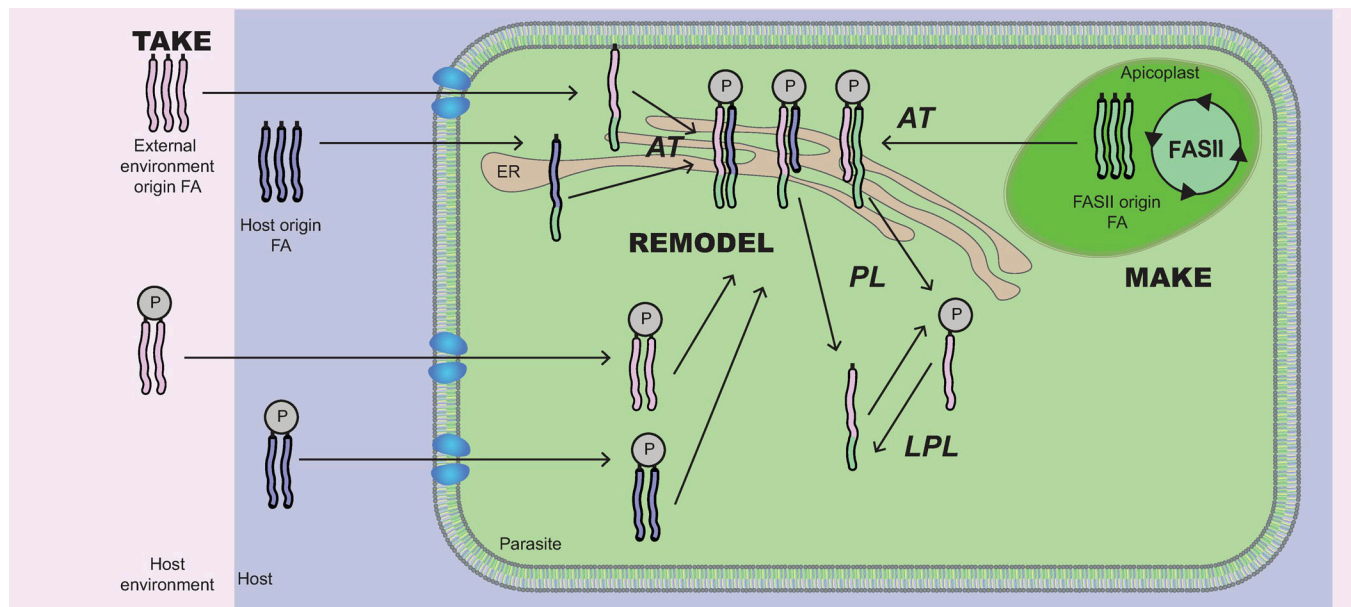


Fig 1. “Make, take, and remodel”; the central dogma explaining how the parasite is able to scavenge lipids from the host environment, the host itself (“Take”) while also synthesize them de novo (“make”). FA elongation and a patchwork assembly mechanism in the ER contribute further to glycerolipid metabolism in the parasite (“remodel”). AT, acyltransferase; FA, fatty acid; LPL, lysophospholipase; PL, phospholipase.

<https://doi.org/10.1371/journal.ppat.1010313.g001>

essentiality is unclear. Unlike tachyzoites, we know that *T. gondii* oocysts rely on FA breakdown to fuel the tricarboxylic acid (TCA) cycle through the production of acetyl-CoA to generate energy rather than glycolysis [12].

Further numerous analyses allowed for the “make and take” central dogma of lipid metabolism in Apicomplexa parasites to be described and accepted [4]. The FASII pathway, in *Plasmodium* parasites fast replicating blood stage, is not critical for parasite survival in nutritionally rich environments because NADH-dependent enoyl-ACP reductase (FabI) and FabB/F can be deleted. It is vital, however, during the mosquito and liver stages of the parasites in the rodent and human species, respectively [13,14].

Additionally, to the apicoplast FASII, another FA synthesis pathway can be found in *T. gondii*, namely the cytosolic eukaryotic type I FA synthase, the FASI. FASI is believed not to be essential in *T. gondii* tachyzoite life stages [15] and is completely absent in *Plasmodium* parasites. The contribution of FASI is yet to be fully determined, but it is believed to be inactive during tachyzoite life stage [15] but could play a more important role during the chronic part of the disease, for the development of bradyzoite life stages. Importantly, the parasite depends on an obligate combination of FAs to generate and maintain parasite lipid homeostasis [5]. Indeed, the parasite uses both host-scavenged FAs and de novo-synthesized FA from the relict plastid, the apicoplast, via its prokaryotic FASII pathway [4], to be assembled together and make the bulk of most parasite membrane lipids [5]. FA pools can be further elongated by the addition of 2-carbons units from acetyl-CoA via the ER-based elongases, ELO1, 2, 3 (Fig 2) [16–18]. Glycerolipids synthesis, which leads to the synthesis of phospholipid, the major membrane lipid classes present in the parasite membranes [19–21], is fueled by this essential influx of FAs from the 2 different sources (“make and take”). The synthesis of glycerolipids is composed of an FA “mix and match” process near the ER/cytosol allowing the parasites to maintain a finely tuned balance between the 2 FA sources [5]. This extraordinarily complex and seemingly redundant presence of 2 FA syntheses pathways is in fact not so complex, but instead reflects the parasite’s versatile and diverse capacities to generate and obtain lipids and precursors, crucial for its survival. Indeed, both FA/lipid scavenging and de novo syntheses pathways are essential and allow the parasite to adapt to the adverse or rich nutritional conditions met within the host. Furthermore, such complex pathway of “take, make, remodel, and adapt to the host” involves numerous proteins, which manipulate lipids as part of the general metabolic homeostasis of the parasite within host nutrient changes. Many of these proteins become essential during tachyzoite life stages, while others become involved and pivotal under certain host nutritional conditions, settings lipid acquisition metabolic programs, accordingly, to host nutrient availability.

Lipids made by the parasite can be influenced by the nutrient environment

Apicomplexa parasites harbor a plant-like plastid acquired from the secondary endosymbiosis of a red algal ancestor [22], the apicoplast (Fig 2). This plastid has lost its photosynthesis ability but kept other essential plant-like metabolic pathways such as the isoprenoid precursor synthesis, i.e., the DOXP pathway, the iron-sulfur cluster synthesis pathway and the prokaryotic type FASII pathway [23]. Bioinformatic reconstruction of the pathway, combined to biochemical analyses, especially using stable isotope ^{13}C labeling, in both *P. falciparum* and *T. gondii*, demonstrated that the parasite imports phosphoenolpyruvate (PEP) acid generated by the parasite glycolysis pathway into the apicoplast using plant-like transporters (APT in *T. gondii* and TPTs in *P. falciparum*) [5,20,24,25]. PEP is then converted to pyruvate by the pyruvate dehydrogenase complex (PDH, which exclusively exists in the apicoplast and not in the mitochondria [26]) after which converts pyruvate to acetyl-CoA, fueling the FA synthesis pathway and

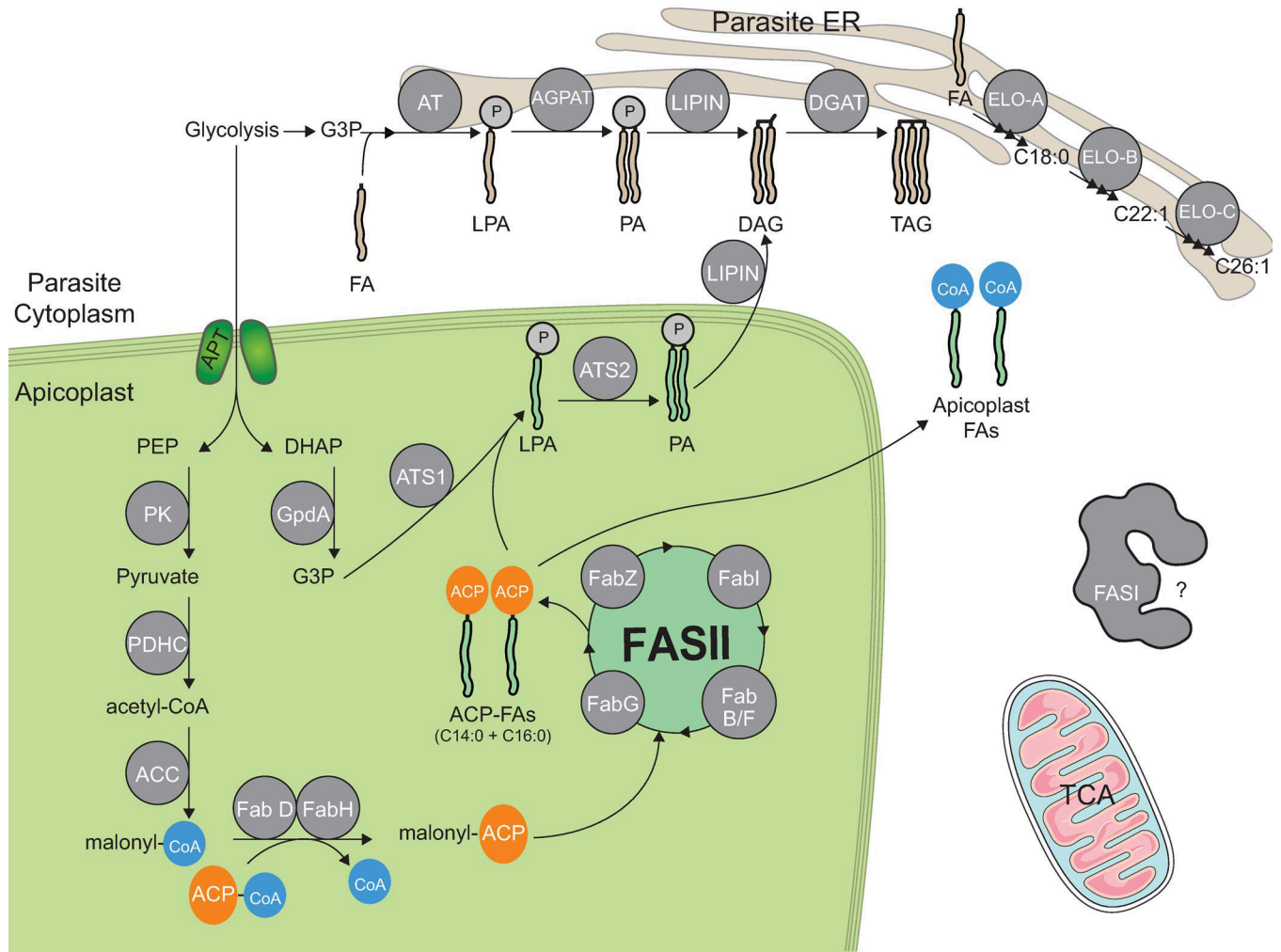


Fig 2. An illustration of the known proteins involved in glycerolipid synthesis in Apicomplexa parasites. PEP and DHAP generated from glycolysis occurring in the cytosol of the parasites enter the apicoplast via the apicoplast phosphate transporter (*TgAPT1*). They are then converted to pyruvate and G3P by a PK and GpdA, respectively. A PDHC (only present in the apicoplast [91]) is responsible for the formation of acetyl-CoA from pyruvate. ACC converts this to malonyl CoA. FabD/H complex leads to the attachment of an ACP and the loss of CoA resulting in ACP-malonyl. The FASII complex (comprised of FabG/B/F/I/Z) are responsible for the formation of short FA chains, mainly C14:0 and C16:0 fatty acyl (FA) ACP-chains. Esterification of FA-ACP from FASII or FA-CoAs from scavenged FAs on a G3P backbone (i.e., acylation) can occur in both the apicoplast by a plant-like acyltransferase *TgATS1* [5], and/or at the ER by a GPAT [93]. It is the first step for the de novo synthesis of all glycerolipids and results in the synthesis of LPA. LPA can be further acylated with another FA chain resulting in PA by ATS2-apicoplast or AGPAT-based ER [6]. LIPIN is responsible for the dephosphorylation of PA into DAG [39]. DAG can be further acylated into TAG by DGATs [94]. Elongation of FA chains can occur in the elongation pathway in the ER via ELO-A/B/C [16]. FASI is present in *T. gondii* parasite and not essential during tachyzoite stages and has not been further characterized [15]. ACC, acetyl-CoA carboxylase; ACP, acyl-carrier protein; DAG, diacylglycerol; DGAT, DAG acyltransferase; DHAP, dihydroxyacetone phosphate; FA, fatty acid; GpdA, glyceraldehyde-3-phosphate dehydrogenase; G3P, glycerol-3-phosphate; LPA, lysophosphatidic acid; PA, phosphatidic acid; PDHC, pyruvate dehydrogenase complex; PEP, phosphoenolpyruvate; PK, pyruvate kinase; TAG, triacylglycerol.

<https://doi.org/10.1371/journal.ppat.1010313.g002>

its 4 core proteins (FabB/F, FabG, FabZ, and FabI) allowing the elongation of the growing FA chain [27]. The FASII pathway produces relatively “short” FA chains, mainly C12:0, C14:0, C16:0, and very little C18:0 [5,16]. The identification and characterization of 2 plant-like acyltransferases (so-called ATS1/ApiG3PAT and ATS2) located within the apicoplast revealed the capacity of Apicomplexa parasites to sequentially synthesize then esterify activated FA chains (i.e., Acyl-CoA/ACP) onto a glycerol-3-phosphate backbone resulting in the formation of lysophosphatidic acid (LPA) and, thereafter, phosphatidic acid (PA) [5,6,14,28]. Inducible disruption of *TgATS1* is lethal to tachyzoites and causes a drastic reduction of phospholipid content

(approximately 50% reduction) including bulk phospholipid synthesis, leading to the disturbance of most parasite organelles while highly affecting the apicoplast membrane integrity. Nevertheless, *TgATS1* disruption (lethal) versus *TgATS2* disruption (nonlethal) revealed that LPA C14:0 is a major apicoplast product essential for the parasite survival and addition of exogenous LPA C14:0 on *ATS1* mutant can rescue the parasite growth compare to LPA C16:0. Similar results were obtained by disrupting the *ATS1* of *P. falciparum* during liver stage, emphasizing the critical role of the apicoplast lipid synthesis during the important life stage for parasite propagation [28]. In the original chloroplast, acyltransferases are purposed to galactoglycerolipid synthesis essential for chloroplast biogenesis and photosynthetic activity [29] but the lack of such lipids in malaria and toxoplasmosis parasites [19,30] and the repurpose of *ATS1/2* [5,6] illustrate the remodeling of the organisms to be conform to an parasitic intracellular lifestyle.

The FA synthesis capacity in the apicoplast is also dependent on host nutrient availability. In *P. falciparum*, it was shown that the FASII pathway in the apicoplast is essential during liver and mosquito stage while being dispensable during blood stages [13,31,32]. Contrastingly, transcriptomics analyses in malaria patients showed that under starved conditions, the expression of the apicoplast FASII was highly up-regulated in the human host, suggesting that the pathway could be more versatile than originally thought [33]. It was shown that under minimal lipid environment, which still sustain normal parasite growth, the apicoplast FASII could be metabolically (re)activated and generate medium size FA (C14:0) de novo within the parasite [20,34].

This emphasizes the parasite's ability to sense host conditions and alter its own metabolic processes to optimize its own development and propagation according to the host environment. In *Toxoplasma*, nutrient availability directly influences the synthetic processes of the apicoplast's FASII [35–38]. For example, in harsh/low host nutritional conditions, stable isotope labeling of the FASII products showed that FASII is metabolically up-regulated and capable of producing significantly more FAs (C14:0) to compensate for the lack of lipids in the external environment. A similar mechanism was revealed in *P. falciparum* blood stages where FASII is reactivated under low host lipid environment, becoming critical for parasite survival in blood stages under these conditions over a long period. Likewise, FASII activity can also be reduced to compensate for elevated levels of FA/lipids scavenged from the host to maintain lipid homeostasis, normal parasite propagation, and avoid death by lipotoxicity [39].

Recent findings have shown that FASII disruption by antibiotics (triclosan; [11]) or gene deletion dehydrogenase complex (PDH), malonyl-CoA-[acyl carrier protein] transacylase (FabD) [40], and FabZ [37] leads to an inhibition of parasite growth, which can be rescued with the supplementation of myristic and palmitic acids, confirmation that these acyl chains are the main end products of the pathway. This was similarly observed in the *ATS1* mutant, which is rescued after LPA C14:0 supplementation. This illustrated essentiality of host lipid scavenging and the parasite's ability to compensate for FASII disruption.

Unlike *Plasmodium* and *Toxoplasma*, *Cryptosporidium* behaves atypically where in *it* undergoes sexual and asexual stages in a single host and lacks the apicoplast. Intracellular FA synthesis relies on the giant eukaryotic type I FA synthetase (FASI), which is also conserved in *Toxoplasma* but inactive during rapid tachyzoite life stages and completely absent in *Plasmodium*. Host scavenged "short" FA chains C16:0 are used in *CpFASI* as a substrate for synthesis of "longer" FA chain up to C22:0 that are then involved in lipid and membrane remodeling. Further, this parasite also possesses typical Apicomplexa elongases, but for elongation up to 2 carbons (not 6) from host-scavenged FAs. The absence of FASII and that the substrate of *CpFASI* is a host-derived FA, suggests that the parasite is not able to perform synthesis of de novo full-length FA chains and it solely relies on its scavenging capacities [41].

Fatty acids are also directly scavenged from the host and extracellular environment

Parasite also obtain lipids by scavenging the host cell and its extracellular environment [42–44]. Using radioisotope-labeled lipids or precursors, and fluorescently labeled lipids, it has been shown that scavenged host lipids can be actively imported into the parasite and its organelles including the plasma membrane and the endomembrane system of the parasite [42]. These studies first showed how the parasite can import FA, PLs, and cholesterol. Sphingolipids, which are essential for parasite replication, are another important class of lipids actively scavenged by the parasite from host Golgi-derived vesicles despite the presence of a nonessential sphingomyelin synthase in *Toxoplasma* [45,46]. Furthermore, the cellular and metabolic fate of the scavenged lipids remained unknown. Recent studies showed that *Toxoplasma* can scavenge membrane/lipid material from host lipid droplets hijacked by the parasite [47,48], FA from the host mitochondria [49], and that oleic acid (C18:1) is an important scavenged FA that can kill the parasite by lipotoxicity [50]. Collectively, the existing data were suggesting that the parasite needs to scavenge lipids for survival as confirmed by disruption of the apicoplast FASII and/or complementation by external FA sources [5,6,16,37,40]. The use of metabolic labeling and lipidomic have now shed more light on the nature and the cellular destiny for such imported FA. Amiar and colleagues showed that most major phospholipid classes (PC, PE, and PI) and their molecular species were generated from an obligatory combination of FA directly scavenged from the host. Yet, this was using an indirect method labeling de novo-made FA from the apicoplast, and an actual approach to directly quantify the FA “scavenger” was missing. Dass and colleagues addressed this issue by directly fueling the host FASII pathway with ^{13}C glucose to generate its own ^{13}C labeled FA and phospholipids. Using such approaches allowed for monitoring and quantification of the scavenging capacity and deciphered the first parasite scavenged lipidome. This confirmed that very long chain FAs are scavenged [16]. Tachyzoites scavenge considerably more medium and long chain FAs than previously thought, notably unsaturated FAs such as palmitoleic acid (C16:1), oleic acid (C18:1), and paullinic acid (C20:1) [39]. Certain lipids and FAs are not produced by the parasite and must be obtained from the host of their environment [42,44,51]. Most importantly, this approach determined that the parasite constantly scavenges host FAs, which are then stored as triacylglycerol (TAG) in parasite lipid droplets, and then timely mobilized when the parasite most need them during parasite division. Altogether, this allows a constant access to lipid resources without the parasite being affected by potential lipotoxic death. However, using radioisotope and fluorescently labeled lipids, it has also been shown that, beyond being directed to lipid droplets, recruited host lipids can be directed also enter into the endomembrane system of the parasite [52].

Expectingly, the host nutrient environment strongly governs the scavenging capacity of *Toxoplasma* tachyzoites as well as the de novo lipid synthesis capacity. Amiar and colleagues have further shown that under host starvation, the parasites can stimulate “overscavenging,” inducing the formation of giant multivesicular bodies made from deep modifications of host organelles, further directed toward the parasite vacuole and which content is imported in the PV [6]. The identity and composition of giant multivesicular bodies (gMVBs) are still unknown at this stage. However, electron microscopy strongly suggest that they originate mainly from the host nuclear envelope/ER and may somehow allow the parasite to increase its lipid scavenging capacity in the absence of nutrient-rich serum. Further research is required to fully characterize their role in host–parasite interactions specific to the host-nutrient environment.

Mi-ichi and colleagues reported that palmitic acid (C16:0) and oleic acid (C18:1) is the sole combination of FAs for intraerythrocytic asexual proliferation of *P. falciparum* parasites

[34,53]. These FAs can be further activated to acyl-CoAs by 4 acyl-CoA synthetase (ACS) found in *Plasmodium* sp. genome. Intriguingly, *P. falciparum* harbor an additional 9 ACSs, which happen to be encoded in the subtelomeric regions where a high level of recombination occurs such as the *var* genes [54]. This emphasizes their importance for the survival of these life stages [27,54]. Of these ACSs, 2 of them have an apicoplast targeting sequence, but their localization and role in FA synthesis remain unclear. Recently, ACS11 as shown to be critical for parasites survival and been proposed as an interesting drug target, with existing MMV compounds [55].

Exogenous FAs, phospholipids, and those released by phospholipases (PLA2) can be recycled and used in phospholipid and neutral lipid assembly [56–58]. Recent work by 2 independent studies have also shown that *Pf*PLA2 is essential for gametocytogenesis during blood stages [57] and the fertilization process during mosquito stages [59]. Collectively, these studies emphasize that the synthesis of endogenous FAs is not essential for parasite growth and may in fact solely rely on exogenous FAs in blood stage parasites.

Other classes of lipids also need to be directly scavenged from the host and host environment

T. gondii and *Plasmodium* parasites are auxotroph for cholesterol and must be scavenged from the host or their environment [60,61]. Nishikawa and colleagues identified an acyl-CoA: cholesterol acyltransferase localized to the *T. gondii* parasite ER that produces sterol esters and forms lipid bodies (Fig 3). Upon depletion of this protein, free FAs' levels increased. They were also able to determine that in a host lipoprotein-free environment, there was a decrease in lipid droplet numbers of the parasite. This indicates that the host lipid availability governs neutral lipid synthesis in *Toxoplasma* [62]. Recently, *T. gondii* serine hydrolases with esterase and thioesterase activities have been identified and could be acting upon lipids to release FA chains. This also highlights the potential for targeting parasite hydrolases against lipids for therapeutic applications against the parasite [63].

The process by which *Plasmodium* parasites take up cholesterol is still largely unknown. Malaria parasites have moderate need of sterols for optimal development in liver stages, but they can adapt to survive in cholesterol-restrictive conditions by exploitation of accessible sterols derived from alternative sources in hepatocytes to maintain proper infectivity [64]. Recently, a *Pf*Niemann–Pick Type C1-Related protein (*Pf*NCR1) was suggested as an essential molecule for cholesterol transfer intraerythrocytic stage parasites [65]. Tomographic imaging results suggest that *P. falciparum* initially takes up external cholesterol and/or membrane cholesterol from the inner erythrocyte membrane, after which budding lipid membranes are elongated, migrate to the cytosol, and may fuse with and/or pass through the PVM to eventually reach the parasite body [66].

Lipid scavenging mechanisms

Identification of proteins and pathways involved in the scavenging of host lipids remain scarce due to the highly divergent and poorly conserved nature of such effectors in *Toxoplasma* and *Plasmodium* parasites. The parasite is able to manipulate the hosts microtubules (Fig 3) to redirect Rab vesicles from the host Golgi network toward the PV [67]. Together with the action of GRA proteins (GRA2, GRA6 . . .), they then generate an extensive tubular network called the intravacuolar network (IVN) in the parasite parasitophorous vacuole, which contributes to host-lipid scavenging and is dependent from parasite-dense granule proteins [52]. Host lipid droplets and vesicles can also be endocytosed through this parasite-made network due to their Rab7 coating, which is redirected by the parasite. *Plasmodium* asexual blood stages are also

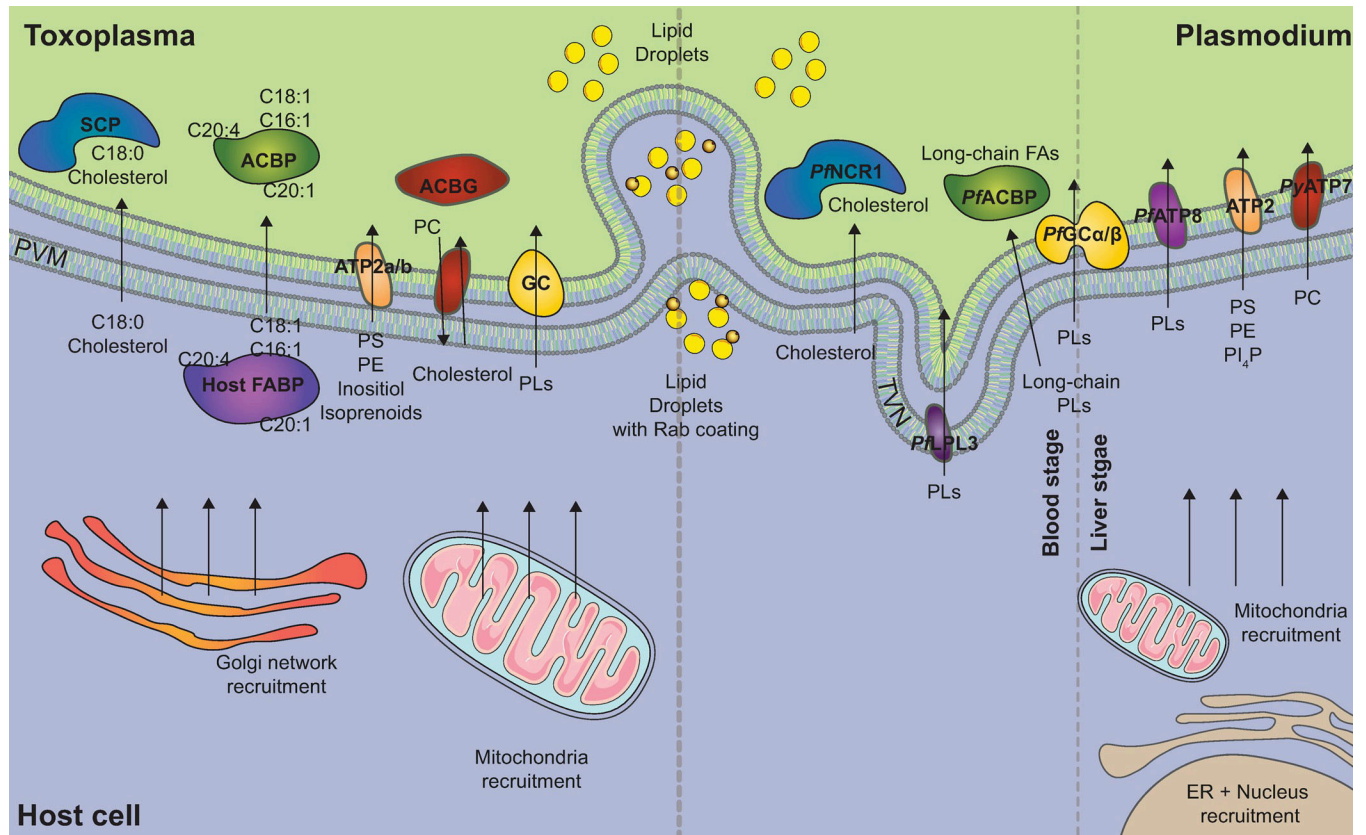


Fig 3. Scavenging mechanisms known in *T. gondii* (left) and *Plasmodium* sp. (right) parasites. *Toxoplasma* (left): *T. gondii* infection displays active recruitment of the host Golgi network and mitochondria to the parasite and is important in nutrient scavenging. Host lipid droplets can be endocytosed into the parasite through the PVM due to their Rab7 coating. Rab vesicles also facilitate the formation of the intravacuolar network found in the PVM. Stearic acid (C18:0) and cholesterol are taken up from the host via an SCP and host FABPs and parasite ACBPs modulate the importation of acyl chains into the parasite and to specific organelles. ABCGs are responsible for the influx/efflux of PC and cholesterol between the host and the parasite. Other lipid transporters are responsible for the scavenging of PS, PE (*TgP4-ATPase1-3*), choline, sphingolipids, inositol, and isoprenoids; all involved in lipid metabolism. GC is an atypical flippase whose exact mechanism is not yet known but is proposed to be a PL transporter. *Plasmodium* (right): Lipid droplet scavenging occurs in a similar manner to that in *Toxoplasma* parasites. Malarial infection displays active recruitment of the host ER/nucleus and mitochondria to the parasite (not in blood stages). It is suspected that *PfNCR1* is important in cholesterol transport from the host. *PfLPL3* localized to the intravacuolar TVN. *PfLPL3* allows to hydrolyze host phospholipids to generate FA then used for DAG/TAG formation 3 *PfACBPs* have been identified that show an affinity to transporting phosphorylated long-chain fatty acyl chains (PLs only). A GC protein also exists in *Plasmodium* (*PfGCα/β*) coupled to a P4 ATPase. ATP8 (in *P. falciparum*) and ATP2 (In *P. falciparum/chabaudi/berghei*) responsible for the scavenging of an assortment of PLs. *PyATP2* is responsible for PC transport into the parasite. ABCG, ATP-binding cassette G family transporter; ACBP, acyl-CoA binding protein; DAG, diacylglycerol; FA, fatty acid; FABP, fatty acyl binding protein; GC, guanylate cyclase; PC, phosphatidylcholine; PE, phosphatidylethanolamine; *PfNCR1*, *PfNiemann–Pick Type C1-Related protein*; PL, phospholipid; PS, phosphatidylserine; PVM, parasitophorous vacuole membrane; SCP, sterol carrier protein; TAG, triacylglycerol; TVN, tubulovesicular network.

<https://doi.org/10.1371/journal.ppat.1010313.g003>

capable for generating trafficking network within the host cell, via extensions of the PVM into the red blood cell cytosol, also known as the tubulovesicular network (TVN), which can promote nutrient exchange including lipids. Indeed, a recent study showed that the parasite expresses a lysophospholipase (LPL) (i.e., lipid-hydrolyzing enzyme) that locates at the TVN to generate FA used for timely membrane biogenesis during schizogony [68]. It has also been shown that the loss of a phospholipase can inhibit the parasites ability to scavenge lipids and further suggests that host lipids are immediately recycled at the point parasite entry at host–parasite interface [47].

The host cell mitochondria and Golgi network have shown to be actively recruited/move toward the PVM right after infection and can contribute to lipid homeostasis [49,61]. Host mitochondria are recruited in close vicinity to the parasite parasitophorous vacuole during

Toxoplasma infection and limit the parasites' ability to uptake FA, but it is also suggested that host mitochondria are involved in innate immunity against parasite infection [49]. In host cells lacking mitochondrial fusion, there is an increase in FA uptake [49], hence also pointing that beyond limiting FA supply, mitochondria is also an active source of FA for the parasite. The PVM's highly porous nature, which allows molecules up to 1.9 kDa into the parasite from the host cytoplasm, is accredited to the secreted parasite proteins GRA17 and GRA23 [69,70]. The parasite can mediate these processes of lipid uptake involving many different host-pathogen interactions through tubular networks and escort proteins. A sterol carrier protein (SCP) called *TgHAD-2SCP2* is able to transport cholesterol and oleic acid to be incorporated into neutral lipids [71]. *Toxoplasma* also has 6 ATP-binding cassette G family transporter (ABCG), which localizes differentially within the parasite and are shown to be involved in phospholipid and cholesterol import/efflux [72]. Not only can these parasites scavenge FA, but they can also recruit whole phospholipids [42,73] and neutral lipid stores directly from the host [47]. Phospholipid synthesis is facilitated by the scavenging of precursors such as serine, ethanolamine, and choline from the host environment. These polar headgroups are used by the parasite for the production of phosphatidylserine (PS), phosphatidylethanolamine (PE), and phosphatidylcholine (PC) [55,74]. Chen and colleagues have shown that PE and PS are able to be taken up directly from the host environment, unlike PC that thus has to be generated directly by the parasite from host-scavenged and or de novo-made precursors [75]. A very recent study suggests that parasite lysophospholipase could be used to generate the phosphocholine for parasite PC synthesis from existing lysolipids from the host during *P. falciparum* asexual blood stages [68].

PLs and FA are amphipathic molecules, meaning they can disrupt the membrane as they are recruited from the host to the parasite. This dilemma is overcome by carrier proteins such as acyl-CoA binding proteins (ACBPs) and FA binding proteins (FABPs) are such protein classes, which bind to fatty acyl esters and transport them across various cellular compartments [76]. The genome of *Toxoplasma* has no FABP but encodes for 2 ACBPs and are involved in lipid signaling and metabolism. In the absence of the cytosol *TgACBP1*, there is a decreased abundance of C18:1, which is predominantly scavenged from the host [73]. The mitochondrial *TgACBP2* plays a key role in cardiolipin metabolism and is critical of the growth and virulence of type II parasites [77]. Both proteins under starvation showed no deleterious effect on tachyzoite growth, indicating it is unlikely they are involved in nutrient adaptation. ATP-dependent PL transporters for PS and PE are present in the plasma membrane of tachyzoites [75].

The *P. falciparum* genome annotation revealed the existence of 3 putative ACBPs [78]. Kumar and colleagues show that *PfACBPs* have a higher binding affinity to long-chain fatty acyl-CoAs than short chains. They also show that they can bind to phosphorylated lipids but not to the unphosphorylated lipid esters, such as DAG and TAG, suggesting phospholipid transport rather than that of FAs/neutral lipids. Their roles in intracellular transport or host scavenging is still not fully elucidated [79].

To cross membranes in an efficient manner, lipids can be channeled by transporters such as flippases. In *P. falciparum* parasites, there are 5 flippases whose role and putative redundancy are currently fragmented [80,81]. *Plasmodium chabaudi* ATP2 has been identified as an essential lipid flippase responsible for PS and PE transport [82]. Homologs in other *Plasmodium* sp. exist but without confirmation of function. Recently, the *Plasmodium yoelii* ATP7 ATPase has been characterized as a phospholipid transporter responsible for the uptake of PC across the plasma membrane in mosquito stage ookinetes [83]. Both *Toxoplasma* and *Plasmodium* sp. possess atypical flippases with dual domains, named GC (*TgGC* and *PfGC* α + *PfGC* β) consisting of a guanylate cyclase (GC) domain coupled to a P-4 ATPase (flippases). Both are involved in the processes of parasite invasion, egress, and microneme secretion

through cGMP and lipid signaling. Briefly, both enzymes can generate cGMP, which activates PKG and a signaling cascade, which includes calcium release and activation of calcium-dependent protein kinases (CDPKs). The flippase domain of GCs are known to be essential; however, their exact mechanism in the above mentioned process is unclear [55,84,85]. In a study that monitored the in vitro virulence traits of a lab-adapted *T. gondii* strain, the early fixation of a P4 flippase gene SNP supported a critical role of lipid homeostasis [35]. Other flippases have been identified in *Toxoplasma*, but their roles have not been fully elucidated [75].

In general, *Toxoplasma* tachyzoite-infected cells are biologically flexible at many levels (genome, epigenetic, transcriptional, protein, and metabolic) to increase their ability to acquire nutrients from their environment and provide them to the parasite. As a good example at the lipid level, once within a cell, tachyzoites increase host synthesis of neutral lipids (TAG) and host lipid droplet numbers [48,49]. This lipid “hijacking” is facilitated via changes at the transcriptional levels of the host, such as the up-regulation of key host enzymes involved in TAG production like acylglycerol-3-phosphate acyltransferase (AGPAT2), acyl-CoA: diacylglycerol acyltransferase (DGAT2), and FA binding transport proteins like FABP3 and FABP5. Similarly, under starvation, parasites exhibit an increase in lipid storage abundance [6]. The low nutritional condition is sensed by the parasite, which attempts to compensate by the up-regulation of FASII lipid synthesis using glucose. The effector TgASP5, a Golgi-resident aspartyl protease, has been shown to play a role during FBS starvation [6].

Neutral lipids can be acquired from the host through endocytosis via the *T. gondii* parasite PVM. IVN had Rab7 coating onto their membranes. It is also proposed that probable interaction between Rab effectors and proteins present on PVM in order to promote this event of scavenging [47]. A separate study also should show that LPA accumulates in vesicles that are trafficked through the parasites secretory pathway, suggesting that there is convergence between lipid uptake and the endocytic pathway [86]. The ATS2 (protein involved in LPA to PA conversion) KO mutant has also shown evidence of aberrant endocytosis at the plasma membrane; however, it is presently unclear which, if any, nutrients are taken up by endocytosis during intracellular development [6].

Globally, *Plasmodium* parasites are believed not to take up lipids by typical endocytosis pathways, but characterization of PfEHD and PfLPL1 could suggest that, like *T. gondii* parasites, neutral lipids are acquired via endocytosis [87,88]. During *P. berghei* liver stage development, there is host cell mitochondria recruitment at the PVM, like in *Toxoplasma*, but in this context to mediate lipoic acid scavenging, which is required for parasite growth [89].

The balance between membrane biogenesis, lipid storage, and lipotoxicity in nutrient adaptation

Lipid storage is essential in maintaining this lipid homeostasis within the parasite and is used for the prevention of lipotoxicity or as an efficient energy source in suboptimal growth/culture conditions (Fig 4). The latter can be achieved through the process of β -oxidation in which lipids, in the form of FA, imported into the mitochondria or the peroxisomes, and then broken down into acetyl-CoA. These pool of acetyl-CoAs can then enter the mitochondrial TCA cycle and leads to energy production. The presence of β -oxidation is highly debated in the Apicomplexa field, and many questions [90,91] still exist about the fate of DAG/TAG and the dependence of this process on the host and its proteins/nutrient condition (NB: It is believed that *Toxoplasma* possess a complete beta oxidation pathway in its mitochondrion but lacks the canonical transporter allowing to initiate beta-oxidation, the Carnitine palmitoyl transferase CPT1; the situation is more complex in *P. falciparum* where not only CPT1 is missing but also some other members of the beta-oxidation pathway).

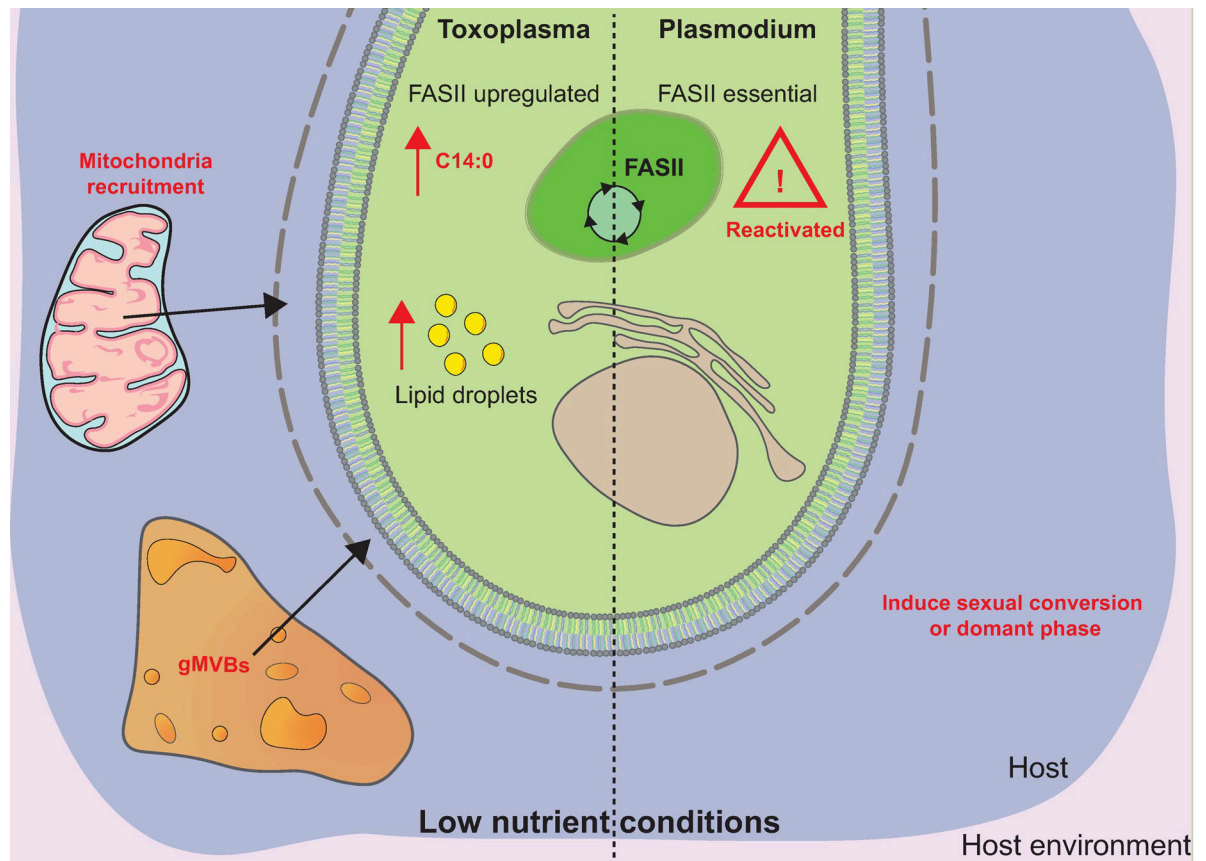


Fig 4. Cellular changes in parasite (*Toxoplasma*: left; *Plasmodium* sp.: right) in low nutrient conditions. Mitochondria recruitment and gMVBs are apparent and exacerbated in low nutrient conditions of *Toxoplasma* tachyzoites. The metabolic up-regulation of FASII (resulting in the increase production of C14:0), along with an increase in parasite lipid droplets, is characteristic of low nutritional conditions in the host. In similar conditions, when nutrients are limited in the host environment, *Plasmodium falciparum* asexual blood stages can up-regulate the metabolic activity of the apicoplast FASII, rendering it essential in these conditions. The lack of LPC in the host environment leads to sexual conversion of the parasite. Very little is known about the adaptation of this parasite to changing lipid statuses. gMVB, giant multivesicular body; LPC, lysophosphatidylcholine.

<https://doi.org/10.1371/journal.ppat.1010313.g004>

A recent study by Primo and colleagues has demonstrated that laboratory adaptation of *T. gondii* GT1 strain results in augmented phenotypes driven by selection pressures in the nutrient content of the extracellular environment. They also identified medium chain FAs to be the limiting factor in the extracellular environment, which provided insight into the contribution of FAs in parasite virulence. Lab adaptation evolution experiments performed in 1% FBS, as opposed to 10% FBS showed an up-regulation of genes involved in FA metabolism, specifically those in the FASII pathway. This reiterates the importance of these genes in parasite survival in harsh conditions [35].

The physiological fluctuations of the host nutrient environment are modulated between the equilibrium of both FASII and host-scavenged lipids. Lipids taken up from the host and made de novo by the parasite are reshuffled and remodeled in many different compartments (ER/cytosol/vesicles, etc.) of the parasites by a variety of proteins. Amiar and colleagues demonstrated that disrupting LPA production through its plant-like acyltransferase in the apicoplast leads to a severe impairment of the PL bulk content and composition that leads to a drastic reduction of the abundance of both PC (major membrane component) and PI by at least 50%. To reveal the origin of the PL FA chains, stable isotope labeling of was used in combination

with LC-MS based lipidomic analyses (labeled = apicoplast; unlabeled = host). It was revealed that 70% of FA chains (mainly short chains) from both PC and PI are from the apicoplast, while the remaining 30% are from the host. The importance of this ratio of make/take lipids is important to grasp as it is severely altered depending on the nutrient availability and strongly indicates the membrane remodeling ability of Apicomplexa parasites [4,16,21,36,92].

To allow for the remodeling of these lipids, Apicomplexa parasites possess a so-called eukaryotic glycerol-3-phosphate acyltransferase (GPAT; Fig 2), which has been located in the ER (*Plasmodium*) able to assemble LPA [14,93]. This GPAT seems capable of generating LPA with a high specificity for C16:0 and C16:1, both of which originating either from de novo synthesis or being scavenged from the host. In *Toxoplasma*, a putative GPAT and 1-acylglycerol-3-phosphate acyltransferase (AGPAT) locating the parasite ER [6] have been identified but not characterized yet, suggesting that the parasite could be able to reassemble host and de novo lipids in an “eukaryotic” manner to fuel membrane biogenesis. The eukaryotic-type AGPAT was also found in the *Plasmodium* ER, and both the *Toxoplasma* and *Plasmodium* homologs seem essential for the parasite survival [6,14]. On another hand, parasites are also able to massively reroute host-scavenged lipids from membrane to storage to maintain parasite survival through active division in a timely regulation and to prevent parasite death by lipotoxicity. Indeed, recent findings showed that a PA phosphatase in *T. gondii* (TgLIPIN) can act as a “switch” and a “metabolic scale” by converting PA to diacylglycerol (DAG), ultimately sustaining bulk TAG synthesis by fueling DAG to diacylglycerol acyltransferase (DGAT) affecting formation of parasite lipid droplets [39,94]. DAG can also be converted to cytidine diphosphate-diacylglycerol (CDP-DAG, pools that are present in the apicoplast or the ER), which serves as a major precursor for phospholipid synthesis [95]. In a low lipid environment, the deletion of TgLIPIN in the parasite leads to a decrease in lipid droplets and TAG levels, ultimately leading to gross membrane malformations and parasite death by lipotoxicity. Intriguingly, this effect is exacerbated in a high host lipid environment when the TgLIPIN is depleted (i.e., the more host lipid in the absence of TgLIPIN, more membrane, less TAG, high parasite death rate) the unlike wild-type parasites, which growth and survival is typically favored under higher host lipid/nutrient content [39]. This imbalance leads to an accumulation of free FAs, which are indicative and causative of lipotoxicity, and ultimately leads to the parasite’s death. It is interesting to note that gMVBs are highly formed under suppression of this protein in both low and high nutrient environment. The formation of gMVBs was previously observed to form solely under low host nutritional conditions, as seen by Amiar and colleagues (Fig 4). The parasite thus seems tricked into a false environment of low lipid levels, thinking that no lipids are available for the conversion of PA to DAG and for the formation of storage lipid droplets/TAGs. The parasite thus seems to overcompensate by continuing to scavenge host lipids that leads to an accumulation of PA, which unnaturally fuels PLs synthesis, then diverged into the endomembrane system of the parasite, affecting the membrane/structural integrity of the parasite.

Furthermore, phospholipases are suspected to play a crucial role in the recycling and reshuffling of lipids (Fig 4). Phospholipases are lipolytic enzymes that hydrolyze phospholipid substrates at specific ester bonds, releasing lysolipids and FA. TgPL2 is one such phospholipase that localizes to the apicoplast and regulates PC and lysophosphatidylcholine (LPC) levels in the parasite [96]. This protein seems to be crucial in the lipid homeostasis of the apicoplast since its deletion leads to rapid organelle loss. Different LPLs can serve to generate FA that sources TAG and DAG synthesis, but their specific localization allows different function. PflLPL1 is a dynamic protein of *P. falciparum*, which transits from parasite periphery/PVM into cytosolic vesicles that ends in a compartment closely localized to the food vacuole and rich in neutral lipids. PflLPL1 generates FA that are used to synthesis neutral lipids, DAG, and TAG, which are used to promote hemozoin formation in the food vacuole, thus allowing

essential heme detoxification by using host lipids as substrates. Depletion of *PfLPL1* is deleterious for the *Plasmodium* blood stage but can be rescued by addition of exogenous FA in the culture media, clue of the parasite plasticity. Closer to the host, *PfLPL3* localized to the intravacuolar TVN. *PfLPL3* allows to hydrolyze host phospholipids to generate FA, then used for DAG/TAG formation. These DAG/TAGs are mobilized during blood stages schizogony and thus serve as a tightly controlled reservoir of building blocks for bulk phospholipid synthesis in the parasite. Such process is like what was uncovered through the characterization of *TgLIPIN* in *T. gondii* tachyzoites where host lipids are constantly scavenged, then stored for a timely use for membrane biogenesis specifically during asexual division.

Physiological context

The ability of *T. gondii* to infect any nucleated cell resides in its strength/flexibility to metabolically adapt to their host (Fig 4). These intracellular parasites are in constant competition with their host for nutrient dependencies (not limited to just lipids, but includes other metabolites like glucose and glutamine), which is indirectly dependent on the environmental nutritional conditions [6,97,98]. Amiar and colleagues have also shown that *T. gondii* parasites under a low lipid environment up-regulates the FASII pathway [6]. Moreover, encountering different cell types in an organism has exposed the parasites to a wide panel of environments with different nutrient availability. Endemic areas affected by *Plasmodium*, in many cases, have a population largely affected by malnutrition. Parasites infect different cell types (hepatocytes, erythrocytes) and face certain changes in host nutrient; under amino acid starvation, parasite asexual replication within the red blood cells is reduced, and, instead, parasites enter a hibernating state [99]. Host LPC was revealed to be a critical nutrient that influences parasite growth and differentiation to the sexual stage of blood stages, with high serum levels of LPC responsible for the repression of sexual conversion [100].

Metabolic adaptation in a physiological context of these diseases caused by these parasites is becoming increasingly studied as it may holds the keys to how the parasite can sense and adapt to its host metabolic and nutritional conditions [35]. Phenotypic analyses recently indicated that only traits effected by extracellular host environment conditions evolved in *Toxoplasma* lab-adapted strains, indicating this importance in parasite propagation. Expression of genes involved in FASII pathway and ER FA elongation were up-regulated in extracellular parasites after lab adaptation.

Recent study uncovered the role of a *trans*-FA responsible for the host specificity of *Toxoplasma*. Data show that the accumulation of systemic linoleic acid (18:2) (25% to 46% in cat serum) due to the unusual absence of a $\Delta 6$ desaturase within feline intestines allows parasite oocyst propagation [101]. Such a metabolic lipid environment therefore provides a unique platform for the development of sexual stages otherwise absent in intermediate hosts, including humans. The fact that linoleic acid is toxic for *Toxoplasma* asexual stage tachyzoites also favors sexual stage development in the cat intestine environment. The enzyme $\Delta 6$ desaturase usually catalyzes the conversion of linoleic acid (C18:2) to arachidonic acid (C20:4), which, in turn, can participate in the formation of immune mediators like eicosanoids. Therefore, absence of this enzyme in feline intestines would also rescue the possibility of strong immune response toward parasite sexual stage.

In summary, Apicomplexa lipid metabolism is highly flexible and adapted under different host conditions. Giant strides have been taken in recent years to uncover the complex biology of this parasite and its intimate interactions with the human host. But major questions remain unanswered. Much of this is centered on the cryptic nature of host effectors, which are poorly conserved across eukaryotes and have coevolved specifically in *Toxoplasma* with the human

host. The processes by which parasites scavenge FAs and potentially whole lipids are still in question. Similarly, the proteins responsible for sensing, and adapting to, low host nutritional content are still poorly defined. Recently, a novel kinase *PfKIN1* has been found to bear homology to the *Snf1* protein found to regulate the nutritional response to starvation in yeast [102]. *PfKIN* mutant parasites struggle to adapt to low nutritional environments in *P. berghei* parasites [102]. Future efforts will likely focus on the signaling network responsible for sensing and implementing this response. Furthermore, by establishing that host nutrient content determines the extent of parasite scavenging response and host remodeling, it will be well worth experimenting with different host cell types to establish which genes are essential under which conditions and/or cell types.

Future research on Apicomplexa metabolism will follow the current trend of the parasite's adaptation in different host conditions. It will be important to elucidate this plasticity in different cell types, nutrient conditions, and how it may play a role in stage conversion. Collectively, the work described in this review and successive work is paving the road in identifying novel anti-Apicomplexa therapeutics, specifically concerning the metabolic battle between the host and parasite.

References

1. Jian J. Biosynthesis of lipids. The fundamentals of Biochemistry. 7th ed. S. Chand Publishing; 2004. Available from: http://www.cuchd.in/e-library/resource_library/University_Institutes_of_Sciences/Fundamentals_of_Biochemistry/Chap-25.pdf.
2. World Health Organization. WORLD MALARIA REPORT. 2020:2020. [https://doi.org/10.1002/\(SICI\)1096-8628\(19971128\)73:1<1::AID-AJMG1>3.0.CO;2-Y](https://doi.org/10.1002/(SICI)1096-8628(19971128)73:1<1::AID-AJMG1>3.0.CO;2-Y)
3. Torgerson PR, Mastroiacovo P. The global burden of congenital toxoplasmosis: a systematic review. *Bull World Health Organ.* 2013; 91:501–8. <https://doi.org/10.2471/BLT.12.111732> PMID: 23825877
4. Mazumdar J, Striepen B. Make it or take it: Fatty acid metabolism of apicomplexan parasites. *Eukaryot Cell.* 2007; 6:1727–35. <https://doi.org/10.1128/EC.00255-07> PMID: 17715365
5. Amiar S, MacRae JI, Callahan DL, Dubois D, van Dooren GG, Shears MJ, et al. Apicoplast-Localized Lysophosphatidic Acid Precursor Assembly Is Required for Bulk Phospholipid Synthesis in *Toxoplasma gondii* and Relies on an Algal/Plant-Like Glycerol 3-Phosphate Acyltransferase. *PLoS Pathog.* 2016; 12:1–30. <https://doi.org/10.1371/journal.ppat.1005765> PMID: 27490259
6. Amiar S, Katris NJ, Berry L, Dass S, Duley S, Arnold CS, et al. Division and Adaptation to Host Environment of Apicomplexan Parasites Depend on Apicoplast Lipid Metabolic Plasticity and Host Organelle Remodeling. *Cell Rep* 2020; 30:3778–3792.e9. <https://doi.org/10.1016/j.celrep.2020.02.072> PMID: 32187549
7. Ralph SA, van Dooren GG, Waller RF, Crawford MJ, Fraunholz MJ, Foth BJ, et al. Metabolic maps and functions of the *Plasmodium falciparum* apicoplast. *Nat Rev Microbiol.* Nature Publishing Group; 2004. 203–16. <https://doi.org/10.1038/nrmicro843> PMID: 15083156
8. Waller RF, Keeling PJ, Donald RGK, Striepen B, Handman E, Lang-Unnasch N, et al. Nuclear-encoded proteins target to the plastid in *Toxoplasma gondii* and *Plasmodium falciparum*. *Proc Natl Acad Sci U S A.* 1998; 95:12352–7. <https://doi.org/10.1073/pnas.95.21.12352> PMID: 9770490
9. McFadden GI. Plastid in human parasites. *Nature.* 1996; 381:482. <https://doi.org/10.1038/381482a0> PMID: 8632819
10. Köhler S, Delwiche CF, Denny PW, Tilney LG, Webster P, Wilson RJM, et al. A plastid of probable green algal origin in Apicomplexan parasites. *Science* (80-). 1997; 275:1485–9. <https://doi.org/10.1126/science.275.5305.1485> PMID: 9045615
11. Martins-Duarte ES, Carias M, Vommaro R, Surolija N, de Souza W. Apicoplast fatty acid synthesis is essential for pellicle formation at the end of cytokinesis in *Toxoplasma gondii*. *J Cell Sci.* 2016; 129:3320–31. <https://doi.org/10.1242/jcs.185223> PMID: 27457282
12. Possenti A, Fratini F, Fantozzi L, Pozio E, Dubey JP, Ponzi M, et al. Global proteomic analysis of the oocyst/sporozyte of *Toxoplasma gondii* reveals commitment to a host-independent lifestyle. *BMC Genomics.* 2013; 14:1–18. <https://doi.org/10.1186/1471-2164-14-1> PMID: 23323973
13. van Schaijk BCL, Kumar TRS, Vos MW, Richman A, van Gemert G-J, Li T, et al. Type II fatty acid biosynthesis is essential for *Plasmodium falciparum* sporozoite development in the midgut of *Anopheles* mosquitoes. *Eukaryot Cell.* 2014; 13:550–9. <https://doi.org/10.1128/EC.00264-13> PMID: 24297444

14. Lindner SE, Sartain MJ, Hayes K, Harupa A, Moritz RL, Kappe SHI, et al. Enzymes involved in plastid-targeted phosphatidic acid synthesis are essential for *Plasmodium yoelii* liver-stage development. *Mol Microbiol*. 2014; 91:679–93. <https://doi.org/10.1111/mmi.12485> PMID: 24330260
15. Tymoshenko S, Oppenheim RD, Agren R, Nielsen J, Soldati-Favre D, Hatzimanikatis V. Metabolic Needs and Capabilities of *Toxoplasma gondii* through Combined Computational and Experimental Analysis. *PLoS Comput Biol*. 2015; 11:1–28. <https://doi.org/10.1371/journal.pcbi.1004261> PMID: 26001086
16. Ramakrishnan S, Docampo MD, Macrae JI, Pujol FM, Brooks CF, van Dooren GG, et al. Apicoplast and endoplasmic reticulum cooperate in fatty acid biosynthesis in apicomplexan parasite *Toxoplasma gondii*. *J Biol Chem*. 2012; 287:4957–71. <https://doi.org/10.1074/jbc.M111.310144> PMID: 22179608
17. Dubois D, Fernandes S, Amiar S, Dass S, Katris NJ, Botté CY, et al. *Toxoplasma gondii* acetyl-CoA synthetase is involved in fatty acid elongation (of long fatty acid chains) during tachyzoite life stages. *J Lipid Res*. 2018; 59:994–1004. <https://doi.org/10.1194/jlr.M082891> PMID: 29678960
18. Kloehn J, Oppenheim RD, Siddiqui G, De Bock P-J, Kumar Dogga S, Coute Y, et al. Multi-omics analysis delineates the distinct functions of sub-cellular acetyl-CoA pools in *Toxoplasma gondii*. *BMC Biol*. 2020; 18. <https://doi.org/10.1186/s12915-020-00791-7> PMID: 32546260
19. Welti R, Mui E, Sparks A, Wernimont S, Isaac G, Kirisits M, et al. Lipidomic analysis of *Toxoplasma gondii* reveals unusual polar lipids. *Biochemistry*. 2007; 46:13882–90. <https://doi.org/10.1021/bi7011993> PMID: 17988103
20. Botté CY, Yamaro-botté Y, Rupasinghe TWT, Mullin KA, Macrae JI. Atypical lipid composition in the purified relict plastid (apicoplast) of malaria parasites. *PNAS*. 2013; 110:7506–11. <https://doi.org/10.1073/pnas.1301251110> PMID: 23589867
21. Gulati S, Ekland EH, Ruggles KV, Chan RB, Jayabalasingham B, Zhou B, et al. Profiling the Essential Nature of Lipid Metabolism in Asexual Blood and Gametocyte Stages of *Plasmodium falciparum*. *Cell Host Microbe*. 2015; 18:371–81. <https://doi.org/10.1016/j.chom.2015.08.003> PMID: 26355219
22. Janouškovec J, Horák A, Oborník M, Lukeš J, Keeling PJ. A common red algal origin of the apicomplexan, dinoflagellate, and heterokont plastids. *Proc Natl Acad Sci U S A*. 2010; 107:10949–54. <https://doi.org/10.1073/pnas.1003335107> PMID: 20534454
23. van Dooren GG, Striepen B. The Algal Past and Parasite Present of the Apicoplast. *Annu Rev Microbiol*. 2013; 67:271–89. <https://doi.org/10.1146/annurev-micro-092412-155741> PMID: 23808340
24. Ralph SA, Foth BJ, Hall N, McFadden GI. Evolutionary pressures on apicoplast transit peptides. *Mol Biol Evol*. 2004; 21:2183–94. <https://doi.org/10.1093/molbev/msh233> PMID: 15317876
25. Lim L, Linka M, Mullin KA, Weber APM, McFadden GI. The carbon and energy sources of the non-photosynthetic plastid in the malaria parasite. *FEBS Lett*. 2010; 584:549–54. <https://doi.org/10.1016/j.febslet.2009.11.097> PMID: 19968990
26. Fleige T, Pfaff N, Gross U, Bohne W. Localisation of gluconeogenesis and tricarboxylic acid (TCA)-cycle enzymes and first functional analysis of the TCA cycle in *Toxoplasma gondii* q. *Int J Parasitol*. 2008; 38:1121–32. <https://doi.org/10.1016/j.ijpara.2008.01.007> PMID: 18336823
27. Shears MJ, Botté CY, Mcfadden GI. Fatty acid metabolism in the *Plasmodium* apicoplast: Drugs, doubts and knockouts. *Mol Biochem Parasitol*. 2015; 199:34–50. <https://doi.org/10.1016/j.molbiopara.2015.03.004> PMID: 25841762
28. Shears MJ, Macrae JI, Mollard V, Goodman CD, Sturm A, Orchard LM, et al. Characterization of the *Plasmodium falciparum* and *P. berghei* glycerol 3-phosphate acyltransferase involved in FASII fatty acid utilization in the malaria parasite apicoplast. *Cell Microbiol* 2017; 19. <https://doi.org/10.1111/cmi.12633> PMID: 27324409
29. Kobayashi K, Kondo M, Fukuda H, Nishimura M, Ohta H. Galactolipid synthesis in chloroplast inner envelope is essential for proper thylakoid biogenesis, photosynthesis, and embryogenesis. *Proc Natl Acad Sci U S A*. 2007; 104:17216. <https://doi.org/10.1073/pnas.0704680104> PMID: 17940034
30. Botté C, Saïdani N, Mondragon R, Mondragón M, Isaac G, Mui E, et al. Subcellular localization and dynamics of a digalactolipid-like epitope in *Toxoplasma gondii*. *J Lipid Res*. 2008; 49:746–62. <https://doi.org/10.1194/jlr.M700476-JLR200> PMID: 18182683
31. Yu M, Kumar TRS, Nkrumah LJ, Coppi A, Retzlaff S, Li CD, et al. The Fatty Acid Biosynthesis Enzyme FabI Plays a Key Role in the Development of Liver-Stage Malarial Parasites. *Cell Host Microbe*. 2008; 4:567–78. <https://doi.org/10.1016/j.chom.2008.11.001> PMID: 19064257
32. Vaughan AM O'Neill MT, Tarun AS, Camargo N, Phuong TM, Aly ASI, et al. Type II fatty acid synthesis is essential only for malaria parasite late liver stage development supplementary. *Cell Microbiol*. 2009; 11:506–20. <https://doi.org/10.1111/j.1462-5822.2008.01270.x> PMID: 19068099

33. Daily JP, Scanfeld D, Pochet N, Le Roch K, Plouffe D, Kamal M, et al. Distinct physiological states of *Plasmodium falciparum* in malaria-infected patients. *Nature*. 2007; 450:1091–5. <https://doi.org/10.1038/nature06311> PMID: 18046333
34. Mi-Ichi F, Kano S, Mitamura T. Oleic acid is indispensable for intraerythrocytic proliferation of *Plasmodium falciparum*. *Parasitology*. 2007; 134:1671–7. <https://doi.org/10.1017/S0031182007003137> PMID: 17610764
35. Primo VA, Rezvani Y, Farrell A, Murphy CQ, Lou J, Vajdi A, et al. The Extracellular Milieu of *Toxoplasma*'s Lytic Cycle Drives Lab Adaptation, Primarily by Transcriptional Reprogramming. *mSystems*. 2021; 6.
36. Dass S, Shunmugam S, Berry L, Arnold C-S, Katris NJ, Duley S, et al. *Toxoplasma* LIPIN is essential in channeling host lipid fluxes through membrane biogenesis and lipid storage. *Nat Commun*. 2021; 12. <https://doi.org/10.1038/s41467-021-22956-w> PMID: 34001876
37. Krishnan A, Kloehn J, Lunghi M, Chiappino-Pepe A, Waldman BS, Nicolas D, et al. Functional and Computational Genomics Reveal Unprecedented Flexibility in Stage-Specific *Toxoplasma* Metabolism. *Cell Host Microbe*. 2020;1–17. <https://doi.org/10.1016/j.chom.2020.01.002> PMID: 31991093
38. Xu XP, Elsheikha HM, Liu WG, Zhang ZW, Sun LX, Liang QL, et al. The Role of Type II Fatty Acid Synthesis Enzymes FabZ, ODSCI, and ODSCII in the Pathogenesis of *Toxoplasma gondii* Infection. *Front Microbiol*. 2021; 12:703059. <https://doi.org/10.3389/fmicb.2021.703059> PMID: 34531837
39. Dass S, Shunmugam S, Berry-Sterkers L, Duley S, Arnold CS, Pierrel F, et al. *Toxoplasma* LIPIN is essential in channeling host lipid fluxes between membrane biogenesis and lipid storage, accepted. *Nat Commun*. 2021.
40. Liang X, Cui J, Yang X, Xia N, Li Y, Zhao J, et al. Acquisition of exogenous fatty acids renders apicomplast-based biosynthesis dispensable in tachyzoites of *Toxoplasma*. *J Biol Chem*. 2020; 295:7743–52. <https://doi.org/10.1074/jbc.RA120.013004> PMID: 32341123
41. Zhu G. Current Progress in the Fatty Acid Metabolism in *Cryptosporidium parvum*. *J Eukaryot Microbiol*. 2004; 51:1–2. <https://doi.org/10.1111/j.1550-7408.2004.tb00384.x> PMID: 15352319
42. Charron AJ, Sibley LD. Host cells: Mobilizable lipid resources for the intracellular parasite *Toxoplasma gondii*. *J Cell Sci*. 2002; 115:3049–59. Available from: <https://pubmed.ncbi.nlm.nih.gov/proxy.insermbiblio.inist.fr/12118061/>. PMID: 12118061
43. Tomavo S, Slomianny C, Meissner M, Carruthers VB. Protein Trafficking through the Endosomal System Prepares Intracellular Parasites for a Home Invasion. *PLoS Pathog*. 2013; 9:e1003629. <https://doi.org/10.1371/journal.ppat.1003629> PMID: 24204248
44. Coppens I. Targeting lipid biosynthesis and salvage in apicomplexan parasites for improved chemotherapies. *Nat Rev Microbiol*. 2013; 11:823–35. <https://doi.org/10.1038/nrmicro3139> PMID: 24162026
45. Romano JD, Sonda S, Bergbower E, Smith ME, Coppens I. *Toxoplasma gondii* salvages sphingolipids from the host Golgi through the rerouting of selected Rab vesicles to the parasitophorous vacuole. *Mol Biol Cell*. 2013; 24:1974–95. <https://doi.org/10.1091/mbc.E12-11-0827> PMID: 23615442
46. Pratt S, Wansadhipathi-Kannangara NK, Bruce CR, Mina JG, Shams-Eldin H, Casas J, et al. Sphingolipid synthesis and scavenging in the intracellular apicomplexan parasite, *Toxoplasma gondii*. *Mol Biochem Parasitol*. 2013; 187:43–51. <https://doi.org/10.1016/j.molbiopara.2012.11.007> PMID: 23246819
47. Nolan SJ, Romano JD, Coppens I. Host lipid droplets: An important source of lipids salvaged by the intracellular parasite *Toxoplasma gondii*. *PLoS Pathog*. 2017. <https://doi.org/10.1371/journal.ppat.1006362> PMID: 28570716
48. Hu X, Binns D, Reese ML. The coccidian parasites *Toxoplasma* and *Neospora* dysregulate mammalian lipid droplet biogenesis. *J Biol Chem*. 2017; 292:11009–20. <https://doi.org/10.1074/jbc.M116.768176> PMID: 28487365
49. Pernas L, Bean C, Boothroyd JC. Mitochondria Restrict Growth of the Intracellular Parasite *Toxoplasma gondii* by Limiting Its Uptake of Fatty Acids. *Cell Metab*. 2018; 27:886–897.e4. <https://doi.org/10.1016/j.cmet.2018.02.018> PMID: 29617646
50. Nolan SJ, Romano JD, Kline JT, Coppens I. Novel approaches to kill *Toxoplasma gondii* by exploiting the uncontrolled uptake of unsaturated fatty acids and vulnerability to lipid storage inhibition of the parasite. *Antimicrob Agents Chemother*. 2018;62. <https://doi.org/10.1128/AAC.00347-18> PMID: 30061287
51. Tomavo S, Schwarz RT, Dubremetz JF. Evidence for glycosyl-phosphatidylinositol anchoring of *Toxoplasma gondii* major surface antigens. *Mol Cell Biol*. 1989; 9:4576–80. <https://doi.org/10.1128/mcb.9.10.4576-4580.1989> PMID: 2531282
52. Caffaro CE, Boothroyd JC. Evidence for host cells as the major contributor of lipids in the intravacuolar network of *Toxoplasma*-infected cells. *Eukaryot Cell*. 2011; 10:1095–9. <https://doi.org/10.1128/EC.00002-11> PMID: 21685319

53. Mi-Ichi F, Kita K, Mitamura T. Intraerythrocytic *Plasmodium falciparum* utilize a broad range of serum-derived fatty acids with limited modification for their growth. *Parasitology*. 2006; 133:399–410. <https://doi.org/10.1017/S0031182006000540> PMID: 16780611
54. Bethke LL, Zilversmit M, Nielsen K, Daily J, Volkman SK, Ndiaye D, et al. Duplication, gene conversion, and genetic diversity in the species-specific acyl-CoA synthetase gene family of *Plasmodium falciparum*. *Mol Biochem Parasitol*. 2006; 150:10–24. <https://doi.org/10.1016/j.molbiopara.2006.06.004> PMID: 16860410
55. Bisio H, Krishnan A, Marq J-B, Soldati-Favre D. Toxoplasma gondii phosphatidylserine flippase complex ATP2B-CDC50.4 2 critically participates in microneme exocytosis Running title: Contribution of phosphatidylserine in microneme exocytosis Affiliation. [cited 2021 Dec 13]. <https://doi.org/10.1101/2021.11.25.470034>
56. Flammersfeld A, Lang C, Flieger A, Pradel G. Phospholipases during membrane dynamics in malaria parasites. *Int J Med Microbiol*. 2017 [cited 2018 Jan 26]. <https://doi.org/10.1016/j.ijmm.2017.09.015> PMID: 28988696
57. Flammersfeld A, Panyot A, Yamaro-Botté Y, Aurass P, Przyborski JM, Flieger A, et al. A patatin-like phospholipase functions during gametocyte induction in the malaria parasite *Plasmodium falciparum*. *Cell Microbiol*. 2020;22. <https://doi.org/10.1111/cmi.13146> PMID: 31734953
58. Wilson SK, Knoll LJ. Patatin-like phospholipases in microbial infections with emerging roles in fatty acid metabolism and immune regulation by Apicomplexa. *Mol Microbiol*. 2018; 107:34–46. <https://doi.org/10.1111/mmi.13871> PMID: 29090840
59. Singh P, Alaganan A, More KR, Lorthiois A, Thiberge S, Gorgette O, et al. Role of a patatin-like phospholipase in *Plasmodium falciparum* gametogenesis and malaria transmission. *Proc Natl Acad Sci U S A*. 2019; 116:17498–508. <https://doi.org/10.1073/pnas.1900266116> PMID: 31413195
60. Trigg PI. Sterol metabolism of *Plasmodium*, knowlesi in vitro. *Ann Trop Med Parasitol*. 1968; 62:481–7. <https://doi.org/10.1080/00034983.1968.11686587> PMID: 4977573
61. Coppens I, Sinai AP, Joiner KA. *Toxoplasma gondii* exploits host low-density lipoprotein receptor-mediated endocytosis for cholesterol acquisition. *J Cell Biol*. 2000; 149:167–80. <https://doi.org/10.1083/jcb.149.1.167> PMID: 10747095
62. Nishikawa Y, Quittnat F, Stedman TT, Voelker DR, Choi JY, Zahn M, et al. Host cell lipids control cholesteryl ester synthesis and storage in intracellular *Toxoplasma*. *Cell Microbiol*. 2005; 7:849–67. <https://doi.org/10.1111/j.1462-5822.2005.00518.x> PMID: 15888087
63. Guyard V, Monteiro-Cardoso VF, Omrane M, Sauvanet C, Houcine A, Boulogne C, et al. ORP5 AND ORP8 ORCHESTRATE LIPID DROPLET BIOGENESIS AND MAINTENANCE AT ER-MITOCHONDRIA CONTACT SITES. *bioRxiv* 2021; 2021.11.11.468233. <https://doi.org/10.1101/2021.11.11.468233>
64. Labaied M, Jayabalasingham B, Bano N, Cha S-J, Sandoval J, Guan G, et al. *Plasmodium* salvages cholesterol internalized by LDL and synthesized de novo in the liver. *Cell Microbiol*. 2011; 13:569–86. <https://doi.org/10.1111/j.1462-5822.2010.01555.x> PMID: 21105984
65. Istvan ES, Das S, Bhatnagar S, Beck JR, Owen E, Llinas M, et al. *Plasmodium* niemann-pick type C1-related protein is a druggable target required for parasite membrane homeostasis. *Elife*. 2019; 8. <https://doi.org/10.7554/eLife.40529> PMID: 30888318
66. Hayakawa EH, Yamaguchi K, Mori M, Nardone G. Real-time cholesterol sorting in *Plasmodium falciparum*—erythrocytes as revealed by 3D label-free imaging. *Sci Rep*. 2020:1–12. <https://doi.org/10.1038/s41598-019-56847-4> PMID: 31913322
67. Romano JD, Nolan SJ, Porter C, Ehrenman K, Hartman EJ, Hsia R, et al. The parasite *Toxoplasma* sequesters diverse Rab host vesicles within an intravacuolar network. *J Cell Biol*. 2017; 216:4235–54. <https://doi.org/10.1083/jcb.201701108> PMID: 29070609
68. Sheokand P, Narwal M, Thakur V, Mohammed A. GlnS mediated knock-down of a phospholipase expedite alternate pathway to generate phosphocholine required for phosphatidylcholine synthesis in *Plasmodium falciparum*. *bioRxiv*. 2021 [cited 2021 Jun 18]. <https://doi.org/10.1042/BCJ20200549> PMID: 34133721
69. Schwab JC, Beckers CJM, Joiner KA. The parasitophorous vacuole membrane surrounding intracellular *Toxoplasma gondii* functions as a molecular sieve. *Proc Natl Acad Sci U S A*. 1994; 91:509–13. <https://doi.org/10.1073/pnas.91.2.509> PMID: 8290555
70. Gold DA, Kaplan AD, Lis A, Bett GCL, Rosowski EE, Cirelli KM, et al. The *Toxoplasma* dense granule proteins GRA17 and GRA23 mediate the movement of small molecules between the host and the parasitophorous vacuole. *Cell Host Microbe*. 2015; 17:642–52. <https://doi.org/10.1016/j.chom.2015.04.003> PMID: 25974303

71. Lige B, Sampels V, Coppens I. Characterization of a second sterol-esterifying enzyme in *Toxoplasma* highlights the importance of cholesterol storage pathways for the parasite. *Mol Microbiol*. 2013; 87:951–67. <https://doi.org/10.1111/mmi.12142> PMID: 23374239
72. Ehrenman K, Sehgal A, Lige B, Stedman TT, Joiner KA, Coppens I. Novel roles for ATP-binding cassette G transporters in lipid redistribution in *Toxoplasma*. *Mol Microbiol*. 2010; 76:1232–49. <https://doi.org/10.1111/j.1365-2958.2010.07169.x> PMID: 20487267
73. Fu Y, Cui X, Liu J, Zhang X, Zhang H, Yang C, et al. Synergistic roles of acyl-CoA binding protein (ACBP1) and sterol carrier protein 2 (SCP2) in *Toxoplasma* lipid metabolism. *Cell Microbiol*. 2018; 2:e12970. <https://doi.org/10.1111/cmi.12970> PMID: 30362657
74. Gupta N, Zahn MM, Coppens I, Joiner KA, Voelker DR. Selective disruption of phosphatidylcholine metabolism of the intracellular parasite *Toxoplasma gondii* arrests its growth. *J Biol Chem*. 2005; 280:16345–53. <https://doi.org/10.1074/jbc.M501523200> PMID: 15708856
75. Chen K, Günay-Esiyok Ö, Klingenberg M, Marquardt S, Pomorski TG, Gupta N. Aminoglycerophospholipid flipping and P4-ATPases in *Toxoplasma gondii*. *J Biol Chem*. 2021;296. <https://doi.org/10.1016/j.jbc.2021.100315> PMID: 33485966
76. Neess D, Bek S, Engelsby H, Gallego SF, Faergeman NJ. Long-chain acyl-CoA esters in metabolism and signaling: Role of acyl-CoA binding proteins. *Prog Lipid Res*. 2015; 59:1–25. <https://doi.org/10.1016/j.plipres.2015.04.001> PMID: 25898985
77. Fu Y, Cui X, Fan S, Liu J, Zhang X, Wu Y, et al. Comprehensive Characterization of *Toxoplasma* Acyl Coenzyme A-Binding Protein TgACBP2 and Its Critical Role in Parasite Cardiolipin Metabolism. *Host-Microbe Biol*. 2018; 9:1–20. <https://doi.org/10.1128/mBio.01597-18> PMID: 30352931
78. Kumar A, Ghosh DK, Ali J, Ranjan A. Characterization of Lipid Binding Properties of *Plasmodium falciparum* Acyl-Coenzyme A Binding Proteins and Their Competitive Inhibition by Mefloquine. *ACS Chem Biol*. 2019; 14:901–15. <https://doi.org/10.1021/acscchembio.9b00003> PMID: 30986346
79. Kumar M, Skillman K, Duraisingh MT. Linking nutrient sensing and gene expression in *Plasmodium falciparum* blood-stage parasites. *Mol Microbiol*. 2020. <https://doi.org/10.1111/mmi.14652> PMID: 33236377
80. Kenthirapalan S, Waters AP, Matuschewski K, Kooij TWA. Functional profiles of orphan membrane transporters in the life cycle of the malaria parasite. *Nat Commun* 2016; 7. <https://doi.org/10.1038/ncomms10519> PMID: 26796412
81. Martin RE. The transportome of the malaria parasite. *Biol Rev*. 2019; 8. <https://doi.org/10.1111/brv.12565> PMID: 31701663
82. Lamy A, Macarini-Bruzaferro E, Dieudonné T, Perálvarez-Marín A, Lenoir G, Montigny C, et al. ATP2, The essential P4-ATPase of malaria parasites, catalyzes lipid-stimulated ATP hydrolysis in complex with a Cdc50 β -subunit. *Emerg Microbes Infect*. 2021; 10:132–47. <https://doi.org/10.1080/22221751.2020.1870413> PMID: 33372863
83. Yang Z, Shi Y, Cui H, Yang S, Gao H, Yuan J. A malaria parasite phospholipid flippase safeguards midgut traversal of ookinetes for mosquito transmission. *Sci Adv*. 2021; 7. <https://doi.org/10.1126/sciadv.abf6015> PMID: 34301597
84. Katris NJ, Yamaryo-Botte Y, Janoušková J, Shunmugam S, Arnold CS, Yang ASP, et al. Rapid kinetics of lipid second messengers controlled by a cGMP signalling network coordinates apical complex functions in *Toxoplasma* tachyzoites. *bioRxiv*. 2020:p. 2020.06.19.160341. <https://doi.org/10.1101/2020.06.19.160341>
85. Brown KM, Long S, Sibley LD. Plasma membrane association by N-acylation governs PKG function in *Toxoplasma gondii*. *mBio*. 2017; 8:1–14. <https://doi.org/10.1128/mBio.00375-17> PMID: 28465425
86. Gras S, Jimenez-Ruiz E, Klinger CM, Schneider K, Klingl A, Lemgruber L, et al. An endocytic-secretory cycle participates in *Toxoplasma gondii* in motility. Laub MT, editor. *PLoS Biol*. 2019; 17:e3000060. <https://doi.org/10.1371/journal.pbio.3000060> PMID: 31233488
87. Thakur V, Asad M, Jain S, Hossain ME, Gupta A, Kaur I, et al. Eps15 homology domain containing protein of *Plasmodium falciparum* (PfEHD) associates with endocytosis and vesicular trafficking towards neutral lipid storage site. *Biochim Biophys Acta*. 2015; 1853:2856–69. <https://doi.org/10.1016/j.bbamcr.2015.08.007> PMID: 26284889
88. Asad M, Yamaryo-Botté Y, Hossain ME, Thakur V, Jain S, Datta G, et al. An essential vesicular-trafficking phospholipase mediates neutral lipid synthesis and contributes to hemozoin formation in *Plasmodium falciparum*. *BMC Biol*. 2021; 19:1–22. <https://doi.org/10.1186/s12915-020-00927-9> PMID: 33407428
89. Deschermeier C, Hecht LS, Bach F, Rützel K, Stanway RR, Nagel A, et al. Mitochondrial lipoic acid scavenging is essential for *Plasmodium berghei* liver stage development. *Cell Microbiol*. 2012; 14:416–30. <https://doi.org/10.1111/j.1462-5822.2011.01729.x> PMID: 22128915

90. Moog D, Przyborski JM, Maier UG. Genomic and proteomic evidence for the presence of a peroxisome in the apicomplexan parasite *Toxoplasma gondii* and other coccidia. *Genome Biol Evol*. 2017; 9:3108–21. <https://doi.org/10.1093/gbe/evx231> PMID: 29126146
91. Oppenheim RD, Creek DJ, Macrae JI, Modrzynska KK, Pino P, Limenitakis J, et al. BCKDH: The Missing Link in Apicomplexan Mitochondrial Metabolism Is Required for Full Virulence of *Toxoplasma gondii* and *Plasmodium berghei*. Sibley LD, editor. *PLoS Pathog*. 2014; 10:e1004263. <https://doi.org/10.1371/journal.ppat.1004263> PMID: 25032958
92. Tomčala A, Michálek J, Schneedorferová I, Füssy Z, Gruber A, Vancová M, et al. Fatty Acid Biosynthesis in Chromerids. *Biomolecules*. 2020; 10:1–26. <https://doi.org/10.3390/biom10081102> PMID: 32722284
93. Santiago TC, Zufferey R, Mehra RS, Coleman RA, Ben MC. The *Plasmodium falciparum* PfGatp is an Endoplasmic Reticulum Membrane Protein Important for the Initial Step of Malarial Glycerolipid Synthesis*. *J Biol Chem*. 2004; 279:92222–9232. <https://doi.org/10.1074/jbc.M310502200> PMID: 14668349
94. Quittnat F, Nishikawa Y, Stedman TT, Voelker DR, Choi J-Y, Zahn MM, et al. On the biogenesis of lipid bodies in ancient eukaryotes: synthesis of triacylglycerols by a *Toxoplasma* DGAT1-related enzyme. *Mol Biochem Parasitol*. 2004; 138:107–22. <https://doi.org/10.1016/j.molbiopara.2004.08.004> PMID: 15500922
95. Kong P, Ufermann CM, Zimmermann DLM, Yin Q, Suo X, Helms JB, et al. Two phylogenetically and compartmentally distinct CDP-diacylglycerol synthases cooperate for lipid biogenesis in *Toxoplasma gondii*. *J Biol Chem*. 2017; 292:7145–59. <https://doi.org/10.1074/jbc.M116.765487> PMID: 28314772
96. Lévêque MF, Berry L, Yamaryo-Botté Y, Nguyen HM, Galera M, Botté CY, et al. TgPL2, a patatin-like phospholipase domain-containing protein, is involved in the maintenance of apicoplast lipids homeostasis in *Toxoplasma*. *Mol Microbiol*. 2017; 105:158–74. <https://doi.org/10.1111/mmi.13694> PMID: 28419631
97. Blume M, Seeber F. Metabolic interactions between *Toxoplasma gondii* and its host [version 1; peer review: 2 approved]. *F1000Res*. 2018; 1719. <https://doi.org/10.12688/F1000RESEARCH.16021.1> PMID: 30467519
98. MacRae JI, Sheiner L, Nahid A, Tonkin C, Striepen B, McConville MJ. Mitochondrial metabolism of glucose and glutamine is required for intracellular growth of *Toxoplasma gondii*. *Cell Host Microbe*. 2012; 12:682–92. <https://doi.org/10.1016/j.chom.2012.09.013> PMID: 23159057
99. Babbitt SE, Altenhofen L, Cobbold SA, Istvan ES, Fennell C, Doerig C, et al. *Plasmodium falciparum* responds to amino acid starvation by entering into a hibernatory state. *Proc Natl Acad Sci U S A*. 2012; 109:E3278–87. <https://doi.org/10.1073/pnas.1209823109> PMID: 23112171
100. Brancucci NM, Gerdt JP, Wang CQ, De Niz M, Philip N, Adapa SR, et al. Lysophosphatidylcholine Regulates Sexual Stage Differentiation in the Human Malaria Parasite *Plasmodium falciparum*. *Cell*. 2017; 171:1532–1544.e15. <https://doi.org/10.1016/j.cell.2017.10.020> PMID: 29129376
101. Di Genova BM, Wilson SK, Dubey JP, Knoll LJ. Intestinal delta-6-desaturase activity determines host range for *Toxoplasma* sexual reproduction. *PLoS Biol*. 2019; 17. <https://doi.org/10.1371/JOURNAL.PBIO.3000364> PMID: 31430281
102. Mancio-Silva L, Slavic K, Grilo Ruivo MT, Grosso AR, Modrzynska KK, Vera IM, et al. Nutrient sensing modulates malaria parasite virulence. *Nature*. 2017; 547:213–6. <https://doi.org/10.1038/nature23009> PMID: 28678779